UNIVERSIDAD COMPLUTENSE DE MADRID
FACULTAD DE CIENCIAS FÍSICAS
Departamento de Geofísica y Meteorología

ESTUDIO DE TELECONEXIONES ATMOSFÉRICAS ASOCIADAS A FORZAMIENTOS OCEÁNICOS : INFLUENCIA EN EL CLIMA DE EUROPA

MEMORIA PARA OPTAR AL GRADO DE DOCTOR
PRESENTADA POR

Javier García Serrano

Bajo la dirección de la doctora

María Belén Rodríguez de Fonseca

Madrid, 2014

ISBN: 978-84-695-9681-4

DEPARTAMENTO DE GEOFÍSICA Y METEOROLOGÍA
FACULTAD DE CIENCIAS FÍSICAS
UNIVERSIDAD COMPLUTENSE DE MADRID

ESTUDIO DE TELECONEXIONES ATMOSFÉRICAS ASOCIADAS A FORZAMIENTOS OCEÁNICOS INFLUENCIA EN EL CLIMA DE EUROPA

Javier García Serrano

Memoria de Tesis Doctoral
Dirigida por Dra María Belén Rodríguez de Fonseca

Madrid, 2010

A mis padres, Charo y Antonio

Índice

ACERCAMIENTO

En el estudio del clima y sus características hay toda una rama de investigación dedicada a la *variabilidad climática*. Ésta se entiende como las fluctuaciones que presenta el clima y que se asocian a registros por encima o por debajo de las normales climatológicas. Estos estados normales o climatologías se refieren a condiciones de equilibrio en el sistema medioambiental que han sido relativamente constantes en el tiempo y en el espacio; y se obtienen estadísticamente como valores promedios al evaluar continuamente medidas observacionales durante largos períodos de tiempo. La variabilidad climática actúa sobre los elementos climatológicos; por lo que conocer la climatología es muy importante para entender su variabilidad.

La variabilidad climática comprende el estudio de las desviaciones de una variable analizada respecto a su climatología. Estas desviaciones se conocen como *anomalías*, y su determinación proporciona una distribución temporal de valores a ambos lados del valor promedio. Esta evolución temporal, con valores positivos (por encima) y negativos (por debajo), se conoce como *serie temporal* de anomalías. El análisis de una gran cantidad de estas series, de una o varias variables, revela que el sistema climático y su variabilidad están dominados por un número de fenómenos recurrentes, conocidos como *modos de variabilidad* o *patrones de variabilidad*. La componente oceánica de estos patrones, asociada a las desviaciones en la temperatura de la superficie del mar, es lo que para nosotros constituirá un forzamiento térmico oceánico o, simplemente, *forzamiento oceánico*.

Aunque la región de estudio en la que se centra este trabajo se extiende desde la cuenca oceánica del Atlántico Norte hasta el este del continente europeo; el campo de interés es la *circulación atmosférica global*, el movimiento del aire y sus consecuencias. La variabilidad de la circulación atmosférica es uno de los principales factores que determinan la distribución espacial de elementos climáticos como la precipitación o la temperatura del aire. Por tanto, el conocimiento de los factores que modulan o provocan la variabilidad atmosférica centra especialmente la atención de parte de la comunidad científica. Algunos de estos factores son externos al área de acción de las perturbaciones atmosféricas en el Atlántico Norte y Europa, y tienen su origen en regiones bastante alejadas de donde se dejan sentir sus efectos. Estas relaciones 'a distancia' se conocen como *teleconexiones atmosféricas*, y son las encargadas de propagar las anomalías desde el entorno de forzamiento hasta el dominio de impacto.

Esta Tesis doctoral se centra en el estudio de los mecanismos dinámicos que pueden explicar las conexiones remotas entre diferentes forzamientos oceánicos y la circulación atmosférica anómala en el sector Euro-Atlántico.

Los mecanismos físicos involucrados en estas teleconexiones comprenden una gran variedad de fenómenos atmosféricos. En esta Tesis, el problema se aborda focalizando el análisis en las perturbaciones sobre la atmósfera adyacente a las anomalías oceánicas superficiales, en la propagación de estas perturbaciones desde las regiones de forzamiento hasta la región de interés, en la posible interacción de esta propagación con la dinámica de más alta frecuencia (escala diaria) y menor extensión espacial, y en el impacto final en la variabilidad climática regional, con especial atención en el régimen de lluvias y la temperatura del aire.

Las perturbaciones atmosféricas sobre las anomalías de la superficie del mar implican intensas interacciones aire-océano, donde se ponen en juego flujos de calor y grandes movimientos de masas de aire en toda la columna, mostrando una estructura característica que involucra convergencia o divergencia de vientos de gran escala tanto en superficie como en los niveles más altos (~10-12 km). Estos fuertes movimientos verticales impactan en la circulación general de atmósfera, generando perturbaciones en las células de circulación meridional (Hadley y Ferrel) y zonal (Walker), y mostrando perturbaciones que representan circulaciones cerradas.

Por otro lado, las anomalías en esta convección profunda, y las perturbaciones asociadas en la convergencia/divergencia de la alta troposfera, son también capaces de perturbar la circulación general de carácter zonal (de oeste a este), y desde latitudes tropicales y subtropicales hasta latitudes polares. Estas perturbaciones se conocen como *ondas de Rossby* y son el mecanismo de teleconexión clave a analizar en esta Memoria. Estas ondas propagan las anomalías hasta regiones remotas (en nuestro caso el Atlántico Norte-Europa), dejando a su paso una sucesión de ciclones y anticiclones que generan impactos en el clima regional. Las ondas de Rossby se pueden propagar a lo largo de grandes arcos, con una marcada componente meridional, o zonalmente, 'canalizadas' a lo largo de las corrientes en chorro (vientos intensos del oeste).

Esta Tesis analiza cómo diferentes anomalías oceánicas son capaces de forzar este tipo de teleconexión e influir en el clima Euro-Atlántico. La escala temporal de estudio se centra en la *frecuencia interanual*, es decir, en la variabilidad climática que presenta oscilaciones año a año; siendo el objetivo general subyacente, la búsqueda de teleconexiones atmosféricas asociadas a estos forzamientos y que presenten, por tanto, un cierto carácter predictivo.

El trabajo se ha realizado teniendo en cuenta los meses en los que operan los diversos forzamientos, centrándose en el final del invierno en el caso del Pacífico, en verano en los modos del Atlántico Tropical y a finales de verano-otoño en el Mediterráneo. No obstante, este trabajo también ha tenido en cuenta la influencia del flujo medio (climatológico) en niveles altos de la troposfera del Hemisferio Norte, ya que dicha consideración es determinante a la hora de entender las teleconexiones. De esta forma, el ciclo estacional de las corrientes en chorro determinará el tipo de teleconexión producida desde la región de forzamiento. Es por ello que la propagación de las ondas de Rossby y el impacto sobre la precipitación o la temperatura del aire, en relación con dichos forzamientos, han sido analizadas de forma dinámica en algunos casos, teniendo en cuenta posibles transiciones en las teleconexiones dependiendo del cambio en el flujo medio.

ESTADO DEL ARTE

Como se ha introducido anteriormente, la variabilidad climática de la atmósfera y del océano actúa sobre los elementos climatológicos de cada región particular. Como este trabajo se ha centrado en la propagación de teleconexiones atmosféricas sobre la región Atlántico Norte-Europa, en este capítulo se describe primeramente la climatología del dominio de estudio, poniendo especial hincapié en la circulación atmosférica media de la región. Seguidamente se describe la variabilidad atmosférica del sector Euro-Atlántico, con especial atención a la Oscilación del Atlántico Norte, primer modo de variabilidad climática regional.
Posteriormente se describen los fenómenos de la variabilidad climática global que han sido objeto del trabajo, es decir, los que aquí se han considerado como forzamientos térmicos de las teleconexiones atmosféricas sobre el Atlántico Norte: El Niño-Oscilación del Sur del Pacífico tropical, el Niño Atlántico y el Atlántico Norte Subtropical, y la cuenca oriental del Mar Mediterráneo. Finalmente, en la última sección, se detallan los diferentes mecanismos de teleconexión atmosférica que estos forzamientos térmicos son capaces de generar; centrando la descripción en la propagación extratropical de ondas de Rossby, perturbaciones en la circulación zonal de Walker y en las circulaciones meridionales de Hadley y Ferrel, así como en la interacción entre la propagación extratropical de anomalías y la actividad transitoria eddy.

En este capítulo se presenta el estado actual del consenso científico sobre los fenómenos considerados en este trabajo, mientras que en el siguiente capítulo se analiza el estado actual de debate y las preguntas abiertas relativas a cada objetivo de esta Tesis.

1. Climatología del sector Atlántico Norte-Europa

Como ya se ha comentado, la variabilidad climática actúa sobre el estado medio; es decir, sobre los centros de acción o regiones clave de la climatología. En esta sección se describen dichas regiones sobre el sector Euro-Atlántico.

En la Fig. I.1 se muestran las medias climatológicas para los meses Enero y Julio de la presión al nivel del mar (SLP[1]) y del viento horizontal en superficie (1000hPa) y en la alta troposfera (200hPa). La región Euro-Atlántica se encuentra inmersa entre los cinturones hemisféricos de altas presiones subtropicales y de bajas presiones subpolares. De esta forma, dos de los elementos clave que afectan al clima europeo son el centro de altas presiones de Azores, situado entre el Atlántico Norte subtropical y latitudes medias, y el centro de bajas presiones de Islandia, centrado al sur de Groenlandia en invierno y en el continente en verano. La intensidad relativa entre estos dos sistemas de presión regula el flujo del oeste (*westerlies*) que se adentra en Europa, más intenso en invierno que en verano (Fig. I.1). Este flujo del oeste se extiende sobre la corriente en chorro del Atlántico Norte, la cual está gobernada por la actividad *eddy*[2]. Esta actividad es de muy alta frecuencia y está dominada por la escala sinóptica. Como resultado de los fuertes gradientes térmicos que tienen lugar sobre la costa este de Norte América (Terranova; Fig. I.2), allí se generan intensos flujos de calor *eddy* que producen gran actividad ciclogenética.

1 *Acrónimo del término inglés Sea Level Pressure.*

2 *Término inglés relativo a las perturbaciones turbulentas de escala sinóptica. De aquí en adelante se empleará este vocablo por no considerarse acertada ninguna traducción y por consistencia con el Capítulo IV.*

Esta actividad baroclínica favorece la formación de perturbaciones de presión que se propagan a lo largo de esta corriente en chorro y que intercambian energía con el viento medio a través de flujos de cantidad de movimiento, o flujos de momento. De esta forma, la intensidad relativa entre los sistemas de presión de Azores e Islandia regula también la penetración de las borrascas hacia el norte de Europa, en casos de flujo intenso, o hacia el área Mediterránea, en casos de flujo más débil.

Por su parte, el sistema de altas presiones de Azores también regula la intensidad de los vientos alisios sobre el Atlántico Norte tropical y subtropical, tanto en verano como en invierno (Fig. I.1). Las fluctuaciones en la fuerza de estos vientos afectan de forma considerable al sistema de afloramiento costero de Mauritania.

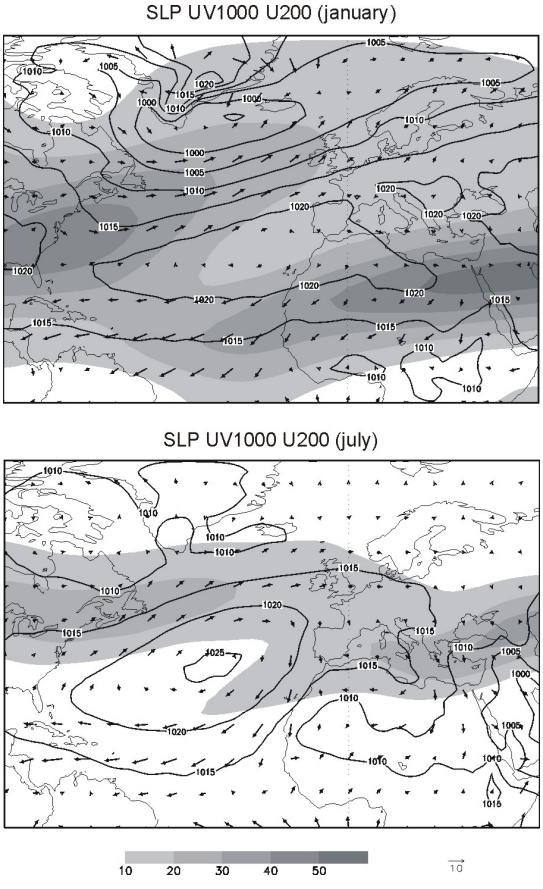

Fig. I.1. Climatología de la presión a nivel del mar (SLP; contornos, hPa), viento en superficie (1000hPa; flechas, m/s) y viento zonal en la alta troposfera (200hPa; sombreado, m/s) sobre el sector Euro-Atlántico.

De forma complementaria, esos vientos alisios del hemisferio Norte convergen con los vientos del Atlántico Sur tropical, de componente sureste, generando lo que se conoce como zona de convergencia inter-tropical (ITCZ[3]). Como se puede apreciar en la Fig. I.1, esta ITCZ sufre un desplazamiento de unos 5º-10º hacia el norte desde su posición ecuatorial en invierno hasta un eje este-oeste que une Brasil y la costa de África occidental en verano. Este desplazamiento latitudinal también es apreciable en el sistema de altas presiones de Azores; así como en la corriente en chorro subtropical, que parte de la costa occidental africana y se adentra por África del Norte en invierno y por el Mar Mediterráneo en verano. Este chorro subtropical, a diferencia de la corriente en chorro del Atlántico Norte, está dominado por la circulación de gran escala y es conducido térmicamente. El aire que asciende por la ITCZ se mueve en dirección ecuador-polo por el calentamiento diferencial terrestre; y gracias a la rotación de la Tierra y a la conservación del momento angular (aceleración de Coriolis) ese flujo posee una gran componente zonal oeste-este en latitudes subtropicales, lo que le confiere una estructura de corriente en chorro (Fig. I.1).

Por otro lado, parte de este aire caliente que asciende en la ITCZ, y que llega hasta latitudes subtropicales, desciende hasta la superficie provocando el sistema de altas presiones de Azores y los vientos alisios, que regresan a latitudes más bajas y que también poseen una componente zonal (en este caso este-oeste) gracias a la aceleración de Coriolis. Esta circulación cerrada y conducida térmicamente, ITCZ-Azores-vientos alisios, configura una celda de circulación conocida como célula de Hadley. Como ya se ha comentado, todo este sistema de circulación sufre desplazamientos latitudinales a lo largo del año; los cuales siguen el ciclo anual de irradiación solar, que se refleja en el ciclo anual de la temperatura de la superficie del mar (SST[4] ; Fig. I.2). Esta evolución anual está marcada por el fuerte gradiente meridional en latitudes medias (40N-50N) y por el máximo relativo durante los meses de verano y principios de otoño. Al desplazamiento latitudinal de los elementos atmosféricos a lo largo del año,

3 Acrónimo del término inglés Inter-tropical Convergence Zone.

4 Acrónimo del término inglés Sea Surface Temperature. En adelante se usará este vocablo por consistencia con la Secc. IV.

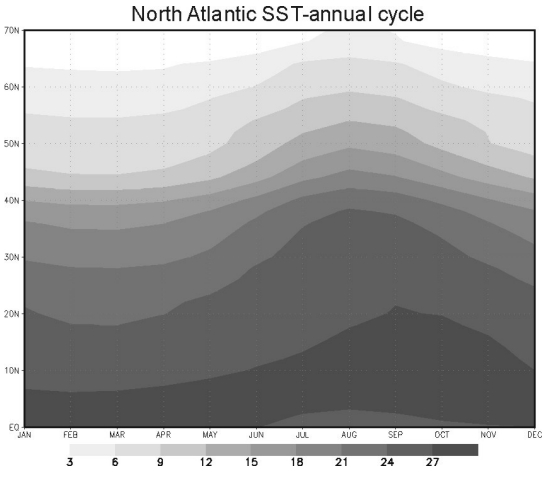

Fig. I.2. Ciclo anual de la SST (ºC) en el Atlántico Norte, promedio zonal 75W-10W.

que coincide con la evolución en la SST, se le conoce como *ciclo estacional* de la circulación atmosférica.

En conjunción con el desplazamiento estacional del chorro subtropical, conducido térmicamente, hay también un desplazamiento estacional del chorro del Atlántico Norte (Fig. I.1) que, como se ha dicho anteriormente, está conducido por la actividad *eddy*. Este chorro extratropical no está confinado en los niveles altos troposféricos, sino que se extiende en toda la profundidad de la troposfera (Fig. I.3). La actividad transitoria *eddy* importa momento del oeste hacia latitudes subpolares, ya que el flujo de momento es positivo en latitudes medias (Fig. I.3). La convergencia de ese flujo de momento *eddy* es compensado por un flujo medio indirecto, en dirección polo-ecuador. Por otro lado, esa convergencia de momento *eddy* en los niveles altos está equilibrada por la fricción en niveles bajos, produciendo vientos del oeste en superficie. Esta aparente celda de circulación indirecta de latitudes medias es conocida como célula de Ferrel, y está conducida por flujos de momento *eddy* en un promedio temporal. Sin embargo, los flujos de calor *eddy* dominan los niveles bajos de la 'célula' fuera de ese promedio y en la atmósfera libre de fricción, de tal forma que el efecto neto de la actividad transitoria es reducir el gradiente térmico entre latitudes tropicales y polares, así como reducir la cizalla vertical en el Atlántico Norte.

Por último, cabe destacar el cambio de régimen en

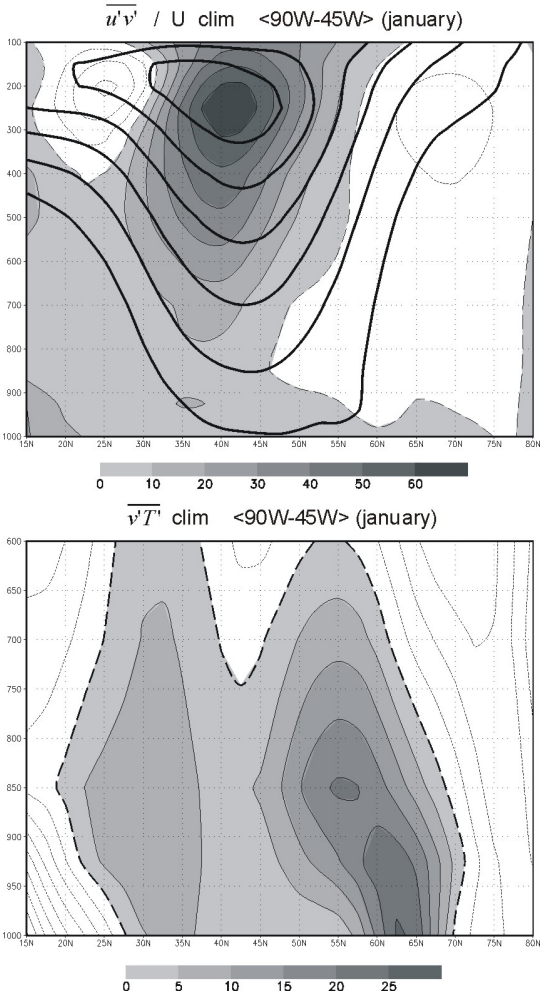

Fig. I.3. a) Viento zonal (contornos, ic=5m/s) y flujos de momento eddy (sombreado, ic=m²/s²; filtro-24h) y b) flujo de calor eddy (ic=5Km/s) en el sector Atlántico Norte; promedio zonal 90W-45W.

la presión atmosférica sobre el área Mediterránea, que, como se puede observar en la Fig.I.1, presenta una alta presión relativa en invierno y una baja presión relativa en verano. Este hecho refleja el efecto del contraste térmico estacional entre la tierra (suelo continental) y el mar.

[Bibliografía: Gill 1982; Peixot y Oort 1992; Holton 1992; Vallis 2006]

2. Variabilidad atmosférica en el sector Atlántico Norte-Europa

La variabilidad de la circulación atmosférica es uno de los principales factores que determinan

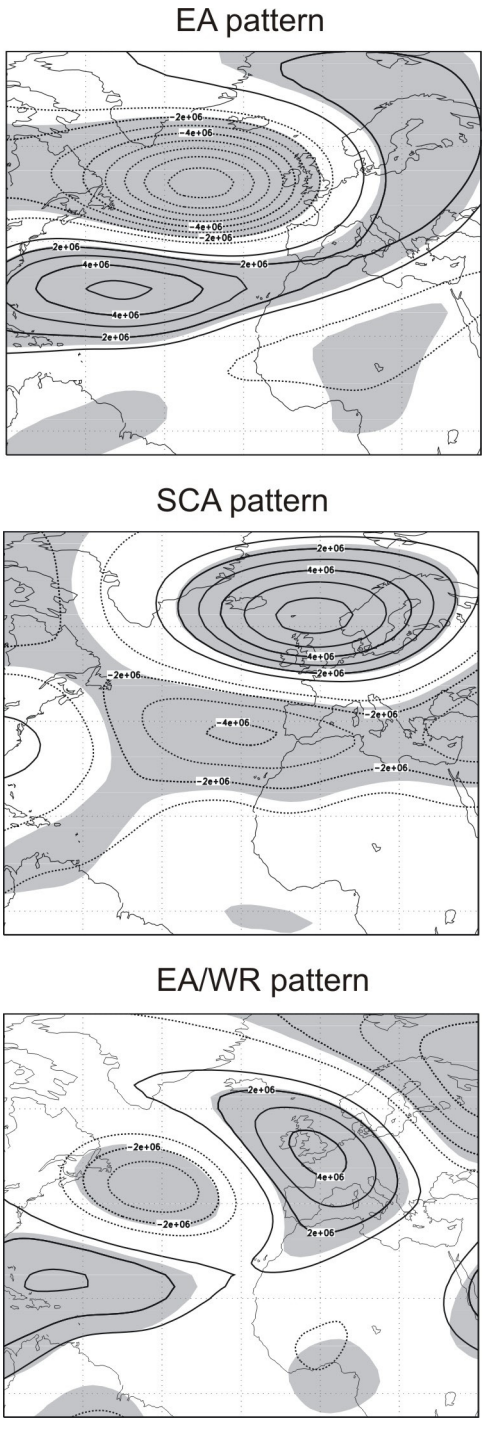

Fig. I.4. Patrones de teleconexión dominantes sobre el Atlántico Norte-Europa (ic=1 10^6 m²/s): EA (11%), SCA (8%), EA/WR (6%).

la distribución espacial de elementos climáticos como la precipitación o la temperatura del aire. De esta forma, la variabilidad climática entre regiones alejadas puede estar relacionada mediante lo que se conoce como *teleconexión atmosférica*. En particular, el clima de Europa está fuertemente influenciado por la Oscilación del Atlántico Norte (Secc. 2.1), siendo ésta el primer patrón de teleconexión de baja frecuencia (Barnston y Livezey 1987). Aun así, existen otros patrones de teleconexión que pueden tener una influencia importante sobre esos elementos climáticos en la región Euro-Atlántica. Aquí se describen las características esenciales de las anomalías de circulación asociadas a los patrones de teleconexión EA (East Atlantic), SCA (Scadinavian) y EA/WR (East Atlantic/West Russian). Una descripción detallada de las anomalías climáticas asociadas a estos patrones, junto con las series temporales de éstos, se puede consultar en la página web de la NOAA[5] , basada en los estudios de Wallace y Gutzler (1981) y Barnston y Livezey (1987). Así mismo, la variabilidad atmosférica en el sector Euro-Atlántico en otras escalas temporales puede consultarse en Sánchez-Gómez y Terray (2005) y Sánchez-Gómez et al. (2008). Muchos han sido los trabajos que han descrito la asociación entre el clima de la Península Ibérica y Europa y estos tres patrones atmosféricos. Entre ellos se pueden citar: Rodríguez-Puebla et al. (1998, 2001); Esteban-Parra et al. (1998); González-Rouco et al. (2000); Sáenz et al. (2001a, 2001b, 2001c); Rodríguez-Fonseca y Serrano (2002); Frías et al. (2005).

La descripción de estos tres patrones de teleconexión se hace aquí a través del análisis EOF de la función de corriente en 200hP sobre la región Euro-Atlántica 90W-40E / 5S-80N y para la estación invernal Nov-Feb (Fig. I.4).

El patrón EA fue descrito por Wallace y Gutzler (1981) y por Barnston y Livezey (1987); y posee principalmente tres centros de acción, siendo la anomalía sobre el Atlántico Norte su centro de acción más intenso, mientras que los otros dos centros de acción forman una anomalía alargada que se extiende desde la costa este de Norteamérica hasta Europa central.

El patrón SCA fue descrito por Barnston y Livezey (1987) como patrón 'Eurasia-1'; y consiste principalmente en un centro de acción sobre la península Escandinava y Mar del Norte, el cual

5 *http://www.cpc.noaa.gov/data/teledoc/telecontents.shtml*

está flanqueado por anomalías más débiles sobre el Atlántico oriental y la región mediterránea.

El patrón EA/WR fue descrito por Barnston y Livezey (1987) como patrón 'Eurasia-2'; y consiste fundamentalmente en cuatro centros de acción que le dan una apariencia de tren de ondas estacionario. Las anomalías de circulación parten del Golfo de Florida, cruzan el Atlántico Norte en latitudes medias, se adentran en el continente europeo por las Islas Británicas, y se extienden hacia el este de Europa y oeste de Asia.

2.1. Oscilación del Atlántico Norte

La *Oscilación del Atlántico Norte* (NAO[6]) es el modo dominante de variabilidad para el clima en el sector Euro-Atlántico a muchas escalas de tiempo (Visbeck et al. 2003), teniendo una alta conexión con los modos de baja frecuencia de la precipitación en Europa (Hurrell 1995). Esta oscilación se define como un intercambio de masa atmosférica entre latitudes subtropicales y polares del Atlántico Norte, correspondiendo a una medida de la intensidad de los sistemas de presión de Azores (altas presiones) e Islandia (bajas presiones). De esta forma, una NAO positiva se asocia a un reforzamiento del anticiclón de Azores y a un ahondamiento de la baja de Islandia; mientras que una NAO negativa se asocia a un debilitamiento de ambos sistemas de presión, o a un desplazamiento de los mismos (Hurrell et al. 2003; Fig I.5). Durante los episodios de alto/+ (bajo/-) índice de la NAO, se produce una reducción (aumento) en el transporte de humedad atmosférica en las regiones mediterráneas y, por tanto, una disminución (incremento) de la precipitación; ocurriendo lo contrario en el norte de Europa (Fig. 1.6). Muchos han sido los trabajos que han descrito los impactos climáticos de la NAO en la Península Ibérica y Europa. Entre ellos se encuentran los estudios de van Loon y Rogers (1978); Hurrell (1995); Hurrell y van Loon (1997); Rodó et al. (1997); Pozo-Vázquez et al. (2000, 2001); Sánchez-Gómez et al. (2001); Castro-Díez et al. (2002); Gámiz-Fortis et al. (2002); Trigo et al. (2002; 2004). En esta introducción, la descripción de la NAO se centra en los procesos atmosféricos que gobiernan su fenomenología. Una revisión de los impactos medioambientales de la NAO y de su circulación atmosférica asociada puede consultarse en Hurrell et al. (2003) y Thompson et al. (2003).

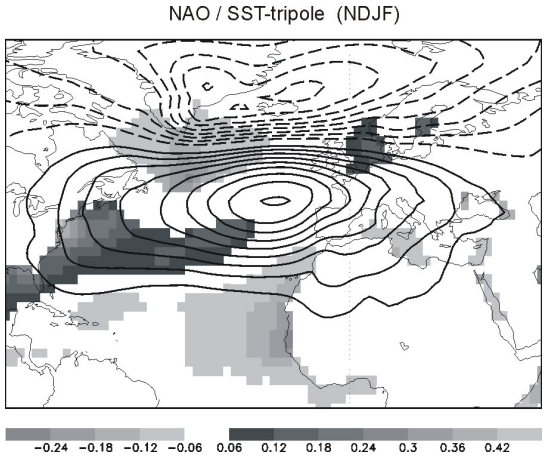

Fig. I.5. Circulación atmosférica (altura del geopotencial en 1000hPa, ci=5m) y anomalías de SST (ºC) asociadas a una NAO positiva; mapas de regresión sobre la segunda componente principal de la función de corriente en 200hPa (14%).

Hasta escalas interanuales, la NAO debe su existencia, no a interacciones acopladas océano-atmósfera, sino a la dinámica intrínseca de la atmósfera extratropical. Simulaciones numéricas del sistema climático han demostrado que los procesos atmosféricos por sí solos son suficientes para generar un patrón de variabilidad tipo NAO (Hurrell et al. 2003). Resultados de estudios teóricos y de modelización sugieren que las anomalías de SST de latitudes medias tienen un impacto muy débil sobre la NAO, por lo menos a escalas estacionales y anuales (e.g. Kushnir et al. 2002; Czaja et al. 2003). No obstante, varios trabajos mantienen que la variabilidad de la TAV[7] puede tener una relativa importancia en la predictabilidad de la NAO (Czaja y Frankignoul 1999, 2002; Drévillon et al. 2001; Rodríguez-Fonseca y Castro 2002; Drévillon et al. 2003; Cassou et al. 2004; Frankignoul y Kestenare 2005; Rodríguez-Fonseca et al. 2006; Peng et al. 2005).

La dinámica de la NAO está controlada por la variabilidad de los *stormtracks*[8] en el Atlántico Norte (Hurrell 1995; Hurrell et al. 2003). Fluctuaciones en la NAO están fuertemente acopladas a la intensidad del vórtice polar

6 *Acrónimo del término inglés North Atlantic Oscillation.*

7 *Acrónimo del término inglés Tropical Atlantic Variability.*

8 *Término inglés que se refiere a la 'trayectoria de los ciclones extratropicales de escala sinóptica'. En esta memoria se empleará preferentemente el vocablo inglés por conveniencia y por consistencia con el capítulo IV.*

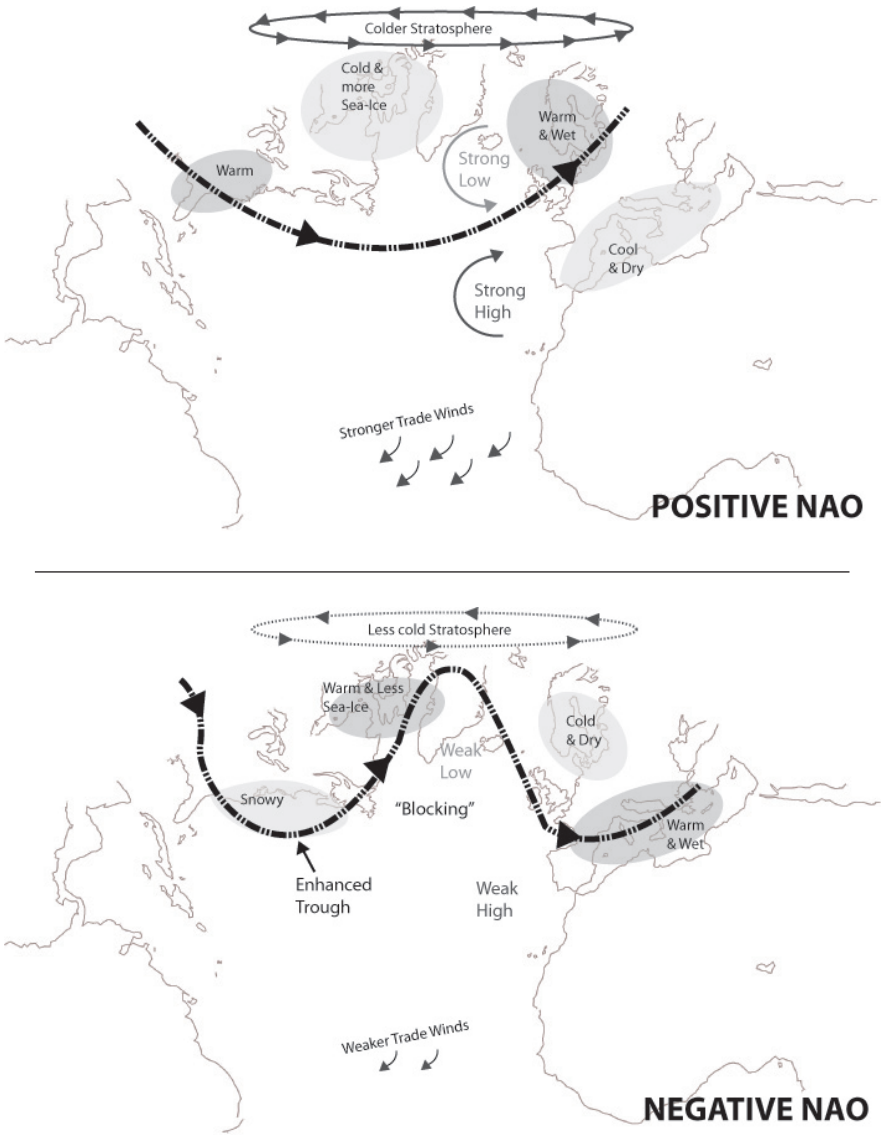

Fig. I.6. Condiciones atmosféricas e impactos climáticos de la fase positiva y negativa de la NAO.

estratosférico: una fase positiva de la NAO corresponde a un vórtice más frío y más fuerte, asociado con vientos troposféricos del oeste anómalos sobre los 55ºN, y viceversa (e.g. Ambaum y Hoskins 2002). Fluctuaciones en la NAO también están acopladas con la circulación en los trópicos: una NAO positiva corresponde a unos vientos alisios más fuertes sobre el Atlántico, anomalías negativas en la temperatura troposférica tropical, vientos anómalos del oeste en el ecuador centrados a 200hPa, y anomalías positivas de temperatura en niveles estratosféricos; lo que provoca un debilitamiento en el afloramiento de ondas desde la tropopausa tropical (Thompson y Wallace 2000). En latitudes medias y altas del Atlántico Norte, la corriente en chorro que canaliza los *stormtracks* está conducida por la convergencia o divergencia de flujo de momento *eddy*. Esta corriente es más débil que la corriente en chorro subtropical, y se encuentra sobre la zona de ciclogénesis, zona de generación de ondas baroclínicas; por lo que la variabilidad de esta corriente conducida por *eddies* se caracteriza por desplazamientos meridionales del flujo zonal (meandros) (Thompson et al. 2003).

De forma contemporánea al patrón atmosférico NAO, la circulación oceánica en el Atlántico Norte se ve anómalamente perturbada a través cambios en los giros oceánicos superficiales asociados al sistema de altas presiones de Azores (giro subtropical) y al sistema de bajas presiones de Islandia (giro subpolar). Este forzamiento atmosférico imprime en la cuenca atlántica un patrón oceánico conocido como *Tripolo* (Sutton y Allen 1997; Fig. I.5). Este patrón tripolar anómalo de SST posee tres centros de acción: uno en el Atlántico tropical, sobre el afloramiento de Mauritania; otro en latitudes medias, al este de la costa de Norte América; y un tercero en latitudes subpolares, sobre el Mar del Labrador. Estas anomalías de SST están causadas por flujos anómalos de calor latente y sensible, flujos anómalos de momento asociados a cambios en el esfuerzo del viento, anomalías en el transporte de Ekman, y efectos de advección por parte de las corrientes oceánicas medias, sobre todo de la corriente del Golfo-Atlántico Norte (Visbeck et al. 2003). A escala estacional e inter-anual la respuesta oceánica a la NAO se puede entender por tanto, y en primer orden, como una respuesta en la capa de mezcla. Por el contrario, a escala decadal (o superior) la respuesta oceánica implica cambios en la dinámica oceánica y perturbaciones en la circulación termohalina, que apuntan a un mayor papel en la realimentación océano-atmósfera asociado a la NAO (Visbeck et al. 2003).

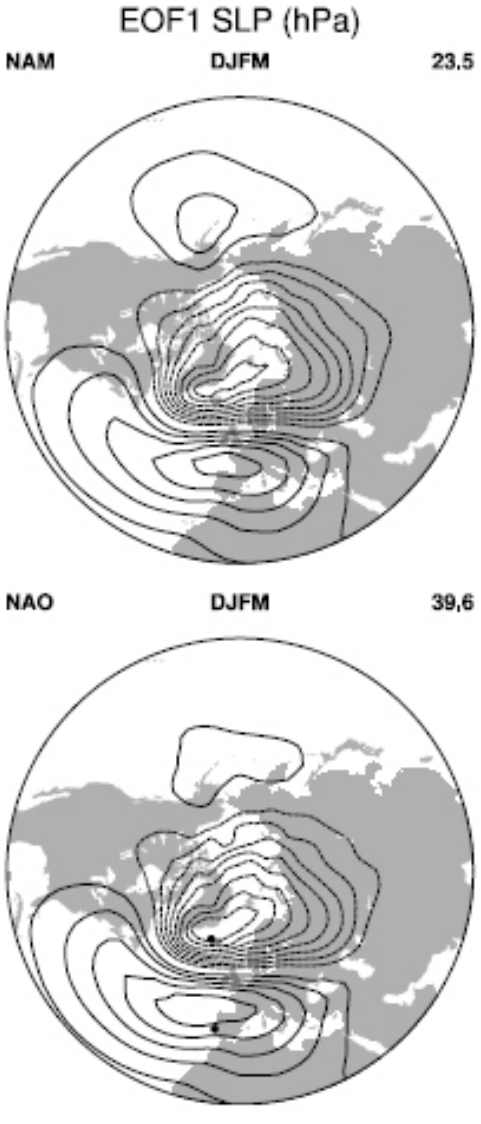

Fig. I.7. Modo anular (arriba) y patrón NAO (abajo) entendidos como primera EOF de SLP en el hemisferio Norte (20N-90N) y sector Euro-Atlántico (90W-40E), respectivamente. [Extraído de Hurrell et al. (2003)]

También en debate continúa el paradigma de considerar la NAO como parte de un fenómeno hemisférico conocido como Oscilación Ártica (AO[9] ; Fig. I.7). Dos perspectivas han sido propuestas para explicar el patrón global AO, en el que la NAO representa una regionalización o 'parte' de un fenómeno de mayor escala. La primera considera la AO como un modo anular a escala hemisférica, el cual representa una oscilación entre latitudes polares y latitudes medias del Atlántico Norte y Pacífico Norte, y que recibe el nombre de NAM[10] (e.g. Wallace 2000). La segunda perspectiva considera que la AO no constituye un modo anular, sino un modo no-anular, en el que la NAO es parte de una onda de Rossby estacionaria de número de onda 5 que se establece a través del efecto guía de onda de las corrientes en chorro del oeste (Branstator 2002; Watanabe 2004). No obstante, numerosos trabajos han mostrado la incompatibilidad de una dinámica común entre el sistema de altas presiones de Azores (Atlántico Norte) y el sistema de bajas presiones de Aleutianas (Pacífico Norte)(e.g. Deser 2000; Ambaum et al. 2001; Itoh 2002), y una teoría unificadora es todavía necesaria (consultar Thompson et al. 2003 para una revisión del debate).

9 Acrónimo del término inglés Artic Oscillation.

10 Acrónimo del términos inglés Northern Hemisphere Annular Mode.

3. Forzamientos oceánicos

3.1. El Niño y la Oscilación del Sur

El fenómeno de *El Niño-Oscilación del Sur* (ENSO[11]) es la fuente más importante de variabilidad en el sistema climático global (Peixoto y Oort 1992). Este sistema acoplado océano-atmósfera se caracteriza por calentamientos (El Niño) o enfriamientos (La Niña) anómalos de las aguas superficiales del Pacífico ecuatorial centro-oriental, en conjunción con una masiva subida o bajada de las presiones atmosféricas entre las regiones del este y el oeste del Pacífico tropical (Chang y Battisti 1998).

La componente oceánica de ENSO se caracteriza por anomalías en la temperatura de la superficie del mar (SST) que se extienden por todo el centro-este del Pacífico tropical, con forma de 'punta de flecha' y partiendo de las costas de Sudamérica (Fig. I.8a). La evolución completa de la SST a lo largo de un ciclo ENSO puede consultarse en Wang (2002a). La componente atmosférica de ENSO, la Oscilación del Sur, comprende el intercambio de masa atmosférica entre el Pacífico tropical sur-oriental y el Pacífico ecuatorial occidental (Fig. I.8b). El acoplamiento de estas dos componentes está regulado por el mecanismo de realimentación propuesto por Bjerknes (1969), que involucra la interacción entre la dinámica oceánica, la convección atmosférica y los vientos superficiales (Chang y Battisti 1998). De este modo, una anomalía inicial positiva de SST en el Pacífico oriental cambia el gradiente este-oeste de SST dentro de la cuenca, y así la fuerza de la circulación zonal asociada a la Oscilación del Sur (la célula de Walker), lo que resulta en un debilitamiento de los vientos alisios a lo largo del cinturón ecuatorial. Este cambio en el régimen de vientos alisios conduce, a su vez, a cambios en la circulación oceánica subsuperficial (termoclina) y en el afloramiento costero, lo que lleva a un reforzamiento de la anomalía inicial de SST (Fig. I.8). Este mecanismo de realimentación positivo conduce al Pacífico ecuatorial a un estado de calentamiento anómalo, es decir a un episodio El Niño. Anomalías e interacciones de signo contrario conducen a un estado anómalo de enfriamiento, es decir, a un episodio La Niña.

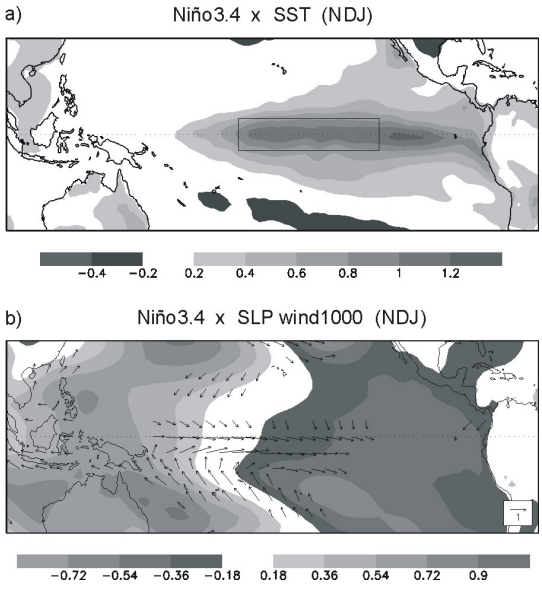

Fig. I.8. a) Mapa de regresión de la SST (ºC) sobre el índice Niño3.4 (rectángulo; 5S-5N / 170W-120W) durante la fase madura de ENSO (Nov-Dic-Ene; Wang 2002a). b) Igual que a) pero para la presión a nivel del mar (SLP; hPa) y el viento en 1000hPa (m/s; mostrado sólo donde el módulo es mayor que 0.5m/s).

Como se ha dicho, ENSO es la señal más importante de la variabilidad del sistema climático, y en particular a escala interanual; siendo el índice de SST Niño3.4 (promedio de SST en la región 5S-5N, 170W-120E; Fig. I.8a) una de las medidas más convenientes de su variación temporal (Sterl et al. 2007). Las anomalías de SST asociadas a ENSO producen cambios tanto en la atmósfera local (e.g. Wang 2002a, 2005) como en la circulación global de la atmósfera (e.g. Trenberth et al. 1998). A las alteraciones climáticas remotas asociadas a ENSO, que suceden lejos de la región de forzamiento (el Pacífico tropical), se les conoce como teleconexiones ENSO. Éstas han sido ampliamente estudiadas (Ropelewski y Halpert 1986, 1987, 1989, 1996; Kiladis y Diaz 1989; Kiladis y Weickmann 1992; Sánchez-Gómez et al. 2001; Frías et al. 2010), aunque todavía no todas pueden ser explicadas dinámicamente (e.g. Trenberth et al. 1998; Alexander et al. 2002); siendo la teleconexión invernal con el sector Euro-Atlántico uno de los objetivos abordados en este trabajo (Secc. II.1).

11 *Acrónimo del término inglés El Niño-Southern Oscillation.*

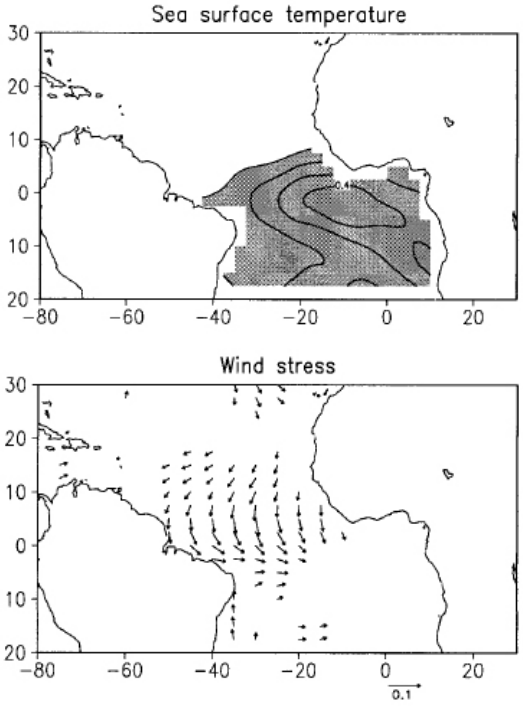

Fig. I.9. Anomalías de el modo Niño Atlántico; SST (ºC; arriba) y esfuerzo del viento (dyn/cm²; abajo; mostrado anomalías mayores de 0.02 dyn/cm²). [Adaptado de Ruiz-Barradas et al. (2000)]

3.2. Variabilidad del Atlántico Tropical

La *Variabilidad del Atlántico Tropical* (TAV[12]) a escalas interanuales y decadales comprende, principalmente, dos modos de variabilidad: el *modo Ecuatorial* y el *modo Dipolar* o *Meridional* (Servain et al. 1999). El primero, el modo ecuatorial, es una estructura de variabilidad climática caracterizada por variaciones anómalas de SST en el Atlántico ecuatorial, con un comportamiento equivalente a ENSO pero más débil (Zebiak 1993). Este modo está regulado dinámicamente por el mecanismo de realimentación de Bjerknes (Huang y Shukla 2005). El segundo, el modo meridional, se caracteriza por anomalías en el gradiente interhemisférico de SST (Carton et al. 1996, Chang et al. 1997), de forma que en un episodio típico aparecen anomalías de distinto signo a ambos lados de la ITCZ. A diferencia del modo ecuatorial, el modo meridional está regulado por el mecanismo de realimentación termodinámico WES[13] (Huang y Shukla 2005).

12 Acrónimo del término inglés Tropical Atlantic Variavility, la cual comprende el estudio de los cambios e interacciones en la ITCZ, vientos alisios y SST en la región del Atlántico Tropical.

13 Acrónimo del término inglés Wind-Evaporation-SST.

Además de estos dos mecanismos regionales de interacción océano-atmósfera, la TAV está fuertemente influida por forzamientos remotos, como el fenómeno ENSO y la Oscilación del Atlántico Norte (e.g. Ruiz-Barradas et al. 2000; Xie y Carton 2004; Huang y Shukla 2005; Chang et al. 2006).

3.2.a. El Modo Ecuatorial / Niño Atlántico

El modo Ecuatorial del Atlántico o *Niño Atlántico* es el primer modo de variabilidad de SST de la TAV desde primavera hasta otoño (Huang y Shukla 2005). Como ya se ha dicho, este modo está dominado por el mecanismo de realimentación positivo de Bjerknes (Bjerknes 1969; Zebiak 1993; Wang 2006; Keenlyside and Latif 2007). Así, en su fase positiva, este modo se caracteriza por una relajación en los vientos alisios que inducen una redistribución de las aguas cálidas a lo largo del cinturón ecuatorial, así como un debilitamiento en la pendiente de la termoclina y en el gradiente zonal

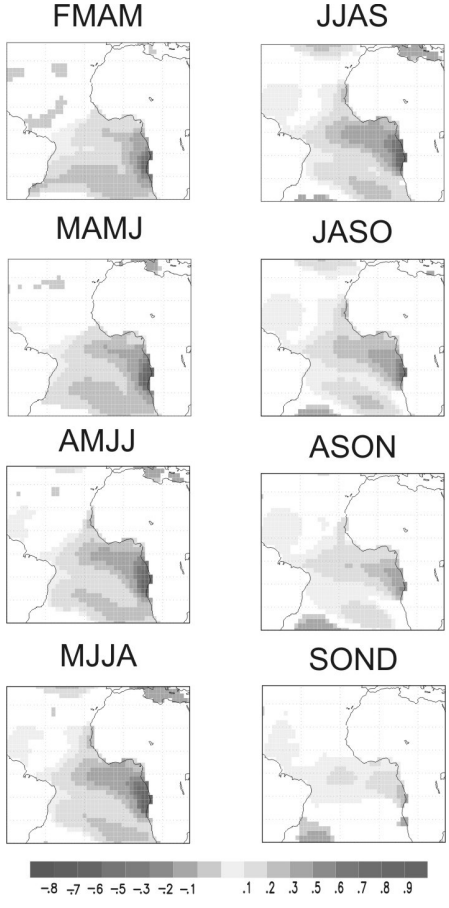

Fig. I.10. Secuencia EMCA de SST (ºC) asociada al Niño Atlántico. [Adaptado de Polo et al. (2008)]

del contenido de calor (Fig. I.9); produciéndose un desplazamiento hacia sur-este de la convección profunda (también en Carton et al. 1996; Ruiz-Barradas et al. 2000; Wang 2002b, 2005).

En este trabajo se ha analizado el Niño Atlántico perteneciente al clima reciente (Secc. II.2), desde finales de los años 70, debido a las tendencias observadas en el Atlántico tropical durante las últimas décadas (Rodríguez-Fonseca et al. 2010). En particular, el Niño Atlántico reciente ha sido descrito por Polo et al. (2008). Este modo, que tiene su máxima amplitud en verano (Losada et al. 2009a), no persiste hasta el invierno siguiente y no está correlacionado con el Niño Atlántico II, el modo Ecuatorial del Atlántico de principios del invierno (Nov-Dic; Okumura y Xie 2006).

El Niño Atlántico de verano comienza en la región afloramiento de Angola/Benguela, y es causado por anomalías en el esfuerzo del viento costero (invierno-primavera); se propaga hacia el norte y el oeste a través de ondas de Rossby oceánicas durante su fase de transición (primavera-verano); y su decaimiento está forzado por flujos anómalos de calor latente y por ondas de Kelvin oceánicas (verano-otoño) (Fig. I.10; Polo et al. 2008). En los últimos años se ha encontrado que este Niño Atlántico reciente está estadísticamente correlacionado con el posterior desarrollo de un episodio ENSO durante el otoño-invierno siguiente (Keenlyside and Latif 2007; Polo et al. 2008). El mecanismo dinámico que subyace a esta teleconexión inter-tropical ha sido mostrado por Rodríguez-Fonseca et al. (2009), con un modelo atmosférico (AGCM[14]) de complejidad intermedia, mientras que Losada et al. (2009b) lo ha corroborado con un ensemble de 4 modelos AGCM del Estado del Arte. La conexión Niño Atlántico-ENSO, que produciría anomalías de SST de signo contrario entre las cuencas, se produce por perturbaciones en la circulación zonal de Walker entre el Atlántico tropical y el Pacífico tropical.

3.2.b. El Modo Meridional

Este modo de variabilidad de la TAV consiste, esencialmente, en anomalías de SST en la región del Atlántico Norte Subtropical (SNA[15]), las cuales

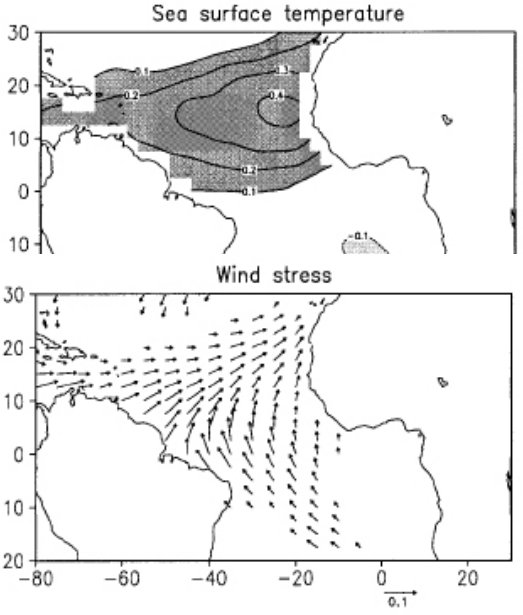

Fig. I.11. Igual que Fig. I.2, pero para el modo Meridional de la TAV. [Adaptado de Ruiz-Barradas et al. (2000)]

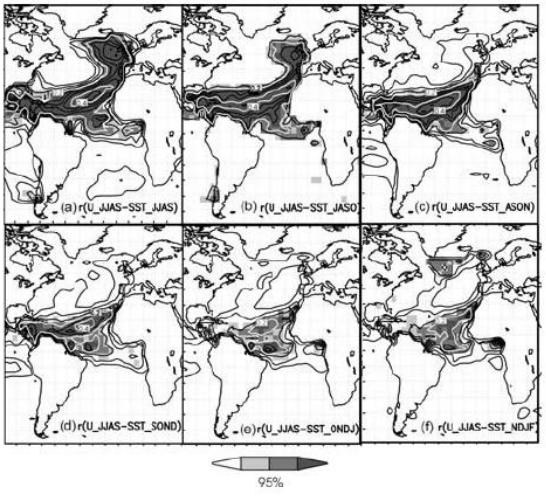

Fig. I.12. Evolución SST del SNA, como parte del NAH en verano y del NAT en invierno. [Extraído de Rodríguez-Fonseca y Castro (2002)]

están producidas fundamentalmente por cambios en los vientos alisios y en los flujos de calor latente (Fig. I.11), mediados por el mecanismo de realimentación WES (Cayan et al. 1992; Sutton et al. 2000). Este mecanismo mantiene que una anomalía positiva inicial de SST frena los vientos alisios, éstos a su vez extraen menos calor latente del océano y por tanto refuerzan la anomalía inicial.

14 Acrónimo del término inglés Atmospheric General Circulation Model.

15 Acrónimo del término inglés Subtropical North Atlantic.

La región SNA conecta el trópico con latitudes medias, y está estrechamente relacionada con el sistema anticiclónico de Azores. Por lo tanto, este modo está fuertemente influido por la Oscilación del Atlántico Norte y la ITCZ (Xie y Carton 2004), y podría tener un importante impacto climático en el extratrópico (Okumura et al. 2001).

La SST en el SNA comparte variabilidad con dos modos de mayor escala (escala hemisférica) que se extienden por el Atlántico Norte. En verano, el SNA constituye la rama subtropical del *patrón de herradura* (NAH[16]); mientras que en invierno, el SNA es la rama subtropical del *tripolo Atlántico* (NAT[17]), íntimamente ligado a la Oscilación del Atlántico Norte (Secc. 2,1; e.g. Czaja y Frankignoul 1999, 2002). El modo invernal NAT parece ser la evolución del modo de verano NAH (Fig. I.12); y esta evolución parece tener un impacto tanto en la circulación extratropical como en las anomalías climáticas sobre Europa (Rodríguez-Fonseca y Castro 2002; Cassou et al. 2004; Frankignoul y Kestenare 2005; Rodríguez-Fonseca et al. 2006).
Como en el caso del Niño Atlántico, este trabajo se ha focalizado en el período que cubre el clima reciente, desde finales de los años 70 (Secc. II.3). Dentro de este período, Polo et al. (2005) han mostrado que el modo SNA parece desarrollarse en conjunción con cambios en el sistema de afloramiento de Mauritania/Senegal, y han sugerido que los movimientos oceánicos verticales en la región costera podrían ser importantes para el origen o la persistencia de las anomalías de SST.

3.3. Variabilidad en el Mediterráneo

Los objetivos y el estudio llevados a acabo en este trabajo para la cuenca del Mar Mediterráneo se centran en la estación estival. Xoplaki et al. (2003a, 2003b) han mostrado que los principales modos de variabilidad en verano de la SST del Mediterráneo son dos modos con gradiente zonal: uno con la máxima amplitud en el oeste, sobre los mares Balear y de Liguria (wMED[18]); y otro con la máxima amplitud al este (eMED[19] ; Fig. I.13), sobre los mares Jónico y Egeo.

Del modo wMED se ha sugerido que juega un papel pasivo en la teleconexión del sistema

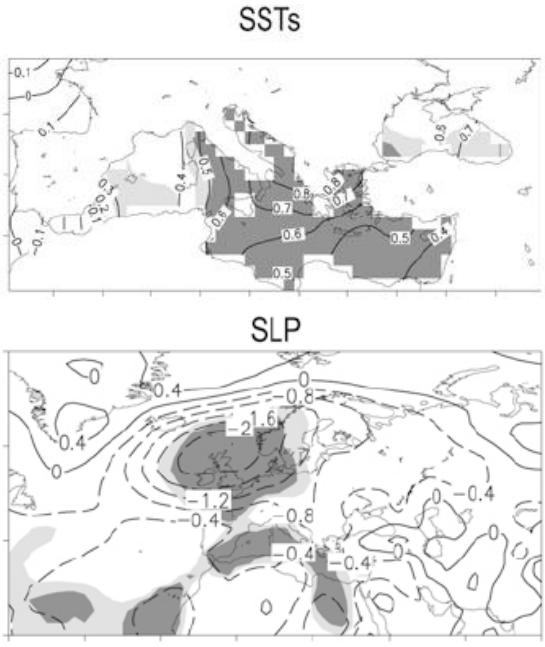

Fig. I.13. Anomalías de SST (ºC) y de presión a nivel del mar (SLP, hPa) asociadas al modo eMED de verano (JJAS). [Adaptado de Xoplaki et al. (2003a)]

Niño Atlántico-Monzón Africano con la cuenca Mediterránea, por tanto asociado a un forzamiento atmosférico de SST (Baldi et al. 2004). Por el contrario, las anomalías de SST del eMED parecen jugar un papel importante en las lluvias monzónicas sobre la región Sudán-Sahel (Rowell 2003; Polo et al. 2008).

Como ha sido mostrado por Xoplaki et al. (2003a, 2003b), el patrón eMED es el primer modo CCA[20] en la región Grecia-Turquía, y el segundo modo CCA en todo el Mediterráneo. Éste, es un modo que captura tanto los 10 veranos más calurosos como los 10 más frescos en el período 1950-1999; y es un modo en el que el contraste térmico tierra-mar es importante. La circulación atmosférica asociada a eMED puede ser identificada como de tipo 'índice bajo'. Los veranos anómalos con temperaturas positivas (negativas) están asociados a subsidencia y estabilidad (convergencia e inestabilidad), advección anómala desde el noreste (suroeste) en niveles medios y altos, y flujo anómalo del oeste (este) en la baja troposfera (Fig. I.13).

16 *Acrónimo del término inglés North Atlantic Horseshoe.*
17 *Acrónimo del término inglés North Atlantic Tripole.*
18 *Acrónimo del término inglés western-Mediterranean.*
19 *Acrónimo del término inglés eastern-Mediterranean.*
20 *Acrónimo del término inglés Canonical Correlation Analysis.*

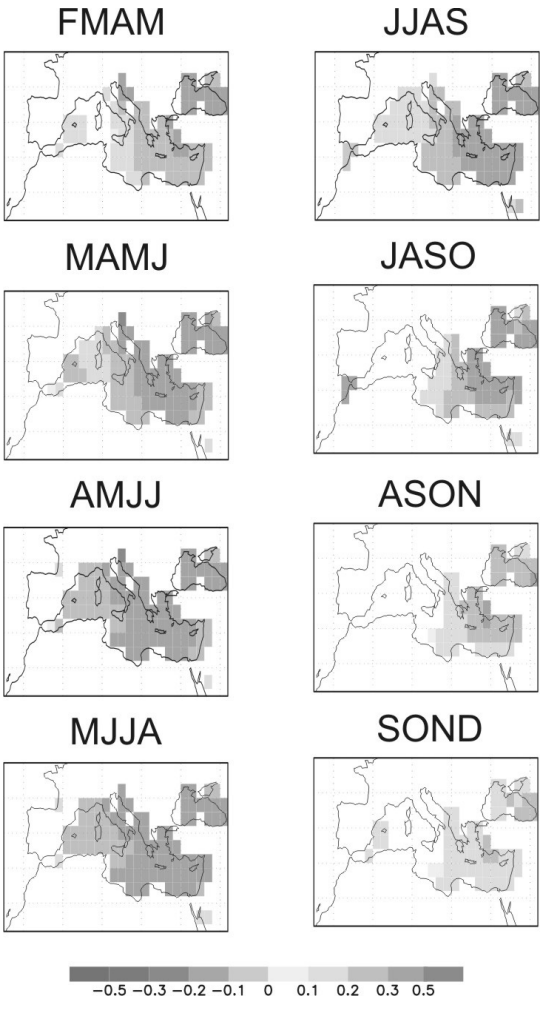

Fig. I.14. Secuencia EMCA de SST (ºC) asociada al patrón eMED. [Adaptado de Polo et al. (2008)]

El objetivo abordado en este trabajo, con relación al Mediterráneo, concierne al análisis de la respuesta atmosférica global ante un forzamiento del eMED (Secc. II.4). El patrón de SST en el que se basa este trabajo es el obtenido por Polo et al. (2008), en el que se describe la evolución temporal del eMED, cubriendo tanto su desarrollo (primavera-verano) como su decaimiento (verano-otoño) (Fig. I.14). Nuestro estudio, al igual que el de Polo et al. (2008), está centrado en el clima reciente (1979-2005).

4. Fundamentos de las teleconexiones atmosféricas

Por *teleconexión atmosférica* se entiende una relación causal entre la variabilidad atmosférica de regiones alejadas, la cual implica un régimen climático anómalo en las zonas afectadas. Por lo general, la distancia entre esas regiones alejadas es del orden de miles de kilómetros; y las perturbaciones climáticas que se dan lugar suelen tener carácter opuesto, unas de otras, en zonas afectadas contiguas.

La importancia de las teleconexiones atmosféricas reside en varios motivos. Entre ellos, la propia definición, ya que cambios en las regiones de forzamiento (e.g. ENSO, TAV, eMED) pueden influir en áreas muy alejadas de estas. Segundo, dado el potencial predictivo y el largo tiempo de decaimiento de las anomalías de SST asociadas a esos forzamientos oceánicos, las teleconexiones pueden ser utilizadas para hacer predicciones estacionales o incluso anuales y decadales. Tercero, las teleconexiones pueden ser utilizadas también para reconstruir la serie temporal de la variabilidad de esos forzamientos a partir de datos proxy; o viceversa, para inferir anomalías de circulación desde una variabilidad de SST conocida (Sterl et al. 2007).

Las regiones donde se originan estas teleconexiones atmosféricas se conocen como zonas de forzamiento, y suelen estar relacionadas con intensas interacciones océano-atmósfera (Secc. 3). Las anomalías asociadas a estas interacciones tienen un efecto inmediato en la columna atmosférica superior, que implica fuertes movimientos verticales. Éstos impactan en la circulación de gran escala, generando una estructura baroclínica y provocando cambios en la alta troposfera y en la circulación divergente (Secc. 4.2). Por otro lado, estas anomalías en la convergencia/divergencia de la alta troposfera son capaces de perturbar la circulación general de carácter zonal (oeste-este), implicando cambios en la vorticidad y propagando las anomalías por regiones subtropicales y extratropicales (Secc. 4.4.b). Esta propagación, que tiene lugar mediante las llamadas *ondas de Rossby*, interacciona con el flujo medio en el que se dispersa, provocando la reacción de la circulación transitoria de menor escala (Secc. 4.5), y dando como resultado el establecimiento de una teleconexión atmosférica.

En las siguientes subsecciones se describen en detalle los elementos clave que participan en estas teleconexiones, tanto en latitudes tropicales y

subtropicales (Seccs. 4.2, 4.4.a) como en latitudes extratropicales (Seccs. 4.3, 4.4.b, 4.5); mientras que a continuación se describe la base teórica de las ondas de Rossby.

4.1. Ecuación de Vorticidad

Para una atmósfera dominada por movimientos horizontales, donde la advección vertical y los efectos de torsión son despreciables, la ecuación de movimiento se puede expresar como la *Ecuación de Vorticidad Barotrópica*, o sencillamente *Ecuación de Vorticidad* (Holton 1992):

$$\frac{d}{dt}(\zeta + f) + (\zeta + f)\nabla \cdot \vec{v} = 0$$

donde $\nabla \cdot \vec{v}$ es la divergencia horizontal del viento, ζ es la vorticidad relativa, local (en cada punto), y f es la vorticidad planetaria o parámetro de Coriolis $f = 2\Omega sen(\varphi)$, con φ la latitud y Ω la frecuencia de rotación de la Tierra. A través del teorema de Helmholtz, el flujo atmosférico se puede representar como suma de la componente rotacional (v_ψ) y divergente (v_χ)(Sardeshmuhk and Hoskins 1985, 1987):

$$\vec{v} = \vec{v}_\psi + \vec{v}_\chi = \vec{k} \times \nabla\psi + \nabla\chi$$

donde ψ es la función de corriente y χ el potencial de velocidad. De esta forma, la ecuación de vorticidad se puede representar como:

$$\frac{\partial \zeta}{\partial t} + \vec{v}_\psi \cdot \nabla(\zeta + f) =$$
$$-(\zeta + f)\nabla \cdot \vec{v}_\chi - \vec{v}_\chi \cdot \nabla(\zeta + f)$$

Los términos a la izquierda de la igualdad, parte dominada por la circulación rotacional, describen la propagación de ondas de Rossby; mientras que los términos de la derecha, la parte dominada por la circulación divergente, representa las fuentes de esas ondas (Sardeshmuhk and Hoskins 1988).

En regiones extratropicales, lejos de las regiones de forzamiento, la propagación de anomalías vía ondas de Rossby queda bien representada por modelos de vorticidad barotrópica no-divergente (Secc. 4.4.b; Hoskins and Karoly 1981; Branstator 1983; Hoskins and Ambrizzi 1993):

$$\frac{d}{dt}(\zeta + f) = 0$$

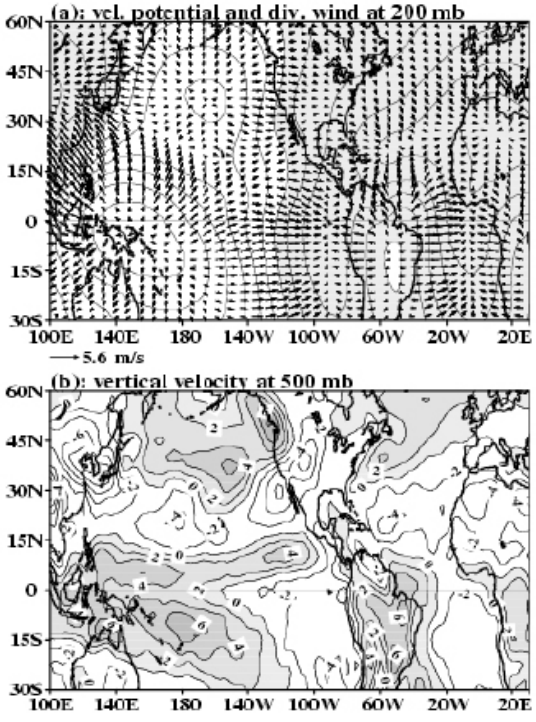

Fig. I.15. Climatología del potencial de velocidad y del viento divergente en 200hPa (a) y de ω en 500hPa (b) en Enero. [Adaptado de Wang (2005)]

De esta forma, las *ondas de Rossby* son aquellos movimientos atmosféricos que conservan la vorticidad absoluta: suma de la vorticidad relativa y la planetaria.

En latitudes tropicales, donde las fuentes de ondas de Rossby resultan de la conversión de perturbaciones en la circulación divergente en anomalías barotrópicas, los modelos puramente baroclínicos representan bien la respuesta atmosférica (Matsuno 1966; Gill 1980). Esta repuesta se caracteriza por ondas zonales que emergen hacia el este (Kelvin) y el oeste (Rossby) de la región de forzamiento (Secc. 4.4.a).
Una revisión de la validez y aplicación de estos modelos puede consultarse en Lee et al. (2009).

4.2. Circulación divergente / Walker y Hadley

La ecuación de continuidad implica que:

$$\nabla \cdot \vec{v}_\chi + \frac{\partial \omega}{\partial p} = 0$$

donde ω es la velocidad vertical en coordenadas de presión y p es la presión (Holton 1992). Si se integra esa ecuación entre la presión en superficie

(p_s) y un nivel p, se obtiene la expresión:

$$\omega(p) = \int_{p}^{p_s} (\nabla \cdot \vec{v}_\chi) dp$$

donde $\omega(p_s)$=0 Pa/s.

Por tanto, en regiones tropicales, donde los calentamientos atmosféricos y oceánicos inducen importantes perturbaciones en la convergencia/ divergencia horizontal, estas anomalías representan intensos movimientos verticales (sistemas convectivos). Estas perturbaciones en la circulación divergente, por consiguiente, también caracterizarán las fuentes de ondas de Rossby.

Como se ha indicado antes, el flujo horizontal se puede descomponer en una parte rotacional (asociada a la función de corriente ψ) y una parte divergente (asociada al potencial de velocidad χ). La primera parte, por definición, no contribuye al campo divergente atmosférico, y por tanto tampoco a los movimientos verticales (ya que es no-divergente). Como es bien conocido, la atmósfera tropical conducida térmicamente comprende dos tipos de circulación: una zonal, conocida como

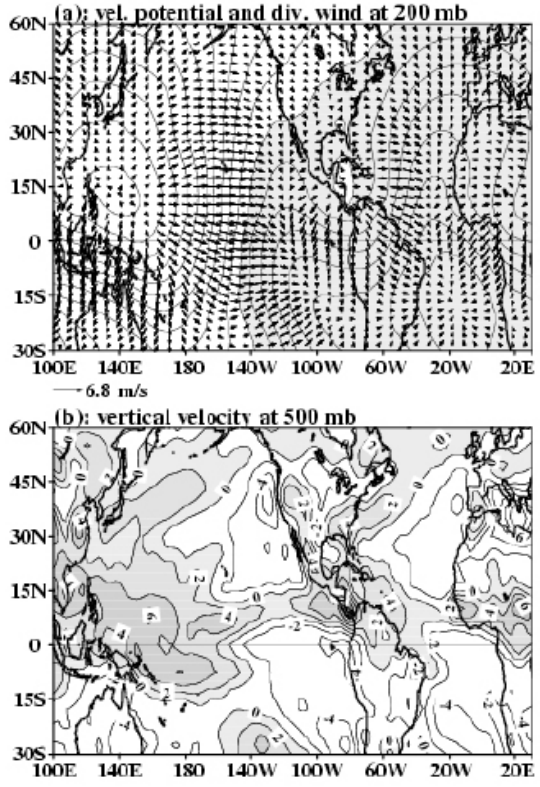

Fig. I.16. Igual que Fig. I.15, pero para Julio.

circulación Walker; y otra meridional, conocida como circulación Hadley (e.g. Krishnamurti 1971; Krishnamurti et al. 1973). Así, el análisis de la circulación divergente, campo divergente (χ,v_χ) y movimientos verticales (ω), es esencial para describir la circulación conducida térmicamente (Figs. I.15, I.16; Wang 2002a, 2002b, 2005).

La circulación de Walker fue primeramente postulada por Bjerknes (1969), y focalizada en el Pacífico tropical. Ahora se sabe que la circulación zonal presenta diferentes células a lo largo del cinturón tropical (Krishnamurti 1971; Krishnamurti et al. 1973). La célula del Pacífico, una circulación en el plano zonal-vertical, es parte del fenómeno Oscilación del Sur (ENSO; Secc. 3.1) y fue bautizada por Bjerknes como 'circulación de Walker' en homenaje a los estudios de Gilbert Walker (1923, 1924, 1928). Esta circulación de Walker Pacífica se caracteriza por ascenso de aire en el Pacífico oeste, flujo oeste-este en los niveles altos, y descenso de aire en el Pacífico este, volviendo hacia la otra parte de la cuenca con dirección este-oeste en los niveles bajos. Por su parte, la célula de Walker Atlántica tiene el mismo tipo de circulación oeste-este en niveles altos y este-oeste en niveles bajos, pero con el aire ascendiendo en Sudamérica y descendiendo en al Atlántico ecuatorial (Figs. I.15, I.16). Desplazamientos latitudinales pueden observarse entre verano e invierno asociados al ciclo estacional de la ITCZ (también en Fig. I.1).

La células de Hadley son también conducidas térmicamente, al igual que las de Walker, aunque éstas tienen una orientación meridional y se sitúan entre el trópico y el subtrópico. El aire caliente tropical asciende, fluye ecuador-polo en los niveles altos hasta la regiones subtropicales, se enfría, desciende y vuelve al trópico en los niveles bajos (Figs. I.15, I.16). Como se ha descrito en la Sección 1, las células de Hadley se generan por el calentamiento diferencial terrestre (ciclo anual) y el contraste térmico asociado ecuador-polo, mientras que su extensión latitudinal está controlada por la rotación de la Tierra y la conservación del momento angular (aceleración de Coriolis).

4.3. Circulación indirecta / Ferrel

Como también se ha descrito en la Sección 1, las células de Ferrel son circulaciones meridionales aunque éstas no son conducidas térmicamente

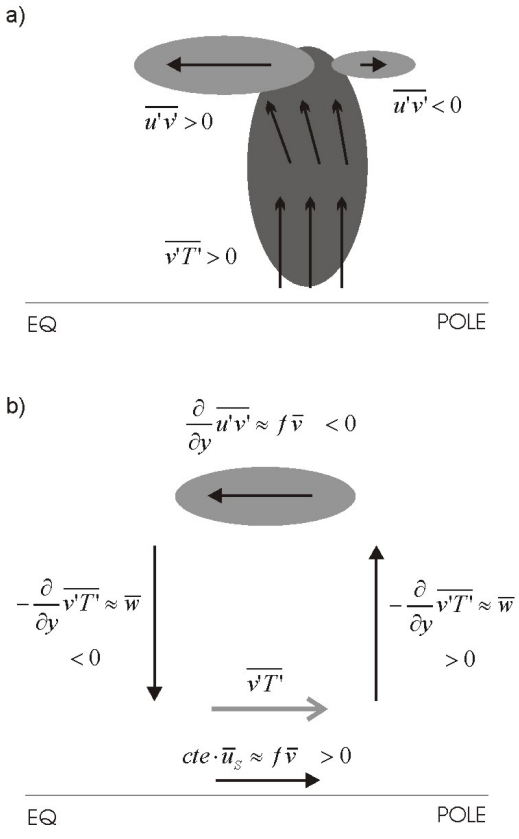

Fig. I.17. (a) Esquema del vector de Eliassen-Palm (flechas) y los flujos eddy de calor (sombreado oscuro) y momento (sombreado claro). (b) Esquema de la célula de Ferrel.

sino por la circulación transitoria *eddy*. Las células de Ferrel constituyen unas celdas de circulación indirecta: el aire asciende en regiones extratropicales y desciende en las regiones subtropicales. Como se ha mostrado en la Fig. I.3, el flujo de momento *eddy* es positivo en latitudes medias, mientras que la convergencia (divergencia) de ese flujo tiene una orientación ecuador-polo (polo-ecuador) (Peixoto y Oort 1992). Ese flujo de momento *eddy,* $\overline{u'v'}$, se puede expresar también a través de la componente meridional del vector de Eliassen-Palm (Edmon et al. 1980):

$$F_y = -\overline{u'v'}$$

El vector de Eliassen-Palm y su divergencia son dos diagnósticos fundamentales para analizar los procesos asociados a la actividad transitoria *eddy*: por ejemplo, cuantifica el transporte de momento del oeste (indicando la dirección opuesta al transporte), también es una medida de la transferencia neta de actividad de onda, y su divergencia indica el forzamiento *eddy* del flujo-zonal medio (Edmon et al. 1980). Así, la deposición por parte de los *eddies* de momento del oeste en latitudes altas y en la alta troposfera, se ve transportado a los niveles bajos gracias a la reducción del gradiente térmico ecuador-polo y de la cizalla vertical como consecuencia del flujo *eddy* de calor en la dirección meridional (Figs. I.3, I.17a).

Por otra parte, fuera de la capa límite planetaria donde los efectos de fricción son notables, es decir, en la atmósfera libre, el balance de momento y la ecuación de la termodinámica se pueden aproximar como (e.g. Peixoto y Oort 1992; Vallis 2006):

$$f\,\overline{v} \approx \frac{\partial}{\partial y}\overline{u'v'}$$

$$\overline{w} \approx -\frac{\partial}{\partial y}\overline{v'T'}$$

donde f es el parámetro de Coriolis, $\overline{v}$ y $\overline{w}$ el flujo medio, $\overline{u'v'}$ el flujo de momento *eddy* y $\overline{v'T'}$ el flujo de calor *eddy*. Así, de acuerdo a la Fig. I.3, la región de convergencia de flujo de momento *eddy* debe ser compensada por un flujo medio en dirección polo-ecuador, es decir en sentido indirecto; mientras que esa misma convergencia en altura se disipa en superficie a través de fricción, generando vientos del oeste en latitudes medias. De esta forma, la circulación de Ferrel es conducida por los flujos de momento *eddy*. No obstante, el transporte de calor *eddy* también es positivo hacia los polos (Fig. I.3), reduciendo el gradiente térmico meridional y la cizalla vertical; por lo que también generaría una circulación tipo Ferrel (Fig. I.17b; e.g. Peixoto y Oort 1992; Vallis 2006).

4.4. Circulación rotacional

4.4.a. Ondas equatoriales / Rossby y Kelvin

Como se ha introducido en la Sección 4.1, la respuesta atmosférica a un forzamiento oceánico tropical está bien representada por el modelo Matsuno-Gill, el cual considera una estructura vertical puramente baroclínica asociada a una fuente (o sumidero) de calor troposférico (e.g. Davey y Gill 1987).

Este tipo de fuentes de calor producen una onda de Kelvin que se propaga a lo largo del cinturón

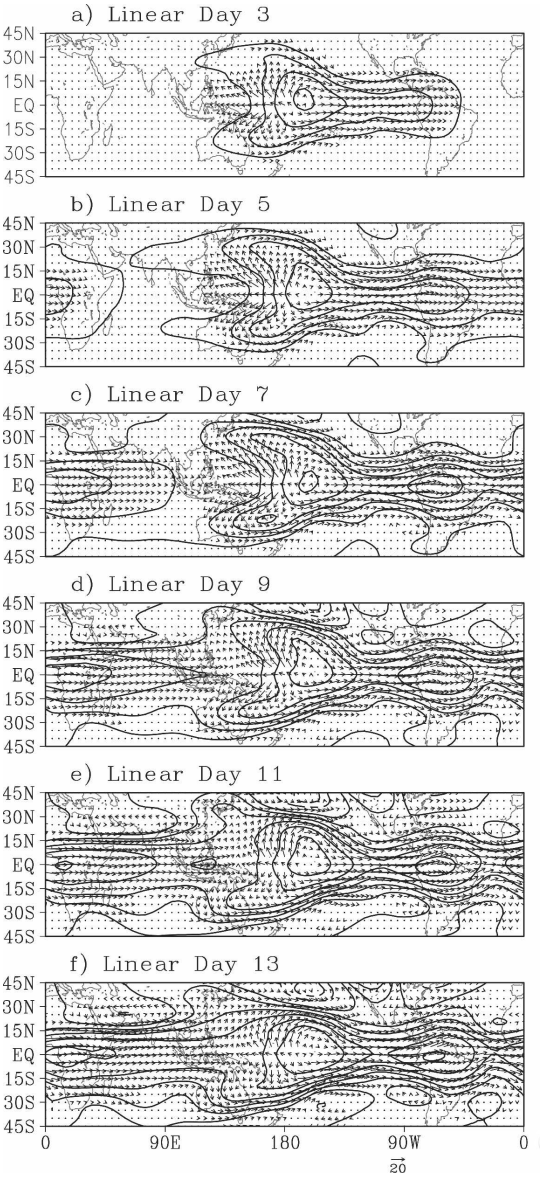

Fig. I.18. Componente lineal El Niño-La Niña de la respuesta atmosférica tropical, geopotencial (m) y viento horizontal (m/s) en 150hPa, a un forzamiento elíptico en el Pacífico central. [Adaptado de Lin et al. (2007)]

tropical en dirección oeste-este; y una onda de Rossby, más lenta, que se propaga también confinada en trópico pero en con dirección este-oeste (Fig. I.18).

Al oeste del forzamiento, la onda de Rossby ecuatorial está asociada a un par de anticiclones (ciclones) en respuesta a un calentamiento (enfriamiento), como es el caso de episodios El Niño (La Niña). Este par de circulaciones anómalas, a ambos lados del ecuador, constituyen los primeros centros de acción de la onda de Rossby extratropical.

Al este del forzamiento, la rápida respuesta de Kelvin se propaga hacia el este, circunscribe todo el ecuador, y acaba interfiriendo con la respuesta de Rossby ecuatorial, reduciendo (dejando casi inalterada) la amplitud de los giros tropicales asociados a El Niño (La Niña) (Lin et al. 2007).

4.4.b. Ondas extratropicales / Rossby

Como ha sido mostrado en trabajos anteriores, el modelo Matsuno-Gill falla completamente en regiones fuera de los trópicos (e.g. Lee et al. 2009). Como demostraron también estudios previos (e.g. Hoskins y Karoly 1981, Horel y Wallace 1981), un calentamiento diabático anómalo, como el asociado a ENSO, excita un tren de ondas de Rossby barotrópico estacionario que se propaga por regiones extratropicales. La limitación del modelo Matsuno-Gill es clara ya que esos patrones de teleconexión son barotrópicos (o equivalente-barotrópicos). Branstator (1983) mostró que un modelo de vorticidad barotrópica no-divergente es el modelo más simple que captura esas teleconexiones forzadas térmicamente. Por tanto, la propagación extratropical de ondas de Rossby está asociada a la conservación de la vorticidad absoluta:

$$\frac{d}{dt}(\zeta + f) = 0$$

Esta ecuación de vorticidad se puede expresar a través de la función de corriente ψ como:

$$\frac{d}{dt}\nabla^2\psi + \beta\frac{\partial\psi}{\partial x} = 0$$

la cual representa una ecuación de onda, cuya solución es una onda plana (2D) del tipo:

$$\psi \approx e^{i(kx+ly-\omega t)}$$

donde k es el número de onda zonal, l el número de onda meridional y ω la frecuencia. De la resolución de la ecuación de vorticidad, se puede obtener la siguiente relación de dispersión para las ondas de Rossby:

$$\omega = kU - k\frac{\beta^*}{k^2 + l^2}$$

donde U es el flujo zonal medio y β^* el gradiente meridional de la vorticidad absoluta:

$$\beta^* = \frac{\partial f}{\partial y} - \frac{\partial^2 U}{\partial y^2} = \beta - \frac{\partial^2 U}{\partial y^2}$$

Por tanto, para condiciones estacionarias (ω=0) se puede definir una dirección de propagación a través del número de onda de Rossby estacionario K_S según (Hoskins y Ambrizzi 1993):

$$K_S^{\ 2} = k^2 + l^2 = \frac{\beta - \frac{\partial^2 U}{\partial y^2}}{U}$$

Desde los trabajos de Hoskins et al. (1977), Hoskins y Karoly (1981), Webster (1982, 1982) y Branstator (1985), la propagación de estas teleconexiones atmosféricas se ha explicado físicamente a través de la dispersión de ondas Rossby, con una marcada orientación meridional (ecuador-polo) en forma de arco (Fig. I.19a). Esta característica propagación Rossby en forma de arco fue ampliamente asumida por la gran cantidad de trabajos centrados en la respuesta atmosférica a ENSO (e.g. Horel y Wallace 1981; Trenberth et al. 1998).

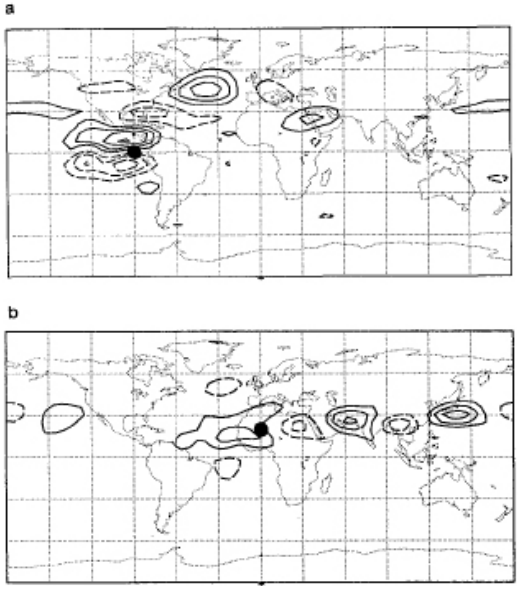

Fig. I.19. Respuesta de un modelo barotrópico a un forzamiento localizado en (a) 90ºW-0ºN (día 6 de integración) y (b) 0ºE-20ºN (día 7 de integración). Anomalías de vorticidad relativa (ic=8 10^{-6}s-1). [Adaptado de Hoskins y Ambrizzi (1993)]

No obstante, esa teoría lineal basada en la ecuación de vorticidad determina el ángulo α de propagación del tren de ondas Rossby en función de un determinado k y del flujo medio en el que se propaga (Hoskins y Ambrizzi 1993):

$$\cos\alpha = \frac{k}{K_S} = k\sqrt{\frac{U}{\beta - \frac{\partial^2 U}{\partial y^2}}}$$

donde α es el ángulo con la dirección oeste-este. Así, cuando el tren de ondas alcanza la latitud donde K_S=k (l=0), la propagación Rossby sufre una reflexión que lo fuerza a descender en latitud, generándose de este modo el típico patrón en arco (Fig. I.19a).

En cambio, cuando los efectos refractivos del flujo medio son tenidos en cuenta, la propagación Rossby puede presentar otra apariencia. Ésta está determinada por el efecto 'guía de onda' o 'de confinamiento' de las corrientes en chorro del oeste (Hoskins y Karoly 1981; Branstator 1983; Hsu y Lin 1992; Hoskins y Ambrizzi 1993; Ambrizzi et al. 1995; Branstator 2002; Ding y Wang 2005). Esta propagación se caracteriza por una marcada orientación zonal, de oeste a este (Fig. I.19b), y no produce anomalías en la media-zonal (Branstator 2002). El análisis de Hoskins y Karoly (1981) sobre el número de onda estacionario mostró que ondas con K_S =6 estarían meridionalmente confinadas alrededor de los 30ºN, donde se sitúa el máximo de las corrientes en chorro. El trabajo de Branstator (1983) mostró, adicionalmente, que este efecto 'guía de onda' también se produce en las corrientes confinadas longitudinalmente a una región.

Esencialmente, se puede comprobar que para un determinado número de onda zonal k, a mayor flujo zonal medio U y mayor gradiente meridional de la vorticidad relativa $\partial^2 U/\partial y^2$, menor tiende a ser el ángulo de propagación α. De esta forma, se puede concluir que allí donde las corrientes en chorro sean débiles, la propagación de ondas Rossby tenderá a ser en forma de arco (propagación meridional); mientras que en las regiones donde las corrientes en chorro presenten una gran intensidad, los trenes de onda tenderán a estar confinados meridionalmente (propagación zonal; Fig. I.20) (Branstator 2002). En estas últimas, donde las perturbaciones son

canalizadas en las corrientes en chorro, la energía no es dispersada en una región localizada, sino que es capaz de propagarse más 'aguas abajo' hasta ser disipada. Ésta tendencia hacia una propagación más zonal está, además, reforzada por el hecho de que la velocidad de grupo de las ondas de Rossby (c_g) es proporcional a la velocidad del flujo medio en el que se propagan, la cual es máxima en las corrientes en chorro (Hoskins y Ambrizzi 1993):

$$c_g = 2U\cos\alpha$$

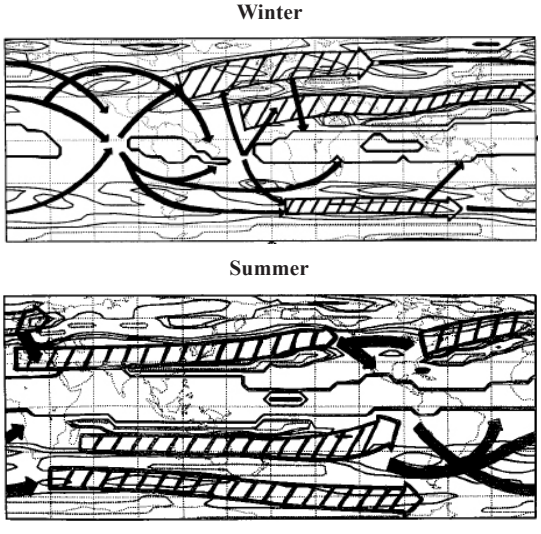

Fig. I.20. Esquemas de las guías de onda (flechas gruesas) y propagaciones preferentes (flechas estrechas) de las teleconexiones Rossby. [Adaptados de Hoskins y Ambrizzi (1993) y Ambrizzi et al. (1995)]

Dinámicamente, aun falta una pieza clave para entender la propagación extratropical de ondas de Rossby. Ésta resulta de la conversión de los modos baroclínicos inducidos térmicamente (Matsuno-Gill) en anomalías barotrópicas (e.g. Branstator 1983; Hoskins y Ambrizzi 1993). Las regiones donde esta conversión se lleva a cabo se conocen como fuentes de ondas de Rossby (RWS[21]). Estas fuentes de ondas están descritas por los términos de la ecuación de vorticidad que dependen del flujo divergente:

$$RWS = -(\zeta + f)\nabla\cdot\vec{v}_\chi - \vec{v}_\chi\cdot\nabla(\zeta + f)$$

donde el primer término está asociado a la divergencia horizontal del flujo, y el segundo a la advección de vorticidad por el viento divergente.

Sardeshmukh y Hoskins (1988) y Qin y Robinson (1993) describieron y analizaron ampliamente estas fuentes y su interpretación física. La versión lineal de esas RWS se puede obtener al descomponer su expresión teniendo en cuenta una perturbación en el flujo (v'_χ, ζ') y un estado medio, generalmente la media climatológica ($\overline{v_\chi}, \overline{\zeta}$). De esta forma, como mostraron Qin y Robinson (1993), las fuentes de ondas de Rossby se pueden separar en dos partes, una centrada en la región de forzamiento (TRWS[22]) y otra que se extiende por un círculo de latitud alrededor de 30ºN y tiene un máximo al noreste del máximo de TRWS (ERWS[23]):

$$TRWS = -\vec{v}_\chi'\cdot\nabla(\overline{\zeta} + f)$$

$$ERWS = -(\overline{\zeta} + f)\nabla\cdot\vec{v}_\chi'$$

de forma que los términos de propagación en la ecuación de vorticidad están equilibrados de forma diferente en los trópicos y en los extratrópicos. El resto de términos lineales y los no-lineales son despreciables. El término TRWS representa la advección de vorticidad absoluta por el viento divergente anómalo, por lo que será máximo en las inmediaciones de las corrientes en chorro (Sardeshmukh y Hoskins 1988). El término ERWS es importante para la respuesta estacionaria en latitudes medias, y se puede entender con dinámica cuasi-geostrófica (Qin y Robinson 1993).

4.5. Interacción eddy-flujo medio

Los fenómenos transitorios, con una escala temporal típica de varios días, consisten fundamentalmente en ondas baroclínicas migratorias. Las relaciones entre estas perturbaciones y el flujo estacionario han sido descritas por Blackmon et al. (1977) y Trenberth (1991), entre otros. Es conocido que estas ondas baroclínicas, *eddies* transitorios, son particularmente activas en las regiones oceánicas situadas al final de las corrientes en chorro, tanto en el Atlántico Norte como en el Pacífico Norte (Fig. I.21). Las rutas seguidas por estas ondas, fenómenos de escala sinóptica, son conocidas

21 *Acrónimo del término inglés Rossby Wave Sources.*

22 *Acrónimo del término inglés Tropical Rossby Wave Source.*

23 *Acrónimo del término inglés Extratropical Rossby Wave Source.*

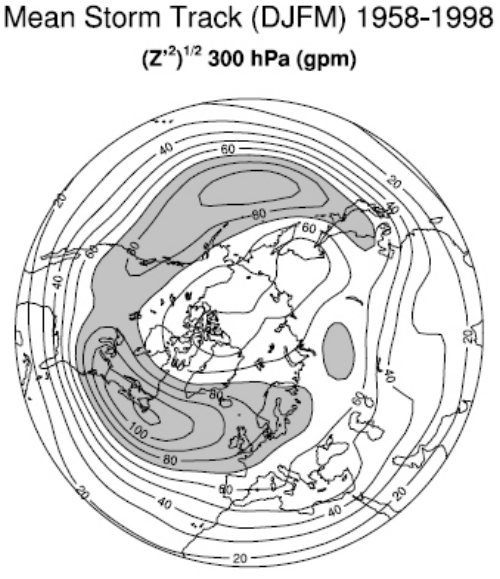

Fig. I.21. Climatología de los storm-tracks durante invierno. [Adaptado de Hurrell et al. (2003)]

como 'trayectorias de las tormentas', o en inglés '*stormtracks*'. Estudios previos mantienen que el origen y la propagación de estos *eddies* transitorios están, en gran medida, gobernados por las regiones de ciclogénesis y por el efecto guía-de-onda del flujo medio (e.g. Chang et al. 2002; Hurrell et al. 2003).

En virtud de los intensos transportes de calor y de vorticidad que tienen lugar en los *stormtracks* a través de los *eddies*, la interacción entre estos fenómenos transitorios y el flujo medio es especialmente acentuada en esas regiones. Como revisó Trenberth et al. (1998), la convergencia de flujos de vorticidad *eddy* refuerza las ondas de Rossby climatológicas (de origen orográfico) y las corrientes en chorro en las regiones de *stormtracks*; mientras que la convergencia de flujos de calor *eddy* disipa esos mismos aspectos estacionarios. Por tanto, ya que la magnitud del forzamiento *eddy* debido a flujos de vorticidad es mayor que la debida a flujos de calor, el efecto neto de las perturbaciones transitorias tiende a reforzar la asimetría zonal del flujo medio.

Las ondas de Rossby estacionarias asociadas a forzamientos térmicos oceánicos (teleconexiones atmosféricas) son reforzadas por los *eddies* transitorios en la alta troposfera. En la baja troposfera, las perturbaciones climáticas (anomalías de temperatura) de esas ondas de Rossby son mantenidas por advección del flujo medio pero disipadas por los *eddies* transitorios. De ese modo, la *interacción eddy-flujo medio* que tiene lugar en los *stormtracks* sugiere que la descripción del efecto de esas ondas transitorias en la respuesta estacionaria a un forzamiento debe ser tenida muy en cuenta, incluyendo su influencia en los flujos de calor en superficie y en los calentamientos diabáticos (e.g. Hoskins and Valdes 1990).

Esta relación, entre los fenómenos transitorios (alta frecuencia) y las anomalías de circulación de gran escala (media-baja frecuencia), ha sido mostrada como muy importante tanto en el entendimiento de la interacción entre escalas como en las teleconexiones atmosféricas (e.g. Hoskins et al. 1983; Trenberth 1986; Hoerling and Ting 1994; Trenberth et al. 1998). En particular, algunos de estos estudios indican que las variaciones en los *stormtrakcs* que acompañan a los cambios en el flujo medio, ejercen una realimentación positiva sobre las perturbaciones de baja frecuencia. También se ha establecido que cambios en el flujo medio, y en las corrientes en chorro asociadas, generan cambios en los patrones de *stormtracks* (Branstator 1995).

La asociación entre la variabilidad de los *stormtracks* y los patrones de teleconexión es ilustrada en la Fig. I.22. Relacionado con la

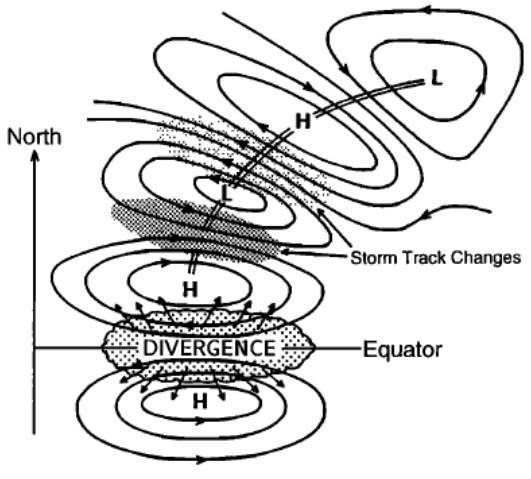

Fig. I.22. Esquema de la interacción de un tren de ondas Rossby y la actividad transitoria-eddy. [Extraído de Trenberth et al. (1998)]

divergencia anómala en altura que se produce ante un calentamiento tropical (Secc. 4.2), aparece una respuesta atmosférica de Gill que produce un par de anticiclones anómalos a ambos lados del ecuador (Secc. 4.4.a), y que provoca la propagación de un tren de ondas de Rossby hacia latitudes medias (Secc. 4.4.b). Esta propagación produce un cambio hacia el sur en el *stormtrack*, asociado con la corriente en chorro subtropical, que genera un aumento de la actividad *eddy* al sur del segundo centro de acción de la onda (ciclón anómalo) y una disminución de la actividad *eddy* al norte de este centro de acción.

Los diagnósticos utilizados en este trabajo para evaluar la interacción '*eddy*-flujo medio' han sido descritos e interpretados por Hoskins et al. (1983) y Trenberth (1986), entre otros:

$$PKE = \frac{1}{2}\left(\overline{u'u' + v'v'}\right)$$

$$E = \left(\frac{1}{2}\overline{v'v' - u'u'}\,, -\overline{u'v'} \right)$$

PKE[24] representa la energía cinética de la perturbación, y es una medida de la actividad de onda. El vector *E* corresponde a las componentes horizontales del flujo de Eliassen-Palm, y describe la interacción entre los *eddies* transitorios y el flujo medio a través de procesos barotrópicos. La componente zonal de *E* proporciona información sobre la forma y las características de propagación de los *eddies*, mientras que la componente meridional describe la realimentación con el flujo medio a través de flujos de momento. La convergencia (divergencia) del vector *E* está asociada con una aceleración (deceleración) del viento zonal medio. En este trabajo, las variables *u'* y *v'* representan las perturbaciones del flujo asociadas a los *eddies*, y se han calculado utilizando el filtro de diferencia-de-24h (Wallace et al. 1988).

24 *Acrónimo de término inglés Perturbation Kinetic Energy.*

MARCOS DE TRABAJO Y OBJETIVOS

En este capítulo se describen en detalle el marco de trabajo, las preguntas abiertas y los objetivos concretos de los análisis llevados a cabo en este estudio. Como se ha introducido anteriormente, el objetivo general que subyace a la Tesis es la búsqueda de señales forzadas por la temperatura de la superficie del mar que tengan un carácter predictivo en su influencia sobre el clima de Europa. Ya que el principal mecanismo de teleconexión considerado ha sido la propagación de ondas de Rossby, las anomalías en la circulación rotacional representa el foco de los diferentes análisis. Los forzamientos oceánicos aquí considerados son fenómenos con una marcada frecuencia interanual en esta covariabilidad, habiéndose descartado por tanto influencias a escala decadal y multidecadal. Esta sección plantea cuatro líneas de investigación: la señal de ENSO en el sector Euro-Atlántico durante los meses invernales posteriores al máximo de El Niño; la respuesta atmosférica durante el decaimiento del Niño Atlántico de verano; el papel del Atlántico Norte Subtropical en la transición *Horseshoe*-Tripolo y su influencia en la NAO invernal; y el impacto de la cuenca este Mediterránea en la circulación hemisférica de verano-otoño. La motivación y las estaciones consideradas para cada forzamiento se describen a continuación.

Este capítulo cita los artículos clave que han motivado esos estudios; para una referencia más exhaustiva consultar las diferentes introducciones de los trabajos (Secc. IV).

1. Teleconexión invernal ENSO-Atlántico Norte

Mientras que el impacto de ENSO en la circulación atmosférica y el clima del sector Pacífico Norte - Norte América es bien conocido (e.g. Trenberth et al. 1998), la influencia de éste sobre la circulación en el Atlántico Norte y el clima europeo es más controvertida. Recientemente, Brönnimann (2007) ha revisado esta teleconexión y ha concluido que, aunque la señal es débil, la conexión es robusta y lineal a finales de invierno y principios de primavera, durante los meses Ene-Feb-Mar. Para condiciones El Niño, esta señal canónica corresponde a un patrón en superficie que proyecta en una fase negativa tipo NAO: anomalías negativas de presión en latitudes medias de la cuenca Atlántica y sobre el continente europeo, y anomalías positivas de presión en latitudes polares del Atlántico Norte (Fig. II.1a). Este patrón atmosférico está asociado a temperaturas anómalamente bajas sobre la Península Escandinava y anómalamente altas en la cuenca Mediterránea y norte de África (Fig. II.1b). Esta teleconexión ENSO también tiene un impacto en el régimen anómalo de precipitación sobre Europa, encontrándose anomalías negativas significativas en el centro-este del continente (Fig. II.1c). Sin embargo, el mecanismo responsable de estas anomalías no está consensuado a día de hoy (Brönnimann 2007).

En los últimos años, y basados en la aparente estructura anular de patrón canónico asociado a ENSO, varios han sido los trabajos que han sugerido una teleconexión estratosférica para explicar esa señal. Esta hipótesis involucra la propagación vertical de ondas planetarias forzadas por ENSO, fundamentalmente de número de onda 1, que alcanzan la estratosfera y debilitan en el vórtice polar (Manzini et al. 2006). Esas perturbaciones producen anomalías positivas en la temperatura del aire, y fomentan la ocurrencia de calentamientos súbitos estratosféricos. El mecanismo se completa con la propagación de las perturbaciones hasta la baja estratosfera, que posteriormente alcanzan la superficie durante el final del invierno, Feb-Mar (Ineson y Scaife 2008;

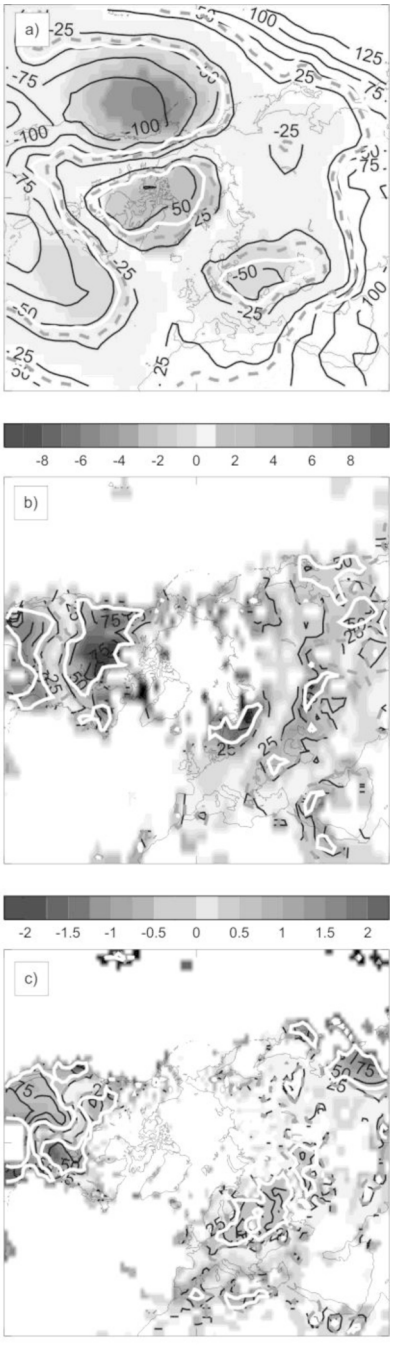

Fig. II.1. Compuesto de anomalías climáticas para episodios El Niño: a) SLP (hPa), b) temperatura del aire en superficie (ºC) y c) precipitación (mm/día). [Adaptada de Ineson y Scaife 2008]

Cagnazzo y Manzini 2009; Bell et al. 2009).

Además de esta teleconexión estratosférica, una ruta puramente troposférica es también esperable (e.g. Alexander et al. 2002). De hecho, varios trabajos han mostrado la propagación de ondas de Rossby por el Atlántico Norte (Trenberth et al. 1998; Shaman Tziperman 2005; Toniazzo y Scaife 2006), aunque ninguno de esos trabajos ha reproducido la estructura tipo-NAO de la señal canónica de ENSO. Por otro lado, estudios con AGCMs han logrado simular una respuesta a ENSO de carácter dipolar en el Atlántico Norte; mientras unos apuntan a un error sistemático del modelo (Cassou y Terray 2001a, 2001b), otros sugieren un papel fundamental de la actividad transitoria-*eddy* para establecer la teleconexión (Merkel y Latif 2002; Pohlmann y Latif 2005). No obstante, todos estos trabajos tienen en común la extensión 'aguas abajo' en la propagación del tren de ondas Rossby, forzado desde el Pacífio tropical y que cruza el Pacífico Norte. Sin embargo, no hay evidencia observacional de este efecto 'aguas abajo' en la generación de esta respuesta tipo-NAO y un mecanismo troposférico que produzca esa señal canónica dipolar en el Atlántico Norte todavía no está claro (Brönnimann 2007).

El objetivo en esta parte del trabajo ha sido intentar aislar la señal canónica de ENSO en el sector Euro-Atlántico usando datos de re-análisis; y focalizar el estudio en el flujo rotacional, el cual representa el medio por el que se propagan las ondas de Rossby. Para ello, se ha analizado la dinámica asociada a los modos de variabilidad obtenidos de un análisis EOF de la función de corriente en 200hPa sobre la región del Atlántico Norte y Europa [Secc. IV.1].

2. Teleconexiones extratropicales del Niño Atántico

Como se ha dicho en la Introducción (Secc. I.3.2a), este trabajo se centra en el Niño Atlántico perteneciente al clima reciente, en el período 1979-2002. Este Niño Atlántico, que ha sido descrito por Polo et al. (2008), tiene su máxima amplitud en verano (Losada et al. 2009a), no persiste hasta el invierno siguiente (Fig. I.10) y no está correlacionado con el Niño Atlántico II, el modo Ecuatorial del Atlántico que ocurre a principios del invierno (Nov-Dic; Okumura y Xie 2006).

En particular, el trabajo estudia la teleconexión del Niño Atlántico con la región extratropical Euro-Atlántica. En estudios previos, cubriendo

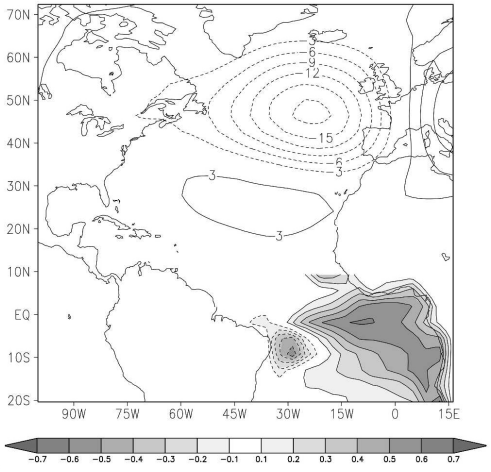

Fig. II.2. Análisis MCA desfasado entre SST tropical (JAS; ºC) y geopotencial en 500hPa (OND; m) de una simulación acoplada de 80-años. [Adaptada de Haarsma y Hazeleger 2007]

el período observacional 1958-2002, se ha mostrado que el Niño Atlántico de verano-otoño está correlacionado negativamente con la NAO invernal: anomalías positivas de SST en el Atlántico ecuatorial precediendo a una fase negativa de la NAO (Czaja y Frankignoul 2002; Drévillon et al. 2003; Peng et al. 2005). Sin embargo, esta relación estadística parece ser artificial, y estar causada por la influencia de ENSO y por la restricción de ortogonalidad del análisis MCA/SVD (Frankignoul y Kestenare 2005). Una vez solventados esos problemas, el análisis de covarianza desfasada parece descartar la influencia del Niño Atlántico en la NAO invernal, y sugiere una relación con el patrón EA (Frankignoul y Kestenare 2005).

En un trabajo posterior usando un AGCM de complejidad intermedia (Haarsma y Hazeleger 2007), la conexión Niño Atlántico-EA ha sido simulada (Fig. II.2) y se ha sugerido que el patrón EA sobre el Atlántico Norte es parte de la respuesta circumglobal forzada por las anomalías de SST en el Atlántico ecuatorial. El desfase temporal observado entre las anomalías térmicas y la respuesta atmosférica se ha argumentado a través de la persistencia de la SST y de las condiciones atmosféricas más favorables durante principios del invierno (Oct-Dic), donde la SST es capaz de generar suficiente divergencia tropical como para forzar el tren de ondas Rossby. No obstante, el diseño experimental de Haarsma y Hazeleger (2007), consistente en prescribir las anomalías de SST fijas a lo largo de la simulación, es contrario a las observaciones, en las que el Niño Atlántico de verano decae en el otoño y no persiste hasta el invierno (Polo et al. 2008).

El primer objetivo abordado en esta parte del trabajo ha sido utilizar observaciones y emplear la misma metodología usada en Polo et al. (2008), el análisis EMCA, pero aplicado al predictando, para capturar la evolución temporal de la respuesta atmosférica, incluyendo el análisis de las perturbaciones en la circulación rotacional [Secc. IV.2].
El segundo objetivo consiste en analizar una simulación AGCM en la que se ha prescrito un Niño Atlántico en fase de decaimiento y comparar los resultados con los del primer objetivo [Secc. IV.3].

3. Influencia del Atlántico Norte Subtropical en Europa

Esta parte del trabajo también se ha centrado en la variabilidad del Atlántico tropical para el clima reciente (período 1979-2002), como en Polo et al. (2005, 2008). Trabajos anteriores cubriendo el período observacional 1958-2002 han puesto de manifiesto la relación entre el estado anómalo estival del Atlántico Norte, a través del patrón *Horseshoe* (Secc. I.3.2.b), y la fase de la NAO en el invierno siguiente: anomalías positivas de SST del *Horseshoe* parecen preceder a una fase negativa de la NAO (Czaja y Frankignoul 1999,

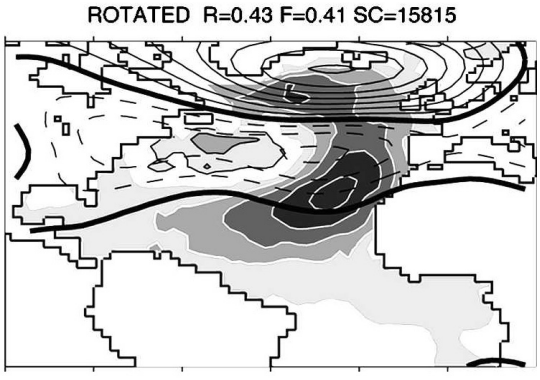

Fig. II.3. Análisis-rotado MCA desfasado entre SST (JJA; ºC) y geopotencial en 500hPa (NDJ; m) sobre la cuenca Atlántica 20ºS-70ºN. [Adaptada de Frankignoul y Kestenare 2005]

2002; Drévillon et al. 2001; Rodwell y Folland 2002). Esta covarianza desfasada entre los dos fenómenos es robusta bajo rotación, y parece confirmar el papel predictivo del Océano Atlántico sobre la variabilidad climática asociada a la NAO (Frankignoul y Kestenare 2005; Fig. II.3). De forma consistente, otros estudios observacionales sugieren la influencia del Atlántico Norte Subtropical de verano, como parte del patrón hemisférico *Horseshoe*, sobre la NAO en invierno (Rodríguez-Fonseca y Castro 2002; Rodríguez-Fonseca et al. 2006; Wainer et al. 2008).

Un experimento de sensibilidad ha simulado la conexión *Horsehoe*-NAO, mostrando la persistencia del patrón hemisférico de SST y su transición al patrón Tripolar acoplado a la NAO (Cassou et al. 2004). Sin embargo, otro trabajo de modelización numérica ha sugerido que el patrón *Horseshoe* de verano es incapaz de forzar la NAO, y que la relación *Horseshoe*-Tripolo es casual no causal (Peng et al. 2005).

Un aspecto a tener en cuenta, y que puede conciliar el debate en la conexión *Horseshoe*-NAO, es el mostrado por Czaja y Frankignoul (1999, 2002) y Rodwell y Folland (2002). Esa consideración radica en la falta de significación estadística de los análisis MCA entre la SST del Atlántico Norte y la NAO para los desfases más cercanos a la estación en la que se considera el patrón atmosférico (Fig. II.4). El problema podría consistir en que el análisis MCA maximiza la covarianza entre la

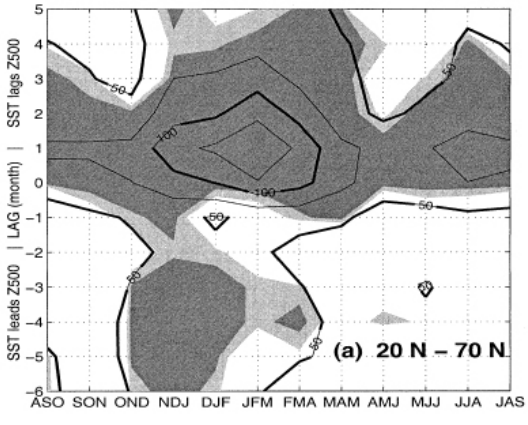

Fig. II.4. Covarianza al cuadrado del primer modo MCA entre la SST Atlántica 20ºN-70ºN y el geopotencial en 500hPa sobre el Atlántico Norte. [Adaptada de Czaja y Frankignoul 2002]

NAO y la SST en cada desfase temporal; y ya que estos trabajos han realizado MCA independientes para cada desfase, en cierto modo se ha asumido la persistencia del patrón SST a lo largo de las estaciones consideradas.

El objetivo abordado en esta parte del trabajo consiste en revisar la conexión entre el Atlántico Norte Subtropical-Horseshoe y la NAO para el clima reciente; pero implementando el análisis EMCA aplicado a la SST del Atlántico tropical fija en verano como predictor y evaluar la evolución temporal de la respuesta atmosférica como predictando, ya que la EMCA tiene en cuenta la dependencia con el ciclo estacional de los modos de covariabilidad [Secc. IV.2].

4. Influencia del Mediterráneo en la circulación global

Al igual que en los objetivos 2 y 3, el estudio llevado acabo en esta parte también se centra en el período 1979-2002 del clima reciente. El punto de partida del trabajo es un resultado mostrado por Polo et al. (2008; Apéndice-A), en el que la variabilidad térmica de la cuenca este del Mar Mediterráneo (patrón eMED; Fig. I.7) está estrechamente relacionada con la precipitación WAM[1] sobre la región Sudán-Sahel: anomalías positivas de SST en el eMED asociadas con un aumento de precipitación en la banda 10N-20N de África del Norte. Este resultado es de especial relevancia en el contexto de las tendencias climáticas, ya que Rodríguez-Fonseca et al. (2010) han mostrado recientemente que el eMED dejó de ser la respuesta a un forzamiento atmosférico remoto, y asociado a las lluvias en Guinea durante el período 1957-1978; pasando a tener un papel activo y aislado sobre el régimen de lluvias del Sahel durante 1979-1998.

En el protocolo de simulaciones del proyecto AMMA[2]-EU, las condiciones de contorno del AGCM (SST prescritas) en los experimentos de sensibilidad llevados a cabo para evaluar el

[1] *Acrónimo del término inglés West African Monsoon.*

[2] *Acrónimo del término inglés African Monsoon Multidisciplinary Analyses.*

impacto del eMED en el régimen monzónico WAM están basadas en el mismo modo SST descrito en Polo et al. (2008). En ese estudio de modelización, los autores han confirmado el forzamiento térmico del eMED sobre las precipitaciones WAM-Sahel (Fontaine et al. 2009).

Como parte de este trabajo, pero de forma complementaria a la Tesis (Apéndice-B), en ese mismo estudio se ha mostrado que la respuesta atmosférica a un calentamiento eMED presenta una respuesta baroclínica sobre la cuenca Mediterránea: bajas presiones anómalas en superficie y altas presiones anómalas en niveles altos. Esta respuesta debilita el flujo climatológico del noreste en la parte oriental del continente africano (Fig. II.5), resultando en un desplazamiento hacia el norte de

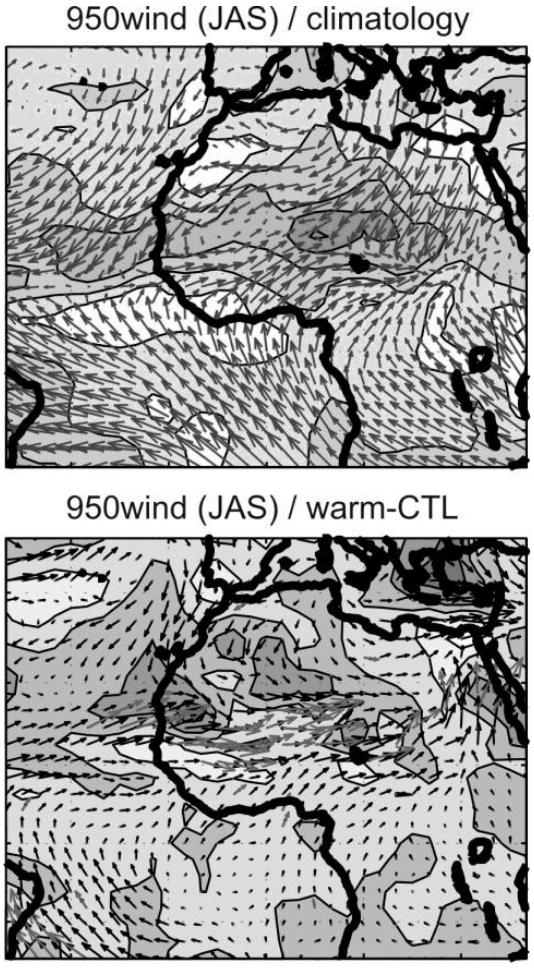

Fig. II.5. Climatología y anomalías de viento en superficie para el experimento con SST positivas en eMED. [Adaptada de Fontaine et al. 2009]

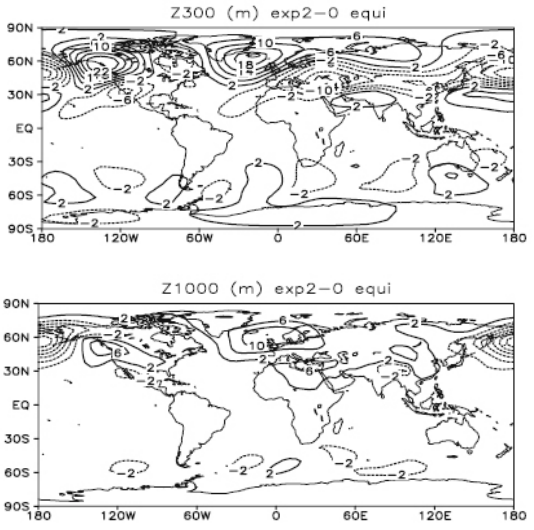

Fig. II.6. Climatología y anomalías de viento en superficie para el experimento con SST positivas en eMED. [Adaptada de Li 2006]

la ITCZ y de las lluvias monzónicas (Fontaine et al. 2009).

Una respuesta atmosférica similar al eMED ha sido encontrada por Li (2006) en una simulación AGCM idealizada en la que se prescribe un enfriamiento de 2K en el patrón eMED y se integra en un enero perpetuo. En ese caso, la respuesta baroclínica regional presenta altas presiones anómalas en superficie y bajas presiones anómalas en altura (Fig. II.6). De forma interesante, la respuesta atmosférica invernal a ese forzamiento en el Mediterráneo también muestra una circulación anómala barotrópica atrapada en las corrientes en chorro del oeste que circunda todo el cinturón de latitudes medias. Este patrón de teleconexión proyecta fuertemente en el patrón circunglobal de Branstator (2002), el cual se explica a través del efecto 'guía de onda' de esas corrientes en chorro, que canalizan la dispersión de la energía y presentan una propagación Rossby prácticamente zonal. En el experimento de Li (2006) dos importantes teleconexiones remotas fueron encontradas: el ahondamiento de la baja de las Aleutianas y el debilitamiento de la baja de Islandia (Fig. II.6).

El objetivo de esta parte del trabajo es doble. Por una parte, analizar la simulación AGCM del protocolo AMMA en la que se prescribe una evolución realista de la SST del patrón eMED (Fontaine et al. 2009) para evaluar si la respuesta baroclínica estival sobre el Mediterráneo tiene un

impacto en la circulación hemisférica.
Como segundo objetivo se han analizado datos procedentes de re-análisis en relación al modo eMED de Polo et al. (2008), para proporcionar una evidencia observacional de la respuesta regional baroclínica y de la hipótesis de respuesta hemisférica atrapada en las corrientes en chorro [Secc. IV.4].

DATOS Y METODOLOGÍA

En este capítulo se describen las diferentes bases de datos utilizadas en los distintos estudios que componen esta Memoria y que pueden agruparse en datos observacionales y datos procedentes de simulaciones con modelos de circulación general de la atmósfera (AGCM). Se describen las variables empleadas así como el cómputo de ciertos diagnósticos calculados para realizar determinados análisis. Asimismo se detalla el tratamiento preliminar que se ha aplicado a los diferentes datos y se desarrolla la metodología seguida en los diferentes estudios. Finalmente se indica cómo se ha llevado a cabo la representación de los resultados, así como la significación estadística de los mismos.

1. Descripción de los datos

A lo largo de esta Memoria, y para la consecución de todos los objetivos, se han analizado variables procedentes fundamentalmente de dos tipos de bases de datos:

- datos procedentes de diferentes re-análisis[1] y de bases de datos de observaciones interpoladas en mallas regulares;
- datos generados artificialmente mediante la integración de un AGCM[2] bajo determinadas condiciones de contorno asociadas a forzamientos oceánicos.

Además, se han calculado, partiendo de algunas variables procedentes de estas bases de datos, otras variables secundarias de cuyo diagnóstico se obtiene información necesaria para la consecución de los objetivos.

1.1. Observaciones. Re-análisis

La totalidad de los campos atmosféricos, excluyendo la precipitación, han sido extraídos del proyecto de re-análisis ERA40 del ECMWF[3]. El sistema de asimilación de datos de ERA40 usa el Sistema de Predicción Integrado (IFS[4]) desarrollado conjuntamente por el ECMWF y Météo-France. Los datos observados son integrados mediante una asimilación variacional de tres dimensiones; y el modelo de asimilación tiene una resolución horizontal espectral T159 y 60 niveles en la vertical (L60).

El re-análisis ERA40 cubre el periodo 01/09/1957-31/08/2002, integrando el re-análisis ERA15 que cubría 1979-1993; y ha producido datos globales cada 6 horas. El proceso de asimilación incluye, entre otros: datos de las sondas satelitales TIROS de la NOAA[5] (TOVS-ATOVS), datos oceánicos producidos por satélites de la NASA (SSM/I), productos derivados de los satélites operativos de la ESA (ERS) y medidas con radiómetros de infrarrojo (VTPR). La información completa y detallada del re-análisis puede consultarse en Uppala et al. (2005), o en http://www.ecmwf.int/research/era/do/get/era-40.

Los datos atmosféricos de ERA40 utilizados en este trabajo tienen una resolución horizontal de 2.5ºx2.5º (144 datos en longitud y 73 en latitud), y cubren 0ºE-357.5ºE / 90ºS-90ºN. Los campos atmosféricos utilizados se encuentran en niveles

1 Un re-análisis es el resultado de un sistema de asimilación de datos que tiene en cuenta medidas in situ y de satélite y constituyen la mejor aproximación al sistema climático observado (Secc. 1.1)

2 Un AGCM es una herramienta óptima para evaluar el forzamiento térmico del océano sobre la circulación atmosférica (Secc. 1.2).

3 Acrónimo del término inglés European Centre for Medium-Range Weather Forecasts.

4 Acrónimo del término inglés Integrated Forecasting System.

5 Acrónimo del término inglés National Oceanic and Atmospheric Administration.

troposféricos, 13 niveles que corresponden a 1000, 925, 850, 775, 700, 600, 500, 400, 300, 250, 200, 150 y 100 hPa. Las variables empleadas han sido: altura de geopotencial, temperatura del aire, viento zonal y meridional, componente vertical del viento en coordenadas de presión (omega), función de corriente, potencial de velocidad, y presión a nivel del mar.

En cuanto a la precipitación, una de las bases de datos de empleada es CMAP[6] , desarrollada en el *Climate Prediction Center* (CPC, Centro de Predicción del Clima) de la NOAA.

Los datos CMAP utilizados corresponden a medias mensuales que se extienden de 01/1979 hasta 12/2002; tienen una resolución espacial de 2.5ºx2.5º en una malla global (144 en longitud y 72 puntos en latitud), y cubren el dominio 1.25ºE-358.75ºE / 88.75ºS-88.75ºN. Los datos CMAP contienen información de 5 tipos de estimaciones satelitales (GPI, OPI, SSM/I-*scattering*, SSM/I-*emission*, MSU) y valores de precipitación del re-análisis NCEP/NCAR. La unidad de los datos CMAP es mm/día, y cubre un rango aproximado de 0-70mm/día. Para más información puede consultarse Xie y Arkin (1997), o http://www.esrl.noaa.gov/psd/data/gridded/data.cmap.html.

La otra base de datos de precipitación empleada es la proveniente de la Universidad de Delaware (EEUU). Los datos utilizados también corresponden a medias mensuales; y cubren el período 01/1950-12/1999. Estos datos de precipitación sólo tienen valores sobre tierra, aunque su resolución es mayor que la de CMAP; correspondiendo a 0.5ºx0.5º y cubriendo el dominio 89.75ºS-89.75ºN / 0.25ºE-359.75ºE (720 puntos en longitud y 360 puntos en latitud). Los datos de la Universidad de Delaware están compuestos por dos archivos de precipitación: el procedente del GHCN (Global Historical Climate Network) y el archivo de Legates&Willmott. Información más detallada se puede obtener de Legates y Willmott (1990), o en http://www.esrl.noaa.gov/psd/data/gridded/data.UDel_AirT_Precip.html.

La última base de datos observacional considerada, es la base de SST ERSST[7] de la NOAA, la cual es una reconstrucción de datos históricos de temperatura de la superficie del mar mediante sofisticados métodos estadísticos. Los datos utilizados son medias mensuales, y provienen de un conjunto que se extiende desde 01/1854 hasta la actualidad. Los datos ERSST poseen una resolución de 2ºx2º y cubren el dominio 88ºS-88ºN / 0ºE-358ºE (180 puntos en longitud y 89 puntos en latitud). Están construidos en base a los datos de SST de la ICOADS[8] , y han sido mejorados mediante técnicas estadísticas que permiten reconstrucciones estables usando datos con poca densidad espacial. Para más información consultar en Smith y Reynolds (2003), o en http://www.esrl.noaa.gov/psd/data/gridded/data.noaa.ersst.html.

1.2. Simulaciones

Un Modelo Global de Clima, y en particular un Modelo de Circulación General de la Atmósfera, o AGCM[9] , es, a diferencia de modelos regionales o conceptuales, una herramienta para la investigación del *clima global* y la exploración de sus fluctuaciones. Un AGCM es una representación espacial y temporal aproximada de los principales procesos físicos que ocurren en la atmósfera y de sus interacciones con las demás componentes del sistema climático. De su resolución (integración de las ecuaciones que lo componen) se obtiene la evolución temporal y espacial (tridimensional) del sistema, en función de las condiciones iniciales y de contorno elegidas y de los valores de ciertos parámetros climáticos (por ejemplo, la concentración de CO_2 o la irradiación solar), así como de ciertas parametrizaciones físicas que no resuelve el modelo y que se estiman (por ejemplo, procesos convectivos o microfísica de nubes). Una parte importante de estas condiciones de contorno con las que se integra un AGCM corresponde al estado del océano; en particular, a la temperatura de la superficie del mar (SST). Con la manipulación y diseño de estas condiciones de contorno, a las que se le denomina *SST prescritas*, se puede integrar un AGCM con diferentes propósitos. En particular, las simulaciones o experimentos numéricos analizados en este trabajo se conocen como *experimentos de sensibilidad*, y están planteados mediante *simulaciones por conjunto* (*ensemble simulations* en inglés) (McGuffie y Henderson-

6 Acrónimo del término inglés CPC Merged Analysis of Precipitation (Análisis de Precipitación Combinada del CPC).

7 Acrónimo del término Extended Reconstructed SST.

8 Acrónimo de International Comprehensive Ocean-Atmosphere Data Set.

9 Acrónimo del termino ingles Atmospheric General Circulation Model o Atmospheric Global Climate Model.

Sellers 2005).

Un experimento de sensibilidad es un diseño experimental en el que las condiciones de contorno prescritas se definen con el objetivo de conocer y evaluar la respuesta atmosférica a unas anomalías específicas de SST. Por lo general, estas SSTs constituyen el único forzamiento anómalo del modelo AGCM, y se definen de tal forma que el patrón anómalo de SST se superpone a la climatología de las condiciones de contorno. No obstante este diseño experimental tiene sus limitaciones, las cuales son inherentes al concepto de modelo de atmósfera (AGCM). Una es que la simulación AGCM considera que la fuente térmica anómala, el patrón de SST prescrito, tiene capacidad calorífica infinita, lo cual es contrario a las observaciones. Otra es que en una simulación AGCM, en sí, la atmósfera no extrae calor del océano, efecto fundamental de las interacciones océano-atmósfera que configuran la variabilidad climática. Sin embargo, los estudios mediante simulaciones AGCM son una herramienta única para analizar la respuesta puramente atmosférica a un forzamiento oceánico, por lo que poseen un interés excepcional para el análisis de los mecanismos de teleconexión atmosférica.

Una simulación por conjuntos es un diseño experimental que consta de diferentes integraciones numéricas con las mismas condiciones de borde. Las distintas integraciones se diferencian entre sí solamente en las condiciones iniciales del sistema. A cada una de estas integraciones se le conoce como 'miembro' de la simulación por conjuntos. En el caso de los AGCMs, la finalidad de estos diseños experimentales es aislar la señal atmosférica forzada por las anomalías de SST prescritas, minimizando la influencia de la variabilidad atmosférica interna del modelo; es decir, filtrando la señal forzada del ruido.

Las simulaciones analizadas en este trabajo se han realizado en el marco del proyecto europeo AMMA-EU, y con el modelo de atmósfera de la Universidad de Los Ángeles, UCLA-AGCM (Mechoso et al. 2000). Este modelo es un AGCM del Estado del Arte, y su atmósfera se extiende desde la superficie terrestre hasta una altura de 50km. El UCLA-AGCM predice el viento horizontal, la temperatura potencial, la razón de mezcla del vapor de agua, las razones de mezcla del agua precipitable y del hielo en nube, la profundidad de la capa límite planetaria y la presión en superficie, así como la temperatura superficial y la cubierta de nieve. El modelo UCLA-AGCM utilizado en los experimentos de sensibilidad del protocolo AMMA-EU es la versión 7.3, que tiene una resolución horizontal de 2º en latitud (89 puntos) y 2.5º en longitud (144 puntos), cubriendo el dominio 180ºW-177.5ºE / 88ºS-88ºN , y 29 niveles en la vertical. Información más completa y detallada puede encontrarse en Ritcher et al. (2008), o en http://www.atmos.ucla.edu/~mechoso/esm/agcm.html.

Haciendo uso del UCLA-AGCM v7.3, en este trabajo se han analizado dos simulaciones AGCM: una relativa al Niño Atlántico (Seccs. I.3.2.a, II.2) y otra a la cuenca oriental del Mediterráneo (eMED; Secc. I.3.3, II.4). Las condiciones de contorno empleadas en ambos experimentos de sensibilidad, pertenecientes al protocolo AMMA-EU, están basadas en los resultados de Polo et al. (2008). En particular, están basadas en los coeficientes de expansión del análisis EMCA realizado para Atlántico y el Mediterráneo. En el caso del eMED, y como parte de esta Memoria (aunque de forma paralela a la Tesis), se han realizado parte de las simulaciones del ejercicio de intercomparación del proyecto AMMA-EU. Las condiciones de contorno de estas simulaciones fueron diseñadas mediante compuestos de SST para eventos por encima/debajo de +1/-1 desviación estándar en el coeficiente de expansión eMED de Polo et al. (2008). De esta forma, la simulación con anomalías cálidas fue creada a partir de un patrón de forzamiento obtenido al restar el compuesto de eventos positivos de aquel procedente de los eventos negativos. Multiplicando por –1 dicho patrón se obtuvieron las condiciones de contorno para SSTs frías. Finalmente, se multiplicó el patrón de forzamiento por 2 para obtener una respuesta atmosférica más robusta. Las anomalías de SST de estas condiciones de contorno fueron obtenidas de la base de datos ERSST y calculadas para el período reciente 1979-2005. Los experimentos constaban de 10 miembros (10 integraciones), con objeto de realizar un *ensemble*. Una descripción más detallada de la simulación para el forzamiento eMED, así como los campos de SST prescritos, puede consultarse en Fontaine et al. (2009; Apéndice-B). Un diseño experimental similar fue desarrollado para la simulación con el forzamiento

Niño Atlántico, cuyo detalle y campos de SST prescritos pueden consultarse en Losada et al. (2009a).

1.3. Cálculo de diagnósticos

Actividad transitoria

Esta actividad tiene una marcada escala espacial sinóptica y una variabilidad de muy alta frecuencia. Como se ha descrito en el capítulo I, los diagnósticos calculados en este trabajo son:

$$PKE = \frac{1}{2}\left(\overline{u'u' + v'v'}\right)$$

$$E = \left(\frac{1}{2}\overline{v'v' - u'u'}\,, -\overline{u'v'} \right)$$

$$\overline{v'T'}$$

donde *PKE* es la energía cinética de las perturbaciones, *E* es la componente horizontal del vector de Eliassen-Palm y $\overline{v'T'}$ es la componente meridional del flujo de calor *eddy*. Para el cálculo de estos diagnósticos, en este trabajo se han considerados datos diarios de (*u,v,T*), y se han computado las anomalías (*u',v',T'*) a través del filtro de 24-horas, que consiste en la diferencia entre dos días consecutivos de la serie de datos; de esta forma, representando esencialmente la variabilidad atmosférica de escala sinóptica (Wallace et al. 1988). Posteriormente se han calculado, para cada día, las covarianzas entre las variables (e.g. *u'v'* o *v'v'*); y finalmente se han realizado promedios mensuales de estas covarianzas (e.g. $\overline{u'v'}$ o $\overline{v'T'}$). A partir de estos datos mensuales se ha procedido igual que en el resto de las variables atmosféricas empleadas (Secc. 2.1).

Variables indirectas

La función de corriente y el potencial de velocidad son potenciales de flujo de los que se deriva el viento rotacional y el viento divergente (Secc. I.4.1), así como la componente tropical de las fuentes de ondas de Rossby (Secc. I.4.4.b), tal que:

$$\left(u_\psi, v_\psi\right) = \left(-\frac{\partial \psi}{\partial y}, \frac{\partial \psi}{\partial x} \right)$$

$$\left(u_\chi, v_\chi\right) = \left(\frac{\partial \chi}{\partial x}, \frac{\partial \chi}{\partial y} \right)$$

$$TRWS = -u_\chi' \frac{\partial \bar{\zeta}}{\partial x} - v_\chi' \frac{\partial}{\partial y}\left(\bar{\zeta} + f\right)$$

Estas variables derivadas no se obtienen directamente del reanalisis ERA40 y han sido calculadas implementando un esquema de diferencias finitas en un dominio cerrado y de paso de malla regular (ERA40, 2.5ºx2.5º). Los puntos de malla en las fronteras han sido calculados mediante diferencias adelantadas o retrasadas, según corresponda, y los puntos del interior mediante diferencias centradas (Llorente y Pérez 1998), siguiendo el siguiente esquema numérico:

$$\frac{\partial F}{\partial x} = \begin{cases} \dfrac{F(i, j+1) - F(i, j)}{\Delta x} & dif.\ adelantada \\ \dfrac{F(i, j+1) - F(i, j-1)}{2\Delta x} & dif.\ centrada \\ \dfrac{F(i, j) - F(i, j-1)}{\Delta x} & dif.\ retrasada \end{cases}$$

$$\frac{\partial F}{\partial y} = \begin{cases} \dfrac{F(i+1, j) - F(i, j)}{\Delta y} & dif.\ adelantada \\ \dfrac{F(i+1, j) - F(i-1, j)}{2\Delta y} & dif.\ centrada \\ \dfrac{F(i, j) - F(i-1, j)}{\Delta y} & dif.\ retrasada \end{cases}$$

2. Tratamiento de los datos

Como se ha dicho anteriormente, a lo largo de este trabajo se han analizado fundamentalmente datos observacionales y de simulaciones AGCM. En ambos casos se analizará la variabilidad atmosférica asociada a una media climatológica o a una simulación de control sin forzamiento. Sin embargo, la forma de calcular dicha desviación respecto a un estado medio es distinta y requiere de la aclaración de ciertos matices.

2.1 Cálculo de anomalías

En el caso de analizar la variabilidad de la atmósfera ante un determinado forzamiento mediante las salidas de una simulación numérica, el procesado de los datos es sencillo. En esta Memoria,

los patrones de anomalías se han calculado sustrayendo el promedio de una simulación control (integraciones sin SST anómala) al promedio de la salida de los experimentos de sensibilidad (integraciones con SST anómala). Es decir, se ha calculado por separado el promedio del conjunto de miembros de sensibilidad y el promedio del conjunto de miembros de control, y posteriormente se ha computado su diferencia. De ese modo, los patrones de anomalías asociados a la respuesta atmosférica representan perturbaciones por encima (anomalías positivas) o por debajo (anomalías negativas) del comportamiento medio de la atmósfera del AGCM sin forzamiento.

Para el caso de datos procedentes de observaciones, el cálculo de anomalías representa un filtro de los datos originales. Al igual que en el caso de las simulaciones AGCM, la escala temporal seleccionada es la frecuencia interanual, es decir, año a año. Con objeto de estudiar esa variabilidad interanual, de los datos mensuales de los que se parte se ha sustraído la media climatológica de cada mes a analizar, eliminando de esta forma la influencia del ciclo anual (e.g. Xoplaki et al. 2003a).

2.2 Pre-procesado

Cuando se trabaja con datos globales hay que tener en cuenta que las áreas en geometría esférica no son iguales que si se trabaja con geometría cartesiana, no siendo tan acentuada dicha diferencia cerca del ecuador y acentuándose cuando se llega a los polos. Este hecho se enfatiza, además, al realizar un análisis discriminante de la matriz de varianza o covarianza (Secc. 3). Para asegurar que áreas iguales en una variable tengan el mismo peso en la matriz de varianza o covarianza, y teniendo en cuenta la forma esférica de la Tierra, cada valor de la matriz de anomalías de esa variable debe ser multiplicado por la raíz cuadrada del coseno de la latitud de ese punto (Thompson y Wallace 2000).

Como se ha indicado en el capítulo anterior (Secc. II.1), en esta Memoria se presentan los resultados de realizar un análisis discriminante sobre la matriz de varianza de la función de corriente (Secc. IV.1). La función de corriente, potencial del flujo rotacional, se obtiene como solución de un problema elíptico: la integración de la ecuación de Poisson para la función de corriente ψ, siendo la vorticidad relativa ζ el término independiente (e.g. Sardeshmukh and Hoskins 1987),

$$\nabla^2\psi = \zeta$$

donde ∇^2 representa el operador Laplaciano. La solución de este problema se debe ajustar a las condiciones de frontera especificadas, y generalmente se impone que la media global de la función de corriente sea igual a cero (e.g. Uppala et al. 2005). Esta condición introduce una variabilidad 'artificial' si el estudio se realiza sobre un área limitada de la esfera terrestre, ya que indica que localmente esta variable puede verse influenciada por regiones de fuera del dominio de estudio. Esa variabilidad matemática, 'no física', se reduce sustrayendo el promedio espacial sobre el dominio considerado a cada punto del dominio y para cada paso de tiempo. Esta metodología sería también aplicable a un análisis discriminante sobre el potencial de velocidad, potencial del flujo divergente (e.g. Sardeshmukh and Hoskins 1987).

3. Métodos de análisis discriminante

Las técnicas de análisis discriminante son una herramienta muy importante para el estudio de la variabilidad climática. El objetivo de estas metodologías es la síntesis o reducción de información pero sin la pérdida de las condiciones originales de variabilidad. Es decir, ya que los datos climáticos suelen tener una gran dimensión espacial y temporal, estos análisis discriminantes tratan de comprimir los datos de manera que se obtengan unas determinadas direcciones relevantes del espacio de fases original (von Storch y Zwiers 2001). Los análisis discriminantes utilizados en esta Tesis se basan en la reducción de información en la dimensión espacial de un campo o variable, o de dos campos que co-varían. Para ello, como se explicará más adelante, se diagonaliza la matriz de varianza o de covarianza, respectivamente. El resultado de este cálculo proporciona unas estructuras espaciales, o *patrones espaciales*, que acumulan una gran fracción de varianza o de covarianza en los datos. Matemáticamente, esas estructuras espaciales son la consecuencia de un cambio de base, en el que esos vectores representan las direcciones predominantes de variabilidad en la matriz de anomalías original. De esta forma, mediante la combinación lineal de esas estructuras espaciales se puede reconstruir la

matriz de datos de la que se parte. La alternativa a esta reducción espacial, análisis discriminante en la dimensión temporal, puede consultarse en Drosdowsky (1993) o Huth (1997).

Como se ha dicho antes, estos análisis discriminantes se basan en la discretización de una matriz, la matriz de varianza (para una variable) o la matriz de covarianza (para dos variables que co-varían). La herramienta matemática que proporciona esta reducción dimensional es la *diagonalización* de esa matriz. Sin embargo, esta diagonalización no es el origen de estas técnicas, sino el resultado de un complejo problema de cálculo variacional, el cual incluye una serie de restricciones dadas por la condición de ortonormalidad. Este problema se soluciona aplicando el método de los Multiplicadores de Lagrange sobre una función a maximizar. En el caso de una variable (Secc. 3.1), esta función representa la maximización de la varianza temporal de un campo; y la consecuencia del método es la resolución del *polinomio característico* de la matriz de varianza. Para el caso de dos variables que covarían (Seccs. 3.2, 3.3), la función maximiza las combinaciones lineales de las series temporales de dos campos; y la consecuencia del método es la resolución del polinomio característico de la matriz de covarianza. Una descripción más detallada puede consultarse en von Storch y Zwiers (2001) o Rodríguez-Fonseca (2001). Como resultado final del análisis discriminante, la diagonalización produce un conjunto de direcciones espaciales llamadas *autovectores* y una serie de escalares asociados llamados *autovalores* que aportan el peso (o representatividad) de cada autovector en la matriz original. Así, en ese espacio de autovectores los patrones espaciales asociados a los autovalores son ortogonales entre sí.

3.1. Análisis de componentes principales

El análisis discriminante sobre un sólo campo que se ha aplicado en este trabajo (Secc. II.1) es el Análisis de Componentes Principales (PCA[10]). Como se ha dicho anteriormente, el análisis PCA maximiza la varianza temporal de un campo; y resuelve el polinomio característico de su matriz de varianza. Así, dado un campo espacio-temporal de anomalías C (*ns*, *nt*), donde *ns* indica el número de puntos en el dominio espacial y *nt* el número de tiempos de la serie de cada punto; el análisis PCA diagonaliza la matriz de varianza:

$$VAR = \frac{\sum_{i=1}^{nt} (c_i - \bar{c})^2}{nt - 1}$$

que, matricialmente, se puede indicar como:

$$VAR = \frac{C \cdot C^t}{nt - 1}$$

El problema de autovalores en un PCA, por tanto, se expresa:

$$VAR = E \cdot \lambda \cdot E^t$$

donde la matriz E (*ns*, *ns*) proporciona los autovectores (en columnas) que representan los patrones espaciales linealmente ortogonales, llamados EOFs (Empirical Orthogonal Functions); mientras que los elementos de la matriz diagonal λ son proporcionales a la fracción de varianza (*fvar*) explicada por cada modo *m* sobre la varianza total del campo.

$$f\ \mathrm{var}_m = \frac{\lambda_m}{\sum_{i=1}^{ns} \lambda_i}$$

El número de modos *nm* que se han seleccionado en este trabajo corresponde al conjunto de autovalores que explica alrededor del 80% de la varianza total (Barnett y Preisendorfer 1987). La significación estadística de las EOFs se ha evaluado a través del criterio de North et al. (1982). Éste considera que el grado de separación requerido entre autovectores para establecer la unicidad de cada modo se puede estimar como:

$$\Delta\lambda = \lambda_i - \lambda_{i+1} = \lambda_i \sqrt{\frac{2}{nt}}$$

El análisis PCA se completa a través de las series temporales asociadas a los patrones espaciales, llamadas PCs (Componentes Principales):

$$PCs = \frac{E^t \cdot C}{nt}$$

Estas PCs proporcionan, a lo largo del tiempo,

10 Acrónimo del término inglés Principal Component Analysis.

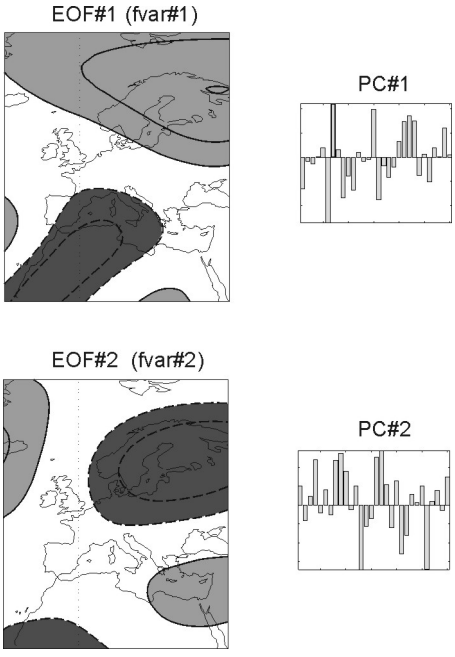

Fig. III.1. Esquema de resultados del análisis PCA, con la representación de dos modos ficticios.

el peso o representatividad de cada EOF en la distribución original de anomalías del campo *C*.

De esta forma, el análisis PCA arroja pares de entidades: un patrón espacial o EOF, y una serie temporal o PC; junto con la fracción de varianza (*fvar*) explicada por cada modo (Fig. III.1). Esta metodología ha sido implementada en el capítulo IV.1. Información más detallada sobre PCA puede encontrarse en von Storch (1995) y von Storch and Zwiers (1999). Las limitaciones del análisis PCA pueden ser consultadas en North et al. (1982) y Dommenget y Latif (2002); mientras que el ejercicio de rotación de EOFs para asegurar la interpretación física puede encontrarse en Richman (1986), Jolliffe (1987) y Barnston y Livezey (1987).

3.2. Análisis de máxima covarianza

El análisis discriminante sobre dos campos aplicado en este trabajo se llama EMCA[11] , el cual es una extensión del análisis llamado MCA (Maximum Covariance Analysis).

Como se ha dicho anteriormente, el análisis MCA maximiza las combinaciones lineales de las series temporales de dos campos; y resuelve el polinomio característico de su matriz de covarianza. Así, dados dos campos espacio-temporales de anomalías *C* (*ns1*, *nt*) y *B* (*ns2*, *nt*); el análisis MCA equivale a diagonalizar la matriz de covarianza:

$$COV = \frac{\sum_{i=1}^{nt} (c_i - \bar{c})(b_i - \bar{b})}{nt - 1}$$

$$COV = \frac{C \cdot B^t}{nt - 1}$$

Por tanto, en este caso, el problema de autovalores se puede expresar como:

$$COV = L \cdot \lambda \cdot R^t$$

donde la matriz *L* (*ns1*, *n*) proporciona los vectores singulares (por columnas) de los modos asociados al campo *C* y la matriz *R* (*ns2*, *n*) proporciona los vectores singulares (también por columnas) asociados al campo *B,* siendo *n* el valor mínimo entre *ns1* y *ns2*; mientras que los elementos de la matriz diagonal λ (*n*, *n*) son proporcionales a la fracción de covarianza cuadrática (*scf*[12]) explicada por cada modo *m*:

$$scf_m = \frac{\lambda_m^{\,2}}{\sum_{i=1}^{\min(ns1,ns2)} \lambda_i^{\,2}}$$

El valor de la *scf* indica, también, la aportación relativa de cada modo en la variabilidad conjunta entre los campos considerados. La significación estadística de la *scf* ha sido estimada a través de un test de Monte-Carlo (Secc. 6.3).

Las series temporales asociadas a cada modo MCA se denominan *coeficientes de expansión*, y se calculan según:

$$U = \frac{L^t \cdot C}{nt} \qquad V = \frac{R^t \cdot B}{nt}$$

Como se ha descrito antes, las combinaciones lineales entre estos coeficientes de expansión representan la función a maximizar en el problema

11 Acrónimo del término inglés Extended-Maximum Covariance Analysis.

12 Acrónimo del término inglés squared covariance fraction.

de los Multiplicadores de Lagrange asociado al método MCA. Por tanto, otro parámetro importante de este análisis es el coeficiente *ruv,* que representa el coeficiente correlación entre las series temporales asociadas a cada campo. Así, *ruv* indica el grado de relación lineal entre cada par de modos MCA; mientras que el cuadrado de *ruv* proporciona una medida de la varianza de un campo explicada por el otro.

De este forma, el resultado del análisis MCA consta de dos pares de entidades para cada modo: un mapa espacial y un coeficiente de expansión del campo *C*; y otro mapa espacial y otro coeficiente de expansión asociado al campo *B*; junto con la *scf* explicada y el *ruv* asociado (Fig. III.2). Al igual que para los modos PCA, los resultados de los modos MCA se representan mediante mapas de regresión (Secc. 5). Si se utiliza la serie temporal de un campo para proyectarla en la matriz de anomalías espacio-temporal del campo covariante, a este mapa se le denomina *mapa de regresión heterogéneo*; si se proyecta una serie temporal sobre su propio campo de anomalías, se le llama *mapa de regresión homogéneo*. Para más información referente al análisis MCA consultar Bretherton et al. (1992) y Wallace et a. (1992). Las limitaciones de este análisis pueden extraerse de Cherry (1997) y Hu (1997); mientras que el ejercicio de rotación de los modos para asegurar la interpretación física de MCA puede encontrarse en Cheng y Dunkerton (1995) y Frankignoul y Kestenare (2005).

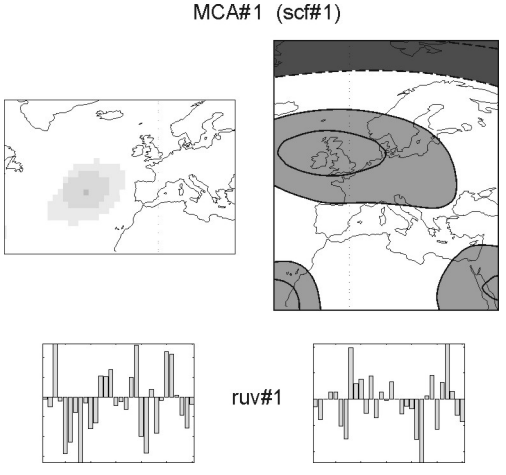

Fig. III.2. Esquema de resultados del análisis MCA; con la representación de un modo ficticio, mapas de regresión homogéneos y coeficientes de expansión.

3.3. Análisis de máxima covarianza extendido

Una de las principales utilidades del análisis MCA es el analizar la covariabilidad entre campos en los que se hace la hipótesis de causalidad: en la que un campo *predictor* influye y determina parte de la variabilidad de un campo a predecir o *predictando*. En nuestro caso, siguiendo los resultados de Rodríguez-Fonseca y Castro (2002), Frankignoul y Kestenare (2005) y Rodríguez-Fonseca et al. (2006), se hace la hipótesis de que el océano Atlántico tropical tiene un cierto carácter predictivo sobre la circulación atmosférica y la precipitación invernal del sector Euro-Atlántico (Secc. II.2, II.3). A diferencia de Rodríguez-Fonseca y Castro (2002) y Frankignoul y Kestenare (2005) que realizaron diferentes MCAs desfasando la SST (hasta el verano anterior) y fijando la variable atmosférica en invierno, aquí se ha optado por la metodología desarrollada en Polo et al. (2008) que tiene en cuenta la dependencia de las variables con el ciclo estacional. Esta metodología, llamada EMCA (Extended-MCA), consiste en introducir diferentes desfases temporales en uno de los campos del análisis MCA. Por su parte, Polo et al. (2008) introdujeron desfases en el campo predictor, la SST. En este trabajo se han introducido desfases en el campo a predecir, la precipitación. En particular, se ha fijado la SST del Atlántico tropical en verano (predictor; jun-sep) y se han introducido 6 tiempos desfasando un mes la estación estival hasta el final del invierno, dic-mar (predictando; jjas + 6, *nlag*=7; Fig. III.3).

De esta forma, si la matriz de anomalías de SST tiene dimensiones (*ns1*, *nt*) y la de precipitación PCP (*ns2*, *nt*), la matriz de covarianza del análisis EMCA tiene dimensiones (*ns1*, *nlag* x *ns2*). Ejemplos de la aplicación del análisis EMCA al campo predictor pueden encontrarse en Polo et al. (2008; ver también Figs. I.3, I.7). Más información sobre esta metodología puede consultarse en Polo (2008).

4. Regresión múltiple

Como se verá posteriormente, a lo largo del primer capítulo de resultados (Secc. IV.1), en este trabajo se han realizado dos regresiones múltiples para reconstruir o modelar la serie temporal de dos modos canónicos de variabilidad: la Oscilación del

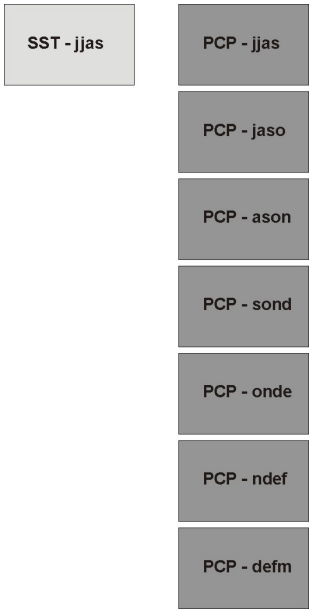

Fig. III.3. Esquema del análisis EMCA implementado entre la SST estival del Atlántico tropical y la secuencia de precipitación del sector Euro-Atlántico.

Atlántico Norte, entendida como primera EOF de la presión a nivel del mar en el Atlántico Norte; y la Oscilación Ártica, entendida como primera EOF de la presión a nivel del mar en el hemisferio Norte (ver también Secc. I.2.1).

La regresión múltiple es un método estadístico para estimar un modelo paramétrico en la relación entre una variable dependiente (o variable a predecir) y una o varias variables independientes (o predictores). El *modelo de regresión lineal múltiple* empleado en esta Memoria es la regresión paso-a-paso[13] (von Storch y Zwiers 2001).

En particular, las series temporales modeladas en este trabajo se han reconstruido en base a las dos primeras EOFs (PC1, PC2) de la función de corriente en el Atlántico Norte-Europa. De esta forma, el problema de regresión múltiple constituye el modelado de una serie temporal mediante una función polinómica en el tiempo:

$$SLP\#1 = a_0 + a_1 PC1 + a_2 PC2$$

Así, los tres parámetros libres a_0, a_1 y a_2 deben ser estimados desde los datos. Esta estimación se ha realizado mediante el método de mínimos cuadrados; la cual, en este caso, es sencilla ya que el modelo de regresión múltiple es lineal en sus parámetros (von Storch y Zwiers 2001). La regresión paso-a-paso es una aplicación iterativa de pasos de selección hacia delante y eliminación hacia atrás, cuyo objetivo es maximizar el valor del coeficiente de correlación múltiple. A medida que la selección hacia delante progresa, los factores seleccionados van incorporándose al modelo; mientras que la eliminación hacia atrás se realiza después de cada paso de selección para así eliminar variables redundantes del modelo. Aunque en este trabajo se ha empleado el modelo de regresión múltiple paso-a-paso, el avance de la computación está permitiendo actualmente el empleo de otros modelos, como es la *regresión por todos los subconjuntos* (von Storch y Zwiers 2001).

5. Representación de los resultados

A continuación se describe la metodología de representación de los resultados observacionales; la cual incluye *mapas de regresión* y *mapas de correlación*. Los mapas de regresión se computan mediante el producto matricial de una matriz espacio-temporal de anomalías por una serie temporal. Una matriz espacio-temporal es aquella creada como compilación de las anomalías en un dominio espacial a lo largo del tiempo: una matriz que contiene la evolución temporal de cada punto de malla del dominio, y que por lo general tiene dimensiones (*ns*, *nt*), donde *ns* es la dimensión espacial y *nt* la dimensión temporal (Fig. III.4).

Las series temporales analizadas en este trabajo, y con las que se han generado los mapas de regresión, son series temporales que corresponden a componentes principales (PCs) o a coeficientes de expansión EMCA; y por lo general son vectores que tienen dimensión (*nt*, 1). Así, estos mapas se emplean para conocer como se comporta una determinada variable en la dirección marcada por una serie temporal, ya sea un índice de teleconexión o una PC. Y ya que estas series temporales suelen estar estandarizadas, estos mapas de regresión representan la amplitud de las anomalías de una determinada variable por desviación estándar de la serie temporal empleada.

13 *Traducción del término inglés stepwise.*

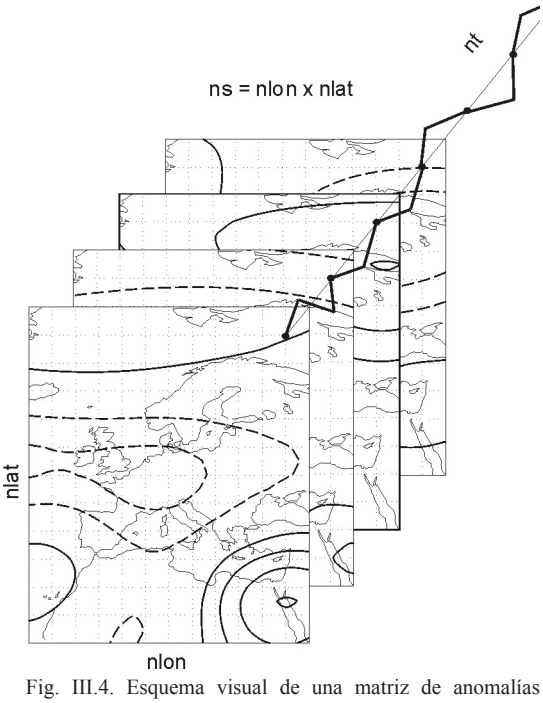

Fig. III.4. Esquema visual de una matriz de anomalías espacio-temporal de dimensiones (ns, nt).

Dado un campo de anomalías *C* y una serie temporal *ST*, el mapa de regresión viene dado por:

$$regres\ (ns,1) = C\ (ns,nt) \times ST\ (nt,1)$$

por tanto, el mapa de regresión tiene sólo dimensiones espaciales (*ns*, 1). Como puede comprobarse, ese producto matricial corresponde al producto escalar de la serie temporal de cada punto de malla con la serie temporal *ST*; por lo que en realidad un *mapa de regresión* representa un mapa de proyección, la proyección de un campo de anomalías (*ns*, *nt*) sobre una serie temporal (*nt*, 1).

Por otro lado, los mapas de correlación representan la distribución espacial del coeficiente de correlación lineal *r* calculado entre la serie temporal de cada punto de la malla *ns* y la serie *ST*:

$$correl_i\ (1,1) = r\left(C_i(1,nt), ST\,(nt,1)\right)$$

De esta forma, toda la información de un mapa de regresión está supeditada a la significación estadística del mapa de correlación; es decir, que el análisis del mapa de regresión se debe realizar para aquellas regiones donde el mapa de correlación sea significativo.

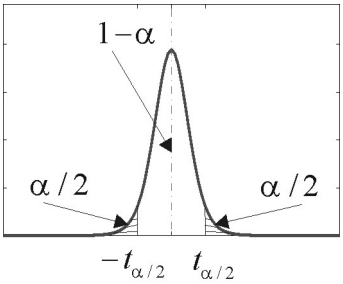

Fig. III.5. Esquema de la distribución *t* de Student para un test bilateral, con la región de aceptación 1-α y las colas de rechazo α/2.

6. Análisis de la significación estadística

Uno de los análisis más importantes en el tratamiento de datos climáticos es el análisis de la significación estadística de los resultados, el cual se hace mediante un contraste de hipótesis. Esta hipótesis (estadística) es una 'afirmación' que se hace sobre alguna característica de las poblaciones a estudiar, y se suele denominar como *Ho* o *hipótesis nula*; mientras que la *hipótesis alternativa* se suele indicar como H_1. La mayoría de los tests que se han realizado en este trabajo han sido de tipo test-bilateral paramétrico, y el estadístico calculado de las poblaciones se ha comparado con la distribución continua de probabilidad *t* de Student (Fig. III.5). Esta distribución tiende a la curva normal tipificada cuando aumenta el número de grados de libertad del sistema (*n*), siendo la distribución normal una buena aproximación, en general, cuando $n \geq 30$ (Gorgas et al. 2009). En cualquiera de los tests bilaterales realizados, la hipótesis nula *Ho* se ha rechazado (aceptado) con un nivel α (1-α) de significación (confianza) si:

$$rechaza \quad |t| \geq t_{\alpha/2}$$
$$acepta \quad |t| < t_{\alpha/2}$$

6.1. Coeficiente de correlación

A lo largo de los objetivos de este trabajo, casi todos los análisis de datos observacionales han sido mediante mapas de regresión. Como se ha dicho en la Secc. 5, estos mapas de regresión consisten básicamente en el producto escalar (o proyección) de la serie temporal de cada punto de malla de la matriz de anomalías con la serie temporal a analizar, una componente principal (PCA) o un coeficiente de expansión (EMCA). Por

tanto, la significación estadística de estos mapas de regresión ha sido realizada mediante un contraste de hipótesis aplicado al coeficiente de correlación entre estas series temporales; aplicado, por tanto, a cada punto del mapa de correlación. De esta forma, la hipótesis nula en estos casos ha sido que la correlación poblacional (ρ) sea nula; es decir, que las series temporales no estarían correlacionadas entre sí de aceptarse la hipótesis nula:

$$Ho: \quad \rho = 0$$
$$H_1: \quad \rho \neq 0$$

Ho: se acepta si $|t| < t_{\alpha/2, n-2}$

$$\text{con } t = \frac{r\sqrt{n-2}}{\sqrt{1-r^2}}$$

donde *n* es el número de grados de libertad del sistema, en nuestro caso el número de tiempos o dimensión temporal de los datos (*nt*); *r* el coeficiente de correlación entre las series; *t* el estadístico de Student; y α el nivel de significación, que en los análisis observacionales ha sido 0.02 (nivel de confianza del 98%).

6.2. Igualdad de medias

Para los resultados de las simulaciones, el test bilateral utilizado ha sido el de igualdad de medias con varianzas desconocidas (pero iguales). El contraste de hipótesis ha sido aplicado entre las medias poblacionales de los experimentos de sensibilidad (μ_{exp}) y las simulaciones de control (μ_{ctl}). De esta forma, la hipótesis nula en estos casos ha sido que la media poblacional sea igual; es decir, que no habría diferencias significativas entre la simulación con y sin forzamiento si se aceptase la hipótesis nula:

$$Ho: \quad \mu_{\exp} = \mu_{ctl}$$
$$H_1: \quad \mu_{\exp} \neq \mu_{ctl}$$

Ho se acepta si $|t| < t_{\alpha/2, n+m-2}$

$$\text{con } t = \frac{\overline{Z}_{\exp} - \overline{Z}_{ctl}}{S_P\sqrt{\frac{1}{n}+\frac{1}{m}}}$$

$$S_P^2 = \frac{(n-1)S_{\exp}^2 + (m-1)S_{ctl}^2}{n+m-2}$$

donde *n* es el número de grados de libertad del experimento de sensibilidad y *m* de la simulación control; *Z* el campo a analizar; *t* el estadístico a calcular; S_{exp} y S_{ctl} las varianzas muestrales del experimento de sensibilidad y de la simulación control respectivamente; y α el nivel de significación, que en los análisis AGCM ha sido 0.05 (nivel de confianza del 95%).

6.3. Test de Monte-Carlo

De forma alternativa a la práctica totalidad de los análisis llevados a cabo en este trabajo, para la significación estadística de los modos EMCA (secc. IV.2) se ha realizado un test estadístico unilateral no-paramétrico. Esta validación estadística corresponde al test de Monte-Carlo, y ha sido aplicado sobre la fracción de covarianza cuadrática (*scf*) por cada modo EMCA. La particularidad del test no-paramétrico es que la función de distribución del estadístico se genera para cada caso, en particular, mediante permutaciones aleatorias de la característica de la población a validar (Fig. III.6).

En este caso, el contraste de hipótesis se reduce a:

$$\text{si } \theta > \theta_k, \text{ siendo } k\frac{100}{p} = (1-\alpha)100$$

θ (característica muestral) es estadísticamente significativo con α; siendo *p* el número de permutaciones y *k* la posición de θ_k.

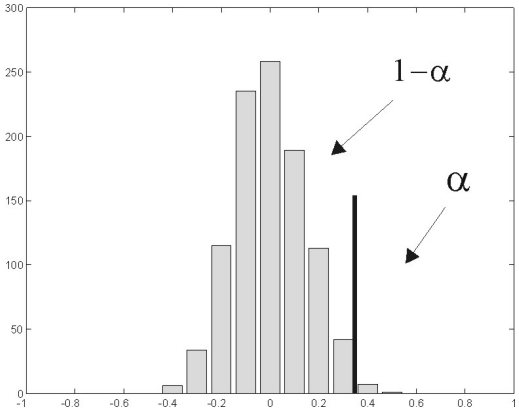

Fig. III.6. Función de distribución de Monte-Carlo para un coeficiente de correlación ficticio con 1000 permutaciones; frecuencia de correlaciones en el eje de ordenadas.

[Bibliografía: von Storch y Zwiers 2001]

RESULTADOS

A lo largo de este capítulo se encuentran los cuatro artículos que componen esta Memoria, los cuales resumen el trabajo de Tesis desarrollado entre 2005 y 2010. De forma paralela a esta Memoria, en el Apéndice se encuentran otros dos artículos que complementan los estudios aquí mostrados y en los que el autor ha colaborado.

IV.1.

Circulación atmosférica rotacional durante el invierno del Atlántico Norte-Europa: la influencia de ENSO

García-Serrano, J., B. Rodríguez-Fonseca, I. Bladé, P. Zurita-Gotor y A. de la Cámara (2010): Rotational atmospheric circulation during North Atlantic-European winter: the influence of ENSO. Clim. Dyn., CLIDY-D-10-00043 (under review).

Los modos de variabilidad dominante del flujo rotacional sobre el Atlántico Norte-Europa son examinados a través de un análisis de componentes principales (PCA/EOF) de la función de corriente en 200hPa a mediados del invierno boreal (meses Ene-Feb). Los resultados revelan que, cuando esta norma es usada, el modo dominante (EOF1) no corresponde con la tradicional Oscilación del Atlántico Norte (NAO, EOF2), sino que es la manifestación regional del modo EOF dominante de la función de corriente hemisférica. La regresión de este modo sobre el campo de SST muestra una clara y significativa señal de El Niño, sin anomalía significativa en el Atlántico; mientras que las anomalías de geopotencial en la alta troposfera recuerdan al patrón Trópico/Hemisferio Norte (TNH). Al este de América del Norte, este tren de ondas tipo-TNH produce un patrón meridional tipo dipolo en los niveles bajos. Pese a la similitud de este patrón con la NAO (EOF2), las dinámicas de estos dos modos son muy diferentes, de tal forma que sólo EOF2 está asociada a un desplazamiento latitudinal de la trayectoria de las perturbaciones sinópticas en el Atlántico Norte. Así, la elección de la norma función de corriente en el análisis EOF permite separar dos fenómenos diferentes que pueden producir anomalías dipolares de presión en superficie sobre el Atlántico Norte, aunque éstas tienen impactos distintos en el clima europeo.

Estos dos modos también difieren en su contribución a la variabilidad en los niveles bajos: mientras que la NAO-EOF2 está fundamentalmente confinada al Atlántico Norte, el TNH-EOF1 tiene un carácter mucho más global y anular. En los niveles altos, NAO-EOF2 también produce un patrón global, aunque no-anular, en amplio acuerdo con la 'teleconexión circunglobal'.

Rotational Atmospheric Circulation During North Atlantic-European Winter: The Influence of ENSO

J. García-Serrano(1), B. Rodríguez-Fonseca(1), I. Bladé(2), P. Zurita-Gotor(1), A. de la Cámara(1)

(1) Departamento de Geofísica y Meteorología, UCM, Madrid, Spain
(2) Departament d'Astronomia i Meteorologia, UB, Barcelona, Spain

(CLIDY-D-10-00043, under review)

ABSTRACT

The dominant variability modes of the North Atlantic-European rotational flow are examined by applying a principal component analysis (PCA/EOF) to the 200hPa streamfunction mid-winter anomalies (Jan-Feb monthly means). The results reveal that, when this norm is used, the leading mode (EOF1) does not correspond to the traditional North Atlantic Oscillation (NAO, EOF2) but is the local manifestation of the leading hemispheric streamfunction EOF. The regression of this regional mode onto the global SST field exhibits a clear and significant El Niño signature, with no signal over the Atlantic, while the associated upper height anomalies resemble the Tropical/Northern Hemisphere (TNH) pattern. East of North America, this TNH-like wavetrain produces a meridional dipole-like pattern at lower levels. Although this pattern in some ways resembles the NAO (EOF2), the dynamics of these two modes are very different in that only EOF2 is associated with a latitudinal shift of the North Atlantic stormtrack. Thus, the choice of the streamfunction norm in the EOF analysis allows to separate two different phenomena that can produce similar dipolar surface pressure anomalies over the North Atlantic but that have different impact on European climate.

These two modes also differ on their contribution to variability at lower levels: while NAO-EOF2 is mostly confined to the North Atlantic, TNH-EOF1 has a more annular, global character. At upper levels NAO-EOF2 also produces a global pattern, but with no annular structure, in broad agreement with the "circumglobal teleconnection".

1. Introduction

The forcing and propagation of Rossby waves is known to be the primary mechanism by which anomalous tropical diabatic heating can influence temperate latitudes (Hoskins and Karoly 1981; Horel and Wallace 1981; Shukla and Wallace 1983; Branstator 1983; Hoskins and Ambrizzi 1993; Trenberth et al. 1998). This fundamental link between anomalous tropical circulation and changes in the extratropical circulation can be most succinctly described in term of non-divergent (or rotational) barotropic theory (Hoskins and Karoly 1981; Webster 1981; Sardeshmukh and Hoskins 1988).

Yet, although a great number of studies have analyzed the atmospheric circulation variability over the North Atlantic-European (NAE) sector, none of them has focused on the upper level anomalous rotational circulation (Wang 2005). This is in spite of abundant observational and modelling evidence indicating the existence of forced Rossby wavetrains over NAE associated with either tropical Atlantic variability (TAV) (e.g.; Sutton et al. 2000; Cassou and Terray 2001a; Terray and Cassou 2002; Drévillon et al. 2003; Cassou et al. 2004; Peng et al. 2005; Haarsma and Hazeleger 2007; García-Serrano et al. 2008, 2010) or the El Niño-Southern Oscillation (ENSO) (e.g.; Fraederich 1994; Trenberth et al. 1998; Cassou and Terray 2001a; Shaman and Tziperman 2005; Toniazzo and Scaife 2006).

The motivation of this work is twofold. Our first goal is to characterize the rotational atmospheric circulation over the NAE sector at upper-levels, which has not yet been documented. Additionally, we seek to associate the dominant patterns of rotational variability to some of the remote sources suggested in the literature, such as the tropical Atlantic or the tropical Pacific (El Niño). Another major objective of this study will be to compare the dynamics involved in the ENSO-NAE teleconnection and the internal variability that produces the North Atlantic Oscillation (NAO).

As we shall see, the dynamical signatures of these phenomena are very different despite some similarity in their surface patterns.

Brönnimann (2007) has recently revisited the relationship between ENSO and the NAE circulation and concluded that the linear response to ENSO in this sector is modest but robust. The canonical signal for El Niño conditions consists of a dipolar surface pressure pattern that resembles the negative NAO phase and is accompanied by low (high) surface temperatures over northern Europe (Mediterranean region), together with above-normal (below-normal) precipitation in central (northwestern) Europe. However, the dynamical mechanism responsible for this teleconnection has been elusive to date. Some model studies have examined the possibility that transient-eddy activity in the North Atlantic basin may generate a NAO-like signal in response to the downstream extension of the ENSO wavetrain propagating across the North Pacific-North America (e.g.; Cassou and Terray 2001a, 2001b; Merkel and Latif 2002; Pohlmann and Latif 2005). However, no clear evidence has been found in observations supporting the association between ENSO and the NAO via that downstream effect (Brönnimann 2007). On the other hand, Toniazzo and Scaife (2006) have suggested the existence a secondary ENSO wavetrain emanating from the tropical Atlantic towards Europe, which could account for some deviations from the El Niño canonical teleconnection. For their part, Ineson and Scaife (2008) have achieved a successful simulation of the dipolar ENSO teleconnection over the NAE sector that relies on a dynamically active stratosphere. The mechanism involves disturbances propagating downward from the middle-upper stratosphere to the lower stratosphere, subsequently reaching the surface during late winter. This teleconnection requires prior upward propagation of ENSO-forced ultra-long planetary waves into the stratosphere (Manzini et al. 2006) and seems to occur during episodes of sudden stratospheric warming (Ineson and Scaife 2008; Cagnazzo and Manzini 2009; Bell et al. 2009). In addition to this stratospheric pathway, a tropospheric pathway could be expected (Alexander et al. 2002; Brönnimann 2007). Our manuscript aims to provide further insight into this issue.

This work is based on a Principal Component analysis (PCA or EOF) of the streamfunction field at 200hPa over the NAE region. Other studies have also chosen to use the streamfunction (rather than geopotential height) as the primary variable for analysis of teleconnections (e.g.; Kang and Lau 1986; Hsu and Lin 1992; Ambrizzi et al. 1995; Trenberth et al. 1998; Kidson 1999; Revell et al. 2001; Ambaum et al. 2001; Kidson et al. 2002; Branstator 2002). Our choice of this variable is motivated not only by the direct association between the rotational circulation and the streamfunction field but also by the fact that geopotential anomalies often fail to reveal the tropical circulation changes that lead to the extratropical wavetrains. Furthermore, given our focus on the linkages between the tropical and midlatitude circulations, the upper tropospheric level of 200hPa has been selected because it relates more directly to vorticity sources in the divergent flow. Thus, our work complements previous studies by DeWeaver and Nigam (2000), Cassou and Terray (2001a, 2001b), Aumbum et al. (2001), Sutton and Hodson (2003), and Thompson et al. (2003), among others.

The datasets and diagnostic tools used are described in the next section. The description of the rotational modes and a discussion of their associated dynamics are presented in section 3.1. Next, the contribution of these modes to the leading regional and hemispheric SLP EOFs is investigated (section 3.2). A discussion of the results follows in section 4, while section 5 summarizes the main conclusions.

2. Data and methodology

In order to characterize the rotational atmospheric circulation over the Euro-Atlantic sector, a principal component analysis (PCA/EOF; von Storch and Zwiers 2001) of the 200hPa anomalous winter streamfunction is performed. The domain used for the PCA is the NAE region (5ºS-5ºN / 90ºW-40ºE). PCA provides a set of spatial patterns (empirical orthogonal functions, EOFs) and associated standardized time series (principal components, PC). The information associated with each PCA mode is completed by the corresponding fraction of explained variance (fvar).

As will be shown, the dominant NAE streamfunction EOF is tightly associated with ENSO. Consistently, the teleconnection between ENSO and the NAE anomalous circulation

represents the main research topic of this paper, together with the comparison with the NAO.

Moron and Gouirand (2003) and Gouirand and Moron (2003) have shown that there is a strong intraseasonal modulation of the ENSO-influence on the NAE wintertime circulation. In addition, Toniazzo and Scaife (2006) and Gouirand et al. (2007) have noted that the ENSO-related circulation is weak over the North Atlantic during early winter and much stronger during mid/late-winter. Finally, a recent paper by Bladé et al. (2008) has shown that even in the North Pacific the "canonical" TNH extratropical response to ENSO is not completely established until January. For all these reasons, we chose to apply PCA to January-February (JF) streamfunction monthly anomalies.

The 200hPa monthly streamfunction field (ψ200) used was obtained from the ECMWF-ERA40 reanalysis (Uppala et al. 2005) with a 2.5ºx2.5º lat-lon spatial resolution and covering the 1957/58-2001/02 period. Data pre-processing includes: i) multiplying the value at each grid-point by the square root of the cosine of latitude, to ensure that equal areas are having the same weight in the covariance matrix (Thompson and Wallace 2000); ii) subtracting the area-average over the NAE domain from each grid-point at each time step, to remove unphysical fluctuations in this quantity.

The PCA results are presented in terms of regression maps, obtained by projecting the anomaly fields onto the PC associated with each mode. Statistical significance is assessed using a two-tailed Student's t-test for correlation at the 98% confidence level. Regressed circulation anomalies have been computed for sea level pressure (SLP) and geopotential height at 1000, 500 and 200 hPa (ERA40). Additionally, daily horizontal wind and air temperature between 1000 and 100 hPa (ERA40) have been used to compute transient eddy forcings. To diagnose the lower tropospheric signals associated with the EOF modes, ERA40 air temperature at 850hPa and University of Delaware precipitation (Legates and Willmott 1990) are also analyzed. The SST data included in the analysis is taken from the NOAA Extended Reconstruction (Smith and Reynolds 2003). All monthly anomalies are calculated by subtracting the monthly climatology.

3. Two rotational dynamics, one surface signature

3.1. PCA results

Figure 1 shows the two leading EOF modes of the wintertime NAE streamfunction at 200hPa (EOF1/PC1, Fig. 1a-b; EOF2/PC2, Fig. 1c-d). These modes account for 24% and 19% of the mid-winter variance, respectively. At the onset, one may have expected the NAO to appear as the leading mode, since that pattern has been widely documented as the dominant mode of North Atlantic atmospheric variability (e.g.; Thompson et al. 2003). However, an NAO-like spatial structure appears here only as the second EOF (EOF2), while the leading mode (EOF1) is associated with ENSO, as discussed in the following subsection.

These two EOFs are robust to changes in the domain definition and do not change when the domain boundaries are varied by 10º in the four cardinal directions (not shown). The North et al. (1982) criterion reveals that these two ψ200 leading patterns represent two well separated modes, as is also the case for the third and fourth EOFs (Fig. 2), which correspond to the East Atlantic pattern (EA; fvar=13%) and the Scandinavian pattern (SCA; fvar=8%).

A remarkable feature of these regional results is that when performing the same analysis using geopotential height at 200hPa (Z200) instead of streamfunction, the same modes appear except for EOF1. The dominant patterns of Z200 variability can be identified as the NAO (29%), the SCA (17%) and the EA (15%). Interestingly, the leading Z200 EOF is temporally correlated with both EOF1 (0.51) and EOF2 (0.74) of the streamfunction field, indicating that this leading height EOF shares common features with both leading streamfunction EOFs.

In order to confirm that that the leading EOF of the streamfunction field is a real mode rather than an artefact of computing the streamfunction over a limited domain, we repeated the analysis by extending the domain to the entire northern hemisphere (5ºS-80ºN/0º-357.5ºE). The leading hemispheric streamfunction mode (not shown) corresponds to the regional one in Fig. 1a: the temporal correlation between their PCs is 0.90; the spatial correlation between regional EOF1 and the regional regression of hemispheric EOF-1 is 0.96; and, conversely, the spatial correlation between hemispheric EOF-1 and the hemispheric

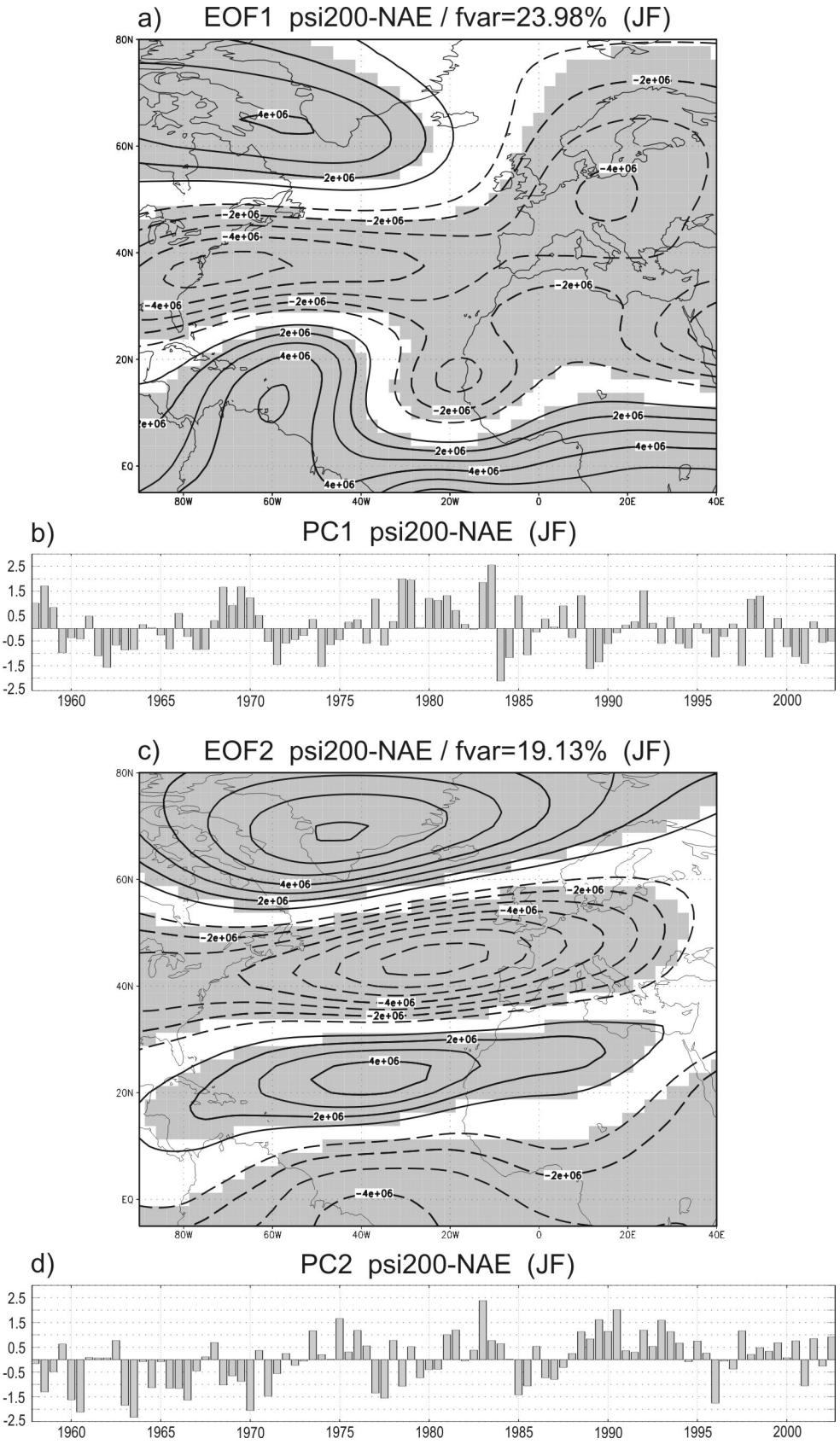
a) EOF1 psi200-NAE / fvar=23.98% (JF)
80N
60N
40N
20N
EQ
80W
60W
40W
20W
0
20E
40E
-2e+06
4e+06
b) PC1 psi200-NAE (JF)
2.5
1.5
0.5
-0.5
-1.5
-2.5
1960
1965
1970
1975
1980
1985
1990
1995
2000
c) EOF2 psi200-NAE / fvar=19.13% (JF)
d) PC2 psi200-NAE (JF)

regression of regional EOF1 is 0.97.

Additionally, our hemispheric streamfunction EOFs compare well to those obtained by DeWeaver and Nigam (2000) using Z200 global anomalies, albeit in a different order. Their global Z200 EOFs successively describe the NAO (here, the third hemispheric ψ200 EOF, 8%), an ENSO-related mode very similar to our leading hemispheric ψ200 EOF (31%), and the Pacific-North America pattern (PNA; here the second hemispheric ψ200 EOF, 11%) (Fig. 2). The different ordering is consistent with the fact that the streamfunction norm emphasizes lower latitudes compared to the geopotential norm.

In the next subsection, the leading rotational mode is examined in more details, while in the following subsection the two leading modes will be compared.

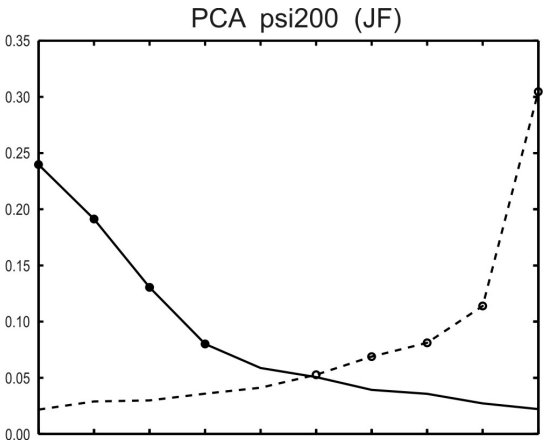

Figure 2. Fraction of the explained variance for each eigenvalue from the PCA applied to JF ψ200 over NAE (solid; left-to-right) and Northern Hemisphere (dashed; right-to-left). Highlighted scores (circles) correspond to rotational modes that are well separated according to the criteria of North et al. (1982).

a. Description of the leading mode

The spatial distribution of the leading regional ψ200 pattern (EOF1; Fig. 1a) is characterized by elongated streamfunction anomalies of one sign extending from eastern North America (35ºN-70ºW) to central Europe (50ºN-15ºE). This structure is accompanied by an anomaly centre of the opposite sign to the north, between Greenland and Canada (65ºN-55º/60ºW). Complementary to this regional pattern, the hemispheric projection of upper level geopotential height onto this mode shows a wavetrain emanating from the tropical Pacific that propagates over the North Pacific-American sector (Fig. 3a). The three centres of action of this wavetrain are organized as in the canonical Tropical-Northern Hemisphere (TNH) pattern (Mo and Livezey 1986; Barnston and Livezey 1987; Livezey and Mo 1987; Trenberth et al. 1998), which is the atmospheric response to ENSO forcing (Robertson and Ghil 1999; Straus and Shukla 2002; DeWeaver and Nigam 2002; Bladé et al. 2008). The corresponding regressions of geopotential height at 500hPa (Z500, Fig. 3b) and at 1000hPa (Z1000, Fig. 3c) reveal that the centres of action of this TNH-like pattern are quasi barotropic with a slight westward tilt, a feature characteristic of stationary Rossby wavetrains (Lau 1979; Hsu and Wallace 1985). In the Atlantic sector, this eastward displacement of the surface signature relative to the upper level signal is very apparent, conferring it a negative NAO-like appearance which is consistent with the "canonical" ENSO signal observed in this sector (Brönnimann 2007).

Associated with this extratropical wavetrain, there are twin upper level anticyclonic anomalies straddling the equator located roughly at 150ºW (Figs. 3a,b), reflecting the tropical Gill-type response to diabatic heating. This thermal forcing can be inferred from the corresponding SST regression (Fig. 4a), which yields a noticeable anomalous warm tongue over the central-eastern Pacific surrounded by cold SST anomalies. All these results lead us to identify EOF1 (Fig. 1a) as the NAE signature of the atmospheric response to El Niño forcing. This relationship is confirmed by the correlation between PC1 and the Niño3.4 index, which is 0.57. Notice also that the SST regression map has no significant signal in the Atlantic basin (except in the Gulf of Mexico/eastern North American coast).

In addition to the two centres of action of EOF1 located over the North Atlantic basin, which, as we have seen, correspond to the tail of the TNH pattern, a third center is present over the European continent (Figs. 1a). This centre of action also has a quasi-barotropic structure (Fig. 3), suggesting that this anomaly might be due to a split of the

Figure 1. (a) Leading and (c) second leading ψ200-JF empirical orthogonal functions (EOF1/EOF2; contours, ci=106 ms-2) over NAE region (5S-80N/90W-40E). (b, d) Associated principal components (PC1/PC2). Statistically significant areas, according to a t-test at the 98% level, are shaded.

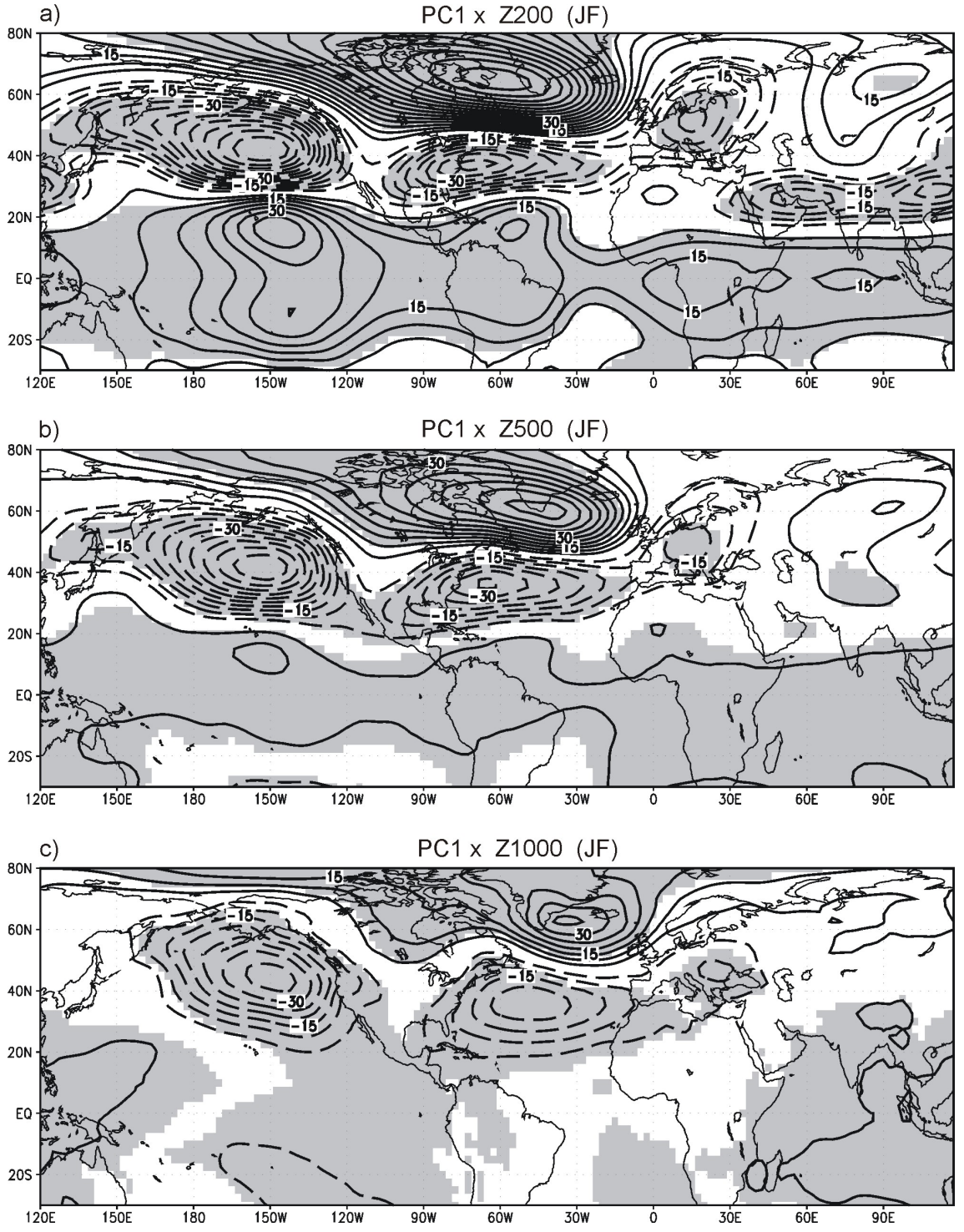

Figure 3. Regression maps of geopotential height at 200hPa (Z200; top), 500hPa (Z500; middle) and 1000hPa (Z1000; bottom) onto PC1. Magnitudes correspond to one std dev of the time series. Statistically significant areas, according to a t-test at the 98% level, are shaded.

ENSO wavetrain originating in the tropical Pacific, with the other branch propagating into the tropical Atlantic.

Both the main wavetrain and the notion of a wavetrain split are in good agreement with the ENSO pattern and wave activity flux shown in Karoly et al. (1989) for midwinter (Jan-Feb; their Fig. 4). In that paper, the authors used a diagnostic derived by Plumb (1985) to investigate the propagation of stationary wave activity associated with ENSO. As in Karoly et al. (1989), we have computed the wave activity flux directly from the zonally asymmetric part of a regression map, specifically from the Z200 regressed anomalies (Fig. 3a). Fig. 5 depicts the result of this calculation using anomalies poleward of 20N to avoid ageostrophic wind effects. Our diagnostic resembles Karoly et al.(1989)'s stationary wave activity plot, exhibiting strong propagation poleward and eastward away from the forcing region, the central tropical Pacific. Interestingly, although some of the wave activity flux turns equatorward around eastern North America, a second branch propagates across the North Atlantic at high latitudes, turning equatorward over eastern Europe. This result supports our hypothesis of

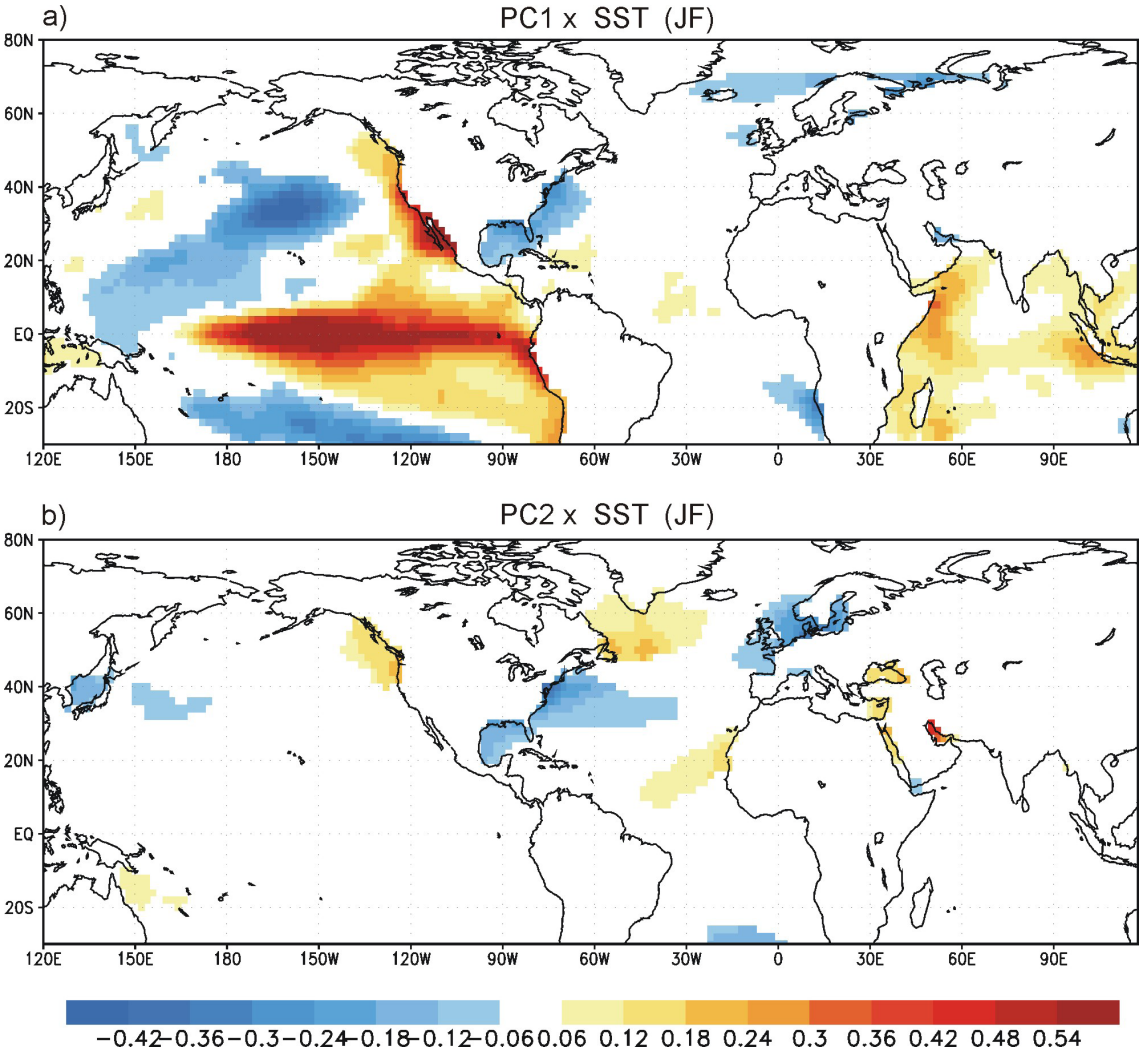

Figure 4. Regression maps of global SST (shaded, ºC) onto PC1 (a) and PC2 (b). Magnitudes correspond to one std dev of the time series. Statistically significant areas, according to a t-test at the 98% level, are gridded for SST.

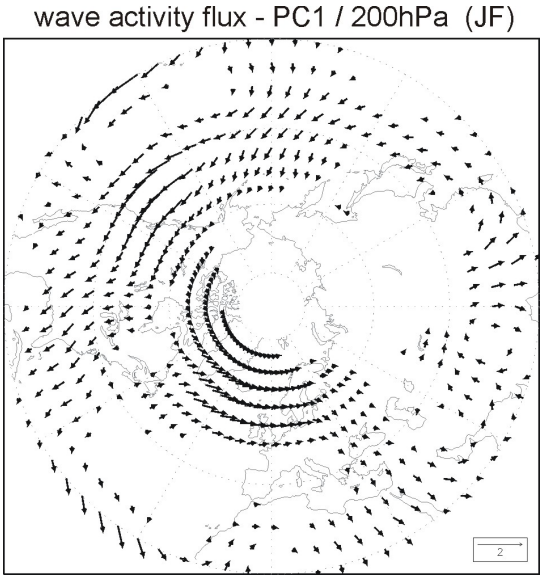

Figure 5. Horizontal wave activity flux associated with the asymmetric part of the regression map of Z200 onto PC1 (Fig. 3a). Shown are anomalies larger than 0.5 m2/s2. This diagnostic has been computed according to Karoly et al. (1989).

a split in the midwinter ENSO wavetrain upon reaching the NAE sector.

Given this scenario, we argue that the leading streamfunction mode is related to forced tropical Pacific variability and ENSO. In the next subsection we compare the eddy-mean flow interaction for this mode (EOF1) and for the second mode (EOF2), with the aim of distinguishing the internal and forced components of the rotational circulation.

b. The nature of the leading mode vs the second mode

We now focus on EOF2 (Fig. 1c), which is characterized by a zonally symmetric structure with three centers of action located over the tropical Atlantic, the midlatitudes (about 45ºN) and the polar region. The global Z200 regression onto this EOF exhibits the same centers of action in the North Atlantic, as well as negative anomalies in the North Pacific (Fig. 6a). As we descend towards the surface (Z500, Z1000) the Pacific and the tropical centers weaken noticeably and the circulation, now confined to the Atlantic sector, displays a meridional seesaw between middle and polar latitudes reminiscent of the NAO (Figs. 6b-c). We will discuss in section 4 why EOF2 is more hemispheric at upper levels despite the regional character of its low level circulation.

The SST pattern obtained by regressing the global SST onto PC2 (Fig. 4b) adds very relevant information. This oceanic pattern is confined to the Atlantic sector and resembles the North Atlantic Tripole pattern, which is known to be the oceanic signature of the NAO (e.g.; Visbeck et al. 2003). Consistently, the corresponding SST regression for negative lags shows a much weaker and non significant signal (not shown). These results suggest that EOF2 arises from internal atmospheric dynamics.

It is noteworthy that the SST regression maps for the two leading NAE streamfunction modes separate the oceanic imprint of the rotational circulation so cleanly, confining one to the Pacific (Fig. 4a) and the other to the Atlantic (Fig. 4b): EOF1 is associated with El Niño, while EOF2 is tied to the North Atlantic Tripole. As far as we are aware, this is the first study in which the decomposition of the atmospheric circulation variability into orthogonal modes accomplishes a separation of the associated oceanic anomalies in the Pacific and Atlantic basins, as identified in previous studies (e.g.; Watanabe and Kimoto 1999; Cassou and Terray 2001a, 2001b; Sutton and Hodson 2003). This result is particularly interesting given that the surface atmospheric signature of the two modes in the Atlantic sector is very similar (Figs. 3c and 6c).

In order to assess the role of internal dynamics and eddy-mean flow interaction for these two rotational modes and to further explore the extent to which EOF1 and EOF2 involve different dynamics over the NAE region, Fig. 7 shows the perturbation kinetic energy (PKE) and the horizontal components of the Eliassen-Palm vector (E-vector). The former is a measure of wave activity, while the latter encapsulates the interaction between transient eddies and mean flow through barotropic processes (Hoskins et al. 1983; Trenberth 1986):

$$PKE = \frac{1}{2}\left(\overline{u'u'} + \overline{v'v'}\right); \qquad E = \left(\frac{1}{2}\overline{v'v'} - \overline{u'u'}, -\overline{u'v'}\right)$$

The zonal component of the E-vector provides information about the shape and propagation characteristics of eddies; the meridional one describes the feedback on the mean flow. The convergence (divergence) of the E-vector is associated with the eddy-induced acceleration (deceleration) of the mean zonal wind. Here, the time-mean covariances have been computed by

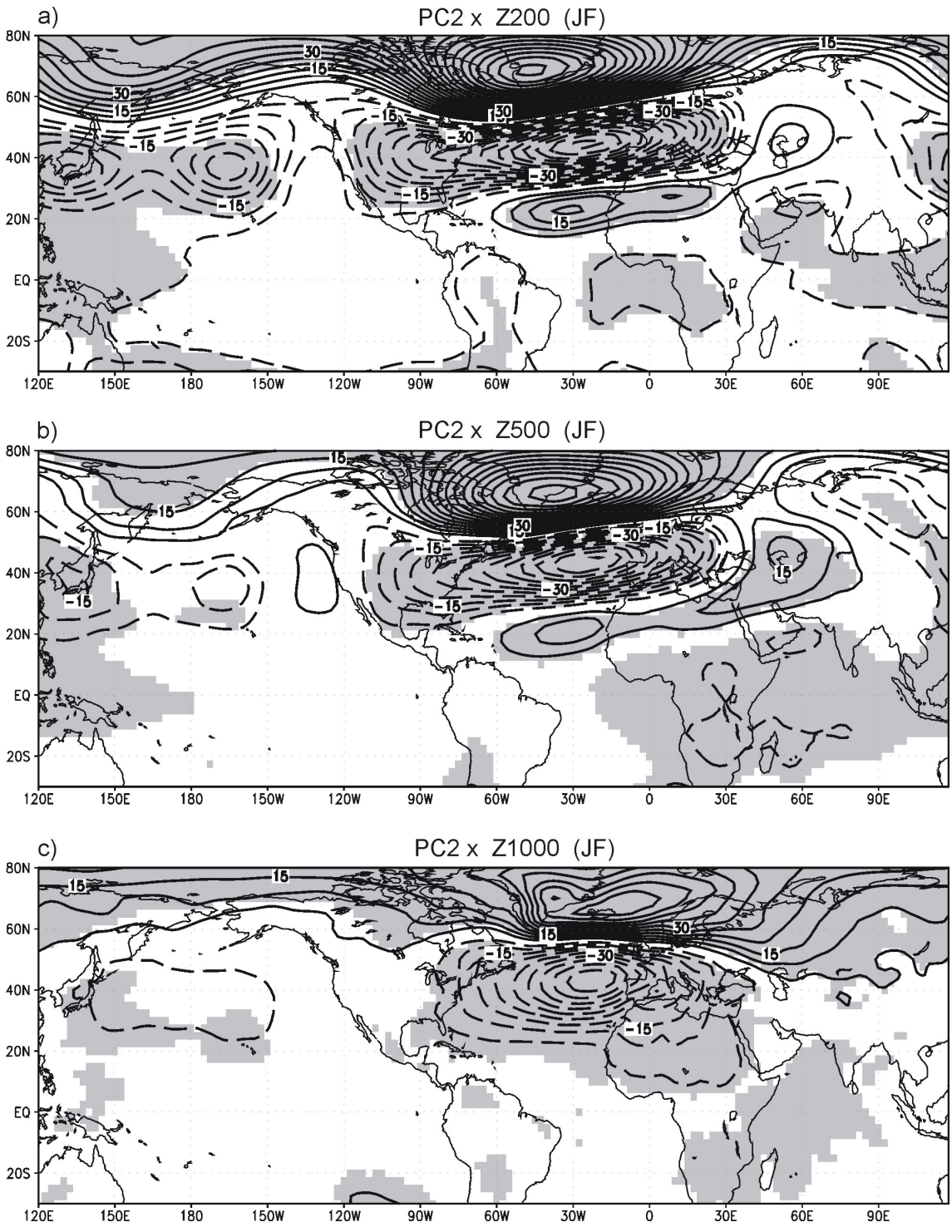

Figure 6. Same as Fig. 3 but using PC2.

filtering daily horizontal wind at 200hPa using the 24h-difference filter (Wallace et al. 1988; Chang and Fu 2002) and computing monthly averages. The regressions maps were obtained by subtracting the monthly climatologies and projecting the resulting anomalies onto PC1 (Fig. 7a) and PC2 (Fig. 7b). Regressed U200 anomalies (contours) are also represented in Fig. 7.

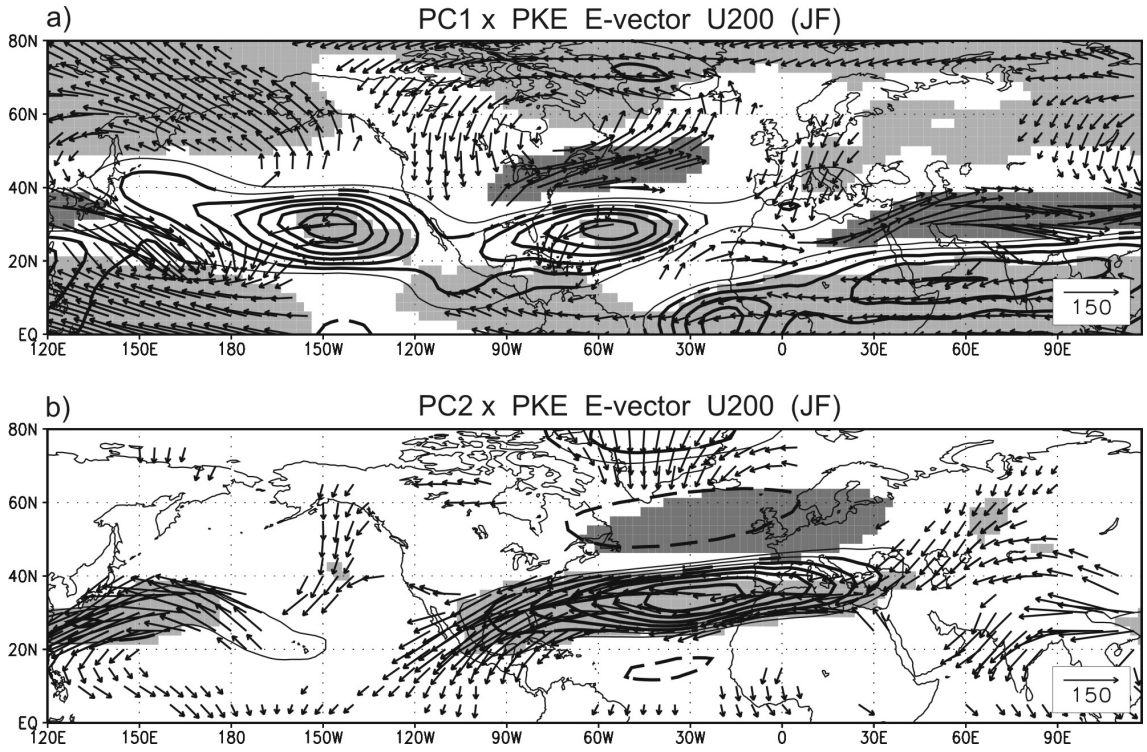

Figure 7. Regression maps of perturbation kinetic energy (PKE; shading; only plotted the sign, dark/light representing negative/positive), horizontal component of the Eliassen-Palm flux (E-vector; arrows; m2/s2) and zonal wind at 200hPa (U200; contours; ci=1m/s) onto PC1 (a) and PC2 (b). Magnitudes correspond to one std dev of the time series. Statistically significant areas, according to a t-test at the 98% level, are gridded for PKE and E-vector and bolded for U200.

In the North Atlantic basin, the E-vector associated with EOF1 (Fig. 7a) displays a weak meridional divergence around the Florida Gulf coast (at 30ºN). This is accompanied by an anomalous PKE dipole on either side of the divergence axis and implies both a southward displacement of the subtropical jet and a reinforcement of the mean westerly flow. However, the U200 anomaly in the western subtropical Atlantic exhibits a more prominent acceleration than might be expected based on the anomalous transient flux alone; moreover, this acceleration is apparent along the entire subtropical Pacific. Given De Weaver and Nigam (2000)'s finding that the response of the global circulation to ENSO is dominated by the zonal-mean intensification of the subtropical jets, we conclude that the EOF1-related U200 anomalies in the NAE region (Fig. 7a) reflect a zonal wind acceleration on the global scale (Figs. 3). For this mode then, changes in the eddies may reinforce and help maintain the upper tropospheric zonal wind anomalies but do not seem to be the main driving force.

In contrast, the eddy momentum transport for EOF2 (Fig. 7b) clearly tends to decelerate the westerly mean flow in the exit region of the North Atlantic jet. This is indicated by the presence of anomalous E-vector convergence over the northeastern Atlantic and a strong dipolar PKE anomaly overlaying the U200 anomalies in the NAE sector. These anomalies reflect a southward shift of the North Atlantic jet and associated stormtracks and suggest a link between the EOF2-based NAO pattern (Figs. 1c, 6) and high-frequency eddies, as represented by the synoptic storm track (Rogers 1990, 1997; Hoskins and Valdes 1990).

In order to complete the picture of the differing roles of eddy activity for the two rotational modes, we analyze the changes in the meridional heat flux by transient eddies ($\overline{v'T'}$) in the North Atlantic basin associated with EOF1 (Fig. 8a) and EOF2 (Fig. 8b). The eddy heat flux is proportional to the vertical component of the Eliassen-Palm flux (e.g.; Andrews et al. 1987) and therefore indicative of vertical wave propagation. Additionally, the heat flux at low levels is associated with a divergence of the Eliassen-Palm flux, hence with wave activity

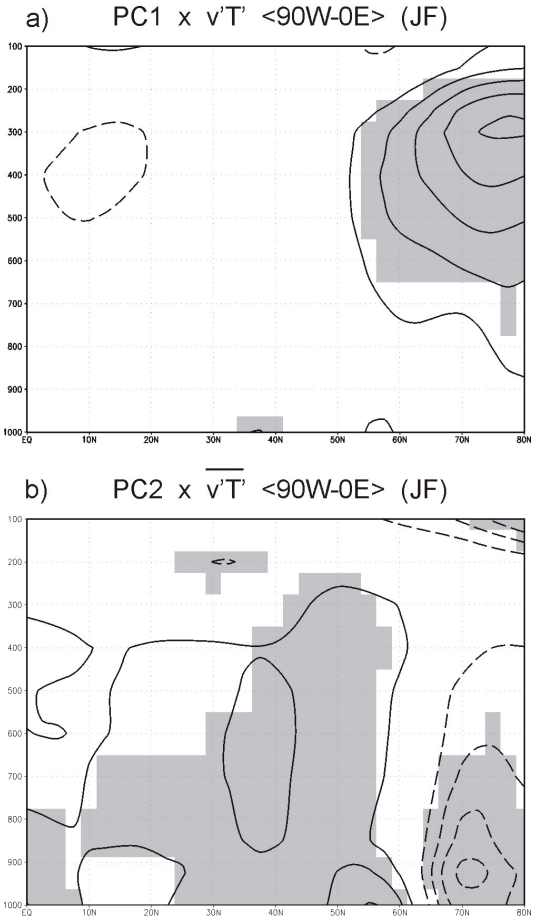

Figure 8. Regression maps of transient heat flux (Km/s) onto PC1 (a) and PC2 (b). Magnitudes correspond to one std dev of the time series. Statistically significant areas, according to a t-test at the 98% level, are gridded for contours.

generation via baroclinic processes (Wallace et al. 1988).

As expected, EOF2 shows decreased generation of baroclinic activity at high latitudes, compensated by enhanced generation between 45ºN-60ºN (Fig. 8b). This dipole-like anomaly implies that the North Atlantic stormtrack is weakened and shifted to the south, as expected during the negative phase of the NAO (e.g.; Hurrell 1995), here represented by EOF2 (Fig. 6c, 7b). In contrast, EOF1 is only associated with positive anomalies at upper-levels and over polar latitudes (Fig. 8a). This suggests that the EOF1-based ENSO signal has little impact on cyclogenesis over the North Atlantic. Instead, the anomalous positive transient heat flux at upper levels is indicative of enhanced upward propagation of waves into the stratosphere, presumably resulting from the changes in the background flow seen in Fig. 7b.

All these results lead us to conclude that the regional rotational atmospheric variability over the NAE is mainly explained by two independent structures at upper-levels, one associated with the response to ENSO and the other with internal variability over the North Atlantic. These two modes of variability project onto a similar dipolar surface structure (Figs. 3c and 6c), implying that the same surface signature may be produced by two different dynamics.

We next discuss the impacts of these two rotational modes onto the NAE sector. Figure 9 shows the regression maps of anomalous precipitation (top) and air temperature at 850hPa (T850; bottom) onto the PC1 and PC2 time series. As expected from the resemblance between their surface geopotential signatures (Figs. 3c, 6c), both EOFs are characterized by a pair of anomalous T850 dipolar anomalies on either side of the North Atlantic basin (Figs. 9c-d). EOF1 produces strong positive (negative) T850 anomalies along the northern (southern) east coast of North America, associated with the equatorward branch of the TNH wavetrain, while weaker negative anomalies appear over the Norwegian and Baltic seas in conjunction with the eastward branch of this wavetrain (Fig. 9c). A weak secondary wavetrain forced by ENSO but originating in the tropical Atlantic (Toniazzo and Scaife 2006) could be responsible for the subtropical warming over Africa (Figs. 1a, 3a,b). All these features are in close agreement with the expected ENSO influence on low level air temperature in the NAE sector, as described in the introduction.

Despite the overall similarity between Figs. 9c and 9d, the regression onto EOF2 more closely resembles the North Atlantic quadrupolar air temperature anomaly associated with a negative NAO phase (Fig. 9d; van Loon and Rogers 1978; Hurrell 1995; Hurrell and van Loon 1997), reflecting the impact of cold continental (warm maritime) air advection over a broad area of northern Europe and North America (Greenland-northeastern Canada and North Africa-Mediterranean Sea). Still, except from a slight difference in phase and a stronger intensity, the T850 pattern for this mode is qualitatively similar to that for EOF1, consistent with the similarity in the surface circulation patterns.

In contrast, the precipitation fields associated with both forms of rotational variability exhibit more discrepancies. During its positive phase,

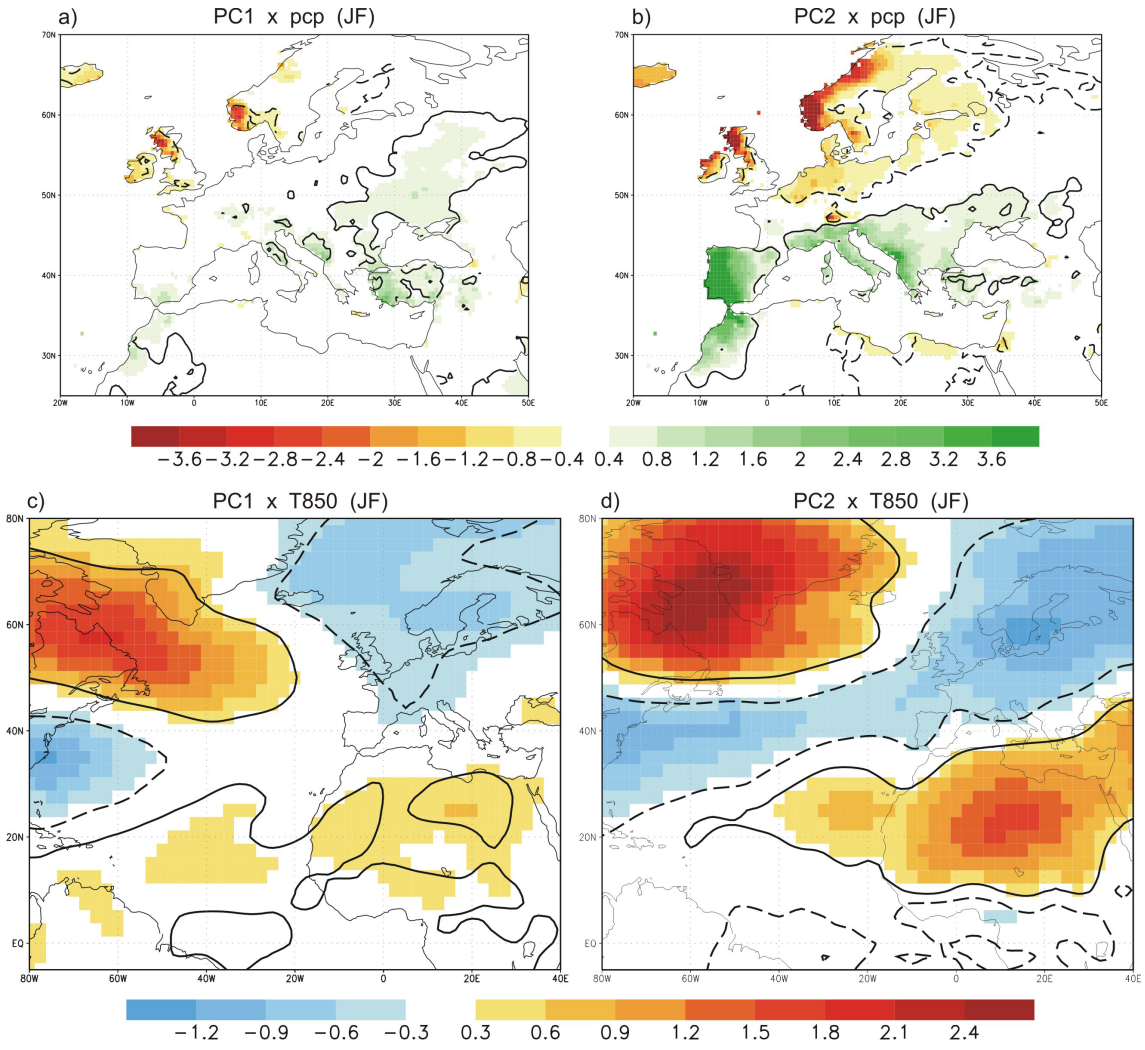

Figure 9. Regression maps of precipitation (pcp; top, cm/month) and air temperature at 850hPa (T850; bottom, ºC) onto PC1 (left) and PC2 (right). Magnitudes correspond to one std dev of the time series. Statistically significant areas, according to a t-test at the 98% level, are contoured.

EOF1 produces weak negative rainfall anomalies over northwestern Europe and positive ones in the northern flank of the eastern Mediterranean and central-eastern Europe (Fig. 9a). The former seems to be associated with advection of cold and dry polar air through the northernmost node, while the latter could be explained in terms of the quasi-barotropic cyclonic circulation over the continent (Figs. 1a, 3). As for the NAO-like mode, EOF2 produces an anomalous dipolar rainfall distribution over Europe (Fig. 9b), associated with the meridional shift of the synoptic stormtrack in the North Atlantic basin (Fig. 7b, 8b), consistent with the results of Hurrell (1995) and Hurrell and van Loon (1997). Although the precipitation patterns share some common features, the magnitude of the anomalies is much larger for the NAO mode than for the ENSO mode, despite the similarity of their surface circulations. This is consistent with the notion that the precipitation anomalies for EOF2 arise from changes in the stormtracks, rather than from changes in the mean circulation. As noted above (Fig. 7), the strengthening of the subtropical jet is associated with a stormtrack shift only in the case of EOF2 and not for EOF1.

3.2. Modeling the surface signature

As discussed in the previous section, there is a high degree of similarity in the Z1000 regressions of EOF1 and EOF2 over the North Atlantic (Figs. 3c, 6c), in spite of the dynamical differences between the anomalous rotational circulations

described by these EOFs. The resemblance is confirmed by the 0.78 correlation coefficient between both Z1000 regression maps in the NAE-domain. A close inspection, however, reveals differences in the location of the midlatitude centers of action, as these are centered west/east of 30ºW and south/north of 40ºN for the PC1/PC2 regressions. These offsets can also be seen at upper levels (Figs. 1a, 3, 7a/Figs. 1c, 6, 7b) and explain the phase differences in the air temperature and precipitation patterns (Fig. 9).

The differences between the Z1000 regressions in the North Pacific basin are more remarkable. EOF2 is associated with a very weak negative anomaly over the central/western North Pacific (Fig. 6c), supporting the conclusion of Deser (2000) and Ambaum et al. (2001) that the NAO is not correlated with Pacific variability. In contrast, EOF1 shows an anomalous deepening of the Aleutian low (Fig. 3c) so that in some ways this pattern is reminiscent of the Artic Oscillation or Northern Annular mode (AO/NAM). This characteristic of the surface signature of EOF1 leads us to wonder whether this mode may explain some aspects of the AO/NAM paradigm (Thompson and Wallace 1998, 2000; Wallace 2000).

To investigate this issue we will now try to reconstruct the time series of the dominant regional (NAO) and hemispheric (NAM) surface variability modes using PC1 and PC2, aiming to quantify the contribution of our rotational patterns to the NAO and the NAM modes. Following Wallace and Thompson (2002) and earlier works, we compute the leading EOFs of monthly JF SLP for both the Euro-Atlantic sector (EOF_NAE) and for the entire Northern Hemisphere (EOF_GLOB), which correspond to the so-called 'NAO' (Fig. 10a) and 'NAM' (Fig. 10b), respectively. These two regional and hemispheric modes explain 42% and 23% of their respective variance. As a first step, we linearly fit the corresponding time series (PC_NAE and PC_GLOB) to PC2 using least squares linear regression methodology (REGs) and regress the reconstructed series onto the hemispheric SLP field (Figs. 10c,d). Next, we improve the fit by adding PC1 as a new independent variable in the least squares regression model (multiple-linear regression, REGm) and obtain another pair of reconstructed time series and associated hemispheric SLP projections (Figs. 10g,h). The differences between the original leading SLP EOFS (EOF_NAE and EOF_GLOB) and the reconstructed patterns obtained with our fits are also shown (Figs. 10e,f; and 10i,,j respectively).

The regional EOF_NAE of SLP is very well captured by EOF2 (cf. Figs. 10a and 10c) and the explained variance reaches 67% (in terms of the square correlation coefficient of the linear fit); even so, Fig. 10e suggests that more contributions must be taken into account to recover the entire NAE dipolar variability. On the other hand, the linear reconstruction of EOF_GLOB (Fig. 10d) using only PC2 does not capture the Aleutian centre of action of this mode, a result that seems to indicate that the annular mode (Fig. 10b) cannot be dynamically understood in the same way as the regional NAO oscillation. Indeed, the fitting using only PC2 explains less than half of the total variance in this case (46%). Hence, the latitudinal shifts in the Atlantic eddy-driven jet that characterize EOF2 do not appear to be connected to variability of the Aleutian low (Fig. 10f). Interestingly, the difference pattern shown in Fig. 10f strongly resembles the EOF1 signature in the Z1000 field (Fig. 3c), although the amplitude of the anomalies is not comparable. This resemblance supports our hypothesis that the ENSO-related EOF1 is a key ingredient of the AO/NAM paradigm.

Noticeable features emerge when introducing PC1 in the regression. For EOF_NAE, a weak strengthening, together with a slight westward expansion, is apparent in the centers of action of the Azores-Iceland seesaw (Fig. 10g). Although adding the ENSO-related mode (EOF1) barely alters the regressed structure in the Euro-Atlantic sector, it does introduce large changes in the North Pacific basin. SLP anomalies in the North Pacific now appear that are correlated (anticorrelated) with North Atlantic middle (subpolar) latitudes (Fig. 10g). For EOF_GLOB, the inclusion of PC1 clearly improves the deficient representation of the Aleutian centre using simple regression (Fig. 10h). The increase in explained variance upon including PC1 is larger for the global than for the regional reconstruction (29% against 14%). This result stresses the contribution of the ENSO signal to the NAM. Indeed, the lack of structure in the difference map between EOF_GLOB and the global reconstruction (Fig. 10j) suggests that the ENSO wavetrain crossing the North Pacific-American sector is part of the NAM. Although Wallace and Thompson (2002) ruled out any contribution to the NAM from the PNA

a) EOF_NAE SLP (fvar=42%)

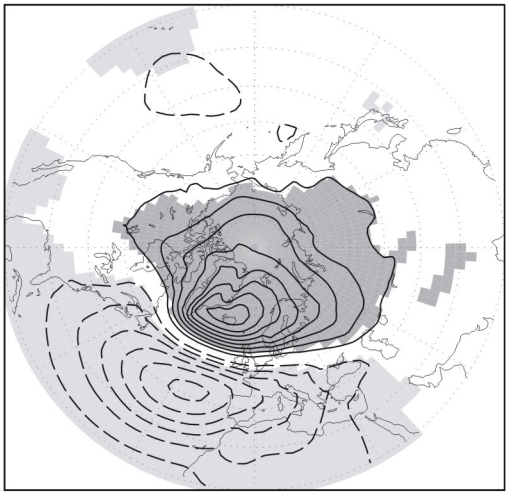

b) EOF_GLOB SLP (fvar=23%)

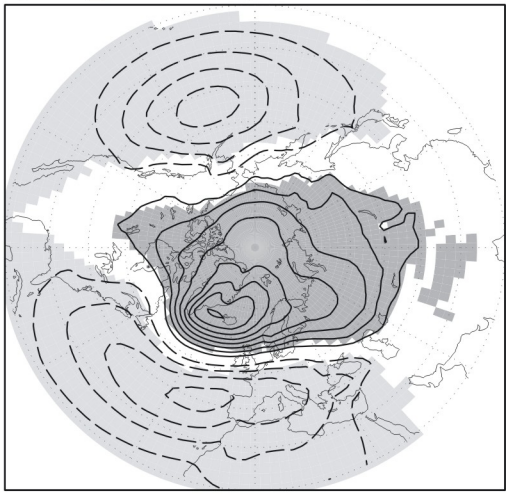

c) REGs_NAE = 0.82*PC2

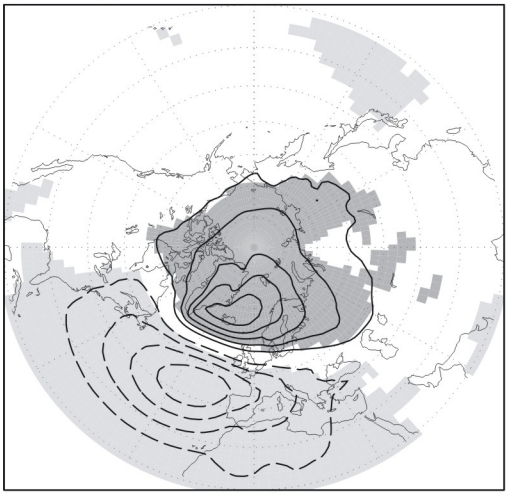

d) REGs_GLOB = 0.68*PC2

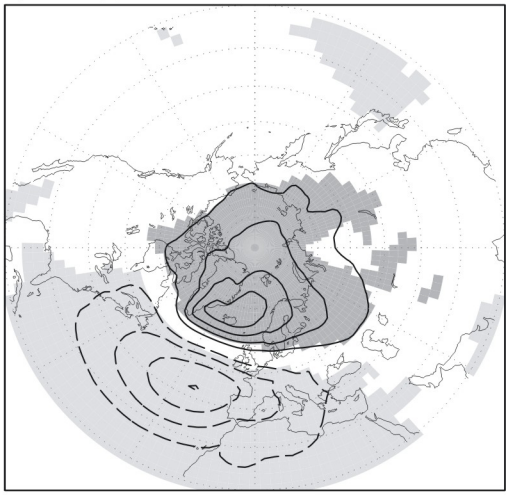

e) diff EOF_NAE - REGs_NAE

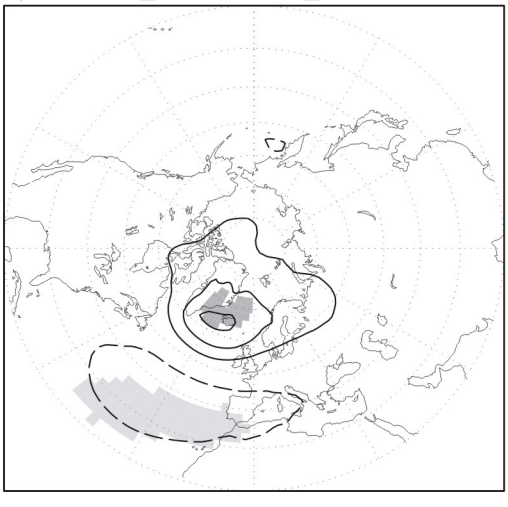

f) diff EOF_GLOB - REGs_GLOB

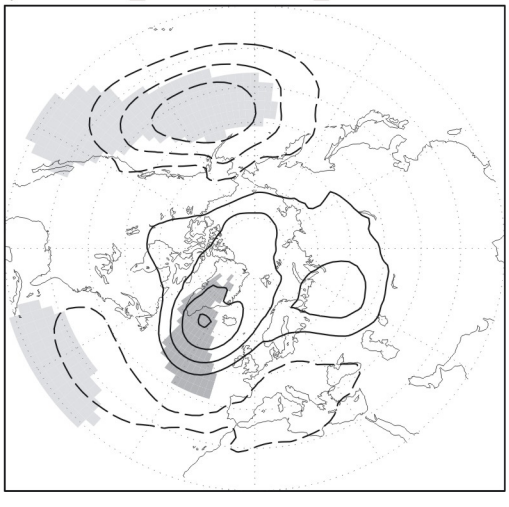

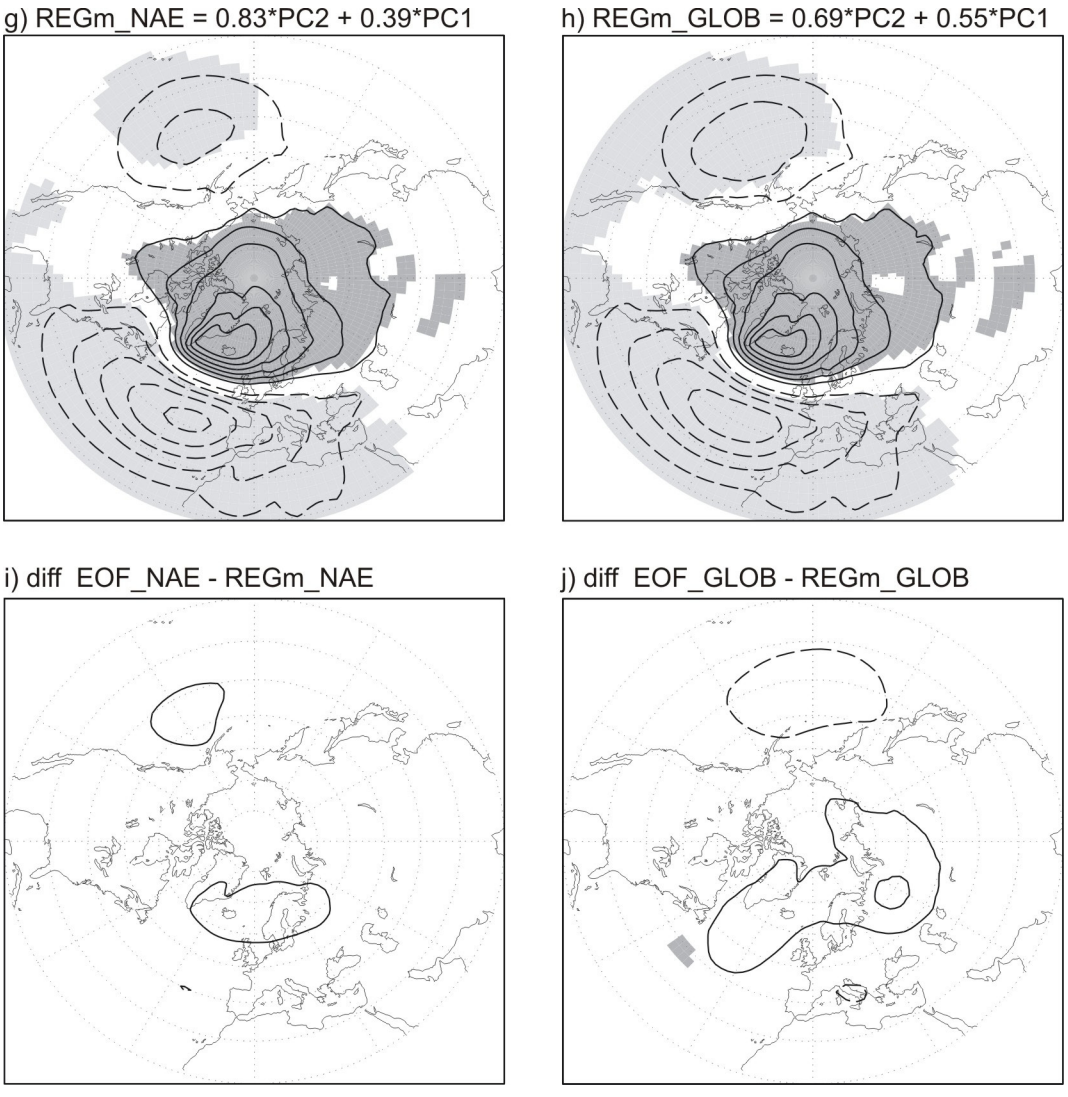

Figure 10, Cont. g) Reconstruction of a) with PC2 and PC1 by applying multiple least squares linear regression (REGm). h) Same as g) but applied to b). i) and j) Difference between a) and g), and b) and h) respectively.

mode, known to be primarily driven by internal atmospheric variability (e.g., Straus and Shukla 2002), this work presents another possible candidate: the El Niño-forced TNH wavetrain. This conclusion would go along with works that have suggested an impact of ENSO on the annular mode (Quadrelli and Wallace 2002).

Figure 10. a) Leading EOF of the JF SLP anomalies in the North Atlantic-European sector (20-70N / 90W-40E; fvar=43%). b) Leading EOF of the JF SLP anomalies in the Northern Hemisphere (20-70N; fvar=23%). c) Reconstruction of a) with PC2 by applying simple least squares linear regression (REGs). d) Same as c) but applied to b). e) and f) Difference between a) and c), and b) and d) respectively.

4. Discussion

In light of the evidences presented in Section 3.1, we argue that the two leading EOFs of NAE streamfunction represent two well differentiated teleconnection dynamics. The first mode, associated with ENSO, displays variability of global scale: SST-forced tropical disturbances trigger a Rossby wavetrain that crosses the North Pacific/North America region and reaches the North Atlantic. This wavetrain then apparently splits into two branches, one directed towards the tropical Atlantic that impacts the subtropical Atlantic jet and another one that yields a quasi-barotropic anomalous circulation over Europe.

The second EOF, associated with the NAO, arises from intrinsic Atlantic storm track variability: midlatitude dynamics control the meridional structure of the eddy-driven jet variability and induce latitudinal shifts in synoptic activity.

This interpretation disagrees with a number of previous works, particularly with those arguing that the Euro-Atlantic winter atmospheric response to ENSO is linked to the NAO through changes in the North Atlantic westerly flow and/or synoptic activity (Cassou and Terray 2001a, 2001b; Merkel and Latif 2002; Moron and Gouirand 2003; Gouirand and Moron 2003; Pohlmann and Latif 2005). Our results instead support other studies suggesting that the ENSO-NAE teleconnection is not related to NAO and that they constitute two separate patterns (van Oldenborgh et al. 2000; DeWeaver and Nigam 2000; Rodwell and Folland 2002; Wang 2002; DeWeaver and Nigam 2002).

One of the main conclusions of this work is that the ENSO signal on NAE winter climate should not be interpreted in terms of the NAO even though its surface signature may be reminiscent of the NAO pattern (cf. Figs. 3c and 6c). The evidence presented here suggests that the dynamics involved in the generation of the ENSO signal in the NAE are very different from the dynamics that characterize the NAO. Thus we feel that a more proper description for this ENSO signal would be a dipole-like response in the North Atlantic rather than an NAO-like response. Nevertheless, in as much as this dipole does resemble the NAO, our results are consistent with previous works subjectively describing the ENSO impact on the Euro-Atlantic sector in terms of a NAO-like signal. Indeed, Figure 3c shows that EOF1 is very similar to the 'canonical' winter signal over the NAE associated with ENSO, as reviewed in Brönnimann (2007). Moreover, our interpretation that this surface dipole-like pattern is simply the downstream propagation of the quasi-barotropic TNH pattern could explain the observed (Moron and Gouirand 2003; Brönnimann 2007) and simulated (Gouirand et al. 2007) intraseasonal modulation of the ENSO impact on the Euro-Atlantic circulation between early and late winter, since this TNH wavetrain is not established until midwinter (Bladé et al. 2008).

The additional analyses presented in Section 3.2 could be relevant for the AO/NAM paradigm. Our results indicate that the surface signature of EOF2 (rotational-NAO) strongly projects onto the "classical" (or total) NAO, traditionally defined as the leading regional SLP mode (cf. Figs. 6c and 10a). Transient eddy diagnostics indicate that this regional oscillation (Azores-Iceland seesaw) is basically driven by local eddies (Figs. 7b, 8b), consistent with previous works (e.g.; Thompson et al. 2003; Vallis and Gerber 2008; Gerber and Vallis 2009). In such scenario, no global longitudinal coherence is expected (Figs. 10c,d). However, with a global forcing such as the TNH wavetrain, more hemispheric (or annular, in appearance) signature could be generated (Figs. 10f,g,h). Additionally, we have shown that the mid-winter total NAO (i.e., the surface dipolar pattern) has a significant contribution from forced variability associated with ENSO (14%). In our view, this results from the fact that, at the surface, the tail of the TNH pattern projects onto the centers of action of the NAO. These "forced" (EOF1-related) and "internal" (EOF2-related) contributions add up to explain 83% of the leading mode of NAE SLP variability.

Our results also show that the AO/NAM signal, understood as the leading hemispheric SLP mode (Fig. 10b), has an important contribution from ENSO (EOF1) that accounts for 29% of its variance. These results indicate that the AO/NAM cannot be regarded as a hemispheric extension of the regional NAO oscillation but has a different origin. Thus, this conclusion goes along with Deser (2000) and Itoh (2002) who concluded that the midlatitudes centres of action of the AO/NAM over North Pacific and North Atlantic are not physically related. Thus, we suggest that the annular appearance of this AO/NAM mode results from the linear superposition of distinct variability patterns (including the NAO) dynamically unrelated to each other. This result is in agreement with DeWeaver and Nigam (2000), who found that zonal mean zonal flow dipolar variability is not related to ENSO, and with Aumbaum et al. (2001), who suggested that the independent variations of the zonal winds in the North Pacific and North Atlantic basins is responsible for the apparent AO/NAM mode. Our analysis shows that ENSO-related EOF1 and NAO-related EOF2 explain 76% of the AO/NAM variance, in a multiple regression sense. Other predictors still need to be taken into account in order to recover the full annular variability, and stratospheric effects could have a role (e.g.; Thompson et al. 2002, 2003).

Our claim that NAO-like EOF2 reflects regional

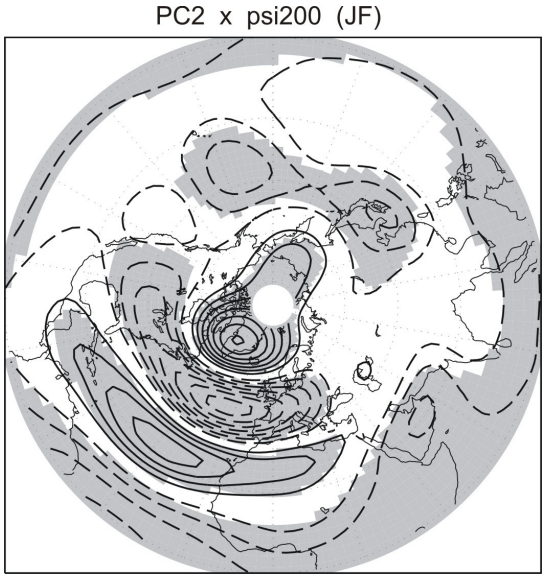

Figure 11. Regression map of the global streamfunction at 200hPa onto PC2 (ci=1x106 m2/s). Magnitudes correspond to one std dev of the time series. Statistically significant areas, according to a t-test at the 98% level, are shaded.

internal variability is supported by the local confinement of the pattern to the North Atlantic basin at lower levels (Fig. 6c). In contrast, the variability associated with this mode has a distinct global signature at upper levels (Fig. 6a). This is consistent with the findings of Branstator (2002) of a global hemispheric NAO signature at upper levels different from the AO/NAM pattern. To make this point, we show in Fig. 11 the regression of the global streamfunction field onto PC2. The resulting pattern compares well with the wavenumber 5 circumglobal pattern found by Branstator (2002). This wave-guided (i.e., non-annular) teleconnection displays centers of action over the eastern North Atlantic, the Arabian Peninsula, the Japanese Islands, the central North Pacific, and North America. Note that the two centers of action in the North Pacific basin are evident throughout the depth of the mid-upper troposphere (Fig. 6). The east-west orientation in the anomalous horizontal component of the Eliassen-Palm flux (Fig. 7b) indicates zonally elongated perturbations along the entire subtropical belt and suggests a tendency for the response to eddy forcing in the Atlantic basin to be guided along the shifted North Atlantic and North African/Asian subtropical jets. This hypothesized mechanism for exciting the recurrent circumglobal pattern, however, requires further investigation.

5. Conclusions

In this paper we have analyzed upper level NAE streamfunction aiming to describe the rotational variability, which could have a remotely forced component. Although upper level streamfunction has been studied many times, an examination of the regional rotational circulation has not been attempted before, as far as we are aware. There are reasons for that as the streamfunction field represents the solution of an elliptic problem (e.g.; Sardeshmukh and Hoskins 1987) and thus is unavoidably influenced by remote influences outside the domain of study. Care was taken to eliminate these influences in our analysis by subtracting the domain average of the streamfunction from each grid-point at all time steps. Moreover, to the extent that the extratropical wind is nearly geostrophic, remote influences should be small because of the local geostrophic closure relating streamfunction and geopotential height. The main difference between these two variables then is the presence of the Coriolis parameter in the definition of geostrophic streamfunction, which implies that the streamfunction norm will tend to emphasize lower latitude variability compared to the geopotential norm. This is helpful for detecting variability forced from the tropics such as that associated with ENSO and indeed application of this norm has allowed us to produce some novel results, summarized below.

- The leading rotational mode of upper level streamfunction in mid-winter in the NAE sector describes the remote ENSO influence (EOF1; fvar=24%). This is in contrast with most previous regional studies based on geopotential height or SLP, in which the NAO tends to be more ubiquitous, but is consistent with the results obtained using streamfunction and a global domain. Indeed, our leading regional (NAE) EOF may be regarded as the local component of the leading hemispheric mode. The pattern corresponds to the tail of the TNH wavetrain emanating from the tropical Pacific and produces a surface dipolar structure in the North Atlantic that is reminiscent of the NAO. We argue, however, that this response should not be described as a NAO-like pattern, because of the different underlying dynamics.

- The second streamfunction mode (EOF2; fvar=19%) has a more regional structure at lower levels, where it displays the classical Azores-Iceland seesaw, which leads us to identify this

mode with a purely rotational NAO. Analysis of the dynamics of this mode suggests an important role for internal variability, through the meridional shift of the stormtracks and eddy-driven jet. It is interesting that the regression of EOF1 and EOF2 onto sea surface temperature separates the signals in the Pacific and Atlantic oceans very cleanly. The Pacific SST signal supports the association of EOF1 with ENSO, while the Atlantic signal (related to EOF2) resembles the well-known North Atlantic Tripole. Note that although EOF2 explains less variance than EOF1 (when using the streamfunction norm), it has a stronger impact on European climate, especially in the precipitation field. We attribute this to the fact that EOF2 variability is associated with a shift in the stormtracks whereas EOF1 is not.

- Additional analyses concerning the surface signatures of EOF1 (ENSO-forced variability) and EOF2 (NAO-related variability) have shown that the latter accounts for most of the variability of the leading regional EOF of SLP, whereas both patterns contribute to the leading hemispheric pattern, the so-called AO/NAM mode. The small but significant contribution of EOF1 to the regional SLP mode is interpreted as due to the fact that the tail of the TNH wavetrain projects onto the centers of action of this leading surface pattern (NAO). The fact that both EOF1 and EOF2 contribute to the AO/NAM pattern indicates that this hemispheric SLP pattern may be a combination of different regional (NAO) and large scale (ENSO) phenomena. Finally we have shown that, despite its regional character at lower levels, EOF2 has a hemispheric structure at upper levels, reminiscent of the global circumglobal pattern discussed by Branstator (2002).

Acknowledgments.

We are grateful to Dr Adam Scaife (Met Office-Hadley Centre, UK), Dr Tercio Ambrizzi (Universidade de Sao Paulo, Brazil) and Dr David Karoly (University of Melbourne, Australia) for useful discussions, and to Dr Paul Berrisford (University of Reading, UK) for kindly providing the ERA40 datasets. We also thank two anonymous reviewers for their invaluable help in the first version of this paper. This research was supported by the national CGL2005-06600-C03-02 and CGL2006-04471 projects of the Spanish Ministry of Education and Science. PZG is supported by the Ramón y Cajal program and AdlC is supported by a FPI-UCM grant.

References

Alexander M A, Bladé I, Newman M, Lanzante J R, Lau N-C, Scott J D (2002) The atmospheric bridge: the influence of ENSO teleconnections on air-sea interaction over the global oceans. J Clim 15:2205-2231.

Ambaum M H P, Hoskins B J, Stephenson D B (2001) Arctic Oscillation or North Atlantic Oscillation? J Clim 14:3495-3507.

Ambrizzi T, Hoskins B J, Hsu H-H (1995) Rossby wave propagation and teleconnection patterns in the austral winter. J Atmos Sci 52:3661-3672.

Andrews D G, Holton J R, Leovy C B (1987) Middle atmospheric dynamics. Academic Press, London.

Barnston A G, Livezey R E (1987) Classification, seasonality and persistence of low-frequency atmospheric circulation patterns. Mon Wea Rev 115:1083-1126.

Bell C J, Gray L J, Charlton-Perez A J, Joshi M M, Scaife A A (2009) Stratospheric communication of El Niño teleconnections to European winter. J Clim 22:4083-4096.

Bladé I, Newman M, Alexander M A, Scott J D (2008) The late fall extratropical response to ENSO: sensitivity to coupling and convection in the tropical West Pacific. J Clim 21:6101-6118.

Branstator G (1983) Horizontal energy propagation in a barotropic atmosphere with meridional and zonal structure. J Atmos Sci 40:1689-1708.

Branstator G (2002) Circumglobal teleconnections, the jetstream waveguide, and the North Atlantic Oscillation. J Clim 15:1983-1910.

Brönnimann S (2007) The impact of El Niño/Southern Oscillation on European climate. Rev Geophys 45:RG3003. doi: 10.1029/2006RG000199.

Cagnazzo C, Manzini E (2009) Impact of the stratosphere on the winter tropospheric teleconnections between ENSO and the North Atlantic and European region. J Clim 22:1223-1238.

Cassou C, Terray L (2001a) Oceanic forcing of the wintertime low-frequency atmospheric variability in the North Atlantic European sector: a study with the ARPEGE model. J Clim 14:4266-4291.

Cassou C, Terray L (2001b) Dual influence of Atlantic and Pacific SST anomalies on the North Atlantic/Europe winter climate. Geophys Res Lett 28:3195-3198.

Cassou C, Desert C, Terray L, Hurrell J W, Drévillon M (2004) Summer sea surface temperature conditions in the North Atlantic and their impact upon the atmospheric

circulation in early winter. J Clim 17:3349-3363.

Chang E K M, Fu Y (2002) Interdecadal variations in Northern Hemisphere winter storm track intensity. J Clim 15:642-658.

Deser c (2000) On the teleconnectivity of the "Artic Oscillation". Geophys Res Lett 27:779-782.

DeWeaver E, Nigam S (2000) Do stationary waves drive the zonal-mean jet anomalies of the Northern winter?. J Clim 13:2160-2176.

DeWeaver E, Nigam S (2002) Linearity in ENSO's atmospheric response. J Clim 15:2446-2461.

Drévillon M, Cassou C, Terray L (2003) Model study of the North Atlantic region atmospheric response to autumn tropical Atlantic sea-surface-temperature anomalies. Q J R Meteorol Soc 129:2591-2611.

Fraederich K (1994) An ENSO impact on Europe? Tellus 46A:541–552.

García-Serrano J, Losada T, Rodríguez-Fonseca B, Polo I (2008) Tropical Atlantic variability modes (1979–2002). Part II: time-evolving atmospheric circulation related to SST-forced tropical convection. J Clim 21:6476-6497.

García-Serrano J, Losada T, Rodríguez-Fonseca B (2010) Extratropical atmospheric response to the Atlantic Niño damping. J Clim (JCLI-3640, under review).

Gerber E P, Vallis G K (2009) On the zonal structure of the North Atlantic Oscillation and annular modes. J Atmos Sci 66:332-352.

Gouirand I, Moron V (2003) Variability of the impact of El Niño-Southern Oscillation

on sea-level pressure anomalies over the North Atlantic in january to march (1874-1996). Int J Climatol 23.1549-1566.

Gouirand I, Moron V, Zorita E (2007) Teleconnections between ENSO and North Atlantic in an ECHO-G simulation of the 1000-1990. Geophys Res Lett 34:L06705. doi: 10.1029/2006GL028852.

Haarsma R J, Hazeleger W (2007) Extratropical atmospheric response to equatorial Atlantic cold tongue anomalies. J Clim 20:2076-2091.

Horel JD, Wallace M J (1981) Planetary scale atmospheric phenomena associated with the Southern Oscillation. Mon Wea Rev 109:813-829.

Hoskins B J, Ambrizzi T (1993) Rossby wave propagation on a realistic longitudinally varying flow. J Atmos Sci 50:1661-1671.

Hoskins B J, Karoly D J (1981) The steady linear response of a spherical atmosphere to thermal and orographic forcing. J Atmos Sci 38:1179-1196.

Hoskins B J, James I N, White G H (1983) The shape, propagation and mean-flow interaction of large-scale weather systems. J Atmos Sci 40:1595-1612.

Hoskins B J, Valdes P J (1990) On the existence of storm-tracks. J Atmos Sci 47:1854-1864.

Hsu H-H, Lin S-H (1992) Global teleconnections in the 250-mb streamfunction field during the North Hemisphere winter. Mon Wea Rev 120:1169-1190.

Hsu H-H, Wallace J M (1985) Vertical structure of wintertime teleconnection patterns. J Atmos Sci 42:1693-1710.

Hurrell J W (1995) Decadal trends in the North Atlantic Oscillation: regional temperatures and precipitation. Science 269:676-679.

Hurrell J W, van Loon H (1997) Decadal variations in climate associated with the North Atlantic Oscillation. Clim Chang 36:301-326.

Ineson S, Scaife A A (2008) The role of the stratosphere in the European climate response to ENSO. Nat Geosci. doi: 10.1038/NGEO381.

Itoh H (2002) True versus apparent Artic Oscillation. Geophys Res Lett 29:1268. doi: 10.1029/2001GL013978.

Kang I-S, Lau N-C (1986) Principal modes of atmospheric variability in model atmospheres with and without anomalous sea surface temperature forcing in the tropical Pacific. J Atmos Sci 43:2719-2735.

Karoly D J, Plumb R A, Ting M (1989) Examples of the horizontal propagation of quasi-stationary waves. J Atmos sci 46:2802-2811.

Kidson J W (1999) Principal modes of Southern Hemisphere low-frequency variability obtained from NCEP–NCAR reanalyses. J Clim 12:2808-2830.

Kidson J W, Revell M J, Bhaskaran B, Mullan A B, Renwick J A (2002) Convection patterns in the Tropical Pacific and their influence on the atmospheric circulation at higher latitudes. J Clim 15:137-159.

Lau N-C (1979) The observed structure of the tropospheric stationary waves and the local balances of vorticity and heat. J Atmos Sci 36:996-1016.

Legates D R, Willmott C J (1990) Mean seasonal and spatial variability global surface air temperature. Theor Appl Climatol 41:11-21.

Livezey R E, Mo K C (1987) Tropical-extratropical teleconnections during the Northern Hemisphere winter. Part II: Relationships between monthly mean Northern Hemisphere circulation patterns and proxies for tropical convection. Mon Wea Rev 115:3115-3132.

Manzini E, Giorgetta M A, Esch M, Kornblueh, Roeckner E (2006) The influence of sea surface temperature on the Northern winter stratosphere: ensembles simulations with the MAECHAM5 model. J Clim 19:3863-3881.

Merkel U, Latif M (2002) A high resolution AGCM study of the El Niño impact on the North Atlantic/European sector. Geophys Res Lett 29:1291. doi: 10.1029/2001GL013726.

Mo K C, Livezey R E (1986) Tropical-extratropical geopotential height teleconnections during the Northern Hemisphere winter. Mon Wea Rev 114:2488-2515.

Moron V, Guirand I (2003) Seasonal modulation of the El Niño–Southern Oscillation relationship with sea level pressure anomalies over the North Atlantic in october–march 1873–1996. Int J Climatol 23:143-155.

North G R, Bell T L, Cahalan R F, Moeng F J (1982) Sampling errors in the estimation of Empirical Orthogonal Functions. Mon Wea Rev 110:699-706.

Peng S, Robinson W A, Li S, Hoerling M P (2005) Tropical Atlantic SST forcing of coupled North Atlantic seasonal responses. J Clim 18:480-496.

Plumb R A (1985) On the three-dimensional propagation of stationary waves. J Atmos Sci 42:217-229.

Pohlmann H, Latif M (2005) Atlantic versus Indo-Pacific influence on Atlantic-European climate. Geophys Res Lett 32:L05707. doi: 10.1029/2004GL021316.

Quadrelli R, Wallace J M (2002) Dependence of the structure of the Northern Hemisphere annular mode on the polarity of ENSO. Geophys Res Lett 29:2132. doi: 10.1029/2002GL015807.

Revell M J, Kidson J W, Kiladis G N (2001) Interpreting low-frequency modes of Southern Hemisphere atmospheric variability as the rotational response to divergent forcing. Mon Wea Rev 129:2416-2425.

Robertson A W, Ghil M (1999) Large-scale weather regimes and local climate over the western United States. J Clim 12:1796-1813.

Rodwell M J, Folland C K (2002) Atlantic air-sea interaction and seasonal predictability. Q J R Meteorol Soc 128:1413-1443.

Rogers J C (1990) Patterns of low-frequency monthly sea level pressure variability (1899-1986) and associated wave cyclone frequencies. J Clim 3:1364-1379.

Rogers J C (1997) North Atlantic storm track variability and its association to the North Atlantic Oscillation and climate variability of northern Europe. J Clim 10:1635-1647.

Sardeshmukh P D, Hoskins B J (1987) On the derivation of the divergent flow from the rotational flow: the c problem. Q J R Meteorol Soc 113:339-360.

Sardeshmukh P D, Hoskins B J (1988) The generation of global rotational flow by steady idealized tropical divergence. J Atmos Sci 45:1228-1251.

Shaman J, Tziperman E (2005) The effect of ENSO on Tibetan Plateau snow depth: a stationary wave teleconnection mechanism and implications for the South Asian monsoons. J Clim 18:2067-2079.

Shukla J, Wallace J M (1983) Numerical simulation of the atmospheric response to equatorial Pacific sea surface temperature anomalies. J Atmos Sci 40:1613-1630.

Smith T M, Reynolds R W (2003) Extended reconstruction of global sea surface temperatures based on COADS data (1854-1997). J Clim 16:1495-1510.

Straus D M, Shukla J (2002) Does ENSO force the PNA?. J Clim 15:2340-2358.

Sutton R T, Hodson D L R (2003) Influence of the ocean on North Atlantic climate variability 1871-1999. J Clim 16:3296-3313.

Sutton R T, Norton W A, Jewson S P (2000) The North Atlantic Oscillation - what role for the ocean? Atmos Sci Lett 1:89-100.

Terray L, Cassou C (2002) Tropical Atlantic sea surface temperature forcing of quasi-decadal climate variability over the North Atlantic-Europe region. J Clim 15:3170-3187.

Thompson D W J, Wallace J M (1998) The Arctic Oscillation signature in the wintertime geopotential height and temperature fields. Geophys Res Lett 25:1297-1300.

Thompson D W J, Wallace J M (2000) Annular modes in the extratropical circulation. Part I: month-to-month variability. J Clim 13:1000-1016.

Thompson D W J, Baldwin M P, Wallace J M (2002) Stratospheric connection to Northern Hemisphere wintertime weather: implications for prediction. J Clim 15:1421-1428.

Thompson D W J, Lee S, Baldwin M P (2003) Atmospheric processes governing the Northern Hemisphere Annular Mode/North Atlantic Oscillation. In: Hurrell J W, Kushnir Y, Ottersen G, Visbeck M (eds) The North Atlantic Oscillation: climate significance and environmental impact. Geophys Monogr Ser 134:81–112.

Toniazzo T, Scaife A A (2006) The influence of ENSO on winter North Atlantic climate. Geophys Res Lett 33:L24704. doi: 10.1029/2006GL027881.

Trenberth K E (1986) An assessment of the impact of transient eddies on the zonal flow during a blocking episode using localized Eliassen-Palm flux diagnostics. J Atmos Sci 43:2070-2087.

Trenberth K E, Branstator G W, Karoly D, Kumar A, Lau N-C, Ropelewski C (1998) Progress during TOGA in understanding and modeling global teleconnections associated with tropical seas surface temperatures. J Geophys Res 103:14291-14324.

Uppala S M and co-authors (2005) The ERA-40 re-analysis. Q J R Meteorol Soc 131:2961-3012.

Vallis G K, Gerber E P (2008) Local and hemispheric dynamics of the North Atlantic Oscillation, annular patterns and the zonal index. Dyn Atmos Ocean 44:184-212.

van Loon H, Rogers J C (1978) The seesaw in winter temperatures between Greenland and northern Europe. Part I: General descriptions. Mon Wea Rev 106:296-310.

van Oldenborgh G J, Burgers G, Klein Tank A (2000) On the El Niño teleconnection to spring precipitation in Europe. Int J Climatol 20:565-574.

Visbeck M, Chassignet E P, Curry R G, Delworth T L, Dickson R R, Krahmann G (2003) The ocean's response to North Atlantic Oscillation variability. In: Hurrell J W, Kushnir Y, Ottersen G, Visbeck M (eds) The North Atlantic

Oscillation: climate significance and environmental impact. Geophys Monogr Ser 134:113–145.

von Storch H, Zwiers F W (2001) Statistical analysis in climate research. Cambridge University Press, UK.

Wallace J M (2000) North Atlantic Oscillation/annular mode: Two paradigms-one phenomenon. Q J R Meteorol Soc 126:791-805.

Wallace J M, Lim G H, Blackmon M L (1988) Relationship between cyclone tracks, anticyclone tracks and baroclinic waveguides. J Atmos Sci 45:439-462.

Wallace J M, Thompson D W (2002) The Pacific center of action of the Northern Hemisphere Annular Mode: real or artifac?. J Clim 15:1987-1991.

Wang C (2002) Atmospheric circulation cells associated with the El niño-Southern Oscillation. J Clim 15:399-419.

Wang C (2005) ENSO, Atlantic climate variability and the Walker and Hadley circulations. In: Diaz H F, Bradley R S (eds) The Hadley Circulation: Present, Past and Future. Kluwer Academic Publishers, pp 173-202.

Watanabe M, Kimoto M (1999) Tropical-extratropical connection in the Atlantic atmosphere-ocean variability. Geophys Res Lett 26:2247-2250.

Webster P J (1981) Mechanisms determining the atmospheric response to sea surface temperature anomalies. J Atmos Sci 38:554-571.

IV.2.

Modos de variabilidad del Atlántico Tropical (1979-2002). Parte II: evolución temporal de la circulación atmosférica relacionada con la convección tropical forzada por SST

García-Serrano, J., T, Losada, B. Rodríguez-Fonseca e I. Polo (2008): Tropical Atlantic variability modes (1979-2002). Part II: time-evolving atmospheric circulation related to SST-forced tropical convection. J. Clim., 21, 6476-6497.

Las formas en las que la convección profunda sobre el Atlántico tropical afecta a la variabilidad climática de latitudes medias a través de la circulación meridional, teleconexión tipo onda y la interacción onda-flujo medio, son analizadas para el periodo 1979-2002, siguiendo la evolución de la precipitación anómala en el Atlántico Norte desde el verano hasta finales del invierno. De esta forma, los dos modos dominantes de covariabilidad entre la temperatura de la superficie del mar (SST) en el verano del Atlántico tropical y la precipitación anómala Euro-Atlántica de verano a invierno son analizados usando la misma metodología de máxima covarianza extendida desarrollada en la Parte I (ver Apéndice-A). Este trabajo actualiza los resultados mostrados por otros autores, cuyos estudios están basados en diferentes bases de datos y se extiende hasta los 1950s. Para este fin, la base de datos del Análisis Combinado de Precipitación (CMAP) del Centro de Predicción del Clima (CPC), la cual incluye medidas sobre océano, es usada para proporcionar una perspectiva completa de los patrones interanuales de precipitación durante las últimas décadas.

El primer modo, que explica más del 40% de la fracción de covarianza cuadrática, involucra anomalías de SST relacionadas con el Modo Ecuatorial o Niño Atlántico. Su respuesta atmosférica muestra variaciones en las circulaciones de Hadley y Ferrel, reforzando, respectivamente, las células de circulación directa e indirecta; desplazamientos anómalos en la circulación de Walker; y la excitación de ondas de Rossby que quedan atrapadas en la corriente en chorro de África del Norte-Asia. El segundo modo, que explica el 15% de la fracción de covarianza, está asociado con el patrón de Herradura en verano y con el Tripolo en invierno. Las anomalías de circulación atmosférica asociadas incluyen un forzamiento térmico local (alterando la célula de Hadley); perturbaciones en la ITCZ; y una respuesta tipo onda desde la región del Caribe.

El método usado en este trabajo resalta la dependencia estacional de los modos, en contraste con previos trabajos que no tienen en cuenta la evolución mes a mes de los mismos. Los resultados añaden nueva y valiosa información para el entendimiento de estos modos desde el importante periodo a partir de la década de los 80'.

Tropical Atlantic Variability Modes (1979–2002). Part II: Time-Evolving Atmospheric Circulation Related to SST-Forced Tropical Convection

JAVIER GARCÍA-SERRANO, TERESA LOSADA, BELÉN RODRÍGUEZ-FONSECA, AND IRENE POLO

Departamento de Geofísica y Meteorología, UCM, Madrid, Spain

(Manuscript received 13 August 2007, in final form 27 February 2008)

ABSTRACT

The ways in which deep convection over the tropical Atlantic affects the midlatitude climate variability through meridional circulation, planetary wave teleconnection, and wave–mean flow interaction is examined for the 1979–2002 period, by following the North Atlantic anomalous rainfall evolution from summer to late winter. In this way, the first two covariability modes between anomalous summer tropical Atlantic sea surface temperature (SST) and anomalous summer–late-winter precipitation over the North Atlantic basin are analyzed using the same methodology of extended maximum covariance analysis developed for Part I. This work updates the results given by other authors, whose studies are based on different datasets dating back to the 1950s. To this end, the Climate Prediction Center (CPC) Merged Analysis of Precipitation (CMAP) dataset, which includes measures over the ocean, is used to give a complete picture of the interannual rainfall patterns for the last decades.

The first mode, which accounts for more than 40% of the squared covariance fraction (SCF), involves SST anomalies related to the equatorial mode or Atlantic Niño. Its atmospheric response shows variations of the Atlantic Hadley and Ferrel circulations, reinforcing the direct and indirect circulation cells, respectively, displacements of the Atlantic Walker circulation, and the excitation of Rossby waves, which are trapped in the North African–Asian jet. The second mode, which accounts for 15% of the SCF, is associated with the summer horseshoe and winter tripole SST patterns. The related atmospheric circulation anomalies include direct thermal forcing (altering the local Hadley cell), perturbations in the ITCZ, and wavelike responses from the Caribbean region.

The method used in this work highlights the seasonal dependence of the modes, in contrast to previous work that neglects to take into account the month-to-month evolution of these modes. The results add new and valuable information to the understanding of these modes from the important period back to the 1980s.

1. Introduction

The study of the dynamics of the teleconnections between the tropics and extratropics continue to be a priority in climate research. Several studies have focused on the atmospheric link between tropical Atlantic variability (TAV) and midlatitude climate on seasonal to decadal time scales (e.g., Kushnir 1994; Mehta and Delworth 1995; Sutton and Allen 1997; Czaja and Frankignoul 1999).

The study of atmospheric teleconnections involves the following different processes and mechanisms: first, the excitation of Rossby waves by tropical convection and its associated divergent outflow in regions of strong vorticity gradient, characterized by the rotational component of the flow (Hoskins and Karoly 1981; Sardeshmukh and Hoskins 1988), and second, the deep vertical motion through the divergent part of the flow; these induced anomalies are thermally driven and associated with alterations in the zonal (Walker) and meridional (Hadley) circulations (Krishnamurti 1971; Krishnamurti et al. 1973). The perturbations that propagate to the extratropics are further influenced by interactions with asymmetries in the zonal mean flow and with the midlatitude storm tracks (Hoskins et al. 1983; Simmons et al. 1983; Trenberth 1986).

The dominant modes of SST variability in the tropical Atlantic Ocean are the *equatorial mode* or *Atlantic Niño* and the *Atlantic meridional* pattern. Previous studies show that the equatorial mode owes its interannual variations to the Bjerknes positive feedback

Corresponding author address: Javier García-Serrano, Facultad de C. C. Físicas, Departamento de Geofísica y Meteorología, UCM, Av/Complutense, 28040 Madrid, Spain.
E-mail: javigarcia@fis.ucm.es

DOI: 10.1175/2008JCLI2191.1

mechanism (Zebiak 1993; Keenlyside and Latif 2007), while the Atlantic dipole is not a coupled ocean–atmosphere variability mode (Sutton et al. 2000). The equatorial mode is characterized by anomalous SST and heat content at the eastern equatorial basin, and the displacement of the convective region southward and eastward (Zebiak 1993; Ruiz-Barradas et al. 2000; Vauclair et al. 2004). The Atlantic meridional pattern shows SST anomalies of opposite sign at both sides of the equator. Some studies maintain that it constitutes an intrinsic mode of variability (e.g., Chang et al. 1997; Servain et al. 1999), while others support that the two lobes are independent modes (e.g., Dommenget and Latif 2000; Wang 2002). In either case, the centers of action represent an interhemispheric SST gradient and its subtropical northern branch shares SST anomalies with the North Atlantic horseshoe (NAH; Czaja and Frankignoul 2002) during summer and with the North Atlantic tripole (NAT; Sutton and Allen 1997) during winter.

Several modeling and observational studies suggest an influence of the summer tropical Atlantic SST on the fall–winter North Atlantic Oscillation (NAO), though the nature of this connection is still unclear. Proposed mechanisms involve the excitation of Rossby waves toward Europe from the Amazon–Caribbean (Drévillon et al. 2003) or the central tropical Atlantic (Peng et al. 2005), and a direct response to the extratropical SST anomalies added to changes in storm activity (Cassou et al. 2004).

The transition between the summer NAH and the winter NAT is an important issue still under debate, as is the oceanic forcing in winter atmospheric circulation. Some studies suggest NAH as the SST forcing (Czaja and Frankignoul 1999, 2002; Drévillon et al. 2001; Cassou et al. 2004; Frankignoul and Kestenare 2005), while others fundamentally point to subtropical North Atlantic SST anomalies (Rodríguez-Fonseca and Castro 2002; Polo et al. 2005; Rodríguez-Fonseca et al. 2006), in agreement with the dominant tropical forcing (Sutton et al. 2001; Terray and Cassou 2002). In contrary, different works point to the equatorial SST anomalies as the responsible oceanic forcing for the NAO (Drévillon et al. 2003; Peng et al. 2005) or the East Atlantic pattern (Frankignoul and Kestenare 2005; Haarsma and Hazeleger 2007).

The coupled low-frequency variability involved in the connection between the North Atlantic–European atmospheric circulation and the tropical SST anomalies is, thus, controversial and requires further investigation. Therefore, we consider that a clear and robust observational evidence of the tropical–extratropical teleconnections is necessary.

In Polo et al. (2008, hereafter Part I), the authors addressed the study of these TAV modes associated with West African rainfall from boreal early spring to late summer; this paper studies the principal mechanisms of the tropical–extratropical atmospheric connection for both the Atlantic Niño damping and the horseshoe–tripole transition from summer to late winter.

To investigate the TAV SST impact on the tropical convection and the tropical–extratropical teleconnections from summer to winter described above, we perform an extended maximum covariance analysis (EMCA) between summer tropical Atlantic SST and summer–winter North Atlantic precipitation fields.

The paper is organized as follows: the data and methods used are described in the next section; summer–late-winter precipitation sequences related to TAV modes are described in section 3a, and the tropospheric circulation anomalies associated with these sequences are discussed in section 3b; section 4 summarizes the concluding remarks.

2. Data and methodology

The 1979–2002 monthly Climate Prediction Center (CPC) Merged Analysis of Precipitation (CMAP; Xie and Arkin 1997) and extended Reynolds SST (Smith and Reynolds 2003) have been used to study the main coupled modes between summer [June–September (JJAS)] tropical Atlantic SST anomalies (from 30°S to 38°N, and from 60°W to 34°E) and Atlantic anomalous precipitation (PCP; from 30°S to 70°N, and from 90°W to 35°E). To quantify the anomalous rainfall and compare it with the Part I results, precipitation anomalies have been standardized. Monthly SST and PCP anomalies are calculated by subtracting the monthly SST climatology for the period of study and removing the linear trend.

The 1979–2002 period is very reliable in the sense of data accuracy because satellite data are included in the precipitation dataset and provide information of the precipitation over the ocean, which allows us to follow the deep convection over the basin. In addition to this, several recent papers have addressed the changes in the observed climate trends from the 1970s (Vecchi et al. 2006; Hansen et al. 2006; Seidel et al. 2008). This makes the revision of previous studies an interesting task, in order to determine the possible change in the issues already described for longer periods of time.

To study the dynamical mechanisms involved in the teleconnections found, different atmospheric fields are extracted from the 40-yr European Centre for Medium-Range Weather Forecasts (ECMWF) Re-Analysis (ERA-40) project (Uppala et al. 2005) for 1979–2002.

The monthly anomalies have been calculated by sustracting the monthly mean climatology for that period. The variables used are as follows: horizontal wind at 925 and 200 hPa, vertical velocity at 500 hPa, geopotential height from 1000 to 100 hPa, and streamfunction and velocity potential at 200 hPa. Rotational and divergent components of the upper-tropospheric flow are computed by applying a finite-difference scheme to the streamfunction and velocity potential, respectively.

The EMCA methodology implemented in the first part of the study is also applied in this study. It is an extension of the maximum covariance analysis (MCA; Bretherton et al. 1992; Frankignoul and Kestenare 2005) but considers more than one time lag in one of the arrays. In this way, we can isolate in the same mode the whole sequence of significant covariant precipitation patterns in relation to the JJAS anomalous SST, obtaining the whole picture of the evolution of the rainfall from summer to winter [JJAS–December–March (DJFM)]. Also, this new methodology increases the number of time series in the analysis, having as many time series per point as time lags used in the analysis and assuring the statistical significance.

We have used this kind of statistical methodology with the aim of taking into account the intrannual evolution of the interannual variability modes. In this way, the EMCA method highlights the seasonal dependence of these modes. In contrast, previous work lacks in taking into account the month-to-month evolution of these modes, maximizing lagged covariability independent of the other adjacent seasons and presuming the persistence of the anomalies to be a function of time. Thus, we think that the EMCA results could be more robust, particularly regarding the time dependence of a mode's evolution.

The results are shown in terms of homogeneous and heterogeneous regression maps for the summer SST and the PCP sequence, respectively. The SST homogeneous maps show the amplitude of the projection (for each grid point) of the JJAS SST expansion coefficient (EC) on the gridpoint anomaly time series of the SST. The PCP heterogeneous maps show the amplitude of the projection of the JJAS SST EC on the gridpoint anomaly time series (for each of the lags) of the precipitation. Only those areas that are 98% statistically significant with a t test are mapped. The squared covariance fraction (SCF), a measure of the fraction of covariability explained by each mode, and the correlation coefficient between the independent and dependent ECs (RUV), completes the information for each mode. To test whether the results are statistically significant and the SST–PCP link that is found is not random, we check the results using a Monte Carlo test, shuffling and applying the EMCA 100 times. The probability density function (PDF) of the SCF that arises from these 100 realizations is compared to the nonshuffled EMCA SCF score, giving a significance level (SL) for the connection found.

3. Results

a. SST–precipitation patterns

In this section, the first two EMCA modes between the summer and winter precipitation sequence and the summer SST are described, with the aim of finding those tropical Atlantic SST patterns that could be responsible of the rainfall anomalies over the Atlantic region. This description gives us some insights about possible extratropical teleconnections through tropical convection.

1) FIRST MODE: THE EQUATORIAL MODE

The leading ECMA mode (Fig. 1h) is characterized by a JJAS SST pattern that resembles the well-known equatorial mode (Zebiak 1993); indeed, the correlation coefficient between its EC and ATL3 SST index (Zebiak 1993 average over the region 3°S–3°N, 20°W–0°), during JJAS is 0.93. This mode coincides with the leading mode described in Part I, with a correlation of 0.91. Their first mode has its origin at the southeastern tropical Atlantic basin during the previous late boreal winter season; it evolves into an anomalous SST tongue in summer (related to the equatorial mode), and damps in early winter because of a dynamically active ocean, together with the contribution of the anomalous heat fluxes; finally, this mode leads in an opposite way the winter anomalous SSTs at the equatorial Pacific.

For positive SST anomalies this pattern is associated with a wide band of positive anomalous precipitation that, in JJAS, covers the entire equatorial Atlantic, accompanied by drier conditions at both sides of the band (Fig. 1a).

Figures 1b–g show the rest of precipitation sequence of this mode, from July–October (JASO) to DJFM. In JASO (Fig. 1b), the anomalous rainfall pattern is similar to that of JJAS, but the rainfall equatorial band seems to split into two regions, western and eastern of 20°W. The negative precipitation anomalies at both sides of the equatorial band decay. In August–November (ASON; Fig. 1c), the split of the rainfall equatorial band is clearer and tropical convection over the Gulf of Guinea weakens, while anomalous rainfall increases over northern South America. In contrast, during the following lagged season [September–

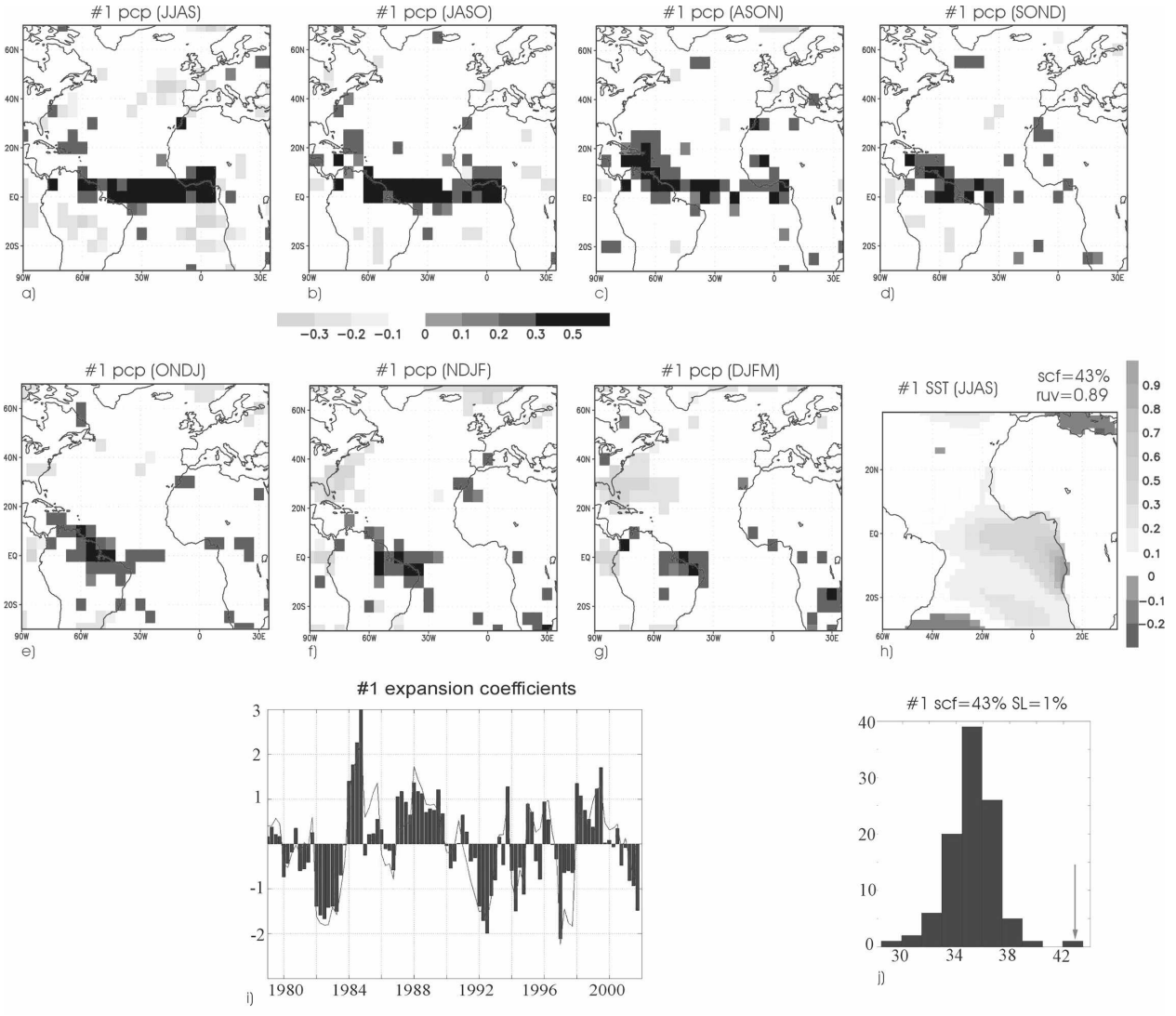

FIG. 1. (a)–(h) Regression maps of the summer–winter precipitation and the summer SST onto the leading SST expansion coefficient obtained from the EMCA between the anomalous summer tropical Atlantic SST (°C, JJAS) and summer–winter monthly Atlantic standardized anomalous precipitation (mm day^{-1}; JJAS–DJFM). Only 98% of the statistically significant areas (evaluated with a *t* test) are shaded. Square covariance fraction explained by this mode (SCF) and linear correlation between expansion coefficients (RUV) is indicated. (i) Standardized SST (bars) and precipitation (continuous line) expansion coefficients corresponding to the first EMCA mode. (j) Probability density function of the SCF from 100 Monte Carlo tests (histogram) is compared with the original EMCA SCF score (arrow) to show its significance level (SL).

December (SOND)], the last rainfall anomalies suffer a decrease in magnitude, while the anomalous rainfall along the Guinean coast has nearly disappeared. In October–January (ONDJ; Fig. 1e), the precipitation anomaly over northern Brazil continues its southern confinement. Negative rainfall anomalies arise over the Gulf of Florida, which could be indicating the upper inflow convergence along the northern subtropical latitudes. Figure 1f shows a strengthening of the negative precipitation anomalies over the Gulf of Florida during November–February (NDJF). The South America positive rainfall anomaly is reduced spatially to northeastern Brazil. Finally, during DJFM, the Amazonian positive rainfall anomalies show the major spatial confinement to northeastern Brazil (equator–10°S, 55°–30°W).

The JJAS SST anomalies associated with the rainfall anomalous sequence described above are confined to the tropical Atlantic. The same analysis considering the whole Atlantic basin (not shown) results in a SST anomaly pattern that is significant just for the tropical region. The correlation between the SST ECs of the

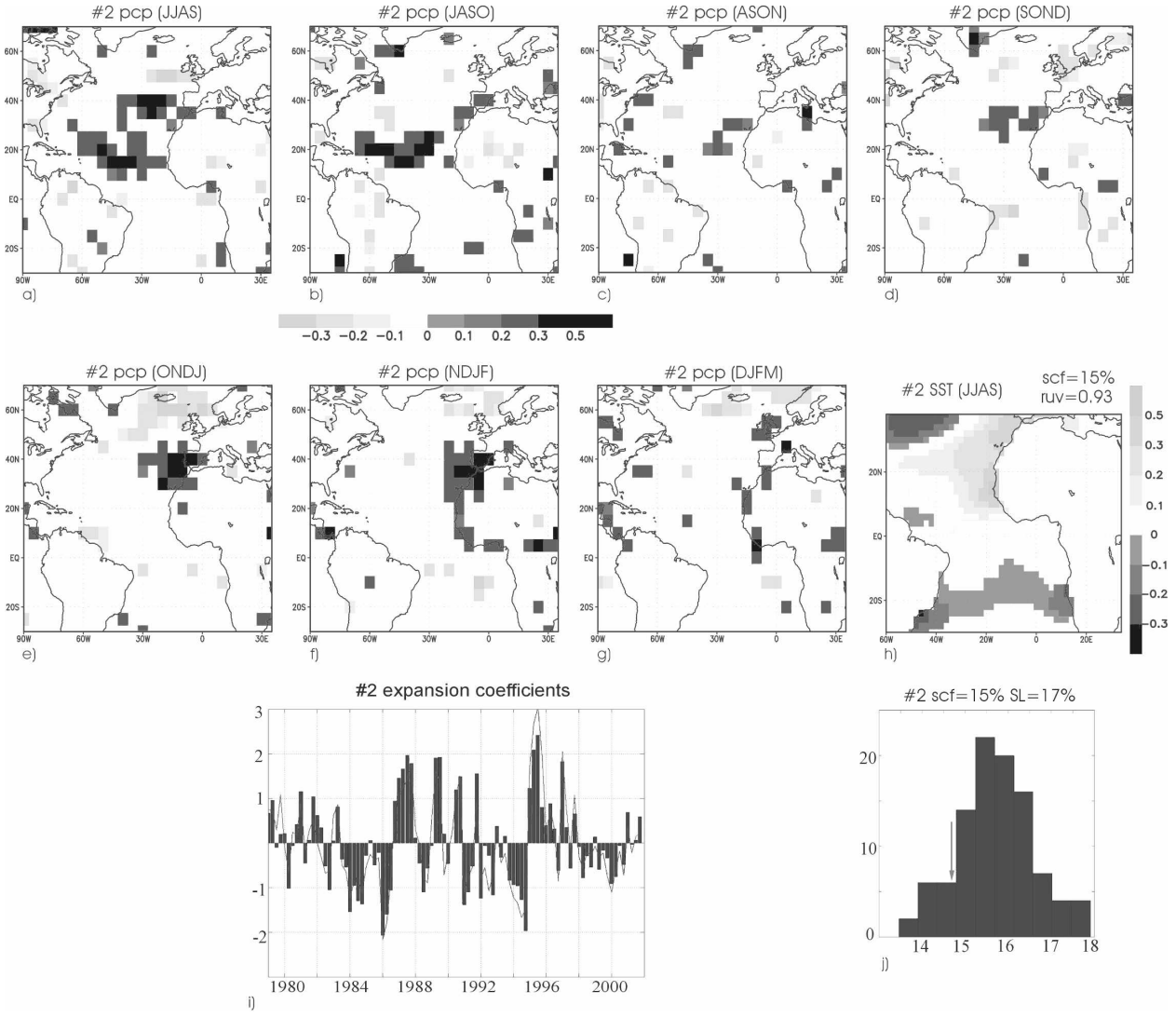

FIG. 2. Same as Fig. 1, but for the second SST–precipitation EMCA covariability mode.

leading modes of this two analysis is 0.99; meaning that this is a very robust mode in the sense of spatial domain. Moreover, the PDF of SCF shows a 1% significance level for this leading mode (Fig. 1j), which reveals the pattern robustness.

2) SECOND MODE: SUBTROPICAL NORTH ATLANTIC

The second ECMA mode (Fig. 2), which explains 15% of the squared covariance, with 17% significance level for the SCF (Fig. 2j), relates the SST over the subtropical North Atlantic (SNA) to a sequence of rainfall patterns that are significant over SNA from summer to autumn and over Europe from autumn to winter. The PCP and SST expansion coefficients are very well correlated (RUV = 0.93).

The SST EMCA second mode, projected onto the whole Atlantic Ocean (see Fig. 8), points out a more global Atlantic structure, identified as the well-known NAH pattern. Moreover, when computing the ECMA considering the whole Atlantic basin (not shown) the obtained pattern reveals the same NAH SST mode (0.93 correlation).

Figure 2a shows the spatial distribution of the summer (JJAS) precipitation anomalies over the North Atlantic connected with the contemporaneous SST NAH. It displays positive anomalies over a broad tropical–subtropical region from the Mauritanian coast to the Caribbean Sea (10°–25°N, 60°–15°W). In JASO (Fig. 2b), the North Atlantic rainfall dipole at the midlatitudes disappears, and the spatial extension of the subtropical positive precipitation band is reduced. In

ASON (Fig. 2c) the tropical–subtropical positive anomaly of the North Atlantic basin vanishes. From SOND to DJFM an anomalous rainfall dipole pattern between southwestern and northwestern Europe appears (Figs. 2d–g). Even so, strictly speaking, only the fourth and fifth lags (ONDJ and NDJF; see Figs. 2e,f) display the following precipitation NAO signature over the North Atlantic–European region: positive (negative) rainfall anomaly covering the Iberian Peninsula and northwestern Africa (northern latitudes). Indeed, the correlation coefficient between the second SST EMCA EC and NAO index (Hurrell 1995) is statistically significant only during these two seasons (-0.40 and -0.25, respectively).

During late winter (DJFM), the positive precipitation anomaly has moved to the north, and it is located over western-central Europe, although with a general decreasing in magnitude; and the negative anomalies suffer a slightly northeastward displacement.

The dynamical mechanisms between the tropics and extratropics associated with the EMCA modes will be discussed in section 3b(2).

b. Atmospheric response to SST anomalies

We have used the SST EMCA ECs as a time index that collects the complete information of the summer–winter time-evolving precipitation mode. Now, we compute regression maps of atmospheric variables to illustrate the dynamical mechanisms associated with the evidence of precipitation-related teleconnections.

1) THE DECAY OF THE ATLANTIC NIÑO

To illustrate how the Atlantic Niño is able to significantly force rainfall anomalies through tropical deep convection, the regression maps of the leading SST EMCA EC onto the 500-hPa anomalous vertical velocity (w500) and the 200-hPa upper-troposphere divergent wind are shown in Fig. 3. The dynamical information associated with thermally driven vertical movements is completed in Fig. 4, with the projection onto the 925-hPa wind field and SST. The horizontal upper-tropospheric response is characterized by regressing this SST EMCA EC onto the streamfunction and its derived rotational wind at 200 hPa (Fig. 5). The tropical component of the Rossby wave sources (TRWS; Sardeshmukh and Hoskins 1988; Qin and Robinson 1993), which comprises the advection of the climatological absolute vorticity by the anomalous divergent wind, is also shown in Fig. 3.

As found by Wang (2002, 2005), Fig. 3a shows how the Atlantic Walker circulation is extended eastward during the peak phase of the Atlantic Niño (JJAS). The anomalous ascending motion is located in the equatorial Atlantic between 60°W and 0°E, while its summer climatological behavior is associated with upward motions around 60°–50°W and downward motions over 20°W–0°E. Also, observational and model results have shown that the effect of the anomalously warm (cool) cold tongue on the West African summer precipitation consists of a southward (northward) migration of the monsoon ITCZ rainband and above (below)-normal rainfall along the coast of the Gulf of Guinea (Fontaine et al. 1999; Okumura and Xie 2004). These results are reproduced in Figs. 1a, 3a, and 4a; the equatorial eastern Atlantic shows anomalous northwesterly trade winds and upper-tropospheric anomalous divergent outflow, involving positive precipitation anomalies over the region.

Consequently, this mode is associated with variations in the descending Hadley branches of both hemispheres, which are responsible for the negative precipitation anomalies in the northern subtropical midlatitudes (30°–45°N) and tropical latitudes in the South Atlantic (5°–20°S; see Figs. 1a and 3a). Also, Fig. 5a shows how the upper-tropospheric response is dominated by anomalous anticyclonic circulations, according to the subsidence over those regions.

During JASO and ASON, the anomalous rainfall moves away from the Gulf of Guinea (Figs. 1b,c), ascending motions weakens over this region, and upper-tropospheric divergent outflow migrates westward (Figs. 3b,c). SST anomalies also show a relaxation in the eastern tropical Atlantic (Figs. 4b,c). In fact, the correlation between SST EMCA and ATL3 declines rapidly (0.93 in JJAS, 0.72 in JASO, 0.53 in ASON, and 0.37 in SOND). SOND is the last season in which SST anomalies cover the entire equatorial Atlantic (Fig. 4d).

The growth of the equatorial SST interannual variations owes its existence to the Bjerknes positive ocean–atmosphere feedback mechanism that involves ocean dynamics, atmospheric convection, and equatorial winds over the ocean basin (Zebiak 1993; Keenlyside and Latif 2007; Part I). The surface convergence and upper divergence, associated with deep convection, tend to move in the direction of positive thermal forcing (Figs. 3a and 4a). Hence, if the Bjerknes positive feedback weakens, then the mode decays. As expected, Fig. 4 shows how surface winds tend to displace tropical convection toward South America, so the Atlantic Walker circulation comes back to its climatological position (Figs. 3b–g and 4b–g).

Evidence of this damping mode is illustrated in Fig. 6, which shows the correlation coefficient scores between the SST EMCA EC and the Atlantic Walker and Hadley circulation indices created by Wang (2002) for six

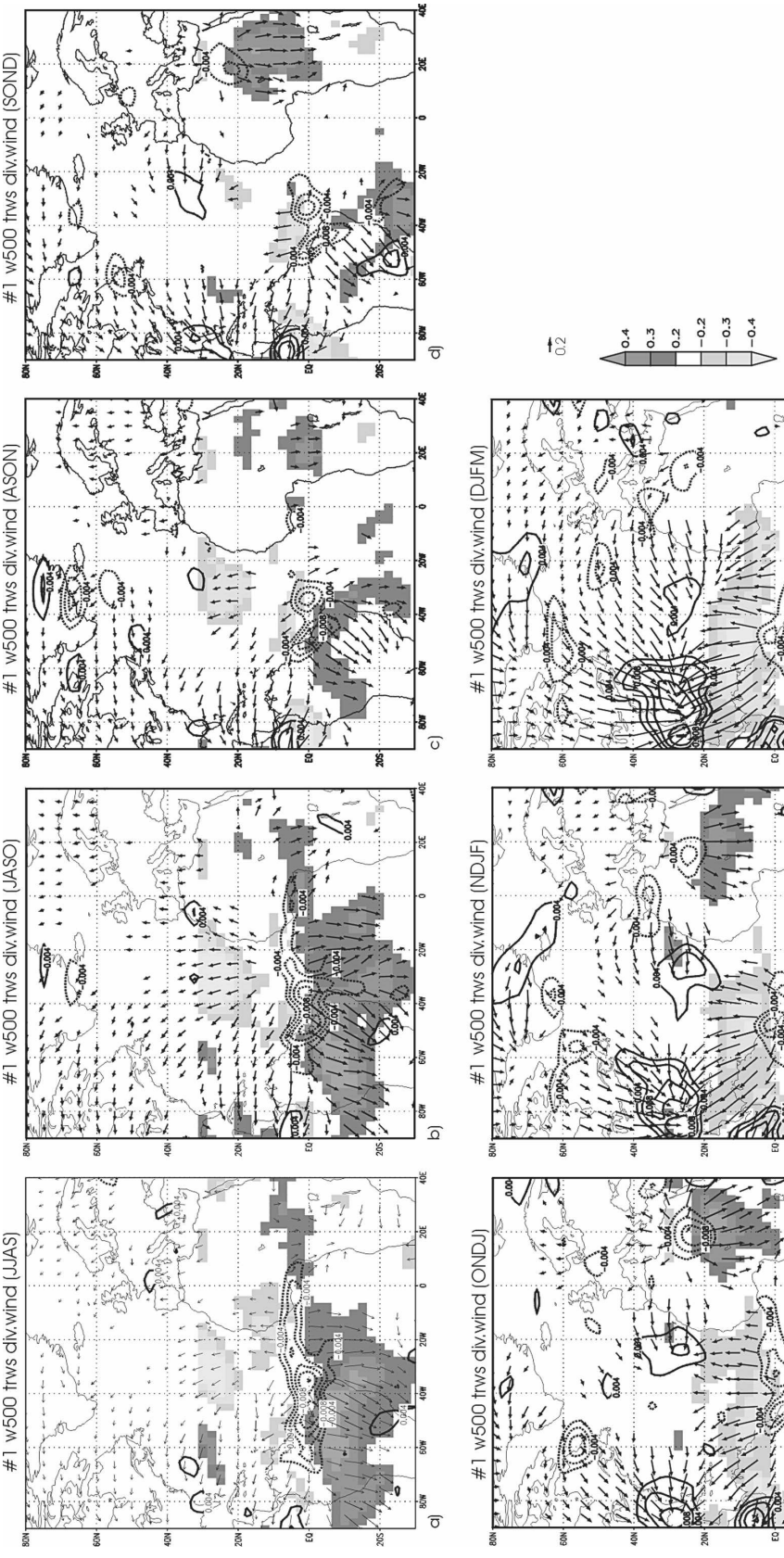

FIG. 3. Regression maps of 500-hPa vertical velocity (w500; contours, ci = 0.002 hPa s^{-1}) and 200-hPa divergent wind (arrows, m s^{-1}), together with the correlation maps of 200-hPa TRWS (shaded) onto the leading SST EMCA standardized expansion coefficient from JJAS to DJFM. Only 98% statistically significant areas (evaluated with a *t* test) are plotted (for divergent wind, vectors in which at least one of the components is statistically significant are shown).

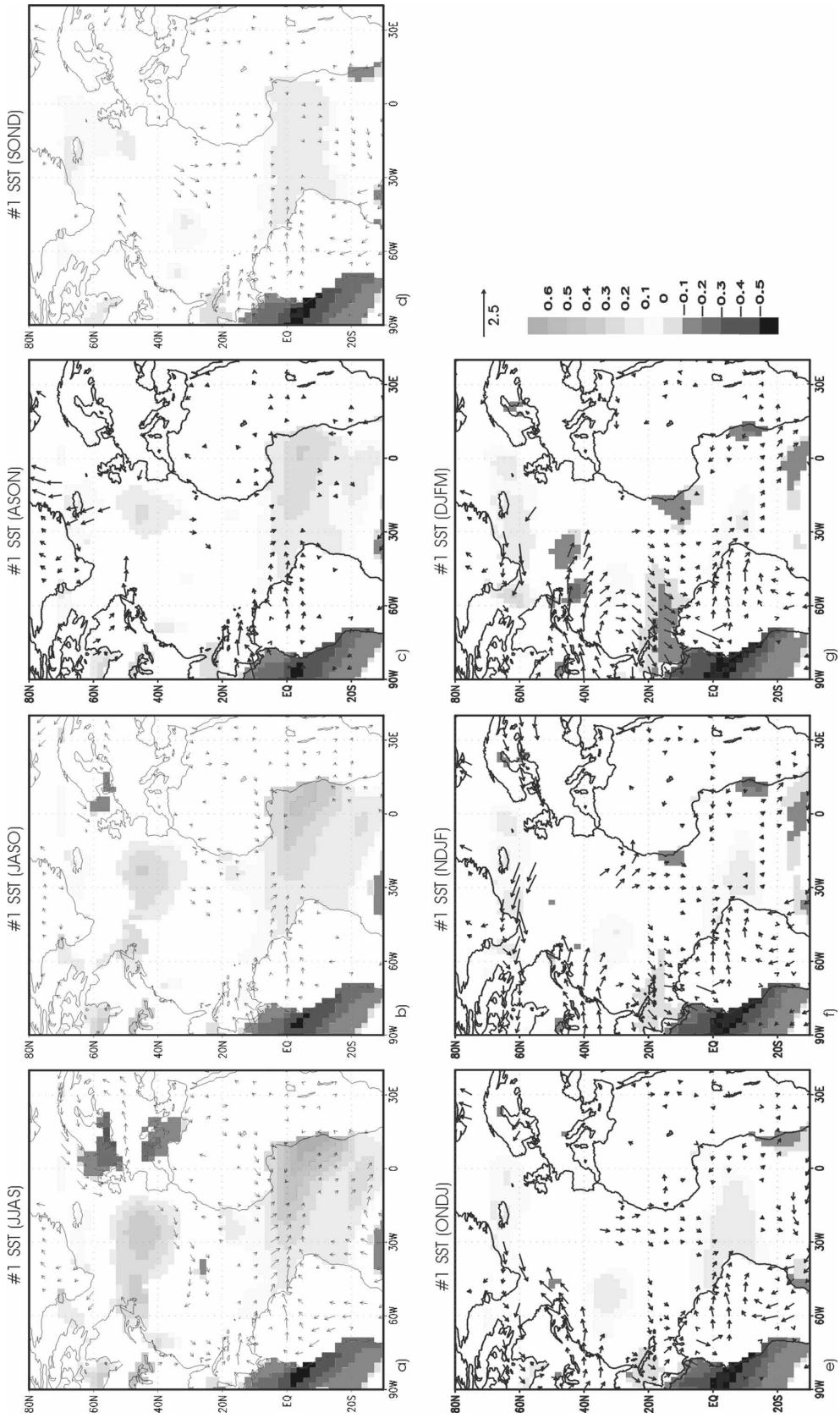

FIG. 4. Regression maps of SST (shaded, °C) and 925-hPa horizontal wind (arrows, m s^{-1}) onto the first SST EMCA standardized expansion coefficient from JJAS to DJFM. Only 98% statistically significant areas (evaluated with a *t* test) are plotted (for surface wind, vectors in which at least one of the components is statistically significant are shown).

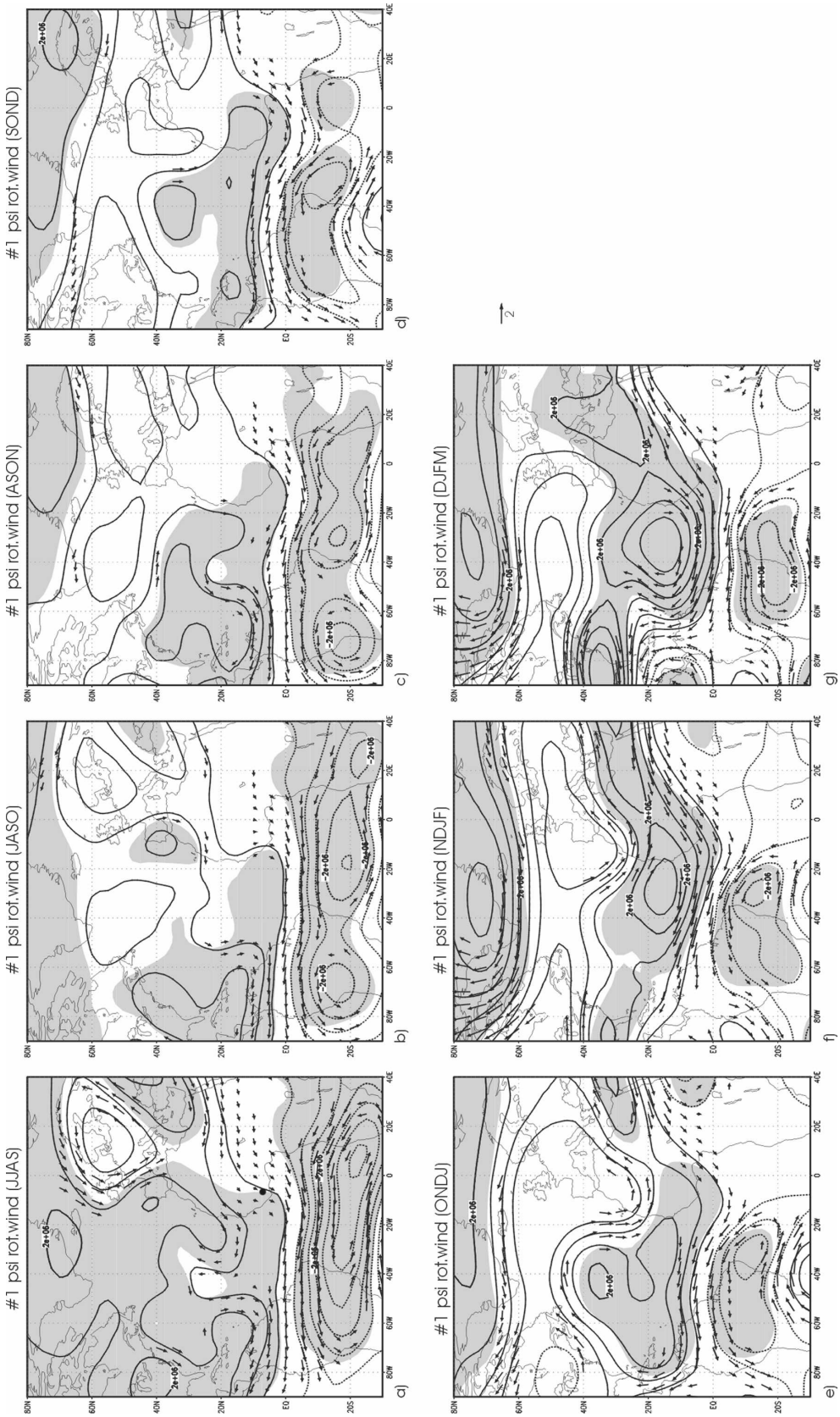

FIG. 5. Regression maps of the streamfunction (contours, ci = 0.5×10^6 m s^{-2}) and rotational wind (arrows, m s^{-1}) at 200 hPa onto the first SST EMCA standardized expansion coefficient from JJAS to DJFM. Statistically significant areas greater than 98% (evaluated with a *t* test) for streamfunction are shaded. For rotational wind, vectors in which at least one of the components is 98% statistically significant are shown.

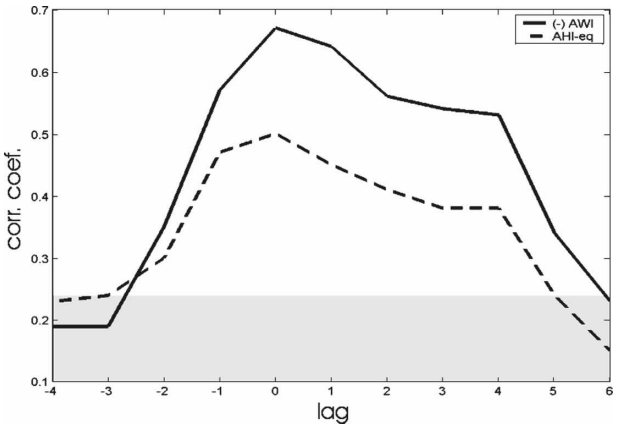

FIG. 6. Time evolution of the linear correlation between the first SST EMCA expansion coefficient (JJAS, lag 0) and the Atlantic Walker circulation index (solid line) and Hadley circulation index [dashed line; AWI and AHI respectively, as defined by Wang (2002)]. The time axis is centered in the JJAS monthly sequence (lag 0), lagging 1 month backward (negative lags) and forward (positive lags), to cover the spring–winter transition (FMAM–DJFM). Shading represents 98% statistical significance threshold.

different positive lags (from JASO to DJFM) and four different negative lags [from February–May (FMAM) to May–August (MJJA)], with JJAS being the period corresponding to lag 0. The correlation curves indicate that the anomalous upward motion and divergent outflow gradually increase over the equatorial Atlantic basin. Thus, during the spring–summer transition (negative lags), the SST EMCA equatorial mode is associated with an extension of the Atlantic Walker circulation and a strengthening of the Atlantic Hadley circulation. The maximum correlation appears for lag 0 (JJAS), with −0.67 for the Atlantic Walker index and 0.50 for the Atlantic Hadley index. Later, correlation curves decrease toward the statistical significance threshold. Such a feature is interpreted as the decrease of the anomalous ascending movements over the equatorial Atlantic, associated with the progressive westward displacement of the divergent circulations from the summer maximum location (Figs. 3a–g).

Regarding the atmospheric extratropical impacts of the Atlantic Niño, vertical velocity anomalies depict a strengthening of the direct subsidence over the Florida Gulf Coast starting in ASON (Fig. 3c), and are more clearly defined from SOND to DJFM (Figs. 3d–g). The associated sequence of negative precipitation anomalies confirms these results during ONDJ–DJFM (Figs. 1e–g), reflecting the local Atlantic Hadley enhancement (divergent wind; see Figs. 3e–g). A continuous energy source is required to maintain the divergent meridional circulation in an anomalous state. This source could be linked to the Atlantic SST warming but, although the SST regression maps show the presence of SST anomalies off the northeastern Brazilian coast during all the lags, they clearly decay from ONDJ to DJFM (Figs. 4e–g), accompanied by a damping of the precipitation over the Amazon region (Figs. 1e–g), associated with a weakening of vertical movements (Figs. 3e–g). For this reason, such a feature is not enough to explain the increase of negative rainfall anomalies over the Florida Gulf Coast during the three last EMCA seasons.

Because the weakening of the ascending motion over eastern Brazil does not support the progressive subtropical reinforcement, we expect another contributing mechanism to maintain the increasing amplitude of the upper convergent inflow over the subtropical western Atlantic in ONDJ–DJFM (Figs. 3e–g). The analysis of the Rossby wave dynamics (Fig. 5) could give us some insight. But, given that theory predicts that there is not possible poleward rotational propagation following a latitudinal circle (Hoskins and Karoly 1981), the horizontal projection (at 200 hPa) of the Rossby response is unable to support the time-evolving subtropical precipitation pattern (Figs. 1e–g).

To diagnose the physical mechanisms involved in the midlatitude response, a study of the internal atmospheric variability (transient dynamics) is performed. The horizontal components of the Eliassen–Palm vector (**E** vector) gives the following description of the interaction between synoptic transient eddies and the mean flow resulting from barotropic processes (Hoskins et al. 1983; Trenberth 1986):

$$\mathbf{E} = \left(\frac{1}{2} \overline{v'v' - u'u'},\ -\overline{u'v'} \right).$$

The convergence (divergence) of **E** depicts the eddy-induced tendency to decrease (increase) the mean zonal wind. Here we compute the **E**-vector components for the horizontal wind-filtered daily data using the 24-h difference filter described in Wallace et al. (1988).

Figure 7 shows its regression over the North Atlantic region from SOND to DJFM. In the midlatitudes, the **E**-vector field shows both a clear north–south orientation and a convergence (divergence) in the region about 30°N (50°N) (Figs. 7b–d). Hence, regressed eddy momentum transports tend to decelerate (accelerate) the westerly mean flow along subtropical (subpolar) latitudes. These findings are in good agreement with the upper wind anomaly depicted in the regression maps of the SST EMCA expansion coefficient onto the zonal wind at 200 hPa from early to late winter (ONDJ–DJFM; see Fig. 7). In spite of the weak amplitude of the transient activity (especially during NDJF), the eddy–

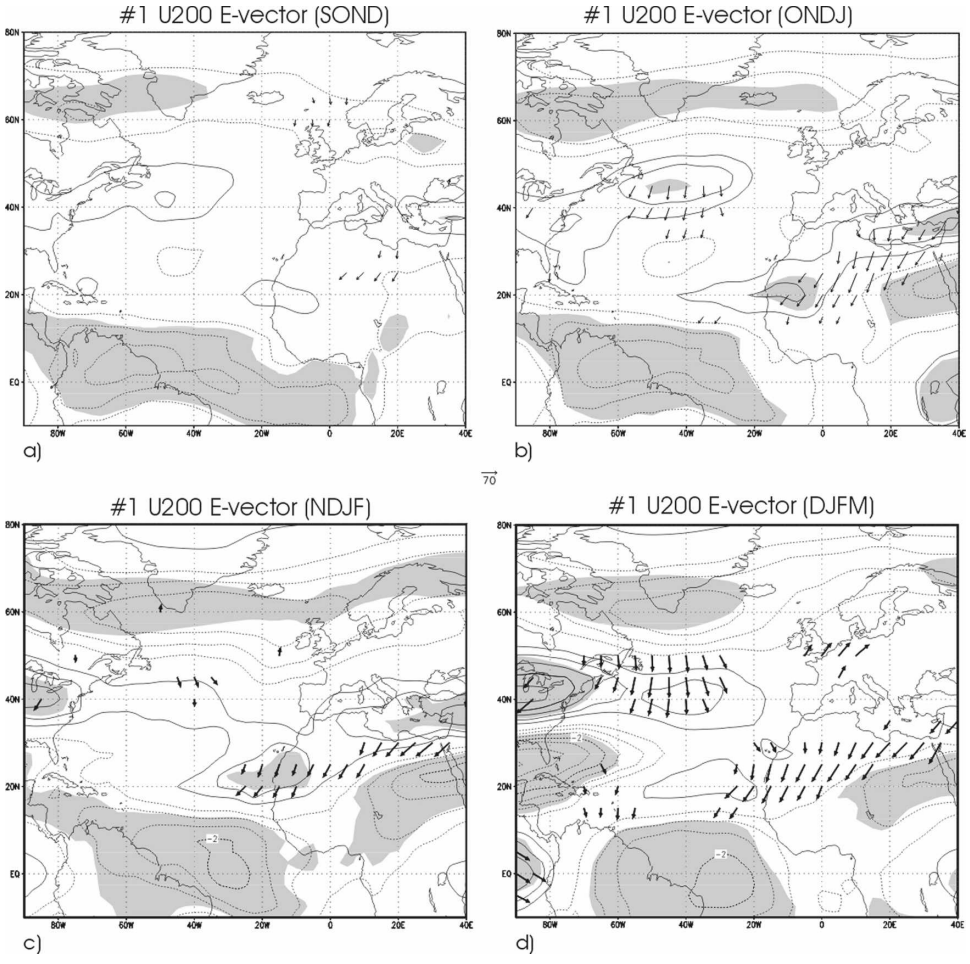

FIG. 7. Regression maps of the 200-hPa zonal wind (U200; contours, ci = 0.5 m s^{-1}) and horizontal components of the Eliassen–Palm flux (**E** vector; arrows, m^2 s^{-2}) onto the leading SST EMCA standardized expansion coefficient from SOND to DJFM. Statistically significant areas greater than 98% (evaluated with a *t* test) for U200 are shaded. For **E** vector, vectors in which at least one of the components is 98% statistically significant are shown.

mean flow interaction is acting like it does in its climatological direction (Edmon et al. 1980; Hoskins et al. 1983) and, hence, reinforcing the indirect midlatitude Ferrel circulation [poleward westerly injection, equatorward easterly injection; see Held and Hoskins (1985)]. Such a feature, although weak, could also be contributing to the excited subsidence in the subtropical Atlantic region.

Because none of the possible sources detailed above can totally explain the reinforcement of the subsidence over Florida, an external forcing must also be acting. Figure 4 depicts the presence of a La Niña SST condition (with steady amplitude) related to the positive phase of the equatorial mode. The lead–lagged connection between Atlantic and Pacific El Niño has been discussed in Part I. ENSO anomalies could be transferred to the Atlantic sector either via the atmospheric bridge (Wang 2002, 2005) or through the Pacific–North America (PNA) (Enfield and Mayer 1997; Giannini et al. 2001), mechanisms that involve reinforced subsidence over subtropical latitudes. Nevertheless, the atmospheric bridge needs a more prominent upper divergence over northern South America, and the only significant temporal correlation between the SST EMCA EC and the PNA index (Wallace and Gutzler 1981) occurs during DJFM ($r = -0.30$). Moreover, the rainfall anomalies associated with the first EMCA mode do not reproduce the observed ENSO impacts in the tropical Atlantic, which are associated with more pronounced and northern equator–flanking Amazon precipitation and much weaker rainfall over Florida (Giannini et al. 2000, 2001; Alexander et al. 2002). The correlation coefficient between Niño-3.4 (Philip and van Oldenborgh 2006) and SST EMCA EC is statisti-

cally significant during all lags (~ -0.4); although latter values are lower compared to the correlation with the ATL3 index. These results point to an important role of ENSO in the atmospheric response found on the EMCA analysis. It seems like both equatorial coupled phenomena have an impact on the autumn–winter anomalous precipitation dipole in the western subtropical Atlantic. Prescribed SST simulations with an AGCM are needed to quantify this impact.

Finally, over the northern African subtropical latitudes, another region of barotropic conversion of energy from the transient eddies to mean flow is present during whole SOND–DJFM transition (Figs. 7a–d). There, the transient dynamics are primarily active in the region of the North Africa–Asian jet (Hoskins and Ambrizzi 1993). The **E** vector exhibits a divergence (convergence) above (below) 20°N inland; thus, the North Africa–Asian jet stream suffers an increase of the zonal wind velocity (Fig. 7). Contrary to the North Atlantic midlatitude transient forcing, here the **E** vectors show an east–west orientation indicating a clear zonally elongated axis of Rossby perturbations (Kiladis 1998).

The TRWS are represented in Fig. 3 (shaded areas), indicating the upper-tropospheric divergent wind efficiency to disturb the mean flow downstream. Figure 3 shows upper-tropospheric divergent outflow in the equatorial western Atlantic (over the South American coast) being the effective TRWS extended along the subtropical central-eastern Atlantic from SOND to DJFM (Figs. 3d–g). Then, a Rossby wave train is excited by the vorticity source at the entrance of the North Africa–Asian jet, propagating eastward from the tropical eastern Atlantic. The results indicate that anomalies remain trapped in a narrow meridional band and propagate zonally along the waveguide jet (Figs. 5d–g and 7).

Previous studies (Sardeshmukh and Hoskins 1988; Branstator 2002; Shaman and Tziperman 2005) seems to corroborate the teleconnection presented here, also supporting the suggested response of the sensitivity experiments by Haarsma and Hazeleger (2007).

2) HORSESHOE TO ATLANTIC TRIPOLE TRANSITION

Figures 8–10 show the regression, from summer (JJAS) to late winter (DJFM), of the second SST EMCA EC onto different variables: Fig. 8 shows the regression onto the Atlantic SST and surface winds anomalies, while the regression onto the divergent and rotational components of the circulation are shown in Figs. 9 and 10, respectively.

In section 3a(2) it was shown that the oceanic pattern associated with this mode resembles the well-defined NAH during JJAS (Fig. 8a).

From JASO the pattern weakens progressively, with the positive subtropical lobe being the only one practically persisting in ASON. In SOND, cold SST anomalies over central North Atlantic are reinforced and slightly displaced toward the east, and warm anomalies emerge off Newfoundland; also, there is a weakening of the trade winds in the eastern warmer subtropical basin (Fig. 8d). At this stage, the anomalous SST pattern resembles that obtained in the winter SST EMCA regressions more than the JJAS-associated one; results of Czaja and Frankignoul (2002) also point to this feature.

In ONDJ, the subtropical positive anomalies strengthen again as well as the negative anomalies in the central Atlantic, and positive anomalies at high latitude cover the whole basin width. The anomalous SST pattern now resembles the NAT pattern, just as the atmospheric projection resembles the NAO (Figs. 2e, 9e, and 10e). This NAT pattern, which persists until DJFM, peaks in NDJF, supporting the Czaja and Frankignoul (2002) and Rodwell and Folland (2002) results of the main atmospheric forcing of the NAT during winter. Thus, we also find that the maximum covariance is reached, with the atmosphere (ONDJ NAO) leading the ocean by 1 month (NDJF SST).

During JJAS there is a weakening of the Azores high–related winds (Fig. 8a) and, in turn, the trades (Cassou et al. 2004). During JASO and ASON (Figs. 8b,c), the midlatitude circulation becomes anticyclonic, and the weakening of the trades persists over the subtropical warm SSTs, though it is confined to a narrower subtropical band. In SOND the first stage of an anomalous cyclonic circulation arises in the midlatitudes, and it is totally formed in ONDJ, centered on 40°N–20°W, corresponding with the equivalent barotropic structure of the NAO seesaw (Figs. 8d,e). During ASON and SOND, a reduction of the trade winds over the warm SST remains, and could act to extract less heat from the tropical western Atlantic, thus reinforcing the SST anomalies, in agreement with results of Chang et al. (1997) and Okumura et al. (2001). The regression of the latent heat flux onto the second mode EC (not shown) shows positive values (atmosphere gains heat) over the tropical Atlantic, except in the Caribbean Sea during ASON; thus, the latent heat flux at this stage mostly acts to damp the SST anomalies everywhere but in the western tropical basin. During SOND, the negative latent heat flux anomalies extend to the central tropical Atlantic; the SST anomalies in the western tropical Atlantic could be reinforced now by the heat flux. Nevertheless, the reinforcement of the SST anomalies in the subtropical North Atlantic would be just partially ex-

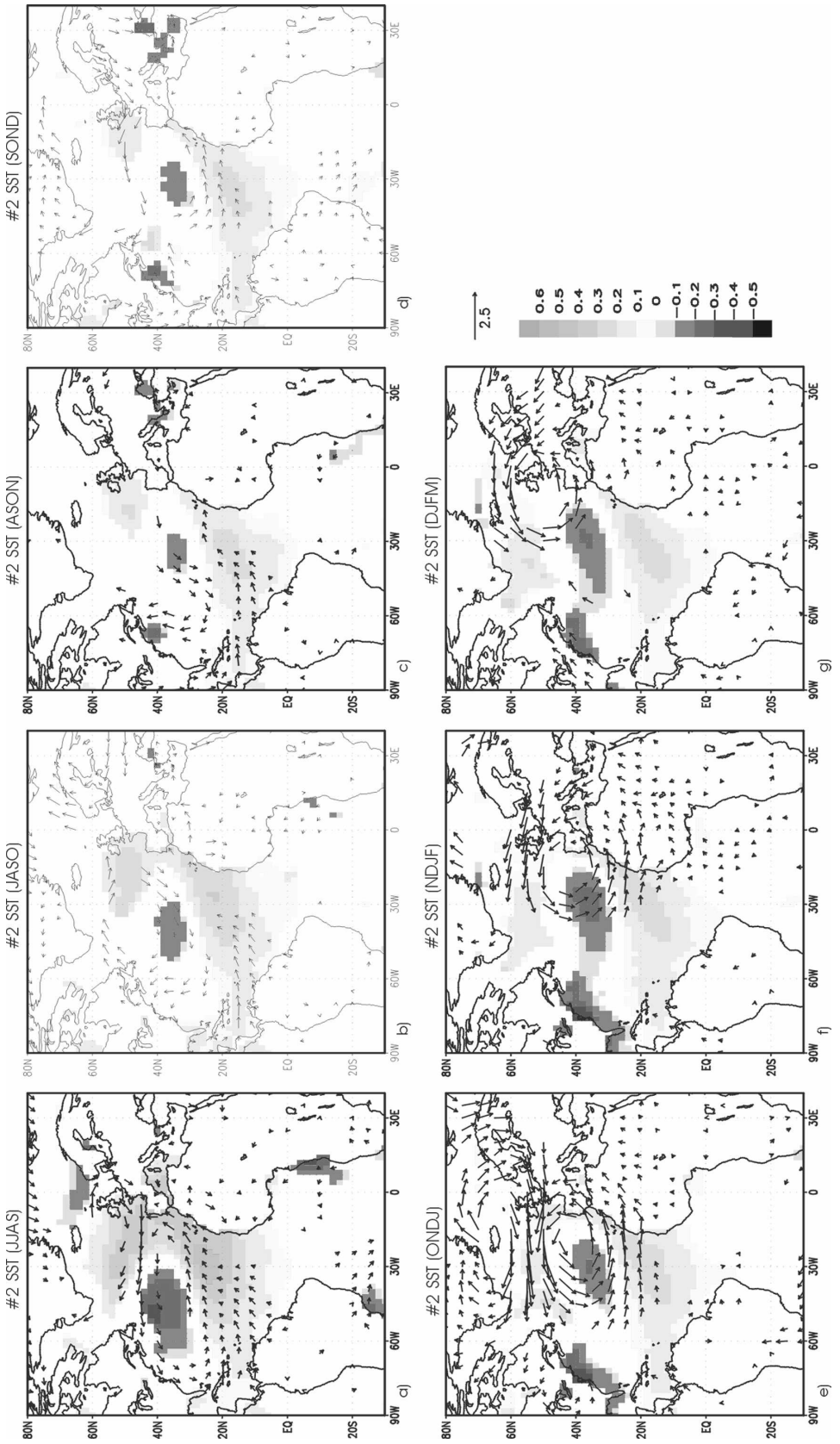

FIG. 8. Same as Fig. 4, but for the second SST EMCA mode.

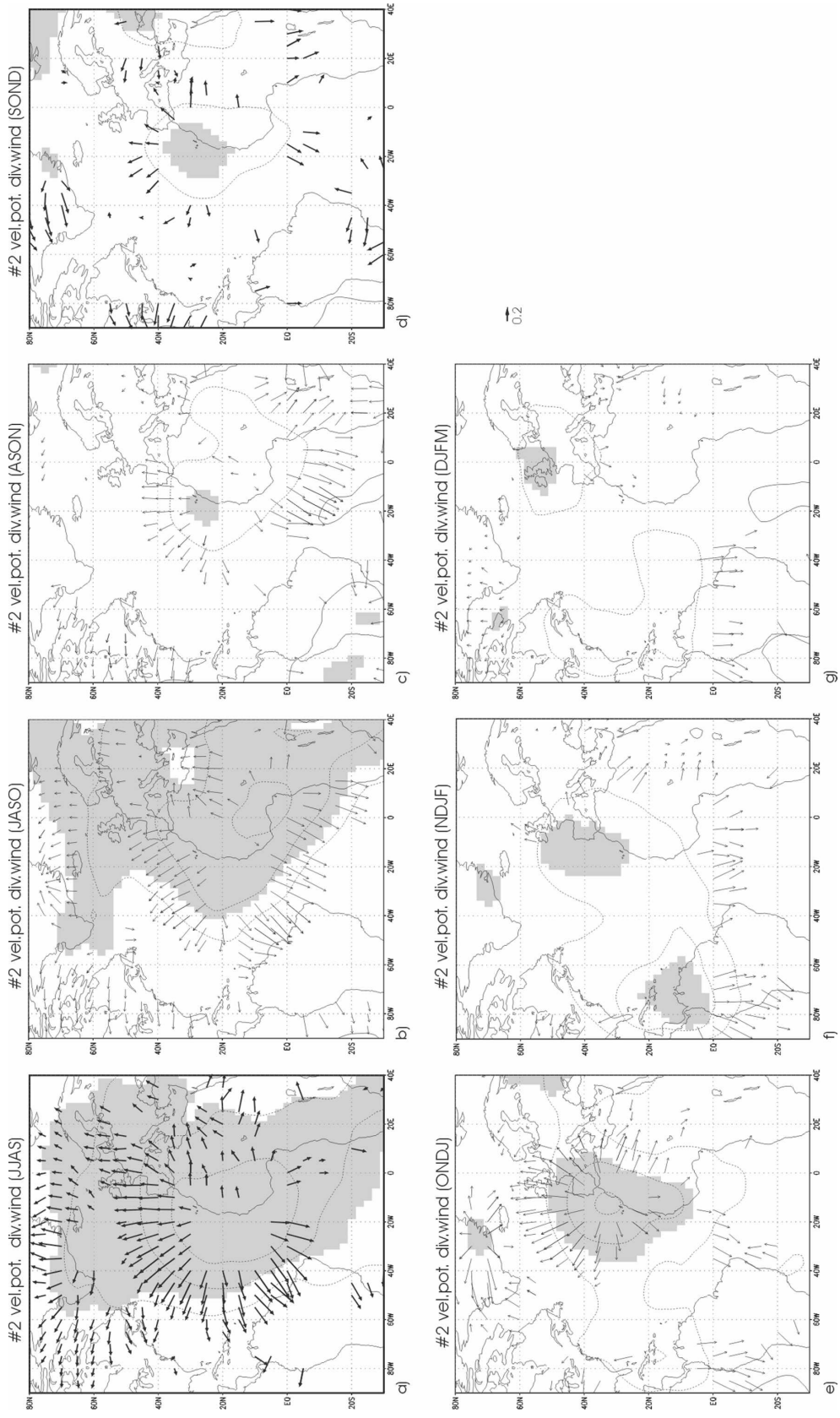

FIG. 9. Regression maps of the 200-hPa velocity potential (contours, ci = 0.2×10^6 m s^{-2}) and divergent wind (arrows, m s^{-1}) onto the second SST EMCA standardized expansion coefficient from JJAS to DJFM. Statistically significant areas greater than 98% (evaluated with a *t* test) for velocity potential are shaded. For divergent wind, vectors in which at least one of the components is 98% statistically significant are shown.

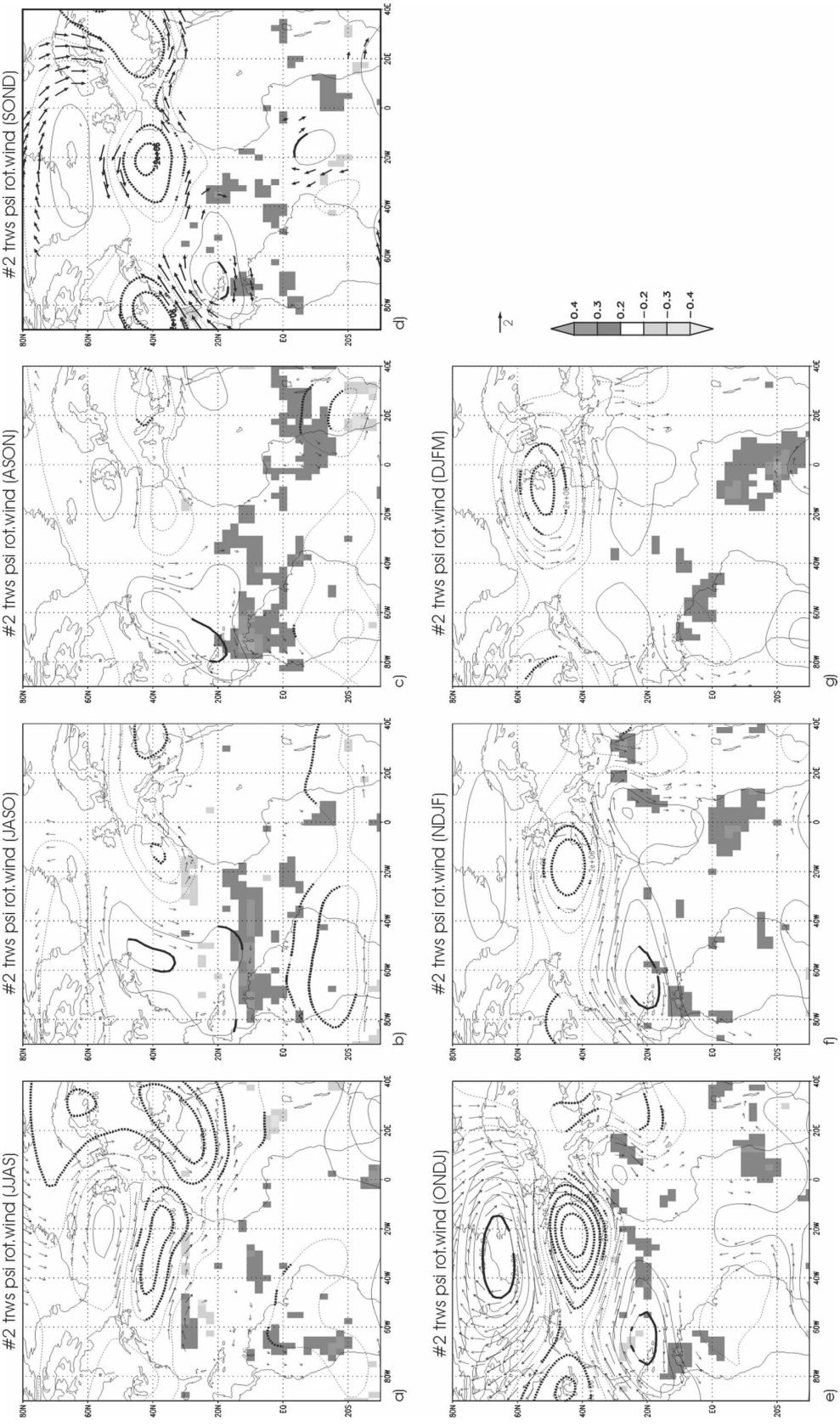

FIG. 10. Regression maps of the streamfunction (contours, ci = 0.5×10^6 m s^{-2}) and rotational wind (arrows, m s^{-1}) at 200 hPa, and correlation maps of 200-hPa tropical Rossby wave sources (TRWS; shaded) onto the second SST EMCA standardized expansion coefficient from JJAS to DJFM. Statistically significant areas greater than 98% (evaluated with a *t* test) for streamfunction are bold. For rotational wind, vectors in which at least one of the components is 98% statistically significant are shown.

plained by this mechanism and further investigation is required, maybe using a couple model, in order to totally understand it.

Our results show the nonpersistence of the whole North Atlantic anomaly structure throughout the late summer to early winter in relation to the North Atlantic precipitation variability, contrary to Drévillon et al. (2001), Czaja and Frankignoul (2002), Cassou et al. (2004), and Frankignoul and Kestenare (2005), who pointed out that the summer NAH and its persistence could be considered as an isolated forcing of the winter NAO. In the same way, the transition of the NAH to NAT does not correspond to the dominating evolution of the equatorial Atlantic SST anomaly, as suggested by Peng et al. (2005).

However, the summer NAH exhibits a strong covariability with the next winter NAO-like pattern, as described in the above studies. Our results point out this relationship (Figs. 2e, 8e, 9e, and 10e), although we include a prior transition toward the winter NAT. Indeed, from the summer NAH it seems that the more effective oceanic forcing of the extratropical winter precipitation is confined to the subtropical North Atlantic (SNA), in accordance with Rodríguez-Fonseca and Castro (2002) and Rodríguez-Fonseca et al. (2006). Such a feature also is partially in accordance with Peng et al. (2005) who affirmed that the NAH SST is not effective in forcing the following NAO. In our opinion, both the NAH–NAO connection and the NAH–NAT transition are not casual, but causal. Thus, we suggest that the EMCA statistical tool is filtering the summer NAH SST anomaly information, which is really connected to the winter NAO (or NAT SST).

We want to understand the NAH damping from JJAS to ASON and how the Atlantic tripole appears in ONDJ. In JJAS, the warm SST anomaly over the SNA produces anomalous convection over this region, which generates anomalous divergent wind aloft and anomalous convergence over the Amazon basin, associated with negative rainfall anomalies (Figs. 2a, 8a, and 9a). This anomalous upper-troposphere convergence over the Amazon persists in JASO and slightly remains in ASON, in agreement with the negative precipitation anomalies over this region (Figs. 2a–c, 9a–c). Similar results are found by Wang (2002, 2005), who relates positive SNA SST anomalies to an inversion of the direct Hadley circulation.

In JASO, the anomalous convergence over the Amazon (Fig. 9b) efficiently modulates the mean flow and triggers a Rossby wave (Figs. 10b,c). The anomalous midlatitude anticyclonic circulation is well defined and could be responsible of the anomalous low rainfall located at 35°N, 55°W (Figs. 2b,c). This anomalous high could act to damp the anomalous surface westerlies and produce the weakening of the horseshoe pattern until ASON (Figs. 8b,c and 10b,c).

Anomalous TRWS, associated with large upper convergence, are present in northern South America during JASO and ASON (Figs. 10b,c), supporting the above statement. From SOND this TRWS weakens and is localized over northwestern South America, persisting like this during ONDJ–NDJF. Because the upper convergence over the Amazon basin is weaker in ASON than in JASO (Figs. 9b,c), the associated Rossby response is also weaker in this season, although the anomalous anticyclonic circulation remains in the midlatitudes (Figs. 8c and 10c).

During JASO and ASON, significant positive anomalous precipitation are present in the eastern Atlantic (20°–30°N; see Figs. 2b,c). This could be related to a Gill-type response to the anomalous warm SST centered at 15°N, with a local baroclinic structure over the warm SST and a barotropic structure to the north (not shown for these seasons).

During SOND, and more clearly in ONDJ–NDJF, the subtropical warm SST anomalies lead to a direct response of the atmosphere that resembles the Gill solution for oceanic forcing in the tropics: baroclinic in the tropics and equivalent barotropic in the extratropics (Figs. 11a–c,e–g). The geopotential anomalies for the atmospheric column show anomalous low pressure in the midlatitudes and anomalous high pressure farther north, strongly resembling a negative phase of the NAO (Figs. 8e, 9e, and 10e). The precipitation anomalies confirm this negative NAO structure, being positive in the Iberian Peninsula and northern Africa and negative over northern Europe (Figs. 2d–f).

The divergent wind pattern shows anomalous divergence over the Caribbean Sea, which is very weak in SOND but clearer in ONDJ–NDJF (Figs. 9d–f). This can be indicative of a migration of the Hadley ITCZ farther north than its climatological position for this season (around 10°N instead of 0°N), which triggers another Rossby wave associated with high pressure in the upper troposphere (divergence) over the Caribbean Sea and low pressure (cyclonic circulation) in the midlatitudes (Figs. 8d–f). This mechanism is in accordance with the simulations of Terray and Cassou (2002). Our suggestion is that the effects of the Rossby wave triggered from the Caribbean Sea and the response to the warm SST in the eastern part of the Atlantic basin add each other, producing a clear enhancement of the precipitation anomalies in the Iberian Peninsula and northern Africa during winter (Figs. 2d–f).

Although these processes seem to be at work during the SOND–NDJF evolution (Figs. 9d–f, 10d–f, 11),

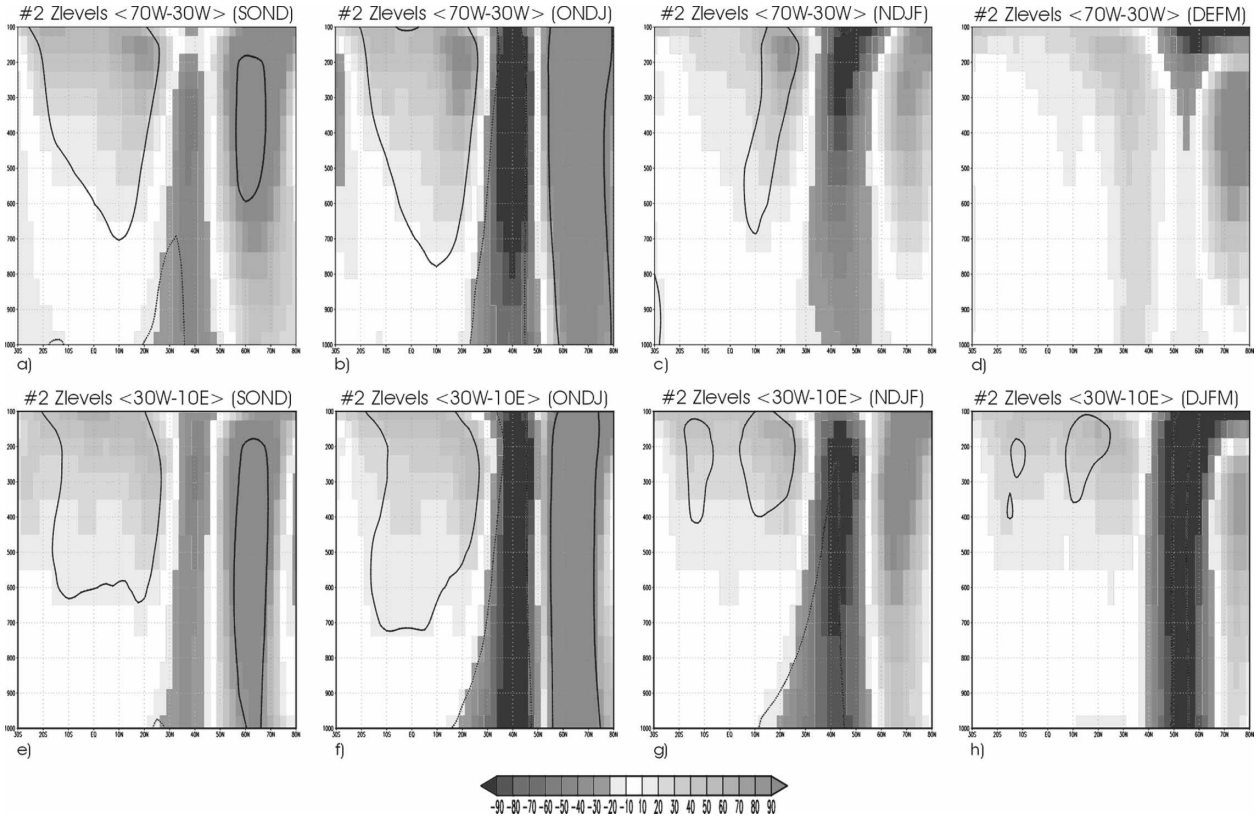

FIG. 11. Regression latitude by height profiles (30°S–80°N, 1000–100 hPa) of anomalous geopotential heights (shaded, m) onto the second SST EMCA standardized expansion coefficient from SOND to DJFM: (top) averaged over 70°–30°W, and (bottom) averaged over 30°W–10°E. Contours represent statistical significance greater than 98% (evaluated with a *t* test).

some effect is clearly dominating the midlatitude atmospheric response from ONDJ to determine the NAO phase structure (the second SST EMCA EC is correlated with the NAO index only during ONDJ and NDJF). From early winter, there is a reinforcement of the anomalous meridional SST gradient at the midlatitudes off of Newfoundland (Figs. 8e,f), which could have an influence on the precipitation pattern. Losada et al. (2007) have suggested that the anomalous extratropical SST gradient lead to an increase in the kinetic energy of the transient eddies that is transferred to the mean flow in the upper troposphere.

To quantify the activity of transients and associated eddy–mean flow interactions, the regression of the second mode over the anomalous horizontal Eliassen–Palm flux (**E** vector) is computed. Figure 12 shows these results from SOND to DJFM, together with the regression of the anomalous 200-hPa zonal wind. The behavior of the anomalous **E** vector varies from autumn to late winter, possibly, as stated by other works (Peng et al. 1995; Cassou et al. 2004), because of the influence of the background state on the efficiency of the eddy–mean flow interaction.

In SOND (Fig. 12a), the anomalous **E** shows divergence around 50°N and convergence around 20°–30°N. Thus, transient activity can be interpreted as a deceleration of the subtropical jet and acceleration of the flow farther north. From ONDJ to DJFM (Figs. 12b–d), **E** is divergent around 40°N, with the **E** vector pointing to the pole and giving an acceleration of the jet over the midlatitudes with a more zonal extension.

We argue that, during SOND, the synoptic eddy activity counteracts the effects of the SST direct forcing Rossby mechanism explained above, so the anomalous atmospheric cyclonic circulation is weak at this stage. During ONDJ, the transients accelerate the jet around 30°–40°N because of barotropic conversion (Fig. 12b), adding its action to the other two and leading to a strong anomalous cyclonic circulation in the midlatitudes. Consequently, the exchange of air mass between the Azores and Iceland is disturbed and a negative phase of the NAO is completely established.

During NDJF, the anomalous 200-hPa zonal wind around 30°N is weaker (Fig. 12c) and the negative lobe of the precipitation anomalous dipole diminishes (Fig. 2f). Because the Rossby wave activity does not signifi-

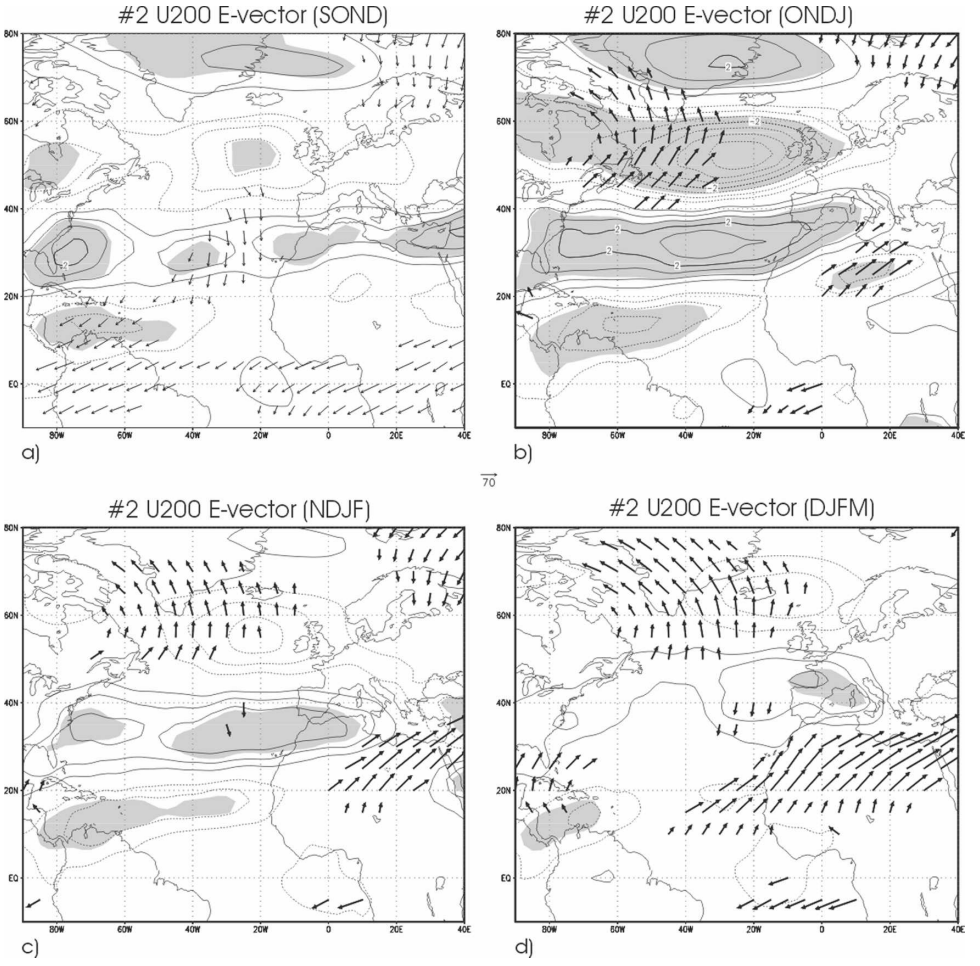

FIG. 12. Same as Fig. 7, but for the second SST EMCA mode.

cantly change compared with ONDJ (Figs. 9e,f and 10e,f), the effective transient flux (Fig. 12c) again seems to be the dominant factor in the NAO-like seesaw (Figs. 2f and 11c–g): the westerly eddy forcing of the mean horizontal circulation (E divergence) is located northward (50°N), and is less effective in forcing a negative NAO phase. However, the midlatitude rainfall anomalies persist in magnitude and location (Fig. 2e,f), supporting the theory that the tropical influence in the NAO pattern is not negligible (Figs. 10f and 11g).

During DJFM, neither rotational wind anomalies, nor TRWS appear over the Caribbean (Fig. 10g). Positive precipitation anomalies are located over the United Kingdom (Fig. 2g), in the region of anomalous cyclonic circulation (Fig. 8g). They might be caused, in part, by the remote effect of the positive SST anomalies in the eastern subtropical Atlantic because there is a Gill-type response in this part of the column (Figs. 11d–h). The streamfunction and eastward TRWS distribution in this area (Fig. 10g) could be indicative of a direct Rossby wave that would be responsible of the cyclonic circulation located over western Europe. The divergence of the **E** vector around 45°–50°N (Fig. 12d) indicates transference of energy to the Atlantic jet, which would strengthen the anomalous circulation generated by the Rossby wave.

4. Conclusions

The different ways in which SST-forced tropical convection can trigger teleconnections are analyzed in this study by describing the atmospheric response associated with the first two coupled modes between the summer tropical Atlantic SST and North Atlantic summer–late-winter time-evolving anomalous precipitation.

This impact of the summer tropical SST anomalies is analyzed applying the EMCA, which is developed and described in Part I and is an extension of the maximum covariance analysis (MCA). Part I has investigated the modes of boreal early spring to late-summer anomalous

tropical Atlantic SST related to the summer West African rainfall anomalies. Analogously, in the present study, the EMCA has allowed us to determine modes characterized by a time sequence of anomalous precipitation structures related to the summer tropical Atlantic SST variability, improving our understanding of the role of tropical convection and its subsequent extratropical connection.

The analysis has been done for the 1979–2002 period, for which important changes in the observed climate trends have been documented, using an enhance dataset with information over the ocean.

The above-mentioned features have made this work an interesting task that revises previous studies in order to determine the possible change in the issues already described for longer periods of time and different methodologies.

The leading SST–precipitation EMCA mode is associated with the equatorial mode or Atlantic Niño, whose origin and associated air–sea interaction processes have been already analyzed in Part I. In the present paper, this SST mode has been related to a precipitation anomalous band that, during the peak phase (JJAS), covers the whole tropical Atlantic basin from the Brazilian coast to the Gulf of Guinea, affecting the position of the ascendant branch of the Atlantic Walker circulation, the Atlantic Hadley cell, and the displacement of the ITCZ. As the eastern equatorial SST anomalies decay, the precipitation and vertical motions associated with the Atlantic Walker cell come back to its climatological location, generating large upper-tropospheric divergence over northern South America. This upper divergent outflow, located over the remaining SST anomalies (SOND–DJFM), leads the extratropical climate by both zonal and meridional circulation. Zonally, generating Rossby waves that appear to be trapped in the North Africa–Asian jet supports the hypothesis of a circumglobal response to the equatorial mode suggested by Haarsma and Hazeleger (2006); these waves and the transient eddy feedback can reinforce the wind velocity within the jet. Meridionally, the subtropical subsidence is coherent with the transient activity of midlatitude synoptic eddies, because the eddy momentum convergence reinforces the indirect circulation in the western North Atlantic. However, all of these features are not enough to explain the more pronounced subtropical Atlantic rainfall anomalies during the ONDJ–DJFM lags, and a forcing from other basins must be at work. The EMCA results point at the possibility of a remote Pacific ENSO influence (Fig. 4). Albeit the constant Pacific SST amplitude, the temporal correlations between the EMCA EC and the Niño-3.4 and PNA time series are weak, and the autumn–winter time-evolving precipitation anomalies are not exactly like the ones described as the tropical Atlantic response to ENSO. Thus, although it seems that both Pacific and Atlantic Niños have an influence on the Florida–Amazon anomalous rainfall regions, model simulations are required to clarify the impact of the interaction between both basins. Results of simulations done in the framework of the African Monsoon Multidisciplinary Analysis (AMMA)-European Union (EU) project will be the scope of future studies in order to clarify these hypotheses.

One of the novelties of this work resides in the fact of its consideration of the summer to late-winter precipitation sequence in relation to the Atlantic Niño as an entire mode, which complements other authors' findings (Fontaine et al. 1999; Wang 2002; Okumura and Xie 2004; Wang 2005). Our results reveal that the summer Atlantic Niño pattern and its autumn–winter damping are ineffective in forcing a correlated response over Europe.

Regarding the second SST–PCP EMCA mode, the authors associate it with a thermal forcing located over the Subtropical North Atlantic during all lagged seasons. This SST anomaly is part of a complete North Atlantic pattern that is present in summer (horseshoe, NAH) and winter (tripole, NAT).

The associated EMCA precipitation anomalies cover the tropical North Atlantic during the summer–fall transition (JJAS–ASON) and the North Atlantic–European sector during the fall–late-winter transition (SOND–DJFM). During the first stage, with the damping of the horseshoe, the rainfall pattern decays in the tropical–subtropical Atlantic. The responsible mechanism involves changes in tropical convection, the weakening of the Atlantic Hadley cell, and the emergence of a Rossby wave train from the Caribbean–Central America that affects the midlatitude circulation, damping the NAH SST anomaly via anticyclonic barotropic circulation (JJAS–ASON). In SOND, the SST anomaly weakly resembles the NAT, and the subtropical forcing leads to a displacement of the ITCZ and changes in the upper divergence over northwestern South America. Such anomalous outflow forces another Rossby wave train of opposite polarity from the Caribbean, affecting the trade winds (cyclonic barotropic circulation), which also acts during ONDJ–NDJF. That SOND SST pattern, associated with a dipolelike precipitation anomaly in Europe, is previous to the NAO pattern. Later, during ONDJ–NDJF, the transient eddy activity adds its effects by affecting the airmass exchange between the Azores high and Iceland low through changes in the

zonal extension of the subtropical Atlantic jet. Finally, in DJFM, the dipolar precipitation anomaly is displaced northward. The anomalous circulation seems to be the response of the atmosphere to the subtropical SST anomaly, adding the direct Gill and forced Rossby responses, not via perturbations in the ITCZ. The transient activity acts as a positive feedback inducing a large cyclonic anomaly over western Europe.

The above EMCA results, concerning the second EMCA, provide outstanding future research lines. Cassou et al. (2004) evidenced that the NAH's origin could be interpreted as the remote footprint of tropical atmospheric changes, and here we suggest that the damping shown by the NAH through the JASO–ASON transition could be understood as a decaying forced by alterations in the Atlantic Hadley cell, and associated with the subtropical warming, via Rossby wave extension from the Amazon convergence zone.

The second EMCA mode shows that the damp in the SST could be due to the negative feedback produced in response to tropical atmosphere alterations. This feature could also explain the gap in the covariance between autumn NAH and winter NAO found in previous studies (Czaja and Frankignoul 1999, 2002; Rodwell and Folland 2002; Frankignoul and Kestenare 2005).

We have also addressed the possibility of a positive feedback between the NAT pattern and the NAO. Note that this feedback begins before the established NAO phase: the SOND tropical emerging Rossby wave train associated with oncoming SST in the NAT occurs just in the previous season to the winter NAO (ONDJ). Thus, this work also points at tropical atmospheric perturbations as contributors in exciting the midlatitude transient activity (final responsible of the NAO event).

This study has explored the potential predictability of European fall–winter climate on the basis of the knowledge of summer tropical Atlantic variability modes. Although the above relationships are robust and physically coherent regarding temporal and spatial structures, we cannot forget that we are following a linear approach through all of the study, thereby missing all of the asymmetric remote effects of the tropical convection. Further modeling studies are required to elucidate the potential connections described above, as well as investigate the nonlinear atmospheric response to the tropical forcing.

Acknowledgments. This research was supported by the European Project AMMA-EU and the national CGL2005-06600-C03-02 and CGL2006-04471 projects of the Spanish MEC. We wish to thank Dr. C. Roberto Mechoso (UCLA) and Dr. Pablo Zurita (UCM) for useful discussions and comments regarding this study. The comments of two anonymous reviewers helped to improve the manuscript. The ERA-40 datasets were kindly provided by Dr. Paul Berrisford (University of Reading).

REFERENCES

Alexander, M. A., I. Bladé, M. Newman, J. R. Lanzante, N.-C. Lau, and J. D. Scott, 2002: The atmospheric bridge: The influence of ENSO teleconnections on air–sea interaction over the global oceans. *J. Climate,* **15,** 2205–2231.

Branstator, G., 2002: Circumglobal teleconnections, the jet stream waveguide, and the North Atlantic Oscillation. *J. Climate,* **15,** 1893–1910.

Bretherton, S. B., C. Smith, and J. M. Wallace, 1992: An intercomparation of methods for finding coupled patterns in climate data. *J. Climate,* **5,** 541–560.

Cassou, C., C. Desert, L. Terray, J. W. Hurrell, and M. Drévillon, 2004: Summer sea surface temperature conditions in the North Atlantic and their impact upon the atmospheric circulation in early winter. *J. Climate,* **17,** 3349–3363.

Chang, P., L. Ji, and H. Li, 1997: A decadal climate variation in the tropical Atlantic Ocean from thermodynamic air–sea interactions. *Nature,* **385,** 516–518.

Czaja, A., and C. Frankignoul, 1999: Influence of the North Atlantic SST on the atmospheric circulation. *Geophys. Res. Lett.,* **26,** 2969–2972.

——, and ——, 2002: Observed impact of Atlantic SST anomalies on the North Atlantic Oscillation. *J. Climate,* **15,** 606–623.

Dommenget, D., and M. Latif, 2000: Interannual to decadal variability in the tropical Atlantic. *J. Climate,* **13,** 777–792.

Drévillon, M., L. Terray, P. Rogel, and C. Cassou, 2001: Midlatitude Atlantic SST influence on Europe winter climate variability in the NCEP Reanalysis. *Climate Dyn.,* **18,** 331–344.

——, C. Cassou, and L. Terray, 2003: Model study of the North Atlantic region atmospheric response to autumn tropical Atlantic sea-surface-temperature anomalies. *Quart. J. Roy. Meteor. Soc.,* **129,** 2591–2611.

Edmon, H. J., B. J. Hoskins, and M. E. McIntyre, 1980: Eliassen–Palm cross sections for the troposphere. *J. Atmos. Sci.,* **37,** 2600–2616.

Enfield, D. B., and D. A. Mayer, 1997: Tropical Atlantic sea surface temperature variability and its relation to El Niño–Southern Oscillation. *J. Geophys. Res.,* **102,** 929–945.

Fontaine, B., N. Philippon, and P. Camberlin, 1999: An improvement of June-September rainfall forecasting in the Sahel based upon region April-May moist static energy content (1968-1997). *Geophys. Res. Lett.,* **26,** 2041–2044.

Frankignoul, C., and E. Kestenare, 2005: Air–sea interactions in the tropical Atlantic: A view based on lagged rotated maximum covariance analysis. *J. Climate,* **18,** 3874–3890.

Giannini, A., Y. Kushnir, and M. A. Cane, 2000: Interannual variability of Caribbean rainfall, ENSO, and the Atlantic Ocean. *J. Climate,* **13,** 297–311.

——, J. C. H. Chiang, M. A. Cane, Y. Kushnir, and R. Seager, 2001: The ENSO teleconnection to the tropical Atlantic Ocean: Contribution of the remote and local SSTs to rainfall variability in the tropical Americas. *J. Climate,* **14,** 4530–4544.

Haarsma, R. J., and W. Hazeleger, 2007: Extratropical atmo-

spheric response to equatorial Atlantic cold tongue anomalies. *J. Climate,* **20,** 2076–2091.

Hansen, J., M. Sato, R. Ruedy, K. Lo, D. W. Lea, and M. Medina-Elizade, 2006: Global temperature change. *Proc. Natl. Acad. Sci. USA,* **103,** 14 288–14 293.

Held, I. M., and B. J. Hoskins, 1985: Large-scale eddies and the general circulation of the troposphere. *Advances in Geophysics,* Vol. 28A, Academic Press, 3–31.

Hoskins, B. J., and D. J. Karoly, 1981: The steady linear response of a spherical atmosphere to thermal and orographic forcing. *J. Atmos. Sci.,* **38,** 1179–1196.

——, and T. Ambrizzi, 1993: Rossby wave propagation on a realistic longitudinally varying flow. *J. Atmos. Sci.,* **50,** 1661–1671.

——, I. N. James, and G. H. White, 1983: The shape, propagation, and mean-flow interaction of large-scale weather systems. *J. Atmos. Sci.,* **40,** 1595–1612.

Hurrell, J. W., 1995: Decadal trends in the North Atlantic Oscillation: Regional temperatures and precipitation. *Science,* **269,** 676–679.

Keenlyside, N. S., and M. Latif, 2007: Understanding equatorial Atlantic interannual variability. *J. Climate,* **20,** 131–142.

Kiladis, G. N., 1998: Observations of Rossby waves linked to convection of the eastern tropical Pacific. *J. Atmos. Sci.,* **55,** 321–339.

Krishnamurti, T. N., 1971: Tropical east-west circulations during the northern summer. *J. Atmos. Sci.,* **28,** 1342–1347.

——, M. Kanamitsu, W. J. Koss, and J. D. Lee, 1973: Tropical east-west circulations during the northern winter. *J. Atmos. Sci.,* **30,** 780–787.

Kushnir, Y., 1994: Interdecadal variations in North Atlantic sea surface temperature and associated atmospheric conditions. *J. Climate,* **7,** 141–157.

Losada, T., B. Rodríguez-Fonseca, C. R. Mechoso, and H.-Y. Ma, 2007: Impacts of SST anomalies on the North Atlantic atmospheric circulation: A case study for the northern winter 1995/1996. *Climate Dyn.,* **29,** 807–819.

Mehta, V. M., and T. Delworth, 1995: Decadal variability of the tropical Atlantic Ocean surface temperature in shipboard measurements and in a global ocean–atmosphere model. *J. Climate,* **8,** 172–190.

Okumura, Y., and S.-P. Xie, 2004: Interaction of the Atlantic equatorial cold tongue and the African monsoon. *J. Climate,* **17,** 3589–3602.

——, ——, A. Numaguti, and Y. Tanimoto, 2001: Tropical Atlantic air-sea interaction and its influence on the NAO. *Geophys. Res. Lett.,* **28,** 1507–1510.

Peng, S., L. A. Mysak, H. Ritchie, J. Derome, and B. Dugas, 1995: The differences between early and midwinter atmospheric response to sea surface temperature anomalies in the northwest Atlantic. *J. Climate,* **8,** 137–157.

——, W. A. Robinson, S. Li, and M. P. Hoerling, 2005: Tropical Atlantic SST forcing of coupled North Atlantic seasonal responses. *J. Climate,* **18,** 480–496.

Philip, S., and G. J. van Oldenborgh, 2006: Shifts in ENSO coupling processes under global warming. *Geophys. Res. Lett.,* **33,** L11704, doi:10.1029/2006GL026196.

Polo, I., B. Rodríguez-Fonseca, and J. Sheinbaum, 2005: Northwest Africa upwelling and the Atlantic climate variability. *Geophys. Res. Lett.,* **32,** L23702, doi:10.1029/2005GL023883.

——, ——, T. Losada, and J. García-Serrano, 2008: Tropical Atlantic Variability Modes (1979–2002). Part I: Time-evolving SST modes related to West African rainfall. *J. Climate,* **21,** 6457–6475.

Qin, J., and W. A. Robinson, 1993: On the Rossby wave source and the steady linear response to tropical forcing. *J. Atmos. Sci.,* **50,** 1819–1823.

Rodríguez-Fonseca, B., and M. Castro, 2002: On the connection between winter anomalous precipitation in the Iberian Peninsula and North West Africa and the summer subtropical Atlantic sea surface temperature. *Geophys. Res. Lett.,* **29,** 1863, doi:10.1029/2001GL014421.

——, I. Polo, E. Serrano, and M. Castro, 2006: Evaluation of the North Atlantic SST forcing on the European and northern African winter climate. *Int. J. Climatol.,* **25,** 179–191.

Rodwell, M. J., and C. K. Folland, 2002: Atlantic air-sea interaction and seasonal predictability. *Quart. J. Roy. Meteor. Soc.,* **128,** 1413–1443.

Ruiz-Barradas, A., J. A. Carton, and Y. S. Nigam, 2000: Structure of interannual-to-decadal climate variability in the tropical Atlantic sector. *J. Climate,* **13,** 3286–3297.

Sardeshmukh, P. D., and B. J. Hoskins, 1988: The generation of global rotational flow by steady idealized tropical divergence. *J. Atmos. Sci.,* **45,** 1228–1251.

Seidel, D. J., Q. Fu, W. J. Randel, and T. J. Reichler, 2008: Widening of the tropical belt in a changing climate. *Nature Geosci.,* **1,** 21–24.

Servain, J., I. Wainer, J. P. McCreary, and A. Dessier, 1999: Relationship between the equatorial and meridional modes of climatic variability in the tropical Atlantic. *Geophys. Res. Lett.,* **26,** 485–488.

Shaman, J., and E. Tziperman, 2005: The effect of ENSO on Tibetan Plateau snow depth: A stationary wave teleconnection mechanism and implications for the South Asian monsoons. *J. Climate,* **18,** 2067–2079.

Simmons, A. J., J. M. Wallace, and G. W. Branstator, 1983: Barotropic wave propagation and instability, and atmospheric teleconnections patterns. *J. Atmos. Sci.,* **40,** 1363–1392.

Smith, T. M., and R. W. Reynolds, 2003: Extended reconstruction of global sea surface temperatures based on COADS data (1854–1997). *J. Climate,* **16,** 1495–1510.

Sutton, R. T., and M. R. Allen, 1997: Decadal predictability in North Atlantic sea surface temperature and climate. *Nature,* **388,** 563–567.

——, S. P. Jewson, and D. P. Rowell, 2000: Elements of climate variability in the tropical Atlantic region. *J. Climate,* **13,** 3261–3284.

——, W. Norton, and S. Jewson, 2001: The North Atlantic Oscillation—What role for the ocean? *Atmos. Sci. Lett.,* **1,** 89–100.

Terray, L., and C. Cassou, 2002: Tropical Atlantic sea surface temperature forcing of quasi-decadal climate variability over the North Atlantic–Europe region. *J. Climate,* **15,** 3170–3187.

Trenberth, K. E., 1986: An assessment of the impact of transient eddies on the zonal flow during a blocking episode using localized Eliassen–Palm flux diagnostics. *J. Atmos. Sci.,* **43,** 2070–2087.

Uppala, S. M., and Coauthors, 2005: The ERA-40 re-analysis. *Quart. J. Roy. Meteor. Soc.,* **131,** 2961–3012.

Vauclair, F., Y. du Penhoat, and G. Reverdin, 2004: Heat and mass budgets of the warm upper layer of the tropical Atlantic Ocean in 1979–99. *J. Phys. Oceanogr.,* **34,** 903–919.

Vecchi, G. A., B. J. Soden, A. T. Wittenberg, I. M. Held, A. Leetmaa, and M. J. Harrison, 2006: Weakening of tropical Pacific atmospheric circulation due to anthropogenic forcing. *Nature,* **441,** 73–76.

Wallace, J. M., and D. S. Gutzler, 1981: Teleconnections in the geopotential height field during the Northern Hemisphere winter. *Mon. Wea. Rev.,* **109,** 784–812.

——, G. H. Lim, and M. L. Blackmon, 1988: Relationship between cyclone tracks, anticyclone tracks, and baroclinic waveguides. *J. Atmos. Sci.,* **45,** 439–462.

Wang, C., 2002: Atlantic climate variability and its associated atmospheric circulation cells. *J. Climate,* **15,** 1516–1536.

——, 2005: ENSO, Atlantic climate variability and the Walker and Hadley circulations. *The Hadley Circulation: Present, Past and Future,* H. F. Diaz and R. S. Bradley, Eds., Cambridge University Press, 173–202.

Xie, P., and P. A. Arkin, 1997: Global precipitation: A 17-year monthly analysis based on gauge observations, satellite estimates, and numerical model outputs. *Bull. Amer. Meteor. Soc.,* **78,** 2539–2558.

Zebiak, S. E., 1993: Air–sea interaction in the equatorial Atlantic region. *J. Climate,* **6,** 1567–1586.

IV.3.

Respuesta atmosférica extratropical al decaimiento del Niño Atlántico

García-Serrano, J., T. Losada y B. Rodríguez-Fonseca (2010): Extratropical atmospheric response to the Atlantic Niño camping. J. Clim., JCLI-3640 (accepted).

El Niño Atlántico o Modo Ecuatorial del Atlántico (EM) es el fenómeno de variabilidad acoplada dominante en la cuenca tropical atlántica durante el verano boreal. Este trabajo se centra en el período 1979-2005, donde se ha mostrado como el EM ha cambiado, evolucionando en el tiempo desde el este al oeste de la cuenca sin persistir hasta el siguiente invierno. En el trabajo mostrado en la sección anterior (IV.2) se han propuesto tres hipótesis sobre el decaimiento de este modo: i) el confinamiento de la convección profunda sobre el noreste de Brasil, siguiendo el decaimiento del forzamiento térmico; ii) una anomalía negativa de precipitación sobre el Golfo de Florida que se amplifica en el tiempo; y, iii) la excitación de ondas de Rossby forzadas por la divergencia anómala remanente en la alta troposfera, que son atrapadas en la corriente en chorro subtropical pero que no muestran una respuesta robusta en el sector europeo.

En este trabajo se ha analizado la respuesta al EM mediante una simulación por conjuntos (10 miembros) con el AGCM-UCLA, evaluando la respuesta atmosférica al decaimiento del Niño Atlántico de verano. Los resultados de este experimento de sensibilidad apoyan que la primera y la última hipótesis pueden ser interpretadas en términos de un forzamiento térmico Atlántico; mientras que las anomalías negativas de precipitación sobre la cuenca oeste subtropical requieren de un forzamiento externo al Atlántico tropical. Estudios previos apuntan al desarrollo contemporáneo de un episodio El Niño como potencial influencia.

Extratropical Atmospheric Response to the Atlantic Niño Damping

Javier García-Serrano, Teresa Losada, Belén Rodríguez-Fonseca

Departamento de Geofísica y Meteorología, UCM, Madrid, Spain

(JCLI- 3640, accepted)

ABSTRACT

The Atlantic Niño or Atlantic Equatorial Mode (EM) is the dominant coupled variability phenomenon in the tropical Atlantic basin during boreal summer. This work focuses on the 1979-2005 period, when it has been shown how the EM has changed, evolving in time from east to west and without persisting until the following winter. In a previous observational work, the authors proposed three main issues along the damping of this mode: i) the continuous confinement of deep convection over northeasten Brazil following the thermal-forcing decay; ii) an increasing dipole-like precipitation anomaly with dry conditions in the Florida Gulf; and, iii) the excitation of Rossby waves forced by the remaining upper-tropospheric divergence which are trapped into the subtropical jet, but do not show a robust response on the European sector.

In this work, a 10-members ensemble simulation for the recent EM with the UCLA-AGCM model has been analysed for assessing the evolution of the atmospheric response to the summer Atlantic Niño damping. Results from the sensitivity experiment support that the former and the latter hypotheses can be interpreted in terms of Atlantic thermal forcing; whilst the negative rainfall anomalies in the western subtropical-basin requires an external forcing outside tropical Atlantic. Prior studies point at the peaking Pacific El Niño as potential player.

1. Introduction

The Atlantic Niño or Atlantic Equatorial Mode (EM) is the dominant tropical Atlantic SST (sea surface temperature) variability mode during boreal summer (Xie and Carton 2004; Huang and Shukla 2005). The Atlantic Niño is an ocean-atmosphere coupled mode in which the Bjerknes feedback operates by means of relaxation/reinforcement of the tropical trade winds, redistribution of warm waters in the equatorial belt, and changes in the equatorial thermocline slope and heat content zonal gradient (Zebiak 1993; Keenlyside and Latif 2007).

Many others works have described the characteristics of this summer mode (Carton et al. 1996; Sutton et al. 2000; Ruíz-Barradas et al. 2000; Frankignoul and Kestenare 2005a), as well as its local (Vizy and Cook 2002; Losada et al. 2009a) and remote tropical impacts (Wang 2006; Kucharski et al. 2007, 2008, 2009; Losada et al. 2009b; Rodríguez-Fonseca et al. 2009).

Nevertheless, few works have paid attention to extratropical teleconnections of the Atlantic Niño, and a systematic description of the forced atmospheric response to time-evolving EM has not yet been documented. While some of the studies conclude that the influence of summer equatorial Atlantic on mid-winter North Atlantic Oscillation (NAO) was artificial, and that the horseshoe SST pattern and the Atlantic Niño mode are independent one to each other (Frankignoul and Kestenare 2005b; García-Serrano et al. 2008); others point to a lagged effect of the EM on the North Atlantic region through the propagation of Rossby waves either from the Amazon region (Drévillon et al. 2003) or from the central-eastern part of the tropical Atlantic basin (Peng et al. 2005).

In this work, we focus on the 1979-2005 period, as it has been show how the summer-peaking Atlantic Niño does not persist into winter (Polo et al. 2008), and it is not correlated with the early-winter Atlantic Niño II (Okumura and Xie 2006). Here we will focus on the atmospheric response to this recent mode described in Polo et al. (2008), which starts at the Angola/Benguela upwelling region and is caused by alongshore wind stress anomalies; it propagates westward via Rossby oceanic waves during the transition phase (spring-summer); while the ending is forced by anomalous latent heat fluxes and Kelvin oceanic waves propagation from an off-equatorial forcing

(summer-autumn).

In a focal study, Haarsma and Hazeleger (2007) recaptured the Atlantic Niño-East Atlantic pattern lagged-relationship previously suggested by Frankignoul and Kestenare (2005b). The amplitude of their equatorial Atlantic SST anomaly was, however, fixed in throughout the year, which is contrary to what was described for the after-70's observed Atlantic Niño (Polo et al. 2008; García-Serrano et al. 2008). Even so, keeping the amplitude constant provides information about the sensitivity of the atmospheric response to the seasonal cycle. They proposed that the early-winter North Atlantic response is part of a circumglobal teleconnection initiated in the tropical Atlantic and enhanced at extratropical latitudes by transient-eddy feedback.

García-Serrano et al. (2008) described the tropical-extratropical interaction in the course of the equatorial SST damping, for the same period of study (1979-2005), evidencing the anomalous displacement of the Atlantic Walker ascending branch from the marine summertime extension (offshore Brazil-Gulf of Guinea) to inland wintertime location (southeastern part of the Amazonia). Here we have reploted three lagged seasons in Fig. 1 (a-c) showing the anomalous rainfall and SST during late-summer (Jul-Oct; JASO), late-autumn (Sep-Dec; SOND) and winter (Nov-Feb; NDJF). In JASO, the rainfall equatorial band seems to split into two regions, west and east of 20W (Fig. 1a). In SOND, when the anomalous SST has evolved to reach the whole equatorial area in equal proportions, the anomalous tropical convection over South America weakens but reaches western longitudes (always north of equator), while the anomalous rainfall along the Guinean coast has nearly disappeared (Fig. 1b). Finally in NDJF, the positive SST anomaly is localized offshore eastern Brazil at southern latitudes, and a negative precipitation anomaly arises over the Gulf of Florida, while South America positive rainfall anomaly is reduced spatially to latitudes south of equator (0-10S; Fig. 1c).

In this context, and according to that time evolution, three main hypotheses were suggested for the EM damping (García-Serrano et al. 2008): the restoring of the deep convection to its climatological location; the reinforcement of the local Hadley circulation in the western tropical Atlantic, resulting in dry conditions over the Florida Gulf; and the excitation of Rossby waves during autumn-winter which are trapped into the North African-Asian jet.

Related to the first issue, the westward displacement of the anomalous ascending branch of the local Walker cell from peak phase (May-Jun) to mature phase (Jul-Aug-Sep) has been assessed in Losada et al. (2009b) using an AGCM (atmospheric general circulation model) experiment. The present work will focus both on the subsequent tropical-convection decay and the assessment of the other two observational results by analysing the same dedicated AGCM experiment (Losada et al. 2009a; see Section 2; Fig. 1d-f).

The paper is organized as follows: some details of the simulation and the AGCM model used are presented in the next section; the outputs are analysed in section 3; while the summary and conclusions will be shown in section 4.

2. Experimental setup

In order to study the atmospheric response to the Equatorial Mode damping, the UCLA AGCM was forced with the leading time-varying anomalous tropical Atlantic SST pattern from the extended-maximum covariance analysis (EMCA) described in Polo et al. (2008). This AGCM design was adopted by the AMMA (African Monsoon multidisciplinary analyses) community in an intercomparison protocol. In this project, four AGCMs took part in the exercise but only the UCLA model enlarged its integration to winter after monsoonal season.

The version of the model used in this work is the v7.3 (Ritcher et al. 2008), in its high-resolution configuration (2ºlat x 2.5ºlon, 29 sigma levels in the vertical). The methodology used in this study consisted in the performance of a 10-member ensemble simulation in which the anomalous pattern was composed by choosing extreme events of the leading observed EMCA SST expansion coefficient (Polo et al. 2008): positive minus negative multiplied by two (Fig. 1d-f) was added to the 1979-2005 climatological SSTs (Smith and Reynolds 2003). We will refer to this simulation as EMP; further details of the characteristics and computation of the anomalous pattern used can be found in Losada et al. (2009a).

The results obtained from the EMP simulation will be compared with a 10-year long control run,

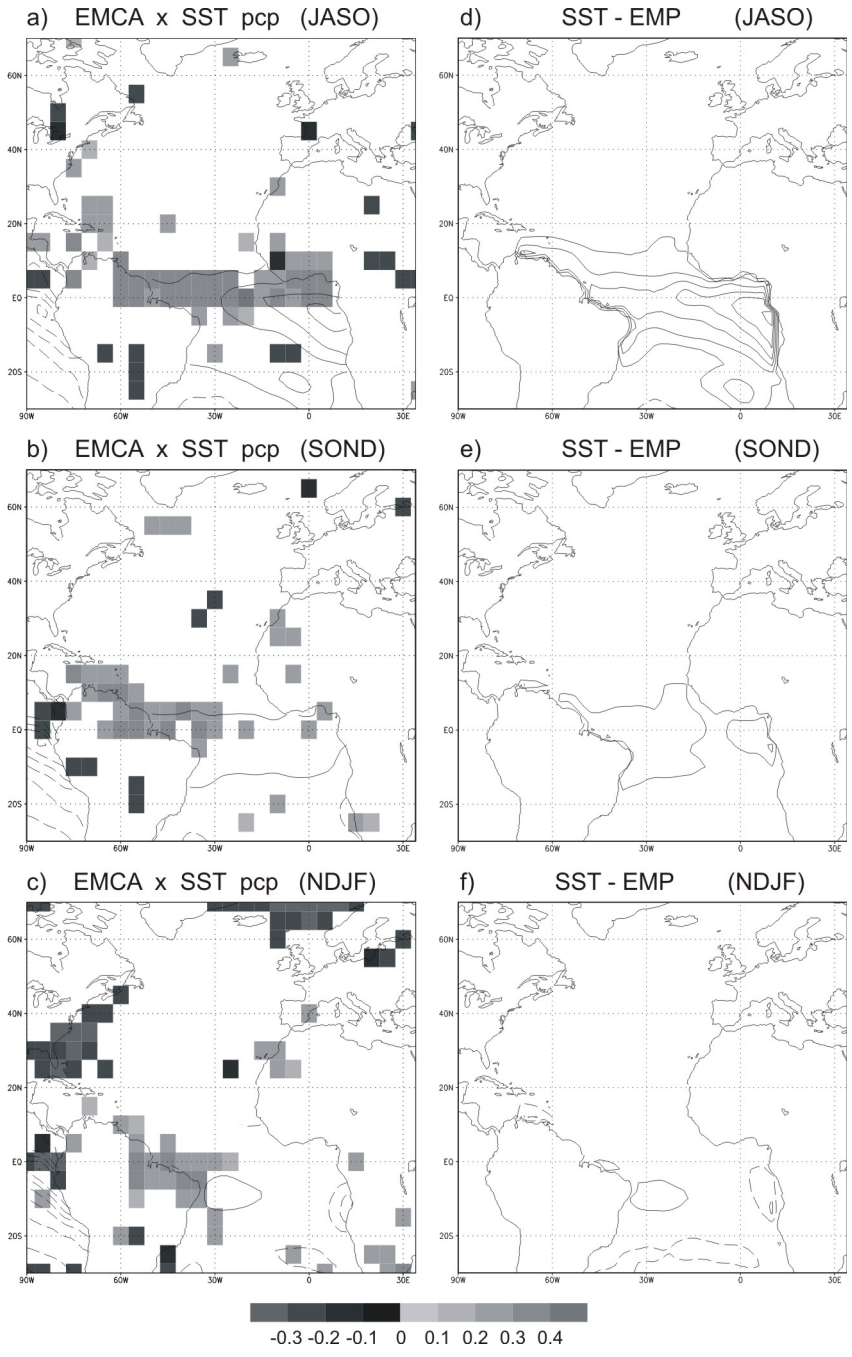

Figure 1. [left] Homogeneous and heterogeneous regression maps of respectively SST (contours; ci=0.1 ºC) and standardized precipitation (shaded) onto the observed EMCA SST expansion coefficient as in García-Serrano et al. (2008) for JASO, SOND, and NDJF. [right] Boundary conditions (SST; ci=0.3 ºC) of the time-varying prescribed EMP AGCM-simulation.

performed using monthly climatological SSTs averaged from 1979 to 2005. Throughout the whole work we will refer as the anomalous model response to Atlantic Niño to the difference between the control and the EMP runs. The significance of the response will be assessed by applying a t-test of equal means (von Storch and Zwiers 2001) at 95% of confidence level.

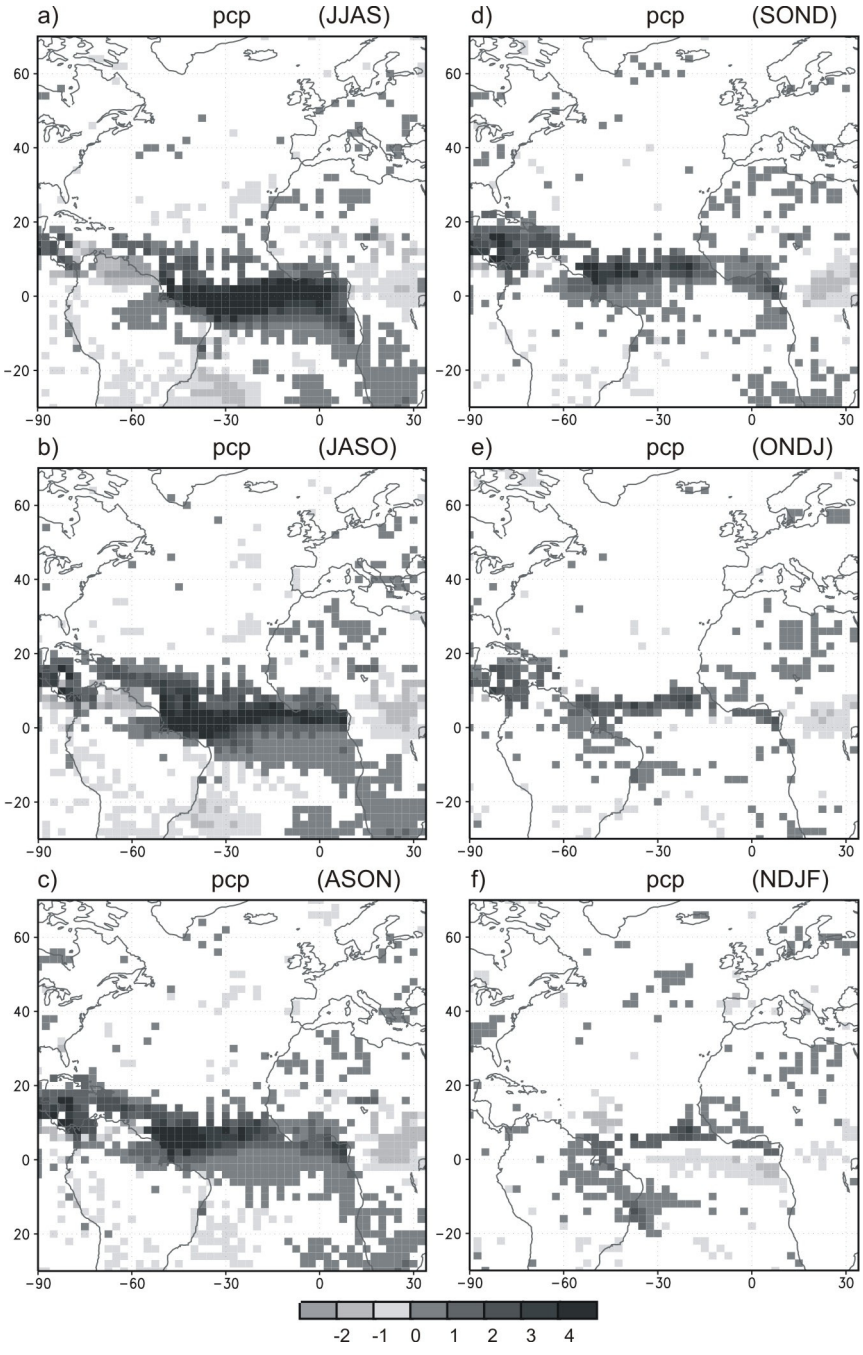

Figure 2. JJAS to NDJF ensemble-mean of precipitation (mm/day) from the EMP simulation.

3. Results

Fig. 2 represents the anomalous precipitation sequence derived from the ensemble mean of the EMP simulation. No clear rainfall pattern appears outside the tropics, in the Euro-Atlantic region, throughout the lagged seasons. As also shown in observations, the precipitation response to the Atlantic Niño damping is confined over the tropical Atlantic basin. Indeed the simulated deep-convection tightly resembles the observed evolution: covering the whole tropical band during summer (JJAS; Fig. 2a), depicting the subsequent rainfall decay during autumn (Fig. 2b-d), and

providing the final confinement of precipitation over South America in wintertime (Fig. 2e-g). Even so, it is important to mention that EMP experiment seems to be overestimating the rainfall anomalies. This feature could be explained by the magnitude of the prescribed anomalous SST itself, as the anomalous SST pattern calculated from the EMCA described in Polo et al. (2008) was multiplied by a factor of 2 in order to better capture the atmospheric response to the Atlantic Niño (see Losada et al. 2009a for further details about the experimental setup). In addition, UCLA AGCM precipitation response tends to be stronger than the observed and other models (Losada et al. 2009a; Mohíno et al. 2009).

In JJAS and JASO, positive rainfall anomalies spread out from offshore northeastern Brazil to African equatorial coastline, while negative ones are localized over northern South American continent. A weakening in the amplitude of both anomalies is noticeable from summer (JJAS; Fig. 2a) to late-summer (JASO; Fig. 2b), reflecting the first stage on the decay of the atmospheric response to SST-damping. In the subsequent season, during autumn (ASON; Fig. 2c), inland dry conditions almost vanish and anomalous deep tropical rainfall strongly weakens over the Guinean Gulf. A northward displacement of the latter is also appreciable, as well as positive precipitation anomalies over Central America-Caribbean appear to be enhanced. Later, in SOND (Fig. 2d), a general decrease in the positive precipitation anomalies goes along with the Atlantic Niño SST damping (Fig. 1e). At this stage it is worthy pointing out how anomalous convection in the central tropical Atlantic is north of equator. During early-winter (ONDJ; Fig. 2e), positive precipitation anomalies over southern Caribbean clearly weakens, disappearing in NDJF (Fig. 2f). Also in ONDJ, anomalous wet conditions appear in the eastern south-tropical Brazil covering the latitudinal window eq-10S, which tightly enhance during winter (NDJF). Related to this remaining anomalous deep convection is compensated divergent circulation (anomalous convergence; not shown), resulting in dry conditions offshore northern Brazil (east of 20W) and along the central-eastern equatorial Atlantic (Fig. 2e-f). Note that the observed subtropical subsidence over western Atlantic basin (Gulf of Florida) is not associated with the Atlantic Niño.

The simulated atmospheric response to the Atlantic Niño damping is shown in Fig. 3 through the streamfunction (contours) and derived rotational wind (arrows) at 200hPa deviations of the ensemble mean from the control run. It points out several features. First, a Rossby wave poleward propagation to central Europe seems to occur during the mature phase of the Atlantic Niño (JJAS; Fig. 3a). During the first stages of the SST decay (JASO, ASON), the forced Rossby wave-like response arches along the eastern North Atlantic basin and it finally ends up trapped into the North African-Asian jet propagating toward western North Pacific (Fig. 3b-c). In the winter hemisphere (Southern Hemisphere), where the atmospheric circulation is more intense, a well-defined arching Rossby wavetrain is present. Notice that model results do not show a robust pattern of anomalous precipitation over North Atlantic-European continent during the three first seasons (Fig 2a-c), which could be likely explained by the fact that we are looking at the summer-autumn hemisphere, where the mean flow is weak, so would be the atmospheric response. Nevertheless, as the atmospheric response over Europe is significant, especially for JJAS and JASO seasons (Fig. 3a-b), the possibility of model dependence in the lack of precipitation response for these seasons can not be ruled out.

Subsequently, from late-autumn (SOND) to winter (NDJF), the simulated atmospheric response remains depicting a Rossby wave-like propagation, but showing a marked zonal orientation from the forcing region. As proposed by Haarsma and Hazeleger (2007), and also suggested by García-Serrano et al. (2008), this SST-forced anomalies propagation appears to constitute disturbances that are meridionally confined along the main subtropical jets, which yield a hemispheric response. According to this circumglobal teleconnection pattern, their energy is not dispersed over broad a region and is able to propagate farther before being dissipated (Branstator 2002). In SOND, an anomalous anticyclonic circulation, which represents a weakening of the Aleutian low (Fig. 3d), emerges over northern North Pacific. This anomaly clearly strengthens in ONDJ (Fig. 3e) and weakens in NDJF (Fig. 3f). Following the structure of the mean flow (see Fig. 4e-f), the circumglobal response reaches Europe through North Atlantic jetstream (Hoskins and Ambrizzi 1993), but it is statistically significant only during early-winter (ONDJ; Fig. 3e).

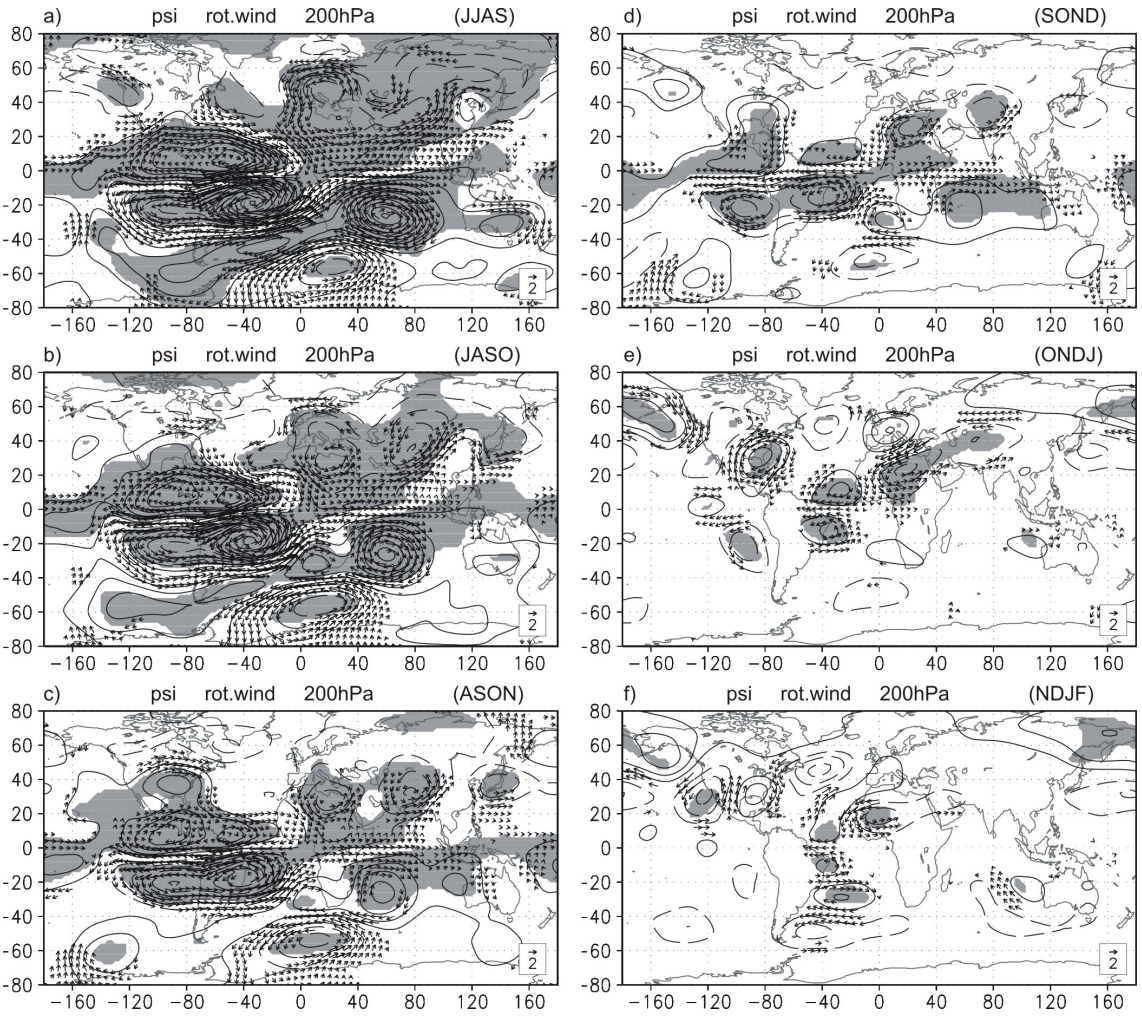

Figure 3. JJAS to NDJF ensemble-mean of streamfunction (contours; ci=106 m2/s) and rotational wind (arrows; m/s) at 200hPa from the EMP simulation.

According to the EMP simulation set-up, the weakening of the atmospheric response goes along with the time-varying equatorial mode; i.e. the Atlantic Niño damping is associated with a continuous reduction in the magnitude of the local Gill-type response. In addition, a close relationship between forced extratropical response and the latitudinal seasonal cycle seems to be operating during the SST damping. Note that the Rossby wavetrain within the North African-Asian jet reveals a southward migration from late-summer (JASO; Fig. 3b) to winter (NDJF; Fig. 3f). This feature is especially noticeable on the waveguide-jet entrance, where the anomalous cyclonic circulation is displaced from 40N (in the Mediterranean basin) in summer, to 15N (over western North Africa) in winter.

In order to better illustrate the seasonality of the atmospheric response to the Atlantic Niño damping, the model climatological wind at 200hPa (arrows) are shown in Fig. 4. Overploted in the figure is the anomalous nondivergent (or rotational) meridional component of the flow at 200hPa (contours), as this variable fairly captures the structure of the waveguided anomalies (Branstator 2002). Another consideration is that low-frequency circulation anomalies tend to be zonally confined to latitudes where the tropospheric jets are centred, while they

Figure 4. JJAS to NDJF ensemble-mean of meridional component of rotational wind at 200hPa (contours; ci=0.5 m/s) from the EMP simulation and climatological flow at 200hPa (arrows; m/s).

a) vrot clim.wind 200hPa (JJAS)

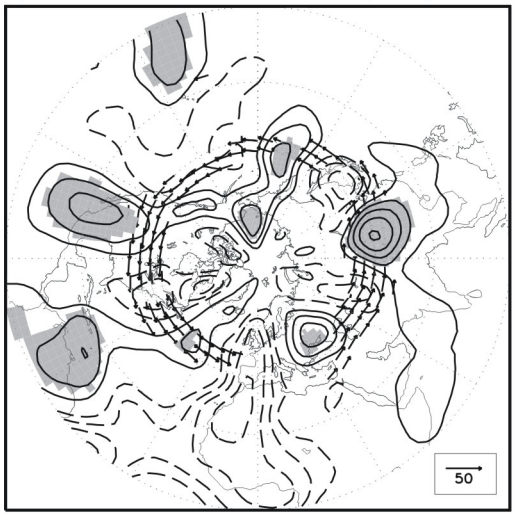

b) vrot clim.wind 200hPa (JASO)

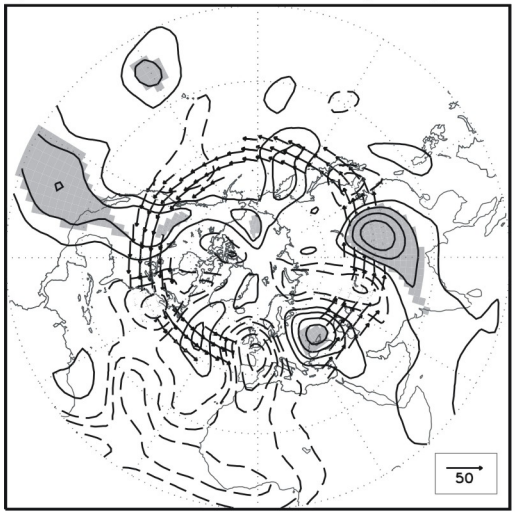

c) vrot clim.wind 200hPa (ASON)

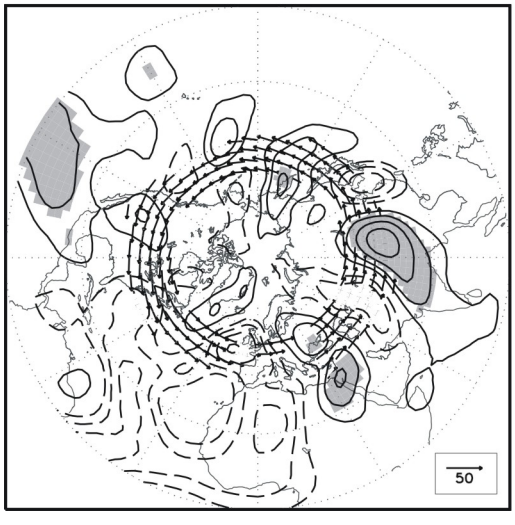

d) vrot clim.wind 200hPa (SOND)

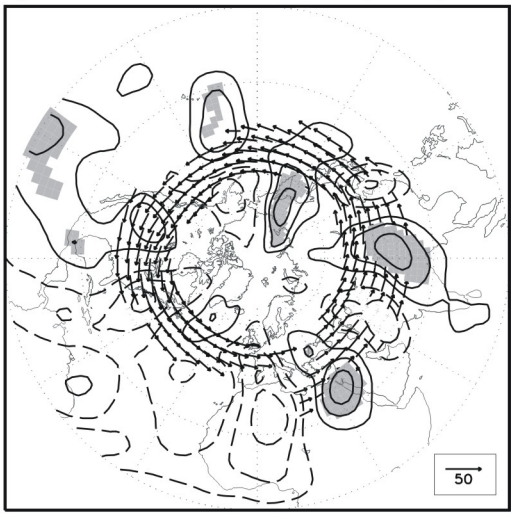

e) vrot clim.wind 200hPa (ONDJ)

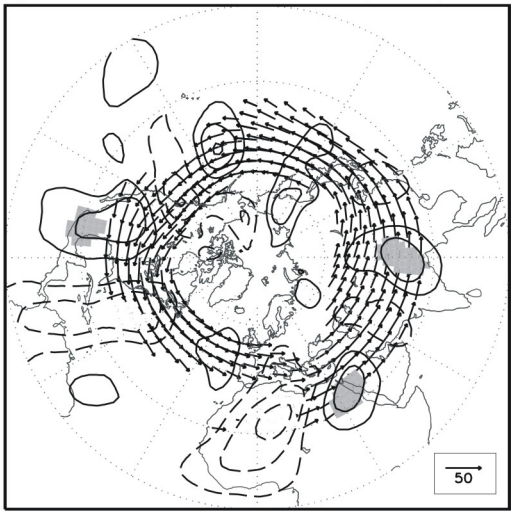

f) vrot clim.wind 200hPa (NDJF)

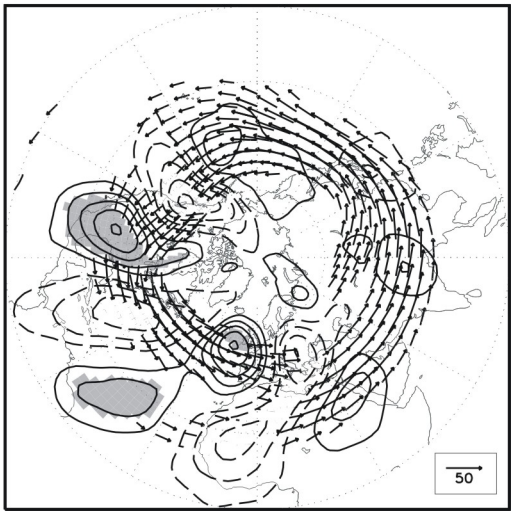

appear to propagate into a more meridional route where the influence of background jets is minimal (Branstator 1983, 2002).

According to Ambrizzi et al. (1995) and Ding and Wang (2005), the Northern Hemisphere jetstreams in summertime (JJAS-to-ASON; Fig. 4a-c) are weaker and more zonal than during winter season (SOND-to-NDJF; Fig. 4d-f). In addition, a clear difference is noticeable in the separation between the North American and Euro-Asian zonal wind maxima from summer (JJAS) to autumn (ASON). In JJAS, the climatological flow over the North Atlantic is the weakest, providing favourable conditions for a meridional propagation of the atmospheric response (Fig. 3a). Following the increase of the North Pacific zonal winds, the North Atlantic background flow strengthens in JASO and ASON (Fig. 4b-c), which would restrict the meridional extension and would force the zonal propagation to central-southern Europe (Fig. 3b-c). Note the weakening of meridional wind anomalies at high latitudes during ASON in comparison with JJAS and JASO.

The absence of circulation anomalies over the polar cap is even better depicted in SOND. At this season, a complete circumglobal teleconnection response may be identified, mainly based on the well-organized wind anomalies over the North Pacific and North Atlantic basins (Fig. 4d). That hemispheric pattern is pretty apparent during early winter (ONDJ; Fig. 4e) and winter (NDJF; Fig. 4f), when the anomalous atmospheric circulation circumscribes the Northern Hemisphere midlatitudes. As can be seen, the spiral shape of the jetstream is marked just in these three seasons, resulting in the singular elongated entrance over northern Africa in SOND and over West African coastline in ONDJ-NDJF. In conjunction with this feature, a progressive latitudinal shift of the subtropical jet occurs from autumn to winter: 40N in ASON, 25N in SOND, 20N in ONDJ, and 15N in NDJF. These two characteristics of the local background flow explain the mechanism underlying the Rossby wavetrain to be trapped into the North African-Asian jet (Fig. 3d-f), as the vorticity source is close to its entrance.

4. Summary and discussion

In this study, we have used an AGCM model (UCLA model) in order to analyze the atmospheric response to the summer Atlantic Niño damping during the last decades of the 20th century. The time period considered here (1979-2005) has a marked importance because several recent climate trends, as various worldwide phenomena have been described within it (e.g.; Fedorov and Philander 2000; Terray and Dominiak 2005; Baines and Folland 2007; Kucharski et al. 2007; Losada et al. 2009b; Rodríguez-Fonseca et al. 2009). Concerning the tropical Atlantic, our previous observational works (Polo et al. 2008; García-Serrano et al. 2008) have shown how, for this period of time, the summer Atlantic Niño is not connected with the early-winter Atlantic Niño, the Atlantic Niño II (Okumura and Xie 2006). Hence, regarding the persistence of the Atlantic Niño into autumn/early-winter, our results are in disagreement with those by Frankignoul and Kestenare (2005b) and Czaja and Frankignoul (2002); thus, being not in accordance with the experimental design of Drévillon et al. (2003), Peng et al. (2005), and Haarsma and Hazeleger (2007).

The EMP simulation has corroborated the observational hypothesis of the restoring effect of the Atlantic Niño damping in deep-convection. The simulated rainfall sequence pointed out the progressive weakening in the eastern part of the basin (Gulf of Guinea) and a clear confinement in the western part, over the Amazon convergence zone, at the end of the Atlantic Niño cycle. This return to the climatological wintertime location of the local convection (see Wang 2002) is accompanied by the evolution of the thermal forcing towards the South American coast, i.e. the decay of the summer SST anomaly (Polo et al. 2008; García-Serrano et al. 2008; Losada et al. 2009a). A recent paper, following a multi-model approach, has shown the first stage in the westward-displacement of the anomalous forced convection between the peak (May-Jun) and mature (Jul-Aug-Sep) phases of the Atlantic Niño (Losada et al. 2009b).

Model results shown here have evidenced that the Atlantic Niño damping is able to trigger a hemispheric teleconnection downstream during late-autumn and winter; and that this anomaly gets trapped into the subtropical jets, as suggested by García-Serrano et al. (2008) following the work of Haarsma and Hazeleger (2007). Even so, regarding the seasonal dependence of the atmospheric response to the Atlantic Niño, our

results agree with those by Haarsma and Hazeleger (2007) just in part. The EMP simulation suggests that the circumglobal atmospheric response is more a function of the zonal mean flow than a dependency of local tropical disturbances. That is, our results indicate that the extratropical Rossby-wave response does not depend on the amplitude of anomalous upper-level divergence, not on the seasonal perturbation of the Atlantic ITCZ. EMP outputs tend to be phase-locked to the seasonal evolution both of the North African-Asian jet entrance over the eastern subtropical Atlantic, and the North Atlantic jet exit over high latitudes. The different Rossby-wave responses to the Atlantic Niño damping show a time-evolution, from an arching pattern in summer, when the jet is weak, to a zonally-trapped propagation in winter, when the jet is strong and close to the anomalous vorticity source. This feature differs from Haarsma and Hazeleger (2007) conclusion, which stated that the ability of SST anomaly in generating sufficiently large upper-tropospheric divergence is the key player in the timing of the response. Even so, our conclusion, using a state-of-the-art AGCM, goes along with the proposed mechanism by Haarsma and Hazeleger (2007), who used an AGCM of intermediate complexity, i.e. the wintertime response to the Atlantic Niño shows a waveguided atmospheric pattern. This conclusion disagrees with the direct (tropical-extratropical) Rossby wavetrain emerging from the Caribbean, proposed by Drévillon et al. (2003), as well as with the one triggered from central-eastern tropical Atlantic to the North Atlantic, described in Peng et al. (2005).

Although our results may be model dependent, and should be taken with caution, the coherence between them and previous observational (García-Serrano et al. 2008) and modelling (Haarsma and Hazeleger 2007) works, gives us confidence on them.

Our modelling evidence of a forced circumglobal teleconnection support the conclusions of other works (Watanabe 2004; Shaman and Tziperman 2005; Li 2006) that the winter circulation anomalies over the eastern Atlantic-Mediterranean region can favour a hemispheric pattern by waveguiding effect of the North African-Asian jet. This feature represents a regional way of exciting the recurrent circumglobal waveguide pattern presented by Branstator (2002).

Nevertheless, although the SST anomalies of the 1979-2005 Atlantic Niño damping are able to produce an extratropical circumglobal response, from a realistic point of view the time declining of the Atlantic Niño observed from the 70's is too weak to generate significant climate anomalies over Europe. This result contrasts with the work of Haarsma and Hazeleger (2007), in which it was stated that the amplitude of the summer/late-summer Atlantic Niño anomalies could be important in the forecasting skill for the North Atlantic-European winter climate, due to the persistence of the mode until early winter. Even so, as the larger the energy release, the larger the trapped energy dispersion, this conclusion does not imply that an Atlantic Niño persistence (e.g. like the EM observed before 1979, or in the future climate) or an Atlantic Niño II episode, might have a stronger impact on Euro-Atlantic sector.

Finally, the model results have revealed that the thermal-forcing evolution of the summer Atlantic Niño does not play an important role in the anomalous dry conditions over the Florida Gulf, as was proposed in the observational study of García-Serrano et al. (2008). As also shown here in Fig. 1, a developing La Niña episode in the tropical Pacific is apparent in conjunction with the Atlantic Niño damping; this feature points at ENSO (El Niño-Southern Oscillation) as potential key player in producing precipitation anomalies over western subtropical basin, instead of the reinforcement of the local Hadley circulation by remaining SST/tropical convection during the last stages of the summer Equatorial Mode. Indeed, previous works have identified a strong correlation between the summer Atlantic Niño and the subsequent wintertime ENSO when focusing on the period of study used in this work, pointing to a leading of the tropical Atlantic on the tropical Pacific (Melice and Servain 2003; Keenlyside and Latif 2007; Polo et al. 2008). More recently, some modelling studies (Rodríguez-Fonseca et al. 2009; Losada et al. 2009b), have also shown how, from the last decades of the 20th century, the Atlantic Equatorial Mode is able to generate an atmospheric response over the tropical Pacific that would favour the development of an anomalous SST pattern of opposite sign in the tropical Pacific, thus confirming the potential link between Atlantic and Pacific equatorial SST anomalies. Whether the link between the tropical basins is the responsible of the precipitation anomalies found over Florida, or if they are just a response to the Pacific anomalies, is something that deserves further investigation and will be the

aim of future work. Likewise, the Atlantic-Pacific connection could have a modulating role on the extratropical atmospheric response to the Atlantic Niño damping, as well as on its influence on the European climate. This is a topic of research that also requires further study and will be the focus of the following work.

Acknowledgments.

We thank Dr. Reindert Haarsma (KNMI, The Netherlands) for his useful discussions and comments. This research was supported by the European AMMA project from the 6th Framework Research Programme, and the national CGL2006-04471 project of the Spanish Ministry of Education and Science.

References

Ambrizzi, T., B. J. Hoskins, and H.-H. Hsu, 1995: Rossby wave propagation and teleconnection patterns in the austral winter. J. Atmos. Sci., 52, 3661-3672.

Baines, P. G., and C. K. Folland, 2007: Evidence for a rapid global climate shift across the late 1960s. J. Clim., 20, 2721-2744.

Branstator, G., 1983: Horizontal energy propagation in a barotropic atmosphere with meridional and zonal structure. J. Atmos. Sci., 40, 1689-1708.

Branstator, G., 2002: Circumglobal teleconnections, the jetstream waveguide, and the North Atlantic Oscillation. J. Clim., 15, 1983-1910.

Carton, J. A., X. Cao, B. S. Giese, and A. M. Da Silva, 1996: Decadal and interannual SST variability in the tropical Atlantic Ocean. J. Phys. Oceanogr., 26, 1165-1175.

Czaja, A., and C. Frankignoul, 2002: Observed impact of Atlantic SST anomalies on the North Atlantic Oscillation. J. Clim., 15, 606-623.

Ding, Q., and B. Wang, 2005: Circumglobal teleconnection in the Northern Hemisphere summer. J. Clim., 18, 3483-3505.

Drévillon, M., C. Cassou, L. Terray, 2003: Model study of the North Atlantic region atmospheric response to autumn tropical Atlantic sea-surface-temperature anomalies. Q. J. R. Meteorol. Soc., 129, 2591-2611.

Fedorov, A., and S. G. Philander, 2000: Is El Niño changing?. Science, 288, 1997-2002.

Frankignoul, C., and E. Kestenare, 2005a: Air-sea interactions in the Tropical Atlantic: a view based on lagged rotated maximum covariance analysis. J. Clim., 18, 3874-3890.

Frankignoul, C., and E. Kestenare, 2005b: Observed Atlantic SST anomaly impact on the NAO: an updated. J. Clim., 18, 4089-4094.

García-Serrano, J., T. Losada, B. Rodríguez-Fonseca, and I. Polo, 2008: Tropical Atlantic variability modes (1979–2002). Part II: time-evolving atmospheric circulation related to SST-forced tropical convection. J. Clim., 21, 6476-6497.

Haarsma, R. J., and W. Hazeleger, 2007: Extratropical atmospheric response to equatorial Atlantic cold tongue anomalies. J. Clim., 20, 2076-2091.

Hoskins, B. J., and T. Ambrizzi, 1993: Rossby wave propagation on a realistic longitudinally varying flow. J. Atmos. Sci., 50, 1661-1671.

Huang, B., and J. Shukla, 2005: Ocean-Atmosphere interactions in the tropical and subtropical Atlantic Ocean. J. Clim., 18, 1652-1672.

Keenlyside, N. S., and M. Latif, 2007: Understanding equatorial Atlantic interannual variability. J. Clim., 20, 131-142.

Kucharski, F., A. Bracco, J. H. Yoo, and F. Molteni, 2007: Low-frequency variability of the Indian monsoon-ENSO relationship and the tropical Atlantic: the 'weakening' of the 1980s and 1990s. J. Clim., 20, 4255-4266.

Kucharski, F., A. Bracco, J. H. Yoo, and F. Molteni, 2008: Atlantic forced component of the Indian monsoon interannual variability. Gephys. Res. Lett., 35, L04706, doi : 10.1029/2007GL033037.

Kucharski, F., A. Bracco, J. H. Yoo, A. Tompkins, L. Feudale, P. Ruti, and A. Dell'Aquila, 2009: A Gill-Matsuno-type mechanism explains the Tropical Atlantic influence on African and Indian monsoon rainfall. Q. J. R. Meteorol. Soc., 135, 569-579.

Li, L. Z. X., 2006 : Atmospheric GCM response to an idealized anomaly of the Mediterranean sea surface temperature. Clim. Dyn., doi: 10.1007/s00382-006-0152-6.

Losada, T., B. Rodríguez-Fonseca, S. Janicot, S. Gervois, F. Chauvin, and P. Ruti, 2009a: A multimodel approach to the Atlantic Equatorial mode. Impact on the West African monson. Clim. Dyn., doi: 10.1007/s00382-009-0625-5.

Losada, T., B. Rodríguez-Fonseca, I. Polo, S. Janicot, S. Gervois, F. Chauvin, and P. Ruti, 2009b: Tropical response to the Atlantic Equatorial mode: AGCM multimodel approach. Clim. Dyn., doi: 10.1007/s00382-009-0624-6.

Melice, J. L., and J. Servain, 2003: The tropical Atlantic meridional SST gradient index and its relationships with the SOI, NAO and Southern Ocean. Clim. Dyn., 20, 447-464, doi: 10.1007/s00382-002-0289-x.

Mohino, E., B. Rodríguez-Fonseca, C. R. Mechoso, S. Gervois, P. Ruti, and F. Chauvin, 2009: West African monsoon precipitation response to Equatorial Pacific sea surface temperature anomalies. Dynamical mechanims. Clim. Dyn. (under review).

Okumura, Y., and S.-P. Xie, 2006: Some overlooked features of Tropical Atlantic climate leading to a new Niño-like phenomenon. J. Clim., 19, 5859-5874.

Peng, S., W. A. Robinson, S. Li, and M. P. Hoerling, 2005: Tropical Atlantic SST forcing of coupled North Atlantic seasonal responses. J. Clim., 18, 480-496.

Polo, I., B. Rodríguez-Fonseca, T. Losada, and J. García-Serrano, 2008: Tropical Atlantic variability modes (1979-2002). Part I: time-evolving SST modes related to West African rainfall. J. Clim., 21, 6457-6475.

Ritcher, I., C. R. Mechoso, and A. W. Robertson, 2008: What determines the position and intensity of the South Atlantic anticyclone in austral winter?. J. Clim., 21, 214-229.

Rodríguez-Fonseca, B., I. Polo, J. García-Serrano, T. Losada, E. Mohino, C. R. Mechoso, and F. Kucharski, 2009: Are Atlantic Niños enhancing Pacific ENSO events in recent decades?. Geophys. Res. Lett., 36, L20705, doi: 10.1029/2009GL040048.

Ruíz-Barradas, A., J. A. Carton, and S. Nigam, 2000: Structure of interannual-to-decadal climate variability in the Tropical Atlantic sector. J. Clim., 13, 3285-3297.

Shaman, J., and E. Tziperman, 2005: The effect of ENSO on Tibetan Plateau snow depth: a stationary wave teleconnection mechanism and implications for the South Asian monsoons. J. Clim., 18, 2067-2079.

Smith, T. M., and R. W. Reynolds, 2003: Extended reconstruction of global sea surface temperatures based on COADS data (1854-1997). J. Clim., 16, 1495-1510.

Sutton, R. T., S. P. Jewson, and D. P. Rowell, 2000: The elements of climate variability in the Tropical Atlantic region. J. Clim., 13, 3261-3284.

Terray, P., and S. Dominiak, 2005: Indian Ocean sea surface temperature and El Niño-Southern Oscillation: a new perspective. J. Clim., 18, 1351-1368.

Vizy, E. K., and K. H. Cook, 2002: Development and application of a mesoscale climate model for the tropics: influence of sea surface temperature anomalies on the West African monsoon. J. Geophys. Res., 107, D3, 4026, doi: 10.1029/2001JD000686.

von Storch, H., and F. W. Zwiers, 2001: Statistical analysis in climate research. Cambridge University Press, UK.

Wang, C., 2006: An overlooked feature of tropical climate: inter-Pacific-Atlantic variability. Geophys. Res. Lett., 33, L12702, doi: 10.1029/2006GL026324.

Watanabe, M., 2004: Asian jet waveguide and downstream extension of the North Atlantic Oscillation. J. Clim., 17, 4674-4691.

Xie, S.-P., and J. A. Carton, 2004: Tropical Atlantic variability: patterns, mechanisms, and impacts. In Earth Climate: The Ocean-Atmosphere interaction, C. Wang, S.-P. Xie, and J. A. Carton (eds.), Geophys. Monograph., AGU, Washington DC.

Zebiak, S. E., 1993: Air-sea interaction in the equatorial Atlantic region. J. Clim., 6, 1567-1586.

IV.4.

Respuesta atmosférica de gran-escala a las anomalías estivales en el Mediterráneo Oriental

García-Serrano, J., I. Polo, B. Rodríguez-Fonseca y T. Losada (2010): Large-scale atmospheric response to Eastern Mediterranean summer SST anomalies. Clim. Dyn., (submitted).

Estudios recientes han mostrado que el estado anómalo de la superficie del Mar Mediterráneo oriental influye fuertemente en el sistema monzónico de África Occidental, no sólo aumentando el contenido de humedad en la baja troposfera sino también forzando anomalías en la circulación. Observaciones y experimentos de sensibilidad son analizados aquí para dar evidencias de una respuesta atmosférica de gran escala asociada a esas anomalías en la superficie del Mediterráneo, cuyo máximo está al este de la cuenca. Los resultados apoyan la hipótesis de un patrón hemisférico iniciado en dicha región, mostrando tanto una respuesta baroclínica local como una circulación circunglobal barotrópica. Este patrón de teleconexión atmosférica se extiende a lo largo de las latitudes medias del Hemisferio Norte, reflejando el efecto guía de onda de las corrientes en chorro del oeste, y presenta un impacto en superficie sobre el Pacífico Norte y Euro-Asia.

Large-Scale Atmospheric Response to Eastern Mediterranean Summer SST Anomalies

Javier García-Serrano, Irene Polo, Belén Rodríguez-Fonseca, Teresa Losada

Departamento de Geofísica y Meteorología, UCM, Madrid, Spain

(Climate Dynamics, submitted)

ABSTRACT

Recent studies have shown that anomalous state of the Mediterranean Sea strongly influences the summer African monsoon system, not only enhancing the humidity content of the lower troposphere but also forcing circulation anomalies. Observations and modelling experiments are analysed in order to give evidences of a large-scale atmospheric response associated with those Mediterranean surface anomalies, which maximum is over the eastern basin. Results support the hypothesis of a hemispheric pattern initiated in the Mediterranean basin, pointing out both a local baroclinic response and a barotropic circumglobal circulation. This atmospheric teleconnection pattern extends to the entire Northern Hemisphere midlatitudes, reflecting the waveguide effect of the westerly jet, and it has a surface impact on the North Pacific and Euro-Asia.

1. Introduction

The Mediterranean sea surface temperature (SST) is a small region in the water masses system, but it seems to have a notable role in some climatic phenomena. On the one hand, a number of works have evidenced the Mediterranean thermal-forcing of the West African Monsoon (WAM), in particular of the summertime Sahelian rainfall (Rowell 2003; Fontaine et al. 2003; Jung et al. 2006; Polo et al. 2008). In addition to these studies, which had a marked regional point of view in the relationship, Fontaine et al. (2009) have added large-scale features in the Mediterranean-Sahel covariability, showing forced changes in the Atlantic ITCZ (inter-tropical convergence zone) and a baroclinic structure over southeastern Mediterranean basin. Moreover, they reported a weakening of the climatological northeasterly flow east of 10E, over Egypt, associated with the low-level convergence found in the southeastern Mediterranean basin. This is consistent with both low-level pressure anomalies described in the observational work by Raicich et al. (2003) and decrease in the north-easterly climatological winds, depending on the thermal contrast between African continent and the Mediterranean Sea, suggested from an idealized 2D-model by Peyrillé et al. (2007).

On the other hand, and during boreal winter, other works have pointed out the importance of the Mediterranean basin in favouring the establishment of a hemispheric pattern which resembles the Artic Oscillation (Kodera and Kuroda 2003; Watanabe 2004). Diagnoses using a linear barotropic model, shown by Watanabe (2004), indicate the downstream propagation of Rossby waves trapped on the North African-Asian jet (Hoskins and Ambrizzi 1993; Ambrizzi et al. 1995) which is effectively excited by the anomalous upper-level convergence over the Mediterranean. In addition, and also following the relevant outcomes by Branstator (2002), Li (2006) hypothesised and demonstrated the ability of the Mediterranean winter SST anomalies in forcing a global-waveguided atmospheric response. Two remarkable remote signals were shown: the deepening of the Aleutian Low in the North Pacific and the weakening of the Iceland Low in the North Atlantic. The main objective of this work is to investigate whether this teleconnection can be also acting during summertime since the impact of the Mediterranean summer SST on the global atmospheric circulation has not yet been well documented. On this subject, Ding and Wang (2005) have evidenced a recurrent summer

circumglobal pattern, similar to that found by Branstator (2002) for winter, thereby giving certain robustness to our hypothesis.

As shown by Xoplaki et al. (2003a, b) and Fontaine et al. (2009), the Mediterranean SST variability has two well separated summer modes: first, a zonal mode with higher SST scores in the western part of the basin, over the Balearic and Ligurian seas; and second, another zonal mode but with maximum amplitude in the eastern part, over the Jonian and Aegean seas. The former has been suggested to have a more passive role in the Mediterranean-WAM connection (Baldi et al. 2004), while the latter is tightly linked to anomalous Sahelian regime (Rowell 2003; Fontaine et al. 2009).

The starting point of this work comes from a recent paper of the authors (Polo et al. 2008), in which the active role of the summer Mediterranean SST (eastern pattern) onto the WAM variability shows an evolution with a realistic persistence from early-spring to late-autumn, recovering the same June to September (JJAS) surface mode found by Xoplaki et al. (2003a, b). Monsoonal precipitation associated with these SST anomalies, confined over the eastern part of the basin, has been identified during late-summer (Fontaine et al. 2009). Hence, the focus of the study is on JJAS season and one month-lag forward (July to October; JASO). The corresponding SST anomalies shown in Polo et al. (2008) are reproduced in Fig. 1.

This work constitutes a further step in the understanding of the connections between Mediterranean and climate variability, leaving the Mediterranean-WAM link aside and focusing the study on the anomalous atmospheric circulation in response to the surface thermal forcing. In particular, the main scope of the present manuscript is to investigate the mechanism involved in the summer global-teleconnection associated with the eastern Mediterranean mode (Fig. 1).

The atmospheric and SST fields used in the work are detailed in the next section; followed by a description of the observational (Section 3) and modelling (Section 4) results, and a discussion of these findings (Section 5).

2. Datasets

Using an extended-maximum covariance analysis (EMCA) Polo et al. (2008) described the time-varying Mediterranean SST anomalies, from February-to-March (FMAM) until September-to-December (SOND), associated with JJAS-summer WAM. They found that the first time-evolving SST mode reveals both the development and the damping of the eastern Mediterranean pattern; while related precipitation anomalies project onto the Sahel rainfall season. In that study, the 1979-2002 monthly Climate Prediction Center (CPC) Merged Analysis of Precipitation (CMAP; Xie and Arkin 1997) and Extended-Reynolds SST (Smith and Reynolds 2003) were used (also in Fig. 1). The implemented EMCA methodology is an extension of the classical Maximum Covariance Analysis (MCA or SVD; Bretherton et al. 1992) by introducing more than one time-lag in one of the field. This kind of statistical method was used with the aim of taking into account the monthly evolution of the interannual covariability SST mode, whereby EMCA highlights the seasonal dependence of the significant covariant SST patterns (also in García-Serrano et al. 2008).

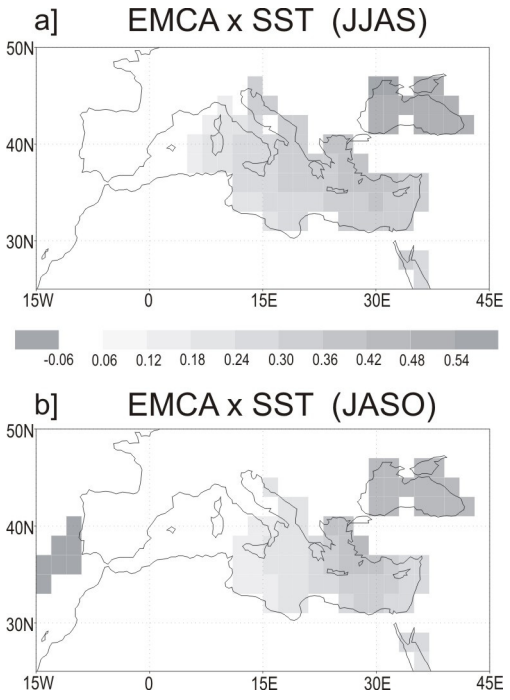

Figure 1. Regression maps of JJAS (a) and JASO (b) SST (ºC) onto the first SST EMCA expansion coefficient between FMAM-to-SOND Mediterranean SST (28N-46N/7W-42E) and JJAS West African precipitation (5S-32N/21.25W-33.75E). Only 98% statistically significant areas are plotted. [Adapted from Polo et al. 2008]

Complementary to this, a sensitivity experiment is analysed using an atmospheric general circulation model (AGCM) with boundary conditions derived from Polo et al. (2008). The aim of the simulation was to investigate the above-mentioned evidences, isolating the influence of the Mediterranean Sea on WAM. The experimental setup as well as the forcing fields is described in detail by Fontaine et al. (2009). The sensitivity simulation considered here was performed with the UCLA AGCM model (Ritcher et al. 2008) version 7.3 with a horizontal resolution of 2º lat x 2.5º lon and 29 sigma levels.

Both works (Polo et al. 2008; Fontaine et al. 2009) were conducted in the frame of the AMMA-EU project (African Monsoon Multidisciplinary Analyses); while the present manuscript attempts to get new insights into the global approach of the atmospheric response to Mediterranean summer SST anomalies. In that project, four AGCMs took part in the intercomparison exercise but only the UCLA model enlarged its integration to autumn after monsoonal season.

Observational results are presented in terms of regression maps, obtained by projecting different fields onto the first EMCA SST expansion coefficient (as in Polo et al. 2008). To study the atmospheric circulation involved in the teleconnection found, zonal wind at 200hPa (U200), geopotential height from 1000 to 100 hPa, and streamfunction at 200hPa are extracted from the 40-years ECMWF re-analysis project (Uppala et al. 2005) for the period 1979-2002. Statistical significance is addressed using a correlation two-tailed Student's t-test at 98% confidence level.

Model data comes from the ensemble of 10 runs where each member differs in its atmospheric initial conditions. The SST-forcing fields were added to 1979-2005 climatology; and the anomalous model response is referred as the difference between the corresponding sensitivity experiment and the control run (see Fontaine et al. 2009). In this case, air temperature at 850hPa and streamfunction at 850hPa and 200hPa together with U200 are used; while the statistically significant areas are obtained according to an equal means Student's t-test at 95% confidence level.

3. Results

3.1. Observed circulation

In order to gain an insight into the anomalous global circulation related to eastern Mediterranean SST mode (Fig. 1), Fig. 2 shows the regression maps of the geopotential height vertical profile (1000-100hPa), averaged along the Mediterranean Sea axis (30N-40N), onto the EMCA-SST expansion coefficient for JJAS (Fig. 2a) and JASO (Fig. 2c). These longitude-by-height profiles reveal a clear and useful picture. Consistent with the surface warming showed in Figs. 1a-b are evident the negative geopotential anomalies over the Mediterranean region, reflecting the low-level convergence associated with a thermal sea-air interaction. This result is in close agreement with Raicich et al. (2003) and Fontaine (2009). As it can be also seen, such a lower-tropospheric response is accompanied by positive geopotential anomalies (anticyclonic circulation) in the upper-troposphere, involving a local baroclinic structure. Although this kind of atmospheric feature is more proper to subtropical and tropical regions, a similar response in the Mediterranean was found by Li (2006) in his wintertime sensitivity experiment. Following those arguments, it is also shown that, except for this local baroclinic anomaly, the atmospheric circulation yields a quasi-barotropic structure worldwide along the Northern Hemisphere midlatitudes. This result supports the hypothesis of a summer circumglobal pattern initiated in the Mediterranean Sea.

Persistent positive anomaly (anticyclonic circulation) appears in the North Pacific basin, roughly over 150E-150W (Figs. 2a, c). Anticyclonic anomalies are also apparent over the North American continent, east of 120W, and in the North Atlantic Ocean, east of 60W. The statistical significance of these anomalies seems to indicate that there is a more downward penetration during JJAS than during JASO. On its part, without a significant change between JJAS and JASO, positive geopotential anomalies also appear at mid-high levels over 120E, in the eastern part of China-Mongolia.

An interesting point must be highlighted. Two consecutive seasons have been chosen with the aim of providing a reliable observational evidence of the anomalous atmospheric circulation associated with the Mediterranean thermal forcing, because it is difficult to test solely on the basis of observational analysis. In fact, it is worthy to mention that there is no observational evidence so far of the winter hemispheric response to Mediterranean SST-forcing found by Li (2006). Since the atmospheric

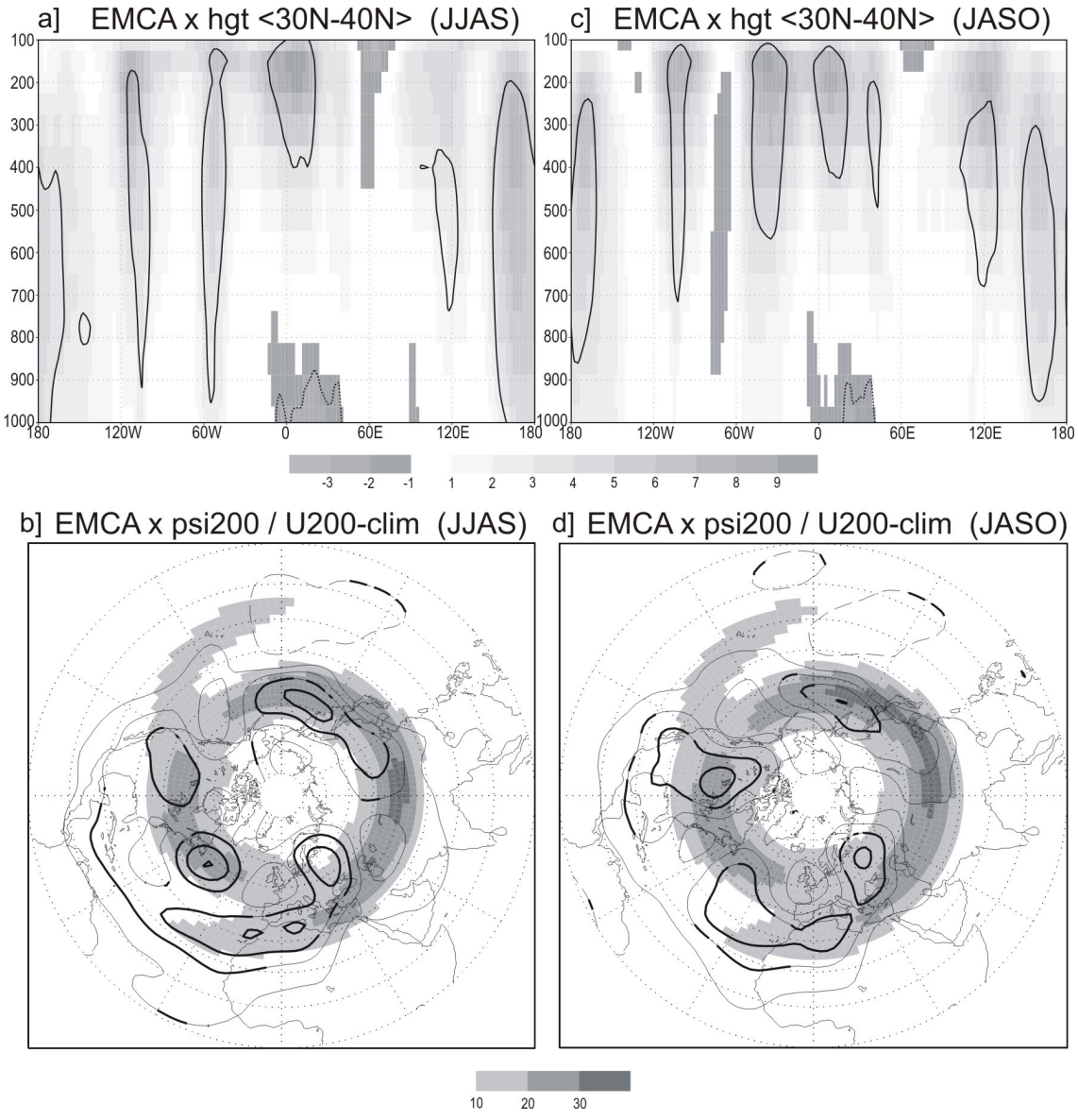

Figure 2. Regression vertical profiles of geopotential height averaged over 30N-40N (a,c; shaded,m) and regression maps of streamfunction at 200hPa (b,d;contours,ci=5m) onto the first SST EMCA expansion coefficient during JJAS (left) and JASO (right). Observational climatology of zonal wind at 200hPa is also plotted in bottom panels for each season (shaded, m/s). Statistically significant areas at 98% level are contoured (bolded) in top (bottom) panels.

JJAS-JASO anomalies are fairly identical one to each other (Figs. 2a, c) the possible circumglobal teleconnection could be reflecting the Rossby wavetrain propagation from a stationary vorticity source. Additionally, due to the atmosphere has not inertia, these results seem to indicate that the local baroclinic anomaly and downstream propagation are thermally-driven.

The hypothesis by which the eastern Mediterranean SST pattern is capable of triggering a global atmospheric response will be addressed in the next section through the AGCM sensitivity experiment. As previously reported, the variability of the thermal low over the eastern Mediterranean (Maheras et al. 1999) also produces a local baroclinic structure (Ferranti and Viterbo 2006; Fischer et al. 2007; Haarsma et al. 2009), which could also excite a hemispheric teleconnection; however, this is out of the scope of the present study.

In order to test the waveguiding mechanism proposed for the atmospheric circulation related to the Mediterranean warming, trapped anomalies propagation has to be evidenced. Fig. 2b and Fig. 2d show the regressed streamfunction anomalies at 200hPa (ψ200; contours) and the mean westerly jet (shaded) in the two EMCA seasons, JJAS and JASO respectively. It is clearly seen that ψ200 anomalies are mostly confined along a wide-latitudinal band (40N-50N), extending to the entire Northern Hemisphere midlatitudes and reflecting the downstream extension into the westerly jet. Concretely, this circumglobal pattern has a zonal wavenumber-5 presenting prominent centres of action. A persisting anomalous anticyclone dominates the north-eastern Europe, which is the only one within 50N-60N belt following the spiral shape of the mean flow (Ding and Wang 2005). An elongated lobe reaches from eastern Eurasia to western North Pacific, with two clear centres in JJAS and only one significant in JASO. Another positive ψ200 anomaly appears over North America, which reinforces in JASO; while, the anomalous anticyclonic circulation in the North Atlantic basin weakens from late-summer (JJAS) to early-autumn (JASO).

These results bear a strong resemblance to the circumglobal teleconnection revealed by Ambrizzi et al. (1995) and Ding and Wang (2005) in its spatial structure and the locations of the centres, thereby supporting the dynamics suggested for the hemispheric pattern in Figs. 2a,c. This wavetrain pattern is also reminiscent of that one from wintertime simulation performed by Li (2006), adding a confident degree to the interpretation in terms of Mediterranean forcing. Finally, the spatial structure shown in Fig. 2b-d closely resembles the mid-upper tropospheric pattern found by Xoplaki et al. (2003a, b) over the Euro-Mediterranean area associated with the eastern-SST mode.

3.2. Model evidence

The first simulation analysed is that one performed with positive SST anomalies, hereafter referred to as AGCM-P (Fig. 3); whereas the negative case prescribing the opposite in sign anomaly, indicated as AGCM-N (Fig. 4), is discussed later.

Accompanying the ensemble-mean of ψ200 anomalies (contours) is the U200 climatology (shaded) of the UCLA-AGCM model for late-summer (JJAS; Figs. 3a, 4a) and early-autumn (JASO; Figs. 3c, 4c). As can be seen, the model underestimates the subtropical branches of the observed main jetstreams over the North Pacific and North Atlantic basins during JJAS (Fig. 2b versus Fig. 3a); while this feature is better captured in JASO (Fig. 2d). The zonal extension and the latitudinal location of the jets are well represented in the climatological model-flow for both seasons; although the wind maximum in the North American continent is overestimated and that one over Asia is underestimated. In general terms, the UCLA-AGCM depicts quite reliable zonal wind climatology at upper-levels.

The bottom panel of Fig. 3 presents the ensemble-mean of ψ850 (streamfunction at 850hPa) anomalies for JJAS (Fig. 3b) and JASO (Fig. 3d) from the AGCM-P simulation. According to Fontaine et al. (2009), a clear baroclinic structure appears over the eastern part of the Mediterranean area during both seasons: negative streamfunction anomalies at low-levels and positive ones at high-levels. Based on the experimental design (AGCM study), this local response is associated with a SST-forcing, i.e. the eastern Mediterranean pattern.

Following the Fontaine et al.'s (2009) arguments, this local low-level anomalous convergence reduces the sea-continent thermal contrast and forces the weakening of the climatological northeasterly winds in the African continent, resulting in anomalous southwesterly flow (not shown). This would favour the northward intrusion of warm and dry air from central North Africa. Although reduced, the remaining northeasterly flow would also produce the advection of anomalous air temperature from the Mediterranean. In conjunction, these near-surface disturbances would yield an anomalous warming over northeast Africa. This feature is illustrated here by means of the ensemble-mean of T850 (air temperature at 850hPa) anomalies (shaded in Figs. 3b-d). This regional impact of the eastern Mediterranean SST pattern was not reported by Fontaine et al. (2009); it is new and will be a subject for future investigation.

As also shown in observations (Fig. 2b-d), the positive ψ200 anomaly related to the baroclinic structure consists of an extended centre of action at 30E (Figs. 3a-c). A close inspection to ψ200 and ψ850 (Figs. 3a-b,c-d) anomalous patterns reveal that this latitudinally elongated anticyclone has two different centres: one over the eastern Mediterranean basin, and other over the

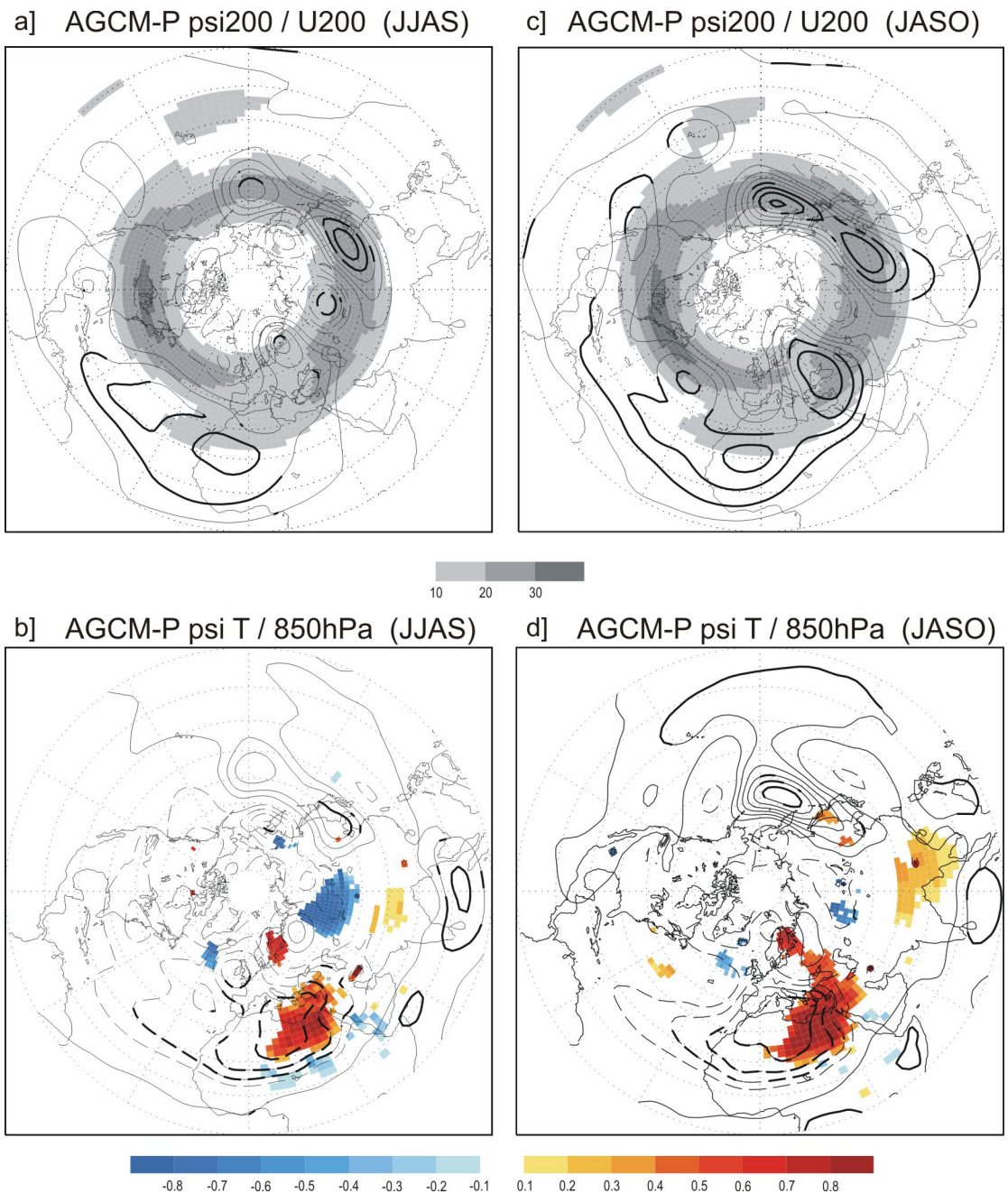

Figure 3. JJAS (left) and JASO (right) ensemble-mean of streamfunction at 200hPa (a,c;contours,ci=0.5 106 m2/s) and 850hPa (b,d;contours,ci=0.2 106 m2/s) from the Mediterranean positive-SST runs. Model climatology of zonal wind at 200hPa is plotted in top panels for each season (shaded, m/s). Ensemble-mean of air temperature at 850hPa is shown in bottom panel for each season (shaded, ºC). Statistically significant areas at 98% level are bolded for contours and gridded for shading.

northeastern Europe. The former rightly depicts the local SST-forced baroclinic structure; and the latter points out a quasi-barotropic structure, showing the characteristic westward-upward tilt of stationary Rossby wavetrain propagation (Lau 1979; Hsu and Wallace 1985). This result indicates that anomalous anticyclonic circulation over northeastern Europe is consequence of the circumscribed atmospheric response. Note that circulation anomalies follow the southwest-northeast orientation of the North Atlantic jet. At low-levels, this quasi-barotropic positive anomaly

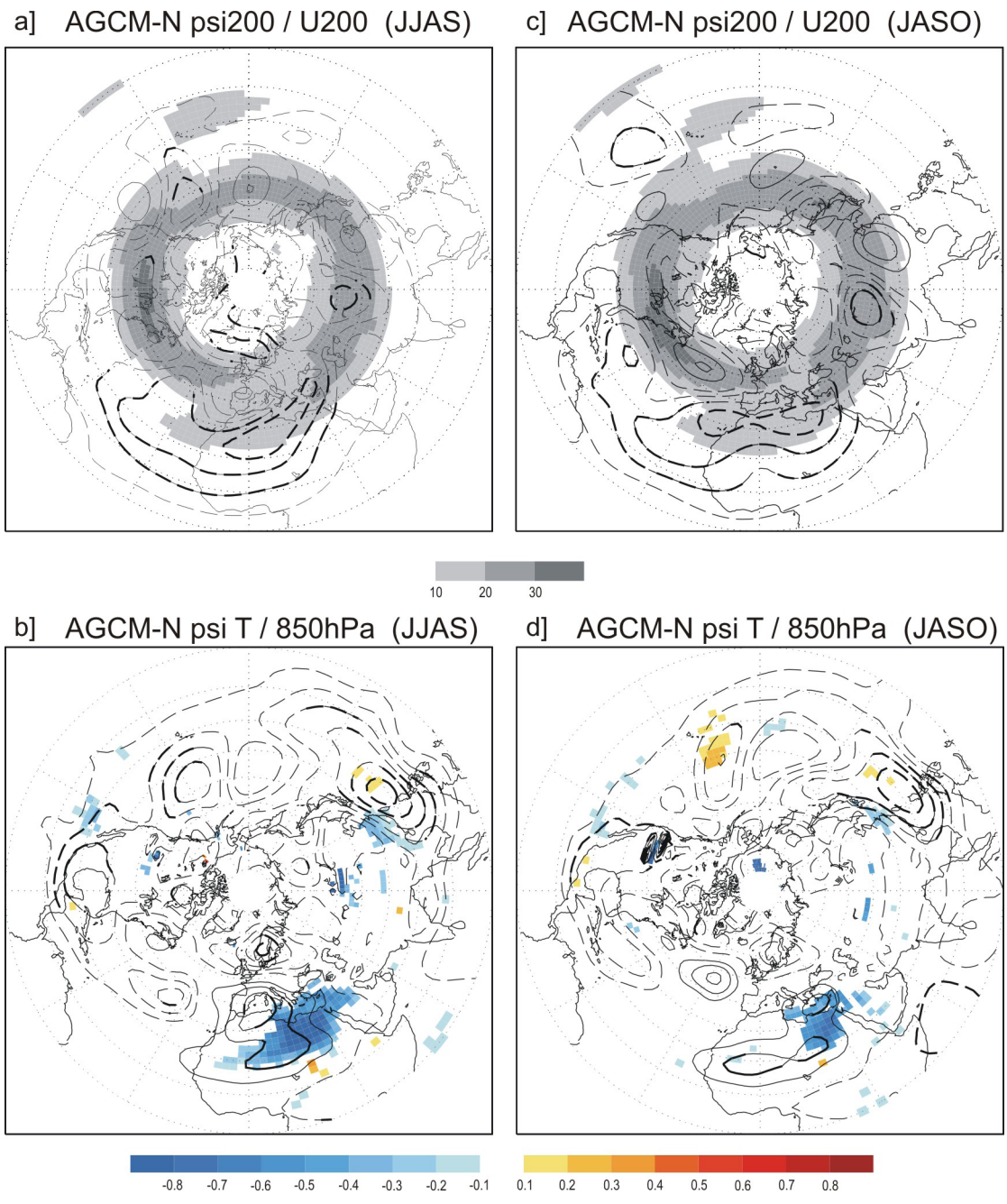

Figure 4. As Fig. 3 but for the Mediterranean negative-SST runs.

produces above-normal air temperatures in the Scandinavian Peninsula (Figs. 3b-d).

From an hemispheric approach, the upper-tropospheric response to AGCM-P strongly projects onto the observed anomalous circulation, in both JJAS (Figs. 2b, 3a) and JASO (Figs. 2d, 3c). The simulated atmospheric responses also reveal a wavenumber-5 pattern, although the centres of action in North America and the North Atlantic are lesser evident during late-summer than early-autumn.

Downstream of the baroclinic response, a clear anomalous cyclone appears in the middle of Eurasian continent. At upper-levels, this centre of action is statistically significant only in JJAS. However, at low-levels, the associated cyclonic

circulation (not significant) produces negative T850 anomalies east of Caspian Sea in both seasons, although stronger during late-summer (Figs. 3b-d). Further downstream, the circumglobal pattern shows persistent and deep positive ψ200 anomalies over eastern Asia and western North Pacific. The centre of action over China-Mongolia region remains unaltered between JJAS and JASO, while the corresponding in the North Pacific basin reinforces in JASO (Figs. 3a-c). At low-levels, those streamfunction anomalies seem to project onto one signature surrounding the Japanese islands. This barotropic anomaly yields significant positive T850 anomalies only during early-autumn (Figs. 3b-d).

Upstream of the baroclinic response, the large-scale anomalous circulation meanders in the North Atlantic basin showing a clear anomalous cyclone over western Europe (Figs. 3a-c). The associated negative circulation anomalies at low-levels advect cold air from higher latitudes into central North Atlantic both in JJAS and JASO (Figs. 3b-d). Also noticeable is the stronger meridional component in the meandering during early-autumn, resulting in a clear anomalous anticyclone at 200hPa (Fig. 3c) and positive T850 anomalies over western midlatitudes (Fig. 3d).

In case of cold SST-conditions over the eastern Mediterranean, the AGCM-N simulation, the opposite in sign local baroclinic structure is rightly produced: positive streamfunction anomalies at 850hPa (anticyclonic circulation; Figs. 4b-d) and negative streamfunction anomalies at 200hPa (cyclonic circulation; Figs. 4a-c). This atmospheric structure is associated with anomalous subsidence at low-levels. In this way, the opposite regional impact is observed over northeastern Africa (Figs. 4b-d). The reverse in T850 anomalies would be related to both, enhanced southwestward flow in the direction of the climatological winds, and to northeasterly advection of anomalous air temperature from the Mediterranean Sea. Further research is needed to resolve this issue.

At upper-levels, the atmospheric response in AGCM-N shows a clear circumglobal pattern along the entire Northern Hemisphere (Figs. 4a-c). Indeed, this hemispheric pattern is prettier apparent than in AGCM-P (Figs. 3a-c); although the statistical significance of the circulation anomalies is reduced. This waveguided response remains having a zonal wavenumber-5 structure. Following the main westerly jets, the atmospheric response presents anomalous cyclonic circulations in the middle of Eurasia, over Japan, central-eastern North Pacific, North America, and the Euro-Atlantic sector. The amplitude and the significant score of each centre of action strongly depend on the season considered.

The simulated large-scale response significantly impacts on the Tibetan Plateau, with a slight strengthening from JJAS to JASO (Figs. 4a-c). This anomalous circulation downstream of the baroclinic response yields, however, a scarce impact at low-levels (Figs. 4b-d). The meandering of the trapped anomalies along the North Pacific basin project on a more significant ψ850 signature in JJAS than in JASO; whilst the associated air temperature impact reveals a clearer wave-like pattern in JASO than in JJAS. In the North Atlantic-European region, the tail of the circumglobal response shows a deep cyclonic anomaly over the Scandinavian Peninsula during both seasons (Figs. 4a-c). Nevertheless, it is significant only in JJAS; whereas no significant T850 anomaly is found at any time (Figs. 4b-d).

4. Summary

In this study, we have used the AGCM-UCLA model in order to analyze the atmospheric response to the eastern Mediterranean summer SST anomalies during the last decades of the 20th century. The time period considered here (1979-2005) has a marked importance because several recent climate trends, related to various worldwide phenomena, have been described within it (e.g.; Fedorov and Philander 2000; Terray and Dominiak 2005; Baines and Folland 2007; Kucharski et al. 2007; Losada et al. 2009b; Rodríguez-Fonseca et al. 2009). Concerning the Mediterranean basin, recent works show how the Mediterranean-WAM link has given up being the imprint of a remote forcing on WAM variability; and how the Mediterranean Sea is playing a role as isolated entity (Mohíno et al. 2010; Rodríguez-Fonseca et al. 2010). Hence, special attention has to be paid to improve our understanding of the relation between the Mediterranean SST variability and the climate. This may lead to untapped predictability sources and contribute to the success of seasonal forecasting system.

In this study, we have shown from observations that the eastern Mediterranean summer-

early autumn SST is associated with both a local baroclinic structure over the basin and a quasi-barotropic anomalous circulation along the Northern Hemisphere midlatitudes. Our hypotheses were that the former can be forced by the Mediterranean SST itself, and the latter reflects the waveguiding effect of the climatological westerly jetstreams.

According to Fontaine et al. (2009), model results shown here have confirmed that eastern Mediterranean basin is able to trigger a local baroclinic response during late-summer (JJAS) and early-autumn (JASO); which presents low-level convergence (subsidence) and upper-level anticyclonic (cyclonic) circulation anomalies over the Mediterranean-northern Africa region associated with warm (cold) SST conditions. This baroclinic response seems to produce a regional climate impact in the Egypt-Niger sector. However, this relationship is out of scope of this work and deserves further investigation. Indeed, we have explored the dynamics of the large-scale atmospheric circulation related to that local baroclinic response.

Contrary to Fontaine et al. (2009), who found an asymmetry in the Mediterranean-WAM link between positive and negative SSTs, AGCM results shown here suggest that eastern Mediterranean SST anomalies have a not negligible influence on the hemispheric atmospheric circulation in both thermal phases. The atmospheric response forced by the eastern Mediterranean basin has a horizontal structure with a zonal wavenumber-5, which strongly projects on the recurrent circumglobal teleconnection pattern found by Ding and Wang (2005). The model waveguided response consists of circulation anomalies trapped within the main westerly jets, which circumscribe the entire midlatitudes belt and have a reduced meridional component. The influence of the Mediterranean-forced teleconnection on the hemispheric circulation reveals centres of action, downstream of the baroclinic response, over middle Eurasia and western North Pacific following the North African-Asian jet. Further downstream, along the tail of the atmospheric teleconnection, the eastern Mediterranean SST affects the circulation over the Euro-Atlantic sector following the North Atlantic jet.

The model evidences shown here, together with conclusion by Black and Sutton (2007) for the western Mediterranean pattern, suggest that the summer Mediterranean Sea may play an important role in the development of climate anomalies over Europe. On the other hand, our result complements those by Li (2006) who described the ability of the eastern Mediterranean SST to initiate a global atmospheric teleconnection during wintertime.

Nevertheless, dedicated modelling efforts are required in order to provide further support to our evidences. First, a larger number of members in the ensemble exercise are needed than in the AMMA-experiment protocol (10 members) with the aim of assessing a more significant (and robust) signal. Second, a transient approach (daily sequence) in the experimental set-up would be useful to better illustrate the mechanism controlling the circumglobal response to Mediterranean SST (as Li 2006). Third, a couple ocean-atmosphere GCM experiment with an initial-value approach of the forcing (as Wu et al. 2007) would correct the limited conclusions from AGCMs, which in turn would allow to track the evolution of SST and associated atmospheric response.

Derived from the results shown here, further study requires the potential changes in the North African-Asian jet configuration (Baldi et al. 2006, 2009) by means of different impact during warm and cold summertime conditions in the Mediterranean Sea. This is envisaged from the apparent slant seen in the remote impacts of the warm-SST on the Euro-Atlantic sector and of the cold-SST on the North Pacific basin.

The model results reported here support the conclusions of others (Watanabe 2004; Li 2006) that the circulation anomalies over the Mediterranean basin can favour a hemispheric pattern by waveguiding effect of the North African-Asian jet. This feature is also consistent with Jung et al. (2006), who found wave-like disturbances along northern midlatitudes prescribing summer SST anomalies over the western part of the Mediterranean Sea.

From this scenario, it is arguably that the variability of the thermal low over eastern Mediterranean (Maheras et al. 1999) could also initiate a global atmospheric teleconnection influencing the weather and the climate for remote regions, as it presents a baroclinic structure (Haarsma et al. 2009). Such a baroclinic pattern is also reminiscent of the climate change response over the Mediterranean area in summertime (Haarsma et al. 2009), implicating that this potential hemispheric circulation may be important in future

climate. On the other hand, the continental-scale wave pattern associated with this type of thermal low (Ferranti and Viterbo 2006; Fisher et al. 2007) could represent a regional signature of an excited circumglobal response. Likewise, similar baroclinic structures in the Mediterranean basin remotely forced from the Indian Ocean (Rodwell and Hoskins 1996; Black and Sutton 2007) may trigger a Rossby wavetrain downstream along the subtropical jets.

Finally it is worth noting that our results, and also following all above-mentioned suggestions, emphasize the importance of Mediterranean Sea for the success of seasonal forecasting skill, in both statistical and dynamical models.

Acknowledgments.

We thank Dr. Jucundus Jacobeit (U. of Augsburg, Germany) and Dr. Laurent Li (LMD-IPSL, France) for their constructive comments on the preliminary study presented in the 2nd ESF-MedCLIVAR Workshop. Thanks to Dr. Reindert Haarsma (KNMI, The Netherlands) for his advertisement on the mean-flow shape during summertime and comments concerning the baroclinic structure associated with the eastern Mediterranean thermal low. This research was supported by the European AMMA project from the 6th Framework Research Programme, and the national CGL2006-04471 and 2008-00050084028 (MOVAC) projects of the Spanish Government. J. G.-S. greatfully acknowledge the founds from the ESF-MedCLIVAR Programme of grants (EG/1694).

References

Ambrizzi T, Hoskins B J, Hsu H-H (1995) Rossby wave propagation and teleconnection patterns in the austral winter. J Atmos Sci 52:3661-3672.

Baines P G, Folland C K (2007) Evidence for a rapid global climate shift across the late 1960s. J Clim 20:2721-2744.

Baldi M, Meneguzzo F, Dalu G A, Maracchi G, Pasqui M, Capecchi V, Crisci A, Piani F (2004) Guinea Gulf SST and Mediterranean summer climate: analysis of the interannual variability. In Proceedings of the 84th AMS Conference 11.11. http://ams.confex.com/ams/84Annual/techprogram/programexpanded_187.htm

Baldi M, Cesarone F, Dalu G A, Maracchi G, Pasqui M (2006) Heat-waves in the Mediterranean: a local feature or a large scale effect?. Int J Climatol 26:1477-1487. doi: 10.1002/joc.1389.

Baldi M, Gaetani M, Dalu G A, Maracchi G (2009) Jetstream and seasonal anomalies in the Mediterranean. Boll Geofis XXXI 1-4:51-69.

Black E, Sutton R (2007) The influence of oceanic conditions on the hot European summer of 2003. Clim Dyn 28:53-66.

Branstator G (2002) Circumglobal teleconnections, the jetstream waveguide, and the North Atlantic Oscillation. J Clim 15:1983-1910.

Bretherton S B, Smith C, Wallace J M (1992) An intercomparison of methods for finding coupled patterns in climate data. J Clim 5:541-560.

Ding Q, Wang B (2005) Circumglobal teleconnection in the Northern Hemisphere summer. J Clim 18:3483-3505.

Fedorov A, Philander S G (2000) Is El Niño changing?. Science 288:1997-2002.

Ferranti L, Viterbo P (2006) The European summer of 2003: sensitivity to soil water initial conditions. J Clim 19:3659-3680.

Fischer E M, Seneviratne S I, Vidale P L, Lüthi D, Schär C (2007) Soil moisture-atmosphere interactions during the 2003 European summer heat wave. J Clim 20:5081-5099.

Fontaine B, Roucou P, Trzaska S (2003) Atmospheric water cycle and moisture fluxes in the West African monsoon: mean annual cycles and relationship using NCEP/NCAR reanalysis. Geophys Res Lett 30:1117. doi: 10.1029/2002GL015834.

Fontaine B, García-Serrano J, Roucou P, Rodríguez-Fonseca B, Losada T, Chauvin F, Gervois S, Sijikumar S, Ruti P, Janicot S (2009) Impacts of warm and cold situations in the Mediterranean basins on the West African monsoon: observed connection patterns (1979-2006) and climate simulations. Clim Dyn. doi: 10.1007/s00382-009-0599-3.

García-Serrano J, Losada T, Rodríguez-Fonseca B, Polo I (2008) Tropical Atlantic variability modes (1979–2002). Part II: time-evolving atmospheric circulation related to SST-forced tropical convection. J Clim 21:6476-6497.

Haarsma R J, Selten F, Hurk H v, Hazeleger W, Wang X (2009) Drier Mediterranean soils due to greenhouse warming bring easterly winds over summertime central Europe. Geophys Res Lett 36:4. doi: 10.1029/2008GL036617.

Hoskins B J, Ambrizzi T (1993) Rossby wave propagation on a realistic longitudinally varying flow. J Atmos Sci 50:1661-1671.

Hsu H-H, Wallace J M (1985) Vertical structure of wintertime teleconnection patterns. J Atmios Sci 42:1693-1710.

Jung T, Ferranti L, Tompkins A M (2006) Response to the summer of 2003 Mediterranean SST anomalies over Europe and Africa. J Clim 19:5439-5454.

Kodera K, Kuroda Y (2003) Regional and hemispheric

circulation patterns in the Northern hemisphere winter, or the NAO and the AO. Geophys Res Lett 30:1934. doi: 10.1029/2003GL017290.

Kucharski F, Bracco A, Yoo J H, Molteni F (2007) Low-frequency variability of the Indian monsoon-ENSO relationship and the tropical Atlantic: the 'weakening' of the 1980s and 1990s. J Clim, 20, 4255-4266.

Lau N-C (1979) The observed structure of the tropospheric stationary waves and the local balances of vorticity and heat. J Atmos Sci 36:996-1016.

Li L Z X (2006) Atmospheric GCM response to an idealized anomaly of the Mediterranean sea surface temperature. Clim Dyn. doi: 10.1007/s00382-006-0152-6.

Losada T, Rodríguez-Fonseca B, Polo I, Janicot S, Gervois S, Chauvin F, Ruti P (2009) Tropical response to the Atlantic Equatorial mode: AGCM multimodel approach. Clim Dyn. doi: 10.1007/s00382-009-0624-6.

Maheras P, Xoplaki E, Davies T, Martin-Vide J, Bariendos M, Alcoforado M J (1999) Warm and cold monthly anomalies across the Mediterranean basin and their relationship with circulation: 1860-1990. Int J Climatol 19:1697-1715.

Mohino E, Rodríguez-Fonseca B, Losada T, Gervois S, Janicot S, Bader J, Ruti P, Chauvin F (2010) Inter-annual SST-forced signals on West African rainfall from AGCM simulations. Part I: model intercomparison and multidecadal changes. Clim Dyn (submitted).

Peyrillé P, Lafore J P, Redelsperger J L (2007) An idealized two-dimensional framework to study the West African monsoon. Part I: validation and key controlling factors. J Atmos Sci 64:2765-2782.

Polo I, Rodríguez-Fonseca B, Losada T, García-Serrano J (2008) Tropical Atlantic variability modes (1979-2002). Part I: time-evolving SST modes related to West African rainfall. J Clim 21:6457-6475.

Raicich F, Pinardi N, Navarra A (2003) Teleconnections between Indian monsoon and Sahel rainfall and the Mediterranean. Int J Climatol 23:173-186.

Ritcher I, Mechoso C R, Robertson A W (2008) What determines the position and intensity of the South Atlantic anticyclone in austral winter?. J Clim 21:214-229.

Rodríguez-Fonseca B, Polo I, García-Serrano J, Losada T, Mohino E, Mechoso C R, Kucharski F (2009) Are Atlantic Niños enhancing Pacific ENSO events in recent decades?. Geophys Res Lett 36:L20705. doi: 10.1029/2009GL040048.

Rodríguez-Fonseca B, Losada T, Mohino E, Janicot S (2010) Inter-annual SST-forced signals on West African rainfall from AGCM simulations. Part I: understanding a global tropical SST mode. Clim Dyn (submitted).

Rodwell M J, Hoskins B J (1996) Monsoons and the dynamics of deserts. Q J R Meteorol Soc 122:1385-1404.

Rowell D P (2003) The impact of the Mediterranean SSTs on the Sahelian rainfall season. J Clim 16:849-862.

Smith T M, Reynolds R W (2003) Extended reconstruction of global sea surface temperatures based on COADS data (1854-1997). J Clim 16:1495-1510.

Terray P, Dominiak S (2005) Indian Ocean sea surface temperature and El Niño-Southern Oscillation: a new perspective. J Clim 18:1351-1368.

Watanabe M (2004) Asian jet waveguide and downstream extension of the North Atlantic Oscillation. J Clim 17:4674-4691.

Wu L, He F, Liu Z, Li C (2007) Atmospheric teleconnections of Tropical Atlantic Variability: interhemispheric, tropical-extratropical, and cross-basin interactions. J Clim 20:856-870.

Xie P, Arkin P A (1997) Global precipitation: a 17-year monthly analysis based on gauge observations, satellite estimates, and numerical model outputs. Bull Amer Meteor Soc 78:2539-2558.

Xoplaki E, González-Rouco J F, Gyalistras, Luterbacher J, Rickli R, Wanner H (2003a) Interannual summer air temperature variability over Greece and its connection to the large-scale atmospheric circulation and Mediterranean SSTs 1950-1999. Clim Dyn 20:537-554.

Xoplaki E, González-Rouco J F, Luterbacher J, Wanner H (2003b) Mediterranean summer air temperature variability and its connection to the large-scale atmospheric circulation and SSTs. Clim Dyn 20:723-739.

DISCUSIÓN

El objetivo de esta Tesis ha sido el responder a preguntas abiertas acerca de las teleconexiones atmosféricas forzadas por cambios en las temperaturas de la superficie del mar y su influencia en el clima de Europa. A continuación se reflexiona y discute acerca de los aspectos comunes que hemos aprendido dentro de este objetivo general. En el capítulo siguiente se sintetizan las principales conclusiones de todos los resultados alcanzados a lo largo de la Memoria, de los cuales algunos se alejan de ese objetivo general y no parecen, por tanto, en esta discusión integradora.

Los trabajos presentados en esta Memoria han tratado de aclarar los mecanismos dinámicos que subyacen en la variabilidad del clima en el sector Euro-Atlántico. Se trata de una región situada en las latitudes extratropicales del Hemisferio Norte donde la mayor parte de la variabilidad es de origen interno y está dominada por *eddies*. Eso hace difícil discernir en las observaciones el origen externo de la variabilidad climática regional. No obstante, las teleconexiones atmosféricas vía ondas de Rossby proporcionan un mecanismo plausible para explicar influencias remotas. Como se presentó en la introducción (Fig. I.20), la propagación de estas ondas está determinada por las características del flujo medio o viento promedio en niveles altos troposféricos.

Una de las características más significativas de la Circulación General de la Atmósfera es la gran diferencia que existe entre el patrón del flujo medio en el hemisferio de invierno en comparación con el correspondiente al verano. En particular, y para nuestros intereses, en el invierno del Hemisferio Norte (invierno boreal) la circulación atmosférica en la alta troposfera es mucho más intensa que durante la estación estival (verano boreal). Así, mientras que en verano las corrientes en chorro poseen su máximo entre 30-40 m/s, en invierno ese máximo llega alcanzar los 60-70m/s. Esta contrastada diferencia en la velocidad del viento es consecuencia del ciclo anual de la irradiación solar, marcado por la presencia de las estaciones. En el invierno boreal el gradiente térmico ecuador-polo es más acentuado y por tanto el flujo atmosférico es más intenso (e inestable), mientras que el contraste térmico entre el océano y el suelo continental favorece la asimetría zonal de esos vientos. Por el contrario, durante el verano, el gradiente térmico meridional es menor y el flujo medio más débil (e.g. Peixoto y Oort 1992).

Igual que en la Fig. I.1 se ha descrito esta característica desde el punto de vista regional del Atlántico Norte, la Fig. V.1 muestra la climatología de la componente zonal del viento en 200hPa para Enero (invierno) y Julio (verano), donde se pone de manifiesto esa diferencia estacional en al intensidad del flujo bajo una perspectiva global.

Como se ha descrito en la introducción (Secc. I.4.2.b), la propagación de las ondas de Rossby depende fuertemente del flujo medio por el que se propagan. Así, se conoce que allí donde las corrientes en chorro son débiles, la propagación de ondas de Rossby tiende a ser en forma de arco (propagación meridional); mientras que en las regiones donde las corrientes en chorro presentan una gran intensidad, los trenes de onda tienden a estar confinados meridionalmente (propagación zonal) (Hoskins y Karoly 1981; Branstator 1983, 2002; Hoskins y Ambrizzi 1993; Ambrizzi et al. 1995).

A lo largo de este trabajo, los mecanismos de propagación de ondas de Rossby propuestos para los diferentes forzamientos oceánicos parecen

estar de acuerdo con esta descripción. Como se discute a continuación, dependiendo de la estación considerada, un forzamiento similar puede llegar a tener dos respuestas atmosféricas bastante diferentes. Asimismo, distintos forzamientos pueden excitar mecanismos de propagación muy parecidos. Para facilitar la comparación, se especifican las partes de las corrientes en chorro del Hemisferio Norte en las que se centra la discusión. De acuerdo con Hoskins y Ambrizzi (1993), que centraron su estudio en el invierno boreal, y con Ambrizzi et al. (1995), que focalizaron el análisis en el verano boreal, aquí se definen dos corrientes en chorro o jets: la corriente en chorro del Norte de África y Asia o *NAA-jet* (North African-Asian jet), muy zonal y que se sitúa en latitudes subtropicales durante el invierno y en latitudes medias durante el verano; y la corriente en chorro del Atlántico Norte o *NA-jet* (North Atlantic jet), que es conducida por la actividad transitoria y presenta una clara inclinación suroeste-noreste aunque más marcada en invierno que en verano.

Con respecto a la estación estival, los resultados apuntan a una clara influencia del flujo medio sobre la propagación de ondas de Rossby. Como se ha presentado en la Sección IV. 3, el Niño Atlántico de verano (ATL NIÑO en Fig. V.1), que está en su fase madura, genera una respuesta de Gill en el Atlántico tropical que presenta dos anticiclones anómalos a ambos lados del ecuador. La propagación extratropical de esta señal se extiende por el Atlántico Norte y penetra en Europa hacia el centro del continente. Como se puede apreciar en la distribución climatológica del viento zonal el 200hPa (U200), esa interacción trópico-extratrópico tiene lugar a través de la región intermedia entre el NA-jet y el NAA-jet, donde la corriente en chorro del oeste es más débil sobre el Atlántico Norte. Aunque hasta ahora no haya más evidencias con las que comparar esta señal extratropical forzada desde el Atlántico ecuatorial, es interesante resaltar como Cassou et al. (2004) encuentran una propagación similar para un forzamiento atmosférico localizado en la cuenca del Amazonas. Aunque los autores también recaen en lo débil del flujo medio estival en el Atlántico Norte, sus resultados sugieren a la vez una propagación de Rossby extratropical a través de la cuenca atlántica.

Siguiendo con el verano y para el caso del forzamiento térmico situado en la cuenca oriental del Mediterráneo (eMED en Fig. V.1), los resultados del estudio observacional y de la simulación AGCM analizada sugieren que la repuesta local baroclínica forzada por eMED presenta una propagación aguas abajo guiada a través de las dos corrientes en chorro del Hemisferio Norte (Secc. IV.4). En particular, como se puede apreciar en la Fig. V.1, la perturbación atmosférica asociada a eMED se localiza sobre la entrada del NAA-jet de verano. Tal y como aparece esquematizado en la Fig. V.1, la dispersión de la energía a través de la propagación del tren de ondas de Rossby se canalizaría primeramente a lo largo del NAA-jet, para atravesar el Pacífico Norte y adentrarse en el Atlántico Norte, guiada ya por el NA-jet. Aunque tampoco existen estudio previos que apoyen el forzamiento de esta propagación hemisférica estival asociada a eMED, Jung et al. (2006) han mostrado una respuesta atmosférica similar asociada al patrón wMED (western Mediterranean). Así mismo, Ambrizzi et al. (1995) y Ding y Wang (2005) han revelado la existencia de un patrón atmosférico canónico asociado al efecto guía de onda de las corrientes en chorro durante el verano boreal, dando de este modo cierta robustez a los resultados aquí mostrados (Secc. IV.4).

Durante la estación invernal, los resultados también están de acuerdo con esa influencia del flujo medio sobre la propagación de ondas de Rossby anómalas estacionarias. Como se ha mostrado en la Sección IV.3, el decaimiento del Niño Atlántico durante el otoño-invierno siguiente a su fase madura es capaz de generar una respuesta de Gill sobre el Atlántico tropical, cuya propagación extratropical a través de un tren de ondas de Rossby queda atrapada en las corrientes en chorro del oeste y circunda todo el cinturón de latitudes medias. Como se presenta en la Fig. V.1, y a diferencia de la respuesta atmosférica al Niño Atlántico en verano, la circulación anómala asociada a la respuesta local en invierno se localiza a la entrada del NAA-jet, el cual canaliza la dispersión de la energía y produce una respuesta hemisférica que recorre también el NA-jet. Este mecanismo es enteramente consistente con la simulación AGCM llevada a cabo por Haarsma y Hazeleger (2007) con un modelo de complejidad intermedia, y en la que se propone esa respuesta atmosférica circunglobal basada en el efecto guía de onda del NAA-jet (Hoskins y Ambrizzi 1993; Branstator

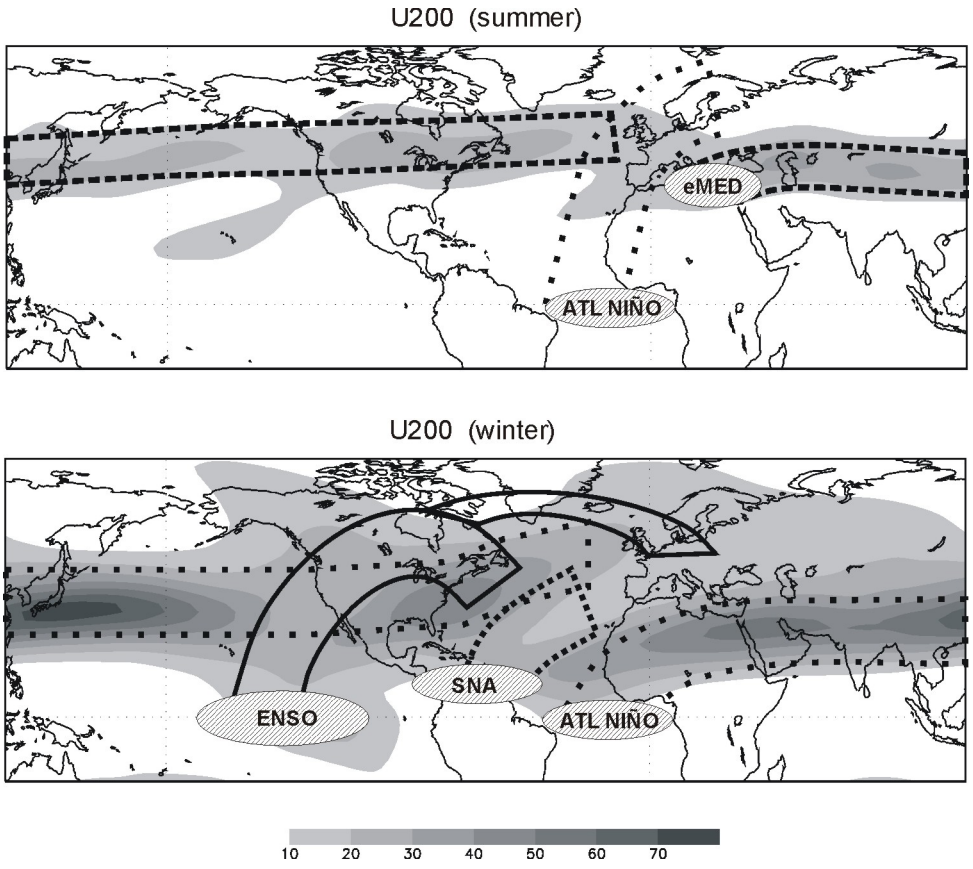

Fig. V.1. Esquema que resume la propagación de los trenes de ondas de Rossby asociados al Niño Atlántico (ATL NIÑO), al Atlántico Norte Subtropical (SNA), a la cuenca oriental del Mediterráneo (eMED) y al fenómeno ENSO; en sombreado, de fondo, las corrientes en chorro del oeste para verano (Julio) e invierno (Enero) en función de la climatología del viento zonal en 200hPa (m/s).

2002). Estos resultados también están apoyados por estudios previos que muestran el mismo tipo de respuesta hemisférica atrapada en los NAA-jet / NA-jet aunque forzada por el eMED invernal (Li 2006) y por la respuesta remota a ENSO en el Atlántico tropical (Shaman y Tziperman 2005).

Por su parte, el mecanismo propuesto en respuesta al forzamiento en el Atlántico Norte Subtropical (SNA en Fig. V.1) se caracteriza por una propagación mucho más meridional, en forma de arco, que es excitada desde el Amazonas y que cruza el Atlántico Norte hacia Europa. La propagación de este tren de ondas de Rossby desde el Atlántico tropical se produce como consecuencia de las perturbaciones forzadas sobre la ITCZ local, que consisten en una retención del desplazamiento estacional hacia el sur y por tanto de una divergencia anómala sobre la cuenca amazónica (Terray y Cassou 2002). Como está esquematizado en la Fig. V.1, la dispersión extratropical de la energía mediante el tren de ondas de Rossby se produce a través del intermedio entre el NA-jet y el NAA-jet y, por tanto, sobre la región donde los vientos del oeste son más débiles en el Atlántico Norte. Esta conclusión está de acuerdo con varios trabajos con AGCM que han estudiado la interacción trópico-extratrópico asociada al SNA (e.g. Sutton et al. 2001; Terray y Cassou 2002; Losada et al. 2007).

Finalmente, y de acuerdo con varios trabajos previos que han analizado la respuesta atmosférica a ENSO (e.g. Blackmon et al. 1983; Branstator 1985; Karoly et al. 1989; DeWeaver y Nigam 2002; Bladé et al. 2008), el estudio basado en datos observacionales presentado en la Sección IV.1 muestra cómo la circulación anómala asociada a ENSO en invierno proyecta fuertemente en un tren de ondas de Rossby conocido como TNH (Tropical/Northern Hemisphere). Este patrón de teleconexión es forzado desde el Pacífico tropical y se propaga sobre el Pacífico Norte y

Norteamérica a través del intermedio entre el final del NAA-jet y el NA-jet (Fig. V.1). La división de este tren de ondas en el Atlántico Norte, cuya rama más oriental alcanza el continente europeo, es totalmente consistente con trabajos como los de Blackmon et al. (1983) o Karoly et al. (1989) y podría explicarse a través de la guía de onda NA-jet / Europa del Norte mostrada por Hoskins y Ambrizzi (1993; Fig. I.20)

Como corolario de este trabajo y de acuerdo con todos los resultados aquí discutidos, se puede concluir que el *ciclo estacional de las corrientes en chorro determina gran parte de las características de propagación de los trenes de ondas de Rossby que alcanzan la región Atlántico Norte-Europa como consecuencia de los diferentes forzamientos oceánicos considerados.*

Como se ha comentado anteriormente, esta conclusión está de acuerdo con varios estudios previos basados tanto en datos observacionales como en simulaciones numéricas.

A continuación se profundiza en la consistencia de los resultados mostrados en esta Tesis con las premisas teóricas de la propagación de ondas de Rossby. Para tal fin se computa el ángulo inicial α (con la dirección oeste-este) que presentarían los diferentes trenes de ondas dependiendo de la localización del forzamiento oceánico considerado. Como se mostró en la Secc. I.4.4.b, las características de la propagación de estas ondas están teóricamente determinadas por el flujo medio en el que se propagan. En particular, la excitación de estas ondas queda determinada por el flujo medio en torno a la región de forzamiento.

En condiciones estacionarias (ω=0), la relación de dispersión de las ondas de Rossby proporciona una dirección de propagación en la que el número de onda zonal k permanece constante y el número de onda meridional l varía de acuerdo al flujo medio a través del número de onda estacionario K_S (Hoskins y Karoly 1981; Hoskins y Ambrizzi 1993):

$$K_S^{\,2} = k^2 + l^2 = \frac{\beta - \frac{\partial^2 U}{\partial y^2}}{U}$$

De esta forma, la dirección inicial de propagación en torno a la región de forzamiento viene determinada según:

$$\cos\alpha = \frac{k}{K_S} = k\sqrt{\frac{U}{\beta - \frac{\partial^2 U}{\partial y^2}}}$$

Por tanto, dada una determinada latitud de forzamiento, el ángulo inicial de excitación de las ondas de Rossby será menor (mayor), para un mayor (menor) número de onda k, para un flujo zonal medio U más intenso (débil), o para una variación meridional de la vorticidad relativa climatológica $\partial^2U/\partial y^2$ más acentuada (suave) (Fig. V.2). De esta forma, se. favoreciría una propagación más zonal (meridional).

De acuerdo con los estudios de Hoskins y Karoly (1981), Hosins y Ambrizzi (1993) y Ambrizzi et al. (1995), para el cálculo de α que ahora se presenta, se ha considerado un promedio de k=3-4 (mayor longitud de onda) para las teleconexiones meridionales en arco y k=5-6 (menor longitud de onda) para las teleconexiones zonales atrapadas en las corrientes en chorro.

Para el verano, el ángulo inicial de la propagación extratropical asociada al Niño Atlántico es de

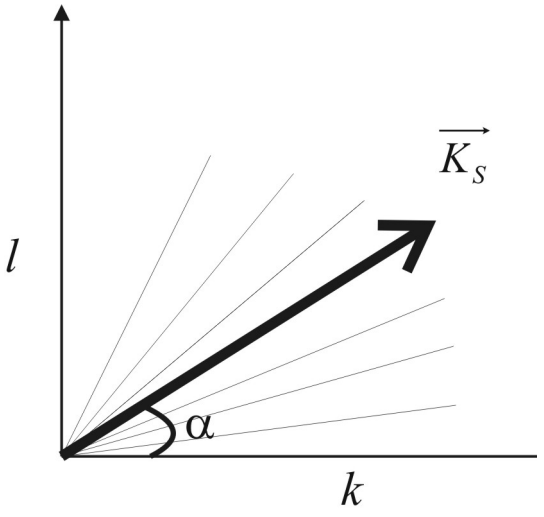

Fig. V.2. Diagrama que representa los números de onda zonal (k) y meridional (l) del tren de ondas de Rossby estacionario, así como el número de onda de Rossby estacionario (K_S) y el ángulo de propagación del tren de ondas (α) con respecto a la dirección oeste-este.

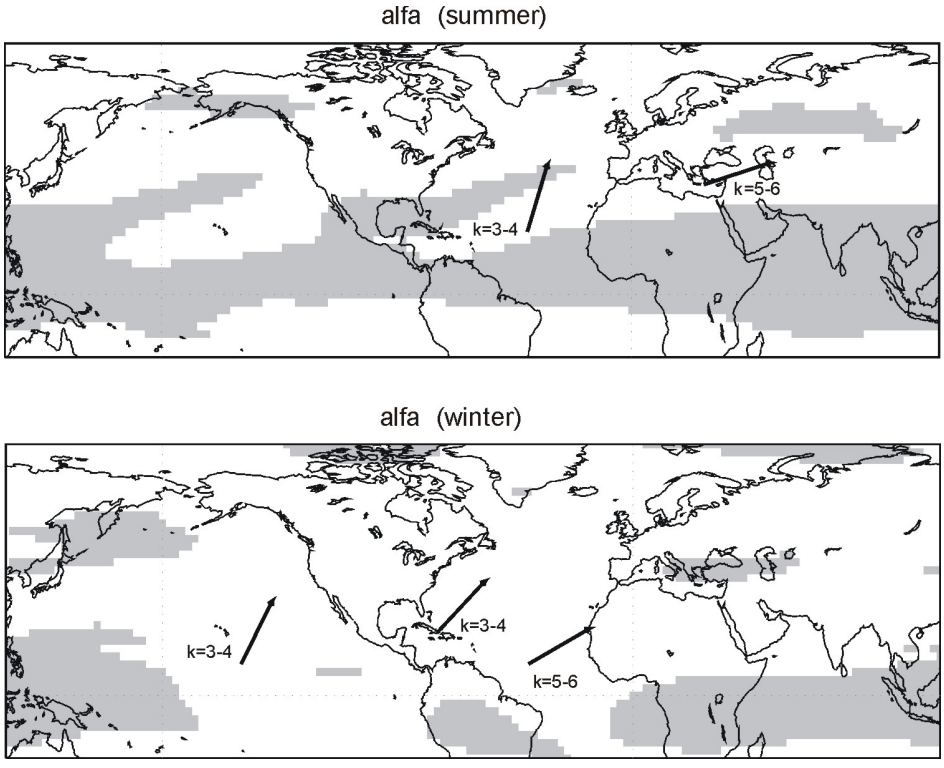

Fig. V.3. Representación de los ángulos iniciales de propagación de los trenes de ondas de Rossby asociados a los forzamientos considerados en esta Tesis (Fig. V.1); en sombreado se muestran las regiones donde el número de onda estacionario *Ks* no está definido.

α=73.4º; corroborando el marcado carácter meridional de la respuesta atmosférica mostrada en los resultados (Seccs. IV.2, IV.3). Para este forzamiento, la región fuente se ha localizado en el punto 20N-40W (Fig. V.3). En el caso del patrón Oriental del Mediterráneo (eMED), el ángulo inicial teórico asociado a una propagación atrapada en las corrientes de chorro sería α=18.1º; que está totalmente de acuerdo con la hipótesis observacional y la respuesta atmosférica mostradas en la Secc. IV.4 sobre la canalización de las anomalías asociadas a la respuesta baroclínica del eMED. Para este forzamiento, la región fuente corresponde al punto 35N-27.5E.

Para el invierno, el ángulo de inclinación de la propagación Rossby asociada con la respuesta de Gill al final del decaimiento del Niño Atlántico sería α=30.2º; lo que confirma el papel del flujo medio en la determinación del patrón de anomalías atrapado en la corriente en chorro NAA-jet. Para este forzamiento, la región fuente se ha situado en 10N-40W. En el caso de la respuesta en arco al Atlántico Norte Subtropical, el cálculo teórico del ángulo inicial de propagación sugiere que el tren de ondas de Rossby emergería con α=47.1º; por tanto, corroborando la hipótesis de una conexión trópico-extratrópico de marcado carácter meridional. La región fuente asociada a este forzamiento del Atlántico Norte ha sido el punto 20N-75W. Finalmente, para la teleconexión invernal ENSO-Europa, el ángulo inicial de la propagación extratropical forzada desde el Pacífico tropical sería α=63.8º; lo que confirma la propagación meridional en arco a través de las corrientes en chorro NAA-jet y NA-jet sobre el Pacífico Norte. La región fuente asociada a ENSO ha sido el punto 10N-150W.

DISCUSSION

The aim of this Thesis has been to answer the open questions concerning some atmospheric teleconnections associated with changes in the sea surface temperature and its influence on the European climate. Next, a reflection and discussion is presented about the commom features learnt from this work regarding this general objective. In the following chapter the main conclusions from the results presented in this Report are summarized, and since some of these results are out of the scope of that general objective are, hence, not reported in the subsequent integrating discussion.

The studies presented in this Report had the aim of clarifying the dynamical mechanisms underlying the climate variability in the Euro-Atlantic sector. This region is localized at extratropical latitudes in the Northern Hemisphere, where the variability is largely driven by internal activity. This feature makes hard to discriminate the external origing in the climate variability on the basis of observations. However, the atmospheric teleconnections via Rossby wave propagation represent a plausible mechanism in order to explain remote influences. As introduced in the State of the Art (Fig. I.20), the propagation of these waves is rightly determined by the mean flow, the averaged wind at upper tropospheric levels.

One of the most significant characteristics of the Atmospheric General Circulation is the marked difference in the mean flow pattern between the summer and winter hemispheres. Concretely, and to our interest, the atmospheric circulation is more intense during wintertime in the Northern Hemisphere (boreal winter) than during summertime (boreal summer): whereas the maximum velocity in the summer westerly jetstreams is roughly 30-40 m/s, this winter maximum reaches 60-70 m/s. This marked difference in the wind velocity is a consequence of the annual cycle in solar irradiation, characterized by the presence of the seasons. During boreal winter, the equatorial-pole thermal gradient is more stressed (and unstable), and the land-sea thermal contrast favours the asymmetries in the zonal flow. Instead, during boreal summer, the meridional thermal gradient is lesser and the mean flow weaker (e.g. Peixoto and Oort 1992).

As also shown in Fig. I.1 from a regional perspective, Fig. V.1 represents the zonal wind climatology at 200hPa for July (summer) and January (winter), where this marked seasonal difference is revealed from a global perpective.

As described in the introduction (Sect. I.4.2.b), the propagation of Rossby waves strongly depends on the mean flow in which these waves propagate. Thus, it is known that where the jetstreams are weak, the Rossby wave propagation tend to be an arching pattern (meridional propagation); whilst in regions where the jetstreams are intense, the Rossby wavetrains tend to be meridionally confined (zonal propagation) (Hoskins and Karoly 1981; Branstator 1983, 2002; Hoskins and Ambrizzi 1993; Ambrizzi et al. 1995).

Along this work, the proposed Rossby wave propagation mechanisms concerning the different forcings seem to be in accordance with this description. Then, as discussed below, it will be shown how depending on the season considered a similar forcing can produce two distinct atmospheric responses; or, how different forcings can excite close propagation mechanisms. In order to facilitate the comparison, next two

separate parts are especified within the westerly jetstreams in the Northern Hemisphere. According to Hoskins and Ambrizzi (1993), who focused the study on boreal winter, and Ambrizzi et al. (1995), who focused the analysis on boreal summer, two jetstreams are defined here: the jetstream along the North African-Asian jet (NAA-jet), quite zonal and localized at subtropical latitudes during winter and at midlatitudes during summer; and the jetstream along the North Atlantic (NA-jet), which is driven by transient activity and presents a clearer soutwest-northeast orientation in winter than in summer.

Regarding summertime, the results shown here point to a clear influence of the mean flow on the Rossby wave propagation. As presented in Sect. IV.3, the summer Atlantic Niño (ATL NIÑO in Fig. V.1), which is in its mature phase, generates a Gill-type response over the tropical Atlantic yielding two anomalous anticyclones straddling the equator. The extratropical propagation of this signal extends through the North Atlantic to central Europe. As can be inferred from the climatological distribution of the zonal wind at 200hPa (U200), this tropical-extratropical interaction takes place between the NA-jet and the NAA-jet, where the westerly jetstream is the weakest in the North Atlantic basin. Although this result can not be compared with previous works, it is important to notice how Cassoou et al. (2004) found a similar propagation anomaly but associated with an atmospheric forcing over the Amazon basin. They also stated the weak condition of the summertime mean flow along the North Atlantic, even so their results indeed suggested an extratropical Rossby propagation through the Atlantic basin.

Also in summer but considering the thermal forcing over the eastern Mediterranean basin (eMED in Fig. V.1), the results both from the observational study and the AGCM simulation suggest that the forced baroclinic response to eMED produce a downstream propagation waveguided along the Northern Hemisphere westerly jets (Sect. IV.4). In particular, as can be seen in Fig. V.1, the atmospheric disturbance associated with eMED is tightly located in the summer NAA-jet entrance. As schematized in Fig. V.1, the energy dispersion through Rossby wavetrain is firstly trapped within the NAA-jet, crossing the North Pacific and reaching the North Atlantic via the NA-jet. Although there are not previous works either supporting this forced hemispheric propagation related to eMED, Jung et al. (2006) showed an atmospheric response quite similar but associated with wMED (western Mediterranean). Likewise, Ambrizzi et al. (1995) and Ding ang Wang (2005) have revealed the existence of a canonical pattern related to the waveguiding effect of the westerly jetstream during summer, giving in that way certain robustness to the results shown here (Sect. IV.4).

Regarding wintertime, the results are also in accordance with the key influence of the mean flow on the anomalous stationary Rossby waves propagation. As shown in Sect. IV.3, the Atlantic Niño damping during autumn-winter after its mature phase is able to force a Gill-type response over the tropical Atlantic, which extratropical propagation via Rossby waves is confined within the westerly jetstreams and enterly circumscribes the midlatitude belt. As presented in Fig. V.1, and in contrast to the summer atmospheric response to the Atlantic Niño, the circulation anomaly associated with the winter local response is rightly located in the NAA-jet entrance, which channels the energy dispersion and produces a hemispheric response also propagating along the NA-jet. This mechanism is enterely consistent with the AGCM simulation performed by Haarsma and Hazeleger (2007) with an intermediate complexity model, in which that circumglobal atmospheric response was proposed on the basis of the waveguiding effect of the NAA-jet (Hoskins and Ambrizzi 1993; Branstator 2002). These results are also supported by previous works showing a similar kind of hemispheric response trapped into both NAA-jet and NA-jet but forced by the winter eMED (Li 2006) and a remote response to ENSO over the tropical Atlantic (Shaman and Tziperman 2005).

On its part, the proposed mechanism in response to the Subtropical North Atlantic forcing (SNA in Fig. V.1) is characterized by a much more meridional propagation, in an arching way, which is triggered from the Amazon and crosses the North Atlantic towards Europe. The propagation of this Rossby wavetrain from the tropical Atlantic is a consequence of the forced perturbations on the local ITCZ, retaining the seasonal southward displacement and yielding divergence anomalies in the Amazonian basin (Terray and Cassou 2002).

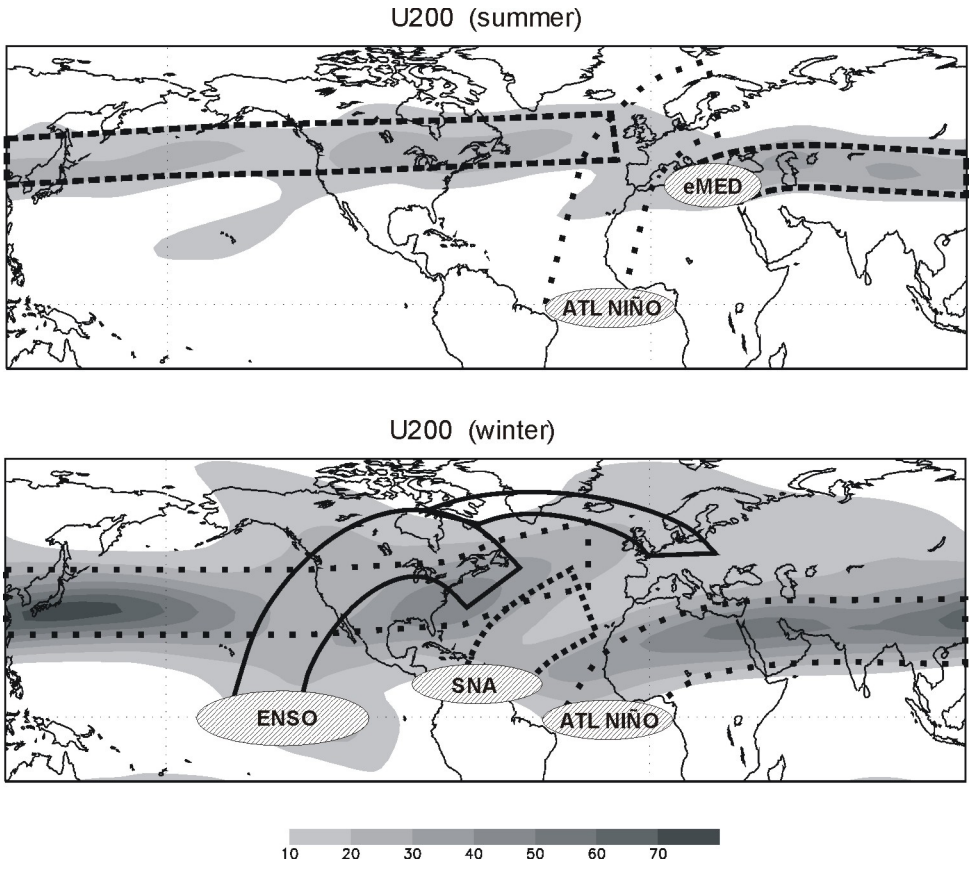

Fig. V.1. Schematic diagram summarizing the Rossby wavetrain propagations associated with the Atlantic Niño (ATL NIÑO), the Subtropical North Atlantic (SNA), the eastern Mediterranean basin (eMED), and the ENSO phenomenon; shading, in background, represents the westerly jetstreams during summer (July) and winter (January) by means of zonal wind climatology at 200hPa (m/s).

As schematized in Fig. V.1, the extratropical energy dispersion via Rossby wavetrain is apparent between the NA-jet and the NAA-jet; hence, through the region in which the westerly winds are the weakest in the winter North Atlantic. This conclusion goes along with a number of AGCM works analysing the tropical-extratropical interaction related to SNA (e.g. Sutton et al. 2001; Terray and Cassou 2002; Losada et al. 2007)

Finally, and accordin to several previous works that have studied the atmospheric response to ENSO (e.g. Blackmon et al. 1983; Branstator 1985; Karoly et al. 1989; DeWeaver and Nigam 2002; Bladé et al. 2008), the observational work presented in Sect. IV.1 shows how the mid-winter anomalous circulation associated to ENSO strongly projects onto the well-known TNH (Tropical/Northern Hemisphere) wavetrain. This teleconnection pattern is forced from the tropical Pacific and propagates crossing the North Pacific and North America between the NAA-jet tail and the NA-jet (Fig. V.1). The wavetrain split in the North Atlantic, which eastern branch reaches the european continent, is enterely consistentn with studies as those by Blackmon et al. (1983) or Karoly et al. (1989), and could be explained via the waveguide of NA-jet / Northern Europe as shown by Hoskins and Ambrizzi (1993; also in Fig. I.20).

A necessary corollary of this work, and according to all above discussed results, is that the *seasonal cycle of the jetstreams determines to a large extent the behaviour of the Rossby wavetrains propagation reaching the North Atlantic-European region in response to the different oceanic forcings considered in this Thesis.*

As described before, this conclusion is in accordance with a great number of previous works based both on observations and numerical integrations. Next, a study is presented concerning theoretical

premises of the Rossby waves propagation in order to further assess the soundness of the results. Concretely, the initial propagation angle α (respect to west-east direction) of the different Rossby wavetrains for each oceanic forcing is computed. As introduced in Sect. I.4.2.b, the characteristics of these propagations are theoretically determined on the basis of the mean flow in which the waves propagate; in particular, the triggering of those waves is determined by means of the mean flow around the forcing region.

At stationary conditions (ω =0), the dispersion relation of Rossby waves provides a propagation direction in which the zonal wavenumber k keeps constant and the meridional wavenumber l varies according to the mean flow through the stationary wavenumber K_S (Hoskins and Karoly 1981; Hoskins and Ambrizzi 1993):

$$K_S^{\,2} = k^2 + l^2 = \frac{\beta - \frac{\partial^2 U}{\partial y^2}}{U}$$

In this way, the initial direction of propagation around the forcing region is determined as:

$$\cos\alpha = \frac{k}{K_S} = k\sqrt{\frac{U}{\beta - \frac{\partial^2 U}{\partial y^2}}}$$

Hence, for a given latitude, the initial angle of Rossby waves triggering will be lesser (larger), favouring a more zonal (meridional) propagation, for a greater (lesser) wavenumber k, giving a zonal mean flow U more intense (weak), and for a meridional variation of climatological realtive vorticity $\partial^2 U/\partial y^2$ more marked (smooth) (Fig. V.2).

According to the works of Hoskins and Karoly (1981), Hosins and Ambrizzi (1993), and Ambrizzi et al. (1995), the calculation of has been averaged between k=3-4 (greater wavelength) in case of arching meridional teleconnections and between k=5-6 (lower wavelength) for zonal teleconnections trapped into the jetstreams.

During summertime, the initial angle of extratropical propagation associated with the mature Atlantic Niño is α=73.4º; supporting the marked meridional behaviour of the atmospheric response shown in the respective results (Sects. IV.2, IV.3). In this forcing, the source region is located at 20N-40W (Fig. V.3). Regarding the Eastern Mediterranean pattern (eMED), the theoretical initial angle associated with a Rossby propagation trapped into the summer NAA-jet would be α=18.1º; which is enterely consistent with both the observational hypothesis and the atmospheric response shown in Sect. IV.4 about the waveguided anomalies in response to the eMED-forced baroclinic structure. In this forcing, the source region corresponds to 35N-27.5E.

During wintertime, the inclination angle of Rossby propagation related to the Gill-type response to damped Atlantic Niño would be α=30.2º; which supports the determinant role of the mean flow in determining the pattern of trapped anomalies within the NAA-jet. In this forcing, the source region has been located at 10N-40W. In the case of the arching response to the Subtropical North Atlantic, the theoretical computation of the initial angle suggests that the Rossby wavetrain would be triggered with α=47.1º; thereby, supporting the hypothesis of a tropical-extratropical connection via marked meridional propagation. The source region associated with this forcing in the North Atlantic has been at 20N-75W. Finally, concerning the ENSO-Europe winter teleconnection, the

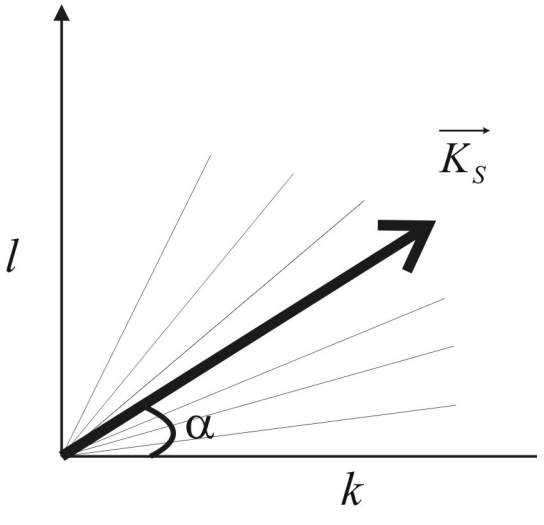

Fig. V.2. Diagram showing the zonal (k) and meridional (l) wavenumbers of the stationary Rossby wavetrain, as well as the stationary Rossby wavenumber K_S and the propagation angle of the wavetrain (α) respect to the west-east direction.

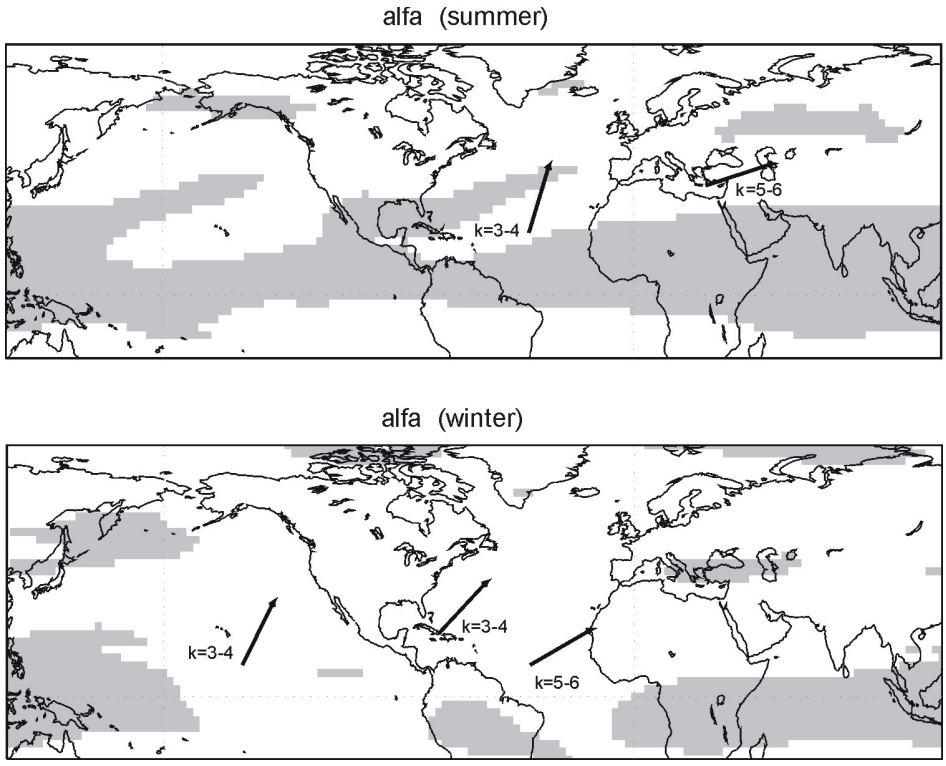

Fig. V.3. Representation of the initial angles of the Rossby wavetrain propagations associated with the oceanic forcings considered in the Thesis (shown in Fig. V.1); shading represents regions in which the stationary Rossby wavenumber *Ks* is not defined (see text for details).

initial angle of the extratropical response forced from the tropical Pacific would be α=63.8º; which is largely consistent with the arching propagation between the NAA-jet tail and the NA-jet in the North Pacific basin. The source region associated with ENSO has been at 10N-150W.

CONCLUSIONES

De acuerdo con los resultados mostrados en el capítulo IV, y con la discusión integradora desarrollada en la sección anterior, las principales conclusiones derivadas de esta Tesis se presentan a continuación. Asimismo, en un marco de continuidad, para cada área de investigación se detallan las líneas de trabajo futuro.

El primer modo rotacional de la función de corriente anómala en invierno (Ene-Feb) sobre el sector Atlántico Norte-Europa describe la influencia remota de ENSO (EOF1), aunque teniendo una débil influencia en la variabilidad climática europea.

- Este modo aparece como la manifestación local de la primera componente principal hemisférica, que corresponde al tren de ondas de Rossby TNH que emerge del Pacífico tropical.

- Este modo tiene una estructura dipolar en superficie sobre el Atlántico Norte, que recuerda a la NAO.

- Esta Tesis defiende, no obstante, que esta respuesta no debe ser descrita como un patrón tipo NAO, ya que su dinámica es muy diferente.

- La señal de SST asociada a este modo corrobora su conexión con ENSO, sin influencia de las cuencas adyacentes.

Como continuación del estudio llevado a cabo en este área, dos tipos de experimentos han sido diseñados para ser realizados con el modelo SPEEDY-AGCM, ahora ubicado en el cluster del Grupo de Investigación. Este AGCM está actualmente en la UCM como resultado de la estancia en el KNMI durante el pasado verano (Apéndice-D). Este AGCM es un modelo sin estratosfera, su nivel atmosférico más alto es 100hPa, y por tanto constituye una herramienta óptima para confirmar la hipótesis observacional de teleconexión troposférica en relación ENSO-Atlántico Norte. La primera simulación, prescribiendo SSTs observadas, está ideada para evaluar si SPEEDY es capaz de capturar esa teleconexión ENSO durante el invierno. El segundo experimento consiste en realizar una simulación transitoria durante Enero, tanto para condiciones El Niño como para La Niña (forzando el modelo con la regresión del índice Niño3.4), con el objetivo de seguir el establecimiento de la respuesta atmosférica tipo TNH.

El segundo modo de la función de corriente en niveles altos (EOF2) presenta la clásica oscilación entre Azores e Islandia, y lleva a identificarlo como una Oscilación del Atlántico Norte (NAO) puramente rotacional.

- La dinámica asociada a este modo involucra esencialmente variabilidad interna, a través de desplazamientos meridionales en la corriente en chorro extratropical.

- La señal atlántica en la SST de este modo recuerda al conocido Tripolo Atlántico.

- EOF2 tiene un gran impacto en el clima europeo, en comparación con EOF1, especialmente en la precipitación, ya que este modo está asociado a cambios en la trayectoria de las perturbaciones sinópticas.

Respecto a la comparación dinámica entre la teleconexión ENSO-Atlántico Norte y la variabilidad interna asociada a la NAO, un paso hacia delante en el entendimiento de estos modos está pensado mediante el cálculo de la misma PCA pero aplicada a dos simulaciones acopladas realizadas con dos versiones del modelo global del MetOffice (HadGEM). Estos datos están disponibles desde la visita a ese centro durante la primavera de 2008 (Apéndice-C). Estas simulaciones consisten en 60 años de integración océano-atmósfera acoplada con condiciones pre-industriales, lo que permite la evaluación de los resultados desde la perspectiva de la variabilidad climática natural.

Los principales modos de SLP, regional y hemisférico, son reconstruidos como combinación lineal de las dos EOFs de la función de corriente; de modo que EOF2 tiene en cuenta la mayoría de la variabilidad regional, mientras que ambos modos contribuyen al llamado modo AO/NAM (variabilidad hemisférica).

- La pequeña pero significativa contribución de EOF1 a la SLP regional se debe a la proyección dipolar en superficie del TNH sobre el Atlántico Norte.

- El hecho de que tanto EOF1 como EOF2 contribuyan al patrón AO/NAM sugiere que este modo es la combinación de diferentes fenómenos locales (NAO) y de gran escala (ENSO).

- A pesar del carácter regional de la EOF2 en superficie, este modo está asociado a un patrón hemisférico en niveles altos que proyecta en el patrón circunglobal de Branstator (2002).

Para continuar con esta línea de investigación, la contribución de ENSO y NAO a las 'oscilaciones' regional y hemisférica, un modelo de regresión múltiple similar al desarrollado para el reanálisis se va a realizar sobre las dos simulaciones acopladas de 60 años de la familia de modelos HadGEM, las versiones HadGEM1 y HadGEM2. Adicionalmente, una simulación transitoria con el SPEEDY-AGCM para el mes de Enero será diseñada para inducir una respuesta tipo NAO, siguiendo el planteamiento experimental de Li y Conil (2003). El objetivo de esta simulación transitoria es evaluar la hipótesis observacional de la excitación regional del patrón circunglobal de Branstator a través de cambios en la actividad eddy del Atlántico Norte.

El primer modo de covariabilidad entre la SST anómala de verano en el Atlántico tropical y la precipitación anómala de verano a invierno en el Atlántico Norte está asociado al Niño Atlántico.

- Durante la fase madura del modo de SST, el patrón anómalo de precipitación cubre toda la banda ecuatorial, afectando la rama ascendente de las circulaciones de Walker y de Hadley.

- Al decaer el modo de SST, la precipitación y los movimientos verticales asociados regresan a su posición climatológica, generando divergencia anómala en los niveles altos troposféricos sobre el norte de Sudamérica.

- Este flujo divergente, localizado sobre las SSTs persistentes, produce anomalías en la región extratropical tanto zonal como meridionalmente.

- Zonalmente, la generación de ondas de Rossby que quedan atrapadas en la corriente en chorro del Norte de África, confirman la hipótesis de una respuesta circunglobal al debilitado Niño Atlántico.

- Meridionalmente, la subsidencia subtropical y la divergencia de momento eddy refuerzan la convergencia en niveles altos sobre la parte occidental del Atlántico Norte.

El análisis de experimentos de sensibilidad para una fase positiva del Niño Atlántico confirma algunas de las hipótesis observacionales.

- La precipitación simulada muestra un debilitamiento progresivo sobre la cuenca este, así como un claro confinamiento sobre la cuenca oeste del Atlántico tropical al final del ciclo del Niño Atlántico.

- El decaimiento del Niño Atlántico es capaz de generar una teleconexión hemisférica aguas abajo del forzamiento durante el otoño-invierno, la cual queda atrapada en la corriente en chorro subtropical.

- Las diferentes propagaciones de ondas de Rossby a lo largo del decaimiento del Niño Atlántico muestran que, para el verano, cuando los chorros son más débiles, la propagación extratropical tiende a ser meridional. Sin embargo, en invierno, la respuesta atmosférica tiende a ser más zonal ya que el flujo medio es más fuerte y la fuente de vorticidad está localizada a la entrada de la corriente en chorro.

- Las anomalías de circulación invernales sobre el este de la región Atlántica-Mediterránea pueden favorecer el patrón circunglobal recurrente de teleconexión encontrado por Branstator (2002) a lo largo de la corriente en chorro del Norte de África y Asia.

- El decaimiento del Niño Atlántico no parece jugar un papel importante en las anomalías de precipitación sobre la cuenca occidental subtropical. El desarrollo de un episodio La Niña en el Pacífico sugiere que ENSO podría producir las anomalías sobre esa parte oeste del Atlántico Norte.

Dos tipos de simulaciones han sido diseñadas para ahondar en las evidencias mostradas durante el decaimiento del Niño Atlántico. El primer diseño experimental consiste en una simulación transitoria usando en mismo UCLA-AGCM, iniciando la integración en diferentes meses (Julio, Septiembre, Noviembre), con el objetivo de seguir el establecimiento de la respuesta atmosférica circunglobal. Un segundo objetivo es analizar la respuesta atmosférica en una simulación AGCM realizada con el modelo UCLA en el marco del proyecto AMMA-EU. Las condiciones de contorno, condiciones que evolucionan en el tiempo, involucran tanto el decaimiento del Niño Atlántico como el desarrollo de un episodio La Niña en el Pacífico (Rodríguez-Fonseca et al. 2010).

El segundo modo de covariabilidad entre la SST anómala de verano en el Atlántico tropical y la precipitación anómala de verano a invierno en el Atlántico Norte está asociado a un forzamiento localizado sobre el Atlántico Norte Subtropical.

- Esa SST anómala es parte del patrón *Horseshoe* del Atlántico Norte en verano y del Tripolo Atlántico en invierno.

- Durante la transición verano-otoño, las anomalías de precipitación cubren latitudes tropicales y subtropicales, y sufren un debilitamiento como consecuencia de cambios en la convección asociados al decaimiento del *Horseshoe*.

- En otoño, la anomalía de SST, que es previa al establecimiento de la NAO, recuerda al Tripolo Atlántico. El forzamiento subtropical retiene el desplazamiento estacional de la ITCZ y produce anomalías en la divergencia sobre el norte de Sudamérica.

- Este flujo divergente anómalo genera un tren de ondas de Rossby desde el Caribe que afecta a los vientos alisios, influyendo, por tanto, en la SST y reforzando el Tripolo.

- Durante la transición otoño-invierno, la precipitación anómala comprende el sector Euro-Atlántico, proyectando en los efectos de la NAO. La actividad transitoria *eddy* añade sus efectos modificando el intercambio de masa atmosférica entre Azores e Islandia, a través de cambios en la extensión de las corrientes en chorro.

- En invierno, la anomalía dipolar de precipitación se desplaza hacia el norte. La circulación atmosférica asociada al calentamiento Subtropical proyecta en una onda de Rossby, mientras que la actividad *eddy* actúa como realimentación positiva reforzando un ciclón anómalo sobre el oeste de Europa.

- Esta Tesis sugiere que el decaimiento del *Horseshoe* podría ser deberse a una realimentación negativa a través de cambios en la atmósfera tropical, aspecto que podría explicar la falta de covariabilidad entre el *Horseshoe* de otoño y la NAO de invierno revelada en estudio previos.

- Esta Tesis también sugiere la posibilidad de una realimentación positiva entre el patrón SST del Tripolo y la NAO, el cual actuaría de forma previa a la ocurrencia de la NAO.

Estos resultados están siendo actualmente evaluados mediante un complejo conjunto de simulaciones AGCM y simulaciones acopladas a un modelo de capa de mezcla con el SPEEDY/O. Estos diseños experimentales incluyen simulaciones con SST prescrita (AGCM) y con flujos de calor prescritos (AGCM-capa de mezcla), así como experimentos de equilibrio y transitorios (Apéndice-D).

La anomalía de SST observada sobre la cuenca oriental del Mediterráneo (eMED) está asociada tanto a una estructura local baroclínica como a una estructura casi-barotrópica a lo largo del cinturón de latitudes medias.

- Resultados de modelo han confirmado esta evidencia observacional, indicando que el eMED es capaz de generar una respuesta baroclínica durante el final de verano, principio de otoño.

- Esta respuesta local es bastante simétrica, mostrando, para un calentamiento en eMED, convergencia en niveles bajos y anomalías anticiclónicas en niveles altos sobre la región Mediterráneo-África del Norte.

- Resultados de modelo sugieren que el eMED impacta en la circulación hemisférica de verano-otoño con una estructura de número de onda 5, que refleja una propagación confinada en las corrientes en chorro.

- Esta circulación hemisférica forzada está caracterizada por centros de acción aguas abajo de la estructura baroclínica que alcanzan el Pacífico Norte guiados por la corriente del Norte de África. Al final de la propagación, las anomalías alcanzan el sector Euro-Atlántico a través de la corriente del Atlántico Norte.

- Esta Tesis sugiere que el Mediterráneo puede ser un predictor no sólo para el clima regional, sino también para las áreas afectadas por la respuesta circunglobal.

Como se indicó en el Resumen del capítulo IV.4, nuevos experimentos de sensibilidad son necesarios para confirmar las evidencias mostradas en esta Memoria. Primero, una simulación transitoria sería útil para entender mejor el mecanismo de la respuesta circunglobal al Mediterráneo oriental; por ejemplo, para evaluar los posibles cambios en la corriente en chorro de África del Norte-Asia a través de los diferentes impactos con SST positiva y negativa. Segundo, una simulación acoplada con un diseño experimental de 'valor-inicial' (como en Wu et al. 2007) corregiría las limitaciones de las simulaciones AGCM, permitiendo seguir la evolución tanto de la SST como de la respuesta atmosférica asociada.

CONCLUSIONS

According to both, the results shown in chapter IV and the integrating discussion presented in the previous section, the main conclusions derived from this Thesis are detailed as follows. Likewise, and based on a framework of continuity, the future research lines are outlined within each investigation topic.

The leading rotational mode of the upper-level anomalous streamfunction in mid-winter (Jan-Feb) in the North Atlantic-European sector describes the remote ENSO influence (EOF1), having a weak influence on the European climate variability.

- This mode appears as the local component of the leading hemispheric mode, corresponding to the tail of the TNH wavetrain emanating from the tropical Pacific.

- This mode has a dipolar structure in the North Atlantic surface level, being reminiscent of the NAO.

- This Thesis defends that this response should not be described as a NAO-like pattern, because of the different underlying dynamics.

- The SST signal associated with this mode supports its connection with ENSO, with no influence of the adjacent basins.

As further study concerning this topic, two types of experiments have been designed to be performed with the SPEEDY-AGCM model, now allocated in the cluster of the Research Group. This AGCM is currently at UCM as result of the visit to the KNMI during the last summer (Appendix-D). This AGCM is a model without stratosphere, its uppest atmospheric level corresponds to 100hPa, hence allowing the assessment of a purely tropospheric pathway in the ENSO-North Atlantic teleconnection. A first simulation, prescribing observed SSTs, is thought to evaluate whether SPEEDY is able to capture the ENSO teleconnection during mid-late winter. A second step consists of performing a transient experiment during January, for both El Niño and La Niña conditions (by regressing the Niño3.4 SST index onto the prescribed observational field), in order to follow the establishment of the TNH-like atmospheric response.

The second mode of the anomalous upper-level streamfunction (EOF2) displays the classical Azores-Iceland seesaw, and leads to identify it as a purely rotational North Atlantic Oscillation (NAO).

- The underlying dynamics associated with this mode involve mainly internal variability, through meridional shifts of the eddy-driven jet.

- The Atlantic SST signal of this pattern resembles the well-known North Atlantic Tripole.

- EOF2 has a stronger impact on European climate, especially in the precipitation field, associated with a shift in the stormtracks.

Concerning the dynamical comparison between the ENSO-North Atlantic teleconnection and the NAO-internal variability, a step forward is going to be done, by computing the same PCA analysis but applied upon two coupled GCM simulations

from two different old versions of the state-of-the-art global model at MetOffice (HadGEM). These datasets are available from the visit to that centre during 2008's spring (Appendix-C). These simulations consist of 60-years fully ocean-atmosphere coupling with pre-industrial conditions, thereby allowing the assessment of the results from a perspective of natural climate variability.

The leading regional and hemispheric EOFs of the SLP are reconstructed as a combination of these two streamfunction EOFs, in which EOF2 accounts for most of the regional SLP variability and both contribute to the so-called AO/NAM mode (hemispheric SLP variability).

- The small but significant contribution of EOF1 to the regional SLP is due to the similar surface projection (dipolar structure) of the TNH over the North Atlantic.

- The fact that both EOF1 and EOF2 contribute to the AO/NAM pattern indicates that this hemispheric SLP structure might be a combination of different regional (NAO) and large-scale (ENSO) phenomena.

- Despite its regional character at lower levels, EOF2 has a hemispheric structure at upper levels, reminiscent of the circumglobal pattern of Branstator (2002).

To continue with this topic, the contribution of ENSO and NAO to regional and global 'oscillations', a similar multiple-regression analysis is thought but applied upon the two 60-years coupled simulations from the HadGEMs family, the so-called HadGEM1 and HadGEM2. Additionally, a transient simulation with the SPEEDY-AGCM for January will be designed in order to induce a NAO-like response, following the experimental set-up of Li and Conil (2003) with a state-of the-art AGCM. The aim of this transient simulations is to further assess the regional excitation of the Branstator's circumglobal pattern from changes in the North Atlantic eddy-activity.

The leading mode of covariability between the summer tropical Atlantic anomalous SST and the summer to winter rainfall variability in the North Atlantic is associated with the Atlantic Niño.

- During the peak phase of the SST mode, the anomalous precipitation pattern appears as a longitudinal band that covers the whole Equatorial basin affecting the position of the ascending branch of the Atlantic Walker and Hadley circulations.

- As the eastern equatorial SST anomalies decay, the corresponding precipitation and vertical motions associated with the Atlantic Walker cell come back to its climatological location generating large upper tropospheric anomalous divergence over northern South America.

- The upper-divergent outflow, located over the remaining SST anomalies leads the extratropical climate in fall and winter by, both, zonal and meridional circulation.

- Zonally, the generation of Rossby waves trapped in the North Africa-Asian jet supports the hypothesis of a circumglobal response to the damped Atlantic Niño.

- Meridionally, the subtropical subsidence and the eddy-momentum divergence reinforce the upper-level convergence in the western North Atlantic.

Sensitivity experiments done for a positive phase of the Atlantic Niño have corroborated some of the observational hypothesis.

- The simulated rainfall shows a progressive weakening in the eastern part of the basin and a clear confinement in the western part at the end of the Atlantic Niño cycle.

- The Atlantic Niño damping is able to trigger a hemispheric downstream teleconnection during late-autumn and winter; which gets trapped into the subtropical jet.

- The different Rossby wave responses to the

Atlantic Niño damping show a time-evolution, from an arching pattern in summer, when the jet is weak, to a zonally-trapped propagation in winter, when the jet is strong and close to the anomalous vorticity source.

- The winter circulation anomalies over the eastern Atlantic-Mediterranean region can favour the recurrent circumglobal teleconnection pattern found by Branstator (2002) along the North African-Asian jet.

- The evolution of the summer Atlantic Niño seems to play a non relevant role in the anomalous dry conditions over the western North Atlantic. A developing La Niña episode is apparent in conjunction with the Atlantic Niño damping; pointing at ENSO as potential key player in producing precipitation anomalies over western subtropical basin.

Two types of simulations have been designed to further study the evidences shown for the Alantic Niño damping. A frist experimental set-up consist of a transient simulation using the same UCLA-AGCM, initializing in different months (July, September, November), in order to follow the establishment of the circumglobal atmospheric response. A second objective is to analyse the atmospheric response from a time-evolving AGCM simulation performed with the UCLA model in the framework of the AMMA project (Rodríguez-Fonseca et al. 2010). This time-evolving run consist of a SST sequence involving both the Atlantic Niño-decay and the Pacific La Niña-development.

The second mode of covariability between the summer tropical Atlantic anomalous SST and the summer to winter rainfall anomalies in the North Atlantic is associated with a thermal forcing located over the Subtropical North Atlantic.

- The SST anomaly is part of the summer North Atlantic Horseshoe and the winter North Atlantic Tripole.

- From summer to fall, the precipitation anomalies, which cover the tropical/ subtropical North Atlantic, get weak as a result of changes in tropical convection associated with the damping of the Horseshoe.

- In fall, the SST anomaly, which is previous to the establishment of the NAO pattern, resembles a weak Atlantic Tripole. The subtropical forcing leads to a displacement of the ITCZ and changes in the anomalous upper divergence over northwestern South America.

- This anomalous outflow forces a Rossby wavetrain from the Caribbean, affecting the trades and the North Atlantic westerly winds, influencing on the SSTs and, thus, reinforcing the tripole.

- During the fall to late-winter transition, the precipitation anomalies cover the North Atlantic-European sector. The transient eddy activity adds its effects by affecting the air-mass exchange between Azores-high and Iceland-low through changes in the zonal extension of the Atlantic jets.

- In winter, the dipolar precipitation anomaly over Europe is displaced northward. The atmospheric response to the eastern Subtropical SST anomaly projects onto a Rossby wave, and the transient activity acts as a positive feedback inducing a large cyclonic anomaly over western Europe.

- This Thesis suggests that the Horseshoe summer to fall transition could be due to the negative feedback produced as response to tropical atmosphere alterations, a feature that could explain the gap in the covariance between autumn Horseshoe and winter NAO found in previous studies.

- This Thesis also suggests the possibility of a positive feedback between the Tripole SST pattern and the NAO, which acts before the NAO occurrence.

These results are currently being assessed by means of a complete set of AGCM and coupled-to-slab-ocean GCM experiments with the SPEEDY/O model. These experimental set-ups include SST-forced (AGCM) and heat flux-forced (slab-ocean-AGCM) long-term equilibrium simulations and transient runs (Appendix-D).

The observed Eastern Mediterranean (eMED) summer-early autumn SST is associated with both, a local baroclinic structure over the basin and a quasi-barotropic anomalous circulation along the Northern Hemisphere midlatitudes.

- Model results have confirmed this observational evidence, indicating that the eMED basin is able to trigger a local baroclinic response during late-summer and early-autumn.

- The local response is close to linear presenting, for a warming in the eMED, a low-level convergence and upper-level anticyclonic circulation anomalies over the Mediterranean-Northern Africa region.

- Model results suggest that eMED SST anomalies impact on the hemispheric atmospheric circulation, with a zonal wavenumber-5 circumglobal structure trapped into the main westerly jets.

- This forced hemispheric circulation is characterized by centres of action, downstream of the baroclinic response, over middle Eurasia and western North Pacific following the North African-Asian jet. Further downstream, along the tail of the atmospheric teleconnection, the eMED SST affects the circulation over the Euro-Atlantic sector following the North Atlantic jet.

- This Thesis suggests the potential role of the summer Mediterranean not only in the regional affected areas, but also as large-scale predictor by the circumglobal response.

As indicated in the Summary of the chapter IV.4, dedicated modelling efforts are required in order to provide further support to these evidences. First, a transient approach in the experimental set-up would be useful to better illustrate the mechanism controlling the circumglobal response to eastern-Mediterraean SST; for instance, to evaluate the potential changes in the North African-Asian jet through different impacts during warm and cold situations. Second, a coupled GCM experiment with an initial-value approach of the forcing (as in Wu et al. 2007) would correct the limited conclusions from AGCMs, which in turn would allow to track the evolution of the SST and associated atmospheric response.

REFERENCIAS

Alexander, M. A., I. Bladé, M. Newman, J. R. Lanzante, N.-C. Lau, J. D. Scott (2002): The atmospheric bridge: the influence of ENSO teleconnections on air-sea interaction over the global oceans. J. Clim., 15, 2205-2231.

Ambaum, M. H. P., B. J. Hoskins y D. B. Stephenson (2001): Arctic Oscillation or North Atlantic Oscillation? J. Clim., 14, 3495-3507.

Ambaum, M. H. P. y B. J. Hoskins (2002): The NAO troposphere-stratosphere. J. Clim., 15, 1969-1978.

Ambrizzi, T., B. J. Hoskins, y H.-H. Hsu (1995) Rossby wave propagation and teleconnection patterns in the austral winter. J. Atmos. Sci., 52, 3661-3672.

Baldi, M., F. Meneguzzo, G. A. Dalu, G. Maracchi, M. Pasqui, V. Capecchi, A. Crisci y F. Piani (2004): Guinea Gulf SST and Mediterranean summer climate: analysis of the interannual variability. In Proceedings of the 84th AMS Conference 11.11.

Barnett, T. P. y R. Preisendorfer (1987): Origins and levels of monthly and seasonal forecast skill for United States surface air temperature determined by canonical correlation analysis. Mon. Wea. Rev., 115, 1825-1850.

Barnston, A. G. y R. E. Livezey (1987): Classification, seasonality and persistence of low-frequency atmospheric circulation patterns. Mon. Wea. Rev., 115, 1083-1126.

Bell, C. J., L. J. Gray, A. J. Charlton-Perez, M.M. Joshi y A. A. Scaife (2009): Stratospheric communication of El Niño teleconnections to European winter. J. Clim., 22, 4083-4096.

Bjerknes, J. (1969): Atmospheric teleconnections from the equatorial Pacific. Mon. Wea. Rev., 97, 163-172.

Blackmon, M.L., J.M. Wallace, N.-C. Lau y S.L. Mullen (1977): An observational study of the northern hemisphere wintertime circulation. J. Atmos. Sci., 34, 1040-1053.

Blackmon, M.L., J. E. Geisler y E. J. Pitcher (1983): A General Circualtion Model study of january climate anomaly patterns associated with interannual variations of equatorial Pacific sea surface temperatures. J. Atmos. Sci., 40, 1410-.

Bladé, I., M. Newman, M. A. Alexander y J. D. Scott (2008): The late fall extratropical response to ENSO: sensitivity to coupling and convection in the tropical West Pacific. J. Clim., 21, 6101-6118.

Branstator, G. (1983): Horizontal energy propagation in a barotropic atmosphere with meridional and zonal structure. J. Atmos. Sci., 40, 1689-1708.

Branstator, G. (1985): Analysis of general circulation model sea surface temperature anomaly simulations using a linear model. Part I: forced solutions. J. Atmos. Sci., 42, 2225-2241.

Branstator, G.W. (1995): Organization of stormtrack anomalies by recurring low-frequency circulation anomalies. J. Atmos. Sci., 52, 207-226.

Branstator, G. (2002): Circumglobal teleconnections, the Jetstream waveguide, and the North Atlantic Oscillation. J. Clim., 15, 1983-1910.

Bretherton, S. B., C. Smith, y J. H. Wallace (1992): An Intercomparation of methods for finding coupled patterns in climate data. J. Clim., 5, 541-560.

Brönnimann S. (2007): The impact of El Niño/Southern Oscillation on European climate. Rev. Geophys., 45, RG3003, doi: 10.1029/2006RG000199.

Cagnazzo, C. y E. Manzini (2009): Impact of the stratosphere on the winter tropospheric teleconnections between ENSO and the North Atlantic and European region. J. Clim., 22, 1223-1238.

Carton, J. A., X. Cao, B. S. Giese y A. M. Da Silva (1996): Decadal and interannual SST variability in the tropical Atlantic

Ocean. J. Phys. Oceanogr., 26, 1165–1175.

Cassou, C. y L. Terray (2001a): Oceanic forcing of the wintertime low-frequency atmospheric variability in the North Atlantic European sector: a study with the ARPEGE model. J. Clim., 14, 4266-4291.

Cassou, C. y L. Terray (2001b): Dual influence of Atlantic and Pacific SST anomalies on the North Atlantic/Europe winter climate. Geophys. Res. Lett., 28, 3195-3198.

Cassou, C., C. Deser, L. Terray, J. W. Hurrell y M. Drévillon (2004): Summer sea surface temperature conditions in the North Atlantic and thier impact upon the atmospheric circulation in early winter. J. Clim., 17, 3349-3363.

Castro-Díez, Y., D. Pozo-Vázquez, F. S. Rodrigo y M. J. Esteban-Parra (2002): NAO and winter temperature variability in southern Europe. Geophys. Res. Lett., 29, doi: 10.1029/2001GL014042.

Cayan, D. R. (1992): Latent and sensible heat flux anomalies over the northern oceans: driving the sea surface temperature. J. Phys.Oceanogr., 22, 859–881.

Chang, E. K. M., S. Lee y K. L. Swanson (2002): Storm track dynamics. J. Clim., 15, 2163-2183.

Chang, P., L. Ji y H. Li (1997): A decadal climate variation in the tropical Atlantic Ocean from thermodynamic air–sea interactions. Nature, 385, 516–518.

Chang, P. y D. S. Battisti (1998): The Physics of El Niño. Physics World, 8, 41-47.

Chang, P., Y. Fang, R. Saravannan, L. Ji y H. Seidel (2006): The cause of the fragile relationship between the Pacific El Niño and the Atlantic Niño. Nature, 443, 324– 328.

Cheng, X. y T. J. Dunkerton (1995): Orthogonal rotation of spatial patterns derived from Singular Value Decomposition analisys. J. Clim., 8, 2631-2643.

Cherry, S. (1997): Some commments on Singular Value Decomposition analysis. J. Clim., 10, 1759-1761.

Czaja, A. y C. Frankignoul (1999): Influence of the North Atlantic SST on the atmospheric circulation. Geophys. Res. Lett., 26, 2969-2972.

Czaja, A. y C. Frankignoul (2002): Observed impact of Atlantic SST anomalies on the North Atlantic Oscillation. J. Clim., 15, 606-623.

Czaja, A., A. W. Robertson, y T. Huck (2003): The role of Atlantic ocean-atmosphere coupling in affecting North Atlantic Oscillation variability. En “The North Atlantic Oscillation: Climatic Significance and Environmental Impact” Geophysical Monograph 134, 147-172.

Davey, M. K. y A. E. Gill (1987): Experiments on tropical circulation with a simple moist model. Quart. J. Roy. Meteor. Soc., 113, 1237–1269.

Deser, C. (2000): On the teleconnectivity of the “Artic Oscillation”. Geophys. Res. Lett., 27, 779-782.

DeWeaver, E. y S. Nigam (2002): Linearity in ENSO’s atmospheric response. J. Clim., 15, 2446-2461.

Ding, Q. y B. Wang (2005): Circumglobal teleconnection in the Northern Hemisphere summer. J. Clim., 18, 3483-3505.

Dommenget, D. y M. Latif (2000): Interannual to decadal variability in the tropical Atlantic. J. Clim., 13, 777-792.

Drévillon, M., L. Terray, P. Rogel y C. Cassou (2001): Mid latitude Atlantic SST influence on Europe winter climate variability in the NCEP Reanalysis. Clim. Dyn., 18, 331-344.

Drévillon, M., C. Cassou y L. Terray (2003): Model study of the North Atlantic region atmospheric response to autumn tropical Atlantic sea-surface-temperature anomalies. Q. J. R. Meteorol. Soc., 129, 2591-2611.

Drosdowsky, W. (1993): An analysis of Australian seasonal rainfall anomalies: 1950–1987. I: Spatial analysis. Int. J. Climatol., 13, 1–30.

Edmon, H. J., B. J. Hoskins y M. E. McIntyre (1980): Eliassen-Palm cross sections for the troposphere. J. Atmos. Sci., 37, 2600-2616.

Esteban-Parra, M. J., F. S. Rodrigo, Y. Castro-Díez (1998): Spatial and temporal patterns of precipitation in Spain for the period 1880–1992. Int. J. Climatol., 18, 1557–1574.

Fontaine, B., J. García-Serrano, P. Roucou, B. Rodríguez-Fonseca, T. Losada, F. Chauvin, S. Gervois, S. Sijikumar, P. Ruti, S. Janicot (2009): Impacts of warm and cold situations in the Mediterranean basins on the West African monsoon: observed connection patterns (1979-2006) and climate simulations. Clim. Dyn., doi 10.1007/s00382-009-0599-3.

Frankignoul C. y E. Kestenare (2005): Observed Atlantic SST anomaly impact on the NAO: an update. J. Clim., 18, 4089-4094.

Frías, M. D., J. Fernández, J. Sáenz y C. Rodríguez-Puebla (2005): Operational predictability of monthly average maximum temperature over the Iberian Peninsula using DEMETER simulations and downscaling. Tellus, 57A, 448-463.

Frías, M. D., S. Herrera, A. S. Cofiño y J. M. Gutiérrez (2010): Assesing the skill of precipitation and temperature seasonal forecasts in Spain: windows of opportunity related to ENSO events. J. Clim., 23, 209-220.

Gámiz-Fortis, S. R., D. Pozo-Vázquez, M. J. Esteban-Parra y Y. Castro-Díez (2002): Spectral characteristics and predictability of the NAO assessed through Singular Spectral Analysis. J. Geophys. Res., 107, doi: 10.1029/2001JD001436.

Gill, A. E. (1980): Some simple solutions for heat-induced tropical circulation. Quart. J. Roy. Meteor. Soc., 106, 447–462.

Gill, A. E. (1982): Atmosphere-Ocean Dynamics. Academic Press, Inc.,.662 pp.

González-Rouco, J. F., H. Heyen, E. Zorita y F. Valero (2000): Agreement between observed rainfall trends and climate change simulations in the southwest of Europe. J. Clim., 13, 976-985.

Gorgas, J., N. Cardiel y J. Zamorano (2009): Estadística básica para estudiantes de Ciencias. Facultad CC Físicas, UCM, Madrid.

Haarsma, R. J. y W. Hazeleger (2007): Extratropical atmospheric response to equatorial Atlantic cold tongue anomalies. J. Clim., 20, 2076–2091.

Hoerling, M.P. y M. Ting (1994): Organization of extratropical transients during E1 Niño. J. Clim., 7, 745-766.

Holton, J. R. (1992): An introduction to dynamic meteorology. volume 48 of International Geophysics Series. Academic Press, third edition.

Horel, J.D. y M. J. Wallace (1981): Planetary scale atmospheric phenomena associated with the Southern Oscillation.Mon. Wea. Rev., 109, 813-829.

Hoskins B. J., A. J. Simmons y D. G. Andrews (1977): Energy dispersion in a barotropic atmosphere. Quart. J. R. Met. Soc., 103, 553-568.

Hoskins, B. J. y D. J. Karoly (1981): The steady linear response of a spherical atmosphere to thermal and orographic forcing. J. Atmos. Sci., 38, 1179-1196.

Hoskins, B.J., I.N. James y G.H. White (1983): The shape, propagation and mean flow interaction of large-scale weather systems. J. Atmos. Sci., 40, 1595-1612.

Hoskins, B. J. y P. J. Valdes (1990): On the existence of storm-tracks. J. Atmos. Sci., 47, 1854-1864.

Hoskins, B. J. y T. Ambrizzi (1993): Rossby wave propagation on a realistic longitudinally varying flow. J. Atmos. Sci., 50, 1661-1671.

Hsu, H.-H. y S.-H. Lin (1992): Global teleconnections in the 250mb streamfunction field during the Northern Hemisphere winter. Mon. Wea. Rev., 120, 1169-1190.

Hu, Q. (1997): On the uniqueness of the Singular Value Decomposition in meteorological applications. J. Clim., 10, 1762-1766.

Huang, B. y J. Shukla (2005): Ocean-atmosphere interactions in the tropical and subtropical Atlantic Ocean. J. Clim., 18, 1652-1672.

Hurrell, J. W. (1995): Decadal trends in the North Atlantic Oscillation: regional temperatures and precipitation. Science, 269, 676-679.

Hurrell, J, W. y H. van Loon (1997): Decadal variations in climate associated with the North Atlantic Oscillation. Clim. Chang., 36, 301-326.

Hurrell, J. W., Y. Kushnir, G. Ottersen, y M. Visbeck (2003): An overview of the North Atlantic Oscillation. En "The North Atlantic Oscillation: Climatic Significance and Environmental Impact" Geophysical Monograph 134, 1-35.

Huth, R. (1997): Continental-scale circulation in the UKHI GCM. J. Clim., 10, 1545–1561.

Ineson, S. y A. A. Scaife (2008): The role of the stratosphere in the European climate response to ENSO. Nature Geosci., doi: 10.1038/NGEO381.

Itoh, H. (2002): True versus apparent Artic Oscillation. Geophys. Res. Lett., 29, 1268. doi: 10.1029/2001GL013978.

Jolliffe, I. T. (1987): Rotation of principal components: Some comments. J. Climatol., 7, 507–510.

Jung, T., L. Ferranti y A. M. Tompkins (2006): Response to the summer of 2003 Mediterranean SST anomalies over Europe and Africa. J. Clim., 19, 5439-5454.

Karoly, D. J., R. A. Plumb y M. Ting (1989): Examples of the horizontal propagation of quasi-stationary waves. J. Atmos. Sci., 46, 2802-2811.

Keenlyside N. S. y M. Latif (2007): Understanding Equatorial Atlantic Interannual Variability. J. Clim., 30, 131-142.

Kiladis, G. N. y H. F. Diaz (1989): Global climatic anomalies associated with extremes in the Southern Oscillation. J. Clim., 2, 1069-1090.

Kiladis, G. N. y K. M. Weickmann (1992): Circulation anomalies associated with tropical convection during Northern winter. Mon. Wea. Rev., 120, 1900-1923.

Krishnamurti, T.N. (1971): Tropical east-west circulations during the northern summer. J. Atmos. Sci., 28, 1342–1347.

Krishnamurti, T.N., M. Kanamitsu, W.J. Koss y J.D. Lee (1973): Tropical east-west circulations during the northern winter. J. Atmos. Sci., 30, 780–787.

Kushnir, Y., W. A. Robinson, I. Blade, N. M. J. Hall, S. Peng, R. Sutton (2002): Atmospheric GCM response to extratropical SST anomalies: synthesis and evaluation, J. Clim., 15, 2232-2256.

Lee, S.-K., C. Wang y B. E. Mapes (2009): A simple atmospheric model of the local and teleconnections responses to tropical heating anoamlies. J. Clim., 22, 272-284.

Legates, D. R. y C. J. Willmott (1990): Mean seasonal and spatial variability global surface air temperature. Theor. Appl. Climatol., 41, 11-21.

Li, Z. X. y S. Conil (2003): Transient response to an atmospheric GCM to North Atlantic SST anoamlies. J. Clim., 16, 3993-3998.

Li, L. Z. X. (2006) : Atmospheric GCM response to an idealized anomaly of the Mediterranean sea surface temperature. Clim. Dyn., doi: 10.1007/s00382-006-0152-6.

Lin, H., J. Derome y G. Brunet (2007): The nonlinear transient atmospheric response to tropical forcing. J. Clim., 20, 5642-5665.

Llorente, M. y V. M. Pérez (1998): Calculo Numérico para Computación en Ciencia e Ingeniería. Ed. Sintesis.362 pp.

Losada, T., B. Rodríguez-Fonseca, C.R. Mechoso y H.-Y. Ma (2007): Impacts of SST anomalies on the North Atlantic atmospheric circulation: a case study for the northern winter 1995/1996. Clim. Dyn., doi 10.1007/s00382-007-0261-x.

Losada, T., B. Rodríguez-Fonseca, S. Janicot, S. Gervois, F. Chauvin y P. Ruti (2009a): A multimodel approach to the Atlantic Equatorial mode. Impact on the West African monson. Clim. Dyn., doi: 10.1007/s00382-009-0625-5.

Losada, T., B. Rodríguez-Fonseca, I. Polo, S. Janicot, S. Gervois, F. Chauvin y P. Ruti (2009b): Tropical response to the Atlantic Equatorial mode: AGCM multimodel approach. Clim. Dyn., doi: 10.1007/s00382-009-0624-6.

Manzini, E., M. A. Giorgetta, M. Esch, Kornblueh, E. Roeckner (2006): The influence of sea surface temperature on the Northern winter stratosphere: ensembles simulations with the MAECHAM5 model. J. Clim., 19, 3863-3881.

Matsuno, T. (1966): Quasi-geostrophic motions in the equatorial area. J. Meteor. Soc. Japan, 44, 25–43.

McGuffie, K. y A. Henderson-Sellers (2005): A climate modelling primer, 3th Edition. John Wiley & Sons Ltd., Inglaterra.

Mechoso, C. R., J.-Y. Yu y A. Arakawa (2000): A coupled GCM pilgrimage: From climate catastrophe to ENSO simulations. General circulation model development: Past, present and future. Proceedings of a Symposium in Honor of Professor Akio Arakawa, D. A. Randall, Ed., Academic Press, pp. 539-575.

Merkel, U. y M. Latif (2002): A high resolution AGCM study of the El Niño impact on the North Atlantic/European sector. Geophys. Res. Lett., 29, 1291, doi: 10.1029/2001GL013726.

North, G. R., T. L. Bell, R. F. Cahalan y F. J. Moeng (1982): Sampling errors in the estimation of Empirical Orthogonal Functions. Mon. Wea. Rev., 110, 699-706.

Okumura, Y., S.-P. Xie, A. Numaguti y Y. Tanimoto (2001): Tropical Atlantic air-sea interaction and its influence on the NAO. Geophys. Res. Lett., 28, 1507-1510.

Okumura, Y. y S.-P. Xie (2006): Some overlooked features

of Tropical Atlantic climate leading to a new Niño-like phenomenon. J. Clim., 19, 5859-5874.

Peixoto, J. P. y A. H. Oort (1992). Physics of Climate. American Institute of Physics, Nueva York, 520 pp.

Peng, S., W. A. Robinson, S. Li y M. P. Hoerling (2005): Tropical Atlantic SST forcing of coupled North Atlantic seasonal responses. J. Clim., 18, 480-496.

Pohlmann, H. y M. Latif (2005): Atlantic versus Indo-Pacific influence on Atlantic-European climate. Geophys. Res. Lett., 32, L05707, doi: 10.1029/2004GL021316.

Polo I., B. Rodríguez-Fonseca y J. Sheinbaum (2005): Northwest Africa upwelling and the Atlantic climate variability, Geophys. Res. Lett., 32, L23702, doi:10.1029/2005GL023883.

Polo, I., B. Rodríguez-Fonseca, T. Losada, J. García-Serrano (2008): Tropical Atlantic variability modes (1979-2002). Part I: time-evolving SST modes related to West African rainfall. J. Clim., 21, 6457-6475.

Polo, I. (2008): Variabilidad del Atlántico Tropical: interacciones océano-atmósfera e impactos en el clima. Tesis Doctoral, UCM, Madrid.

Pozo-Vázquez, D., M. J. Esteban-Parra, F. S. Rodrigo y Y. Castro-Díez (2000): An analysis of the variability of the North Atlantic Oscillation in the time and the frequency domains. Int. J. Climatol., 20, 1675-1692.

Pozo-Vázquez, D., M. J. Esteban-Parra, F. S. Rodrigo y Y. Castro-Díez (2001): A study of NAO variability and its possible non-linear influences on European surface temperatures. Clim. Dyn., 17, 701-715.

Qin, J. y W. A. Robinson (1993): On the Rossby wave source and the steady linear response to tropical forcing. J. Atmos. Sci., 50, 1819-1823.

Richman, M. B. (1986): Rotation of principal components. J. Climatol., 6, 293–335.

Ritcher, I., C. R. Mechoso y A. W. Robertson (2008): What determines the position and intensity of the South Atlantic anticyclone in austral winter?. J. Clim., 21, 214-229.

Rodó , X., E. Baert, y F. Comín (1997): Variations in the seasonal rainfall in Southern Europe during the present century: Relationship with the North Atlantic Oscillation and the El Niño-Southern Oscillation. Clim. Dyn., 13, 275–284.

Rodríguez-Fonseca, B. (2001): Relación entre el régimen de precipitación anómalo en la Península Ibérica y la variabilidad de baja frecuencia del sistema climático en el Atlántico Norte. Tesis Doctorale, UCM, Madrid.

Rodriguez-Fonseca, B. y E. Serrano (2002): Winter 10-day coupled patterns between geopotential height and Iberian Peninsula rainfall using the ECMWF precipitation reanalysis. J. Clim., 15, 1309-1321.

Rodríguez-Fonseca, B. y M. Castro (2002): On the connection between winter anomalous precipitation in the Iberian Peninsula and North West Africa and the summer subtropical Atlantic Sea Surface Temperature. Geophys. Res. Lett., 29, doi:10.1029/2001GL014421.

Rodríguez-Fonseca B., I. Polo, E. Serrano y M. Castro (2006): Evaluation of the north Atlantic SST forcing on the European and northern African winter climate. Int. J. Climatol., 25, doi: 10.1002/7joc.1234.

Rodríguez-Fonseca, B., I. Polo, J. García-Serrano, T. Losada, E. Mohino, C. R. Mechoso y F. Kucharski (2009): Are Atlantic Niños enhancing Pacific ENSO events in recent decades?. Geophys. Res. Lett., 36, L20705, doi: 10.1029/2009GL040048.

Rodríguez-Fonseca, B., S. Janicot, E. Mohino, T. Losada, J. Bader, C. Caminade, F. Chauvin, B. Fontaine, J. García-Serrano, S. Gervois, M. Joly, I. Polo, P. Ruti, P. Roucou y A. Voldoire (2010): Interannual and decadal SST forced responses of the West African Monsoon. Atmos. Sci. Lett., ASL-10-030 (under review).

Rodríguez-Puebla, C., A. H. Encinas, S. Nieto y J. Garmendia (1998): Spatial and temporal patterns of annual precipitation variability over the Iberian Peninsula. Int. J. Climatol., 18, 299-316.

Rodríguez-Puebla, C., A. H. Encinas y J. Sáenz (2001): Winter precipitation over the Iberian Peninsula and its relationship to circulation indices. Hidrol. Earth Syst. Sci., 5, 233-244.

Rodwell, M.R. y C.K. Folland (2002): Atlantic air-sea interaction and seasonal predictability. Quart. J. R. Met. Soc., 128, 1413-1443.

Ropelewski, C. F. y M. S. Halpert (1986): North American precipitation and temperature patterns associated with the El Niño/Southern Oscillation. Mon. Wea. Rev., 114, 2352-2362.

Ropelewski, C. F. y M. S. Halpert (1987): Global and regional scale patterns associated with the El Niño/Southern Oscillation.

Mon. Wea. Rev., 115, 1606-1626.

Ropelewski, C. F. y M. S. Halpert (1989): Precipitation patterns associated with the high index phase of the Southern Oscillation. J. Clim., 2, 268-284.

Ropelewski, C. F. y M. S. Halpert (1996): Quantifying Southern Oscillation-precipitation relationships. J. Clim., 9, 1043-1059.

Rowell, D. P. (2003): The impact of the Mediterranean SSTs on the Sahelian rainfall season. J. Clim., 16, 849-862.

Ruíz-Barradas, A., J. A. Carton y S. Nigam (2000): Structure of interannual-to-decadal climate variability in the tropical Atlantic sector. J. Clim., 13, 3285-3297.

Sáenz, J., J. Zubillaga y C. Rodríguez-Puebla (2001a): Interanual winter temperature variability in the north of the Iberian Peninsula. Clim. Res., 16, 169-179.

Sáenz, J., J. Zubillaga y C. Rodríguez-Puebla (2001b): Interanual variability of the winter precipitation in northern Iberian Peninsula. Int. J. Climatol., 21, 1503-1513.

Sáenz, J., C. Rodríguez-Puebla, J. Fernández y J. Zubillaga y (2001c): Interpretations of interannual winter temperature variations over southwestern Europe. J. Gephys. Res., 106, 20641-20651.

Sánchez-Gómez, E., F. Álvarez-García y M. J. Ortiz-Bevia (2001): Empirical forecasts of 850hPa air temperature anomalies over the North Atlantic. Quart. J. R. Met. Soc., 127, 2761-2786.

Sánchez-Gómez, E. y L. Terray (2005): Large-scale atmospheric dynamics and local intense precipitation episodes. Geophys. Res. Lett., 32, doi:10.1029/2005GL023990.

Sánchez-Gómez, E., L. Terray y B. Joly (2008): Intra-seasonal atmospheric variability and extreme precipitation events in the Euro-Mediterranean region. Geophys. Res. Lett., 35, doi:10.1029/2008GL034515.

Sardeshmukh, P. D. y B. J. Hoskins (1985): Vorticity balances in the tropics during the 1982-83 El Niño-Southern Oscillation event. Quart. J. R. Met. Soc., 111, 261-278.

Sardeshmukh, P. D. y B. J. Hoskins (1987): On the derivation of the divergent flow from the rotational flow: the χ problem. Quart. J. R. Met. Soc., 113, 339-360.

Sardeshmukh, P. D. y B. J. Hoskins (1988): The generation of global rotational flow by steady idealized tropical divergence. J. Atmos. Sci., 45, 1228-1251.

Servain J., I. Wainer, J. P. McCreary y A. Dessier (1999): Relationship between the equatorial and meridional modes of climatic variability in the tropical Atlantic. Geophys. Res. Lett., 26, 485-488.

Shaman, J. y E. Tziperman (2005): The effect of ENSO on Tibetan Plateau snow depth: a stationary wave teleconnection mechanism and implications for the South Asian monsoons. J. Clim., 18, 2067-2079.

Smith, T. M. y R. W. Reynolds (2003): Extended reconstruction of global sea surface temperatures based on COADS data (1854-1997). J. Clim., 16, 1495-1510.

Sutton, R. T. y M. R. Allen (1997) Decadal predictability in North Atlantic sea surface temperature and climate. Nature, 388, 563-567.

Sutton R.T., S. P. Jewson y D. P. Rowell (2000): Elements of climate variability in the tropical Atlantic region. J. Clim., 13, 3261-3284.

Sutton R. T., W. Norton y S. Jewson (2001): The North Atlantic Oscillation —What role for the ocean? Atmos. Sci. Lett., 1, 89–100.

Sterl, A., G. J. van Oldenborgh, W. Wazeleger y G. Burgers (2007): On the robustness of ENSO teleconnections. Clim. Dyn., 29, 469-485.

Terray, L. y C. Cassou (2002): Tropical Atlantic Sea surface temperature forcing of quasi-decadal climate variability over the North Atlantic-Europe region. J. Clim., 15, 3170–3187.

Thompson D. W. J. y J. M. Wallace (2000): Annular modes in the extratropical circulation. Part I: month-to-month variability. J. Clim., 13, 1000–1016.

Thompson, D. W. J., S. Lee y M. P. Baldwin (2003): Atmospheric processes governing the Northern Hemisphere Annular Mode/ North Atlantic Oscillation. En "The North Atlantic Oscillation: Climatic Significance and Environmental Impact" Geophysical Monograph 134, 81-112.

Toniazzo, T. y A. A. Scaife (2006): The influence of ENSO on winter North Atlantic climate. Geophys. Res. Lett., 33, L24704, doi: 10.1029/2006GL027881.

Trenberth, K.E. (1986): An assessment of the impact of

transient eddies on the zonal flow during a blocking episode using localized Eliassen-Palm flux diagnostics. J. Atmos. Sci., 43, 2070-2087.

Trenberth, K.E. (1991): Storm tracks in the southern hemisphere. J. Atmos. Sci., 48, 2159-2178.

Trenberth, K. E., G. W. Branstator, D. Karoly, A. Kumar, N.-C. Lau y C. Ropelewski (1998): Progress during TOGA in understanding and modeling global teleconnections associated with tropical seas surface temperatures. J. Geophys. Res., 103, 14291-14324.

Trigo, R. M., T. J. Osborn y J. Corte-Real (2002): The North Atlantic Oscillation influence on Europe: climate impacts and associated physical mechanisms. Clim. Res., 20, 9-17.

Trigo, R. M., D. Pozo-Vázquez, T. J. Osborn, Y. Castro-Díez, S. Gámiz-Fortis y M. J. Esteban-Parra (2004): North Atlantic Oscillation influence on precipitation, river flow and water resources in the Iberian Peninsula. Int. J. Climatol., 24, 925-944.

Uppala, S. M. y co-authors (2005): The ERA-40 re-analysis. Quart. J. Roy. Meteor. Soc.,131, 2961-3012.

Vallis, G. K. (2006): Atmospheric and Oceanic fluid dynamics. Fundamental and large-scale circulation. Cambridge University Press, New York, 745 pp.

van Loon, H., J. C. Rogers (1978): The seesaw in winter temperatures between Greenland and northern Europe. Part I: General descriptions. Mon. Wea. Rev., 106, 296-310.

Visbeck M., E. P. Chassignet, R. G. Curry, T. L. Delworth, R. R. Dickson y G. Krahmannn (2003): The Ocean's Response to North Atlantic Oscillation Variability. En "The North Atlantic Oscillation: Climatic Significance and Environmental Impact" Geophysical Monograph 134, 113-145.

von Storch, H. (1995): Spatial patterns: EOFs and CCA. En H. von Storch and A. Navarra, editors. Analysis of Climate Variability: Application of Statistical Techniques, Springer Verlag, 227-257.

von Storch, H. y F. W. Zwiers (2001): Statistical analysis in climate research. Cambridge University Press, UK.

Wainer, I., J. Servain y G. Clauzet (2008): Is the decadal variability in the tropical Atlantic a precursor to the NAO?. Ann. Geophys., 26, 4075-4080.

Walker, G. T. (1923): Correlation in seasonal variations of weather VIII: A preliminary study of world weather. Mem. Indian Meteor. Dept., 24, 75–131.

Walker, G. T. (1924): Correlation in seasonal variations of weather IX: A further study of world weather. Mem. Indian Meteor. Dept., 24, 275–332.

Walker, G. T. (1928): World weather III. Mem. Roy. Meteor. Soc., 2, 97–106.

Wallace, J. M. y D. S. Gutzler (1981): Teleconnections in the geopotential height field during the Northern Hemisphere winter. Mon. Wea. Rev., 109, 784–812.

Wallace, J. M., G. H. Lim y M. L. Blackmon (1988): Relationship between cyclone tracks, anticyclone tracks, and baroclinic waveguides. J. Atmos. Sci., 45, 439–462.

Wallace, J. M., C. Smith y C. S. Bretherton (1992): Singular Value Decomposition of wintertime sea surface temperature and 500-mb height anomalies. J. Clim., 5, 561-576.

Wallace J. M. (2000): North Atlantic Oscillation/annular model: two paradigms-one phenomena. Quart. J. Roy. Meteor. Soc., 126, 791–805.

Wang, C. (2002a): Atmospheric circulation cells associated with the El Niño-Southern Oscillation. J. Clim., 15, 399–419.

Wang, C. (2002b): Atlantic climate variability and its associated atmospheric circulation cells. J. Clim., 15, 1516–1536.

Wang, C. (2005): ENSO, Atlantic Climate Variability and the Walker and Hadley Circulations. Revised to the book of the Hadley Circulation: Present, Past and Future, H. F. Diaz and R. S. Bradley, Eds., Cambridge University Press.

Wang, C. (2006): An overlooked feature of tropical climate: inter-Pacific-Atlantic variability. Geophys. Res. Lett., 33, doi:10.1029/2006GL026324.

Watanabe, M. (2004) Asian jet waveguide and downstream extension of the North Atlantic Oscillation. J. Clim., 17, 4674-4691.

Webster, P. J. (1981): Mechanisms determining the atmospheric response to sea surface temperature anomalies. J. Atmos. Sci., 38, 554–571.

Webster, P. J. (1982): Seasonality in the local and remote atmospheric response to sea surface temperature anomalies. J.

Atmos. Sci., 39, 41–52.

Wu, L., F. He, Z. Liu y C. Li (2007): Atmospheric teleconnections of Tropical Atlantic Variability: interhemispheric, tropical-extratropical, and cross-basin interactions. J. Clim., 20, 856-870.

Xie, P. y P.A. Arkin (1997): Global precipitation: A 17-year monthly analysis based on gauge observations, satellite estimates, and numerical model outputs. Bull. Amer. Meteor. Soc., 78, 2539 - 2558.

Xie, S.-P. y J. A. Carton (2004): Tropical Atlantic variability: patterns, mechanisms, and impacts. In Earth Climate: The Ocean-Atmosphere interaction, C. Wang, S.-P. Xie, and J. A. Carton (eds.), Geophys. Monograph., AGU, Washington DC.

Xoplaki, E., J. F. González-Rouco, D. Gyalistras, J. Luterbacher, R. Rickli y H. Wanner (2003a): Interannual summer air temperature variability over Greece and its connection to the large-scale atmospheric circulation and Mediterranean SSTs 1950-1999. Clim. Dyn., 20, 537-554.

Xoplaki, E., J. F. González-Rouco, J. Luterbacher y H. Wanner (2003b): Mediterranean summer air temperature variability and its connection to the large-scale atmospheric circulation and SSTs. Clim. Dyn., 20, 723-739.

Zebiak, S. E. (1993): Air–sea interaction in the equatorial Atlantic region. J. Clim., 6, 1567–1586.

GLOSARIO

AGCM: Atmospheric General Circulation Model

AMMA: African Monsoon Multidisplinary Analyses

AO: Artic Oscillation

CCA: Canonical Correlation Analysis

CMAP: CPC Merged Analysis of Precipitation

CPC: Climate Prediction Center

EA: East Atlantic

EA/WR: East Atlantic/West Russian

ECMWF: European Centre for Medium-Range Weather Forecasts

EMCA: Extended-Maximum Covariance Analysis

eMED: Eastern Mediterranean

ENSO: El Niño-Southern Oscillation

EOF: Empirircal Orthogonal Function

ERA: ECMWF Re-Analysis

ERSST: Extended Reconstructed SST

ERWS: Extratropical Rossby Wave Sources

ESA: European Space Agency

ITCZ: Inter-Tropical Convergence Zone

MCA: Maximum Covariance Analysis

NA-jet: North Atlantic-jet

NAA-jet: North African/Asian-jet

NAH: North Atlantic Horseshoe

NAM: Northern Hemisphere Annular Mode

NASA: National Aeronautics and Space Administration

NAT: North Atlantic Tripole

NAO: North Atlantic Oscillation

NCAR: National Center for Atmospheric Research

NCEP: National Centers for Environmental Prediction

NOAA: National Oceanic and Atmospheric Administration

PC: Principal Component

PCA: Principal Components Analysis

PKE: Perturbation Kinetic Energy

RWS: Rossby Wave Sources

SCA: Scandinavian

SLP: Sea Level Pressure

SNA: Subtropical North Atlantic

SPEEDY: Simplified Parametrizations Primitive Equation Dynamics

SST: Sea Surface Temperature

SVD: Singular Value Decomposition

TAV: Tropical Atlantic Variability

TNH: Tropical/Northern Hemisphere

TRWS: Tropical Rossby Wave Sources

UCLA-AGCM: University of California-Los Ángeles AGCM

WAM: West African Monsoon

WES: Wind-Evaporation-SST

wMED: Western Mediterranean

APÉNDICE A

Modos de variabilidad del Atlántico Tropical (1979-2002). Parte I: Evolución temporal de los modos de SST relacionados con la precipitación de África Occidental

Polo, I., B. Rodríguez-Fonseca, T. Losada y J. García-Serrano.
J. Clim., 21, 6457-6475

Tropical Atlantic Variability Modes (1979–2002). Part I: Time-Evolving SST Modes Related to West African Rainfall

IRENE POLO, BELÉN RODRÍGUEZ-FONSECA, TERESA LOSADA, AND JAVIER GARCÍA-SERRANO

Departamento de Geofísica y Meteorología, UCM, Madrid, Spain

(Manuscript received 28 April 2008, in final form 29 May 2008)

ABSTRACT

This work presents a description of the 1979–2002 tropical Atlantic (TA) SST variability modes coupled to the anomalous West African (WA) rainfall during the monsoon season. The time-evolving SST patterns, with an impact on WA rainfall variability, are analyzed using a new methodology based on maximum covariance analysis. The enhanced Climate Prediction Center (CPC) Merged Analysis of Precipitation (CMAP) dataset, which includes measures over the ocean, gives a complete picture of the interannual WA rainfall patterns for the Sahel dry period. The leading TA SST pattern, related to the Atlantic El Niño, is coupled to anomalous precipitation over the coast of the Gulf of Guinea, which corresponds to the second WA rainfall principal component. The thermodynamics and dynamics involved in the generation, development, and damping of this mode are studied and compared with previous works. The SST mode starts at the Angola/Benguela region and is caused by alongshore wind anomalies. It then propagates westward via Rossby waves and damps because of latent heat flux anomalies and Kelvin wave eastward propagation from an off-equatorial forcing. The second SST mode includes the Mediterranean and the Atlantic Ocean, showing how the Mediterranean SST anomalies are those that are directly associated with the Sahelian rainfall. The global signature of the TA SST patterns is analyzed, adding new insights about the Pacific–Atlantic link in relation to WA rainfall during this period. Also, this global picture suggests that the Mediterranean SST anomalies are a fingerprint of large-scale forcing.

This work updates the results given by other authors, whose studies are based on different datasets dating back to the 1950s, including both the wet and the dry Sahel periods.

1. Introduction

The study of the tropical Atlantic (TA) variability (TAV) is an important challenge for the scientific community because its impacts affect a large rural population, which depends on rain-fed agriculture. TAV implies SST patterns, which are linked to extreme climate conditions over the Atlantic basin, and in particular over West Africa (WA).

At interdecadal time scales, the second part of the twentieth century has known a very unusual evolution of Sahelian rainfall with a 20-yr wet period followed by another 20-yr dry period. Such a long-term downward trend in Sahelian summer rainfall is a unique feature in recent tropical fluctuations, and it has been associated with SST trends in the Atlantic and Indian Oceans (Folland et al. 1986; Shinoda and Kawamura 1994; Bader and Latif 2003; Giannini et al. 2003; Lu and Delworth 2005). Indeed, this observed drought tendency following the 1960s has been well reproduced with models only forced by observed SST (Giannini et al. 2003; Paeth and Hense 2004; Lu and Delworth 2005; Tippett 2006; Tippett and Giannini 2006). In addition, Zhang and Delworth (2006) have pointed out that the Atlantic multidecadal oscillation, which was in its negative phase in the 1980s–90s, can cause the observed multidecadal variations of Sahel summer rainfall, suggesting that the important role of the multidecadal variability in the interpretation of the recent climate change cannot be ignored.

In spite of this recent understanding about WA rainfall at decadal time scales as well as improvements in seasonal prediction, the general circulation models (GCMs) fail to reproduce WA rainfall interannual variability (Moron et al. 2003; Tippett 2006; Tippett and Giannini 2006). Some authors have suggested that the model error observed in the Sahel rainfall could be

Corresponding author address: Irene Polo, Facultad de C.C. Físicas, Departamento de Geofísica y Meteorología, UCM, Av/ Complutense, 28040-Madrid, Spain.
E-mail: ipolo@fis.ucm.es

DOI: 10.1175/2008JCLI2607.1

related to the error in the representation of ocean–atmosphere interaction (Tippett 2006). Faced with this, the SST modulation of the interannual variability of WA rainfall during the Sahel dry period deserves more investigation.

At interannual scales, WA rainfall variability is modulated by both oceanic (between 0° and 10°N) and continental (between 10° and 20°N) convergence, by variations in the ITCZ position and land–atmosphere interactions, respectively. Historically, two main WA rainfall types have been identified: dipole years, in which anomalies of opposite signs appear north and south of 10°N, and nondipole years, with anomalies of the same sign in the whole region (Motha et al. 1980; Janicot 1992; Fontaine and Janicot 1996; Ward 1998). This classification, based on the available in situ precipitation data from land stations over WA, has been useful in order to discriminate some associated processes and SST influences (Fontaine and Janicot 1996; Janicot et al. 1998; Ward 1998). However, it accounts for a large variability occurrence in the different wet and dry decadal periods over the Sahel (Janicot et al. 1996; Ward 1998; Janicot et al. 2001). Some of these studies have suggested that the occurrence of dipole years, which are most closely associated with TA SST, is dominant during the wetter epoch, whereas nondipole years are particularly numerous in the dry Sahel period (Ward 1998; Janicot et al. 2001), when the ENSO is more active in relation to WA rainfall (Janicot et al. 1998; Janicot et al. 2001). Paeth and Stuck (2004) have suggested that warm TA SSTs could enhance the rainfall dipole, which is the prevailing precipitation pattern in the Climatic Research Unit (CRU) observational dataset as well as in the global and regional climate models outputs. However, some discriminant analyses have shown perfect uncoupled rainfall variability modes between the Sahel and the coast of the Gulf of Guinea (GG), associated with different global SST anomalies (Ward 1998; Giannini et al. 2003). This work will present rainfall patterns calculated from the enhanced satellite-based Climate Prediction Center (CPC) Merged Analysis of Precipitation (CMAP) dataset, which includes measures over the ocean, a feature that needs to be discussed with respect to other WA rainfall observational studies.

Regarding rainfall variability on the coast of the GG, it seems to have a very tight ocean–atmosphere coupling at interannual and decadal time scales (Wagner and da Silva 1994; Fontaine and Janicot 1996; Ward 1998; Vizy and Cook 2001; Giannini et al. 2003), linked with the well-known Atlantic El Niño mode (Zebiak 1993; Carton et al. 1996). Vizy and Cook (2001) have shown that such SST events enhance evaporation, and that the southerly flow across the coast of the GG carries more moisture inland, leading to increased precipitation south from the usual latitude of the ITCZ. The Atlantic El Niño mode is characterized by a relaxation in the equatorial trade winds, which induces a redistribution of warm water in the equatorial belt and a weakening in the equatorial thermoclime slope and also in the heat content zonal gradient (Carton et al. 1996; Vauclair et al. 2004). In cold years (dry years in the GG region), the northward ITCZ movements can begin as early as February. Conversely, the warm years (wet years over the GG) are characterized by a reduction of the southerly flow between April and June, followed by a rapid increase later in July (Fontaine et al. 2003). Although the Atlantic El Niño has been investigated from the 1980s, the related air–sea interaction mechanisms are still a current topic (Keenlyside and Latif 2007), mainly because of the lack of reliable ocean data in the TA. This work makes a dedicated effort to address the main question about the development and damping of this SST mode coupled to GG rainfall.

The relation between the Sahelian rainfall and the so-called Atlantic SST meridional mode (Chang et al. 1997) was pointed out to be more important before 1970, during the wet Sahel period (Janicot et al. 1996; Janicot et al. 2001) and at interdecadal time scales (Lamb 1978; Hastenrath 1984). However, the role of the subtropical North Atlantic (SNA) SST on WA rainfall is still unclear. Some authors have suggested that SNA SST plays a passive role with regard to WA rainfall (Ward 1998; Mo et al. 2001). Vizy and Cook (2001) suggest that this region can have less influence over the Sahelian rainfall, mainly because the low-level flow between the SNA and WA is a northeasterly flow, which tends to isolate the continent from SNA, and because horizontal advection is not very effective in the tropics. However, from their GCM simulations, a response to positive SNA and GG SST anomalies results in a westerly low-level flow perturbation that largely impacts WA precipitation (Vizy and Cook 2001).

The possible Sahelian impact from other regions, such as the Mediterranean Sea, has also been supported (Rowell 2001). From AGCM simulations, Rowell (2003) has found positive Mediterranean Sea SST anomalies related to anomalous positive Sahel rainfall through evaporation and southward moisture advection that enhances low-level convergence over the Sahel. Jung et al. (2006) have simulated significant increased Sahelian rainfall for the warm Mediterranean event of 2003, derived from enhanced evaporation in the Mediterranean Sea. Nevertheless, there is still an open question about whether the Mediterranean basin plays an

effective role or it is only a fingerprint of larger-scale forcing.

Regarding the global signature of the TAV, some studies have evidenced an association between ENSO events and the Atlantic El Niño mode (Latif and Grötzner 2000; Wang 2006), and both phenomena are related to WA rainfall patterns (Rowell 2001; Janicot et al. 1998; Janicot et al. 2001). ENSO seems to act by modifying the east–west divergent circulation, which modulates the vertical movements over WA, while the Pacific–Atlantic zonal atmospheric gradient, coupled to the opposite SST anomalies over both oceanic basins, can enhance the WA rainfall response (Janicot et al. 1998). However, the setup of a Pacific–Atlantic zonal atmospheric oscillation in the dry Sahel period could be the result of recent changes in the anomalous SST and WA rainfall trends after 1970. The Pacific–Atlantic relationship has dramatically changed in this recent period (Keenlyside and Latif 2007), and therefore the study of such a relationship is important for understanding the interannual influences over WA.

The aim of this work is to clearly identify and describe the SST modes of variability over the WA adjacent oceans that are coupled to summer WA rainfall during the 1979–2002 period, and their seasonal time evolution (origin, development, and damping). To accomplish this objective, we have developed an extended methodology of the classical maximum covariance analysis (MCA) and applied it to the WA monthly anomalous summer [June–September (JJAS)] precipitation and the monthly TA and Mediterranean SST anomalies from February–May (FMAM) to September–December (SOND). Because the methodology highlights the seasonal dependence of the time-evolving SST, it will give new and valuable insight on the understanding of these interannual variability modes.

The SST patterns found in this paper are being used as boundary conditions in some of the sensitivity experiments that the African Monsoon Multidisciplinary Analysis (AMMA)-European Union (EU) project has planned to perform with different AGCMs, with the aim of understanding the response of the WA rainfall to the SST in the adjacent oceans and its potential predictability. The same extended maximum covariance analysis (EMCA) methodology has been applied in García-Serrano et al. (2008), focusing on the relation between the summer TA SST patterns and summer–winter Atlantic precipitation variability, addressing the TAV–extratropical connection through tropical convection.

In the next section 2, the data and the methodology used in this work are described. Section 3 describes the principal components of the WA rainfall and the main SST–WA rainfall covariability modes. The air–sea interactions related to the leading SST pattern, as well as the global SST signature of every mode, are analyzed. Finally the main conclusions are discussed in section 4.

2. Data and methodology

The 1979–2002 monthly CMAP (Xie and Arkin 1997) and extended reconstructed sea surface temperature (ERSST) dataset (Smith and Reynolds 2003) for the SST variable have been used to study the main coupled modes between summer WA precipitation and TA SST. Regarding data accuracy, 1979–2002 is very reliable period because satellite data are included in the precipitation datasets. Also, the use of these data provides information on the precipitation over the ocean, something important if we want to follow the patterns over the basin. As a first step of the analysis, JJAS monthly standardized precipitation empirical orthogonal functions (EOFs) are computed to quantify the principal modes of WA precipitation during the whole monsoon season. Then, the anomalous SST patterns coupled to the summer WA rainfall variability is described and analyzed. Eight different 4-month sequences, centered in JJAS, and lagging 1 month forward and backward, are computed to find the state of the ocean in relation to the WA rainfall variability. Time series are linearly detrended and anomalies are calculated with respect to the considered period.

To follow and give an interpretation of the air–sea processes related to the leading SST coupled mode, several oceanographic and atmospheric key variables have been analyzed. The oceanic variables are the wind stress [from the Pilot Research Moored Array in the Tropical Atlantic (PIRATA) dataset; see Servain et al. (1998)], the 20°C isotherm depth as tropical thermocline depth proxy [from the Tropical Atlantic Ocean Subsurface Temperature Atlas (TAOSTA) dataset; see Vauclair and du Penhoat (2001)], and the sea level anomalies [SLAs; from the altimetry measures of the Ocean Topography Experiment (TOPEX)/Poseidon in the period of 1993–2001, which is provided by Centre National d'Études Spatiales (CNES) Archiving, Validation, and Interpretation of Satellite Oceanographic data (AVISO)]. The atmospheric variables are the interpolated outgoing longwave radiation [OLR; provided by the National Oceanic and Atmospheric Administration (NOAA)/Office of Oceanic and Atmospheric Research (OAR)/Earth System Research Laboratory (ERSL) Physical Sciences Division (PSD); see Liebmann and Smith 1996], surface heat fluxes, surface winds, and sea level pressure (SLP). The latter surface variables come

from the 40-yr European Centre for Medium-Range Weather Forecasts (ECMWF) Re-Analysis (ERA-40) dataset (Uppala et al. 2005), which includes satellite data from 1973.

The methodology of EMCA (Fig. 1) is developed and implemented in this study. This methodology is an extension of the maximum covariance analysis (Bretherton et al. 1992, Frankignoul and Kestenare 2005; Polo et al. 2005), but considers all of the lagged SST time series in the same array (see Fig. 1, matrix Y). Using EMCA we can isolate, in the same mode, the whole sequence of significant covariant SST patterns in relation to the JJAS precipitation, and accomplish the whole picture of the SST pattern evolution in relation to the precipitation with a realistic persistence feature from boreal late winter to summer. Because the TA SST signals can develop rapidly from early spring to late summer, in our method, a priori, we do not discriminate between the season of the maximum SST covariability and the summer rainfall (in contrast with the classic MCA).

In addition, EMCA gives the opportunity for increasing the number of time series in the analysis, having as many time series per point as time lags used in the analysis, and in this way assesses the statistical significance of the results. As in the classical MCA, each mode comprises different spatial structures (singular vectors) and time series (expansion coefficients) for every involved field in the analysis. The results are shown in terms of homogeneous and heterogeneous regression maps, for the SST sequence and the summer precipitation field, respectively. For each mode, the SST homogeneous map (HM) shows the amplitude of the projection (for each grid point and each lag) of the total SST expansion coefficient onto the TA SST anomalies, giving a measure of the SST anomaly per standard deviation. The precipitation heterogeneous maps (HT) show the amplitude of the projection of the total SST expansion coefficient onto summer WA rainfall anomalies, giving a measure of the precipitation anomalies associated with one standard deviation of the anomalous SST. Only those areas that are 98% statistically significant (evaluated with a t test) are mapped. A measure of the fraction of explained covariability [square covariance fraction (SCF)], and the correlation coefficient (RUV) between the independent and dependent expansion coefficients complete the information for each mode. To quantify the statistical significance of the EMCA, additional statistical information is given. To test if the SST–precipitation link found is not random, we have checked the results using a Monte Carlo test. In this way, the combined action of shuffling and applying the EMCA is performed 100 times. The probability density function of the SCF parameter that arises from these 100 realizations is compared to the nonshuffled EMCA SCF scores, giving a significance level (SL) for the connection found.

3. Results

a. Principal component analysis

In this section, interannual WA rainfall modes (over the region 5°S–32°N, 21.25°W–33.75°E) are computed for the dry Sahel period using the CMAP dataset, with the aim of updating the results given by previous authors. The first two EOFs of WA monthly standardized anomalous precipitation during the rainy season (JJAS), which account for around 20% of the total variance, are shown in Fig. 2. The following third mode has not been considered because its sampling error is larger than the spacing between second and third eigenvectors, which means that the third PC is part of a degenerate multiple (North et al. 1982). The significant precipitation pattern of the leading principal component (PC) shows the anomalous Sahelian rainfall (*Sahelian mode*, see Fig. 2a) as the first mode, with more no-rain than wet periods during the whole sequence. This pattern accounts for 10% of the total variance and its study is of great importance because it explains part of the WA monsoon variability, which is a hot topic for the agriculture and health in developing countries (Sultan et al. 2005). The regression map of the second PC represents the rainfall pattern of the coast of the GG (*Guinean mode*, see Fig. 2b). The pattern exhibits interannual and interdecadal variability, with more dry events over the coast of the GG in the 1990s than in the 1980s.

While other works present the Guinean mode as the leading WA rainfall mode (Giannini et al. 2003), from our results during 1979–2002, most of the rainfall interannual variability is concentrated over the Sahel region, with the Guinean mode being the second EOF. A prior normalization of the rainfall anomalies has confirmed the reversion of the order of the first two modes (not shown). Without the standardization of the rainfall anomalies (as done in Giannini et al. 2003), the rainfall anomalies of the coast of the GG have higher amplitudes and appear as the leading mode.

In addition, although several authors have pointed out that a significant part of the interannual variability of WA anomalous rainfall is due to the opposite evolution between central Sahelian and Guinean rainfall indexes as a dipole pattern (Janicot 1992; Fontaine et al. 1995; Fontaine and Janicot 1996; Ward 1998; Douville et al. 2007), our results separate the Sahelian and the Guinean rainfall in two different modes. Further-

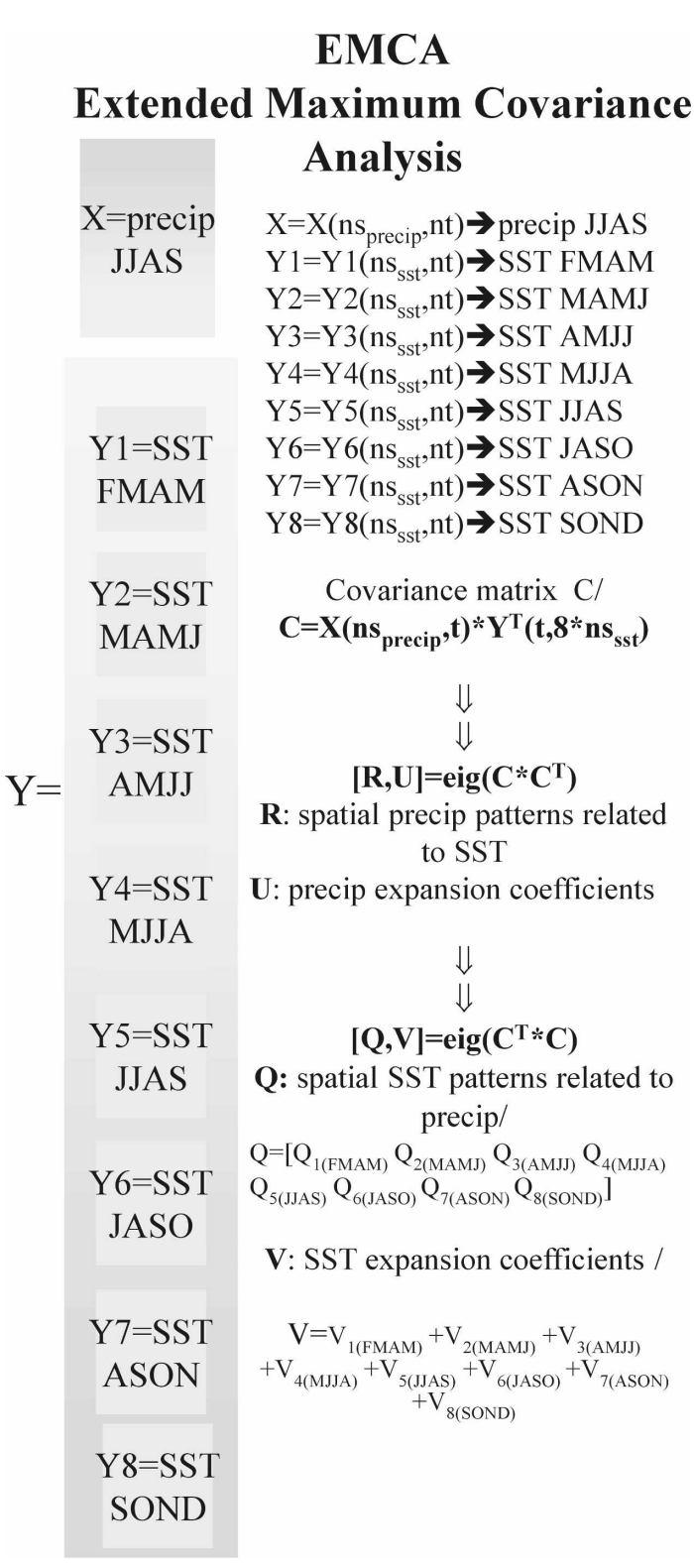

FIG. 1. Scheme of the EMCA used in this study.

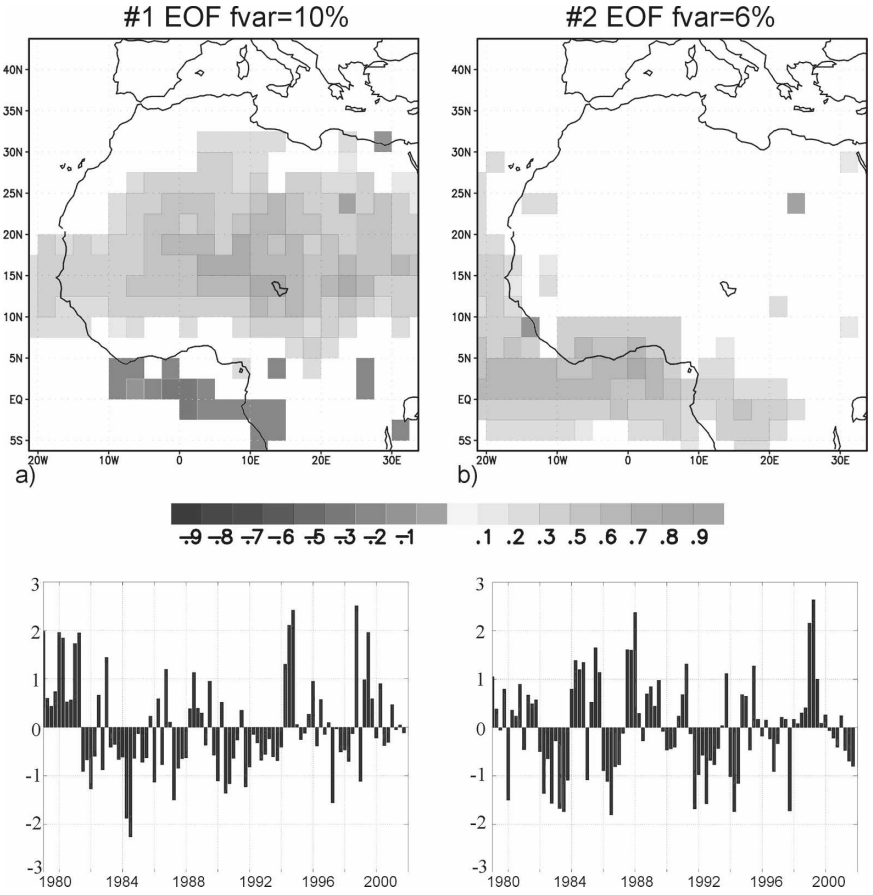

FIG. 2. First two CMAP JJAS precipitation EOFs over WA. Only 98% statistically significant areas (SSA), evaluated with a *t* test, have been shaded. Times series of the associated PCs are in bars.

more, the dipole classification operates under the assumption that both the Sahel and the coast of the GG have the same variability patterns; however, it is clear that they have different variability, especially in the last dry period (Ward 1998). Because the processes associated with both are operating and competing (Ward 1998) for some analysis, the dipole and nondipole subdivisions appear useless. The absence of the dipole pattern in our analysis could be caused by the dataset used; CMAP rainfall comes from satellite data with land–sea continuity and a smaller time span (1979–2002), which is contained in the dry Sahel period. To check this hypothesis, we have analyzed the same patterns considering the CRU dataset for a longer period (1949–96) and for part of the dry period (1975–96). For the same data treatment and for both periods, we have obtained the same uncoupled Sahelian and Guinean modes (not shown). Likewise, standardization produces a reversal of the modes in the sense of percentage of variability. A kind of dipole pattern is found for the second period without standardizing the WA rainfall anomalies, although it has the maximum loadings over the coast of GG region. Therefore, this data treatment dependence reveals that the dipole is not robust enough to be considered as a canonical pattern.

b. SST–precipitation coupled modes

To determine the TA SST patterns related to summer WA precipitation anomalies, we apply EMCA between the TA SST from FMAM to SOND and JJAS WA rainfall. For the leading EMCA mode, which accounts for 31% of the SCF, the SST significant homogeneous regression maps shows positive SST anomalies over the Atlantic equatorial tongue region from the previous spring (AMJJ), related to an increase of summer precipitation along the coast of the GG (Fig. 3, upper panel). The precipitation expansion coefficient of this mode has a strong relation to the Guinean mode in Fig. 2b (0.89 correlation coefficient), and the SST expansion coefficient is very well correlated (0.84 correlation coefficient) with the equatorial Atlantic SST index (ATL3; Zebiak 1993), which describes the Atlan-

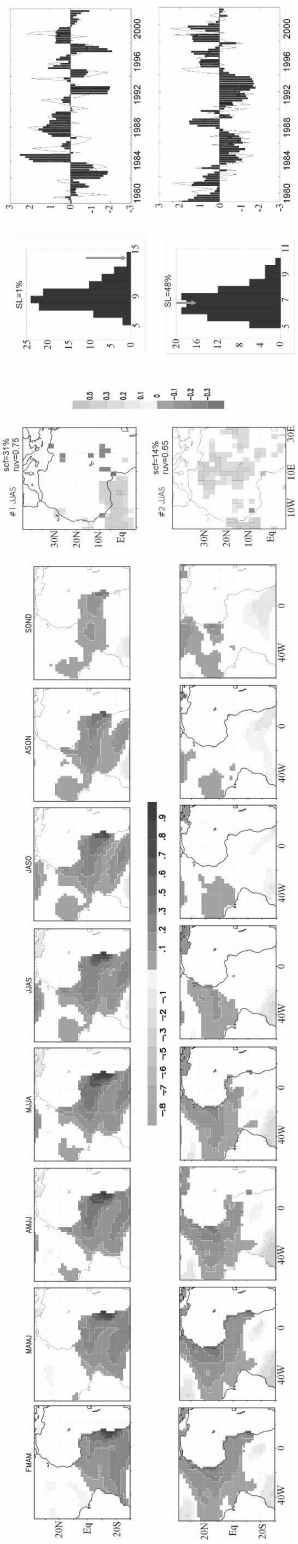

FIG. 3. First two covariability modes obtained from the EMCA between summer WA precipitation and the anomalous SST (°C) 4-month sequences from FMAM to SOND. SSA as in Fig. 2. The probability density function of the SCF from 100 times Monte Carlo tests (histogram) is compared with the original EMCA SCF score (arrow) to show its significance level. The expansion coefficients (SST in bars, precipitation in continuous line) are shown for each mode.

tic El Niño mode. It is important to mention that the Guinean rainfall pattern appears now as the leading mode of covariability with TA SST, implying that an important part of the rainfall variability of the coast of the GG can be explained by TA SST anomalies. Conversely, Sahelian rainfall has been related to more global SST patterns, such as the Pacific (Giannini et al. 2003; Janicot et al. 1998) and Indian or northern basin ocean (Giannini et al. 2003; Ward 1998), and to land surface processes (Douville 2002; Philippon and Fontaine 2002).

The second EMCA mode (Fig. 3, lower panel) represents 14% of the total SCF and describes a spatial pattern with positive summer rainfall anomalies over the Sahel and positive SST anomalies over the SNA and Mediterranean Sea, persisting for some months in advance. The precipitation expansion coefficient has a strong relation to the Sahelian mode in Fig. 2a (0.87 correlation coefficient). Nevertheless, this is not a robust mode because the SL obtained from the Monte Carlo test indicates that the results can be reproduced in half of the shuffled cases. For this reason, this mode will be discussed and recalculated in the next sections.

In the following section, these two covariability modes are intensely analyzed: on the one hand the leading mode, which corresponds to the Guinean rainfall and the Atlantic El Niño, is discussed in terms of air–sea interactions; and on the other hand the second covariability mode will be analyzed and discussed in order to better understand the role of the SNA and Mediterranean Sea SST on the Sahelian rainfall. The global picture of these SST patterns will also be discussed.

1) EQUATORIAL ATLANTIC SST–GUINEAN RAINFALL MODE: AIR–SEA INTERACTIONS

Figure 3 (upper panel, from FMAM to SOND) shows the sequence of SST homogeneous regression maps, related to the Atlantic El Niño or equatorial mode (EM), linked to the Guinean anomalous precipitation. Here, it can be seen that the EM develops from FMAM to JJAS, starting with a maximum of anomalous SST over the Angola/Benguela upwelling region, with a second relative maximum around 20°S. Afterward, the mode shows a strengthening and/or northward (westward) propagation of the coastal (equatorial) anomalies and a weakening of the anomalies in 20°S. Then, the whole mode starts to weaken, disappearing in SOND. The Bjerknes mechanism components in the EM have been analyzed by other authors (Keenlyside and Latif 2007), but there are still some gaps regarding the development and damping of the mode. Therefore, we will analyze the thermodynamics

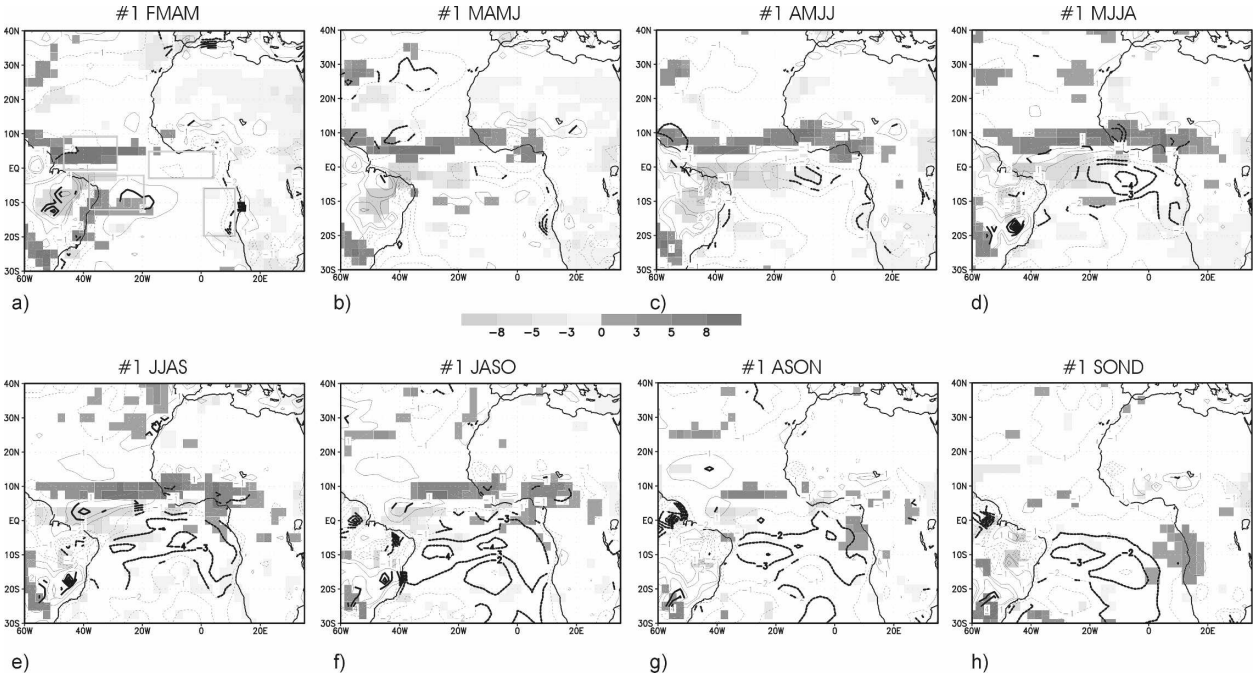

FIG. 4. Regression of the total SST expansion coefficient associated with the leading EMCA mode onto the radiative flux anomalies [shortwave − longwave radiation (W m^{-2}), positive downward], and the latent heat flux anomalies [contour interval (CI) = 1 W m^{-2}, positive downward] for the 4-month sequences from (a) FMAM to (h) SOND. The boxes in (a) are regions considered in the heat balance. SSA as in Fig. 2.

and dynamics involved in the mode's evolution by regressing the SST expansion coefficient onto different thermodynamic and oceanographic variables.

The role of the TA heat fluxes in relation to the EM is investigated in Fig. 4, which shows the balance between the radiative fluxes (shortwave radiation minus longwave) and the turbulent fluxes (latent heat fluxes). Regarding the EM evolution from FMAM to JJAS, heat fluxes are not responsible for the SST anomalies located in the Benguela upwelling region (10°–20°S, 0°–10°E), because the SST warming is concomitant with more evaporation over this region. On the contrary, the west-equatorial North Atlantic warming (0°–10°N, 50°–30°W) can be attributed to an increase of solar radiation (associated with less clouds) and a decrease of evaporation. The damping of the SST anomalies at the southern lobe (0°–10°S; 40°–20°W) starts in MAMJ because of an increase of the latent heat flux to the atmosphere and a decrease of the solar radiation. From JJAS to SOND, negative latent heat flux anomalies could be responsible for the damping at the south of the tongue, while radiative fluxes reduce the SST anomalies at the east, in agreement with Trzaska et al. (2007). From the thermodynamics analysis of the EM, we conclude that, although both negative radiative and latent heat fluxes anomalies could be important in damping the SST in the EM, heat fluxes cannot explain the generation and persistence of the SST anomalies at the southeastern region.

To find an explanation for the SST anomaly generation at the southeastern part of the tongue from the previous winter, regression of the SST expansion coefficient onto the surface winds and the SLP is displayed in Fig. 5. Noticeable is an enhancement of the clockwise circulation, together with a weakening of the subtropical Santa Helena high pressure system from the previous November–February (NDJF) winter sequence. Such a feature could be responsible for the anomalous southeastward surface winds, and hence the SST warming. However, both wind anomalies over the eastern South Atlantic and positive SST anomalies over the Benguela region (not shown) are significant 2 months before negative SLP anomalies from SOND. At that moment, positive SLP anomalies cover the Amazon basin and the equatorial band (Figs. 5a,b) suggests that subsequent weakening of the Santa Helena high could be forced by inversion of the local Hadley cell via an atmospheric bridge. Such a type of mechanism has been proposed in the Northern Hemisphere for explaining the anomalous indirect Atlantic Hadley circulation during the mature and decay phases of El Niño (Wang 2002a,b). However, this result is not totally in agree-

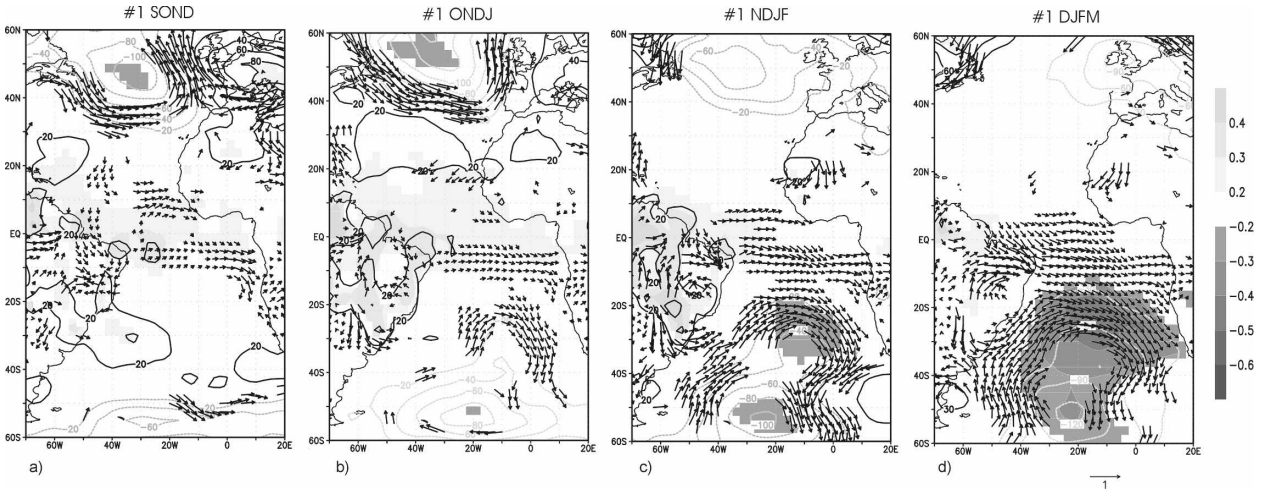

FIG. 5. Regression of the total SST expansion coefficient associated with the leading EMCA mode onto the surface wind anomalies [vectors (m s^{-1})] and the SLP (CI = 20 mbar, SSA as in Fig. 2 have been shaded) for the 4-month sequences from previous (a) SOND to (d) DJFM. SSA as in Fig. 2.

ment with other authors' findings. Trzaska et al. (2007) have shown the EM as a consequence of the subtropical South Atlantic (SSA) SST mode (consistent with Venegas et al. 1997), which is associated with the south Atlantic subtropical high SLP anomalies, and no mention is made of the equatorial contribution.

Despite most of the works being associated with the origin and development of the EM with subtropical atmospheric dynamics, some authors have suggested that Ekman pumping and the wind stirring may also play a role in the SST evolution over the TA (Sterl and Hazeleger 2003; Barreiro et al. 2004). In view of this, the oceanic component is analyzed in Fig. 6, which shows the regression of the leading EMCA mode SST expansion coefficient onto the wind stress and the Ekman pumping. Figure 6a (and Figs. 5a,b) shows how, from the previous winter months, anomalous southward wind stress locally changes the upwelling over the Benguela front, and thus the SST and the thermocline depth over the region (not shown). In particular, in December–March (DJFM), this positive SST anomaly over the southern Atlantic produces a meridional and zonal basin gradient, which increases the northwesterly wind stress over the south Atlantic (Fig. 6b). From DJFM to April–July (AMJJ; see Figs. 6b,e), southeastward anomalous wind stress changes the thermocline slope, rising at the west and sinking at the east in the equator (not shown). In March–June (MAMJ; see Fig. 6d) in the southwest Atlantic, the wind stress curl starts to be anomalously cyclonic, creating upward Ekman pumping and cooling the mixed layer at the west-central basin as the latent heat flux decreases (Fig. 4c). From July to October (JASO), the positive Ekman pumping anomalies are located over the eastern part of the basin, because the southerly alongshore wind starts to be significant over 10°S, helping to damp the mode.

The SLA pattern associated with the EM consists of an anomalous eastern equatorial Atlantic tongue (as the SST) and a western equatorial Atlantic with an opposite sign SLA, in a seesaw-like thermocline configuration (not shown), in agreement with other authors (Wang 2006; Keenlyside and Latif 2007). Because the EM strongly involves subsurface equatorial dynamics through equatorial wave adjustment (Vauclair and du Penhoat 2001; Vauclair et al. 2004; Handoh and Bigg 2000), and because we are looking for a mechanism that could explain the development of the EM (from winter to summer) on the one hand and the fading of the EM (from summer to autumn) on the other, time–longitude plots of SLA have been done for extreme positive and negative events of the expansion coefficient. We have chosen years 1995 and 1997, positive and negative EM years, respectively (see expansion coefficients in Fig. 3, upper panel), following the SLA from 40°W to 10°E and from February to October.

For 1995 (1997), the time–longitude SLA plots (Fig. 7) at 5°S show how the positive (negative) SLA signal at the southeast Atlantic is propagating clearly westward as a Rossby wave (Chelton and Schlax 1996; Polito and Cornillon 1997). This eastern perturbation travels as far as 30°–20°W and does not propagate farther west (Figs. 7a,b, left), because an anomaly of the opposite sign appears. This SLA could be originated and/or reinforced by the Ekman pumping at this longitude, from the AMJJ season, and it is also propagating westward with the same phase speed, cancelling the

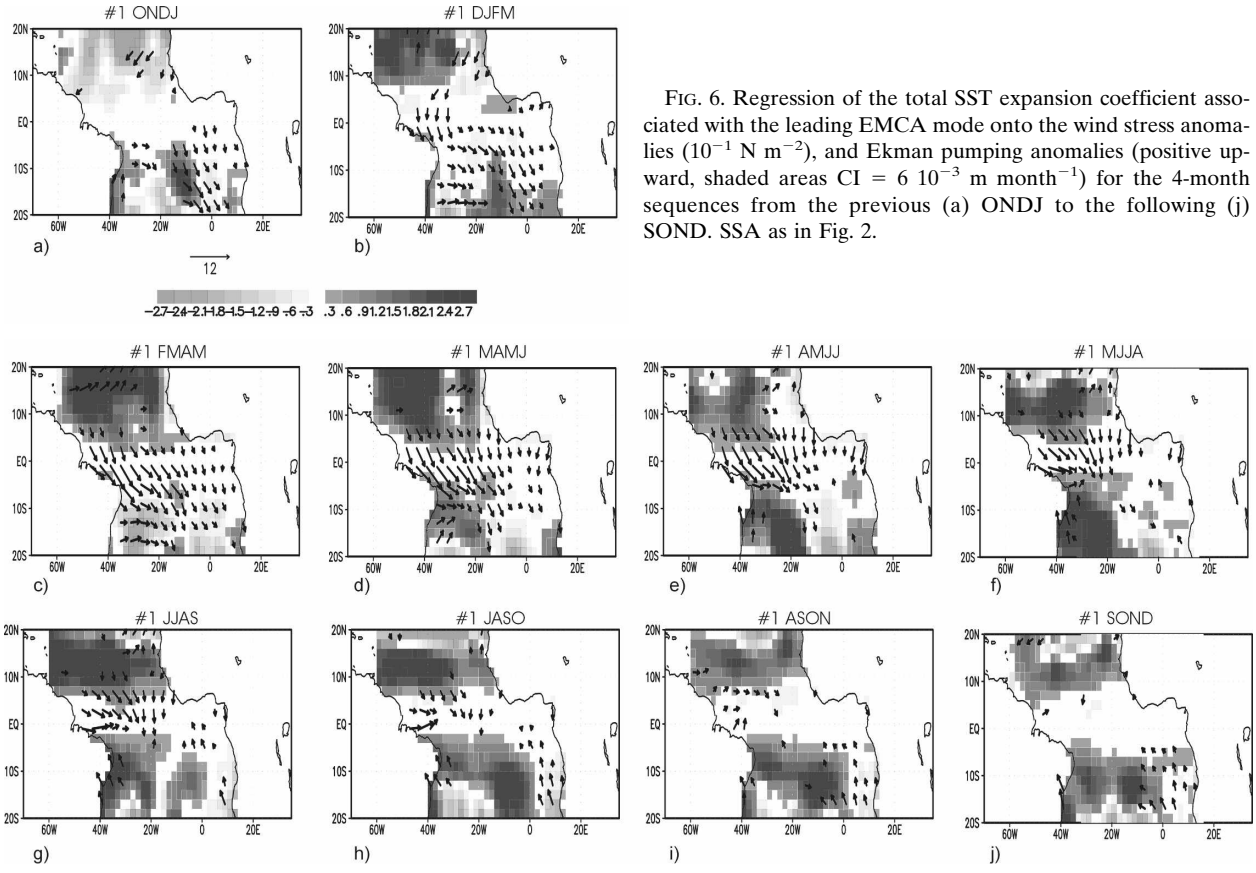

FIG. 6. Regression of the total SST expansion coefficient associated with the leading EMCA mode onto the wind stress anomalies (10^{-1} N m^{-2}), and Ekman pumping anomalies (positive upward, shaded areas CI = 6 10^{-3} m month^{-1}) for the 4-month sequences from the previous (a) ONDJ to the following (j) SOND. SSA as in Fig. 2.

positive (negative) SLA propagation farther west. Simultaneous with the westward upwelling (downwelling) Rossby wave traveling along 5°S (Figs. 7a,b, left), there is an upwelling (downwelling) Rossby wave traveling westward along 5°N latitude (not shown); the wind stress over 30°–20°W is also favoring (inhibiting) the Ekman pumping at both sides of the equator for 1995 (1997). At the beginning of July, this negative (positive) SLA signal appears in the western equatorial Atlantic and is reflected as an eastward Kelvin wave traveling up to September reaching the eastern equator (Figs. 7c,d, right), and helping to damp the EM. The wind stress anomalies over 30°–20°W, the associated Ekman pumping at both sides of the equator (Fig. 6g), and the possible relation to anomalous SLA signal, triggering a Kelvin wave, support the hypotheses proposed by Polo et al. (2008) that Ekman pumping ITCZ shift-induced anomalies are, in part, a source for equatorial Atlantic Kelvin waves.

Although the hypothesis needs to be checked using a model, we have found that the EM starts at the Angola/Benguela upwelling region. The SLAs radiate and propagate westward as Rossby waves, and damp because of the latent heat flux anomalies at the South Atlantic and the Kelvin wave eastward propagation from an off-equatorial forcing. The phase speed for the westward and eastward propagation has been computed with the radon transform technique (Hill et al. 2000). The mean phase speed calculated for the westward propagation at 10°, 5°, and 2.5°S is -0.5 m s^{-1}, and for the equatorial eastward propagation it is around 3 m s^{-1}, corresponding approximately to the first baroclinic mode (Philander 1990; França et al. 2003). Longitudinally, the area around 30°–25°W seems to be a threshold for the first baroclinic Rossby wave. Nevertheless, for both westward Rossby wave and eastward Kelvin wave propagations there is more homogeneity in the middle of the basin (from 20° to 5°W). In addition, other nonlinear processes could interfere in the propagation continuity onshore; however, these tasks are out of the scope of this study and future research lines.

Our results presented above disagree with Latif and Grötzner (2000), Florenchie et al. (2003), and Wang (2006) with regard to the oceanic wave propagation's role in the origin of the equatorial and South Atlantic SST variability. In particular, Florenchie et al. (2003) have suggested that the generation of the Benguela El

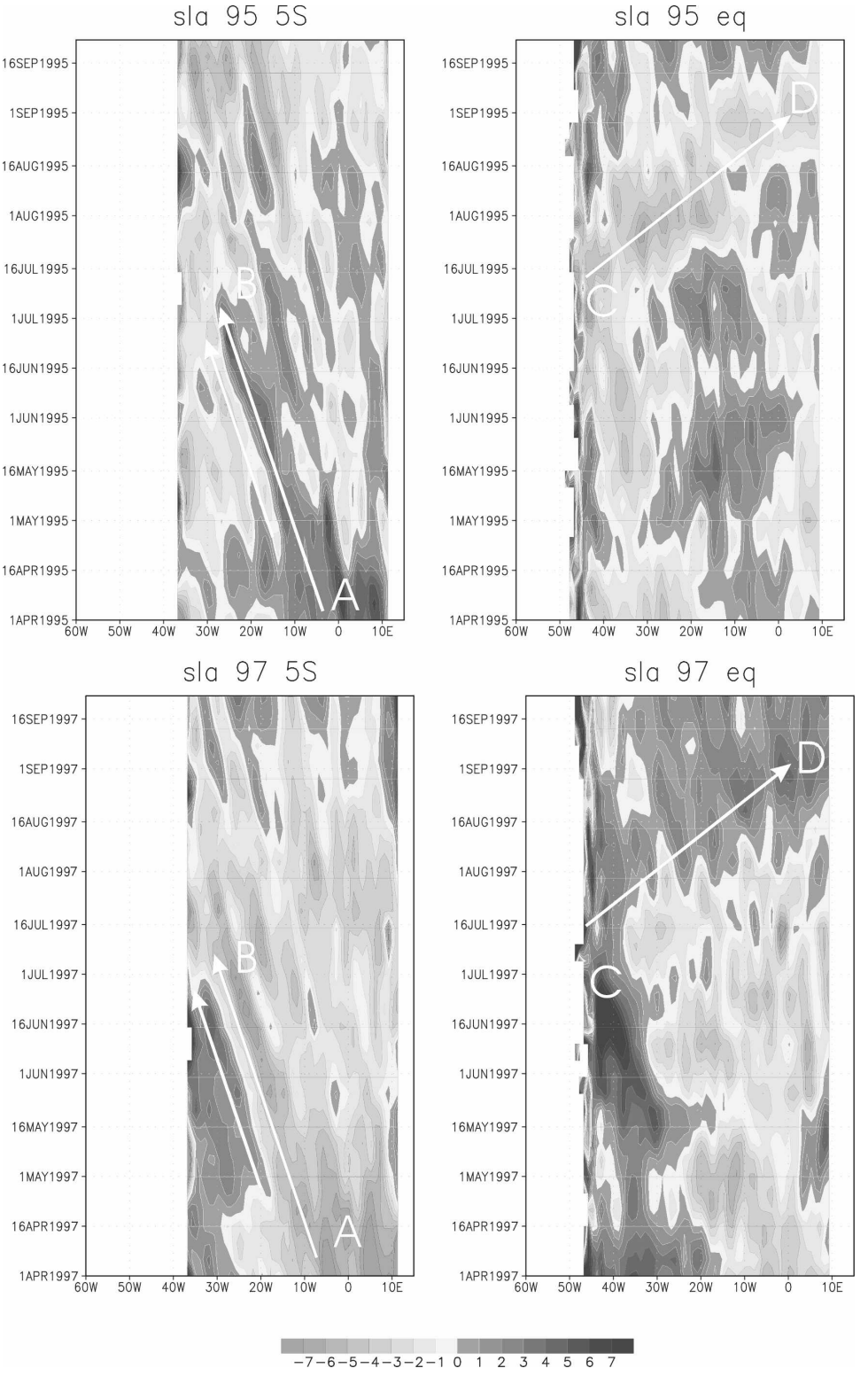

FIG. 7. SLAs (cm) from April to September along (left) 5°S and (right) the equator for (top) 1995 and (bottom) 1997.

Niños could be remotely generated by wind anomalies at the west-central equatorial Atlantic via oceanic Kelvin wave propagation, and Wang (2006) has supported this result. Also, Latif and Grötzner (2000) have showed an eastward SLA propagation from the western equatorial Atlantic in winter that reaches the eastern equatorial Atlantic the next summer when it can be amplified by air–sea interactions and the SST can be modified. Our results show that neither west-equatorial Atlantic SLA in winter nor anomalous winds in the west-central equatorial Atlantic have been found to force Benguela El Niños/EM via Kelvin waves.

Regarding the Pacific–Atlantic connection, Latif and Grötzner (2000) showed how, at quasi-biennal time scales, a winter El Niño event leads an Atlantic El Niño the following summer with no significant simultaneous relationship. Recently, Wang (2006) has discussed the importance of the Pacific–Atlantic SST gradient driving the atmospheric circulation across equatorial South America via the SLP gradient and influencing the tropical climate variability in a feedback way. To assess these relationships between basins, the EM has been regressed onto the global SST and precipitation anomalies (Fig. 8), showing a global rainfall pattern that involves the whole tropical belt. The equatorial Atlantic positive precipitation anomalies from FMAM to AMJJ are related to negative precipitation anomalies over the central Pacific. From JJAS to SOND, the Atlantic El Niño is being damped, with a westward displacement of the global tropical convection anomalies increasing the West Asian precipitation and decreasing the central to eastern Pacific precipitation (La Niña–like pattern). This is more evident when considering the global SST anomalies associated with the EM: SST anomalies decrease from the central to the east Pacific Ocean and increase at the western Pacific (Figs. 8a,d contour lines). To address a possible EM modulation, we have correlated the lagged Niño-3 index with the EMCA SST expansion coefficient (Fig. 8e). The maximum correlation occurs when a warm EM phase in summer leads the Pacific La Niña by 6–8 months during the following winter. This is a very relevant result that points out a different equatorial Pacific–Atlantic connection in the 1979–2002 period: the Atlantic El Niño can lead the Pacific La Niña, and this situation seems to be related to the Guinean rainfall mode instead of Sahelian rainfall. Jury et al. (2002) have found that upper zonal winds in the central Atlantic lead the Niño-3 SST index, particularly in the 1980s and 1990s. They suggest that both the Niño-3 and the Atlantic winds are responding to atmospheric convective forcing in the western Pacific, but that the upper wind reacts more quickly to eastward-shifted convection in the Pacific than the Niño-3 SST, which depends on the comparatively slow eastward propagation of ocean anomalies. These upper winds could force, through the Walker circulation, the SST in the tropical Atlantic to react more quickly that the Niño-3 SST, explaining in this way the relation found between the Atlantic and the Pacific. Melice and Servain (2003) have also shown the south tropical Atlantic leading the Southern Oscillation index (SOI) from 1984 to 1998 by ~4 months, although they do not know how the south tropical Atlantic could be dynamically linked with the Southern Ocean or even if such a link exists. Nevertheless, the importance of the later result in Fig. 8, regarding the recent trends in the Pacific–Atlantic connection, needs further investigation and will be the focus of future studies.

2) Subtropical North Atlantic and Mediterranean Sea SST–Sahelian rainfall mode: A discussion

In JJAS, the second mode in Fig. 3 (lower panel) associates the Sahelian anomalous rainfall with Mediterranean Sea SST anomalies, persisting from FMAM, and SNA SST anomalies, damping from AMJJ. The Mediterranean Sea influence on the WA monsoon regime has already been evidenced (Rowell 2001) and studied with AGCM simulations (Rowell 2003). Regarding SNA, there are some studies suggesting its influence (Paeth and Friederichs 2004; Rodríguez- Fonseca et al. 2006), although there are some authors proposing that SNA SST has a passive role or very limited effects on WA rainfall (Ward 1998; Mo et al. 2001; Vizy and Cook 2001). For this reason, a discussion about the covariability between SNA and the Mediterranean Sea SST anomalies and WA rainfall is considered in this section.

To separate the possible contribution of the Mediterranean Sea SST anomalies from those of the SNA on the summer WA anomalous rainfall, we have performed two different EMCA analyses—one between the Mediterranean Sea and the WA rainfall, and another between the TA and the WA rainfall. The leading EMCA mode, obtained when considering just the Mediterranean SST anomalies (Fig. 9a), explains more than 33% of the covariance and is a very robust mode. The mode relates positive SST over the Mediterranean, maximum at the east, with increasing rainfall over the Sahel, in particular over the 10°–25°N, 5°–25°E region. The correlation of the precipitation expansion coefficient is statistically significant with both, with the first WA rainfall PC in Fig. 2a, and the second EMCA rainfall expansion coefficient in Fig. 3 (0.96 and 0.90, respectively; see Table 1). The same analysis done just for the TA SST presents a second mode (Fig. 9b), with

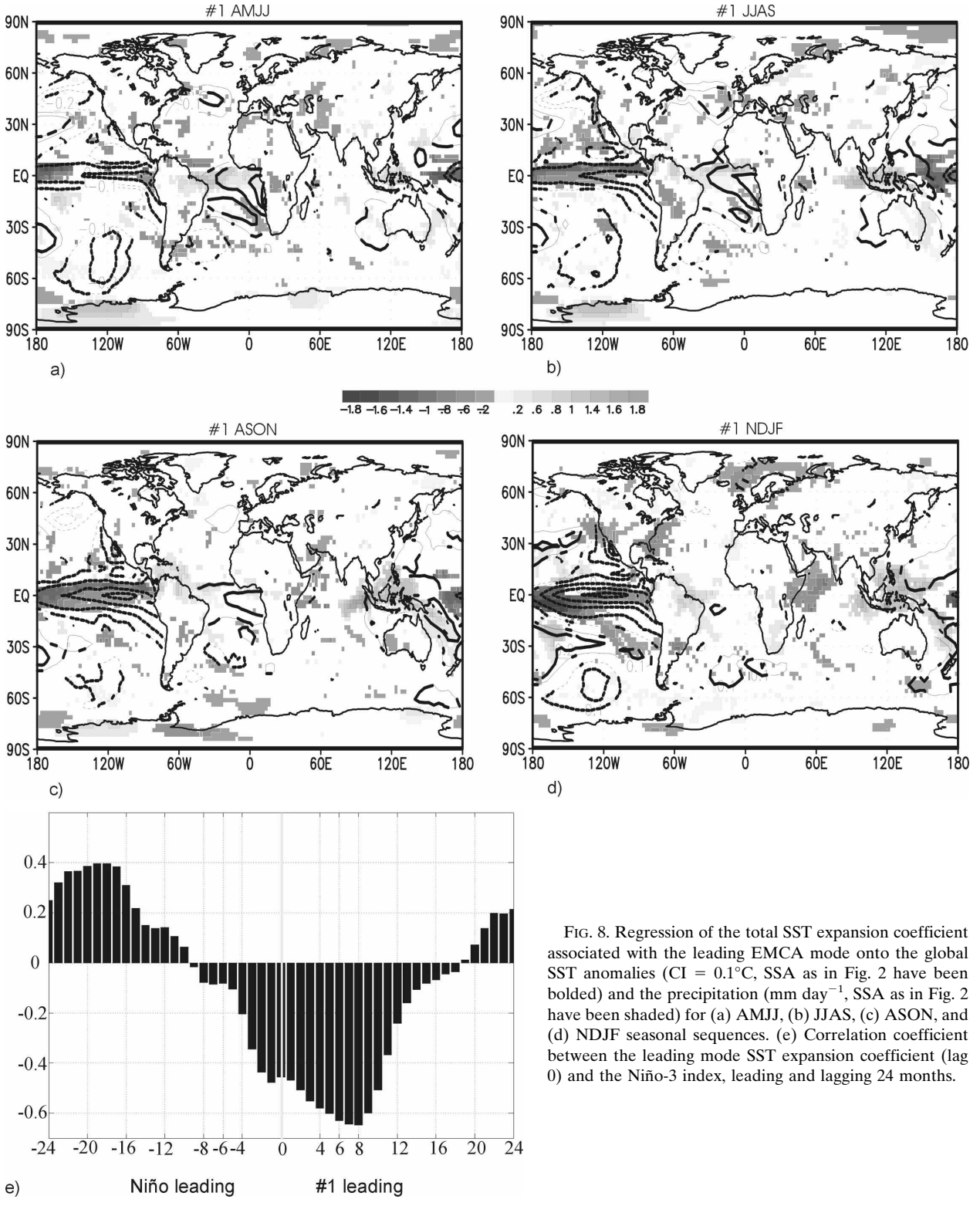

FIG. 8. Regression of the total SST expansion coefficient associated with the leading EMCA mode onto the global SST anomalies (CI = 0.1°C, SSA as in Fig. 2 have been bolded) and the precipitation (mm day^{-1}, SSA as in Fig. 2 have been shaded) for (a) AMJJ, (b) JJAS, (c) ASON, and (d) NDJF seasonal sequences. (e) Correlation coefficient between the leading mode SST expansion coefficient (lag 0) and the Niño-3 index, leading and lagging 24 months.

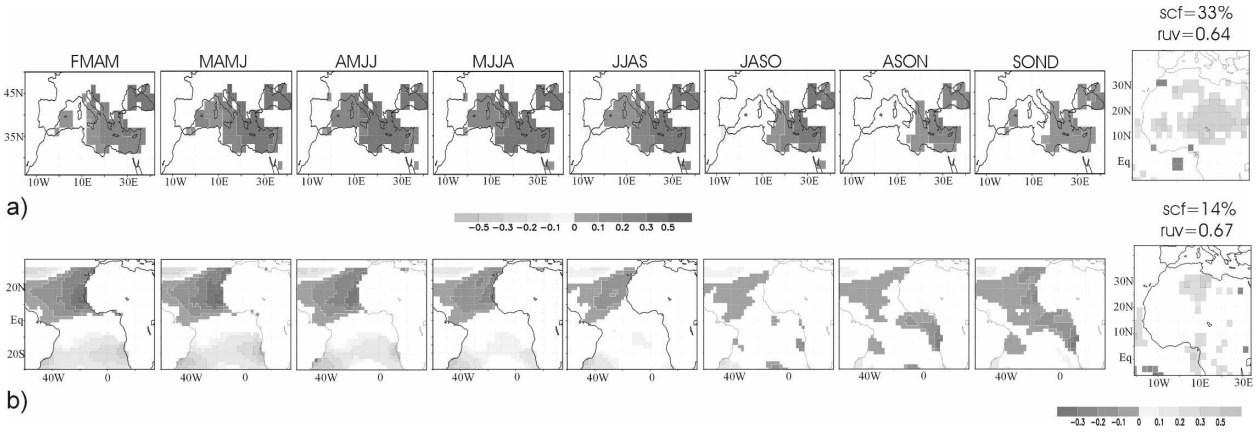

FIG. 9. (a) Leading covariability mode obtained from the EMCA between summer WA precipitation and the anomalous Mediterranean Sea SST 4-month sequences from FMAM to SOND. Only SSA as in Fig. 2 have been shaded. (b) Second covariability mode obtained from the EMCA between summer WA precipitation and the anomalous TA SST (avoiding the Mediterranean Sea) corresponding to the 4-month sequences from FMAM to SOND. Only SSA as in Fig. 2 have been shaded.

maximum loadings over the Congo River basin and the northern Sahel region. This pattern is itself more related to the third mode of variability when including the Mediterranean (not shown; the correlation coefficient between the both SST expansion coefficients is 0.83).

The correlation coefficients between the expansion coefficients of the three analyses are presented in Table 1. The three precipitation EMCA expansion coefficients obtained for the three EMCA analyses (tropical Atlantic + Mediterranean, Mediterranean, and tropical Atlantic) are significantly correlated with the leading WA rainfall PC. However, regarding the SST expansion coefficients, the result from the total analysis (tropical Atlantic + Mediterranean) is very similar to the TA analysis ($r = 0.71$), but is less significant for the Mediterranean Sea analysis ($r = 0.49$), and there is a very poor correlation between TA and the Mediterranean Sea analyses ($r = 0.09$).

These results imply that both the TA and Mediterranean Sea SST anomalies covary with the anomalous WA precipitation, but not necessary in the same way. Indeed, the sum of the SST expansion coefficients of both analyses, considering the SNA and Mediterranean Sea separately (Fig. 9), is very similar to the SST expansion coefficient of the tropical Atlantic + Mediterranean mode (Fig. 3, lower panel), with a correlation coefficient of 0.82 versus the low correlations in Table 1. This linear relationship evidences that the Mediterranean Sea and the SNA SST are independent components of the WA rainfall variability: the Mediterranean Sea SST influences Sahelian rainfall, while SNA SST influences Congo River basin rainfall.

To characterize the large-scale ocean pattern associated with these two modes, the regression of the SST expansion coefficients onto the global SST anomalies is performed (Figs. 10a,b). The analysis reveals that both large-scale patterns are different. On the one hand, tropical SST anomalies related to the Mediterranean mode are confined to the Pacific. On the other hand, for the SNA mode, the whole tropical ocean basin is

TABLE 1. Correlation coefficients between precipitation expansion coefficients (U) and SST expansion coefficients (V) from the different EMCA modes (Fig. 3, lower panel and Fig. 9), and WA rainfall PC modes (Fig. 2).

	Tropical Atlantic (second mode)	Mediterranean Sea (first mode)	First PC WAM	Tropical Atlantic + Mediterranean (third mode)	
Tropical Atlantic + Mediterranean (second mode)	0.75	0.90	0.89		U
	0.71	0.49	0.41		V
Tropical Atlantic (second mode)		0.49	0.49	0.36	U
		0.09	0.12	0.83	V
Mediterranean Sea (first mode)			0.96		U
			0.48		V

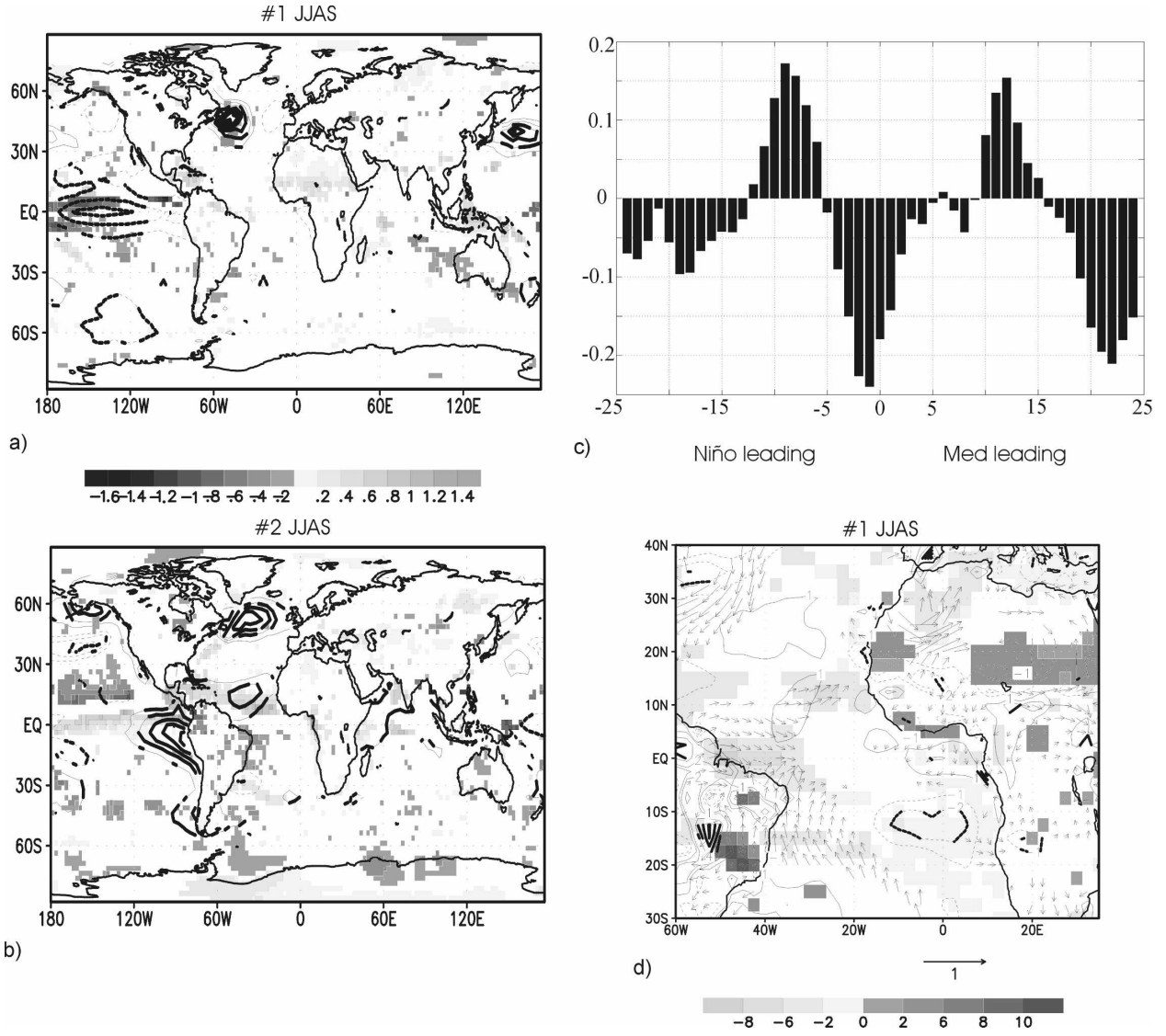

FIG. 10. (a) Regression of the total SST expansion coefficient associated with the Mediterranean Sea EMCA leading mode onto the global SST anomalies (CI = 0.1°C, SSA as in Fig. 2 have been bolded) and the precipitation (mm day^{-1}, SSA as in Fig. 2 have been shaded) for JJAS. Note that SST anomalies over the Mediterranean Sea are significant (same as Fig. 9a), but the contour lines in the global map are not visible enough. (b) Same as (a), but for the total SST expansion coefficient associated with the TA EMCA second mode. (c) Correlation coefficient between the total SST expansion coefficient associated with the Mediterranean Sea EMCA leading mode (lag 0) and the Niño-3 index, leading and lagging 24 months. (d) Regression of the total SST expansion coefficient associated with the Mediterranean Sea EMCA leading mode onto the radiative flux anomalies (shortwave minus longwave radiation, W m^{-2}, positive downward, only SSA as in Fig. 2 have been shaded), the surface wind anomalies (vectors, m s^{-1}, only SSA as in Fig. 2, have been plotted), and the latent heat flux anomalies (CI = 1 W m^{-2}, positive downward, only SSA as in Fig. 2 have been contoured) for the JJAS season.

also significant. The SST signal over the Pacific is also different for both modes: the Mediterranean mode is related to central equatorial Pacific SST, while the SNA mode is related to the central-eastern equatorial Pacific.

The central equatorial Pacific SST signal related to the Mediterranean mode corresponds to the evolution of an extratropical Pacific mode from the previous summer (not shown), but not to a canonical El Niño event. However, the lead–lag correlation analysis between the Mediterranean expansion coefficient and the Niño-3 index shows, with weak but significant scores, a 2-yr correlation cycle that could give some insight into predictability issues (Fig. 10c). Hence, the previously suggested connection between tropical Pacific SST and Sahelian rainfall (Janicot et al. 1996; Janicot et al. 2001)

seems to be pointing at the Mediterranean Sea as a relevant mediator. Thus, the relationship could be interpreted as a tropical Pacific–Mediterranean–Mediterranean–Sahel interaction. The physical mechanisms involved in the remote relation between Mediterranean and Pacific SST anomalies (Fig. 10a) could include atmospheric teleconnections through Rossby waves. In addition, significant simultaneous correlations are found between Pacific decadal oscillation index and the Mediterranean mode. This is an important area of research in progress by the authors through observational and model analyses. However, it is worthwhile to notice that the regression of the leading WA rainfall PC (from Fig. 2a) onto the global SST anomalies is significant only over the Mediterranean Sea region (not shown), giving robust weight to the Mediterranean influence during the dry Sahel period.

Regarding the large-scale SST signal related to the SNA mode, Fig. 10b yields both a North Atlantic pattern, which is reminiscent of the previous winter tripole SST pattern (not shown), and a tropical Pacific pattern, which resembles the decay phase of El Niño (the remaining eastern anomaly accompanied by the opposite western surrounding one). Some authors have pointed out the manner in which ENSO phenomenon can warm the SNA through the Pacific–North America (PNA) pattern and via Atlantic Walker-related anomalies (Wang 2002b; Kushnir et al. 2006), while the NAO modulates trade wind strength and, in turn, SNA SST (Okumura et al. 2001). The regressed precipitation for this SNA mode shows positive anomalous rainfall over the eastern equatorial Pacific, the Western Hemisphere warm pool (Wang 2002b), and the Congo River basin region, and negative loadings over northeastern Brazil.

Our results conclude that interannual Sahelian rainfall variability for the 1979–2002 period is mainly related to Mediterranean SST anomalies, instead of the Pacific basin or SNA region. Figure 10d shows the Mediterranean SST expansion coefficient regressed onto the surface wind, latent heat flux, and radiation flux anomalies for the JJAS season. There is a positive radiative flux anomaly over the Sahel region, which means that the Mediterranean influence is mainly nonconvective. The monsoon flow is weak, and the Harmattan winds over the Sahel are strengthened. This result coincides with those of Rowell (2003), who has shown that in years in which Mediterranean SSTs are warmer than average, increased evaporation leads to an enhanced moisture content of the air that is advected southward by the low-level mean flow across the eastern Sahara into the Sahel, feeding the increased moisture convergence and leading to increased rainfall. Jung et al. (2006) simulates the 2003 Mediterranean warm event, showing how the anomalously high moisture is advected from the Mediterranean by the climatological Harmattan and Etesian winds, where enhanced moisture flux convergence leads to more precipitation. Rowell (2003) also shows how the additional heating over the Sahel could induce a stronger low-level inflow from the TA, which can be an explanation for the appearance of the Mediterranean and SNA SST anomalies together associated with anomalous Sahel rainfall.

4. Conclusions

This work characterizes the most relevant observational TA (and Mediterranean Sea) SST modes coupled to the summer WA rainfall, in order to understand the possible predictability of the interannual WA rainfall variability for the Sahel dry period. We have evidenced the reliability of the precipitation dataset as well as the use of EMCA technique as a tool for resolving time-evolving SST patterns in relation to the anomalous WA rainfall. Using the CMAP rainfall dataset for the 1979–2002 period, the first two summer WA rainfall EOF variability modes have been determined as Sahelian and Guinean rainfall patterns, which appear as uncoupled ones. In contrast to other works that use the CRU dataset, different time periods, and/or different methodologies, no evidence for a dipole pattern is found for this period.

The leading SST–precipitation EMCA mode shows the evolution of the equatorial Atlantic mode associated with anomalous precipitation over the coast of the GG. The SST pattern is persisting for almost the complete sequence. Results suggest that the origin of the SST pattern occurs at the Angola/Benguela upwelling area because of an anomalous alongshore wind stress over this region. The wind anomalies over the southeast Atlantic could be associated with a previous anomalous subsidence over the Amazon basin. The eastern anomalous SST creates a zonal gradient over the equatorial band, changing the thermocline slope. The SLA associated with the SST propagates westward as a Rossby oceanic wave from the southeastern Atlantic as far as the west-central equatorial Atlantic. A different sign SLA anomaly, induced by anomalous Ekman pumping at the west Atlantic, propagates eastward as Kelvin oceanic wave, helping to damp the EM. The latent heat flux anomalies and the reversion of the wind anomalies also contribute to restore the normal conditions over the TA. Nevertheless, in order to assess these hypotheses about the EM air–sea interactions, a coupled model would be needed.

We have also evidenced that the leading TA EMCA mode could be important in driving Pacific anomalies.

This different equatorial Pacific–Atlantic connection during the dry Sahel period implies a less active role of the ENSO events on the Sahelian rainfall anomalies, while the Pacific–Atlantic relationship has more influence on the rainfall over the coast of the GG, because the Walker circulation is anomalous along the entire equatorial band.

Although the Atlantic El Niño mode by itself does not seem to have a large influence on Sahelian rainfall, a seasonal correlation between autumn Guinean rainfall and the following summer Sahel rainfall has been found and evaluated by other authors, mainly as the result of the soil moisture conditions persistence and the developed vegetation interactions (Philippon and Fontaine 2002; Fontaine et al. 2002; Douville et al. 2007).

The second SST–WA rainfall covariability mode relates the anomalous Sahelian rainfall to an anomalous SST pattern over the SNA and Mediterranean Sea. This mode shows how, from AMJJ to JJAS, the warm Mediterranean SST anomalies enhance the Sahel precipitation by more evaporation and southward low-level flow to the Sahel. The westerly winds from the Atlantic are also favored, strengthening the deep and dry convection over the Sahara low. Different EMCA analyses have shown that the Mediterranean SST pattern has the major contribution on Sahel rainfall, while the direct influence of the SNA is not clear. The global SST pattern associated with the Mediterranean Sea mode shows SST anomalies over the central Pacific and North Atlantic. It suggests that the Pacific–Sahel connection could be via the Mediterranean Sea. However, during this period, the Sahelian rainfall variability seems to be influenced only by the Mediterranean Sea (the leading WA rainfall PC regressed onto global SST has shown significant SST anomalies just over the Mediterranean Sea).

This work outlines the TA role over the WA rainfall, indicating that for the 1980s and 1990s the EM is the most relevant mode affecting the GG region and there is no significant link with the Sahelian rainfall. The Mediterranean is shown to affect just over the Sahel precipitation. Nevertheless, there are some constraints that should be outlined. On the one hand, the ocean is not the only factor explaining the WA rainfall variability, and the interaction with land surface processes and the role played by soil moisture and vegetation are also crucial factors (Douville 2002; Philippon and Fontaine 2002). On the other hand, the Atlantic Ocean is not the only basin that influences WA rainfall variability. The role of other ocean basins has been also analyzed in an intercomparison exercise that is being developed in the framework of the AMMA-EU project. In this work, the same analysis for different ocean basins has been done, finding that, for this period, the Mediterranean Sea SST anomalies are the most important in driving Sahel anomalies, while the central Pacific SST and eastern Indian Ocean SST explains less than 10% and 14%, respectively, of the SST–WA rainfall covariability, and the SST evolution of those patterns is not very clear.

Acknowledgments. We thank the editor Dr. Clara Deser, Dr. Carlos Roberto Mechoso, Dr. Elsa Mohino, and anonymous reviewers for their helpful comments. The study was supported by the Global Change and Ecosystems Programme [EU integrated project: African Monsoon Multidisciplinary Analysis (AMMA)]. AMMA has been the beneficiary of a major financial contribution from the European Community's Sixth Framework Research Programme. Detailed information on scientific coordination and funding is available on the AMMA International web site (http://www.amma-international.org). Also, the study has been supported through Spanish MEC project CGL2006-04471.

REFERENCES

Bader, J., and M. Latif, 2003: The impact of decadal-scale Indian Ocean sea surface temperature anomalies on Sahelian rainfall and the North Atlantic Oscillation. *Geophys. Res. Lett.,* **30,** 2169, doi:10.1029/2003GL018426.

Barreiro, M., A. Giannini, P. Chang, and R. Saravanan, 2004: On the role of the South Atlantic atmospheric circulation in tropical Atlantic variability. *Earth's Climate: The Ocean-Atmosphere Interaction, Geophys. Monogr.,* Vol. 147, Amer. Geophys. Union, 143–156.

Bretherton, S. B., C. Smith, and J. H. Wallace, 1992: An intercomparison of methods for finding coupled patterns in climate data. *J. Climate,* **5,** 541–560.

Carton, J. A., X. Cao, B. S. Giese, and A. M. Da Silva, 1996: Decadal and interannual SST variability in the tropical Atlantic Ocean. *J. Phys. Oceanogr.,* **26,** 1165–1175.

Chang, P., L. Ji, and H. Li, 1997: A decadal climate variation in the tropical Atlantic Ocean from thermodynamic air–sea interactions. *Nature,* **385,** 516–518.

Chelton, D. B., and M. G. Schlax, 1996: Global observations of oceanic Rossby waves. *Science,* **272,** 234–238.

Douville, H., 2002: Influence of soil moisture on the Asian and African monsoons. Part II: Interannual variability. *J. Climate,* **15,** 701–720.

——, S. Conil, S. Tyteca, and A. Voldoire, 2007: Soil moisture memory and West African monsoon predictability: Artefact or reality? *Climate Dyn.,* **28,** 723–742.

Florenchie, P., J. R. E. Lutjeharms, C. J. C. Reason, S. Masson, and M. Rouault, 2003: The source of Benguela Niños in the South Atlantic Ocean. *Geophys. Res. Lett.,* **30,** 1505, doi:10.1029/2003GL017172.

Folland, C. K., T. N. Palmer, and D. E. Parker, 1986: Sahel rainfall and worldwide sea temperatures. *Nature,* **320,** 602–607.

Fontaine, B., and S. Janicot, 1996: Sea surface temperature fields associated with West African rainfall anomaly types. *J. Climate,* **9,** 2935–2940.

——, ——, and V. Moron, 1995: Rainfall anomaly patterns and wind field signals over West Africa in August (1958–1989). *J. Climate,* **8,** 1503–1510.

——, N. Philippon, S. Trzaska, and P. Roucou, 2002: Spring to summer changes in the West African monsoon through NCEP/NCAR reanalyses (1968–1998). *J. Geophys. Res.,* **107,** 4186, doi:10.1029/2001JD000834.

——, P. Roucou, and S. Trzaska, 2003: Atmospheric water cycle and moisture fluxes in the West African monsoon: Mean annual cycles and relationship using NCEP/NCAR reanalysis. *Geophys. Res. Lett.,* **30,** 1117, doi:10.1029/2002GL015834.

França, C., I. Wainer, A. R. De Mesquita, and G. J. Goni, 2003: Planetary equatorial trapped waves in the Atlantic Ocean from TOPEX/Poseidon altimetry. *Interhemispheric Water Exchange in the Atlantic Ocean,* G. J. Goni and P. Malanotte-Rizzoli, Eds., Elsevier Oceanography Series, Vol. 68, Elsevier, 213–232.

Frankignoul, C., and E. Kestenare, 2005: Air–sea interactions in the tropical Atlantic: A view based on lagged rotated maximum covariance analysis. *J. Climate,* **18,** 3874–3890.

García-Serrano, J., T. Losada, B. Rodríguez-Fonseca, and I. Polo, 2008: Tropical Atlantic variability modes (1979–2002). Part II: Time-evolving atmospheric circulation related to SST-forced tropical convection. *J. Climate,* **21,** 6476–6497.

Giannini, A., R. Saravannan, and P. Chang, 2003: Oceanic forcing of Sahel rainfall on interannual to interdecadal time scales. *Science,* **302,** 1027–1030.

Handoh, I. C., and G. R. Bigg, 2000: A self-sustaining climate mode in the tropical Atlantic, 1995–97: Observations and modelling. *Quart. J. Roy. Meteor. Soc.,* **126,** 807–821.

Hastenrath, S., 1984: Interannual variability and annual cycle: Mechanisms of circulation and climate in the tropical Atlantic sector. *Mon. Wea. Rev.,* **112,** 1097–1107.

Hill, K. L., I. S. Robinson, and P. Cipollini, 2000: Propagation characteristics of extratropical planetary waves observed in the ATSR global sea surface temperature record. *J. Geophys. Res.,* **105,** 21 927–21 945.

Janicot, S., 1992: Spatiotemporal variability of West African rainfall. Part I: Regionalization and typings. *J. Climate,* **5,** 489–497.

——, V. Moron, and B. Fontaine, 1996: Sahel droughts and ENSO dynamics. *Geophys. Res. Lett.,* **23,** 515–518.

——, A. Harzallah, B. Fontaine, and V. Moron, 1998: West African monsoon dynamics and eastern equatorial Atlantic and Pacific SST anomalies (1970–1988). *J. Climate,* **11,** 1874–1882.

——, S. Trzaska, and I. Poccard, 2001: Summer Sahel-ENSO teleconnection and decadal time scale SST variations. *Climate Dyn.,* **18,** 303–320.

Jung, T., L. Ferranti, and A. M. Tompkins, 2006: Response to the summer of 2003 Mediterranean SST anomalies over Europe and Africa. *J. Climate,* **19,** 5439–5454.

Jury, M. R., D. B. Enfield, and J.-L. Mélice, 2002: Tropical monsoons around Africa: Stability of El Niño–Southern Oscillation associations and links with continental climate. *J. Geophys. Res.,* **107,** 3151, doi:10.1029/2000JC000507.

Keenlyside, N. S., and M. Latif, 2007: Understanding equatorial Atlantic interannual variability. *J. Climate,* **20,** 131–142.

Kushnir, Y., W. A. Robinson, P. Chang, and A. W. Robertson, 2006: The physical basis for predicting Atlantic sector seasonal-to-interannual climate variability. *J. Climate,* **19,** 5949–5970.

Lamb, P. J., 1978: Large-scale tropical Atlantic surface circulation patterns associated with sub-Saharan weather anomalies. *Tellus,* **30,** 240–251.

Latif, M., and A. Grötzner, 2000: On the equatorial Atlantic oscillation and its response to ENSO. *Climate Dyn.,* **16,** 213–218.

Liebmann, B., and C. A. Smith, 1996: Description of a complete (interpolated) outgoing longwave radiation dataset. *Bull. Amer. Meteor. Soc.,* **77,** 1275–1277.

Lu, J., and T. L. Delworth, 2005: Oceanic forcing of the late 20th century Sahel drought. *Geophys. Res. Lett.,* **32,** L22706, doi:10.1029/2005GL023316.

Melice, J. L., and J. Servain, 2003: The tropical Atlantic meridional SST gradient index and its relationships with the SOI, NAO and Southern Ocean. *Climate Dyn.,* **20,** 447–464.

Mo, K., G. D. Bell, and W. M. Thiaw, 2001: Impact of sea surface temperature Anomalies on the Atlantic tropical storm activity and West African rainfall. *J. Atmos. Sci.,* **58,** 3477–3496.

Moron, V., N. Philippon, and B. Fontaine, 2003: Skill of Sahel rainfall variability in four atmospheric GCMs forced by prescribed SST. *Geophys. Res. Lett.,* **30,** 2221, doi:10.1029/2003GL018006.

Motha, R. P., S. K. Leduc, L. T. Steyaert, C. M. Sakamoto, and N. D. Strommen, 1980: Precipitation patterns in West Africa. *Mon. Wea. Rev.,* **108,** 1567–1578.

North, G. R., T. L. Bell, F. Cahalan, and F. J. Moeng, 1982: Sampling errors in the estimation of empirical orthogonal functions. *Mon. Wea. Rev.,* **110,** 699–706.

Okumura, Y., S. P. Xie, A. Numaguti, and Y. Tanimoto, 2001: Tropical Atlantic air–sea interactions and its influence on the NAO. *Geophys. Res. Lett.,* **28,** 1507–1510.

Paeth, H., and P. Friederichs, 2004: Seasonality and time scales in the relationship between global SST and African rainfall. *Climate Dyn.,* **23,** 815–837.

——, and A. Hense, 2004: SST versus climate change signals in West African rainfall: 20th century variations and future projections. *Climatic Change,* **65,** 179–208.

——, and J. Stuck, 2004: The West African dipole in rainfall and its forcing mechanisms in global and regional climate models. *Mausam,* **55,** 561–582.

Philander, S. G. H., 1990: *El Niño, La Niña, and the Southern Oscillation.* International Geophysics Series, Vol. 46, Academic Press, 293 pp.

Philippon, N., and B. Fontaine, 2002: The relationship between the Sahelian and previous second Guinean rainy seasons: A monsoon regulation by soil wetness? *Ann. Geophys.,* **20,** 575–582.

Polito, P. S., and P. Cornillon, 1997: Long baroclinic Rossby waves detected by TOPEX/POSEIDON. *J. Geophys. Res.,* **102,** 3215–3235.

Polo, I., B. Rodríguez-Fonseca, and J. Sheinbaum, 2005: Northwest Africa upwelling and the Atlantic climate variability. *Geophys. Res. Lett.,* **32,** L23702, doi:10.1029/2005GL023883.

——, A. Lazar, and B. Rodríguez-Fonseca, 2008: Oceanic Kelvin waves and tropical Atlantic intraseasonal variability. Part II: Mechanisms and impacts. *J. Geophys. Res.,* **113,** C07009, doi:10.1029/2007JC004495.

Rodríguez-Fonseca, B., I. Polo, E. Serrano, and M. Castro, 2006: Evaluation of the north Atlantic SST forcing on the European and northern African winter climate. *Int. J. Climatol.,* **26,** 179–191, doi:10.1002/joc.1234.

Rowell, D. P., 2001: Teleconnections between the tropical Pacific and the Sahel. *Quart. J. Roy. Meteor. Soc.,* **127,** 1683–1706.

——, 2003: The impact of the Mediterranean SSTs on the Sahelian rainfall season. *J. Climate,* **16,** 849–862.

Servain, J., A. J. Busalacchi, M. J. McPhaden, A. D. Moura, G. Reverdin, M. Vianna, and S. E. Zebiak, 1998: A Pilot Research Moored Array in the Tropical Atlantic (PIRATA). *Bull. Amer. Meteror. Soc.,* **79,** 2019–2032.

Shinoda, M., and R. Kawamura, 1994: Tropical rainbelt, circulation, and sea surface temperatures associated with the Sahelian rainfall trend. *J. Meteor. Soc. Japan,* **72,** 341–357.

Smith, T. M., and R. W. Reynolds, 2003: Extended reconstruction of global sea surface temperatures based on COADS data (1854–1997). *J. Climate,* **16,** 1495–1510.

Sterl, A., and W. Hazeleger, 2003: Coupled variability and air-sea interaction in the South Atlantic Ocean. *Climate Dyn.,* **21,** 559–571, doi:10.1007/s00382-003-0348-y.

Sultan, B., K. Labadi, J. F. Guegan, and S. Janicot, 2005: Climate drives the meningitis epidemics onset in West Africa. *PLoS Med.,* **2,** 43–49.

Tippett, M. K., 2006: Filtering of GCM simulated Sahel precipitation. *Geophys. Res. Lett.,* **33,** L01804, doi:10.1029/2005GL024923.

——, and A. Giannini, 2006: Potentially predictable components of African summer rainfall in a SST-forced GCM simulation. *J. Climate,* **19,** 3133–3144.

Trzaska, S., A. W. Robertson, J. Farrara, and C. R. Mechoso, 2007: South Atlantic variability arising from air-sea coupling: Local mechanisms and tropical–subtropical interactions. *J. Climate,* **20,** 3345–3365.

Uppala, S. M., and Coauthors, 2005: The ERA-40 re-analysis. *Quart. J. Roy. Meteor. Soc.,* **131,** 2961–3012.

Vauclair, F., and Y. du Penhoat, 2001: Interannual variability of the upper layer of the tropical Atlantic Ocean from in situ data between 1979 and 1999. *Climate Dyn.,* **17,** 527–546.

——, ——, and G. Reverdin, 2004: Heat and mass budgets of the warm upper layer of the tropical Atlantic Ocean in 1979–99. *J. Phys. Oceanogr.,* **34,** 903–919.

Venegas, S. A., L. A. Mysak, and D. N. Straub, 1997: Atmosphere–ocean coupled variability in the South Atlantic. *J. Climate,* **10,** 2904–2920.

Vizy, E. K., and K. H. Cook, 2001: Mechanisms by which Gulf of Guinea and eastern North Atlantic sea surface temperature anomalies can influence African rainfall. *J. Climate,* **14,** 795–821.

Wagner, R. G., and A. M. da Silva, 1994: Surface conditions associated with anomalous rainfall in the Guinea coastal region. *Int. J. Climatol.,* **14,** 179–199.

Wang, C., 2002a: Atmospheric circulation cells associated with the El Niño–Southern Oscillation. *J. Climate,* **15,** 399–419.

——, 2002b: Atlantic climate variability and its associated atmospheric circulation cells. *J. Climate,* **15,** 1516–1536.

——, 2006: An overlooked feature of tropical climate: Inter-Pacific-Atlantic variability. *Geophys. Res. Lett.,* **33,** L12702, doi:10.1029/2006GL026324.

Ward, M. N., 1998: Diagnosis and short-lead time prediction of summer rainfall in tropical North Africa at interannual and multidecadal timescales. *J. Climate,* **11,** 3167–3191.

Xie, P., and P. A. Arkin, 1997: Global precipitation: A 17-year monthly analysis based on gauge observations, satellite estimates, and numerical model outputs. *Bull. Amer. Meteor. Soc.,* **78,** 2539–2558.

Zebiak, S. E., 1993: Air–sea interaction in the equatorial Atlantic region. *J. Climate,* **6,** 1567–1586.

Zhang, R., and T. L. Delworth, 2006: The impact of Atlantic multidecadal oscillations on Indian/Sahel rainfall and Atlantic hurricanes. *Geophys. Res. Lett.,* **33,** L17712, doi:10.1029/2006GL026267.

APÉNDICE B

Impactos de condiciones cálidas y frías en las cuencas del Mediterráneo sobre el Monzón de África Occidental: patrones de conexión observados (1979-2006) y simulaciones climaticas

B. Fontaine, J. Garcia-Serrano, P. Roucou, B. Rodriguez-Fonseca, T. Losada, F. Chauvin, S. Gervois, S. Sijikumar, P. Ruti y S. Janicot.
Clim. Dyn., doi 10.1007/s00382-009-0599-3

Clim Dyn
DOI 10.1007/s00382-009-0599-3

Impacts of warm and cold situations in the Mediterranean basins on the West African monsoon: observed connection patterns (1979–2006) and climate simulations

Bernard Fontaine · Javier Garcia-Serrano · Pascal Roucou · Belen Rodriguez-Fonseca · Teresa Losada · Fabrice Chauvin · Sébastien Gervois · Sivarajan Sijikumar · Paolo Ruti · Serge Janicot

Received: 16 December 2008 / Accepted: 19 May 2009

Abstract Using both empirical and numerical ensemble approaches this study focuses on the Mediterranean/West African relationship in northern summer. Statistical analyses utilize skin temperature, sea surface temperature, in situ and satellite rainfall, outgoing longwave radiation (OLR) observations and reanalyzed data winds and specific humidity on isobaric surfaces. Numerical investigations are based on a large set of sensitivity experiments performed on four atmospheric general circulation models (AGCM): ARPEGE-Climat3, ECHAM4, LMDZ4 and UCLA7.3. Model outputs are compared to observations, discussed model by model and with an ensemble (multi-model) approach. As in previous studies the anomalous Mediterranean warm events are associated with specific impacts over the African monsoon region, i.e., a more intense monsoon, enhanced flux convergence and ascendances around the ITCZ, a strengthening of low level moisture advection and a more northward location of ascending motion in West Africa. The results show also new features (1) thermal variability observed in the two Mediterranean basins has unalike impacts, i.e. the western Mediterranean covaries with convection in Gulf of Guinea, while the eastern Mediterranean can be interpreted as Sahelian thermal-forcing; (2) although observations show symmetry between warming and cooling, modelling evidences only support the eastern warming influence; (3) anomalous East warm situations are associated with a more northward migration of the monsoon system accompanied by enhanced southwertely flow and weakened northeasterly climatological wind; (4) the multi-model response shows that anomalous East warm surface temperatures generate an enhancement of the overturning circulation in low and high levels, an increase in TEJ (Tropical Eeasterly Jet) and a decrease in AEJ (African Eeasterly Jet).

This paper is a contribution to the special issue on West African Climate, consisting of papers from the African Multidisciplinary Monsoon Analysis (AMMA) and West African Monsoon Modeling and Evaluation (WAMME) projects, and coordinated by Y. Xue and P. M. Ruti.

B. Fontaine (✉) · P. Roucou · S. Sijikumar
Centre de Recherches de Climatologie,
CNRS/University of Burgundy, Dijon, France
e-mail: fontaine@u-bourgogne.fr

J. Garcia-Serrano · B. Rodriguez-Fonseca · T. Losada
Universidad Complutense de Madrid, Madrid, Spain

S. Gervois · S. Janicot
Institut Pierre-Simon Laplace/LOCEAN, CNRS/IRD/Paris VI,
Paris, France

F. Chauvin
Centre National de Recherches Météorologiques,
CNRS/Météo-France, Toulouse, France

P. Ruti
Environmental and Energy Research Institute, Rome, Italy

1 Introduction

The potential role of surface temperatures over the Mediterranean in West African climate dynamics has been largely less investigated than that of the tropical Atlantic or of the El Nino Southern Oscillation (ENSO) phenomenon. Moreover these investigations are recent and hence only based on a few empirical and/or numerical studies. The seminal work, based on observed (1947–96) data, long-term atmospheric general circulation model (AGCM) simulations and idealized experiments forced by warmer (colder) sea surface temperatures (SSTs) in the Mediterranean, has been published by

Published online: 11 June 2009

Rowell in 2003. It demonstrates that "in years when the Mediterranean is warmer than average the Sahel tends to be wetter than normal" (and vice versa) with a significant positive correlation ($r = +0.47$) between the whole Mediterranean SST and JAS Sahel during 1947–1996.

The same year Fontaine et al. (2003) used observational precipitation data and atmospheric reanalyses on the period 1968–1998 for studying moisture fluxes. They founded that part of the moisture fluxes vertically integrated in the layers 1,000–300 hPa or 1,000–925 hPa advected into the West African Monsoon area originates from the Mediterranean Sea and Central Africa and presents significant relationship with atmospheric water budget over the Sahelian belt during the rainy season. Contemporary, Raicich et al. (2003) found that the Sahel rainfall anticorrelates with sea-level pressure in the southeastern Mediterranean basin, suggesting the physical mechanism might involve variations in the local inter tropical convergence zone (ITCZ).

More recently, Peyrillé et al. (2007) analyzed the effect of changes in SST in the Mediterranean and the Gulf of Guinea using a 2-d zonally-symmetric model (30S to 40°N), in modifying the thermal forcing (5°C warming from May to July). They showed that such a warming moistens the lower layers of the Sahara through advection and reduces the thermal gradient between the Saharan heat low and the Mediterranean, tending to decrease the NE winds (Harmattan). Finally using observations and reanalyses over multi decadal periods, Joly (2008) provided evidence of a significant intensification of the Mediterranean/West African relationship in last years.

However, up to date, there are some intriguing results regarding the thermal forcing of the Mediterranean Sea into the West African monsoon (WAM) system. For instance, Rowell (2003) and Jung et al. (2003) described similar outcomes though using different SST patterns, prescribing thermal anomalies in the eastern and western Mediterranean basins respectively. There are also puzzling features concerning the atmospheric response related to Sahel precipitation, as local circulation anomalies (Raicich et al. 2003; Peyrillé et al. 2007) or 3-D evidences for mechanisms favoring the northward migration of the monsoonal rainbelt (Peyrillé et al. 2007; Peyrillé and Lafore 2007). Indeed these empirical and numerical studies are either cases studies focusing on specific processes (i.e., Peyrillé et al. 2007), or analyzes taking into account the climatic transition which affected West Africa during the second par of the XXth century, i.e., the existence of a succession of anomalously wet years in the 50 and 60 s followed by abnormally dry years in the 70 and 80 s as in Rowell (2003). So the purpose of this study is not to reproduce and discuss previous results for resolving the questions above, but to reexamine the relationship through both historical data covering a period which does not include the negative tendency in West African precipitation between the 50 and 90 s, and a lot of dedicated numerical GCM experiments.

This article focuses on the relationship between surface Mediterranean temperatures and the West African monsoon using Satellite observations and atmospheric reanalyses over the period 1979–2006 along with control and sensitivity experiments performed on 4 GCMs with an ensemble approach. The following section presents briefly the data used while Sect. 3 portrays the basic features of the Mediterranean/African linear relationship through different SVD analyses of the temperature and outgoing longwave radiation (OLR) fields and correlations with observed precipitation. Section 4 focuses on the observed contrasted impacts in Warm and Cold situations over the western and eastern Mediterranean basins to analyze both the linearity of the connection with the OLR signal and its impacts on observed atmospheric dynamics and Hadley circulation. In Sect. 5, we will present different sensitivity experiments relative to the Mediterranean thermal variability performed on four climate models before analyzing the results in terms of rainfall impacts and atmospheric dynamics though an ensemble approach. Section 6 will propose a short discussion before the conclusion.

2 Selected historical datasets

Land-based precipitation data (stations) do not allow accurate description of the West African rainfall variability at short time scales (i.e., lower than 1 month), especially in the recent years. This is mainly due to the anisotropy of the network, the number of stations documenting correctly rain falls being too low, especially along the meridional plane. For example the global surface summary of day dataset (GSOD) exhibits large areas without any station in the Benin, Togo and Burkina Faso positioned over the central parts of West Africa. Moreover some daily values are either not reported, or very underestimated or false which changes the coverage with days, months and years. After the year 2000 the series are too incomplete for analysing accurately the daily or 5-day fields.

So for describing the monthly and seasonal time scales, we selected first the monthly precipitation from the high-resolution gridded CRU TS 2.1 data-set. These files comprise 1224 grids of observed climate, for the period 1901–2002, and cover the global land surface at 0.5 degree resolution (see New et al. 2002; Mitchell et al. 2004). For shorter time scales, rainfall information has been selected from the CPC Merged Analysis of Precipitation (CMAP, Xie and Arkin 1997) and from the Global Precipitation Climatology Project (GPCP, Adler et al. 2003; Xie et al. 2003) estimates on a 2.5 × 2.5 degree latitude/longitude grid at a 5-day time-scale over the period 1979–2006.

These satellite-derived estimates do not describe exactly the real world but have many advantages over current in situ data: they are coherent in space and time at 5-day scale, they have been often described and used and they give access to different information. However in northern summer, the mean precipitation differences (CMAP–GPCP) are positive over land and negative over Ocean with a typical difference of ±0.1 mm/day (Gruber et al. 2000). This could be due to the fact that, by contrast with GPCP, CMAP uses uncorrected rain gauge over land (Gruber et al. 2000). Moreover, Yin et al. (2004) indicate that (1) the GPCP/CMAP spatial correlation is higher over land than over ocean; (2) in general precipitation over ocean represented by the GPCP is more accurate while over land the two products are close. More details can be found in Louvet et al. (2007).

The Sea Surface Temperatures provide from the most current version of the Kaplan dataset produced by taking the MOHSST5 version of the GOSTA data set from the U.K. MET office and using EOF projection, optimal interpolation, Kalman Filter analysis, and an optimal smoother for filling in any missing data. The data set is stored on a 5° × 5° grid.

Skin temperatures and atmospheric data in all the troposphere provide from National Centers for Environmental Prediction (NCEP) and is called NCEP/DOE AMIP-II Reanalysis (R-2) over the period 1979–2006. This dataset can be hence considered as a mix of in situ and satellite observations and modelling. It improves however upon the NCEP/NCAR Reanalysis (R-1) by fixing the errors and by updating the parameterizations of the physical processes. It has been also extensively used and described (Kanamitsu et al. 2002; Maurer et al. 2001 among others). To be very concise one can say that R-2 provides more accurate pictures of soil wetness, near surface temperature and surface hydrology budget over land, and radiation fluxes over Ocean. The new boundary layer and convection schemes have also modified the water vapor profile: R-2 has more moisture in low levels than R-1.

The daily NOAA Interpolated Outgoing Longwave Radiation (OLR) data are used in a 2.5° × 2.5° version where all gaps have been filled with temporal and spatial interpolation as described in Liebmann and Smith (1996). OLR is an interesting additional dataset for our purpose since it measures the direct emission from the surfaces (Earth, clouds). It allows therefore clear depiction between clear-sky regions which concentrate the highest OLR values from the warmest surfaces and deep convective regions where the highest and coldest clouds (cirrus and tops of cumulonimbus) dominate. However OLR values in W/m2 are not direct measurements of deep convection since for example in clear-sky situations, OLR measures the direct emission from the warmer land or oceanic surfaces.

3 Basic features of the Mediterranean/African relationship

The relationship is here examined through several spatial indices and objective field analyses using SSTs, skin temperatures, precipitation and OLR.

3.1 Composite and correlation analyses through observed precipitation

This section illustrates the basic relationship observed at monthly scale using selected spatial indices describing North African rainfall and the Western and Eastern Mediterranean surface temperatures over the recent period 1979–2002. Table 1 presents first the rainfall means in mm observed in North Africa (5–20°N) and in the Sahelian belt (13–18°N) for both the boreal summer (JAS) and the months from May to October. The Warm minus Cold (W − C) differences (see the legend of Table 1 for more details) are displayed in lines 3 and 4. Two important points emerge: (1) in boreal summer the warmest situations in the Mediterranean are associated with rainfall excess over North Africa and the Sahel and are preceded by rainfall deficits in spring; (2) this relationship seems to reinforce when the Eastern Mediterranean and the Sahel band are considered although only the North African index in September can be considered as significantly different.

Table 2 allows us give more details regarding the relative weight of long-term (>8 years) and inter-annual (<8 years) variability in different July–September spatial indexes describing skin temperatures over the West and East Mediterranean, and the GPCP and CMAP rainfall estimates averaged over central Sudan (9–13°N) and the western (17–10°W), central (10°W–10°E) and eastern (10–20°E) Sahel (13–18°N). Several important points can be mentioned. First the strongest significant correlations are generally registered with the GPCP estimates. Second the relationship between Sahelian rainfall and the Mediterranean thermal variability is significantly stronger when thermal variances <8 years are considered, above all in CMAP estimates. Thirdly the mean correlation between skin temperatures in the 2 basins and the Sudan-Sahel rainfall equals +0.31 (9% of variance, not significant taking into account autocorrelation in the series) with unfiltered series but increases to +0.49 (24% significant at $p = 0.05$) when variability lower than 8 year is taken into consideration. Although the difference between these values is not very large, this is rather different from Rowell (2003) who, given the period analyzed (1946–1996), took mainly into consideration the long-term negative trend in West African rainfall: $r = +0.61$ for variability >8 year and +0.31 for <8 year. Notice also that thermal variability in the Eastern Mediterranean explains in mean 20% of the

Table 1 Observed relationship between Mediterranean surface temperatures and North African (5–20°N) and Sahel (13–18°N) rainfall amounts averaged between 15°W and 30°E for the seasons July–September (JAS) and the months May–October

15°W–30°E	JAS	M	J	J	A	S	O
North Africa: 05–20°N							
Mean rainfall amounts (mm)	410	66	95	136	159	115	59
W − C West Medit (%)	+6	−13	−11	−2	+15*	±4	+15
W − C East Medit (%)	+11	**−22****	−2	+4	+13%	±17	+11
Sahelian belt: 13–18°N							
Mean rainfall amounts (mm)	219	8	27	73	101	44	8
W − C West Medit	+16	−22	−21	+12	+24	+3	+55
W − C East Medit	***+22****	*−44**	+3	*+18**	+17	***+39****	+44

Mean rainfall amounts in mm and warm minus cold differences (W − C) in percentages relative to the western and eastern Mediterranean basins. Period 1979–2002. The warmest Mediterranean summers are 1987, 1989, 1990, 1991, 1994, 1999, for the Western basin and 1988, 1994, 1998, 2000, 2001, for the eastern basin The coldest ones are 1979, 1980, 1981, 1984, 1993, 1996, 1997, 2002 for the western basin and 1979, 1981, 1983, 1984, 1991, 1992, 1996, 1997 for the eastern basin. The significant values at $p = 0.1$ (*) and 0.05 (**) using a Student t test are indicated in italic and bold, respectively. Underlined values means that differences are significant with a null hypothesis that the East and West Mediterranean have the same relationship with rainfall'

Table 2 Correlation coefficients between July and September surface temperatures in the Western/Eastern Mediterranean and July–September CMAP and GPCP rainfall estimates averaged over western Sahel (WSAH), central Sahel (CSAH), Eastern Sahel (ESAH) and central Sudan (CSUD) with and without time filtering

	Unfiltered series				Filtered series: variability < 8 years			
	West Medit		East Medit		West Medit		East Medit	
	CMAP	GPCP	CMAP	GPCP	CMAP	GPCP	CMAP	GPCP
WSAH	+07	*+38*	+15	***±65***	+16	+30	***+42***	***+63***
CSAH	+24	+29	***+47***	***±57***	***+41***	***±50***	***±65***	***±66***
ESAH	+18	+10	+31	+37	***±52***	***+44***	***±73***	***±66***
CSUD	−13	***+42***	+01	***±59***	+21	***+42***	***±58***	***±62***

The significant values at $p = 0.1$, 0.05 and 0.01 taking into account time autocorrelations in the series are indicated in italic, bold and underlined, respectively. Period 1979–2006

Sudan-Sahel rainfall total variance while the Western basin explains only 7%.

3.2 Robustness of the relationship

The linear relationship is further analysed by computing several Singular Value decompositions (SVD) between temperature fields and OLR fields over the period 1979–2005. Interpolated OLR data are a practical estimate of convective activity over West Africa, since OLR values <240 W/m^2 depict the occurrence of high clouds closely linked to deep moist convective areas as those which are positioned within ITCZ. These SVDs have been performed both at monthly, 5-day and daily scales in isolation to be not confounded with longer-term variations and using different time filters. The main results are reported in Figs. 1 and 2 and Table 3.

Figure 1 refers to a synchronous (no lag) analysis performed between monthly skin temperatures observed over an extended Mediterranean region (5°W–40°E; 20–45°N) and monthly OLR values referring to an extended WAM region (20°W–40°E; 10°S–20°N). The total covariance equals 32.7% of the total variance and the squared covariance fractions of the two leading modes match 33.4 and 22.5% respectively. The first heterogeneous mode and its related time coefficients are displayed in Fig. 1a, b. They clearly attest the statistical linkage between warm anomalies restricted to Eastern Mediterranean and low OLR anomalies expanding along 10–15°N and eastward to about 10°W. As noticed above, the Eastern Mediterranean concentrates the highest positive loadings, while the western basin and continental regions somewhat northward to the mean ITCZ position accumulates the strongest negative loadings (meaning enhanced deep convection) with the

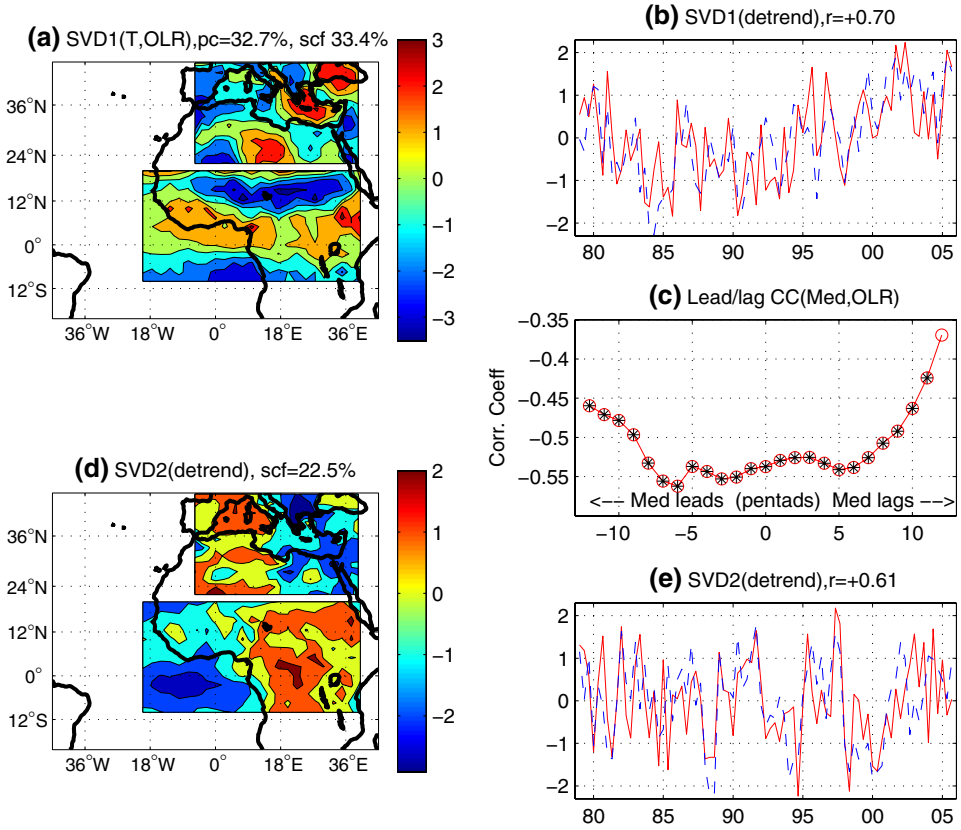

Fig. 1 First and second leading July–September SVD modes performed between skin temperatures in the Mediterranean region and West African OLR values at monthly time step: **a**, **b** (**d**, **e**) describe the first (second) mode in terms of heterogeneous field of covariability and expansion time coefficients while (**c**) displays lead/lag correlation coefficients between a spatial index averaging surface temperatures in the Mediterranean basin (32–40°N; 6–36°W) and OLR values in the Sahel zone (10–20°N; 15°W–30°E). Values significant at $p = 0.05$ taking into account autocorrelations in the series are marked by asters. Period July–September 1979–2006

maximum located in the central and eastern Sahel. Such a result agrees well with those shown by Polo et al. (2008) at monthly-interannual scale, suggesting an active role of the eastern Mediterranean SST into the Sahelian variability. In fact, the coupled OLR and temperature time series in Fig. 1b are largely correlated ($r = +0.70$, significant at $p = 0.01$ taking into account autocorrelation in the series); they display both an in-phase interannual signal and the recent rainfall recovering since the 90 s. When these coefficients are averaged over the successive JAS season its correlation increases to +0.87, while the temperature and OLR time series are positively correlated with JAS rainfall averaged over central (10°W–10°E) Sahel: +0.50 and +0.67, significant at $p = 0.05$ and $p = 0.01$ respectively, taking into account autocorrelation in the series.

By construction the second skin temperature-OLR mode (Fig. 1c, d) is less energetic and registers lower serial correlation between time series ($r = +0.61$, significant at $p = 0.01$ taking into account autocorrelation in the series). However it is the direct complement of the first one: the strongest (positive) temperature loadings are here restricted to the West Mediterranean. A surface warming in this region is linked to lower OLR values (deeper convection) extending both in the Western parts of the Sahel (Senegal, Mali) and over equatorial eastern Atlantic (Gulf of Guinea). When time coefficients are averaged over the JAS seasons the correlation increase to +0.70 ($p = 0.01$), and the temperature and OLR time series are positively correlated with JAS rainfall over the western parts (18–10°W) of the Sahel: +0.31 and +0.43 respectively, this last value being significant at $p = 0.05$.

In fact the Mediterranean/WAM relationship is not purely synchronous as illustrated in Fig. 1c. This diagram displays the lead/lag correlation coefficients computed between spatial indexes averaging OLR values in the Sahel zone (10–20°N; 15°W–30°E) in JAS, at the heart of the rainy season and 3-month surface temperatures in the whole Mediterranean basin (32–40°N; 6–36°W) moving with a 5-day (pentad) time-step before and after JAS. Near all the values are significant at $p = 0.05$ but the strongest correlation is registered when the Mediterranean temperatures are leading OLR by 6 pentads (1 month).

3.3 Evolution of the leading skin temperature/OLR mode at the monthly scale

In order to assess better the robustness of the Mediterranean/WAM lagged relationship, Fig. 2 refers to SVD analyses performed at the monthly scale between Mediterranean skin temperatures and WAM OLR values 1 month later referring to the same domain that in Fig. 1. Here linear trends in the

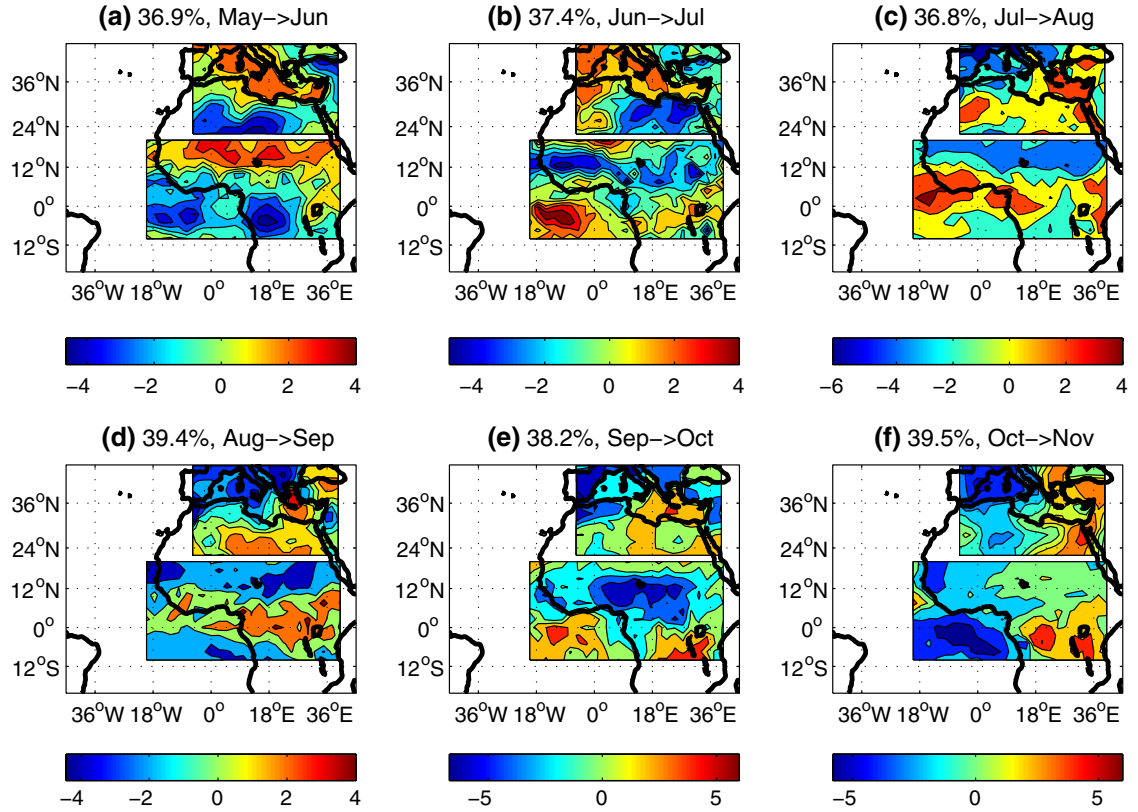

Fig. 2 Monthly evolution of the 1st SVD heterogeneous mode between skin temperature in the Mediterranean region and one-month lagged WAM OLR anomalies; spatial domains as in Fig. 1. The respective covariance fractions in % of total variance are indicated. Period 1979–2006

Table 3 Percentages of covariance and covariance fractions explained by the leading July–September mode (SVD1) at a daily timescale and time correlations (Corr SVD1) with and without linear trend (detrend) and as a function of time filtering in different ranges for capturing the 3–5 days (AEWs), < 10-day (synoptic), 10–90 days (intraseasonal) variability over the period 1979–2006

T, OLR, days	With trend	Detrended	3–5 days	<10 days	10–90 days
% cov/var	**11.5**	17	10.7	8.5	9.9
% SVD1	**51.9**	29	46.2	45.6	43.9
Corr SVD1	**+51**	+42	+48	+41	+26

series have been removed and the display focuses on the May/June to October/November evolution of the lagged temperature/OLR relationship. The results confirm first the statistical linkage between the East Mediterranean and WAM domains shown above (Fig. 1a). Second they show that there is no negative OLR anomaly over the Sahel before June/July (Fig. 2b), confirming the previous dry regime as indicated from Table 1 (in May/June; Fig. 2a). There, warm anomalies are associated with positive values of OLR over Sudan-Sahel, meaning decreased convection. From Jul/Aug to Oct/Nov temperature loadings reinforce on the eastern Mediterranean according to the leading monthly coupled mode (Fig. 1a), while OLR anomalies are related to increased deep motions (Fig. 2c–f).

Once again, the East Mediterranean concentrates the highest positive temperature loadings in connection with WAM deep convection, which points out largest anomalies along 10–15°N and mainly located over inland regions. Also at daily scales, Table 3 summarizes the percentages explained by each leading JAS-mode, time correlation between time series before and after removing all linear trends at each grid point (columns 1–2). In fact the field coupling is slightly lower when the series are detrended with a leading mode, spatially similar to Fig. 2a but less energetic (29 vs. 52% of squared covariance fraction) and positively correlated (+0.42 vs. +0.51). Other columns underline possible connections with oscillatory modes at synoptic scale (<10 days) such as African Easterly Waves (AEW) in the 3–5 day range, when longer-term mean coefficients are removed.

To test the linearity of the connection the next section contrasts the signals observed in warm and cold situations over the Western and Eastern Mediterranean.

4 Contrasted impacts in warm and cold situations

4.1 OLR signal

The mean July–September OLR field displayed in Fig. 3a exhibits high OLR values in the Mediterranean region and low OLR values near the ITCZ mean location since in dry subtropics (no cloud), OLR depends mainly on surface temperatures and is generally greater than 260 W/m^2: any surface warming (cooling) in the lowest levels of the troposphere over the Mediterranean tends to enhance (reduce) OLR values. By contrast, in the vicinity of the ITCZ which concentrates the lowest OLR values (<240 W/m^2 in Fig. 3a) OLR is directly linked to the altitude of clouds (convective towers).

The warm (cold) composites relative to the Western and Eastern Mediterranean are shown in Fig. 3b, c, respectively (Fig. 3d, e). They contrast the 8 warmest and the 8 coldest seasons versus all the remainders (caption in Fig. 3 indicates the selected years). Once again the signal is more significant in Fig. 3c and e, i.e. when the possible thermal forcing involves the East Mediterranean: warm (cold) anomalies in the Eastern basin are associated with lower (higher) OLR values. This denotes an enhancement (a reduction) of deep convection in the monsoon region when the East basin is abnormally warm (cold) and suggests hence the existence of associated signals in atmospheric dynamics.

4.2 Atmospheric dynamics

Vertical cross sections of wind and specific humidity along the 20°–0°W and 0°–30°E meridional planes and relative to the West and East Mediterranean are presented in Fig. 4. Panels a, b show the mean location and intensity of cell circulations along with the regions where specific humidity exceeds 10 g/kg. The northern and southern overturning cells are easily recognizable between the humid Mediterranean and monsoon regions (shading). The southern cell, where the monsoon takes place, includes southerly/northerly horizontal branches in low/high levels and ascending/subsiding branches located respectively by 8–10°N and 20°S. Westward to the 0° meridian the strong ascents are associated with strong northerlies at 200 hPa southward to

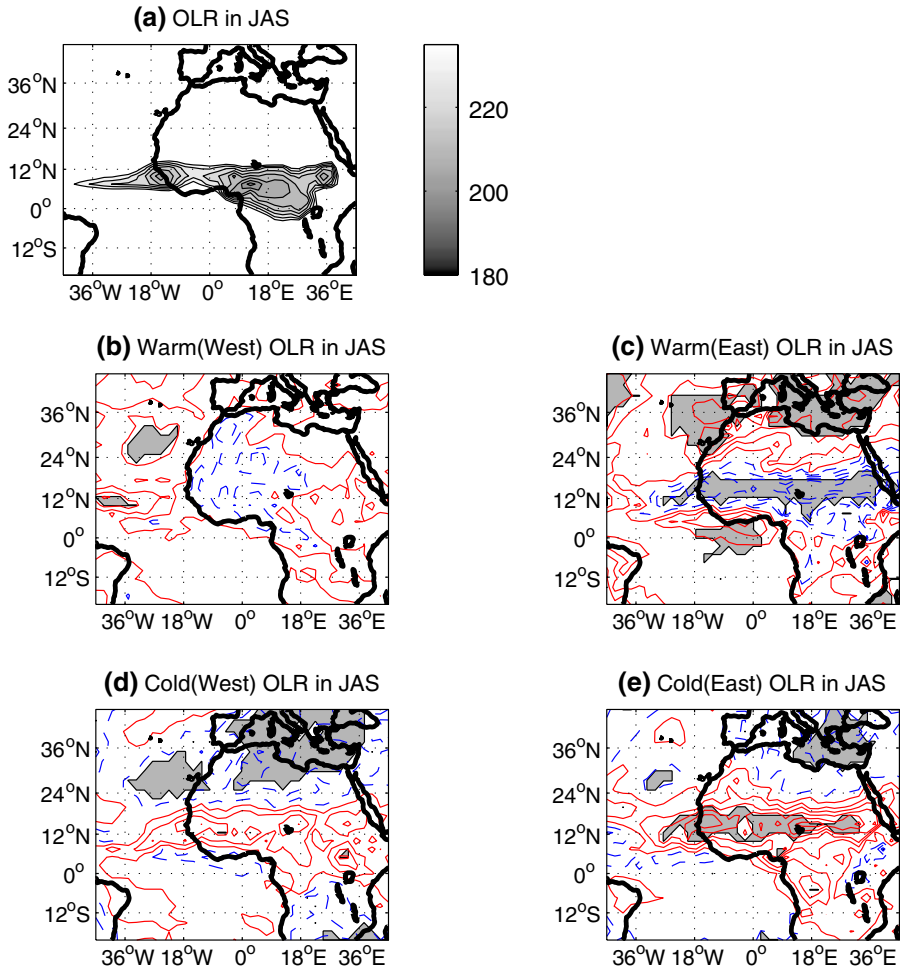

Fig. 3 Warm and cold composites of OLR fields in July–September: (**a**) mean field; (**b**) and (**c**) differences between the warmest situations and all the others relative to the Western and Eastern Mediterranean, respectively; (**d**) and (**e**) as above but for the coldest situations. The warmest JAS seasons are 1987, 1989, 1990, 1991, 1994, 1999, 2003, 2006 for the Western basin and 1988, 1994, 1998, 2000, 2001, 2003, 2005, 2006 for the eastern basin. The coldest ones are 1979, 1980, 1981, 1984, 1993, 1996, 1997, 2002 for the western basin and 1979, 1981, 1983, 1984, 1991, 1992, 1996, 1997 for the eastern basin. The shadings refer to OLR values <240 W/m^2 with a 5 W/m^2 increment (in **a**) and to the significant signals at $p = 0.1$ using a Student t test (in **b**–**e**). Period 1979–2006

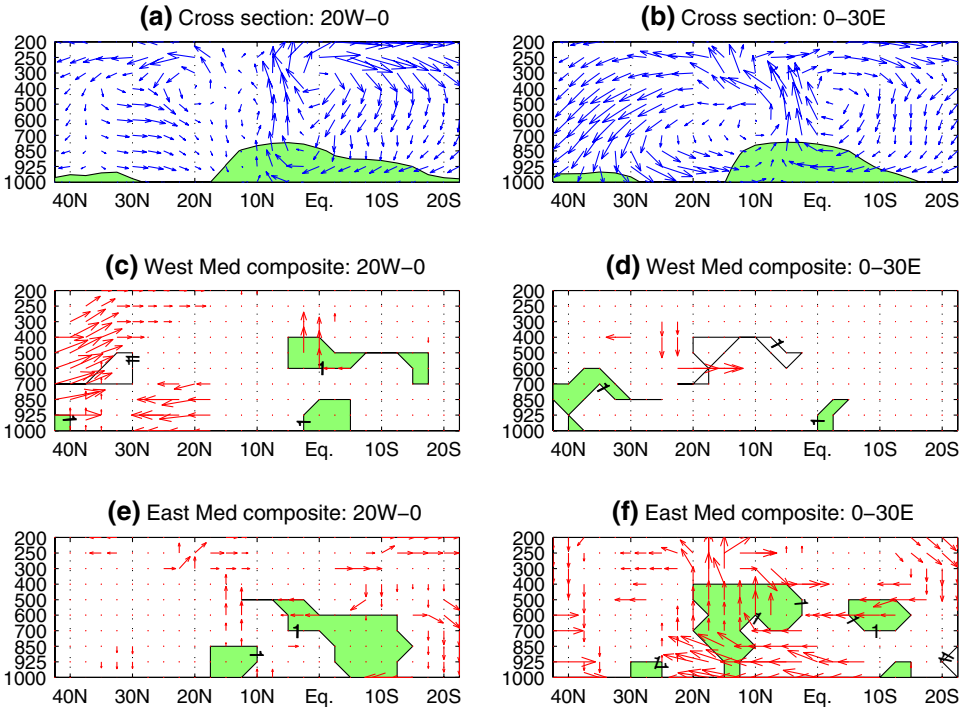

Fig. 4 July–September mean meridional/vertical cross sections and composites of wind and specific humidity along the 20°–0°W (*left*) and 0°–30°E (*right*) meridional planes: (**a**) and (**b**): mean circulation; (**c**, **d**) warm composites relative to the Western Mediterranean; (**e**, **f**) warm composites relative to the Eastern Mediterranean. In (**a**, **b**) the shadings points to the layer where specific humidity >10 g/kg; in (**c**–**f**), *red arrows* and *shadings* refer to the significant signals in wind and specific humidity at $p = 0.1$, respectively, after using a Student *t* test. Period 1979–2006

the equator (Fig. 4a) which tends to fuel monsoon overturning in the southern cell. By contrast eastward to the 0° meridian the ascents fuel preferentially the northerlies in low levels from the Eastern basin and hence the northern cell (Fig. 4b).

Warm composites in Fig. 4c–f exhibit significant signals in both meridional circulation and specific humidity especially. Warm conditions in the Western basin are associated, westward to 0°, with lower-levels convergence and upper-levels ascending motions in the northern subtropical latitudes, and with significant moisture increase (shadings in Fig. 4c) in the low and mid troposphere above the equatorial Atlantic. However only 3% of the area can be considered as significant and there is no clear meridional-connection between the former and the latter. Neither a clear signal appears eastward to 0°. By contrast warm conditions in the Eastern basin reinforce the southern (monsoon) cell circulation between 0° and 30°E (Fig. 4f) with 5% of global field significance): low level advections from the South in temperature and moisture are significantly enhanced, while air ascents within the ITCZ and air descents above the Southern Tropics strengthen. This is accompanied by a significant moisture increase (shading in Fig. 4f) under 400 hPa over the continent (5–20°N). To a lesser extent, but of equal statistical significance, the northern Hadley cell is also reinforced showing a closed circulation.

The results reported in Sects. 3 and 4 are thus compatible with the existence of a significant statistical relationship between the East Mediterranean and the WAM-Sahel region. In order to check whether this is interpretable in terms of Mediterranean forcing, we will analyze multi-model outputs using SST sensitivity experiments performed on 4 AGCMs. This approach allows production of more reliable climate features than a single model method since climate simulations performed on any given model are sensitive to systematic errors, as previously shown by, among others, Bader and Latif (2003) and Giannini et al. (2003).

5 Numerical study

5.1 Description of the sensitivity experiments

Several SST sensitivity experiments linked to normal, warm and cold situations over the Mediterranean have been performed on four AGCMs:

- ARPEGE-Climat Version 3 IPCC-AR4 in truncature 42 with 45 levels run at CNRM (Centre National de Recherches Météorologiques, Météo-France)
- ECHAM Version 4 in truncature 30 with 32 levels run at ENEA (Italian National Agency for New Technologies, Energy and Environment)
- LMDZ Version 4 (96 long, 71 lat and 19 levels) run at IPSL (Institut Paul-Simon Laplace)
- UCLA Version 7.3 (2° long × 2.5°lat, 29 levels) run at UCM (Universidad Complutense de Madrid)

In these experiments the SST anomaly patterns were calculated from observed ERSST dataset (Smith and

Reynolds 2004) and over the period 1979–2005. The African monsoon multidisciplinary analyses (AMMA) community decided that the boundary conditions were based on the expansion coefficient of the leading Extended Maximum Covariance mode between WAM-precipitation (CMAP dataset) and Mediterranean-SST described in Polo et al. (2008). This mode shows strong positive links between the Sahelian rainfall and the spring to summer evolution of the SST anomalies in the eastern Mediterranean. In order to introduce some physical considerations in the SST patterns definitions, a SST composite was constructed by averaging years for which the phasing between SST and African precipitation was maximal. They have been computed chosen those years in which the SST and June–September precipitation expansion coefficients were higher than 1 standard deviation (1984, 1987, 1991, 1992, 1997) and those in which the expansion coefficients were less that −1 standard deviation (1979, 1994, 1999, 2001). In order to amplify the SST signals, it has chosen to compute the difference between the positive-composite and the negative-composite of SST anomalies for defining the positive phase of the thermal forcing; while the negative phase was computed by multiplying the positive phase by −1. The SST anomalous patterns were finally multiplied by two in order to amplify the atmospheric response (Fig. 5). SST conditions have then been prescribed with these anomaly patterns added to the climatology of observed global SST for the period 1979–2005.

The ENEA, IPSL and UCM institutions performed 10 simulations with different initial conditions for each experiment (cold, warm, and control with no superimposed SST anomaly) while CNRM performed 20 simulations, allowing available a total of 150 simulations. However to give each model the same weight, we will consider 10 simulations for each model and each experiment (control, cold and warm), hence $10 \times 4 \times 3 = 120$ simulations. Experiments have been run from 15th of April to 15th of October and each SST pattern have led to a set of 10 runs (20 runs for CNRM). Initial conditions have been taken from a long-term AMIP-type run with conditions representative of the end of the 20th century. A good way to do this was to take conditions around the 15th of April for 10 (or 20 for CNRM) different years in the set of possible initial conditions. The 10 (or 20) years for initial conditions have been taken from years 1979 to 1988 (or 1979–1998 for CNRM).

It is noteworthy that using such prescribed SST as a lower boundary condition implies that the sea acts as a reservoir of infinite heat capacity which is not the case in the real world where the Mediterranean has finite heat capacity. This tends to damp the surface heat fluxes and therefore to decrease the amplitude resulting from the model runs.

5.2 Multi-model rainfall outputs

In order to validate models outputs, Fig. 6 shows the May to September mean monthly rainfall fields averaged over the period 1979–2001 in the CPC merged precipitation and in the control experiments of each model. Nearly all models reproduce well seasonal evolution of the rainbelt both in terms of meridional displacements and of location of rainfall maxima (amounts > 6 mm/day are shaded). However systematic biases exist in each model. For example, the CNRM, IPSL and ENEA simulations tend to underestimate the rainfall amounts while UCLA overestimates. Notice also that the seasonal excursion of the

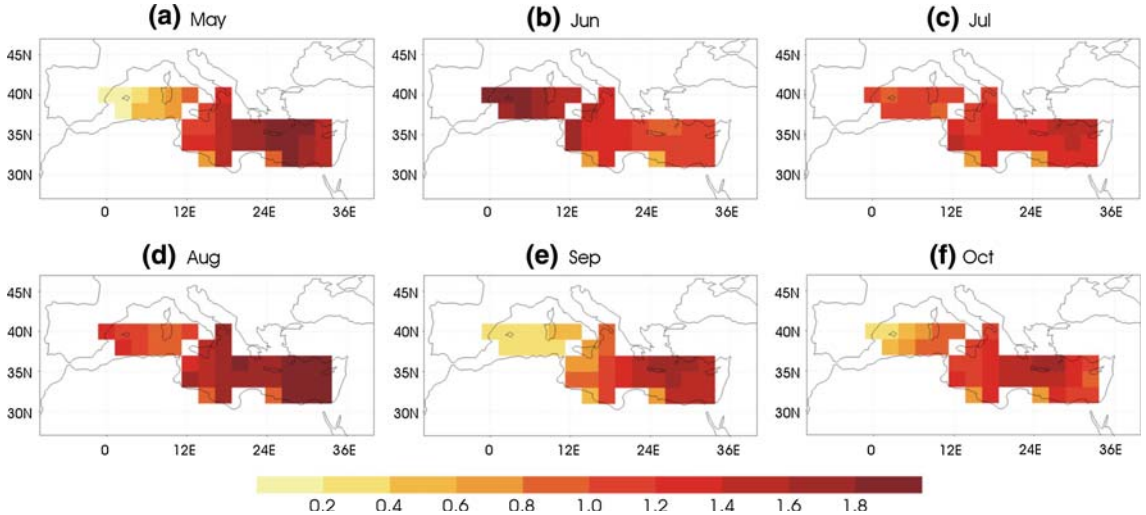

Fig. 5 May–October forcing fields used in the AGCM-sensitivity experiments. SST anomalies are expressed in °C units

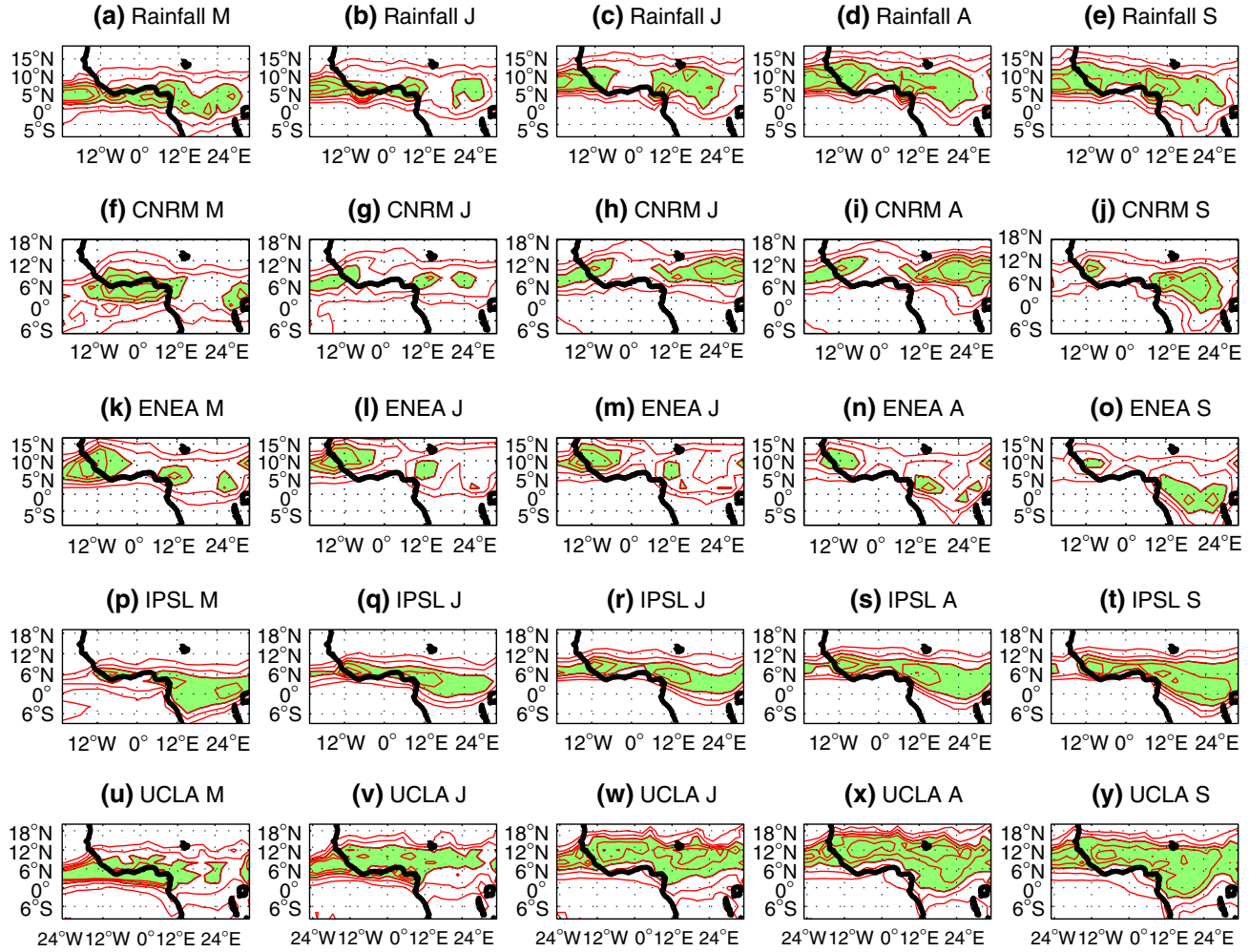

Fig. 6 May–September mean monthly rainfall fields from the CPC merged precipitation (**a–e**) on the period 1989–2001 and from the control experiments of each model CNRM (**f–j**), ENEA (**k–o**), IPSL (**p–t**) and UCLA (**u–y**). Isolines from 2 to 10 mm/day; shadings for values >6 mm/day

rainbelt in latitude is better reproduced in CNRM and UCLA outputs (see also the Hovmoller diagrams for the control runs in Losada et al. 2009; this issue).

The 40 warm (W) and 40 cold (C) experiments limited to the Mediterranean are now compared to the 40 control simulations (CTL = climatology) regarding rainfall outputs from each model. The focus is made on the two main West African rainy seasons, i.e., the first Guinean rainy season in May–June (MJ) and the northern tropical rainy season in July–September (JAS).

Figure 7 displays the W-CTL and C-CTL field differences with superimposed shadings where they are significant. In MJ there is no coherent signal: i.e., the IPSL model produces significant rainfall differences (Fig. 7i, j, with 11 and 5% significant grid points, respectively), but with the same sign in both experiments. In JAS the responses are larger and increase in magnitude and significance. Even so, cold experiments generate fairly unclear results and are not conclusive at all, except with UCLA in Fig. 7o (6%). In contrast, warm experiments produce significant Sahelian rainfall excesses in 3 out 4 models (CNRM, IPSL, UCLA with respectively 10, 18 and 9% significant points), which outputs are in good agreement with our previous empirical results. The precipitation response from ENEA does not yield any significant anomaly, neither from C-CTL (Fig. 7g) nor from W-CTL (Fig. 7h). As shown in Fig. 6k–o, ENEA climatology is unable to simulate the latitudinal migration of the ITCZ-WAM system, and also fails in producing the maximum monsoonal rainfall, i.e. located in MJ instead of JAS (also in Losada et al. 2009, this issue). These features could largely explain the diffuse ENEA response; and, since this model does not reproduce the WAM seasonal cycle we will exclude its outputs in the following sections.

In Fig. 8 statistical distributions of the MJ and JAS rainfall outputs are displayed in standardized values both

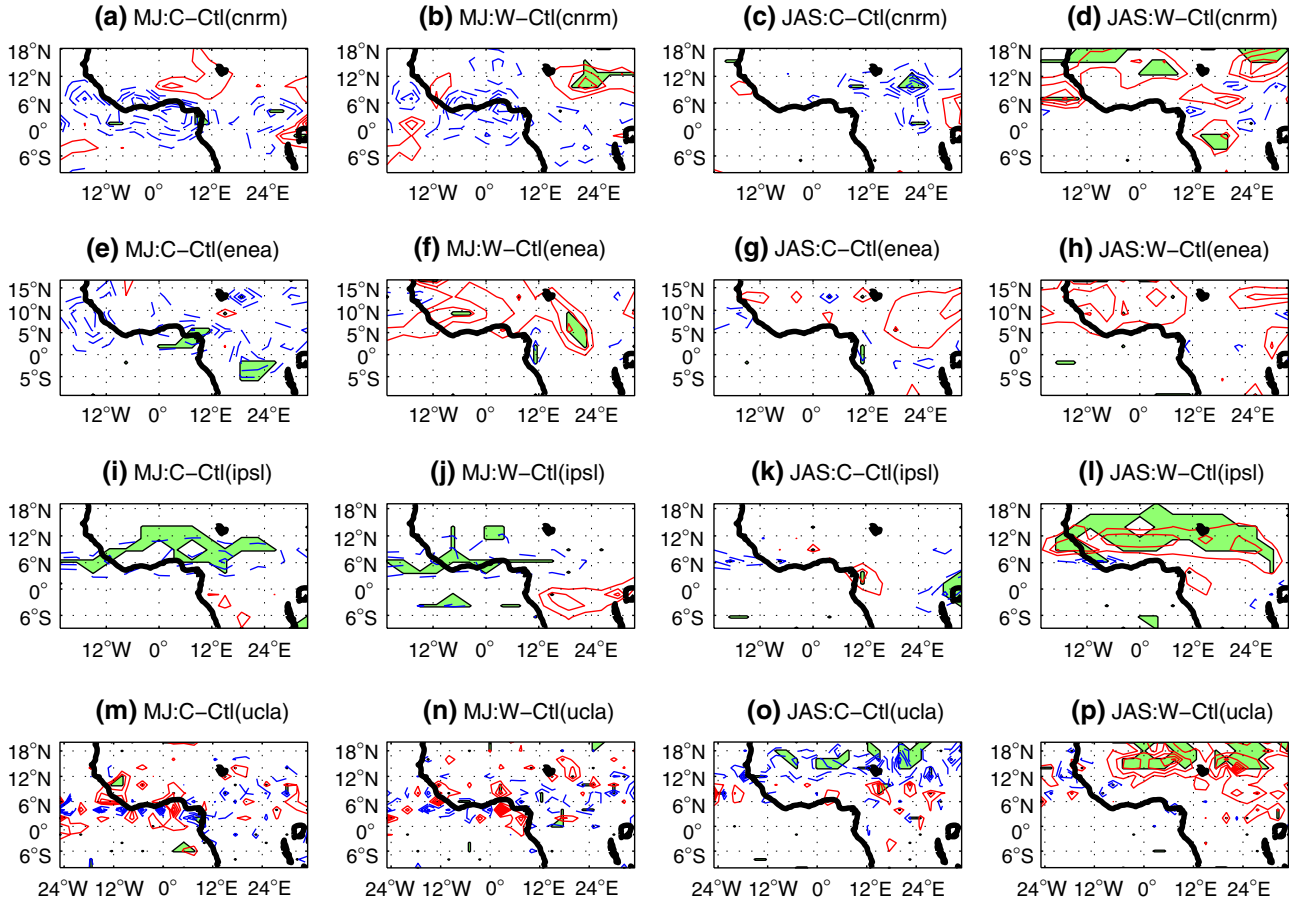

Fig. 7 Cold minus Control and Warm minus Control rainfall differences in May–June (*left part*) and July–September (*right part*) for the different GCMs: *red*/*blue* curves for positive/negative anomalies; shadings are superimposed when differences are significant at $p = 0.05$ regarding a paired-t test

model by model (Fig. 8a, b), and for the mean-ensemble including all the models (Fig. 8c, d). In order to reduce the systematic errors due to each model, the biases have been considered separately for each model and anomalies with respect to the corresponding model climatology have been computed. The histograms refer to a classification in three categories illustrating the relative occurrences of below normal, quasi normal and above normal situations in warm and cold experiments (see the legend).

In MJ (Fig. 8a, c) there is no significant rainfall difference: no model causes a significant dispersion of the rainfall amounts produced by the cold and warm experiments (circles and asters in 8a, respectively). This is similar when using a model-ensemble approach: the histograms relative to the cold and warm simulations (white and blue bars in Fig. 8c, respectively) are alike. In JAS, at the opposite, the same experiments create contrasted responses, i.e., less (more) rainfall in cold (warm) situations. However, there is a more consistent signal in warm outputs than in cold ones: (1) the latter fail 32.5% in distinguishing the precipitation sign, against only 12.5% in the former (Fig. 8b); (2) and, considering 4-models together, the cold (warm) experiments model-ensemble generate a ratio of 9/18 (27/2) between excess/deficits (Fig. 8d). Warm situations in the Mediterranean seem therefore to impact more on West African precipitation in contrast with empirical findings, which showed a symmetrical signal (Fig. 3c, e). For all above, the rest of the work will focus on both the rainy season (JAS) and the forced-response in warm conditions.

5.3 Large-scale wind circulation

Multi-model composites using the anomaly method are now presented for contrasting respectively the 30 cold and 30 warm experiments to the 30 control runs in terms of circulation along the vertical meridional plane (CNRM, UCM, IPSL; excluding ENEA). Figure 9 presents vertical cross sections of wind components (u,v, omega) as simulated by each model averaged along 20°W–30°E where

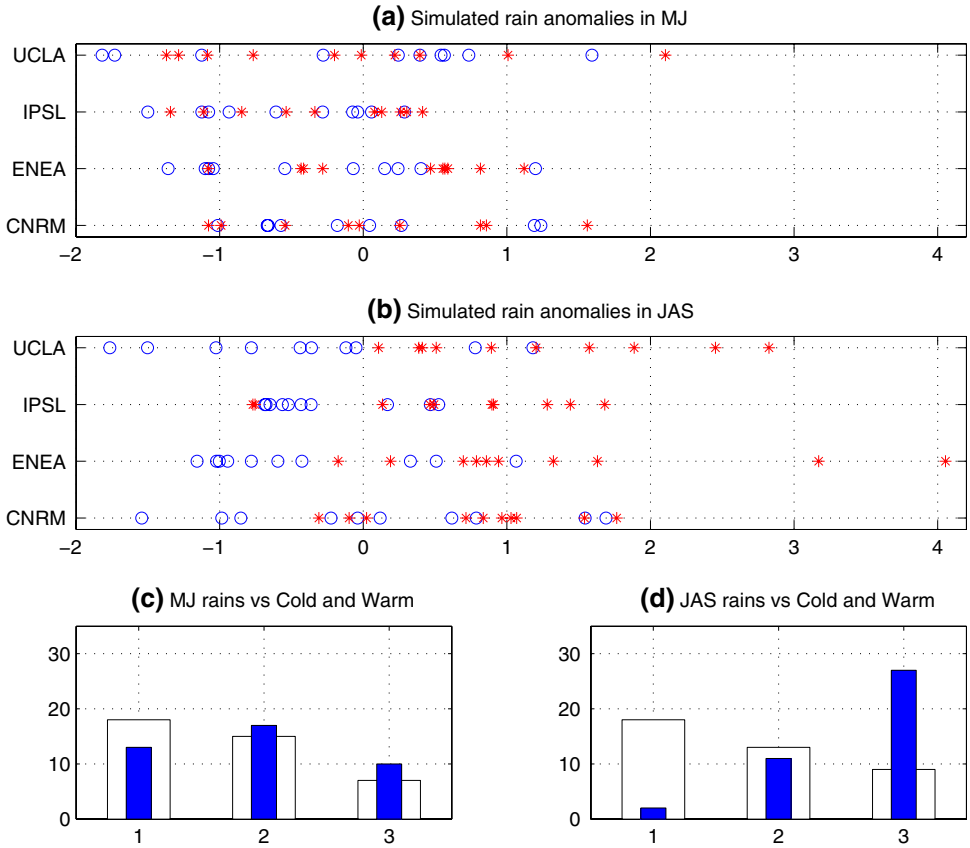

Fig. 8 (*Top*) Simulated rainfall anomalies (vs control) of the West African Index (20°W–30°E; 5–20°N) in standardized values for each GCM: May–June (**a**) and July–September (**b**): circles and asters for cold and warm experiments. (*Bottom*) distributions into 3 classes of the model-ensemble responses relative to the cold and warm (*thin bars*) experiments : *1* = deficits (<−0.5 std), *2* = normal and *3* = excess (>0.5 std)

arrows refer to v and omega and contours to the zonal component: left panels display mean control simulations for each model while diagrams at right refer to the significant warm minus control differences tested with a Student *t* test at $p = 0.05$. Notice first that several basic elements of the mean monsoon circulation are well simulated by the GCMs (Fig. 9a, c, e), i.e., the monsoon cell southward to 20°N fuelled by air ascents over the Sahel domain and SW winds, the northern overturning circulation, the northern subtropical Westerly Jet in high troposphere and also subsidence over the northern subtropics. However there are some discrepancies with the easterly circulation. For example the African Easterly Jet (AEJ) in mid troposphere is strongly underestimated by UCM and CNRM while IPSL underestimates tropical easterly jet (TEJ) maxima in high levels.

Regarding to the W-CTL model responses, the more significant signals are observed in CNRM and UCM simulations (Fig. 9b, d); i.e., note the unclear circulation in IPSL run (Fig. 9f). As shown in observations (Sect. 4.2), it can be seen how CNRM experiment produces a significant reinforcement of both the northern and southern Hadley-cells; while UCM only yields the overturning anomaly of the southern meridional circulation. These features reflect the enhancement of the ITCZ activity, according to one of the Rowell's (2003) feedback mechanism which involves reinforced monsoonal circulation (low-level westerlies and rising motion) responding to the enhanced moisture transport from the Mediterranean. An additional northward displacement of this deeper-ITCZ is also apparent: from 10 to 15°N in CTL to 15–20°N in W-CTL (Fig. 9). In addition to strengthened southwesterly flow associated with increased latent heat (diabatic heating) in the Sahel region, forced by the above anomalous moisture convergence (Rowell 2003); Peyrillé et al. (2007), by using an idealized 2-D model, have suggested that the poleward extent of continental convection is partially explained by the weakening of the climatological northeasterly flow from the Mediterranean (see below, Sect. 5.6). Here, in order to gain insight into the proposed mechanism from 3-D AGCM simulations, Fig. 10 presents jointly the upper (200 hPa, second row) and lower (850 hPa, fourth row) streamfunction anomalies. In 850 hPa response are apparent the alterations in the local-ITCZ (Fig. 10d, h, l): an anomalous cyclone in the WAM domain at CNRM and UCM forcing deep-upward motions; but an anticyclonic anomaly along Central African Republic and Guinean coastline in IPSL.

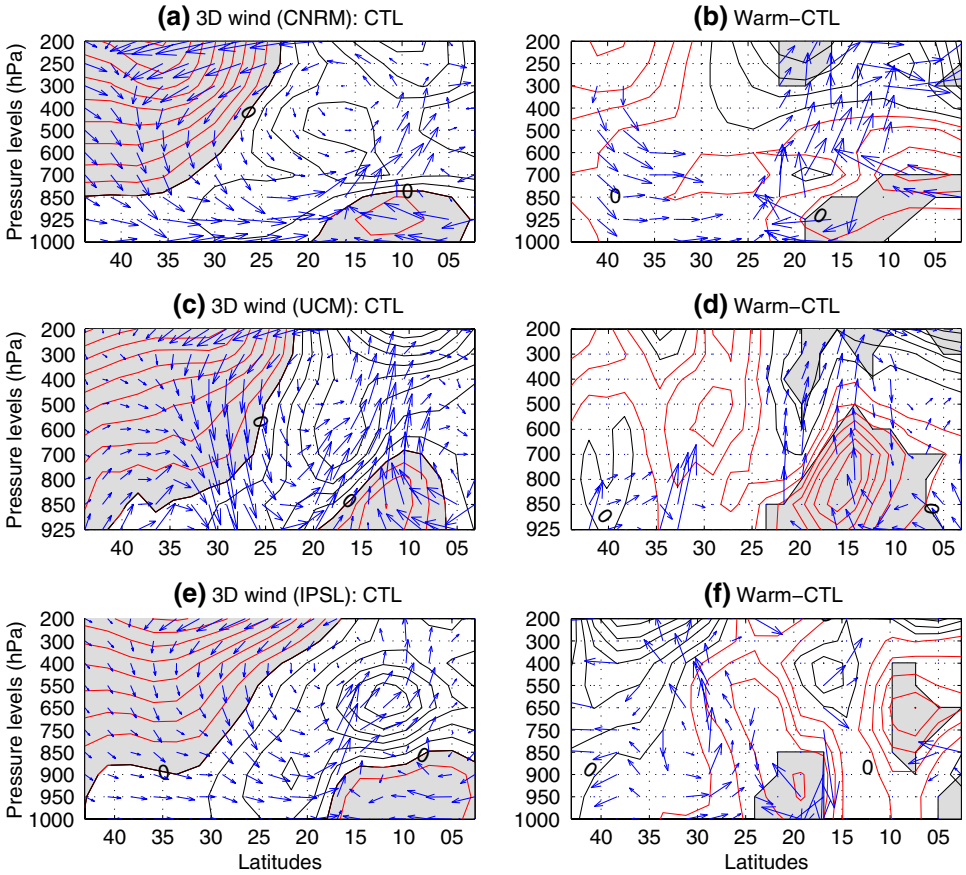

Fig. 9 July–September vertical-meridional cross sections of the 3-D wind field modeled by CNRM (*top*), UCM and IPSL (*bottom*) after averaging the results between 20°W and 30°E. *Arrows* refer to the v and omega components and isolines to the *u* component. Red/black contours each 2 m/s for positive/negative *u* values. *Left* control runs. *Middle* Cold minus control differences with shadings when the zonal wind is positive. *Right* Warm minus control differences. *Arrows* and *shadings* for significant signals from a paired-*t* test at $p = 0.05$

It is also noticeable the low-level negative anomalies surrounding the eastern Mediterranean basin, associated with negative pressure anomalies there and in accordance with the observational work by Raicich et al. (2003). This feature, the low-level convergence anomaly, would go along with Peyrillé et al. (2007) regarding the decrease of NE winds in response to warming of Mediterranean SST (see Sect. 5.6); and partially in contrast to Rowell (2003) and Jung et al. (2006) who found no change in the circulation leading to enhanced monsoon precipitation.

Additionally, this anomalous low-level convergent inflow is associated with positive streamfunction anomalies at upper-levels, revealing a baroclinic structure in the atmosphere (Fig. 10b, f, j): along the whole subtropical belt in CNRM, confined into the eastern Mediterranean in UCM, and isolated over the Arabian Peninsula in IPSL. Similar thermally-driven response to changes in the Mediterranean SST has been reported by Li (2006), who found a circumglobal wintertime-teleconnection initiated in the Mediterranean basin. Experiments analyzed here seem to corroborate this direct global-response to Mediterranean summer forcing (García-Serrano et al. manuscript in preparation); while previous evidences support this finding (Jung et al. 2006).

5.4 Moisture fluxes

Figure 11 a,b focuses better on the zonal and meridional mean moisture fluxes in low and mid troposheric layers using all the CNRM runs, i.e., 20 control and 20 warm simulations. Only the CNRM is chosen for taking advantage of the good vertical resolution of this model (45 vertical levels) particularly in low layers (Salas-Mélia et al. 2005). This approach is not extrapolable to other models but it provides valuable insights.

The moisture transport is mainly organized with a SW maximum at 925 hPa by 10°N (positive values in panels a, b) and an easterly maximum at 700 hPa around 10°N, hence just under and southward to the main AEJ axis, as shown by the negative values in Fig. 11a. Warm-CTL composites in Fig. 11c, d present larger significant signals. In particular the zonal moisture transport by the AEJ is shifted northward (negative/positive dipolar patterns at 700 hPa in Fig. 11c) while in lower levels, negative/positive differences northward/southward to 20°N in Fig. 11c, d reveal a significant increase of northeasterly and southwesterly monsoonal flux. This finding implies an enhanced deep convection in the WAM area. Additional analyzes (not reported here) have shown that the increase

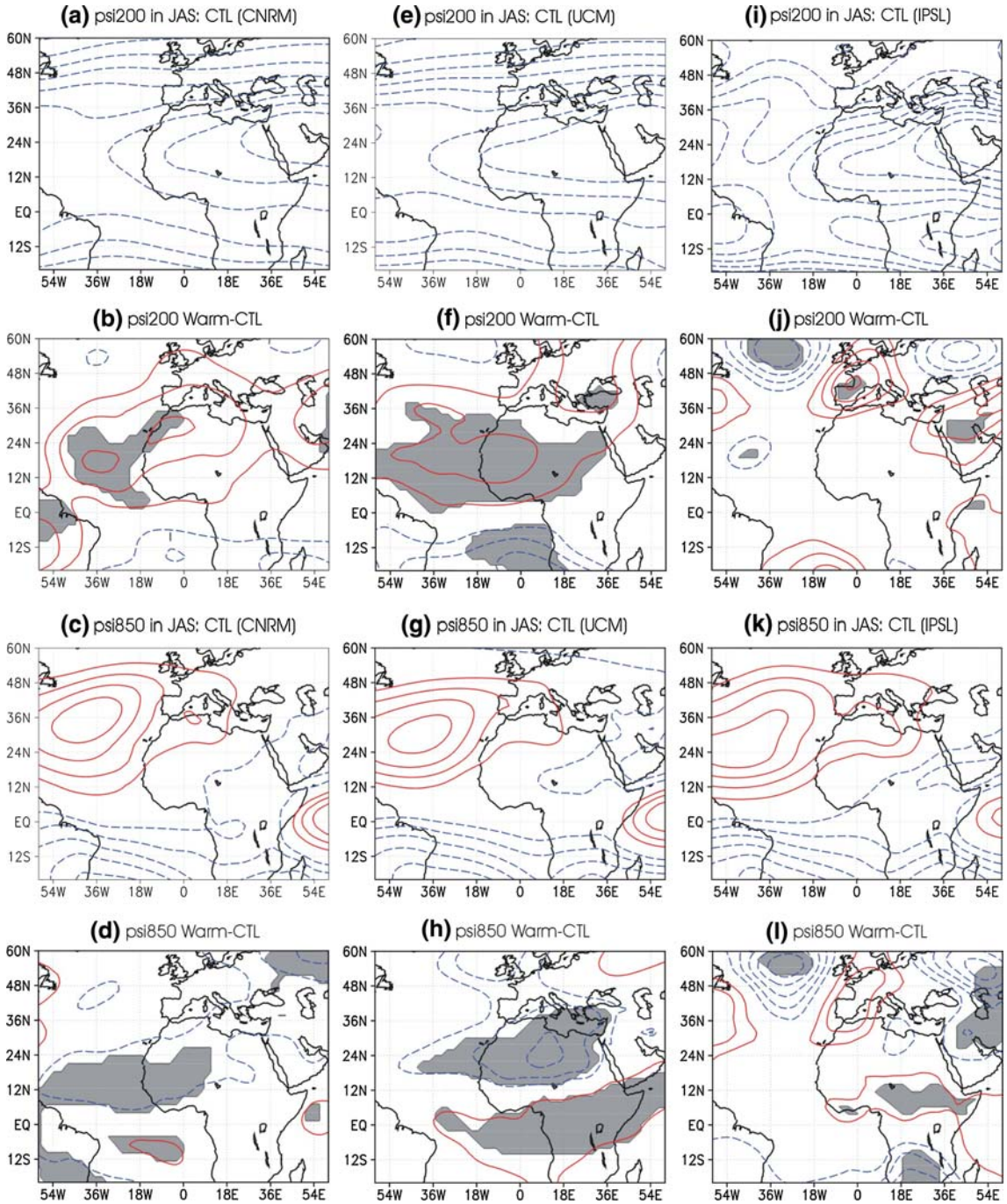

Fig. 10 July–September streamfunction composite at 200 hPa (*first and second rows*) and 850 hPa (*third and fourth rows*) from CNRM (*left*), UCM (*middle*) and IPSL (*right*). *First* (ci = 1.0×10^7 m^2/s) and *Third* (ci = 3.0×10^6 m^2/s) rows: control runs. *Second* (ci = 0.8×10^6 m^2/s) and *Fourth* (ci = 0.3×10^6 m^2/s) rows: warm experiments. Here the *shadings* refer to significant differences regarding a Student t test at $p = 0.05$

in northeasterly moisture flux is mainly due to an augmentation of the specific humidity in low-level over the warmer eastern Mediterranean. This strengthens the flux and together with the reinforcement of the southwest monsoon augments moisture convergence in low levels, according to Rowell (2003). This feedback mechanism would also help to the anomalous northward displacement of the ITCZ, providing above-average precipitation over the Sahel.

5.5 Response in low levels

To assess better the capabilities of the 3 models to reproduce correctly the tropical-subtropical circulation over the

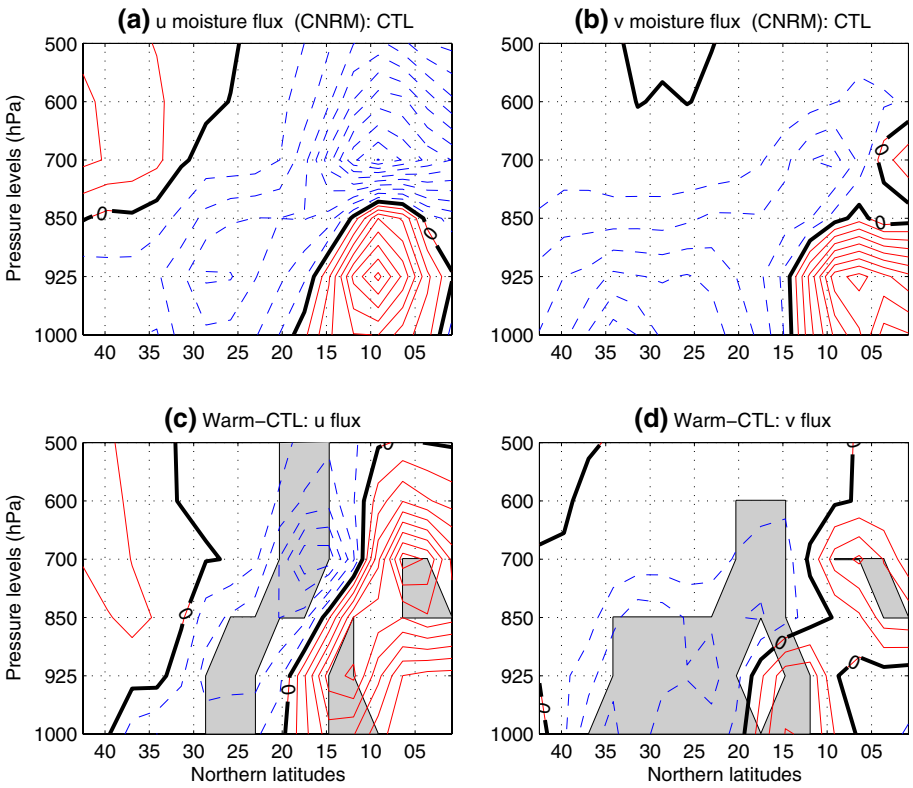

Fig. 11 July–September vertical-meridional cross sections of mean and composite moisture fluxes from CNRM over the longitudinal window 20°W–30°E. (**a**, **b**): u and v mean components from the control runs; (**c**, **d**): composite differences between the warm and control simulations. The *solid (dashed) contours* refer to the positive (negative) differences. In (**c**, **d**), shadings are superimposed when composite differences are significant at $p = 0.10$ regarding a Student t test

Mediterranean-African window, Fig. 12a, c, e displays the mean low level wind fields as produced in the control simulations. The skill of simulations is rather good since several key-elements are reproduced and well located, i.e., Azores and Ste Helena anticyclonic gyres, monsoon and Harmattan systems, ITCZ…

The Warm-CTL significant differences at $p = 0.10$ are presented in Fig. 12b, d, f with shadings when the v component is positive. The 3 models give anomalous surface westerlies over the Sahelian area, although the location of the signals is different from one model to another. Thus, CNRM concentrates the strongest signals over the Atlantic (under 12°N) and the eastern Sahel, UCM over a large part of the West African continent north to the equator and subtropical Atlantic (12–24°N), while IPSL produces significant westerlies in the Sahelian domain but with a similar amplitude south of the equator. Despite these differences, common features emerge from the multi-model approach (Fig. 12g, h). This multi-model ensemble retains large anomalous westerlies coming inland from the Atlantic (Rowell 2003) and reaching the Sahel region, but does not take into account the southerly component from Gulf of Guinea. Additionally, as also shown in each model (Fig. 12b, d, f), the weakening of the climatological northeasterly flow from the eastern Mediterranean is apparent. These anomalous surface winds have a clear southerly component east of 10°E over Egypt. This feature is consistent with the anomalous low-level convergence in the southeastern Mediterranean basin, as discussed above (Fig. 10d, h, l), and is in agreement with Peyrillé et al. (2007) regarding the penetration decrease of the mean circulation depending on the thermal contrast between the African continent and the Mediterranean Sea (or SST-forced in this case).

5.6 Response in mid and high levels

Figures 13 and 14 present the mean and composite wind fields at 600 and 200 hPa, respectively, with shadings where the zonal component is positive (blows eastward). In the top-middle panels are ensemble responses for each model, while in bottom panels are presented the multi-model approach (Figs. 13, 14g, h). At 600–200 hPa the control experiment (Figs. 13, 14a, c, e) reproduces correctly several specific features of the upper and mid level circulation, i.e., the AEJ and TEJ main axes over West Africa, the subtropical westerly jet pattern over the Mediterranean, and at 600 hPa northerlies from the Mediterranean. Warm experiments (Figs. 13, 14b, d, f) cause (1) a significant reduction of subtropical westerlies in high levels south of the equator; (2) a significant increase in TEJ, more clearly seen in each model behaviour than multi-model ensemble, confined to 0 and 15°E; and (3) a relative decrease in AEJ, with clear distinct location in each model which causes a diffuse signal in the multi-model ensemble. All of these features are known to be favourable to the

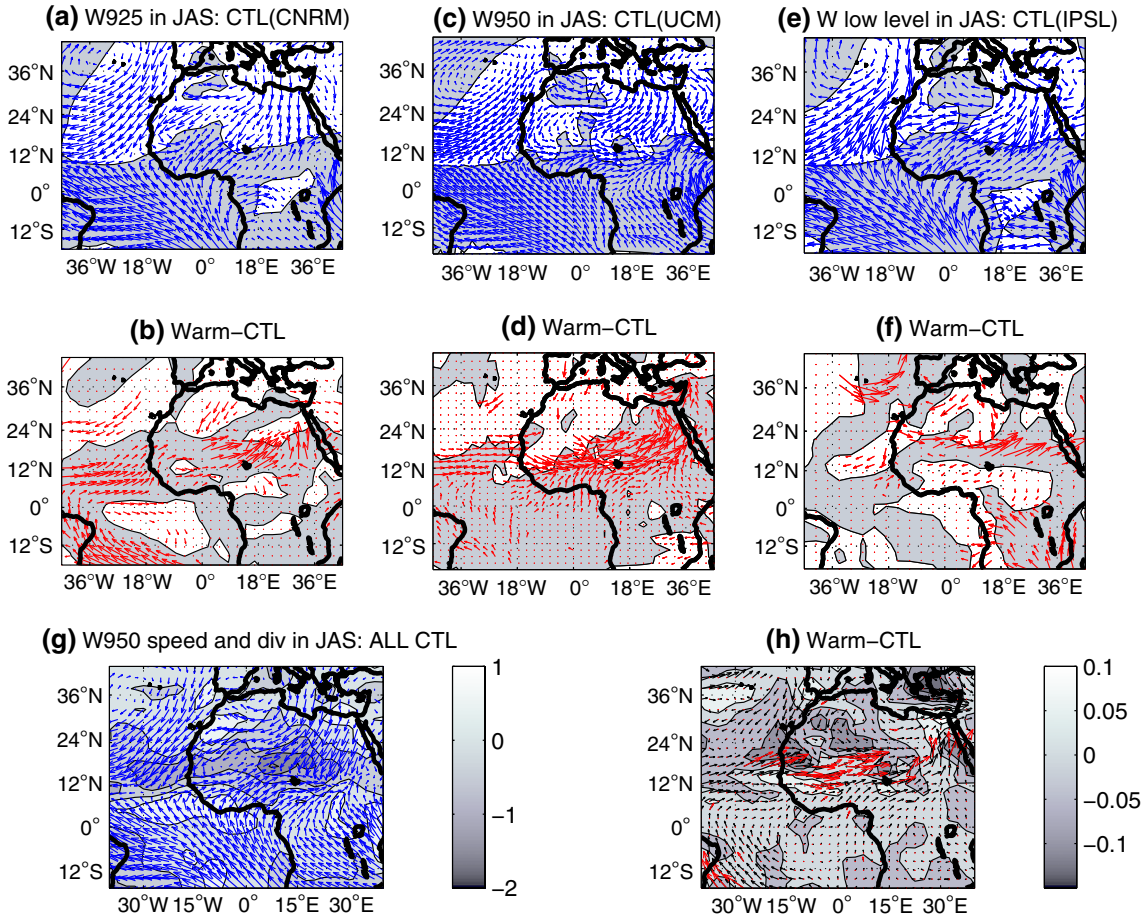

Fig. 12 *Top* July–September mean wind fields in low levels (925 hPa) from CNRM (*left*), UCM (*middle*) and IPSL (*right*) experiments; control runs with positive meridional wind shaded. *Middle*: Warm minus control differences. Here the shadings refer to significant differences regarding a Student t test at $p = 0.10$. *Bottom* Multi-model ensemble of wind (*arrows*) and horizontal divergence (contours) fields at 950 hPa; mean (*left*) and Warm minus Control composite (*right*). Red arrows are superimposed when the differences on (**h**) are significant at $p = 0.10$ regarding a Student t test. Contours refer to the positive (negative) differences in divergence

monsoon circulation (Newell and Kidson 1984; Fontaine et al., 1995).

6 Discussion and conclusion

The purpose of this study was twofold: (1) reexamining the observed relationship between the Mediterranean thermal variability (Western and Eastern basins) and Sudan-Sahel rainfall estimates over the recent period, i.e., not marked by long wet and dry phases (as in the 50–70 s); (2) reporting some rainfall and atmospheric impacts generated by warm JAS anomalies in the Mediterranean Basin using multi-model sensitivity experiments. The results provide from both empirical and numerical ensemble approaches. The analyses use 3 types of datasets: in situ observations (rainfall, sea surface temperature…), satellite estimates (GPCP, CMAP data) and reanalyzed data from the NCEP-DOE AMIP II (winds and specific humidity on isobaric surfaces…).

Considered together the statistical and numerical results let suppose the existence of a thermal forcing of the Mediterranean on the African monsoon. Basically Mediterranean warming, with maximum amplitude in the eastern basin, leads to enhanced moisture convergence and therefore rainfall over Sudan-Sahel latitudes in agreement with Rowell (2003) who reports also a strengthening of moist advection across the Eastern Sahara by the mean flow. Peyrillé et al. (2007) insist more on a reduction of northerlies both in magnitude and extension, compatible with a deeper northward migration of the ITCZ into the continent. In accordance with the latter, Raicich et al. (2003) evidenced that the Sahel monsoonal season is associated with below-normal surface pressure in the eastern Mediterranean. All above has been also verified here, implying that this Mediterranean-WAM connection

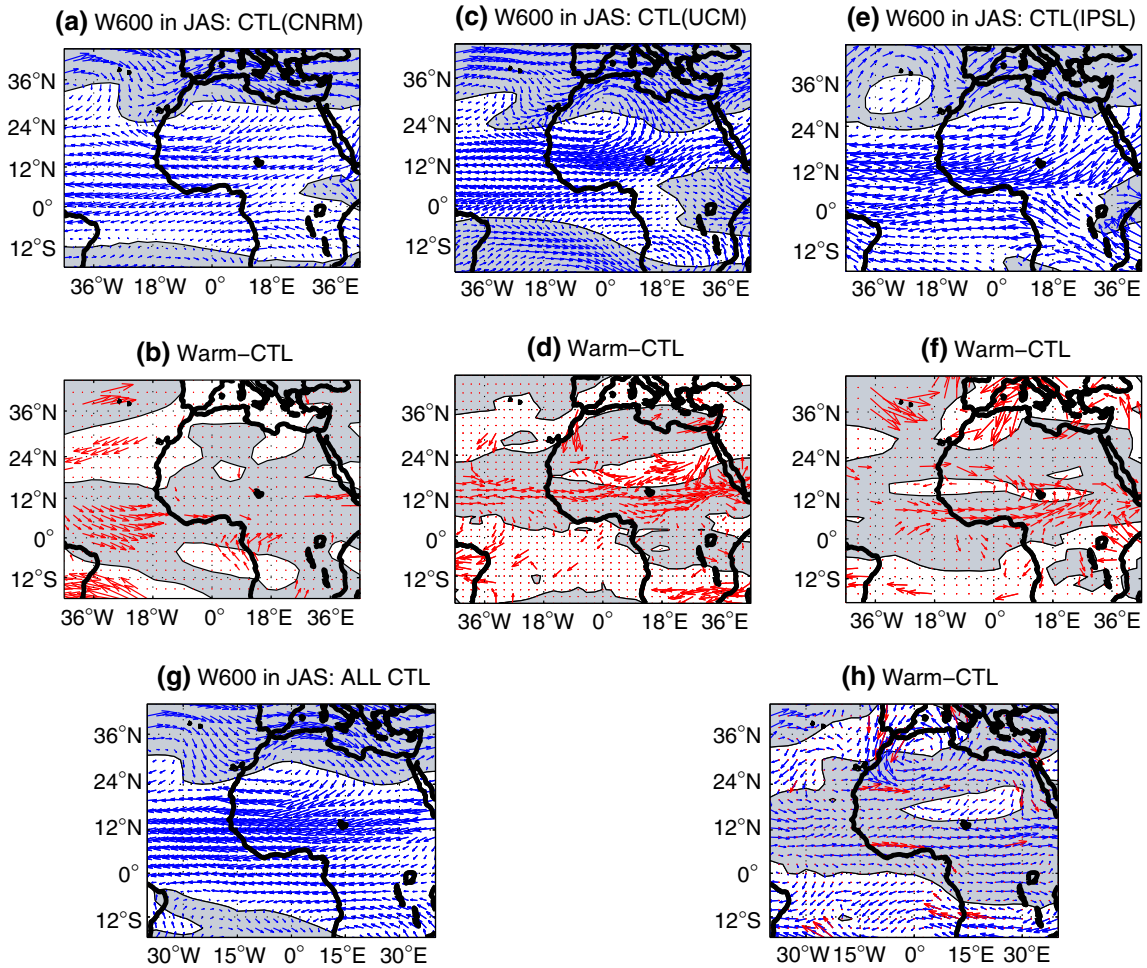

Fig. 13 As Fig. 12 but for horizontal flow at 600 hPa. Shading underline positive values

was robust during recent decades. Thus, when the warming concerns the East basin, a strong link with Sahel precipitation has been found, involving the reinforcement of both the ITCZ-deep motion and westerly transport of humidity thereby, in short, strengthening the main WAM circulation regime. An open question to be addressed concerns the WAM teleconnection with the West basin. Our observational analysis suggests a relationship with deep convection over Gulf of Guinea, possibly related to the Atlantic equatorial SST mode.

The empirical results allowed us to discuss the linearity and significance of the relationship. They can be summarized in 3 points.

(1) The Eastern Mediterranean concentrates the highest SVD temperature variance, while a large continental region, located somewhat northward to the mean ITCZ position, accumulates the strongest loadings in terms of enhanced deep convection and ascendance. This connection has been found in both synchronous and 1 month-lead performances, suggesting an important influence of the East basin on the WAM system.

(2) Additional results have confirmed the existence of a 1 month delay between thermal variability in the Mediterranean and deep convection over Africa. There are also preferred time scales for correlations, i.e., synoptic variability (<10 days) and AEWs (3–5 days). This last connection is mainly observed eastward to the 0° longitude, a region known for a long time as an area of AEW development. These features will be also further analysed in the future through AGCMs and WRF simulations.

(3) When the Eastern basin is abnormally warm the northward migration of the monsoon system and ascendances around the ITCZ reinforce through deeper moist convection south of the Sahara. These air ascents strengthen northerlies at 200 hPa and hence the monsoon cell, air descents above the Southern Tropics and low level moist winds from the South.

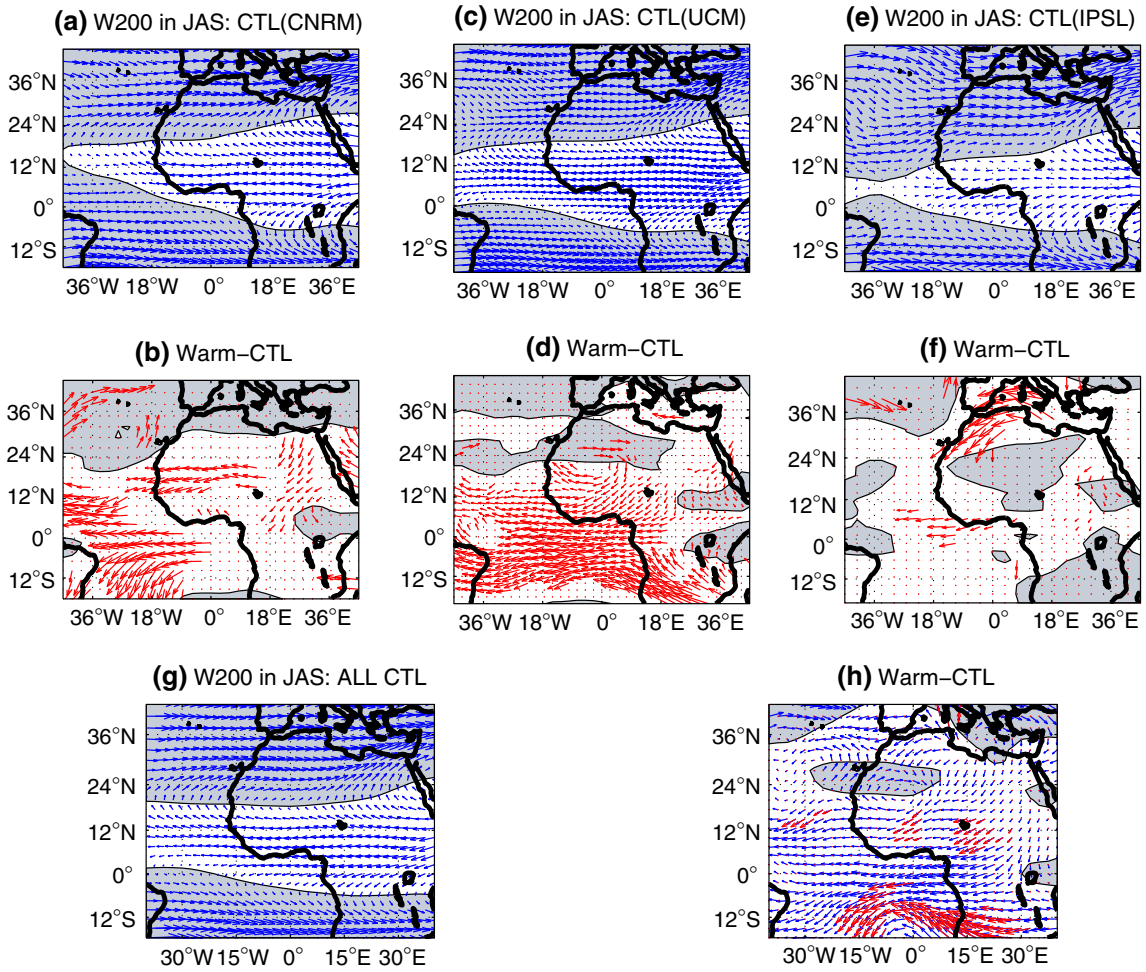

Fig. 14 As Fig. 12 but for horizontal flow at 200 hPa. Shadings underline positive values

This increases moisture transport under 400 hPa over the continent (5–20°N), low level convergence via the SW monsoonal flow in the Sahel zone and hence rainfall surplus just northward to the rain belt in July–September. Additional analyses (not produced here) and Fig. 3 show that the reverse tends to occur in cold situations, in accordance with Rowell (2003).

The *SST sensitivity experiments* linked to normal, warm and cold situations over the Mediterranean and performed on four AGCMs allowed us first to illustrate the relative good accuracy of the models to reproduce the May–September evolution of several key-elements of the monsoon circulation. The more reliable latitudinal-migration of the rainbelt climatology has been found for CNRM and UCM models.

Second, in the models the response between warm and cold situations in the Eastern Mediterranean is not symmetric: the sensitivity experiments showed that warm occurrences impact more on West African precipitation than cold ones. In fact, cold-SST runs have not been conclusive, becoming separated from the linear hypothesis of Rowell (2003). Perhaps, it is because of the AGCM difficulty for well simulating the reduced-latent heat release in cold situations. It is also important to mention that climatological summer SST conditions in the Mediterranean Sea resemble a zonal gradient with maximum located in the eastern basin quite similar to forcing fields prescribed in the simulations (not shown). Hence, the Mediterranean-Sahel connection in cold conditions continues being an issue to be explored. By contrast, the positive empirical relationship between warm SSTs in the Mediterranean and the West African monsoon can be interpreted in terms of thermal Mediterranean forcing.

In this way, warm experiments generate an enhancement of the southern meridional cell in low and high levels, related to reinforced monsoonal southwester lies, a more northward location of its ascending branch (ITCZ) over West Africa in association with more (less) intense monsoon and TEJ (AEJ). It is however important to bear in mind that such changes in the overturning circulation are not necessarily directly forced by Mediterranean SST since the enhanced moisture transport from the Mediterranean

into the Sahel region increases also the latent heat and diabetic heating. This tends to fuel the rising motion in the WAM area and subsequently the downward motion in the overturning circulation.

An integrating picture has been evidenced from AGCM simulations presented here. According to Rowell (2003) and Fontaine et al. (2003), the favoured humidity transport from the Mediterranean Sea into ITCZ is accompanied by both anomalous surface-influx from the tropical Atlantic and reduced export via AEJ at mid-levels (two of the Rowell's feedbacks). The former could help to displace more northward the WAM-deep convection up to the Sahelian region. In addition, another mechanism has been shown contributing to this anomalous poleward ITCZ-extension. Consistent with the lower-tropospheric convergence found in the southeastern Mediterranean basin, which could explain the surface pressure anomalies suggested by Raicich et al. (2003), is the weakening of the climatological northeasterly flow east of 10°E over Egypt. This finding is in agreement with the penetration decrease of the mean circulation depending on the thermal contrast between African continent and the Mediterranean Sea (or SST-forced in the simulations; Peyrillé et al. 2007). This feature reflects a substantial northward migration of the monsonal rainbelt, and hence above-normal precipitation over the Sahel. This result does not contradict the anomalous moisture transport originated in the Mediterranean; since although weakened, the additional evaporation would be advected southward across the eastern Sahara by the flow.

Acknowledgments The authors are very grateful to the anonymous reviewers for their interesting comments, and to the National Center for Atmospheric Research (USA), Climate Prediction Centers and the National Oceanic and Atmospheric Administration for providing the data. J. G.-S. greatfully acknowledge the founds from the ESF-MedCLIVAR Programme of grants (E.G/1694). The study was mainly supported by the Global change and Ecosystems programme (EU Integrated project: African Monsoon Multidisciplinary Analysis (AMMA) and the French component of AMMA. Based on a French initiative, AMMA was built by an international scientific group and is currently funded by a large number of agencies, especially from France, UK, US and Africa. It has been the beneficiary of a major financial contribution from the European Community's Sixth Framework Research Programme. Detailed information on scientific coordination and funding is available on the AMMA International web site http://www.amma-international.org.

References

Adler RF, Huffman GJ, Chang A, Ferraro R, Xie PP, Janowiak J, Rudolf B, Schneider U, Curtis S, Bolvin D, Susskind J, Arkin P, Nelkin E (2003) The version 2 global precipitation climatology project (GPCP) monthly precipitation analysis (1979-present). J Hydrometeorol 4(6):1147–1167. doi:10.1175/1525-7541(2003)004<1147:TVGPCP>2.0.CO;2

Fontaine B, Janicot S, Moron V (1995) Rainfall anomaly patterns and wind field signals over West Africa in August (1958–1989). J Clim 8(6):1503–1510. doi:10.1175/1520-0442(1995)008<1503:RAPAWF>2.0.CO;2

Fontaine B, Roucou P, Trzaska S (2003) Atmospheric water cycle and moisture fluxes in the West African monsoon: mean annual cycles and relationship using NCEP/NCAR reanalyses, Geophys Res Lett, 30, 3, doi: 10.1029-10.1032

Joly M (2008) Rôle des oceans dans la variabilité vclimatique de la mousson ouest africaine, PhD dissertation, 200 pages, CNRM/GAME, Météo-France, Toulouse

Jung T, Ferranti L, Tompkins AM (2003) Response to the Summer of Mediterranean SST Anomalies over Europe and Africa. J Clim 2006(19/20):5439–5454

Kanamitsu M, Ebisuzaki W, Woolen J, Yarg S-K, Hnilo JJ, Fiorino M, Potter GL (2002) NCEP-DOE AMIP-II reanalysis (R-2). Bull Am Meteorol Soc 83:1631–1643. doi:10.1175/BAMS-83-11-1631(2002)083<1631:NAR>2.3.CO;2

Li LZX (2006) Atmospheric GCM response to an idealized anomaly of the Mediterranean Sea surface temperature. Clim Dyn 27:543–552. doi:10.1007/s00382-006-0152-6

Louvet S, Fontaine B, Roucou P (2007) Which rainfall dataset can be used to study African monsoon at intra-seasonal timescale? Technical Note, 3 tables, 10 figures, 27 pages. CRC, Dijon. http://www.ubourgogne.fr/climatologie/AMMA_D1.1.3/other_rainfall_product.htm

Mitchell TD, Carter TR, Jones PD, Hulme M, New M (2004) A comprehensive set of high-resolution grids of monthly climate for Europe and the globe: the observed record (1901–2000) and 16 scenarios (2001–2100). Tyndall working paper 55, Tyndall Centre, UEA, Norwich, UK. http://www.tyndall.ac.uk/

New M, Lister D, Hulme M, Makin I (2002) A high-resolution data set of surface climate over global land areas. Clim Res 21:1–25. doi:10.3354/cr021001

Newell RE, Kidson JE (1984) African mean wind changes between Sahelian wet and dry periods. J Climatol 5:27–33

Peyrillé P, Lafore JP (2007) An idealized two-dimensional framework to study the West African monsoon. Part II: large-scale advection and the diurnal cycle. J Atmos Sci 64:2783–2803. doi:10.1175/JAS4052.1

Peyrillé P, Lafore JP, Redelsperger JL (2007) An idealized two-dimensional framework to study the West African monsoon. Part I: validation and key controlling factors. J Atmos Sci 64:2765–2782. doi:10.1175/JAS3919.1

Polo I, Rodríguez-Fonseca B, Losada T, García-Serrano J (2008) Tropical Atlantic Variability modes (1979–2002). Part I: time-evolving SST modes related to West African rainfall. J Clim (in press). doi:10.1175/2008JCLI2607.1

Raicich F, Pinardi N, Navarra A (2003) Teleconnections between Indian monsoon and Sahel rainfall and the Mediterranean. Int J Climatol 23:173–186. doi:10.1002/joc.862

Rodwell MJ, Hoskins B (1996) Monsoons and the dynamics of deserts. QJR Meteorol Soc 122:1385–1404. doi:10.1002/qj.49712253408

Rowell DP (2003) The Impact of Mediterranean SSTs on the Sahelian Rainfall Season. J Clim 16:849–862. doi:10.1175/1520-0442(2003)016<0849:TIOMSO>2.0.CO;2

Salas-Mélia D, Chauvin F, Déqué M, Douville H, Gueremy JF, Marquet P, Planton S, Royer JF, Tyteca S (2005) Description and validation of the CNRM-CM3 global coupled model, CNRM working note 103., available at http://www.cnrm.meteo.fr/scenario2004/references_eng.html

Xie P, Arkin PA (1997) Global precipitation: a 17-year monthly analysis based on gauge observations, satellite estimates, and numerical model outputs. Bull Am Meteorol Soc 78:2539–2558. doi:10.1175/1520-0477(1997)078<2539:GPAYMA>2.0.CO;2

Xie P, Janowiak JE, Arkin PA, Adler RF, Gruber A, Ferraro R, Huffman GJ, Curtis S (2003) GPCP pentad precipitation analyses: an experimental dataset based on gauge observations and satellite estimates. J Clim 16:2197–2214. doi:10.1175/2769.1

Yin X, Gruber A, Arkin PA (2004) Comparison of the GPCP and CMAP merged gauge satellite monthly precipitation products for the period 1979–2001. J Hydrometeorol 5:1207–1222. doi:10.1175/JHM-392.1

APÉNDICE C

Memoria de Estancia en MetOffice 2008

EG/1694
Con la ayuda de la European Science Fundation- MedCLIVAR

Large-scale atmospheric response to Mediterranean SST anomalies: impacts on the Atlantic climate variability and applications for seasonal forecasting

This project was proposed for the ESF-MedCLIVAR grants to support the scientific visit of Mr. Javier García Serrano, PhD student in the Climate Variability Group at the Universidad Complutense de Madrid (Spain), for spenting 17 weeks at the Met Office-Hadley Centre (United Kingdom). The exchange-visit was joined in the Seasonal Forecasting Group (led by Dr. Alberto Arribas) which is part of the Modelling Climate Variability research area (led by Dr. Adam Scaife).

The visit was framed in one of the five main themes of the ESF-MedCLIVAR Programme: 'Connections between Mediterranean and global climate variability'. The proposed study was also following some of the key CLIVAR research areas, concretely: 'Interannual variability of the African climate system', 'Tropical Atlantic Variability' and 'Regional effects of Climate Change'.

Purpose of the visit

The aim of this exchange grant is to analyse and give evidences of a large-scale atmospheric response to summer Mediterranean sea surface temperature (SST) anomalies with the advice of Adam Scaife's group (Modelling Climate Variability), Richard Graham's group (Climate Applications Development) and Chris Folland's group (Climate Research), who are wellknown by their regional and global teleconnections studies. On the other hand, the Met Office-Hadley Centre is one of the most prestigious meteorological services in seasonal forecast, thereby the results derived from this project could contribute substantially to the improvement of the seasonal prediction system.

The work is based on a preliminary study presented at 2nd ESF-MedCLIVAR Workshop (García-Serrano et al. 2007; enclosed in the Appendix) and constitutes the next step in a new research line of our group (Polo et al. 2008). On the one hand, and regarding the latter paper, Polo et al. shows how the Mediterranean Sea appears to have an isolated active role in the West African Monsoon (WAM) rainfall variability and, concretely, in the Sahelian precipitation anomalies. The results are found for the recent decades, after the so-called *Climate Shift* (e.g. Cane et al. 1997, Seidel et al. 2008), a period for which the Sahelian seasonal rainfall has experimented a longer drought, one of the strongest interdecadal signal on the climate in the 20th century (e.g. Giannini et al. 2003). On the other hand, and besides the impact of the Mediterranean SST on the WAM variability during recent decades (Polo et al. 2008), García-Serrano et al. (2007) points to a possible large-scale atmospheric response to summer Mediterranean SSTs. Such a relevant feature was formulated on the basis of a recent encouraging work by Li (2006), in which the author hypothesizes and demonstrates, for the first time, that winter Mediterranean SST anomalies could force a global atmospheric pattern.

The aim of this exchange grant is to analyse and give evidences of a large-scale atmospheric response to summer Mediterranean sea surface temperature (SST) anomalies with the advice of Adam Scaife's group (Modelling Climate Variability), Richard Graham's group (Climate Applications Development) and Chris Folland's group (Climate Research), who are wellknown by their regional and global teleconnections studies. On the other hand, the Met Office-Hadley Centre is one of the most prestigious meteorological services in seasonal forecast, thereby the results derived from this project could contribute substantially to

the improvement of the seasonal prediction system.

The work is based on a preliminary study presented at 2nd ESF-MedCLIVAR Workshop (García-Serrano et al. 2007; enclosed in the Appendix) and constitutes the next step in a new research line of our group (Polo et al. 2008). On the one hand, and regarding the latter paper, Polo et al. shows how the Mediterranean Sea appears to have an isolated active role in the West African Monsoon (WAM) rainfall variability and, concretely, in the Sahelian precipitation anomalies. The results are found for the recent decades, after the so-called *Climate Shift* (e.g. Cane et al. 1997, Seidel et al. 2008), a period for which the Sahelian seasonal rainfall has experimented a longer drought, one of the strongest interdecadal signal on the climate in the 20th century (e.g. Giannini et al. 2003). On the other hand, and besides the impact of the Mediterranean SST on the WAM variability during recent decades (Polo et al. 2008), García-Serrano et al. (2007) points to a possible large-scale atmospheric response to summer Mediterranean SSTs. Such a relevant feature was formulated on the basis of a recent encouraging work by Li (2006), in which the author hypothesizes and demonstrates, for the first time, that winter Mediterranean SST anomalies could force a global atmospheric pattern.

It is worthy to study the impact on the WAM-Sahel rainfall of this large-scale atmospheric response to Mediterranean SST anomalies because recent studies have shown controversial results when analysing the key role in the long-term drying suffered in the region. The debate is mainly whether the WAM system responds to a thermal forcing (e.g. Giannini et al. 2003) or anthropogenic land-surface modifications (e.g. Held et al. 2005). On the subject, Hoerling et al. (2006) report that a multi-model ensemble forced with 20th century anthropogenic emissions reproduces the long-term variations of Indian Ocean and (less accurately) Atlantic Ocean SST, but fails to reproduce the magnitude of the observed 1950-1980 Sahel drying. It is also important to notice that usually many aspects of Sahel rainfall variability have been linked to SSTs solely over the Indo-Pacific and Atlantic basins (e.g. Held et al. 2005, Biasutti and Giannini 2006), overlooking the potential role of the Mediterranean Sea. Conversely, a number of works have found significant relationships with Mediterranean anomalies (e.g. Raicich et al. 2003, Rowell 2003, Fontaine et al. 2003, Jung et al. 2006, Fontaine et al. 2008). However, these studies have had a marked regional point of view in the connection. On the contrary, this work explores the Mediterranean SST-Sahel rainfall relation with the aim to characterize the large-scale features in the covariability.

Li (2006) made an idealized cooling-experiment of 2K for the Mediterranean to find the above-mention results. In the present work, observations (ERA40), experiments with an AGCM (UCLA model) and two coupled OAGCM (HadGEM-family models) are investigated to test whether the mechanism found in the model study of Li (2006) can be identified also in the real world. In particular, and following the relevant outcomes by Branstator (2002) concerning the circumglobal teleconnections, Li (2006) hypothetised and demonstrated the ability of the Mediterranean SST anomalies in forcing a global-waveguided atmospheric response. Two remarkable remote features were shown: the deepening of the Aleutian Low in the North Pacific and the weakening of the Icelandic Low in the North Atlantic. Also, another two recent works support the importance of the Mediterranean basin, particularly the convergence over the Sea, in favouring the establishment of a hemispheric pattern which resembles the Artic Oscillation (AO) rather than the North Atlantic Oscillation (NAO) (Kodera and Kuroda 2003, Watanabe 2004). Diagnoses using a linear barotropic model, shown by Watanabe (2004), indicate the downstream propagation of Rossby waves trapped on the North African-Asian jet waveguide (hereafter, NAA jet; Hoskins and Ambrizzi 1993) effectively excited by the anomalous upper-level convergence over the Mediterranean.

Very relevant results have been found following the above hypotheses. The consequences derived of the main objective concerns **global teleconnections** and related climate impacts. In this way, the project highlights the **pivotal role of the Mediterranean Sea** not only as local forcing but also **as a large-scale predictor.** The associated phenomena include the influence on the midlatitudes-subtropical basic state (North African-Asian jet), the WAM monsoonal rainfall (Sudan-Sahel region) and the climate variability in the western North Pacific basin (Pacific Decadal Oscillation). All above studies focused the analysis on

boreal wintertime; therefore, this project, regarding the impacts in **summertime**, presents a work that has not been documented yet. In addition, as shown by Xoplaki et al. (2003a-b), a great amount of interannual air temperature variance is associated with the same Mediterranean warming (eastern basin) analyzed in the project: first local EOF-CCA mode (2003a's paper) and second basin-wide EOF-CCA mode (2003b's paper). Hence, the results presented here are also of great interest for the **Mediterranean climate variability itself**.

Description of the work carried out during the visit

During the 17 weeks of the visit, I focused my work on performing numerical experiments and analysing observations and simulations with the aim of supporting the initial hypotheses.

Nevertheless, during the first weeks I tried to learn the basic commands to manage, as well as I could, in the new operative system, the Met Office's system: RedHat distribution of Linux (I used to work in Windows at UCM). In the same way, I also learnt the basic commands for the 'command window' of the Met Office's software for computation (PV-Wave; I used to work with GrADS and Matlab) as well as the digital language of its scripts (.pro, of processor) for manipulating the particular Met Office's data (pp-fields). In addition, I had to learn some UKMO libraries (for PV-Wave) to move our binary and netcdf datasets on pp-field format. In particular, the pp-fields have similar characteristics that netcdf format but with a particular digital weight and much more information in the header. The pp-fields as outputs of the coupled Ocean-Atmosphere GCM (OAGCM) models from HadGEMs family have a very high spatial resolution. Concretely, datasets I have used present 1.875-lon by 1.25-lat (192x144) grid points for atmospheric variables, and higher resolution for oceanic data (360x216): regular-1degree by longitude and roughly irregular-1degree by latitude with 14 levels in depth. During my visit I have worked with two old-versions (currently, it is developing the third version) of the HadGEM-family, particularly with HadGEM-1 (hereafter, HadGEM1) and the simplified Ocean-Atmosphere HadGEM-2, the OA-HadGEM-2 (hereafter, HadGEM2).

At the same time, I completed the bibliography related to this project, as read them. Because the secondary objectives were changing in the course of time, once the hypothesis of global response to Mediterranean SST was established, the bibliography for each issue would request a continue actualization. In general, throughout the exchange-visit, I have compiled a very interesting list of articles not only concerning the Mediterranean climate variability but also regarding dynamics of the teleconnections found, mechanisms involved, climate impacts and potentially-influenced variability modes. Framing on each subject (see References for complete citations):

- Atmospheric circulation associated with the Mediterranean
  Fontaine et al. (2008); Haarsma et al. (2008); Jung et al. (2006); Michaelides (1983); Raicich et al.(2003); Rowell (2003); Xoplaki et al. (2003a); Xoplaki et al. (2003b)

- Wave-mean flow interaction and teleconnection dynamics
  Branstator (2002); Chang et al. (2002); Ding and Wang (2005); Hoskins et al. (1983); Kodera and Kuroda (2003); Rodwell and Hoskins (1996); Trenberth (1986); Watanabe (2004)

- West African Monsoon system
  Biasutti and Giannini (2006); Cook (1999); Fontaine et al. (2003); Giannini et al. (2003); Grist et al. (2002); Held et al. (2005); Hoerling et al. (2006); Hsieh and Cook (2005); Joly et al (2007); Mekonnen et al. (2006); Moron et al. (2004); Nicholson (2008); Nicholson and Grist (2001); Nicholson et al. (2007); Nicholson et al. (2008)

- Pacific Decadal Oscillation
  Barnett et al. (1999); Bond and Harrison (2000); Gershunov and Barnett (1998); Trenberth and Hurrell (1994); Zhang et al. (1997)

Besides the above mentioned co-lateral tasks, the main blocks of work of my visit are :

1. Development of a software to calculate the Rossby wave sources

This work was done during the first 10 weeks of the visit, parallel to the block 3 as a part of the analysis. The script that I developed makes up a current diagnostic in the post-processing of the HadGEMs-outputs as consequence of my exchange-visit.

In this way, the necessary software to calculate two basic 2D-potentials of the flow was performed: the streamfunction (rotational part of the flow) and velocity potential (divergent part of the flow), from the horizontal wind (u,v). This problem has been widely described in the concerning literature (Sardeshmukh and Hoskins 1987, Kundu 1990), and it is commonly named PSI-problem and CHI-problem (both, Poisson equations), respectively:

PSI-problem: $vort = \nabla^2\psi$ CHI-problem: $div = \nabla^2\chi$

where *vort* and *div* represent the third component of the vorticity (the relative vorticity) and the horizontal divergence of the flow; and ψ and χ are indicating the streamfunction and the velocity potential; while ∇^2 identifies the Laplacian operator.

Subsequently, once the 2D-potentials are calculated we are in the position to obtain the derived-components of the flow (the rotational and divergent winds) as well as the Rossby wave sources (RWS), an important diagnostic for analysing both tropical and extratropical teleconnections (Sardeshmukh and Hoskins 1988, Qin and Robinson 1993, Watanabe 2004). For these purposes I also implemented a "finite-differences schema" for regular and horizontal grids (ERA40 and HadGEMs): checking those results provided by UKMO-PV Wave routines (pp_grad), and in order to move the developed scripts on Matlab code (afterwards at UCM).

The first approach to resolve the inversion of the Poisson equations, detailed above, was using the classical recurrence equation called "the four-neighbors schema" applied on the horizontal plane with Drichlet conditions (Fig. 1).

$$\zeta_{i,j} = \left(\psi_{i+1,j} + \psi_{i-1,j} - 2\psi_{i,j}\right)/(\Delta y)^2 \quad + \quad \left(\psi_{i,j+1} + \psi_{i,j-1} - 2\psi_{i,j}\right)/\left(R\cos\varphi_{i,j}\cdot\Delta\lambda\right)^2$$

A great number of white-pages were used to obtain the correct matrix for the Poisson's inversion (with the correct order of the elements for the latitude-longitude order of the data). As it is easily observable in Fig. 1, the results propagate the edge-effects so far from the domain limits so this technique claimed to be improved. For this reason, in a second approach the previous inversion matrix was moved with periodic conditions in longitude, but the resulting 2D flow-potentials remained showing some problems with conditions in the polar caps (not shown). A final approach was to translate the original problem into the time-frequency domain for resolving the problem via spherical harmonics (Fig. 2; Sardeshmukh and Hoskins 1987).

An example of the PV-Wave scripts generated is attached in the Appendix. That script, named 'RWS_ diagnostic.pro', resolve the PSI and CHI problems calling, respectively, the external 'pp_strmfn' and 'pp_velpot' scripts; and calculate both the rotational-divergent components of the wind and the different RWS terms calling the subroutine 'calc_dyn_fields'. Below are shown the streamfunction, rotational wind and tropical-RWS (Fig. 3-top); and the velocity potential, divergent wind and extratropical-RWS (Fig. 3-bottom) for the ERA40 winter climatology at 200hPa. The dominant anomalous RWS terms are the

anomalous tropical-RWS (TRWS), associated with the advection of the climatological vorticity, and the anomalous extratropical-RWS (ERWS), associated with regions of divergence/convergence anomaly (Qin and Robinson 1993):

$$TRWS = -v'_{\chi} \cdot \nabla\left(\bar{\zeta} + f\right) \qquad ERWS = -\left(\bar{\zeta} + f\right)\nabla \cdot v'_{\chi}$$

where v'_{χ} is the anomalous divergent wind, $\bar{\zeta}$ is the climatological relative vorticity and f the planetary vorticity (Coriolis parameter).

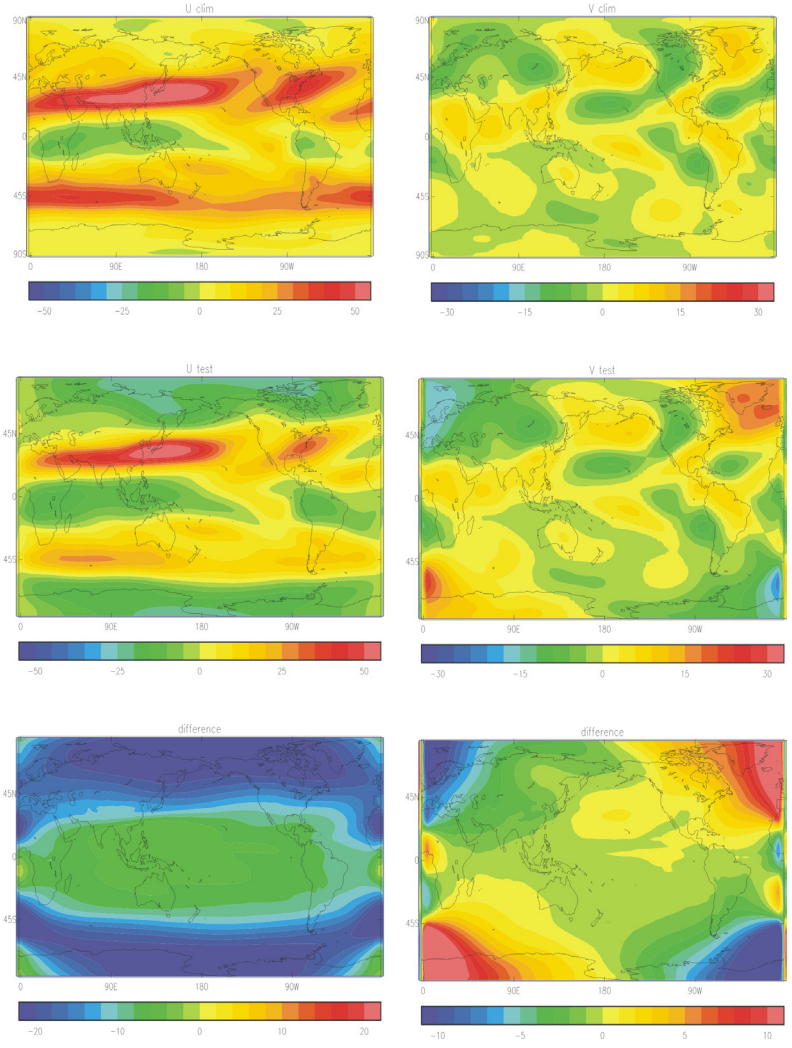

Figure 1. Outcomes after resolving both PSI and CHI problems using Dirichlet boundary conditions. [top] DJF climatological average for zonal (left) and meridional (right) wind at 200hPa from HadGEM2. [middle] Estimation for horizontal 200hPa-wind climatology by adding rotational and divergent parts for each component of the flow; test for zonal (left) and meridional (right) components. [bottom] Difference between original (input, top) and estimated (output, middle) components of the wind climatology at 200hPa.

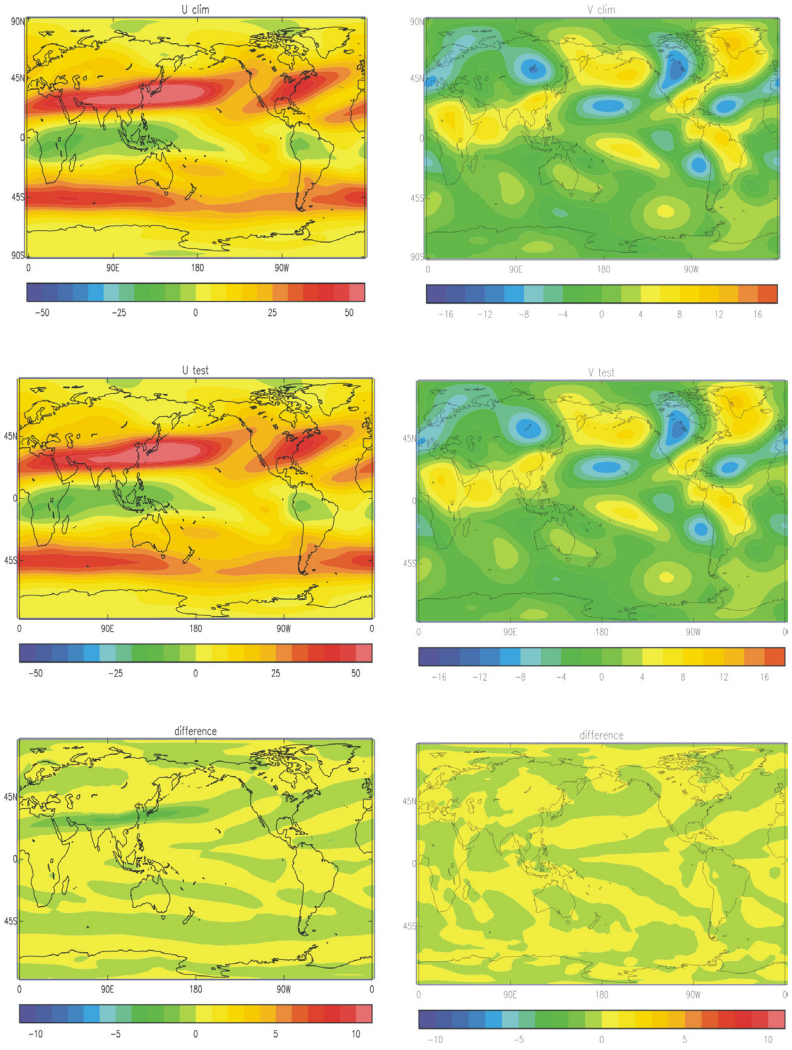

Figure 2. As Figure 1, but after resolving both PSI and CHI problems using spherical harmonics in the time-frequency domain.

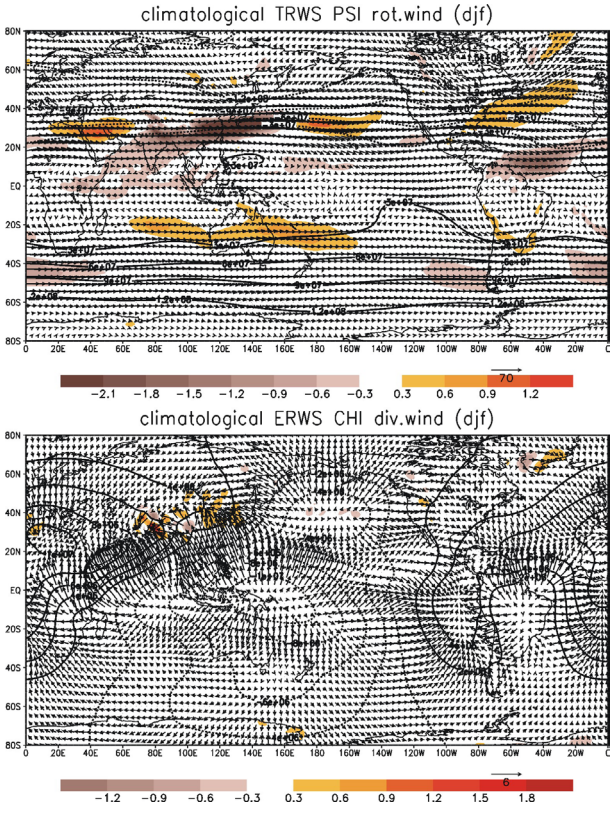

Figure 3. [top] Streamfunction (contours, ci=3 107 m2/s), rotational wind (arrows) and TRWS (shaded, ci=1 10-10 s-2); and [bottom] velocity potential (contours, ci=2 106 m2/s), divergent wind (arrows) and ERWS (shaded, ci=1 10-9 s-2) for the ERA40 DJF climatology at 200hPa.

2. Performance of sensitivity experiments with the UCLA-AGCM

During the first two months of visit I performed a sensitivity experiment for the Mediterranean SST-pattern.

The methodology, which is going to be described below, was discussed and analysed with the Met Office advisors who agreed in the novelty of the simulations that were remotely run, from UK, on the UCM computers. This sensitivity experiment was performed using the UCLA-AGCM model (Mechoso et al. 2000); and it was based on the observational Mediterranean-WAM EMCA mode described in Polo et al. (2008).

This EMCA covariability mode has been found in a recent paper by our group (Polo et al. 2008). The boundary condition used in this sensitivity experiment is based on the expansion coefficient (time series) of the first time-evolving mode between Mediterranean SST (from FMAM to SOND) and JJAS-summer WAM rainfall (also in García-Serrano et al. 2007). This methodology is an extension of the classical Maximum Covariance Analysis (MCA or SVD; Bretherton et al. 1992) by introducing more than one time-lag in one of the field-arrays; with the aim of isolating in the same mode the whole sequence of significant covariant SST patterns in relation to the JJAS anomalous WAM precipitation. In this way, a whole picture

of the evolution of the Mediterranean SST from early-spring (FMAM) to late-autumn (SOND) is obtained.

We have used this kind of statistical methodology with the aim of taking into account the intrannual evolution of the interannual variability SST-mode. Thus, EMCA method highlights the seasonal dependence of the internannual modes obtained. In contrast, previous works lack in taking into account the month-to-month evolution of these modes, maximizing covariability independently of the other adjacent seasons and presuming the persistence of the anomalies as function of time (e.g. Czaja and Frankignoul 2002, Frankignoul and Kestenare 2005, Ding and Wang 2005).

Although the Mediterranean sensitivity experiment has been completed, the corresponding outputs have not been analyzed yet.

3. Study of atmospheric circulation related to the Mediterranean-WAM link

Most of the work done during my visit, coinciding with the main purpose, was focused on investigating the physical mechanisms involved in the summer teleconnections related to the leading ECMA Mediterranean mode. This large-scale response to Mediterranean SST anomalies was analyzed using observations, two OAGCM models (HadGEMs) and one AGCM model (UCLA). The main results related to this third block are described next.

RESULTS

Observations

Description of the Mediterranean mode

As commented above, Polo et al. (2008) have recently found, by applying EMCA, a statistical relation implying an active role of the summer Mediterranean SST onto the WAM variability. In that paper, the EMCA methodology was developed and implemented. The authors use EMCA in order to show the whole picture of the Mediterranean SST pattern evolution in relation to the summer (JJAS) WAM-rainfall with a realistic persistence feature from boreal early spring (FMAM) to late autumn (SOND). Complementary to this, EMCA gives the opportunity of increasing the number of time series in the analysis, having as many time series per point as time lags used, and assessing, in this way, the statistically significance of the results.

Fig. 4 represents the leading EMCA mode, which is the starting point for this study, in order to investigate the underlying dynamics and get new insights in the relationship between Mediterranean SST anomalies and the global climate variability.

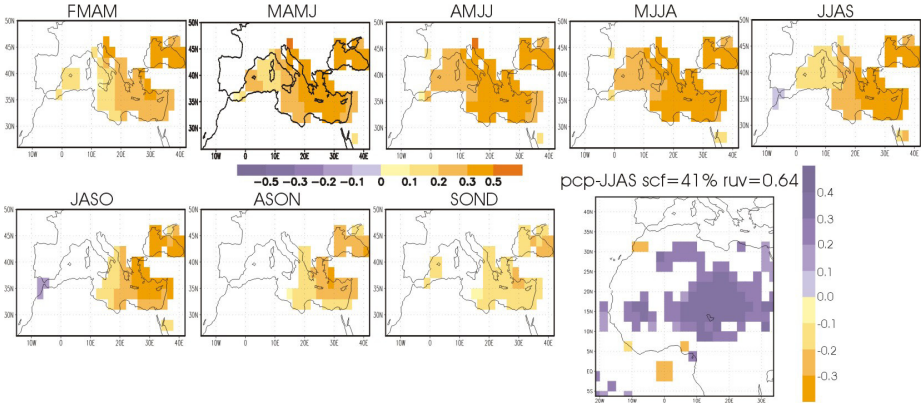

Figure 4. Homogeneous SST (ºC) regression maps for the sequence from early-spring (FMAM) to late-autumn (SOND) obtained from the EMCA analysis. Heterogeneous regression map of the WAM rainfall (JJAS; std anomalies) onto the leading EMCA-SST expansion coefficient. Only 98% statistically significant areas (evaluated with a t-test) are plotted. [as Polo et al. 2008]

This mode is related to persistent positive SST anomalies that peak in MJJA. Concretely, EMCA result shows positive Med SST anomalies confined over the eastern part of the basin, associated with higher than normal WAM rainfall over the Sahel, in particular over the region 15N-25N/5E-30E. This EMCA mode explains more than 40% of the square covariance fraction (scf) and it is a very robust mode, as can be seen after applying 100 Monte Carlo analyses (Fig. 5-bottom).

Also, the correlation of the precipitation expansion coefficient (Fig. 5-top, solid) is statistically significant with the global EMCA SST expansion coefficient (ruv; Fig. 5-top, bars) and the first WAM rainfall EOF (Sahelian mode; Polo et al. 2008): 0.64 and 0.96 respectively. These correlations indicate that the leading EMCA-based WAM pattern, related to the Mediterranean SST, is also the leading WA monsoon-precipitation mode.

Fig. 5 represents the expansion coefficient derived from EMCA for the summer time-varying predictor (Med-SST; bars) and predictand (Sahel-WAM rainfall; solid line). It is apparent the strong decadal signal in the Med-SST time series, according to Xoplaki et al. (2003a-b) in relation to the higher values in the eastern Mediterranean basin. It is also important to notice the covariability between both expansion coefficients, pointing to a stronger relation between the Sahelian rainfall variability and the Mediterranean SST variability for the period 1979-2001 (time-period used here). Even so, the regression of the EMCA-SST expansion coefficient onto the global SST anomalies (see below) reveals that the EMCA-Med mode is associated with central equatorial Pacific SST, rather than central-eastern equatorial Pacific. In fact, the correlation with Niño3.4 is roughly 0.2/0.3 in all time-lags, suggesting that Pacific SST anomalies are not related to a canonical ENSO event. In addition, significant correlations are found between Pacific Decadal Oscillation (PDO) index and the EMCA-Mediterranean mode (discussed below).

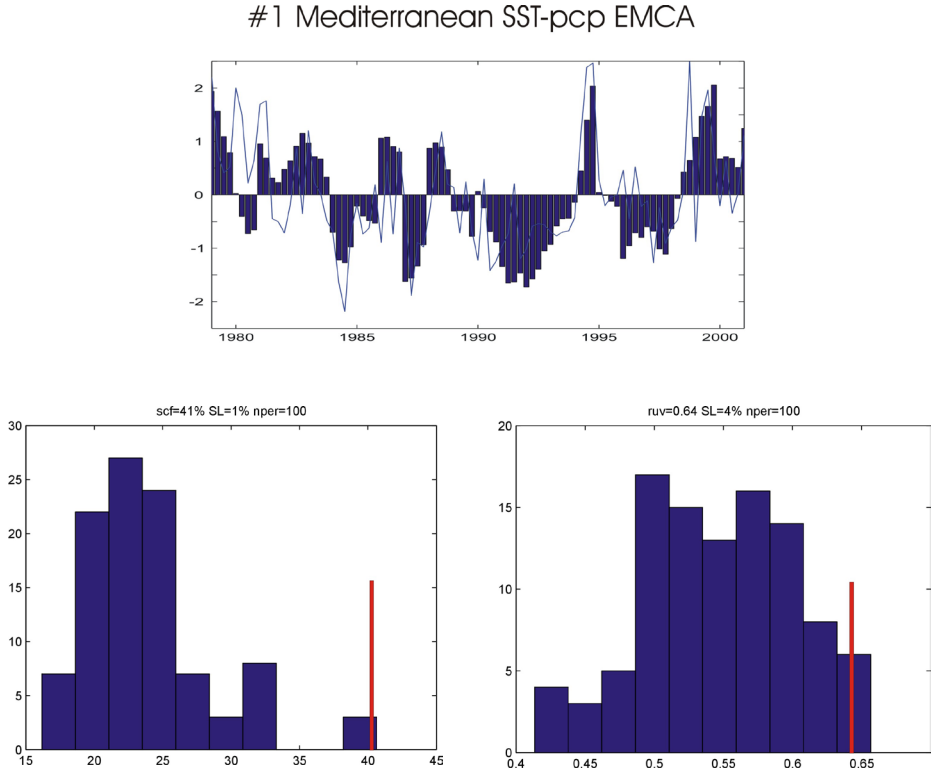

Figure 5. [top] The expansion coefficients corresponding to the leading EMCA mode between Mediterranean SST (NOAA Extended Reconstructed dataset, Smith and Reynolds 2003; bars) and CMAP precipitation (Xie and Arkin 1997; solid line) for the 1979-2001. [bottom] The probability density functions of the scf and ruv from 100 times Montecarlo test (histogram) is compared with the original EMCA scf and ruv scores (red line) to show its significance level (SL; indicated in the title).

Fig. 6 represents the seasonal dependence of the EMCA-Med SST expansion coefficients in relation to the Sahelian mode. On the one hand, the global SST expansion coefficient is obtained by using the whole eigenvector (all lags included) of the covariance matrix and, thus, capturing the complete time-evolving pattern. Hence, the global EMCA-SST is adopted for regressing the EMCA information on different variables/fields (Polo et al. 2008, García-Serrano et al. 2008). On the other hand, the individual SST expansion coefficients are calculated for each SST lag. As expected, it is apparent that the correlation between the Sahelian mode and the global EMCA-SST is comparatively maximum; less than the correlation coefficient using the individual EMCA-expansion coefficients (remember, ruv=0.64).

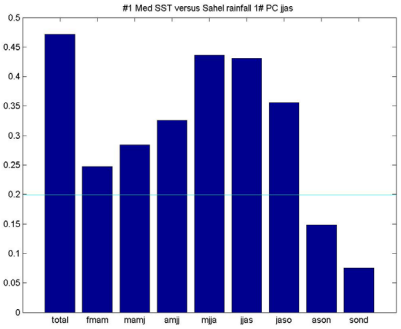

Figure 6. Correlation coefficient between the leading WAM rainfall, the Sahelian mode (Polo et al. 2008), and every SST expansion coefficient obtained from the EMCA-Med; the score associted with the global EMCA-SST time series is indicated in the first column. The horizontal blue line denotes the corresponding Student's t-test threshold for the statistical significance.

From FMAM to AMJJ, the correlation it is low although with significant scores; in MJJA, the correlation is maximum, persisting in JJAS and yielding high values up to JASO; while during ASON and SOND the correlation fails the Student's t-test. At this moment, it is worthy to note that, added to JJAS (contemporary lag to WAM rainfall), above correlation coefficients suggest either a potential predictability skill (in the case of MJJA) or physical relationship between Med-SST anomalies and Sahel precipitation (for the higher scores-related lags). For that reason, hereafter the analysis is mainly focused on one lag backward and one lag forward to JJAS; that is, MJJA-JJAS-JASO EMCA time-sequences .

Atmospheric global response to the Mediterranean mode

In order to find more insights about the anomalous circulation associated to this mode, Fig. 7 shows the regression maps of the streamfunction and rotational wind at 200hPa onto the EMCA-SST expansion coefficient. As indicated above, García-Serrano et al. (2007) proposed a mechanism for explaining the Med-WAM connection. In that work, the streamfunction anomalies from MJJA to JASO show a Med-related upper-tropospheric anomalous anticyclone extending on the adjacent region to the south. This spatial structure closely resemble the mid-upper tropospheric pattern found by Xoplaki et al. (2003a-b) over the Euro-Mediterranean area associated with the eastern-SST anomalies mode.

Since WAM precipitation has a strong component of interannual variability due to the Tropical easterly jet (TEJ; at upper-troposphere) anomalous state (Moron et al. 2004), the suggested mechanism indicates a strengthening of the TEJ, which, together with the climatological northward displacement of the ITCZ, enhances the Sahelian rainfall, following Nicholson and Grist (2001). This interpreation has changed during the recent study, suggesting a large-scale mechanism which involves perturbations in the Hadley cell instead of perturbations in the TEJ, finally not found (discussed below).

In any case, this finding is partially in agreement with Raicich et al. (2003), because it also implies a circulation change in the Mediterranean surrounding region; although their result was remotely forced from

anomalies in the Indian monsoon, whilst our proposal is that anomalous circulation is a direct response to Med-SST anomalies. In contrast, this finding is different from the mechanism found by Rowell (2003) and Jung et al. (2006), who suggested that the Mediterranean influence on WAM system is, via climatological circulation, related to advection of humidity content associated with enhanced evaporation.

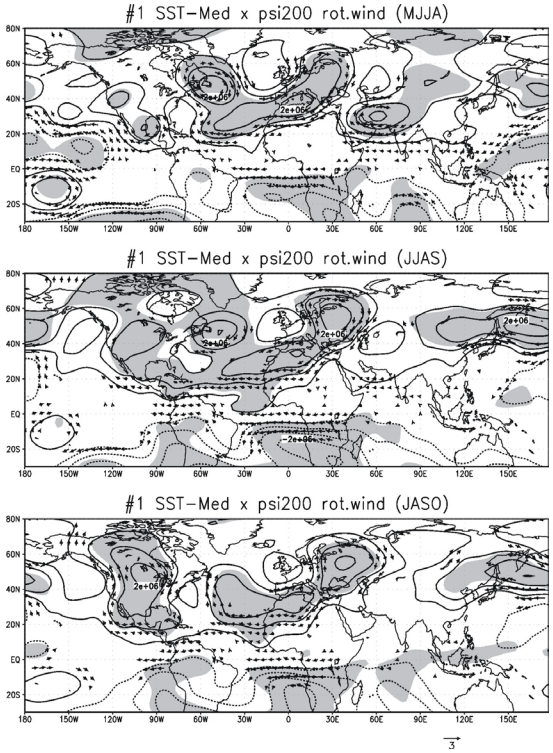

Figure 7. Regression maps of the streamfunction (contours; ci=1x106 m2/s) and rotational wind (arrows; m/s) onto the EMCA-SST expansion coefficient for MJJA [top], JJAS [middle] and JASO [bottom]; ERA40 dataset for 1979-2001 time-period. Magnitudes correspond to one std of the time series. Vectors are restricted to grid points where at least one wind component exceeds the significance level. Statistically significant areas, according to a t-test at the 98% level, are gridded for vectors and shaded for contours.

Another issue which was addressed in García-Serrano et al. (2007) is the answer to the following question: How is the anticyclonic circulation originated and maintained?

There (as in Fig. 7), from a global-scale approach, an almost similar atmospheric anomaly appears over subtropical Atlantic-central Europe during the three selected seasons, involving an extended anticyclone with two closed lobes. In addition, it can be seen that the response has a more global significant signature; indeed, it is apparent that the EMCA-related atmospheric anomalies are essentially confined along the Northern Hemisphere midlatitudes. Also there, the resemblance between 200hPa streamfunction anomaly (Fig. 7) and the simulated wintertime-response shown by Li (2006) made us to suggest that the anticyclonic anomaly is part of a circumglobal teleconnection pattern as a direct response to the Mediterranean warming.

Later, according to the encouraging results by Kodera and Kuroda (2003) and Watanabe (2004), concerning the key role played by the Mediterranean Sea on the hemispheric AO pattern, the explanation became plausible also in observations. Recently, Jung et al. (2006) have simulated a midlatidude wavelike feature extending from Europe to North America in response to summer Mediterranean SST, but forcing with SST anomalies maximum in the western part of the basin, overlooking the relationship between the global circulation and the WAM system. Finally, Ding and Wang (2005) have evidenced a recurrent circumglobal pattern in summertime, similar to that found by Branstator (2002) for winter, and giving

certain robustness to our hypothesis.

Hence, the main task of this study is to investigate the reliability of the large-scale response to Mediterranean SST anomalies in the frame of a hemispheric pattern and based on the EMCA results (for its connection to Sahelian precipitation).

The atmospheric teleconnection patterns that are associated with circumglobal character present low-frequency covariability between very widely separated points, namely the trapping and focusing effects of the time-mean tropospheric jets as they act as waveguide (Hoskins and Ambrizzi 1993, Branstator 2002, Watanabe 2004, Ding and Wang 2005). Theory, observations and model evidences reveal that these effects would not produce zonal mean anomalies but rather zonally oriented chains of perturbations. Next, we analyze the anomalous circulation associated with EMCA-Med in relation to this waveguiding effect.

The first step for testing our hypothesis is to localize the local forcing of the atmospheric pattern. Fig. 8 points out the longitude-by-height profile, averaged over the 30N-40N latitudinal window (along the Mediterranean Sea axis), of the anomalous geopotential height regressed onto the EMCA-SST time series.

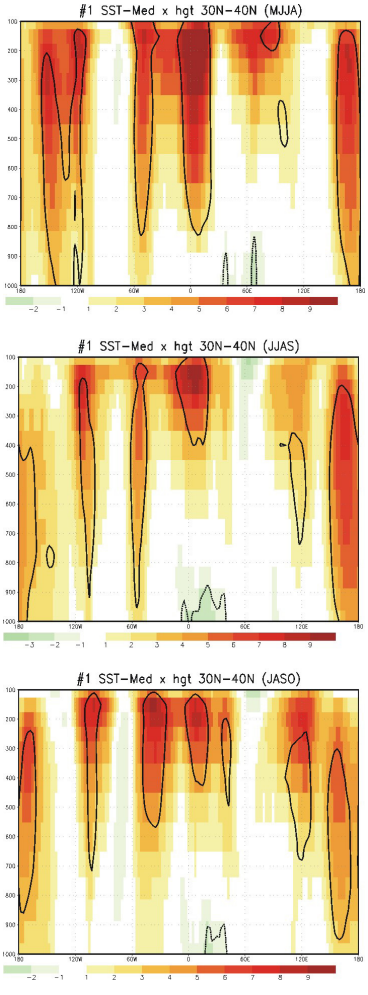

Figure 8. Regression vertical profiles of the EMCA-SST expansion coefficient on the 1000hPa-100hPa anomaloous geopotential height (shaded; m) averaged over 30N-40N; ERA40 dataset for 1979-2001 time-period. Magnitudes correspond to one std dev of the time series. Statistically significant areas, according to a t-test at the 98% level, are contoured.

Consistent with the surface warming showed above (Fig. 4; the Med-SST evolution), it is evident the local geopotential negative anomalies over the Mediterranean basin, reflecting the low-level convergence associated with a thermal sea-air forcing. As can be also seen, such a lower-response is accompanied by positive geopotential anomalies (anticyclonic circulation) in the upper-troposphere, involving a local baroclinic structure (maximum in JJAS). It should be note that, except for this local baroclinic anomaly, the atmospheric circulation shows a quasi-barotropic structure worldwide along the Northern Hemisphere midlatitudes.

Additionally, it is important to notice the persistent positive anomaliy (anticyclonic anomaly too) in the North Pacific basin, roughly over 150E-180E, for the subsequent discussion about the connection with the PDO.

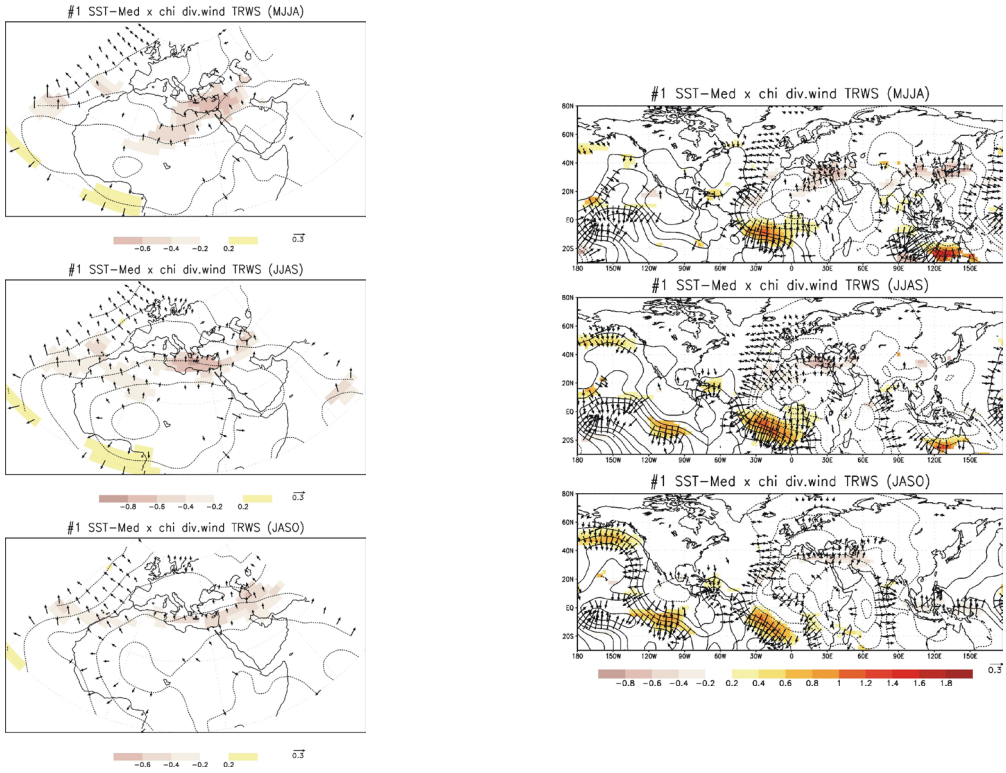

Figure 9. Regression maps of the TRWS (shaded; ci=x10-11 s-2), velocity potential (contours; ci=1 105 m2/s) and divergent wind (arrows; m/s) onto the EMCA-SST expansion coefficient; ERA40 dataset for 1979-2001 time-period. Magnitudes correspond to one std dev of the time series. Vectors are restricted to grid points where at least one wind component exceeds the significance level. Only statistically significant areas, according to a t-test at the 98% level, are plotted.

Once the local atmospheric column has been evidenced as a response for the Mediterranean forcing, we have to analyze the effective upper-tropospheric forcing, related to the latter, in exciting Rossby waves. Thus, from a preliminar study (not shown here) we have found that larger RWS anomalies correspond to TRWS term (associated with baroclinic anomaly; Fig. 9) rather than ERWS term (associated with barotropic anomaly). This finding is in agreement with Sardeshmukh and Hoskins (1988), Qin and Robinson (1993) and Renwick and Revell (1999) who pointed to TRWS as major contributor for this sort of thermal-forcing, reflecting the importance of the strong vorticity gradients in the vecinity of the subtropical jets. According to this, this finding follows, on the one hand, the reasoning of the circumglobal response to Med-SST anomaly (Li 2006; with a clear baroclinic strucutre) and, on the other hand, the hemispheric argument as result of Rossby-waves excitation by the anomalous upper-level convergence over the Mediterranean Sea (Watanabe 2004; barotropic structure related to the NAO/AO).

As can be seen, the largest values of TRWS in the Northern Hemisphere (the Summer Hemisphere) are just over the Mediterranean surrounding region, concretely along the southeast flank of the basin. These anomalies, persisting during the three EMCA-lags, are associated with the strong vorticity gradient in the entrance of the NAA jet, reflecting the effective perturbation of the flow.

Thus, to continue with our hypothesis, the possible circumglobal teleconnection (Fig. 8) would be reflecting the result of Rossby wave propagation from a stationary vorticity source produced by upper-tropospheric convergence (anticyclonic anomaly) over the Mediterranean region of thermally-driven convection (Hoskins and Ambrizzi 1993, Li 2006).

In addition, from the global regression of the divergent fields (Fig. 9-right), it is worthy to note both the perturbation in the local ITCZ over the tropical West Africa (for its connection with the WAM-Sahelian rainfall) and the increasing amplitude of the positive TRWS over the North Pacific (from MJJA to JASO) associated with the upper-tropospheric anticyclone commented above (for its connection with the PDO variability; also Fig. 8).

In order to test our waveguiding mechanism for the atmospheric circulation related to the EMCA-Med warming, we have to evidence the trapped anomalies propagation. Fig. 10 shows the geopotential anomalies at 200hPa (Z200) and the westerly mean jet in the three EMCA seasons. It is evident that the Z200 anomalies are mostly confined along a wide-latitudinal band, extending to the entire Northern Hemisphere midlatitudes and reflecting the downward extension into the westerly jet.

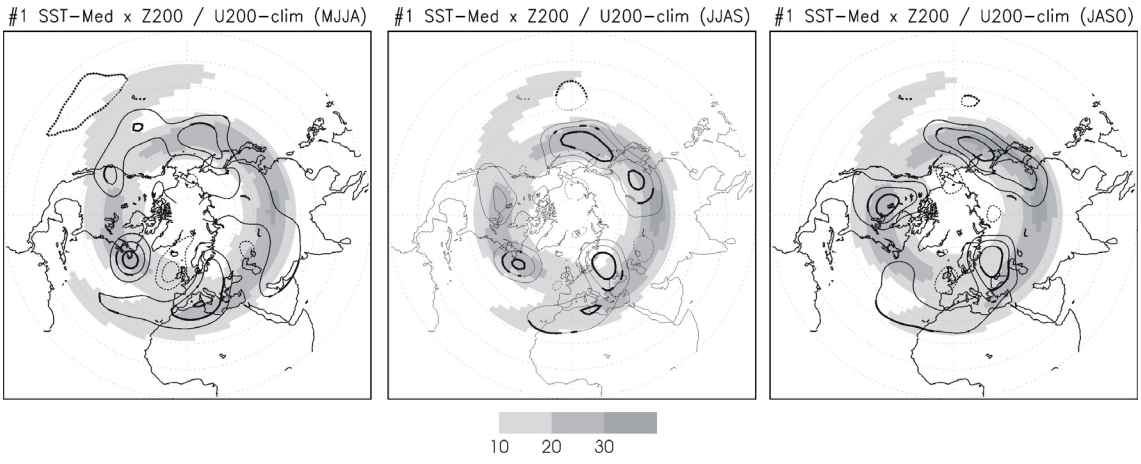

Figure 10. Regression maps of the anomalous geopotential height at 200hPa (contours; ci=5 m) onto the EMCA-SST expansion coefficient overplotted to climatological Northern Hemispehre westerly jet (shaded; ci=10 m/s); ERA40 dataset for 1979-2001 time-period. Regression-magnitudes correspond to one std dev of the time series. Regressed significant areas, according to a t-test at the 98% level, are bolded.

Such a zonally oriented wavetrain is reminescent of that one from the winter simulation by Li (2006). Although this mechanism is more active in winter-spring (Branstator 2002), it seems to be at work also in summer-autumn from the EMCA-Med, according to recent results by Ding and Wang (2005) and Jung et al. (2006).

Following the same line of reasoning of Li (2006), teleconnections with strong zonal characteristics are found trapped into the subtropical jet-stream to the North Pacific and North American continent, propagating further across the North Atlantic towards Northern Europe, following the dominant westerly climatology. These remote anomalies are also evident in the regressions at 700hpa (Fig. 11-left) and surface (Fig. 11-right).

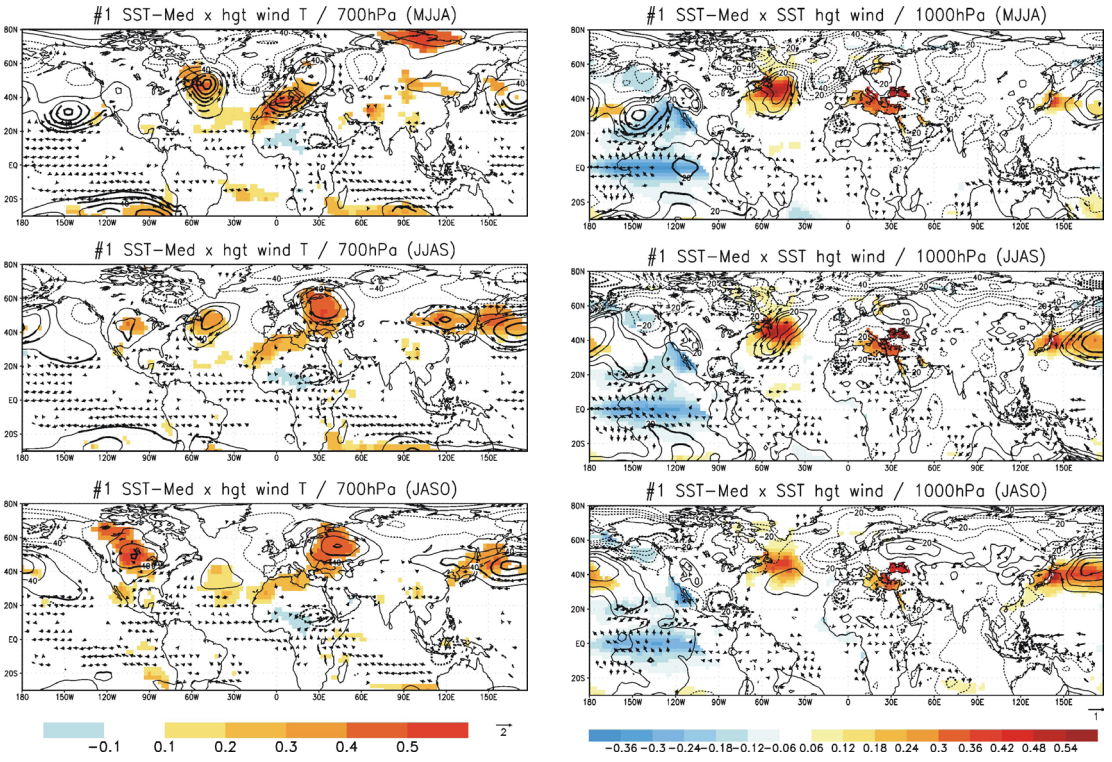

Figure 11. Regression maps of the anomalous geopotential height (contours; m/9.8) and horizontal wind (arrows; m/s) at 700hPa [left] and 1000hPa [right], air temperature at 700hPa (shaded, left; ºC), and SST (shaded, right; ºC) onto the EMCA-SST expansion coefficient. Magnitudes correspond to one std dev of the time series. Vectors are restricted to grid points where at least one wind component exceeds the significance level. Stistically significant areas, according to a t-test at the 98% level, are gridded for shading and vectors and bolded for contours.

As can be seen, the upper-tropospheric wavy anomalous circulation becomes diffuse as approaching the surface. Even so, it is evident the Med-impact on both northeastern oceanic basins. It is also important to notice the significant lower-tropospheric warming over Europe (Fig. 11-left) as result of downstream propagation of Rossby-anomalies at the jet exit of the North Atlantic westerly-stream (Ding and Wang 2005).

Likewise, having found that the EMCA signature of jetstream-trapped covariability between widely spaced points in the summer circulation is quite prominent, it seems possible that this mechanism may influence in the low-frequency of the westerly jet itself. To this aim, we have analized both the eddy activity and the wave-mean interaction.

The actual propagation characteristics of the high-frequency transients themselves can be described by the horizontal component of the Eliassen-Palm flux, the E-vector, which gives a description of the interaction between synoptic eddies and the mean flow due to barotropic processes (Hoskins et al. 1983, Trenberth 1986):

$$\vec{E} = \left(\frac{1}{2} \overline{v'v' - u'u'}, \quad -\overline{u'v'} \right)$$

where a prime denotes a deviation from the time mean and overbars a monthly average. These *u'* and *v'* perturbations are calculated by using the 24-h difference filter described in Wallace et al. (1988). The E-vector is approximately parallel to the group velocity (relative to the mean flow) of barotropic Rossby waves and also gives information about the shape and propagation features of eddies. To measure the amplitude of the transient activity we have calculated the perturbation kinetic energy (PKE; also Matthews and Kiladis 1999a-b):

$$PKE = \frac{1}{2}\left(\overline{u'u' + v'v'}\right)$$

Fig. 12 points out the regressions maps of these diagnostics onto the EMCA-SST expansion coefficient. From PKE results, it is clearly evident that the small regressed amplitude indicates the scarce effect on the time-mean tropospheric jet, according to Branstator (2002) in relation to this sort of teleconections. However, the EMCA-Med circumglobal propagation-pattern is associated with E-vectors showing an east-west orientation, depicting a elongated axis of Rossby perturbations and corfirming the zonally oriented wavetrain. Such a feature, the absence of an apparent meridional component, also reflects that there is not a net influence on the main westerly jetstream.

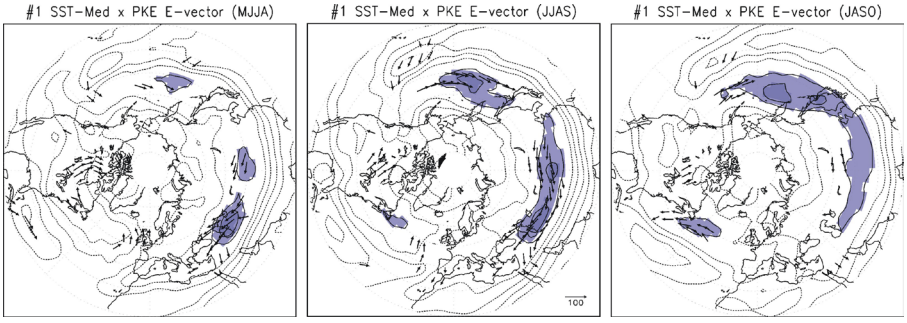

Figure 12. Regression maps of the anomalous PKE (contours; ci= 20 m2/s2) and E-vector (arrows; m2/s2) at 200hPa onto the EMCA-SST expansion coefficient; ERA40 dataset for 1979-2001 time-period. Magnitudes correspond to one std dev of the time series. Vectors are restricted to grid points where at least one wind component exceeds the significance level. Stistically significant areas, according to a t-test at the 98% level, are shaded for contours and gridded for vectors.

According to evidences shown above, there is also a marked influence on the western North Pacific basin, increasing in amplitude in the course of time (from MJJA to JASO). To establish a statistical link between the EMCA-Med circumglobal pattern and the PDO variability, we have calculated the correlation of the EMCA-SST expansion coefficient with the seasonal PDO index[1] (Fig. 13).

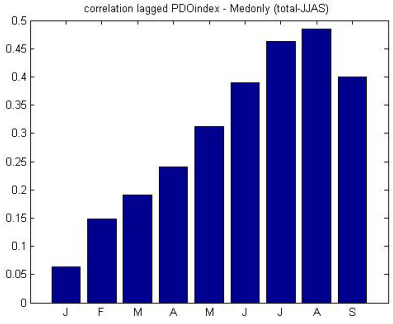

Figure 13. Correlation coefficient between the EMCA-SST time-series and the seasonal PDO index from JFMA to SOND (indicated by the first month of the 4-months sequence).

1 *Obtained from http://www.jisao.washington.edu/pdo/*

As it is evident, and following the same line of reasoning from above results (Figs. 7-to-12), the relationship between the Mediterranean SST time-evolution and the seasonal PDO index strenghthens as the circumglobal teleconnection is likely developed (clearly seen in JJAS-JASO). Even so, as reveled from Fig. 13, the maximum correlation with the North Pacific phenomenon occurs during ASON. However, such a finding is in agreement with the idea of an extratropical atmospheric forcing (remotely triggered from the Mediterraean region) of a midlatitude oceanic anomaly. In short, the barotropic teleconnection centre over the North Pacific, associated with an anomalous anticyclone, results in either an enhanced subsidence in the northeastern basin or a surface anticyclonic circulation, producing less evaporation and warm northward advection thereby increasing both the positive SST anomalies and the connection with PDO variability. This atmosphere-ocean direct mechanism has been determined by several studies (e.g. Bladé 1997, Frankignoul et al. 1998), establishing the time-lag of the forcing in approximately one month, in complete agreement with EMCA-Med results.

This relevant finding opens the possibility of including the Mediterranean anomalous state in the potential predictability on the PDO variability, and, consequently, also on the ENSO variability (e.g., Gershunov and Barnett 1998, Barnett et al. 1999).

Remote link between the Mediterranean mode and the WAM variability

Now, we tackle the remote impact of the EMCA-Med on the WAM system. As it is well known, the Mediterranean is a boundary region that feels both the dynamics of the tropical circulation cells and the mid-latitude stationary waves. Thus, the seasonal cycle is consequently very important, since it regulates the transition from the winter regime, dominated by mid-latitude circulation, to the summer regime, characterized by the tropical dynamics (Raicich et al. 2003). Contemporary to the latter, the WAM monsoon develops its peak phase (Sultan and Janicot 2000, Janicot and Sultan 2001). In accordance with a number of works, due to its particular geographical position under the descending motion of the local Hadley circulation, the Mediterranean Sea is a potential player on the African monsoon season (Fontaine et al. 2003, Raicich et al. 2003, Rowell 2003, Jung et al. 2006, Fontaine et al. 2008).

Fig. 14-left shows the EMCA-Med precipitation related to the WAM-Sahelian rainfall. It is important to bear in mind that the EMCA-precipitaion expansion coefficient (JJAS) is 0.96 correlated with the first WAM-EOF (JJAS), the Sahelian mode (Polo et al. 2008).

On the one hand, and as it is noticeable, the WAM precipitation anomalies associated with EMCA-Med are not restricted to the peak season of the monsoonal rainfall (JJAS); pointing out a clear reminiscent pattern in both MJJA (one negative lag) and JASO (one positive lag), and giving certain robustness to the connection found. Whereas the JJAS positive anomalies extend to the entire Sudan-Sahel area, the lagged ones are practically confined to 20E-surrounding region.

On the other hand, and according to the seasonal correlation coefficients shown in Fig. 6, the EMCA-Med results in this scenario suggest a certain predictability in the influence on WAM system, indicating a possible trigger role of the Mediterranean.

Jointly, the spatial patterns and the temporal relationship (MJJA-to-JASO), could reveal the likely weight in the teleconnection between the Mediterranean-related SST anomaly (maximum over the eastern basin) and the WAM precipitation (Sahel region); pointing the impact to 10E-30E longitudinal band.

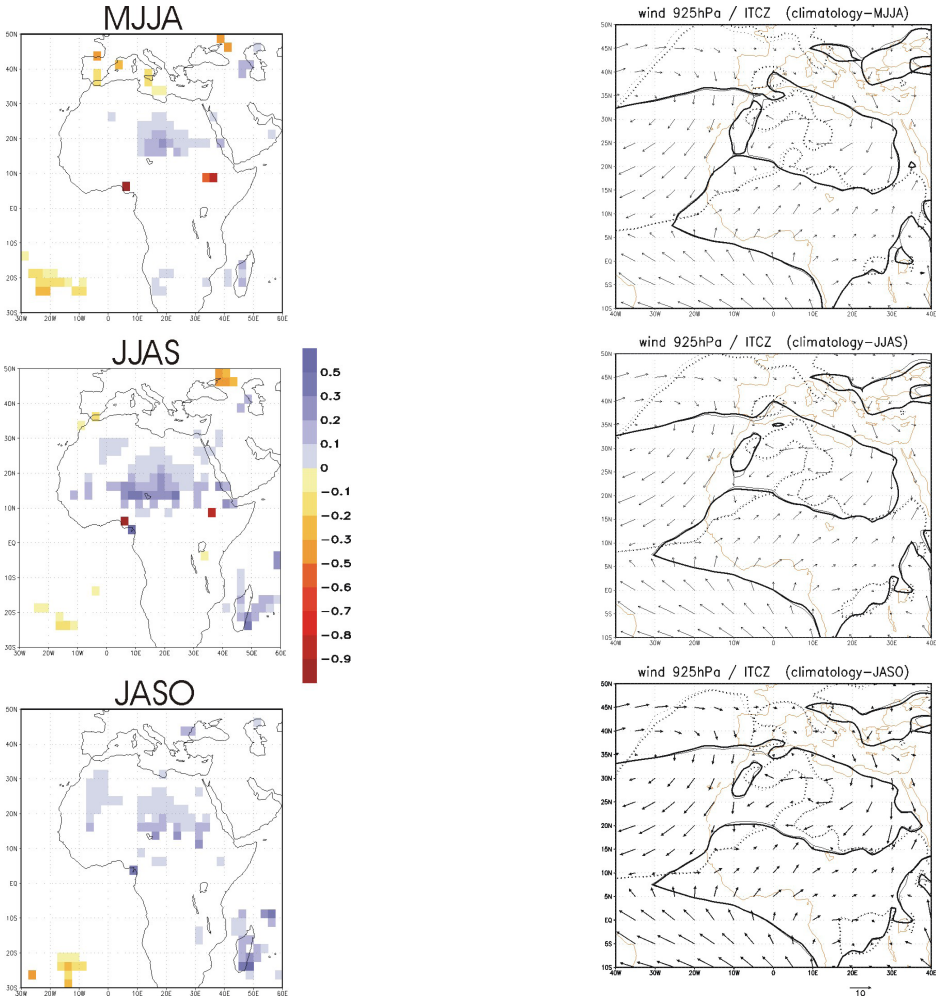

Figure 14. [left] Regression maps of the CMAP precipitation anomalies (mm/day) onto the EMCA-SST expansion coefficient. [right] ERA40 climatology of the 925hPa horizontal wind (arrows); contouring the zonal-zero value (solid) and the meridional-zero value (dashed), as proxy of the ITCZ. Regressed-magnitudes correspond to one std dev of the time series. Only stistically significant areas, according to a t-test at the 98% level, are plotted for rainfall (left pannel).

In the preliminary study (García-Serrano et al. 2007), the authors proposed a mechanism for explaining the Med-WAM relation which had involved the reinforcement of the TEJ (at upper-tropospheric levels). However, such tropical circulation-anomaly is absent in this refined analysis. There, the southward extension of the large-scale anticyclone as response to Med-SST warming (Fig. 7) was suggested as connector-agent with the Sahelian rainfall. On the contrary, the regressed profile of the anomalous zonal wind (averaged between 10E-30E; Fig. 15-right) rules out this hypothesis, because the TEJ is mostly located just over the ITCZ-related deep convection (Grist and Nicholson 2001, Nicholson and Grist 2001). In the same way, there is no evidence for considering the African easterly jet (AEJ; at mid-tropospheric levels) anomaly as precursor of WAM precipitation, since the anomalous easterly wind in that location is maximum during JASO when the Sahelian rainfall vanishes; reflecting that the AEJ anomalous state is a consequence of the ITCZ activity rather than cause (Cook 1999, Hsieh and Cook 2005, Berry and Thorncroft 2005, Hall et al. 2006, Mekonnen et al. 2006).

Above results made us focus the analysis on others elements governing the WAM system, like the ITCZ-associated local Hadley cell and the westerly monsoonal flow. Fig. 14-right and Fig. 15-left show the climatological circulation in the WAM region during the seasonal monsoon regime (from MJJA to

JASO); pointing out, respectively, the horizontal and meridional-vertical circulation climatologies. As established, the meridional-vertical circulation cell (local Hadley cell) shows a dramatic shift between winter and summer, indicating a displacement of the convective area from 5S-5N to the 10N-15N (e.g. Raicich et al. 2003). The low-level southern branch of this Hadley cell is composed of northly wind regimes longitudinally-known as Harmattan (mid-Med) and Etesian (east-Med) (e.g. Jung et al. 2006).

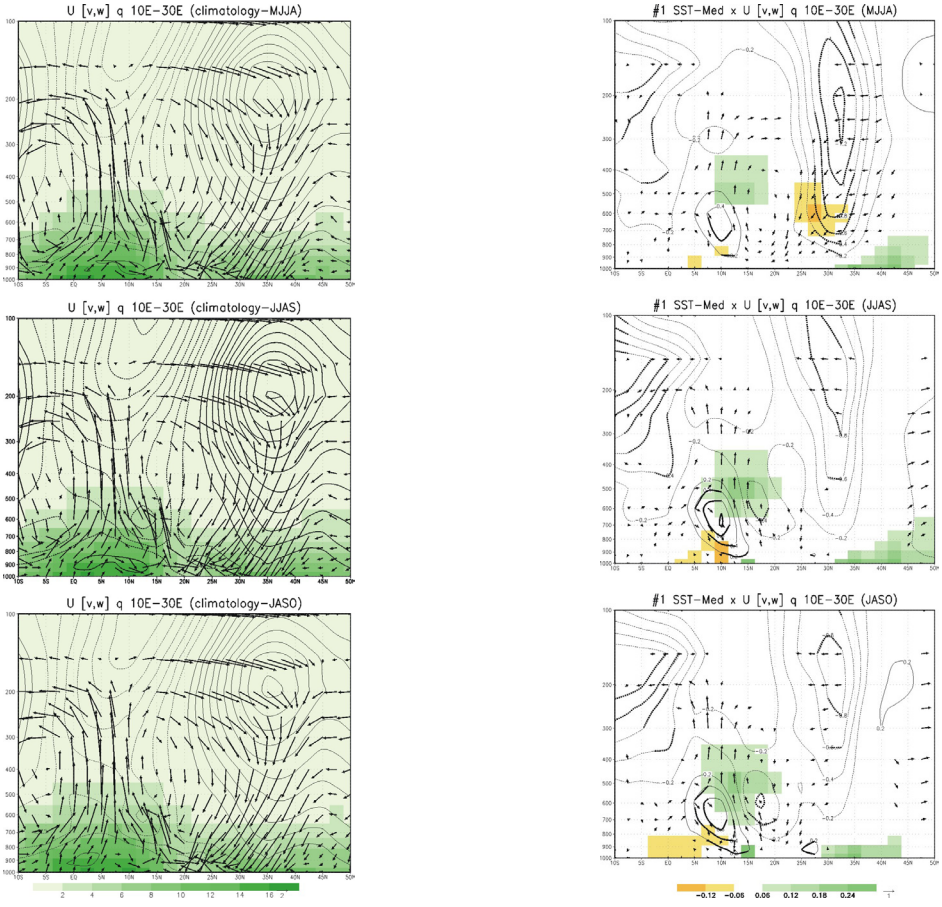

Figure 15. [left] Vertical-profiles climatology of the ERA40 zonal wind (U; contours, m/s), meridional (m/s) and pressure-vertical (x (-100) hPa/s) winds (v,w; arrows) and specific humidity (q; shaded, 1000 x g/g) averaged over 10E-30E. [right] Regression profile-maps of ERA40 U, v, w and q 10E-30E averaged anomalies onto the EMCA-SST expansion coefficient. Regressed-magnitudes correspond to one std dev of the time series. Regressed-vectors are restricted to grid points where at least one wind component exceeds the significance level. Regressed-statistically significant areas, according to a t-test at the 98% level, are gridded for shading and vectors and bolded for contours (right pannel).

Another important climatological-dynamic factor influencing the interannual variability of WAM-Sahelian rainfall is the westerly monsoon flow, or monsoonal flow, in charge of advecting the tropical Atlantic humidity (Fig. 14-right). In fact, these off-equatorial westerlies significantly modulate the Sahel-interannual variability (Grist and Nicholson 2001). Even more, there is evidence indicating that the degree of development of westerlies is the major contrast between wet and dry years (Nicholson and Grist 2001).

As commented above, EMCA-Med analysis is associated with a clear and significant deceleration of the subtropical westerly jet, instead of a perturbation in the TEJ essentially not found (Fig. 15-right). Such a feature, as evidenced from the large-scale approach, is related to the upper-tropospheric anomalous

anticyclone as thermally-driven response to Mediterranean EMCA-SST (Figs. 7, 8, 10).

Additionally, in order to characterize the Sahelian rainfall variability, we can observe contemporary both, an above-normal convergence of moisture occuring into the ITCZ (centred at 500hPa/10N-15N) and a strenghthening and deepening, rather than northward displacement, of the westerly monsoon flow (5N-15N, 900hPa-500hPa). Contrary to the latter, the former is accompanied by an apparent northward migration of the deep-vertical motions [and humidity content]; vertical-axis displaced from 5-7N [7N] to 7-10N [13N] (Fig. 15).

As proposed by Rowell (2003), warmer than average SSTs in the eastern Mediterranean lead to enhanced local evaporation, and hence to enhanced lower-tropospheric humidity there (also in Fig. 15-right). However, from EMCA-Med results there is not evidence of its advection across the arid eastern Sahara, which would feed enhanced moisture convergence over the Sahel and hence enhanced rainfall. Note that, although Rowell's model simulation was performed with a similar SST forcing to EMCA-SST anomaly, his resulting precipitation pattern had the loading scores to the west of 0E with maximum anomaly off African coast (his Fig. 8), completely opposite to findings shown here (Fig. 14-left).

The main features in the EMCA Med-WAM teleconnection, added to anomalous subtropical easterly flow, are the intensification of the ITCZ and the increase of monsoonal westerlies (Fig. 15-right). In the Sahelian rainfall-variability scenario, the latter is closely associated with the former, causing the enhancement of lower-tropospheric moisture advection inland the African continent (Fig. 14-right) and resulting in above-normal rainfall over the Sahel (Fig. 15-left) (e.g. Jung et al. 2006)

According to this, Grist et al. (2002) found that the horizontal shear, rather than the vertical one, is more important in causing the differences between wet and dry years. On the contrary, these results differ from those pointing to the relationship between TEJ and AEJ governs both the extent of the rainbelt and its intensity (Nicholson et al. 2007, Nicholson et al. 2008, Nicholson 2008). Even so, it is should be mentioned that the weakly increased easterly wind in the AEJ during JJAS (Fig. 15-right, middle) could further favour the horizontal shear, thereby likely increasing the instability and allowing African easterly waves (AEWs) to develop downstream. However, we suggest that further increase of Sahelian rainfall based on AEWs activity comes from cumulus convection within the ITCZ (prominent in MJJA-JJAS) and not by shear associated with the AEJ, following the argument by Hsieh and Cook (2005), Berry and Thorncroft (2005) and Mekonnen et al. (2006). Results from GCM simulations (Cook 1999), identifying the cause of the AEJ as the soil moisture distribution, are in agreement with the consequence-role of the AEJ to enhanced Sahelian precipitation.

Consequently, and according to EMCA-Med results, Giannini et al. (2003) pointed out that the SST variability is crucial in determining the sign of rainfall anomalies in the Sahel, whereas coherent land-surface interaction acts to amplify them. Summarizing, the Mediterranean summer SST anomaly has been found strongly correlated with Sahel rainfall anomalies, involving the reinforcement of both ITCZ-deep motion and ocean-land westerly transport of humidity thereby, in short, strenghthening the main WAM circulation regime which leads to enhanced seasonal rainfall.

Finally, one would wonder what is exactly the responsible mechanims in the WAM-Sahel precipitation linked to Mediterranean SST anomaly. To answer this question, and in order to characterize the EMCA-Med large-scale features in the Sahelian rainfall variability, it is important to look at the anomalous state of the local Hadley cell; as noted down by Raicich et al. (2003), who speculated the physical mechanism may involve variations in the WAM-Sahelian ITCZ. In fact, integral with this tropical main aspect is the tropical-extratropical overturning meridional cell, namely the closed meridional-Hadley circulation.

Thus, Fig. 15-right clearly indicates an important contribution to the ITCZ low-level convergence (15N-25N) from the downward-northly Hadley circulation (25N-30N). Indeed, this descending air seems

to be mainly of mid-latitude origin, sinking over the subtropical latitudes related to the anomalous upper-tropospheric easterly jet (200hPa, 30N-35N). To explain this circulation condition, we have referred the model-study of Rodwell and Hoskins (1996). Following this work, we suggest that the anomalous upper-tropospheric anticyclon-associated subtropical easterly flow interacts with the climatological mid-latitudes westerlies causing the air to descend. In such a way, this adiabatic descent, localized over the eastern Sahara and suthern flank of the Mediterranean basin, would be the piece of the puzzle connecting the thermally forced atmospheric response to Med-SST warming (in turn, part of a circumglobal pattern) to above-average Sahelian precipitation anomalies via large-scale circulation of the WAM system (ITCZ-Hadley perturbations).

Model representation

To test the origin of the observational EMCA mode described above for the Mediterranean in relation to the atmospheric response and WAM, different model experiment are needed. On the one hand, to test if the relation comes naturally from the coupled ocean-atmosphere system, we have repeated the analysis with the ocean-atmosphere coupled models currently used at Met Office, applying the same EMCA methodology to the outputs from two different realizations. These are 60-years simulation with the same pre-industrial conditions of two different versions of the HadGEM model, namely the HadGEM1 and HadGEM2. Finally, to test if the relation is SST forced, AGCM experiment with prescribed SSTs are also analysed.

Results from HadGEM1

In HadGEM1, the only statistically significant co-variability mode corresponds to WAM-rainfall anomalies associated with the Guinean Gulf (GG) mode (Fig 16). Such a mode is the leading mode of the EMCA analysis (EMCA1), explains the 51% of the scf between the predictor (FMAM-SOND Med SST) and the predictand (JJAS WAM-rainfall), and has a modest correlation of 0.47 between expansion coefficients. The EMCA1 Med SST associated pattern shows an evolution of the SST anomalies from the western basin in spring (FMAM-AMJJ) to the eastern part in autumn (JASO-SOND). The regression map of the global SST onto the EMCA1-SST expansion coefficient (Fig. 17) has maximum loadings over the equatorial Atlantic (negative SST anomalies); indicating, as expected, the association between GG precipitation and the tropical SST pattern, namely the Atlantic Niño (Janicot et al. 1998, Okumura and Xie 2004, Polo et al. 2008). This result implies that the EMCA1-Med SST pattern would be representing a footprint of the well known coupled phenomenon Atlantic Niño-GG rainfall. Thereby, such a tropical-extratropical relation is linked to an atmospheric teleconnection.

Analyses from lower (1000hPa) and upper (200hPa) tropospheric-levels (Fig. 18) indicate that the Atlantic Niño-Mediterranean relationship could be explained in terms of a quasi-barotropic Rossby wavetrain emanated from the Caribbean region extending along the North Atlantic. Thus, on the one hand, the Atlantic Niño EMCA1-based SST anomalies are associated with above-normal surface pressure anomalies (Z1000) over the eastern equatorial Atlantic and, jointly, negative surface pressure anomalies over Central America; indicating the reinforcement of the seasonal Walker local-cell (Wang 2002, García-Serrano et al. 2008). These perturbations would force an anomalous surface convergent-inflow and an upper-tropospheric divergent-outflow over the Caribbean Sea. Then, on the other hand, the Atlantic Niño EMCA1-based SST anomalies are associated both with positive geopotential anomalies at 200hPa (Z200) in the western tropical Atlantic, reflecting the anomalous vorticity source, and an downstream wavetrain crossing the entire North Atlantic basin towards Europe.

The zonally-oriented SST dipole present at North Atlantic mid-latitudes (Fig. 17), positive (negative) in the western (eastern) part of the basin, may be associated with that Rossby-wave pattern.

Even so, the statistical significance of the teleconnection-centres of action is quite limited (excluding JASO; Fig. 18), hence this proposed mechanism requires further investigation. In fact, another exchange-visit funded by ESF-MedCLIVAR has been recently proposed, from our group at UCM, for continuing this research line.

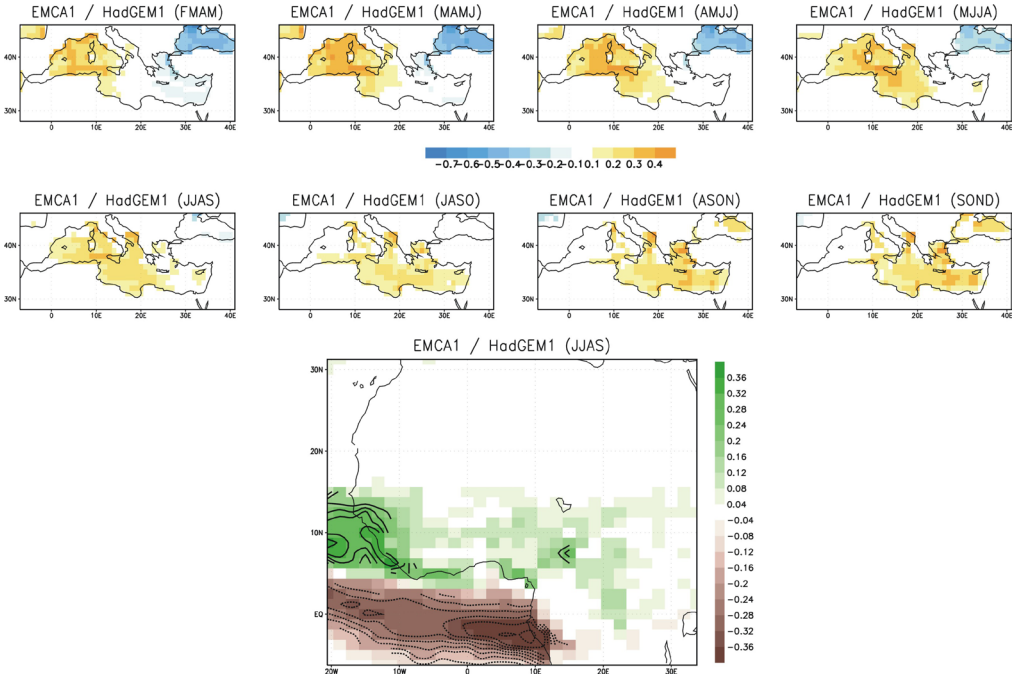

Figure 16. Leading co-variability EMCA mode (EMCA1) between the Mediterranean time-varying SST (FMAM-to-SOND) and JJAS WAM-precipitation applied to 60yrs coupled-run with pre-industrial conditions from HadGEM1. (top-panel) Homogeneous regression maps of Mediterranean SST anomalies (ºC) and (bottom) heterogeneous regression map of the WAM rainfall (std anomalies) onto the EMCA1-SST expansion coefficient. Statistically significant areas, according to a t-test at the 98% level, are gridded for SST and contoured for precipitation.

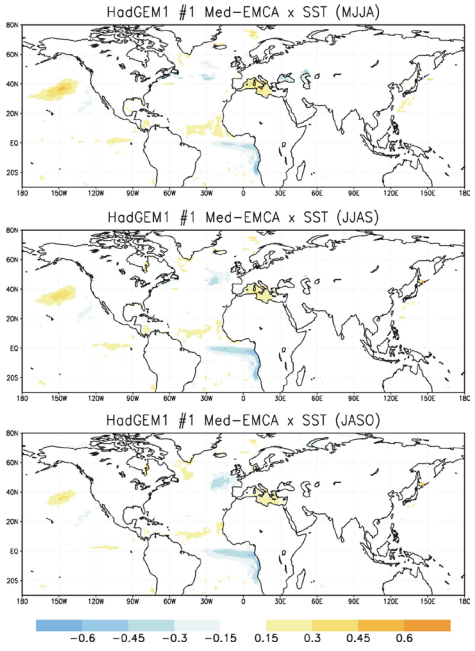

Figure 17. Regression maps of the global SST anomalies (ºC) onto the EMCA1-SST expansion coefficient obtained from 60yrs coupled run with HadGEM1. Magnitudes correspond to one std dev of the time series. Only statistically significant areas, according to a t-test at the 98% level, are plotted.

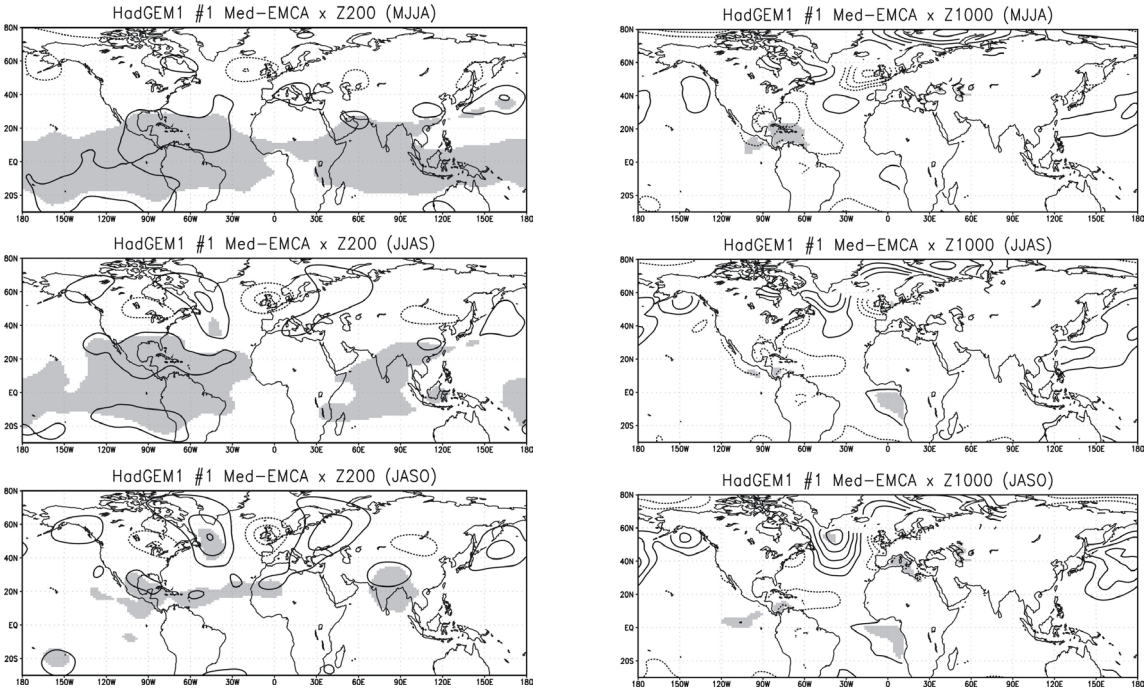

Figure 18. Regression maps of the geopotential height at 200hpa (left; contours, ci= 5hPa) and 1000hPa (right; contours, ci= 1hPa) onto the EMCA1-SST expansion coefficient obtained from 60yrs coupled run with HadGEM1. Magnitudes correspond to one std of the time series. Statistically significant areas, according to a t-test at the 98% level, are shaded.

Results from HadGEM2

Regarding the results from HadGEM2; the above Atlantic Niño-GG rainfall coupled mode and its relation to the Mediterranean time-varying SST pattern, derived from EMCA-HadGEM1, corresponds to the second covariability-mode (EMCA2) after applying EMCA to the 60yrs coupled run of HadGEM2 (Fig. 19). Here, the explained scf between fields is 23%, whereas the correlation coefficient of the expansion coefficients is 0.38. Overall, these covariability measures related to GG anomalous precipitation are rather low in HadGEM2 than HadGEM1, implicating that the remote relationship is more weakly represented. However, the fact that both HadGEMs coupled-models show the Atlantic Niño-GG rainfall connection with Mediterranean summer SST anomaly implies that this relationship is a robust feature.

The leading mode of the Med-EMCA applied to HadGEM2 coupled run (EMCA1; Fig. 20) shows positive precipitation anomalies inland of the GG coastline, roughly over 5W-0E and below 10N. As can be seen, this EMCA1-WAM rainfall pattern, which has a statistical significance quite limited, is so different to the observed Sahelian precipitation anomaly (Figs. 4, 14-left) that it is useless to make comparisons: CMAP-Sahelian rainfall yields positive anomalies east to 0E and between 15N-20N, whilst HadGEM2-EMCA1 depicts above-normal precipitation west to 0E and further into sub-Saharan Africa.

On the contrary, the time-evolving SST pattern in the Mediterranean Sea associated with HadGEM2-EMCA1 points out a common feature regarding Med-EMCA in the observations (Fig. 4), showing the maximum amplitude over the eastern part of the basin. Indeed, according to both observed Med-EMCA (as Polo et al. 2008, her Fig. 9a) and the works by Xoplaki et al. (2003a, her Fig. 6h; 2003b, her Fig. 5c); the HadGEM2-related SST pattern seems to be conditioned by the anomaly in the Black Sea (loading scores), although it also spreads on the Greece-Cyprus surrounding area (Fig. 20).

The above mentioned discrepancy in the Mediterranean-Sahel connection, with similar SST patterns and the different precipitation anomalies, for HadGEM2-EMCA1 and the observed Med-EMCA is an intriguing result. Global regressions using the HadGEM2-EMCA1 SST expansion coefficient give some clues (Fig. 21). The global-SST regression maps (Fig. 21-left) reproduce the observed Med-SST damping during late-summer together with the increasing amplitude of the North Pacific positive SST anomaly (Fig. 11-right). Also it is apparent the increasing negative anomaly in the equatorial Pacific. This finding points again at PDO variability as a phenomenon teleconnected with the Mediterranean SST anomalies; implying very relevant results for the global climate system. The Pacific SST pattern linked to Med-SST differs from the canonical ENSO signal, depicting the maximum equatorial anomalies in the central part of the basin.

The global-Z200 regression clearly shows an anomalous anticyclonic circulation over the maximum SST forcing (Fig. 21-right). The corresponding surface anomalies also show negative pressure anomalies in the Black Sea surrounding region (only statistically significant in MJJA, not shown); indicating, as in the observations, a direct baroclinic response to Med-SST. Likewise, the proposed waveguided atmospheric circulation is present in HadGEM2-EMCA1; resulting in a downstream propagation across the Eurasian continent, trapped into the NAA westerly-jet, that leads to an anticyclonic anomaly over western North Pacific (150E-180) forcing strong subsidence there (MJJA-to-JASO).

Regarding the Med-WAM relationship in HadGEM2-EMCA1, this GG rainfall pattern (Fig. 20) does not seem to be associated with the large-scale atmospheric response to Med-SST anomaly, because the midlatitudes anticyclonic anomaly (at 45N-50N) does not perturb the westerly flow over northern Africa-Mediterranean upper-tropospheric levels (at 25N-35N; not shown). In fact, the HadGEM2-EMCA1 GG anomalous precipitation seems to be more related to the local ITCZ (local vertical motions, at 10N; Sultan and Janicot 2000) than alterations in the local Hadley cell (no evidence of enhanced returning-subsidence has been found; not shown).

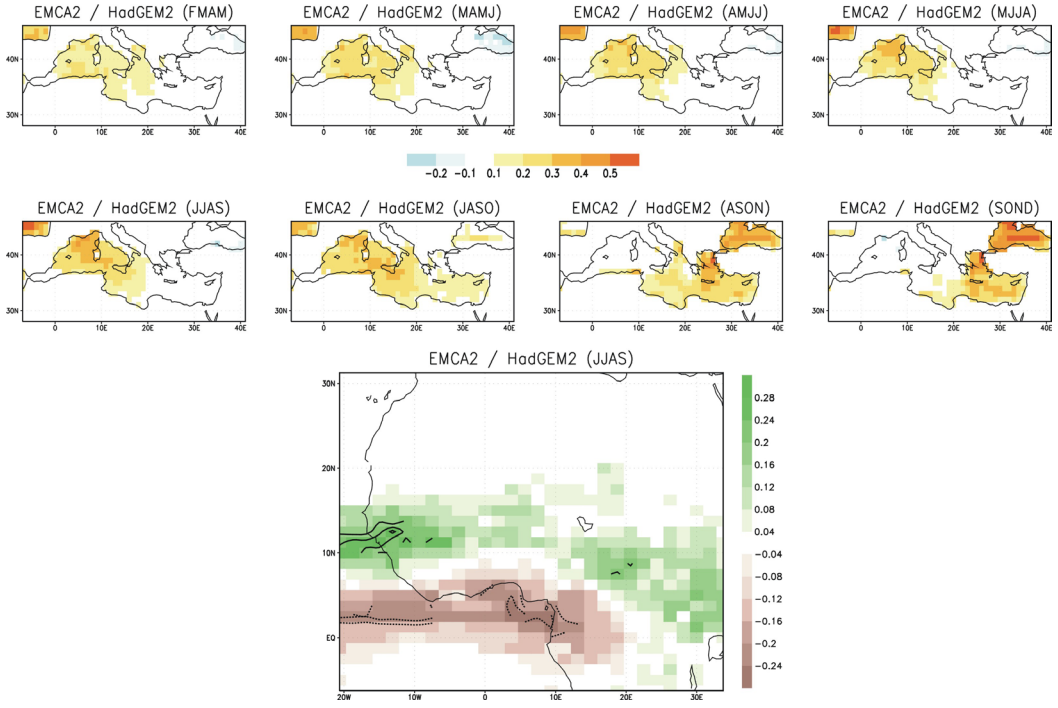

Figure 19. As Fig. 16 but for second EMCA-mode derived from the 60yrs pre-industrial run with HadGEM2.

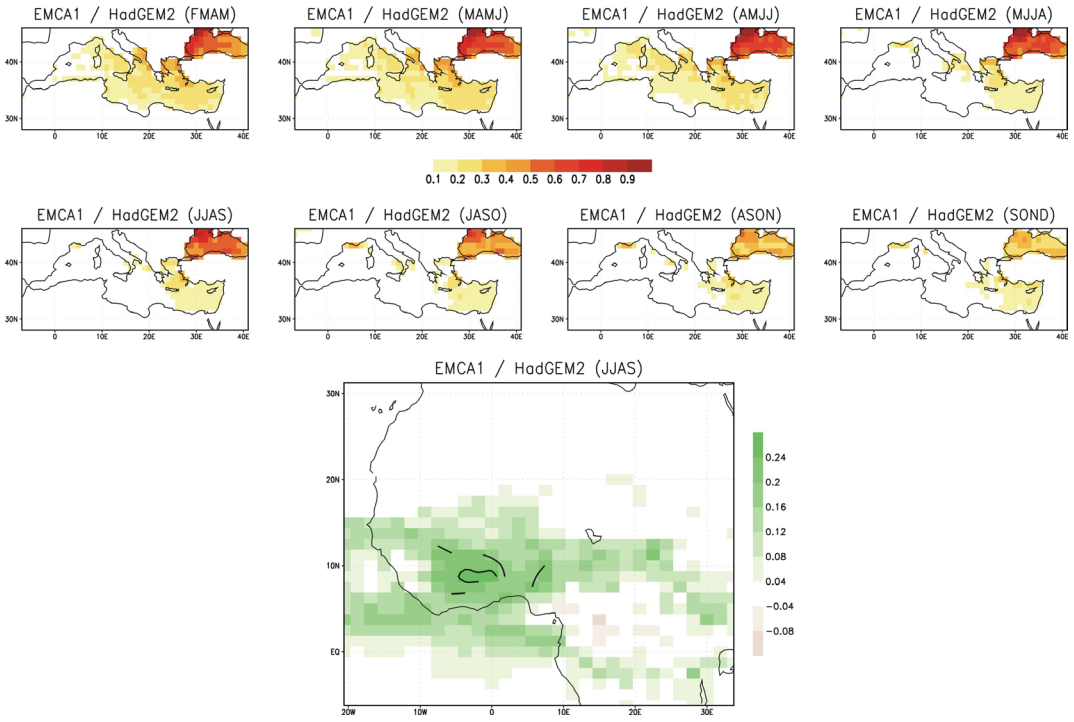

Figure 20. As Fig. 16 but for leading EMCA-mode derived from the 60yrs pre-industrial run with HadGEM2.

Looking at global-SST regression (Fig. 21-left); besides the possible feedback from subtropical North Atlantic (e.g. Rowell 2003, Polo et al. 2008) or the local increased evaporation from weak positive SST anomalies in the equatorial Atlantic, the evolving negative anomaly in the equatorial Pacific could impact on the HadGEM2-EMCA1 WAM rainfall. Following this argument, previous works have evidenced a negative correlation between WAM-rainfall and ENSO-like equatorial SST, resulting in positive precipitation anomalies in conjunction with negative SST anomalies (La Niña conditions; e.g. Janicot et al. 1998). On this respect, Janicot et al. (1998) suggested that the Pacific-WAM teleconnection could be monitored by a Walker-type zonal circulation over the tropical Atlantic. However, there is no evidence for such kind of surface-pressure dipole between the tropical Pacific and Atlantic basins; only positive Z1000 anomalies have been found over the central-eastern Pacific (not shown). Alternately, Rowell (2001) proposed that such a teleconnection could result from anomalous stationary equatorial Kelvin-waves propagating from the Pacific, either through a direct influence of the vertical motions on convection, or through a perturbation in the North Africa anticyclone leading to a moisture advection anomaly. Regardless of these interpretations, the concomitance of negative tropical Pacific SST anomalies with positive ones in the equatorial Atlantic could enhances the inter-basin zonal gradient between the eastern Pacific and tropical Atlantic and, then, would lead to above-normal precipitation anomalies over West Africa.

This Pacific-WAM climate link, including the potential role of the Mediterranean Sea via PDO variability, represents a very daring challenge which must be tackle with designed OAGCM-sensitivity experiments.

This far, there have been no evidence for reproducing in HadGEM's family the eastern Mediterranean SST-Sahelian rainfall connection derived from observations. Not so, HadGEM2 seems to be capturing some indication of large-scale atmospheric response to summer Mediterranean SST anomaly, which is really an encouraging finding.

Regarding the former, it is worthy of noting that Joly et al. (2007) emphasized the OAGCMs' difficulty in simulating the African monsoon rainy-season, particularly the Sahelian rainfall. Thus, from this scenario,

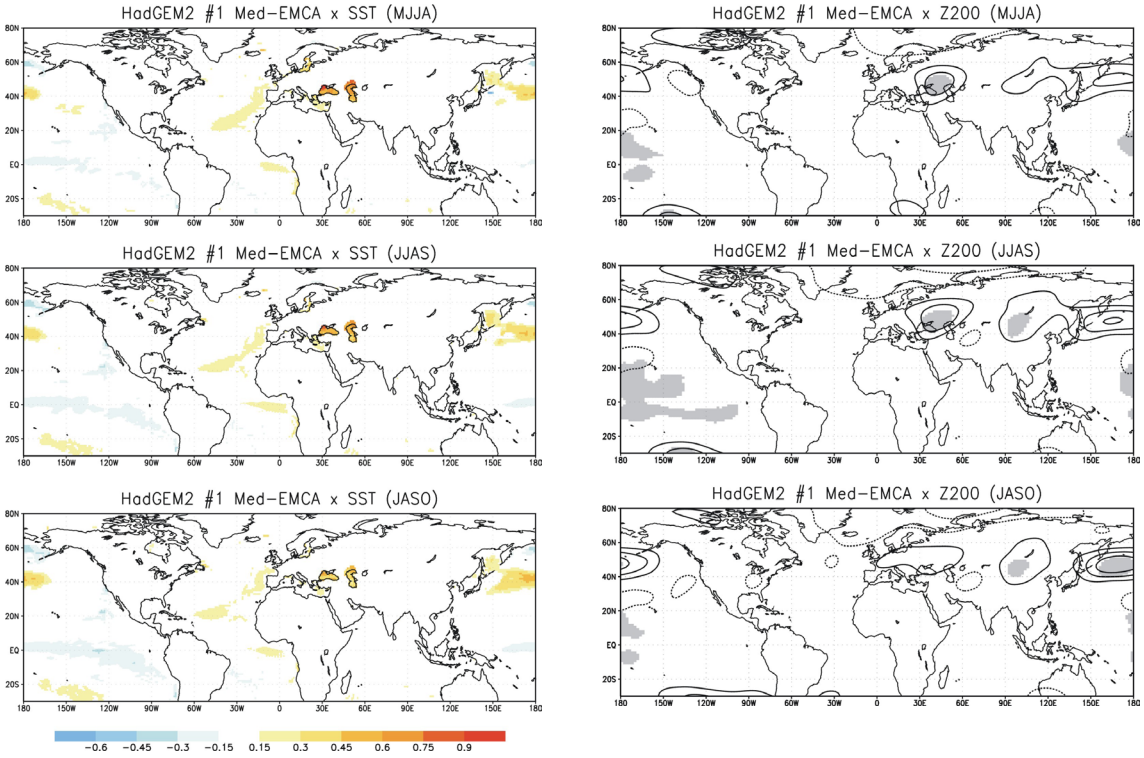

Figure 21. Regression maps of the global SST (left; shaded, ºC) and geopotential height at 200hpa (right; contours, ci= 5hPa) onto the EMCA1-SST expansion coefficient obtained from 60yrs coupled run with HadGEM2. Magnitudes correspond to one std dev of the time series. Statistically significant areas, according to a t-test at the 98% level, are gridded for shading and shaded for contours.

the absence of the Med-Sahel connection in both 60yrs pre-industrial coupled runs (HadGEM1 and HadGEM2) make us think that the observed WAM trends could be partly a response to the anthropogenic forcing, according to Held et al. (2005), Biasutti and Giannini (2006), Joly et al. (2007); and in contrast to Giannini et al. (2003), Hoerling et al. (2006). Even so, it is important to bear in mind that the response of the WAM precipitation is still highly model-dependent (Joly et al. 2007, among others).

This far, there have been no evidence for reproducing in HadGEM's family the eastern Mediterranean SST-Sahelian rainfall connection derived from observations. Not so, HadGEM2 seems to be capturing some indication of large-scale atmospheric response to summer Mediterranean SST anomaly, which is really an encouraging finding.

Regarding the former, it is worthy of noting that Joly et al. (2007) emphasized the OAGCMs' difficulty in simulating the African monsoon rainy-season, particularly the Sahelian rainfall. Thus, from this scenario, the absence of the Med-Sahel connection in both 60yrs pre-industrial coupled runs (HadGEM1 and HadGEM2) make us think that the observed WAM trends could be partly a response to the anthropogenic forcing, according to Held et al. (2005), Biasutti and Giannini (2006), Joly et al. (2007); and in contrast to Giannini et al. (2003), Hoerling et al. (2006). Even so, it is important to bear in mind that the response of the WAM precipitation is still highly model-dependent (Joly et al. 2007, among others).

All above suggests the need for a more detailed validation of the WAM variability, including the overlooked dynamical-link between Mediterranean and the WAM-Sahel rainfall, as well as the large-scale atmospheric response to Med-SST anomalies.

In this respect, validating SST-rainfall teleconnections is particularly attractive for at least two reasons. On the one hand, such teleconnections clearly contribute to the observed climate variability at interannual and multi-decadal time scales and their evolution might therefore influence the twenty-first century climate projections. On the other hand, such teleconnections are mainly controlled by the large-scale atmospheric dynamics and therefore represent much more than a validation of SST and rainfall variability.

Results from an Atmospheric General Circulation model

Next we have applied the same EMCA methodology to an AGCM large-simulation using the UCLA model and prescribing 1979-2005 observed SST. A detailed description of this simulation is given in Mohíno et al. (2008). Note that this AGCM simulation extends the Med-EMCA observational time-period for four years, from 2001 to 2005. Fig. 22 shows the leading covariability mode of the Med-EMCA derived from the UCLA prescribed-run (AGCM-EMCA), which takes into account almost the 45% of the scf and presents a correlation of 0.70 between SST time-varying predictor (FMAM-to-SOND) and WAM-rainfall predictand (JJAS). As in observations, such a performance has been obtained after detrending SST and precipitation dataset, and additionally standardizing the precipitation anomalies.

As can be seen, AGCM-EMCA1 fairly captures the evolution of the Mediterranean SST pattern from observations (Fig. 4), but slightly points out a major weight in the central part of the basin. Regarding the associated WAM anomalies; the AGCM-EMCA yields the Mediterranean-related Sahelian rainfall quite accurately, although with statistical limitations. Excluding the detrending in the model-EMCA computation (Fig. 22, bottom-right), the statistical significance is largely improved (scf=69%; ruv=0.79). However, the climate implications of the difference in forcing the AGCM model with detrended-SST and detrending the outputs after forcing with un-detrended SST is out of the scope of this work. Such a issue requires further investigation (and an additional large-simulation with detrended SST forcing).

Fig. 23 illustrates the structure of the general atmospheric circulation which enables to explain the large-scale Med-teleconnection (Fig. 23-left) and the mechanism between the Mediterranean SST and the West African monsoon (Fig. 23-right).

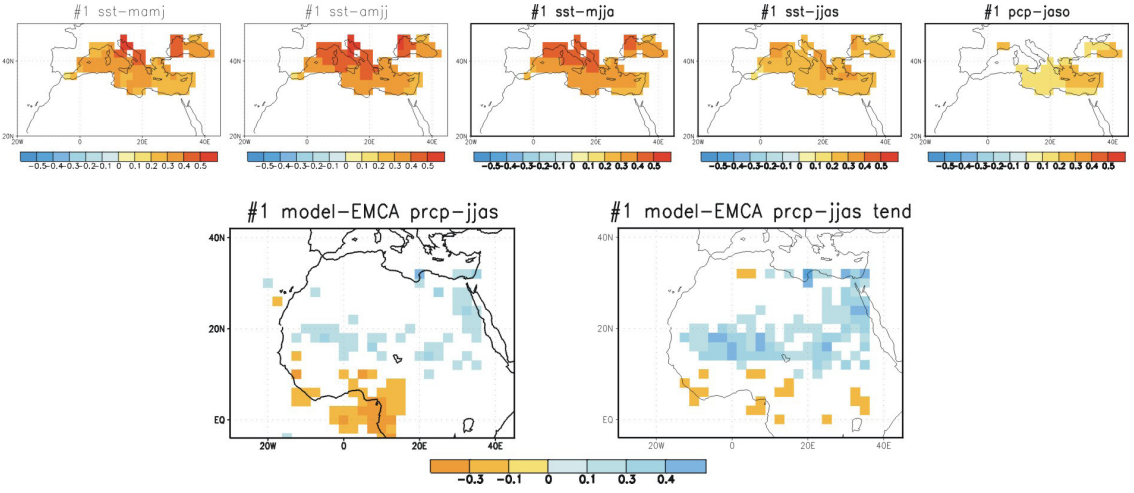

Figure 22. Leading co-variability mode (AGCM-EMCA) of the Mediterranean time-varying SST (FMAM-to-SOND) and JJAS WAM-precipitation EMCA analysis applied to 1979-2005 observed SST UCLA-AGCM simulation. (top) Homogeneous regression maps of Mediterranean SST anomalies (ºC) from MAMJ-to-JASO EMCA-sequences, and (bottom) heterogeneous regression maps of detrended (left) and un-detrended (right) WAM rainfall (std anomalies) onto the corresponding AGCM-EMCA SST expansion coefficient. Only statistically significant areas, according to a t-test at the 98% level, are plotted.

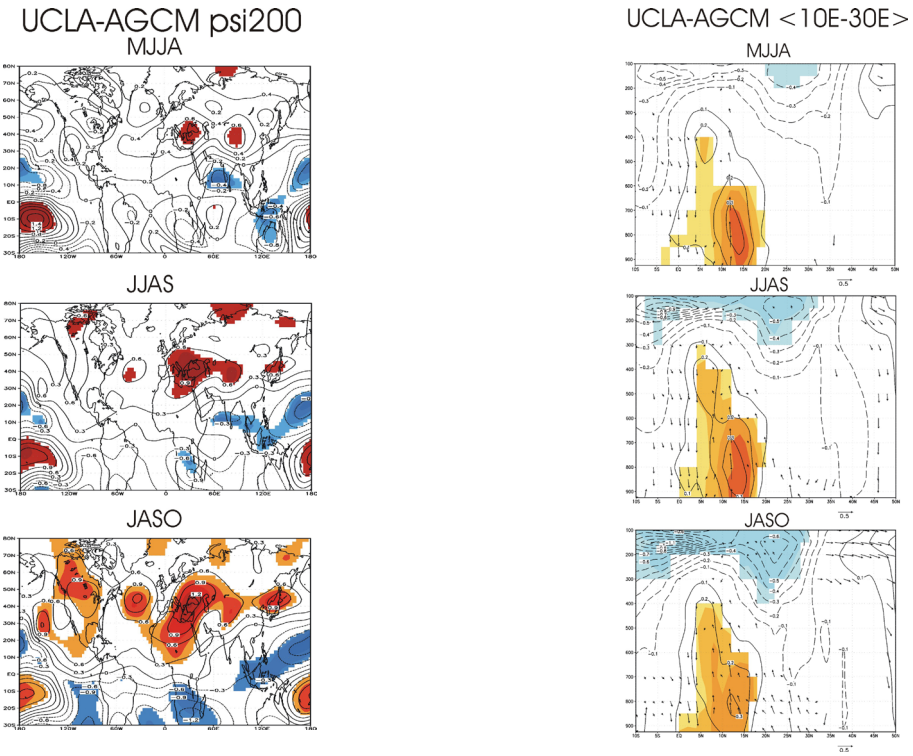

Figure 23. [left] Regression maps of the streamfunction at 200hPa (contours, ci=0.1 106 m2/s); and [right] regressed-vertical profiles of zonal wind (contours, ci=0.1 m/s), meridional (m/s) and omega (x –100, hPa/s) (arrows) onto the AGCM-EMCA SST expansion coefficient. Magnitudes correspond to one std dev of the time series. Statistically significant areas, according to a t-test at the 98% level, are shaded for contours and gridded for vectors.

The former confirms both, the local baroclinic structure in response to summer Med-SST anomaly, low-level convergence (not shown) and upper-tropospheric anomalous anticyclone; and the downstream propagation into the westerly jet as part of the circumglobal teleconnection, with action-centres in Eurasia and over western North Pacific (Japanese islands). Note, as in observations (Fig. 7), the evolution of the local positive streamfunction anomalies over the Mediterranean basin and the time-increasing amplitude of the anomalous anticyclone over Japan (MJJA-to-JASO).

The latter shows the enhanced Sahelian convection and the strong-deep degree of development of the (westerly) monsoonal flow (5N-15N; Fig. 23-right). Also it is evident the influence of the anomalous midlatitudes easterly-flow (related to above anticyclonic response) on the regional WAM climate; entailing the intensification of the overturning anomalous Hadley cell (above all at 25N-35N). This fact represents a first confirmation of the large-scale impact of the Mediterranean Sea on the WAM-Sahel rainfall; implying that the monsoon system becomes more active and precipitation increases (as in observational Fig. 15-right). It is also important to notice the absence of an anomalous state in both the TEJ and AEJ, suggesting its weak role over Sahel.

Future collaboration with host institution

Further work to develop with Met Office-Hadley Centre includes:

- Move the 'RWS_diagnostic' script from PV-Wave (current software) on Interface Definition Language (IDL) programming language (future software)

- Make a profound assessment of deficiencies and uncertainties in the Mediterranean link to WAM-Sahel monsoon in HadGEMs coupled models; for a future report and looking towards improving the HadGEM3-model development

- Use the Extended-MCA technique in the post-processing of seasonal forecasts; it could produce a significant increase in skill

- Study with coupled experiments of the potential connection between the Mediterranean Sea and the Pacific Decadal Oscillation after analysing the EMCA-based sensitivity experiment performed with UCLA-AGCM

Additionally, in the Appendix, I am attaching a letter of introduction from Alberto Arribas, tutor of my exchange-visit at Met Office.

Projected publications/articles resulting or to result from your grant

We are preparing two publications:

"Large-scale atmospheric response to Mediterranean summer SST anomalies" (ready for submitting to Climate Dynamics); showing the observational evidence and testing the hypothesis with AGCM large-simulation.

"Recent impacts of Mediterranean SSTs on West African rainfall variability" (in elaboration for submission). In this paper, Med-EMCA results based on observations and a large-run simulation with the UCLA-AGCM model, at the expense of analysis from the model-sensitivity experiment, are described in relation to the WAM system.

Comments

I thank Jucundus Jacobeit and Laurent Li for their constructive comments on the preliminary study presented in the 2nd ESF-MedCLIVAR Workshop.

I would also like to thank, from Hadley Centre, Stephen Cusack, Adam Scaife, Matthew Collins, Sarah Ineson, Margaret Gordon and Drew Peterson for useful discussions and comments regarding this study. Thanks are also due to Ian Culverwell for his constant help and assistance in pp_routines for computing streamfunction and velocity potential.

I wish to thank Teresa Losada and Irene Polo, at UCM, for technical support and valuable advice on implementation and use of HadGEMs model-data in GrADS and Matlab softwares. I would also like to thank Ellen Degott, from the ESF Office, for her patience and encouragement.

Finally, I would like to express my gratitude to ESF-MedCLIVAR Programme for making this exchange-visit possible. As proof of this fruitful work, apart from possible publications, I have given a seminar concerning the study carried out in the Department of Geophysics and Meteorology in my Faculty (at UCM); I enclose the announcement in the Appendix.

In addition, the reflection about this grant makes me indicate that the visit to a host institution, particularly in the Hadley Centre with its awesome environment, generates so amount of insightful discussions that helps to fall on a great number of different and enriching points of view concerning the study. Really, it was

a very pleasant time for me, although I think that it was not time enough to get used to completely working on the host daily-routine.

References

Barnett, T. P., D. W. Pierce, M. Latif, D. Dommenget, and R. Saravanan (1999): Interdecadal interactions between the tropics and midlatitudes in the Pacific basin. Geophys. Res. Lett., 26: 615-618.

Berry, G. J., and C. D. Thorncroft (2005): Case study of an intense African easterly wave. Mon. Wea. Rev., 133, 752–766.

Biasutti, M and Giannini, A. (2006): Robust Sahel drying in response to late 20th century focings. Geophys. Res. Lett., 33, doi:10.1029/2006GL026067.

Bladé, I. (1997): The influence of midlatitude ocean–atmosphere coupling on the low-frequency variability of a GCM. Part I: No tropical SST forcing. J. Climate, 10, 2087–2106.

Bond, N.A. and D.E. Harrison (2000): The Pacific Decadal Oscillation, air-sea interaction and central north Pacific winter atmospheric regimes. Geophys. Res. Lett., 27(5), 731-734.

Branstator, G. (2002): Circumglobal teleconnections, the jet stream waveguide, and the North Atlantic Oscillation. J. Climate, 15, 1893–1910.

Bretherton, S. B., C. Smith, and J. H. Wallace (1992): An intercomparation of methods for finding coupled patterns in climate data, J. Climate, 5, 541-560.

Cane, M. A., Clement, A. C., Kaplan, A., Kushnir, Y., Pozdnyakov, D., Seager, R., Zebiak, S. E. and Murtugudde, R. (1997): Twentieth- Century Sea Surface Temperature trends. Science 275, 957–960, DOI: 10.1126/science.275.5302.957.

Chang, E. K., S. Lee and K. L. Swanson (2002): Storm track dynamics. J. Climate, 15, 2163-2183.

Cook, K.H. (1999): Generation of the African Easterly Jet and Its Role in Determining West African Precipitation. J. Climate, 12, 1165–1184

Czaja, A. and C. Frankignoul (2002): Observed impact of Atlantic SST anomalies on the North Atlantic Oscillation. J. Climate, 15, 606-623.

Ding, Q. and B. Wang (2005): Circumglobal teleconnections in the Northern Hemisphere summer. J. Climate, 18, 3483-3505.

Douville, H., S. Conil, S. Tyteca and A. Voldoire (2007): Soil moisture memory and West African monsoon predictability: artefact or reality?. Climate Dyn., 28, 723-742.

Fontaine, B., P. Roucou, and S. Trzaska, 2003: Atmospheric water cycle and moisture fluxes in the West African monsoon: mean annual cycles and relationship using NCEP/NCAR reanalyses, Geophys. Res. Lett., 30, 10.1029-10.1032.

Fontaine B., P. Roucou and S. Sivarajan (2008): The relationship between surface temperatures over the Mediterranean and West African monsoon. Part I: observed connection patterns (1979-2006). J. Geophys. Res. Submitted.

Frankignoul C., A. Czaja and B. L'Heveder (1998): Air–Sea Feedback in the North Atlantic and Surface Boundary Conditions for Ocean Models. J. Climate, 11, 2310-2324.

Frankignoul, C. and E. Kestenare (2005): Observed Atlantic SST anomaly impact on the NAO: An update. J. Climate, 18, 4089-

4094.

García-Serrano, J., I. Polo, B. Rodríguez-Fonseca and T. Losada (2007): Summer-fall tropical precipitation related to Mediterranean SST anomalies. Poster presentation at 2nd ESF MedCLIVAR Workshop.

García-Serrano J., T. Losada, B. Rodríguez-Fonseca and I. Polo (2008): Tropical Atlantic Variability modes (1979-2002). Part II: time-evolving atmospheric circulation related to SST-forced tropical convection. J. Climate. DOI: 10.1175/2008JCLI2191.1

Gershunov, A. and T. P. Barnett (1998): Interdecadal modulation of ENSO teleconnections. Bull. Amer. Meteor. Soc., 79, 2715-2725.

Giannini, A., R. Saravanan and P. Chang (2003): Oceanic Forcing of Sahel Rainfall on Interannual to Interdecadal Time Scales. Science., 302, 1027–1030.

Grist, J. P., S. E. Nicholson and A. I. Barcilon (2002): Easterly Waves over Africa. Part II: Observed and Modeled Contrasts between Wet and Dry Years. Mon. Wea. Rev., 130, 212-225.

Haarsma R., F. Selten, N. Weber and M. Kliphuis (2008): Sahel Rainfall variability and response to Greenhouse Warming. Geophys. Res. Lett. (submitted).

Hall, N. M. J., G. Kiladis, and C. Thorncroft (2006): Threedimensional structure and dynamics of African easterly waves. Part II: Dynamical modes. J. Atmos. Sci., 63, 2231–2245.

Held, I. M., T. L. Delworth, J. Lu, K. L. Findell, and T. R. Knutson (2005): Simulation of Sahel drought in the 20th and 21st centuries. Proc. Natl. Acad. Sci., 102, 17.891–17.896.

Hoerling M, Hurrell J, Eischeid J, Phillips A (2006): Detection and Attribution of Twentieth-Century Northern and Southern African Rainfall Change. J Climate, 19, 3989–4008.

Hoskins, B. J., I. N. James and G. H. White, 1983: The shape, prop agation, and mean-flow interaction of large-scale weather sys tems. J. Atrnos. Sci., 40, 1595-1612.

Hoskins, B. J. and T. Ambrizzi (1993): Rossby wave propagation on a realistic longitudinally varying flow. J. Atmos. Sci., 50, 1661-1671.

Hsieh, J.-S. and K. H. Cook (2005): Generation of African Easterly disturbances: relationship to the African Easterly jet. Mon. Wea. Rev., 133, 1311-1327.

Janicot S.and B. Sultan (2001): Intra-seasonal modulation of convection in the West African monsoon. Geophys. Res. Lett., 28, 523-526.

Janicot, S., A. Harzallah, B. Fontaine and V. Moron (1998): West African Monsoon Dynamics and Eastern Equatorial Atlantic and Pacific SSTAnomalies(1970–88). J. Climate, 11,1874-1882.

Joly M., A. Voldoire, H. Douville, P. Terray, and J.-F. Royer (2007): African monsoon teleconnections with tropical SSTs: validation and evolution in a set of IPCC4 simulations. Clim. Dyn., 29, 1-20. doi: 10.1007/s00382-006-0215-8.

Jung, T., L. Ferranti, and A. M. Tompkins (2006): Response to the summer of 2003 Mediterranean SST anomalies over Europe and Africa, J. Climate, 19, 5439–5454.

Kodera, K., and Y. Kuroda (2003): Regional and hemispheric circulation patterns in the northern hemisphere winter, or the NAO and the AO. Geophys. Res. Lett., doi:10.1029/2003GL017290.

Kundu, P.K. (1990): Fluid Mechanics. Academic Press, Inc., 638 pp.

Li LZX (2006): Atmospheric GCM response to an idealized anomaly of the Mediterranean sea surface temperature. Clim Dyn, 27, 543-552.

Matthews, A. J. and G. N. Kiladis (1999a): The Tropical–Extratropical Interaction between High-Frequency Transients and the Madden–Julian Oscillation. Mon. Wea. Rev., 127, 661-677.

Matthews, A. J. and G. N. Kiladis (1999b): Interactions between ENSO, Transient Circulation, and Tropical Convection over the Pacific. J. Climate, 12, 3062-3086.

Mechoso, C. R., J.-Y. Yu and A. Arakawa (2000): A coupled GCM pilgrimage: from climate catastrophe to ENSO simulations. Proceeding of a Symposium in Honor of Prof. Akia Arakawa. Editor D.A. Randall, 539-575.

Mekonnen, A., C. D. Thorncroft and A. R. Aiyyer (2006): Analysis of Convection and Its Association with African Easterly Waves. J. Climate, 19, 5405-5421.

Michaelides, Silas Chr, (1983): Components of large-scale kinetic energy generation during an eastern Mediterranean cyclogenesis. Meteor. and Atmosp. Physics, 32, 247-256.

Mohíno, E., B. Rodríguez-Fonseca, S. Gervois, S. Janicot, T. Losada, J. Bader, P. Ruti (2008): SST-forced signals on West African rainfall from AGCM simulations-PartI: Intercomparison of models. Clim. Dyn., submitted

Moron V., N. Philippon and B. Fontaine (2004): Simulation of West African monsoon circulation in four atmospheric general circulation models forced by prescribed sea surface temperature. J. Geophys. Res., 109, doi:10.1029/2004JD004760.

Nicholson, S. E. (2008): The intensity, location and structure of the tropical rainbelt over west Africa as factors in interannual variability. Int. J. Climatol.., DOI: 10.1002/joc.1507.

Nicholson, S. E. and J. P. Grist (2001) : A conceptual model for understanding rainfall variability in the West African Sahel on interannual and interdecadal timescales. Int. J. Climatol. 21, 1733–1757.

Nicholson, S. E., A. I. Barcilon, M. Challa and J. Baum (2007): Wave Activity on the Tropical Easterly Jet. J. Climate, 64, 2756-2763.

Nicholson, S. E., A. I. Barcilon and M. Challa (2008): An Analysis of West African Dynamics Using a Linearized GCM. J. Atm. Sci., 65, 1182-1203.

Okumura, Y. and S.-P. Xie (2004): Interaction of the Atlantic Equatorial Cold Tongue and the African Monsoon. J. Climate, 17, 3589–3602.

Polo I., B. Rodríguez-Fonseca, T. Losada and J. García-Serrano (2008): Tropical Atlantic Variability modes (1979-2002). Part I: time-evolving SST modes related to West African rainfall. J. Climate, DOI: 10.1175/2008JCLI2607.1 (in press).

Qin, J. and W. A. Robinson, 1993: On the Rossby wave source and the steady linear response to tropical forcing. J. Atmos. Sci., 50, 1819-1823.

Raicich, F., N. Pinardi and A. Navarra (2003): Teleconnections between Indian monsoon and Sahel rainfall and the Mediterranean. Int. J. Climatol. 23, 173–186.

Renwick, J. A. and M. J. Revell (1999): Blocking over the South Pacific and Rossby Wave Propagation. Mon. Wea. Rev., 127,

2233-2247.

Rodwell, M. J. and B. Hoskins (1996): Monsoons and the dynamics of deserts. Q. J. R. Meteorol. Soc., 122, 1385-1404.

Rowell, D. P. (2001): Teleconnections between the tropical Pacific and the Sahel. Q. J. R. Meteorol. Soc., 127, 1683-1706.
Rowell, D. P. (2003): The impact of the Mediterranean SSTs on the Sahelian rainfall season. J. Climate, 16, 849-862.

Sardeshmukh, P. D. and B. Hoskins (1987): On the derivation of the divergent flow from the rotational flow: the chi problem. Q. J. R. Meteorol. Soc., 113, 339-360.

Seidel, D. J., Fu, Q., Randel, W. J. and Reichler, T. J. (2008): Widening of the tropical belt in a changing climate. Nature geoscience 1, 21-24, doi:10.1038/ngeo.2007.38.

Sultan, B. and S. Janicot (2000): Abrupt shift of the ITCZ over West Africa and intra-seasonal variability. Geophys. Res. Lett., 27, 3353-3356.

Trenberth, K. E. (1986): An assessment of the impact of transient eddies on the zonal flow during a blocking episode using localized Eliassen–Palm flux diagnostics. J. Atmos. Sci., 43, 2070–2087.

Trenberth, K.E. and J.W. Hurrell (1994): Decadal atmosphere-ocean variations in the Pacific. Clim. Dyn., 9, 303-319.

Wallace, J. M., G.H. Lim and M. L. Blackmon (1988): Relationship between cyclone tracks, anticyclone tracks, and baroclinic waveguides. J. Atmos. Sci., 45, 439-462.

Wang, C. (2002): Atlantic Climate Variability and Its Associated Atmospheric Circulation Cells. J. Climate, 15, 1516-1536.

Watanabe, M. (2004): Asian Jet Waveguide and a Downstream Extension of the North Atlantic Oscillation. J. Climate, 17, 4674-4691.

Xoplaki, E., J.F. González-Rouco, D. Gyalistras, J. Luterbacher, R. Rickli and H. Wanner (2003a): Interannual summer air temperature variability over Greece and its connection to the large-scale atmospheric circulation and Mediterranean SSTs 1950-1999. Clim. Dyn., 20, 537-554.

Xoplaki, E., J.F. González-Rouco, J. Luterbacher and H. Wanner (2003b): Mediterranean summer air temperature variability and its connection to the large-scale atmospheric circulation and SSTs. Clim. Dyn., 20, 723-739.

Zhang, Y., J.M. Wallace and D.S. Battisti (1997): ENSO-like interdecadal variability: 1900-93. J. Climate, 10, 1004-1020.

APÉNDICE D

Memoria de Estancia en KNMI 2009

TME2008-00927
Con la ayuda del Ministerio de Educación del Gobierno de España

RESUMEN DE ACTIVIDADES DE LA AYUDA *TME2008-00927*
para la Tesis Doctoral (Mención Europea)

Estudio de teleconexiones atmosféricas asociadas a forzamientos oceánicos. Influencia en el clima de Europa

La propuesta original para esta Ayuda era el análisis de una simulación AGCM (atmospheric general circulation model) que se realizó, por parte del Grupo de Investigación del doctorando, dentro del proyecto europeo AMMA (African monsoon multidiscilinary analises). En el marco de este proyecto, un trabajo observacional (García-Serrano et al. 2007) reveló que la cuenca este del Mediterráneo (Fig. 1) era capaz de generar una respuesta baroclínica, típica de latitudes tropicales, en la que la temperatura del mar (TSM[1]) fuerza una convergencia de aire cerca de la superficie asociada a una divergencia de aire en altura. Esta hipótesis fue corroborada con el uso de 3 modelos AGCM en un experimento del protocolo AMMA, el cual se basó en otro trabajo del Grupo de Investigación (Polo et al. 2008). La rápida aceptación del estudio en la revista *Climate Dynamics* (Fontaine et al. 2009) aceleró el trabajo en la hipótesis de partida de esta Ayuda: esa respuesta baroclínica al forzamiento del Mediterráneo puede provocar una respuesta barotrópica (mismo carácter en toda la columna) que queda atrapada en la corriente en chorro subtropical y se propaga zonalmente hasta el océano Pacífico y el Atlántico Norte.

Durante la primavera de este año se ha realizado un intenso trabajo analizando las salidas de la simulación AMMA-AGCM del modelo UCLA; y durante el verano se trabajó en la redacción del artículo que será enviado en breve (García-Serrano et al. 2009). En parte de acuerdo a la propuesta, durante la estancia en el KNMI se han discutido en profundidad los resultados y conclusiones del estudio, así como las líneas abiertas de colaboración en las teleconexiones asociadas la TSM del Mediterráneo.

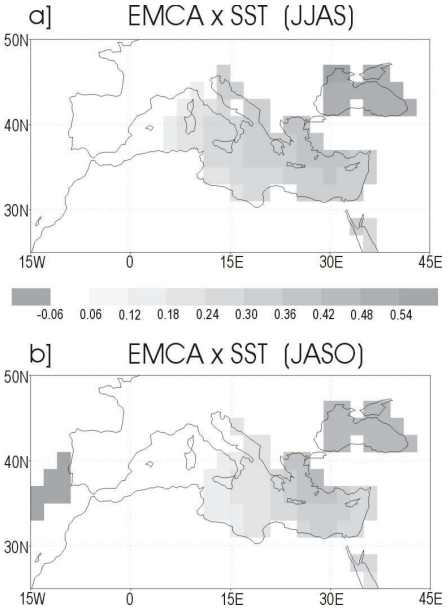

Figura 1. Mapas de regresión de TSM sobre la serie EMCA de Polo et al. (2008).

1 Acrónimo de 'temperatura de la superficie del mar' (TSM)

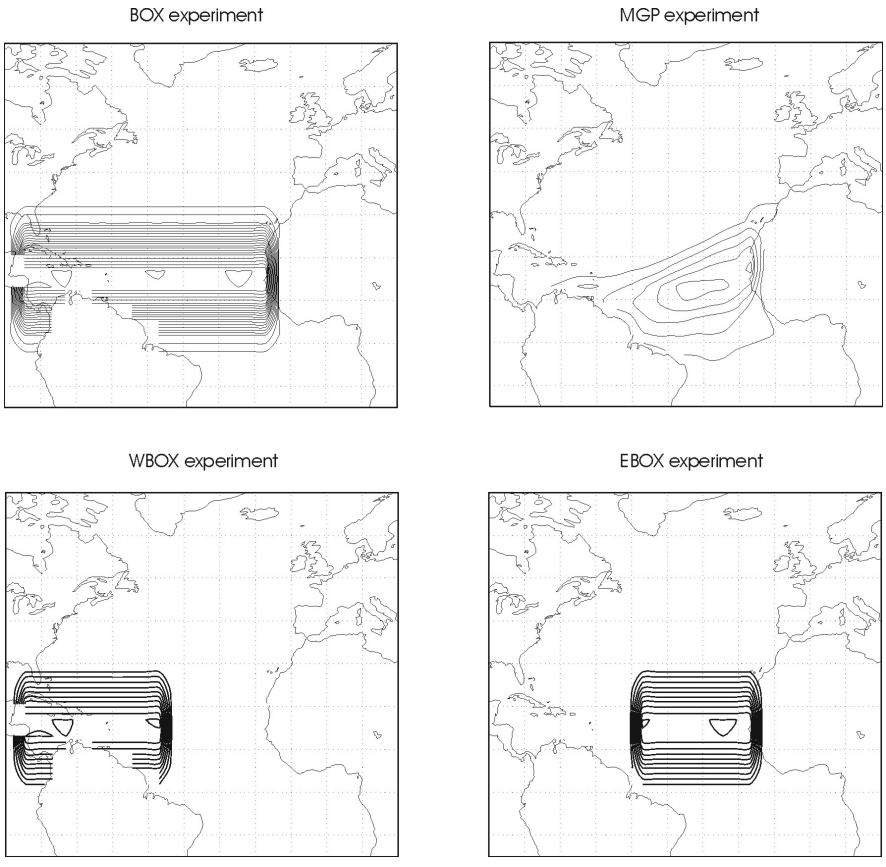

Figura 2. Anomalías de TSM como condiciones de borde en experimentos AGCM y AGCM-SLAB.

El trabajo desarrollado durante la estancia en el KNMI, sin embargo, se centró más en otra línea de investigación de la Tesis Doctoral: el impacto del Atlántico Norte Subtropical en la circulación atmosférica del sector Euro-Atlántico.

El departamento de acogida en el KNMI (Global Climate-division), liderada por el Dr Wilco Hazeleger, tiene una amplia experiencia en el estudio de la variabilidad climática del Atlántico Tropical, la circulación extratropical sobre el océano Atlántico, y el clima en Europa (http://www.knmi.nl/research/). Así mismo, mi supervisor en el KNMI, el Dr Reindert Haarsma, tiene numerosas publicaciones sobre la variabilidad del Atlántico Tropical y su respuesta atmosférica (Haarsma et al. 2003; Hazeleger and Haarsma 2005; Haarsma et al. 2005; Haarsma and Hazeleger 2007), y en particular sobre el modo del Atlántico Subtropical (Breugem et al. 2007).

El modelo AGCM con que el trabajé, y que ahora se está poniendo en marcha en el cluster TROPA del Aula-SUN de la UCM, es un modelo de atmósfera de complejidad intermedia llamado SPEEDY[2] . Este modelo tiene una resolución T30L7; que corresponde con 3.75º en longitud, aprox. 3.7º en latitud y 8 niveles en la vertical (1000-925-850-700-500-300-200-100 hPa).

Durante la estancia trabajé con dos configuraciones de océano acopladas al modelo de atmósfera: i) un modelo de océano pasivo, que sólo proporciona TSM a la atmósfera, y que constituye propiamente lo que se conoce por *AGCM*; ii) y un modelo de capa de mezcla, que proporciona TSM y flujos de calor resultado del acoplamiento océano-atmósfera (OAGCM), que se conoce como *AGCM-SLAB*.

2 *Acrónimo del término inglés 'Simplified Parametrizations Primitive Equation Dynamics'*

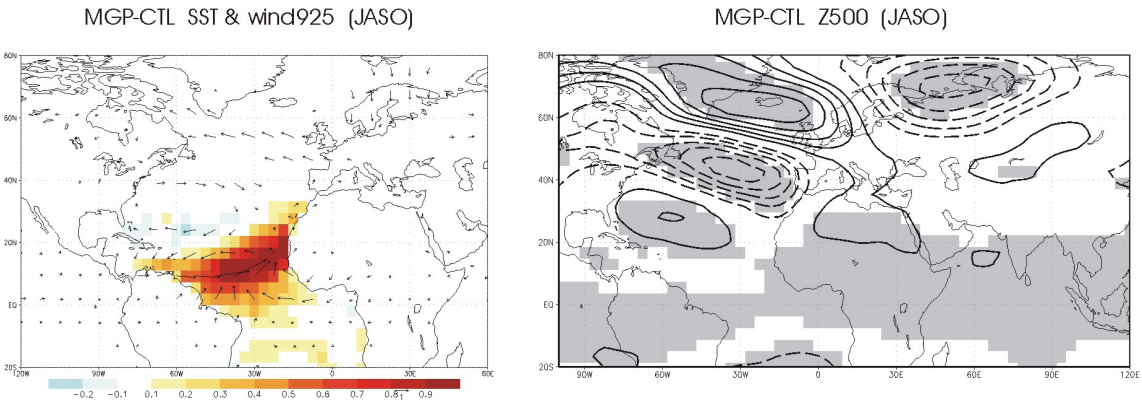

Figura 3. Respuesta atmosférica en 925hPa y 500hPa del AGCM a un SAP (Subtropical Atlantic-positive). La significación estadística del viento en 925hPa (m/s) y de Z500 (i.c.=2m) es 95% (test-t Student).

El punto de partida del trabajo era un estudio anterior basado en observaciones (García-Serrano et al. 2008), en el que se planteó la hipótesis de que la persistencia de anomalías de TSM (desde el verano hasta el invierno) en el Atlántico Norte Subtropical podía forzar un patrón de teleconexión conocido como Oscilación del Atlántico Norte (NAO[3]), el cual tiene un fuerte impacto en el clima de la Península Ibérica (Rodríguez-Fonseca and Castro 2002) y del resto de Europa (Rodríguez-Fonseca et al. 2006).

El primer estudio que se llevó a cabo fue un experimento de sensibilidad en la respuesta atmosférica a un calentamiento en el Atlántico Norte Subtropical; esto es, se prescribió una anomalía de TSM fija a lo largo del año para analizar la respuesta atmosférica en función del ciclo estacional. La anomalía de TSM corresponde al Modo Meridional (MGP; Meridional Grandient-positive; Fig. 2) obtenido por Hazeleger y Haarsma (2005) con el mismo modelo SPEEDY. El experimento se realizó usando el AGCM y el AGCM-SLAB. Ambas simulaciones comprendieron 100 años de integración; y se compararon con otra simulación de 100 años con TSM climatológica (experimento control; CTL).

Los resultados indicaron que el AGCM y el AGCM-acoplado producían la misma respuesta a lo largo del año. Sorprendentemente, la respuesta más débil era en invierno, en contra de la hipótesis (observacional) de partida; mientras que la respuesta más clara era al final del verano-principio de otoño. En la Fig. 3 se muestra la respuesta atmosférica en superficie (izda.) y en altura (dcha.) junto con la TSM anómala en JASO para el AGCM. Se puede apreciar el carácter barotrópico del tren de ondas Rossby que emana del Atlántico Tropical y alcanza el norte de Europa.

Después de este experimento de sensibilidad, se optó por un enfoque más realista: introducir una anomalía de TSM en la capa de mezcla del AGCM-SLAB (de 50 metros en toda la cuenca del Atlántico) en un determinado tiempo, y dejar libre el sistema acoplado OAGCM para que evolucione. Este enfoque está basado en el trabajo de Wu et al. (2007); en el que se introducía una anomalía de 2ºC en forma de caja (BOX; Fig. 2) en una profundidad 0-200m en todo el Atlántico tropical-subtropical el día 1 de Enero, y se corría una simulación de 2 años. Ese experimento se realizó con un modelo complejo de océano (que incluye dinámica oceánica, no sólo una capa de mezcla) y un modelo estado-del-arte de atmósfera (gran resolución horizontal y vertical, y sin simplificaciones en las ecuaciones). Nuestro diseño experimental constaba de 50 miembros (50 condiciones atmosféricas iniciales diferentes), y una temperatura anómala inicial también en forma de caja (máx. 2ºC) en la capa de mezcla (0-50m).

En la Fig. 4 se muestra la respuesta atmosférica del geopotencial en 500hPa (Z500) y la respuesta oceánica (SST[4]) a la evolución del acoplamiento océano-atmósfera para tres estaciones descritas por Wu et al.

3 *Acrónimo del término inglés 'North Atlantic Oscillation'*
4 *Acrónimo inglés de 'sea surface temperature' (SST), que corresponde con TSM*

(2007). De este análisis se desprende que el modelo de atmósfera SPEEDY más el modelo de océano SLAB (configuración AGCM-SLAB) son capaces de reproducir los resultados de un modelo mucho más complejo y más costoso computacionalmente; lo que hace del SPEEDY un modelo muy apto para este estudio. De los resultados de esta simulación se deriva también que con una capa de mezcla de 50m (bastante realista en comparación con 200m) no se puede simular una persistencia de las anomalías de TSM de invierno-a-invierno como la mostrada por Wu et al. (2007).

Para final del invierno-principio de primavera (FMA), la respuesta atmosférica proyecta en el patrón de la NAO; para verano (MJJ) la respuesta corresponde a una onda de Rossby que se propaga por la cuenca oeste del Atlántico Norte; y para el otoño (ce acuerdo con Fig. 3) el tren de ondas Rossby alcanza el continente europeo atravesando el centro del Atlántico Norte.

En este último experimento con AGCM-SLAB (Fig. 4), el diseño experimental consistió en una simulación de 50 miembros que cubrían 2 años de integración. La respuesta atmosférica analizada corresponde a la respuesta 'estacionaria' al acoplamiento océano-atmósfera; es decir, corresponde a la media estacional (tres meses) de la respuesta al forzamiento, que corresponde a una respuesta-en-equilibrio.

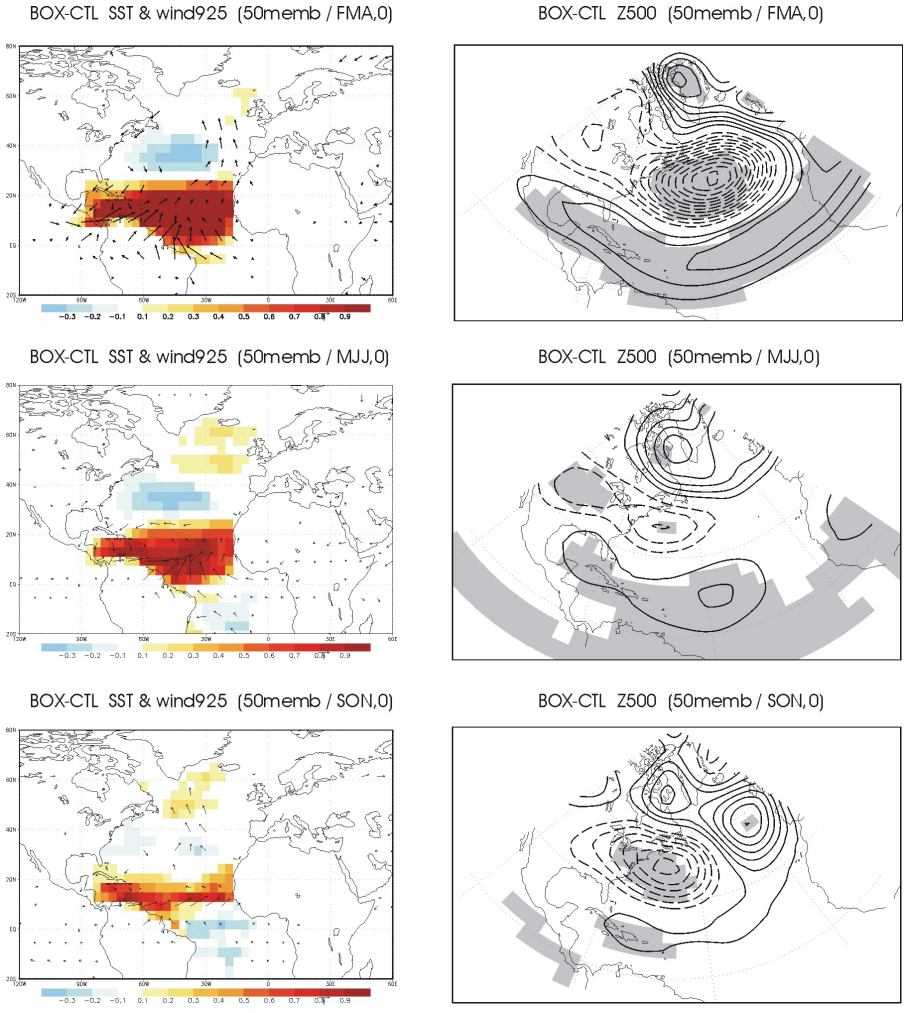

Figura 4. Respuesta oceánica en TSM (izda.), viento en 925 (izda.) y Z500 (dcha.) a una caja de 2ºC en el Atlántico Norte Subtropical (BOX; Fig. 2) prescrita el día 1 de Enero, y AGCM-SLAB evoluciona libre.

En el último tipo de experimentos que lleve a cabo se analizó la respuesta 'transitoria' a un forzamiento; es decir, la respuesta atmosférica antes de alcanzar el equilibrio; en particular, la respuesta diaria al acoplamiento océano-atmósfera. El diseño experimental tuvo por objeto discutir el mecanismo de la respuesta atmosférica a la cuenca oeste (WBOX; Fig. 2) y a la cuenca este (EBOX; Fig. 2) del Atlántico Norte Subtropical del experimento BOX. En estas simulaciones transitorias se redujo el tiempo de integración (de 2 años a 1 mes) pero se aumentó el número de miembros (de 50 miemb. a 200 miemb.). En la Fig. 5 se muestra la respuesta del geopotencial en 300hPa (Z300) para el día 2, día 4 y día 6 de integración para WBOX (izda.) y EBOX (dcha.). Las 200 condiciones atmosféricas diferentes (200 miembros) se obtuvieron de una simulación AGCM control de 200 años; mientras que los experimentos de sensibildad (WBOX, EBOX) se compararon con otra integración control (CTL; 200 miemb.) en la que se prescribieron TSM climatológicas.

De estos experimentos transitorios se desprende que el tren de ondas Rossby emana de regiones diferentes y sigue rutas diferentes como respuesta a los forzamientos en la parte oeste (WBOX) y este (EBOX) del Atlántico Norte Subtropical: la respuesta atmosférica es forzada desde el Caribe y se propaga a lo largo de la corriente en chorro (jet) del Atlántico Norte en el caso WBOX; mientras que se dispara desde el centro-este del Atlántico Tropical y se propaga entre el jet de altas latitudes (corriente en chorro del Atlántico Norte) y el jet subtropical (corriente en chorro del Norte de África) en el caso EBOX.

La estancia del doctorando en la institución del acogida (KNMI) ha dado lugar a la instalación y puesta en marcha del modelo SPEEDY en el cluster TROPA; en el que ahora mismo se trabaja en la compilación del modelo. La fructífera colaboración, derivada de la estancia, entre el KNMI y el Grupo de Investigación del doctorando (TROPA-UCM; http://tropa.fis.ucm.es/) está produciendo importantes resultados y está abriendo nuevas líneas de investigación de las teleconexiones trópico-extratrópico. En este momento se están analizando las últimas simulaciones realizadas en el KNMI y se están preparando las condiciones de borde (TSM) de las primeras simulaciones con SPEEDY (AGCM-SLAB) que se realizarán en la UCM. Los principales resultados derivados de este trabajo conformarán un artículo ya en preparación (García-Serrano et al. 2010).

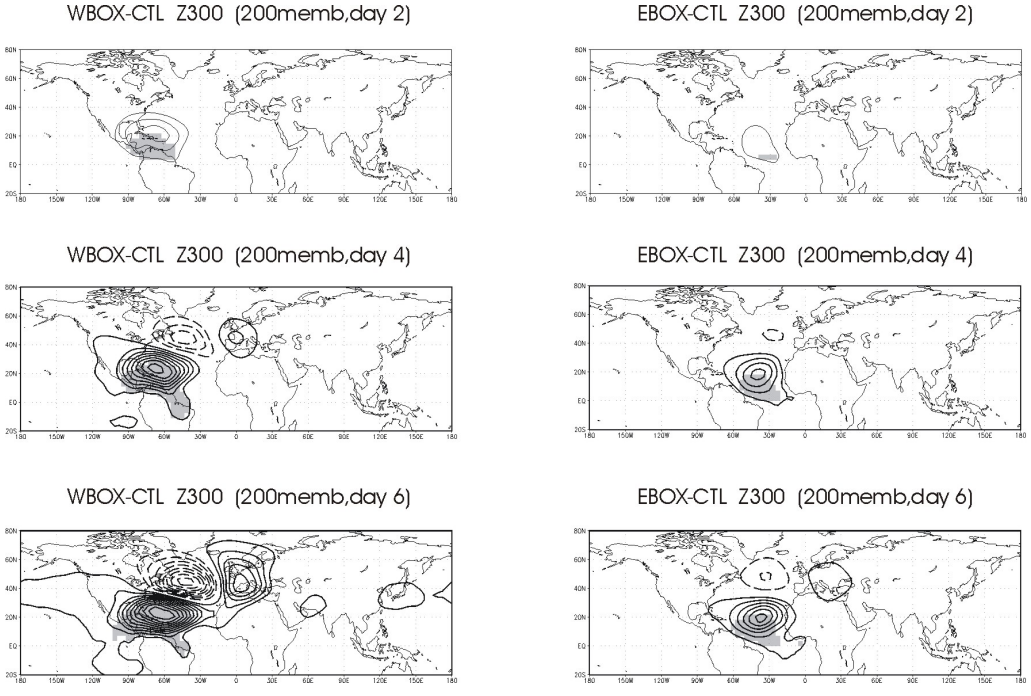

Figura 5. Respuesta atmosférica (Z300) en el día 2, día 4 y día 6 de integración en AGCM-SLAB que evoluciona libre tras el forzamiento WBOX (izda.) y EBOX (dcha.) prescrito el día 1 de Enero.

REFERENCIAS:

Breugem, W.-P., W. Hazeleger, R. J. Haarsma (2007): Mechanism of Northern Tropical Atlantic variability and response to CO2 doubling. J. Clim., 20 (11), 2691-2705.

Fontaine, B., J. García-Serrano, P. Roucou, B. Rodríguez-Fonseca, T. Losada, F. Chauvin, S. Gervois, S. Sijikumar, P. Ruti, S. Janicot (2009): Impacts of warm and cold situations in the Mediterranean basins on the West African monzón: observed connection patterns (1979-2006) and climate simulations. Clim. Dyn., DOI 10.1007/s00382-009-0599-3.

García-Serrano, J., I. Polo, B. Rodríguez-Fonseca, T. Losada (2007): Summer-fall tropical precipitation related to Mediterranean SST anomalies. Poster presentation at 2nd ESF-MedCLIVAR Workshop.

García-Serrano, J., T. Losada, B. Rodríguez-Fonseca, I. Polo (2008): Tropical Atlantic variability modes (1979-2002). Part II: time-evolving atmospheric circulation related to SST-forced. J. Clim., 21 (24), 6476-6497.

García-Serrano, J., I. Polo, B. Rodríguez-Fonseca, T. Losada (2009): Large-scale atmospheric response to Mediterranean summer SST anomalies. Clim. Dyn. (en elaboración).

García-Serrano, J., R. Haarsma, B. Rodríguez-Fonseca (2010): The influence of the Subtropical North Atlantic on the extratropical atmospheric circulation. Clim. Dyn. (en elaboración).

Haarsma, R. J., E. J. D. Campos, F. Molteni (2003): Atmospheric response to South Atlantic SST dipole. Geophys. Res. Lett., 30, 1864, DOI 10.1029/2003GL017829.

Haarsma, R. J., E. J. D. Campos, W. Hazeleger, C. Severejins, A. R. Piola, F. Molteni (2005): Dominant modes of variability in the South Atlantic: a study with a hierarchy of ocean-atmosphere models. J. Clim., 18 (11), 1719-1735.

Haarsma, R. J. and W. Hazeleger (2007): Extratropical atmospheric response to Equatorial Atlantic cold tongue anomalies. J. Clim., 20 (10), 2076-2091.

Hazeleger, W. and R. J. Haarsma (2005): Sensitivity of Tropical Atlantic climate to mixing in a coupled ocean-atmosphere model. Clim. Dyn., 25 (4), 387-399.

Polo, I., B. Rodríguez-Fonseca, T. Losada, J. García-Serrano (2008): Tropical Atlantic variability modes (1979-2002). Part I: time-evolving SST modes related to West African rainfall. J. Clim., 21 (24), 6476-6497.

Rodríguez-Fonseca, B. and M. Castro (2002): On the connection between winter anomalous precipitaion in the Iberian Peninsula and North West Africa and the summer subtropical Atlantic sea surface temperature. Geophys. Res. Lett., 29 (18), 1863, DOI 10.1029/2001GL014421.

Rodríguez-Fonseca, B., I. Polo, E. Serrano, M. Castro (2006): Evaluation of the North Atlantic SST forcing on the European and North African winter climate. Int. J. Climatol., 25, DOI 10.1002/7joc.1234.

Wu, L., F. He, Z. Liu, C. Li (2007): Atmospheric teleconnections of Tropical Atlantic variability: interhemispheric, tropical-extratropical, and cross-basin interactions. J. Clim., 20 (5), 856-870.

AGRADECIMIENTOS

Siempre parece que en esta sección hay que poner todo lo personal que no se ha puesto en el resto de capítulos; yo he intentado que no fuera así, no sé si lo he conseguido. Llegado este momento, siempre tiene uno la sensación de que se le va a olvidar alguien o algo importante; espero que no sea mucho.

Cronológicamente. Juan, Samu, gracias por acompañarme y hacer más llevadera la Licenciatura. Gracias Elvira por decirme que hay algo muy apasionante que se llama Atmósfera. Encarna, sabes que sin ti esto nunca habría visto la luz; mil gracias. Roberto, gracias de corazón por haber perdido tiempo conmigo. Belén, Irene, la primera imagen marca bastante: vosotras totalmente volcadas sobre el ordenador hablando frente a colorbars y contours...uy, esto se puede hacer eterno...bueno, una más: Álvaro compartiendo un vinito en Sevilla diciendo que sé hacer cosas...qué locura!.

Gracias a todos los del Laboratorio y los de fuera de él por haberme hecho sentir bien, muy bien: Teresa, Xavier, Elena, África, Quique, Víctor, Rafa, Ana, Simone, Gianluca, Gregg, Carlos (qué grande!), Carlitos, Oscar, Oscar y Sonia, Salva, Lucía, Marisa, Fidel, Álvaro, Javi, Juan Luis, Pablo, Bea, Dani, Almudena, Tatiana, Paco...(y como en una segunda etapa, imaginaria totalmente)...Blanca, Elsa, Juan, Maurizio, Pablo, Fátima, David, Etor, Esteban, Marta, Bea, Mariano, Jorge, Iñigo, Marta. Gracias en general a todo el Departamento por mostrarme siempre su apoyo (Michel, parece que acabaré leyendo la Tesis con cara de trabajador!).

Belén, sé que al final ha sido complicado...pero siempre mereció la pena; gracias por todo lo que me has enseñado. Irene, gracias por escucharme tantas y cuantas...y por abrirnos algunas veces.

Muchas gracias Alberto por confiar en mí; no sabes lo que eso ha representado. Steve, gracias (saludos a Julie!). Rein, gracias por acogerme y por transmitirme tanto.

Y para variar, los últimos serán los primeros...y más importantes. Para mis padres sobran las palabras, por eso les he dedicado el libro. Lucas, gracias por los años de la Parra; gracias por acercarme el Cálculo y el Álgebra como sólo tú sabes hacer (Nuria, qué suerte tienes!); gracias por soportarme y por hacerme ver que me soportabas; gracias por compartir cosas conmigo. Adri, gracias por hacerme ver que hay otro mundo más allá del de Rossby y del de Fox Mulder; gracias por lo que has hecho con la Tesis!; gracias por todo, te quiero.

Este trabajo ha sido realizado gracias a los proyectos nacionales REN2002-03424, CGL2005-06600-C03-02 (AVACOA), CGL2006-04471 (TROVA) y 2008-00050084028 (MOVAC); al proyecto europeo AMMA; y a las estancias subvencionadas por la ESF-MedCLIVAR (EG/1694) y el Ministerio de Educación (TME2008-00927).